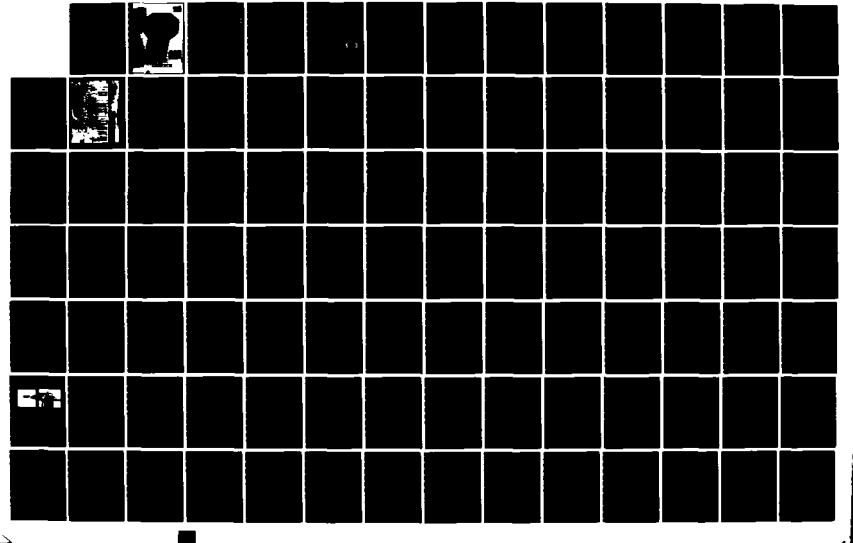
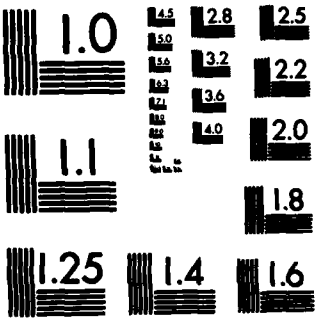
AD-A144 226 PROCEEDINGS OF THE GENERAL MEETING OF THE AMERICAN TOWING TANK CONFERENCE..(U) STEVENS INST OF TECH HOBOKEN NJ DAVIDSON LAB D SAVITSKY ET AL. AUG 83 SIT-DL-TR-13029-VOL-1 N00167-83-M-4062 F/G 20/4 NL

1/7

UNCLASSIFIED





MICROCOPY RESOLUTION TEST CHART
NATIONAL BUREAU OF STANDARDS-1963-A

AD-A144 226

(1)

PROCEEDINGS OF THE

TWENTIETH GENERAL MEETING OF THE

AMERICAN TOWING TANK CONFERENCE

DAVIDSON LABORATORY
STEVENS INSTITUTE OF TECHNOLOGY
HOBOKEN, NEW JERSEY

2-4 AUGUST 1983

DTIC FILE COPY

DTIC
S JUN 8 1984 D

VOLUME I

A A

84 05 16 030

COMPONENT PART NOTICE

THIS PAPER IS A COMPONENT PART OF THE FOLLOWING COMPILATION REPORT:

(TITLE): Proceedings of the General Meeting of the American Towing Tank Conference (20th) Held at Hoboken, New Jersey on 2-4 August 1983. Volume 1.

(SOURCE): Stevens Inst. of Tech., Hoboken, NJ. Davidson Lab.

DTIC ELECTE AUG 22 1984 S D A

TO ORDER THE COMPLETE COMPILATION REPORT USE AD-A144 226.

THE COMPONENT PART IS PROVIDED HERE TO ALLOW USERS ACCESS TO INDIVIDUALLY AUTHORED SECTIONS OF PROCEEDINGS, ANNALS, SYMPOSIA, ETC. HOWEVER, THE COMPONENT SHOULD BE CONSIDERED WITHIN THE CONTEXT OF THE OVERALL COMPILATION REPORT AND NOT AS A STAND-ALONE TECHNICAL REPORT.

THE FOLLOWING COMPONENT PART NUMBERS COMPRISE THE COMPILATION REPORT:

AD#:	TITLE:
AD-P003 803	Wave Cut Tests to Optimize Hull Form Changes.
AD-P003 804	Total Resistance Calculations of Appended Destroyer Hull Forms.
AD-P003 805	Comparisons of Large and Small Models for the Prediction of Resistance.
AD-P003 806	A Comparison of Two Propellers for the Acoustic Research Ship CFAV (Canadian Forces Auxiliary Vessel) Quest.
AD-P003 807	Comparative Performance of Stock and Design Propellers Derived from Propulsion Experiments.
AD-P003 808	Cavitation Inception: A Review-Progress Since 19th ATTC (American Towing Tank Conference).
AD-P003 809	On the Design of Cavitation Susceptibility Meters (C.S.M.s).
AD-P003 810	The Influence of Pressure Gradient on Desinent Cavitation Produced by the Separated Flow from an Isolated Triangular Surface Protrusion.
AD-P003 811	Some Applications of Free Streamline Theory.
AD-P003 812	Numerical Solutions of Lifting Surface Sheet Cavitation: A Review of Research at M.I.T. (Massachusetts Institute of Technology).
AD-P003 813	High Speed Maneuvering of Amphibious Hovercraft.
AD-P003 814	Extended Performance Hydrofoil Program.
AD-P003 815	Planning Surface ¢(F).
AD-P003 816	Planing Patrol Vessel Feasibility Study.
AD-P003 817	Experimental Determination of Low Froude Number Hydrofoil Performance in Calm Water and in Regular Waves.

This document has been approved for public release and sale; its distribution is unlimited.

Codes /or 1

A-1

COMPONENT PART NOTICE (CON'T)

AD#: TITLE:

UNCLASSIFIED

SECURITY CLASSIFICATION OF THIS PAGE (When Data Entered)

REPORT DOCUMENTATION PAGE		READ INSTRUCTIONS BEFORE COMPLETING FORM
1. REPORT NUMBER TR-13029	2. GOVT ACCESSION NO. AD-A144	3. RECIPIENT'S CATALOG NUMBER 226
4. TITLE (and Subtitle) PROCEEDINGS OF THE TWENTIETH GENERAL MEETING OF THE AMERICAN TOWING TANK CONFERENCE		5. TYPE OF REPORT & PERIOD COVERED Final Report August 1983 6. PERFORMING ORG. REPORT NUMBER
7. AUTHOR(s) Edited by: Daniel Savitsky, John F. Dalzell and Mary Palazzo		8. CONTRACT OR GRANT NUMBER(s) NSF Grant MEA-8311237 ONR Grant N00014-83-G-0089 NSRDC Contract N00167-83-M-4062
9. PERFORMING ORGANIZATION NAME AND ADDRESS Davidson Laboratory Stevens Institute of Technology Hoboken, NJ 07030		10. PROGRAM ELEMENT, PROJECT, TASK AREA & WORK UNIT NUMBERS
11. CONTROLLING OFFICE NAME AND ADDRESS David W. Taylor Naval Ship Research and Develop. Center, Bethesda, MD; National Science Foundation, Wash. DC; ONR, Arlington, VA		12. REPORT DATE August 1983 13. NUMBER OF PAGES
14. MONITORING AGENCY NAME & ADDRESS (if different from Controlling Office)		15. SECURITY CLASS. (of this report) UNCLASSIFIED 15a. DECLASSIFICATION/DOWNGRADING SCHEDULE

16. DISTRIBUTION STATEMENT (of this Report)

APPROVED FOR PUBLIC RELEASE: DISTRIBUTION UNLIMITED

17. DISTRIBUTION STATEMENT (of the abstract entered in Block 20, if different from Report)

DTIC
ELECTE
JUN 8 1984
S D
B

18. SUPPLEMENTARY NOTES

19. KEY WORDS (Continue on reverse side if necessary and identify by block number)

Cavitation	High Speed Vehicles
Ice Testing	Propulsion
Seakeeping	Systems and Techniques
Steering and Maneuvering	Resistance and Flow

20. ABSTRACT (Continue on reverse side if necessary and identify by block number)

Collection of contributions for the Proceedings of the 20th American Towing Tank Conference contained in a two (2) volume set.

DD FORM 1 JAN 73 1473 EDITION OF 1 NOV 65 IS OBSOLETE
S/N 0102-014-6601

UNCLASSIFIED

SECURITY CLASSIFICATION OF THIS PAGE (When Data Entered)

PROCEEDINGS OF THE

TWENTIETH GENERAL MEETING OF THE

AMERICAN TOWING TANK CONFERENCE

DAVIDSON LABORATORY
STEVENS INSTITUTE OF TECHNOLOGY
HOBOKEN, NEW JERSEY

2-4 AUGUST 1983

VOLUME I

EDITED BY:

Daniel Savitsky
John F. Dalzell
Mary Palazzo

SPONSORED BY:

Stevens Institute of Technology
National Science Foundation
Office of Naval Research
David W. Taylor Naval Ship Research and Development Center
Society of Naval Architects and Marine Engineers
Maritime Industry Sponsors

PREFACE

The Twentieth meeting of the American Towing Tank Conference was held at Stevens Institute of Technology, Hoboken, New Jersey from the 2nd to the 4th of August, 1983. Approximately 100 delegates and observers from North and South America representing 45 professional establishments and universities attended.

The ATTC is a voluntary association of establishments in the Western Hemisphere having a responsibility in the prediction of hydrodynamic performance of ships, structures, water-borne craft and their appendages and propulsors from tests on scaled models. The Conference is a purely communicative body; it has no authority of financial sponsorship; its membership is voluntary and self-supporting and it assembles on an approximately three year interval in different countries in the Western Hemisphere. Its product is the Conference Proceedings which are published and provided to all registered attendees and made available to others.

It is of interest to note that the founding meeting of the ATTC was also held at Stevens Institute of Technology some 45 years ago on 14th and 15th of April, 1938, and the superintendents of the following six towing tank establishments attended:

U.S. Naval Experimental Model Basin	Washington, DC
National Advisory Committee for Aeronautics	Langley Field, VA
Stevens Institute of Technology	Hoboken, NJ
National Research Council	Ottawa, Canada
Newport News Shipbuilding	Newport News, VA
University of Michigan	Ann Arbor, MI

Only the NACA and Newport News Shipbuilding are no longer active members of the ATTC but the others have been joined by 12 additional organizations for a total of 16 members representing four countries in North and South America. In comparison, the International Towing Tank Conference presently has a membership of 83 Institutions from 32 countries.

The charter members of the first ATTC believed that the foundation of an American association of tank directors would allow for a valuable exchange of ideas, problems, test techniques, standardization of test procedures and enhancement of the value of tank results for the designer and ship operator. Their concern was mainly in estimates of power, relative performance, and model-full size trial correlations. These broad aims are still applicable today as evidenced by the numerous "tankery" papers being presented at the 20th ATTC. The major changes in nearly five decades of existence have been the growth in membership of American towing tanks; the active participation in the Conference of "tankery" researchers in addition to tank superintendents; a strong involvement with the ITTC; and an extensive broadening of technical interests from the limited resistance and propulsion studies of 45 years ago to today's involvement in cavitation, seakeeping, maneuvering, systems and techniques, high speed craft and testing in ice.

The Executive Committee of the 20th ATTC selected individuals to serve as chairmen and to organize committees to report on the technical developments in each of the eight subject areas just described. The summary

of the state of the art and the choice of papers to be presented in each subject area were entirely the chairman's decision. Indeed, the Conference is grateful to the various chairmen who, through an assortment of undefined persuasions, managed to assemble outstanding committee members who provided 50 excellent papers (some of which arrived just hours prior to the welcoming address) and valuable discussions from the members of the Conference. The sheer magnitude of these contributions required a two volume publication of the proceedings containing the following materials:

Volume I
Resistance and Flow
Propulsion
Cavitation
High Speed Craft

Volume II
Ice Testing
Steering and Maneuvering
Seakeeping
Systems and Techniques
General Report (including Business Session)

The Executive Committee of the 20th ATTC extends its thanks and gratitude to those organizations whose financial contributions made this Conference possible. They are identified on the following page of these proceedings. We are also indebted to Prof. Jacques Hadler, Dean at Webb Institute of Naval Architecture, and our dinner speaker, who projected the future roll of towing tanks in "The Uncertain 80's". His speech is included in Volume I.

The Executive Committee is especially grateful to Mr. Seth Hawkins of David W. Taylor Naval Ship Research and Development Center for his guidance and many valuable suggestions which assured the success of our Conference. We also thank Ms. Mary Palazzo, our most efficient and cheerful secretary who handled the correspondence, collated the papers and contributions, arranged the social activities, assisted in travel arrangements and on and on. In all her efforts she was graciously and ably assisted by Ms. Mary Ann McGuire. To many others on the staff of the Davidson Laboratory and Stevens Institute, whose generous contributions of time and suggestions were so valuable, we thank you all.

Daniel Savitsky, Chairman
John F. Dalzell, Secretary

SPONSORS

The Executive Committee of the 20th American Towing Tank Conference extends its thanks to those organizations whose financial contributions made this Conference possible.

David W. Taylor Naval Ship Research
and Development Center

National Science Foundation

Office of Naval Research

Society of Naval Architects
and Marine Engineers

Boeing Marine Systems

C.R. Cushing & Co., Inc.

Gibbs & Cox, Inc.

Marinette Marine Corporation

John F. McMullen Associates, Inc.

Mobil Shipping & Transportation Co.

National Steel & Shipbuilding Co.

Newport News Shipbuilding & Dry Dock Co.

Peterson Builders, Inc.

M. Rosenblatt & Son, Inc.

Tampa Shipyards, Inc.

Tracor, Inc.



Accession For	
NTIS GRA&I	☑
DTIC TAB	☐
Unannounced	☐
Justification	
By	
Distribution/	
Availability Codes	
Dist	Avail and/or Special
A-1	

TABLE OF CONTENTS

VOLUME I

Preface.....iii

Sponsors.....v

Table of Contents.....vi

Program Schedule.....ix

Committees.....x

Group Photograph.....xi

Participants.....xiii

Contributors (Not in Attendance).....xix

PROGRAM:

Resistance and Flow - Chaired by Dr. A. Reed

1. "Progress in Resistance and Flow: A Long Term Perspective," Committee Report.....3

2. "Wave Cut Tests to Optimize Hull Form Changes," L. W. Ward, Webb Institute of Naval Architecture.....29

3. "Total Resistance Calculations of Appended Destroyer Hull Forms," C.H. von Kerczek, F. Stern, C.A. Scragg, Science Applications,Inc. and W. Sandberg, Naval Sea Systems Command.....81

4. "Comparisons of Large and Small Models for the Prediction of Resistance," S.C. Fisher, David W. Taylor Naval Ship Research and Development Center.....93

5. "Mixing-Length Formulations for Turbulent Boundary Layers over Arbitrarily Rough Surfaces," P. S. Granville, David W. Taylor Naval Ship Research and Development Center.....159

AM0560

Propulsion - Chaired by Mr. W.G. Day, Jr.

1. "Propulsion Committee Report".....189

2. "Activities of the ITTC Performance Committee,"
   W.C. Lin, David W. Taylor Naval Ship
   Research and Development Center.....193

3. "A Comparison of Two Propellers for the
   Acoustic Research Ship CFAV Quest,"
   J.L. Kennedy, L.J. Leggat and N.C. Sponagle,
   Defence Research Establishment Atlantic.....197

4. "Comparative Performance of Stock and Design
   Propellers Derived from Propulsion
   Experiments,"
   G. Karafiath and C. Wilson, David W. Taylor
   Naval Ship Research and Development Center.....217

5. "Recent Activities of the ITTC Propeller Committee,"
   T. Brockett, David W. Taylor Naval Ship
   Research and Development Center.....267

Cavitation - Chaired by Dr. J.W. Holl

1. "Cavitation Committee Summary Report"
   B. Parkin, Applied Research Laboratory.....275

2. "Cavitation Inception, A Review-Progress
   Since 19th ATTC,"
   Y.T. Shen, David W. Taylor Naval Ship
   Research and Development Center and
   F. B. Peterson, Naval Sea Systems Command.....277

3. "On the Design of Cavitation Susceptibility
   Meters (C.S.M.'s),"
   L. d'Agostino and A.J. Acosta, California
   Institute of Technology.....307

4. "The Influence of Pressure Gradient on Desinent
   Cavitation Produced by the Separated Flow
   from an Isolated Triangular Surface
   Protrusion,"
   J. W. Holl, M. L. Billet and M. Tada,
   Applied Research Laboratory.....351

5. "Some Applications of Free Streamline Theory,"
   C.C. Hsu, Tracor Hydronautics.....377

6. "Numerical Solutions of Lifting Surface Sheet
   Cavitation, A Review of Research at MIT,"
   R.J. Van Houten, J.E. Kerwin, Massachusetts
   Institute of Technology and J.S. Uhlman,
   Gould, Inc.....393

High Speed Vehicle - Chaired by Dr. D.D. Moran

1. "Committee Report - High Speed Vehicle Committee".....435

2. "High Speed Maneuvering of Amphibious Hovercraft,"
   R.T. Waters, D.D. Moran and R.F. Messalle,
   David W. Taylor Naval Ship Research and
   Development Center.....459

3. "Extended Performance Hydrofoil Program,"
   J.R. Meyer, David W. Taylor Naval Ship Research
   and Development Center.....479

4. "Planing Surface C_F,"
   R. Latorre, University of New Orleans.....489

5. "Planing Patrol Vessel Feasibility Study,"
   T.C. Bertch, U.S. Navy.....495

6. "Experimental Determination of Low Froude Number
   Hydrofoil Performance in Calm Water and in
   Regular Waves,"
   M.B. Wilson, David W. Taylor Naval Ship
   Research and Development Center.....517

7. "Review of Activities of High Speed Marine
   Vehicle Committee of International Towing
   Tank Conference,"
   D. Savitsky, Davidson Laboratory.....577

Banquet Address - Prof. Jacques Hadler

"The Uncertain 80's".....583

PROGRAM SCHEDULE

1 August 1983 (Monday)	Stevens Center (Bissinger Room)
1:00 - 7:30 pm	Registration (Lounge Annex)
6:30 - 7:30 pm	Cocktail Reception
2 August 1983 (Tuesday)	Kidde Building
8:00 - 9:30 am	Registration
9:30 - 10:00 am	Opening Session: Welcome Dr. K.C. Rogers, President Stevens Institute of Technology Introduction: Prof. Daniel Savitsky Chairman, 20th ATTC
10:00 - 10:15 am	Coffee
10:15 - 1:30 pm	Session I: Resistance and Flow Dr. A. Reed, Chairman
12:30 - 1:30 pm	Lunch
1:30 - 3:00 pm	Session II: Propulsion Mr. W.G. Day, Jr., Chairman
3:00 - 3:15 pm	Coffee
3:15 - 4:45 pm	High Speed Craft Dr. D. Moran, Chairman
4:45 - 5:45 pm	Tour: Davidson Laboratory and Demonostration of New Wave Machine Mr. J.F. Dalzell, Secretary
Evening	Free
3 August 1983 (Wednesday)	Kidde Building
9:30 - 10:00 am	Session III: Cavitation Prof. B. Parkin, Chairman
10:00 - 10:15 am	Coffee
10:15 - 12:00 pm	Continuation, Session III
12:00 - 1:30 pm	Lunch
1:30 - 3:00 pm	Session IV: Steering and Maneuvering Prof. W.C. Webster, Chairman
3:00 - 3:15 pm	Coffee
3:15 - 4:00 pm	Continuation, Session IV
4:00 - 5:30 pm	Ice Testing Dr. A. Keinonen, Chairman
6:00 - 10:00 pm	Open Bar and Dinner Bissinger Room, Stevens Center Dinner Speaker: Jacques B. Hadler "The Uncertain 80's"
4 August 1983 (Thursday)	Kidde Building
9:00 - 10:00 am	Session V: Seakeeping Prof. R.F. Beck, Chairman
10:00 - 10:15 am	Coffee
10:15 - 12:00 pm	Continuation, Session V
12:00 - 1:00 pm	Lunch
1:00 - 3:00 pm	Session VI: Systems and Techniques Prof. B. Johnson, Chairman
3:00 - 3:15 pm	Coffee
3:15 - 4:15 pm	Continuation, Session VI
4:15 - 5:00 pm	Business Session: Prof. Daniel Savitsky, Chairman

COMMITTEES OF THE 20th
AMERICAN TOWING TANK CONFERENCE

EXECUTIVE COMMITTEE

Prof. Daniel Savitsky	Chairman 20th ATTC
Mr. John F. Dalzell	Secretary 20th ATTC
Prof. John P. Breslin	Member 17th ITTC Executive Committee
Prof. Armin W. Troesch	University of Michigan (19th ATTC Host)
Prof. Bruce Johnson	Chairman 18th AATTC
Prof. Lawrence Ward	Chairman Hydrodynamics Committee, SNAME
Dr.. William B. Morgan	David W. Taylor Naval Ship Research and Development Center

TECHNICAL COMMITTEES

Resistance and Flow Committee

Dr. Arthur M. Reed, Chairman	Mr. Paul S. Granville
Mr. Howard A. Chatterton	Mr. Edward Numata
Mr. Stuart Cohen	Prof. Lawrence W. Ward

Propulsion Committee

Mr. William G. Day, Jr., Chairman	Prof. Justin E. Kerwin
Mr. Robert J. Boswell	Dr. Paulo C. Leone
Mr. Walter S. Gearhart	Mr. David C. Murdey
Prof. Jacques Hadler	Mr. J. Otto Scherer
Mr. John Hill	

Cavitation Committee

Prof. Blaine R. Parkin, Chairman	Prof. Justin E. Kerwin
Dr. Allan J. Acosta	Dr. F.B. Peterson
Dr. Michael L. Billet	Dr. Young T. Shen
Mr. Luca d'Agostino	Mr. Marshall P. Tulin
Dr. J.W. Holl	Mr. James S. Uhlman
Dr. C.C. Hsu	Prof. R. Van Houten

High Speed Vehicle Committee

Dr. David D. Moran, Chairman	Mr. John R. Meyer, Jr.
Ens. Timothy Bertch	Mr. Eugene Miller
Dr. Donald Blount	Dr. Daniel Savitsky
Prof. Jacques Hadler	Dr. Michael B. Wilson
Dr. Robert Latorre	Mr. Fred W. Wilson

Ice Testing Committee

Dr. Arno Keinonen, Chairman	Dr. Garry Timco
Mr. Ian Glenn	Dr. George Vance
Mr. Lawrence Schultz	Dr. Mary Williams
Dr. Jean-Claude Tatinclaux	

Steering and Maneuvering Committee

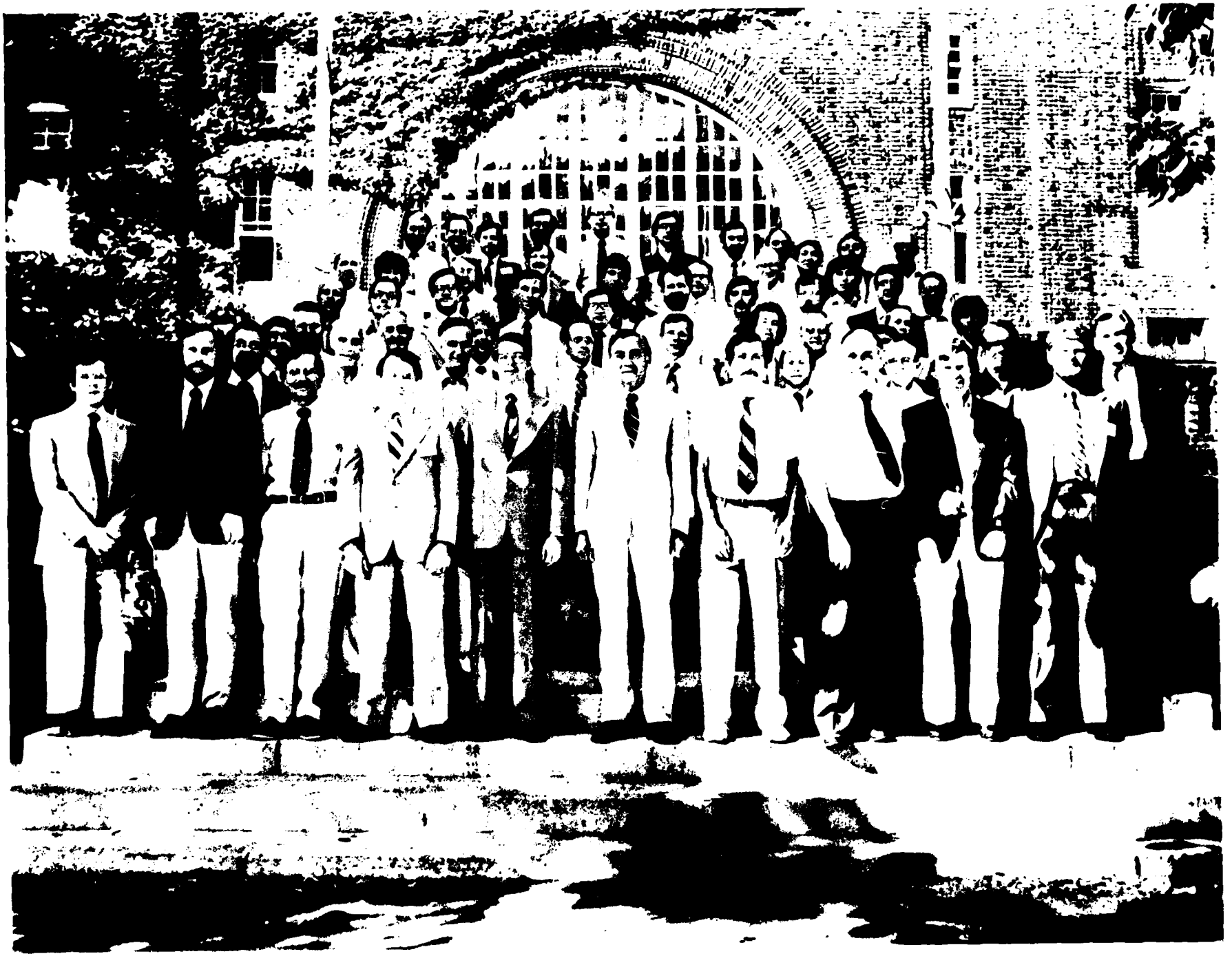
Prof. William C. Webster, Chairman	Mr. Eugene Miller
Prof. R. Bhattacharayya	Prof. Michael G. Parsons
Mr. Frank DeBord, Jr.	Mr. R. Thomas Waters
Dr. Haruzo Eda	

Seakeeping Committee

Prof. Robert F. Beck, Chairman	Mr. John F. Dalzell
Prof. Martin Abkowitz	Dr. Jeff Dillingham
Dr. Roderick A. Barr	Dr. Adrian R.J. Lloyd
Prof. Roger H. Compton	Mr. David C. Murdey
Mr. Geoffrey G. Cox	Prof. J. Randy Paulling

Systems and Techniques Committee

Prof. Bruce Johnson, Chairman	Dr. D. Gospodnetic
Mr. Peter W. Brown	Mr. Michael D. Miles
Mr. Stuart Cohen	Mr. D.R. Mullinix
Dr. Jeffrey T. Dillingham	Dr. R.S. Rothblum
Mr. Alex Goodman	Prof. Armin W. Troesch



PARTICIPANTS

Prof. Martin A. Abkowitz
Massachusetts Institute of Technology
Room 5-319
Department of Ocean Engineering
Cambridge, MA 02139

Mr. Frederick Ashcroft
Ship Hydrodynamics Laboratory
The University of Michigan
Ann Arbor, MI 48109

Prof. Robert F. Beck
204 NA&ME, North Campus
The University of Michigan
Ann Arbor, MI 48109

Ens. Timothy Bertch
Nuclear Power School
7508 F. Serano Circle
Orlando, FL 32807

Dr. Terry E. Brockett
David W. Taylor Naval Ship Research
and Development Center
Code 1522
Bethesda, MD 20084

Mr. Duncan A. Brown
Naval Underwater Systems Center
Bldg. 679, Code 3634
Newport, RI 02841

Mr. J.D. Butler
Department E12, Bldg. 600
Newport News Shipbuilding & Dry Dock Co.
4101 Washington Avenue
Newport News, VA 23607

Dr. Chu Chen
Naval Sea Systems Command
Code 55W3
Washington, DC 20362

Mr. Joseph M. Confoy
U.S. Coast Guard
2100 Second Street, SW
Washington, DC 20593

Mr. Reilly Conrad
Naval Sea Systems Command
Washington, DC 20362

Prof. R.B. Couch
Ship Hydrodynamics Laboratory
The University of Michigan
Ann Arbor, MI 48109

Mr. J.F. Dalzell
Davidson Laboratory
711 Hudson Street
Hoboken, NJ 07030

Mr. Timothy J. Danhieux
Marinette Marine Corp.
Ely Street
Marinette, WI 54143

Mr. William G. Day, Jr.
David W. Taylor Naval Ship Research
and Development Center
Code 1521
Bethesda, MD 20084

Mr. Frank W. DeBord, Jr.
Offshore Technology Corporation
578 Enterprise Street
Escondida, CA 92025

Dr. Haruzo Eda
Davidson Laboratory
711 Hudson Street
Hoboken, NJ 07030

Mr. Robert Falls
Maritime Administration
U.S. Dept. of Transportation
400 7th Street, SW
Washington, DC 20590

Mr. Jeffrey M. Falzarano
U.S. Coast Guard
2100 Second Street, SW
Washington, DC 20593

Mr. Steve Fisher
David W. Taylor Naval Ship Research
and Development Center
Bethesda, MD 20084

Mr. Gerard Fridsma
Davidson Laboratory
711 Hudson Street
Hoboken, NJ 07030

Mr. Patrick Gill
Boeing Marine Systems
Mail Stop 63-29
P.O. Box 3707
Seattle, WA 98124

Mr. Ian Glenn, Sr. Vice President
Arctec Canada Ltd.
311 Legget Drive
Ottawa, Ontario
K2K 1Z8 Canada

Mr. C. Gommers
MARAD
P.O. Box 28
6700 AA Wageningen
The Netherlands

Dr. D. Gospodnetic
National Research Council
2140 Dutton Crescent
Ottawa, Ontario
K1J 6K4 Canada

Mr. Paul S. Granville
David W. Taylor Naval Ship Research
and Development Center
Code 1541
Bethesda, MD 20084

Prof. Jacques Hadler
Webb Institute of Naval Architecture
Crescent Beach Road
Glen Cove, NY 11542

Mr. G.R. Hagen
Designers and Planners
1727 Jefferson Davis Highway
Arlington, VA 22202

Mr. Harry D. Harper
David W. Taylor Naval Ship Research
and Development Center
Bethesda, MD 20084

Dr. J.W. Holl
Applied Research Laboratory
P.O. Box 30
State College, PA 16801

Mr. John Hoste
Offshore Technology Corporation
578 Enterprise Street
Escondido, CA 92025

Mr. Jeff Hough
NAVSEA, Code 03F31
National Center No. 2
Washington, DC 20362

Prof. Jack W. Hoyt
Department of Mechanical Engineering
San Diego State University
San Diego, CA 92182

Dr. Chi-Chao Hsiung
Engineering and Applied Science
Memorial University of Newfoundland
St. Johns, Newfoundland
A1B 3X5 Canada

Prof. Bruce Johnson
Naval Systems Engineering Department
U.S. Naval Academy
Annapolis, MD 21401

Mr. Young R. Joo
Korea Tacoma Marine Ind.
11 Moonachie Road
Moonachie, NJ 07074

Mr. C. Karafiath
David W. Taylor Naval Ship Research
and Development Center
Bethesda, MD 20084

Mr. Robert G. Keane
NAVSEA, Code 6138
Department of the Navy
Washington, DC 20362

Dr. Arno Keinonen, Ice Res. Mgr.
Dome Petroleum Limited (Canmar)
P.O. Box 200
Calgary, Alta
K1A OR6 Canada

Dr. James Kennedy
Defense Research Establishment, Atlantic
P.O. Box 1012
Dartmouth, Nova Scotia
B2Y 3Z7 Canada

Mr. Philip B. Kimball
C.R. Cushing & Co., Inc.
One World Trade Center
New York, NY 10048

Prof. T. Kowalski
University of Rhode Island
Department of Ocean Engineering
Kingston, RI 02881

Mr. Miro Kresic
John J. McMullen Associates, Inc.
One World Trade Center
Suite 3000
New York, NY 10048

Prof. Robert Latorre
University of New Orleans
P.O. Box 1098
New Orleans, LA 70148

Dr. Chung Lee
Mechanics Division
Office of Naval Research
Department of the Navy
800 N. Quincy Street
Arlington, VA 22217

Mr. Wah Lee
David W. Taylor Naval Ship Research
and Development Center
Bethesda, MD 20084

Mr. Alan Libby
CBI Industries
1501 N. Division Street
Plainfield, IL 60544

Mr. A.R.J.M. Lloyd
Naval Systems Engineering Department
U.S. Naval Academy
Annapolis, MD 21401

Dr. T. Glen McKee
Davidson Laboratory
711 Hudson Street
Hoboken, NJ 07030

Mr. John R. Meyer, Jr.
Advanced Hydrofoil Systems Office
Code 1150
David W. Taylor Naval Ship Research
and Development Center
Bethesda, MD 20084

Mr. Michael D. Miles
National Research Council
Mechanical Engineeing Division
Ottawa, Ontario
K1A OR6 Canada

Mr. Eugene Miller
Hydronautics Inc.
7210 Pindell School Road
Laurel, MD 20810

Mr. David Molyneux
National Research Council
Ottawa, Ontario
K1A OR6 Canada

Dr. David D. Moran
David W. Taylor Naval Ship Research
and Development Center
Special Ship & Ocean System Dynamics
Code 1562
Bethesda, MD 20084

Mr. Thomas L. Moran
David W. Taylor Naval Ship Research
and Development Center
Bethesda, MD 20084

Dr. William B. Morgan
David W. Taylor Naval Ship Research
and Development Center
Code 1500
Bethesda, MD 20084

Mr. Lewis E. Motter
David W. Taylor Naval Ship Research
and Development Center
Bethesda, MD 20084

Mr. David C. Murdey
Marine Dynamics and Ship Laboratory
National Research Council
Ottawa, Ontario
K1A OR6 Canada

Mr. Edward Numata
Davidson Laboratory
711 Hudson Street
Hoboken, NJ 07030

Dr. John F. O'Dea
David W. Taylor Naval Ship Research
and Development Center
Code 1524
Bethesda, MD 20084

Mr. B.M. Olson
Gibbs & Cox, Inc.
119 West 31st Street
New York, NY 10001

Mr. Arthur M. Reed
David W. Taylor Naval Ship Research
and Development Center
Code 1506
Bethesda, MD 20084

Dr. Manoel A.S. Reis
Inst. Pasquisas Tecnologicas
Ship and Ocean Research Division
C.P. 7141
CEP 01000 Sao Paulo
Brazil

Dr. R. S. Rothblum
David W. Taylor Naval Ship Research
and Development Center
Code 1508
Bethesda, MD 20084

Mr. Joseph O. Salsich
U.S. Naval Academy
Annapolis, MD 21401

Mr. William Sandberg
Naval Sea Systems Command
Washington, DC 20362

Dr. Daniel Savitsky
Davidson Laboratory
711 Hudson Street
Hoboken, NJ 07030

Mr. Lawrence A. Schultz
Arctec, Inc.
9104 Red Branch Road
Columbia, MD 21045

Dr. Young T. Shen
David W. Taylor Naval Ship Research
and Development Center
Code 1552
Bethesda, MD 20084

Mr. Paul G. Spens
Davidson Laboratory
711 Hudson Street
Hoboken, NJ 07030

Mr. Fred Stern
Science Applications, Inc.
134 Holiday Court, Suite 318
Annapolis, MD 21401

Mr. Jonathan T. Stypinski
Gibbs & Cox, Inc.
119 West 31st Street
New York, NY 10001

Dr. Jean-Claude Tatinclaux
Hydraulic Research Engineer
Cold Regions Res. & Eng. Laboratory
72 Lyme Road
Hanover, NH 03755

Dr. Garry Timco
Hydraulics Laboratory
National Research Council
Building M-32, Montreal Road
Ottawa, Ontario
K1A 0R6 Canada

Prof. Armin W. Troesch
212 NA&ME Bldg., North Campus
The University of Michigan
Ann Arbor, MI 48109

Dr. Steven Tsakonas
Davidson Laboratory
711 Hudson Street
Hoboken, NJ 07030

Dr. Alfred Turnik
American Bureau of Shipping
Hull Department
65 Broadway
New York, NY 10006

Prof. Robert J. Van Houten
Massachusetts Institute of Technology
Room 5-320
Cambridge, MA 02139

Dr. Peter van Oossanen
Maritime Research Inst. Netherlands
P.O. Box 28
6700 AA Wageningen
The Netherlands

Mr. David A. Walden
David W. Taylor Naval Ship Research
and Development Center
Bethesda, MD 20084

Prof. Lawrence W. Ward
Webb Institute of Naval Architecture
Crescent Beach Road
Glen Cove, NY 11542

Mr. Robert Thomas Waters
David W. Taylor Naval Ship Research
and Development Center
Code 1572
Bethesda, MD 20084

Dr. John V. Wehausen
University of California
Department of Naval Architecture
Berkeley, CA 94720

Mr. Joseph M. Wetzel
St. Anthony Falls Hydraulic Lab.
Mississippi River at 3rd Avenue, SE
Minneapolis, MN 55414

Ms. Abigail Wemple
David W. Taylor Naval Ship Research
and Development Center
Bethesda, MD 20084

Dr. Mary Williams
Arctic Vessel and Marine Res. Inst.
National Research Council
Building M-32, Montreal Road
Ottawa, Ontario
K1A 0R6 Canada

Dr. Michael B. Wilson
David W. Taylor Naval Ship Research
and Development Center
Code 1522
Bethesda, MD 20084

Mr. Fred Wilson
Program Development Office
Code 1604
David W. Taylor Naval Ship Research
and Development Center
Bethesda, MD 20084

Mr. B. Wisler
David W. Taylor Naval Ship Research
and Development Center
Bethesda, MD 20084

Mr. John Zselczky
U.S. Naval Academy
Annapolis, MD 21401

CONTRIBUTORS

(Not In Attendance)

Dr. Allan Acosta
California Institute of Technology
Pasadena, CA 91125

Mrs. Susan M. Lee Bales
David W. Taylor Naval Ship Research
and Development Center
Code 1568
Bethesda, MD 20084

Dr. Roderick A. Barr
Hydronautics, Inc.
7210 Pindell School Road
Laurel, MD 20810

Dr. Michael L. Billet
Applied Research Laboratory
Box 30
State College, PA 16801

Dr. David W. Coder
David W. Taylor Naval Ship Research
and Development Center
Code 1543
Bethesda, MD 20084

Prof. Roger H. Compton
Naval Systems Engineering Department
U.S. Naval Academy
Annapolis, MD 21402

Mr. Geoffrey G. Cox
David W. Taylor Naval Ship Research
and Development Center
Code 1568
Bethesda, MD 20084

Dr. William E. Cummins
David W. Taylor Naval Ship Research
and Development Center
Code 1500
Bethesda, MD 20084

Mr. D'Agostino
California Institute of Technology
Pasadena, CA 91125

Mr. D. Friis
Memorial University of Newfoundland
St. Johns, Newfoundland
A1B 3X5 Canada

Dr. Jeffrey T. Dillingham
Offshore Technology Corporation
578 Enterprise Street
Escondido, CA 92025

Mr. Carvel Holton
United Tecnologies Research Center
East Hartford, CT

Dr. C.C. Hsu
Hydronautics, Inc.
7210 Pindell School Road
Laurel, MD 20810

Mr. D. Huminik
David W. Taylor Naval Ship Research
and Development Center
Bethesda, MD 20084

LCDR David H. Humphreys
Naval Engineering Division
U.S. Coast Guard
2100 Second Street, SW
Washington, DC 20593

Mr. M.J. Jeffers
David W. Taylor Naval Ship Research
and Development Center
Bethesda, MD 20084

Mr. Harry Jones
David W. Taylor Naval Ship Research
and Development Center
Bethesda, MD 20084

Mr. G.T. Karppinen
National Research Council
Ottawa, Ontario
K1A OR6 Canada

Mr. C. von Kerczek
Science Applications, Inc.
134 Holiday Court, Suite 318
Annapolis, MD 21401

Prof. Justin E. Kerwin
Massachusetts Institute of Technology
Department of Ocean Engineering
Room 5-324
Cambridge, MA 02139

Dr. L.J. Leggat
Defense Research Establishment Atlantic
P.O. Box 1012
Dartsmouth, Nova Scotia
B2Y 3Z7 Canada

Dr. Wen-Chin Lin
David W. Taylor Naval Ship Research
and Development Center
Code 1524
Bethesda, MD 20084

Mr. R.F. Messalle
David W. Taylor Naval Ship Research
and Development Center
Bethesda, MD 20084

Mr. W. Milne
Memorial University of Newfoundland
St. Johns, Newfoundland
A1B 3X5 Canada

Mr. W.C.E. Nethercote
Defence Research Establishment Atlantic
P.O. Box 1012
Dartmouth, Nova Scotia
B2Y 3Z7 Canada

Prof. Blaine Parkin
Applied Research Laboratory
P.O. Box 30
State College, PA 16801

Prof. J.R. Paulling
Department of Naval Architecture
College of Engineering
University of California
Berkeley, CA 94720

Mr. G.R. Peters
Memorial University of Newfoundland
St. Johns, Newfoundland
A1B 3X5 Canada

Dr. Frank B. Peterson
Naval Sea Systems Command
National Center No. 2
Washington, DC 20362

Mr. F. Phelps
212 NA&ME Building, North Campus
The University of Michigan
Ann Arbor, MI 48109

Mr. C. Scragg
Science Applications, Inc.
134 Holiday Court, Suite 318
Annapolis, MD 21401

Mr. N.C. Sponagle
Defense Research Establishment Atlantic
P.O. Box 1012
Dartmouth, Nova Scotia
B2Y 3Z7 Canada

Mr. M. Tada
Pennsylvania State University
Box 30
State College, PA 16801

Mr. James S. Uhlman
Gould, Inc.
Ocean Systems Division
Middleton, RI

Mr. H.W. Weber
Kempf & Remmers GmbH
Hamburg, West Germany

Mr. C.J. Wilson
David W. Taylor Naval Ship Research
and Development Center
Bethesda, MD 20084

REPORTS OF THE

RESISTANCE AND FLOW

COMMITTEE

Progress in Resistance and Flow:
A Long Term Perspective

Report of the Resistance and Flow Committee

to the 20th ATTC

Committee

Howard Chatterton, USNA
Stuart Cohen, University of Michigan
Paul S. Granville, DTNSRDC
Edward Numata, Davidson Laboratory, Stevens Institute of Technology
L.W. Ward, Webb Institute of Naval Architecture
Arthur M. Reed, DTNSRDC, Chairman

August 2, 1983

INTRODUCTION

The typical committee report to the ATTC discusses the progress which has been made in the three years since the previous meeting. To no one's surprise, this leads to a report which is usually indistinguishable from the previous report. This is due to the fact that ship hydrodynamics, and in particular resistance and flow, are evolutionary rather than revolutionary sciences, or should we say arts.

In an attempt to avoid the pitfall of a report which shows no progress, the committee has chosen to prepare a report which shows the progress which has been made on a longer term basis. The amazing thing is that it really does work, if we look back twenty, twenty-five, or thirty years to see where we are now relative to then, we can see real progress has been made in the area of resistance and flow. To steal a little thunder from one of the upcoming contributions, it has been 36 years since the ATTC friction line (Schoenherr line) was adopted by the ITTC, and 26 years since the ITTC model ship correlation line was adopted. This serves to show that the ATTC has had a significant impact on the prediction of ship resistance worldwide.

In the preparation of their contributions, the committee members have looked at the issue of progress from an institutional perspective. This has led to a wide distribution of significant events. From the United States Naval Academy, we have a report on their new facilities; from the University of Michigan, a summary of the significant experimental studies which have been carried out over the last 20 years; from the David Taylor Naval Ship R&D Center, we have a history of the prediction of the viscous resistance of ships; from Davidson Laboratory, Stevens Institute of Technology, we have a discussion of their success with small models; and finally from Webb Institute of Naval Architecture we have a summary of three advances in facilities and techniques of significance.

UNITED STATES NAVAL ACADEMY

The year 1976 marked a giant step forward in hydromechanics laboratory facilities at the United States Naval Academy.* Prior to this date, equipment for experimental naval architecture was located in Isherwood Hall, and included:

1) A small ship model towing tank: 85-foot length, 6-foot width, 3.5-foot water depth; a gravity towing system and a twin rail powered towing

---

* Extracted from Compton (1977)

carriage capable of a maximum speed of about 7 knots; a pneumatic wave generator capable of producing regular, long-crested waves from 6 inches to 6 feet in length and a maximum height of about 2 inches; electromechanical dynamometry for the measurement of model velocity, model pitch and heave motions; resistance wire and sonic wave height sensors; hot wire and hot film anemometry; an open water propeller boat; assorted accelerometers and pressure transducers; digital and analog data acquisition systems; and a computer terminal attached to the Naval Academy's Honeywell 635 Central Computer Facility.

2) A small circulating water channel with a 16 inch x 16 inch test section and a maximum usable flow velocity of about 10 feet per second; a channel that could be operated as either a free surface channel or a closed, pressure controllable propeller tunnel; a three component strain gage dynamometer available for quantitative force measurement.

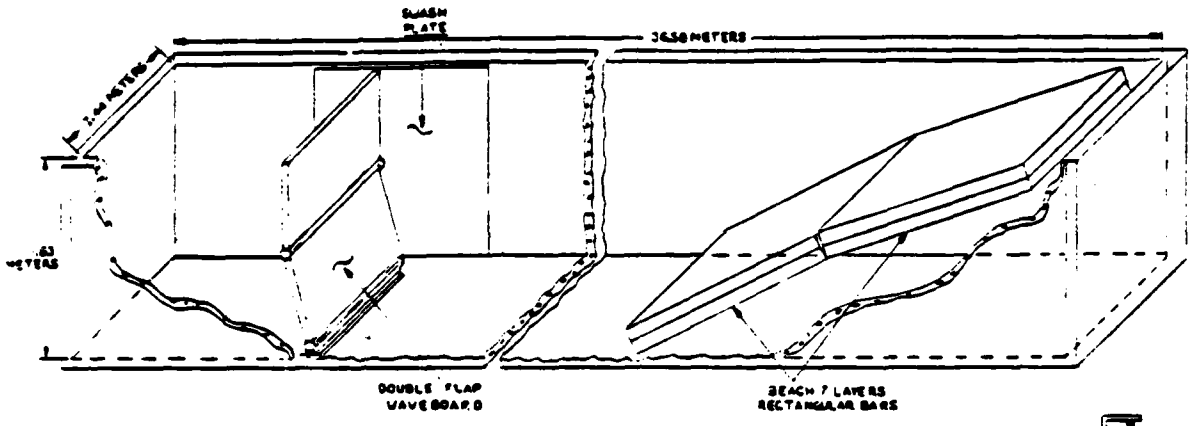
3) A ship stability tank for performing inclining and large angle stability experiments on intact and partially flooded ship models of about 20 foot length.

During the summer of 1976 all three of these facilities were either retired or disassembled and moved to Rickover Hall for updating, reconfiguring, and recommissioning. In September 1976 the 120-foot Ship Model Towing Tank was put into service. The gravity towing system, powered carriage speed control system, all dynamometry, and all data acquisition equipment from Isherwood Hall were modified and reactivated in a longer, wider, and deeper basin. A pictorial diagram of the 120-foot tank arrangement and the laboratory system is shown in Figure 1.

On August 24, 1977, a 380-foot long towing tank was formally dedicated during the 18th American Towing Tank Conference, hosted at the U.S. Naval Academy. The tank arrangement, equipment and instrumentation systems are described in Figure 2. The circulating water channel is a complete redesign retaining only the test section and drive motors of the channel previously located in Isherwood Hall. Arrangement and features of the water channel are described in Figure 3.

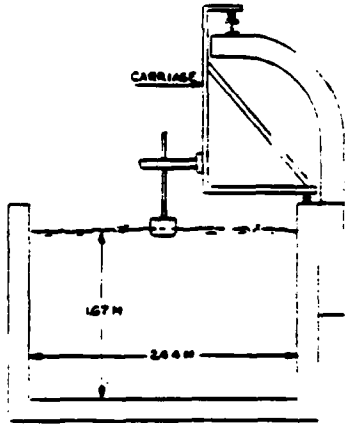
The new facilities in Rickover Hall included a Coastal Engineering Tank and Stability Tank, with characteristics given in Table 1 below.

FIGURE 1 120 FOOT TANK



120 FOOT TANK AND WAVEMAKER SYSTEM

U.S. NAVAL ACADEMY



DESCRIPTION OF CARRIAGE: unmanned

TYPE OF DRIVE SYSTEM AND TOTAL POWER: cable drive motor, 15 Hp digital speed control, manual/computer controlled

MAXIMUM CARRIAGE SPEED: 6 m/s (20 fps)

WAVE GENERATION CAPABILITY: regular, irregular, and transient water waves, max wave height 0.3m x 3m, wave length 0.6m - 10m

WAVEMAKER TYPE AND EXTENT: dual flap servo-hydraulic control 2.4m x 1.7m

BEACH TYPE AND LENGTH: 7 layers of rectangular bars, 4.9m

METHOD IRREGULAR WAVE GENERATION: computer generated, spectral form specified in frequency domain, generated waves are analyzed and spectrum corrected until desired spectral shape is obtained

OTHER CAPABILITIES: the "periodic irregular encountered wave technique for seakeeping test" is based on irregular wave components which are equally spaced in the encounters frequency domain. This reduces the testing time required to the reciprocal of the frequency resolution of the encountered wave harmonics

---

INSTRUMENTATION: PDP 11/50 in control room, PDP 11/05 for wavemaker control, 15 bit A/D converter, variable reluctance force blocks for all force measurements, Hydronautics multi-T signal conditioners, ultrasonic and resistance wave height gauges, graphic display and/or hard copies available immediately upon completion of test run, trailing cable for transmission of data from carriage to shore, general purpose resistance and seakeeping dynamometer

MODEL SIZE RANGE: 1m - 2m

TESTS PERFORMED: resistance in calm water and waves, seakeeping tests, various test of ocean structures, hydrodynamic forces on submerged bodies, foils, etc., flow visualization

OTHER REMARKS: extensive software developed for standard test data base, shares computer with 128m towing tank, gravity towing capability

---

PUBLISHED DESCRIPTION: none

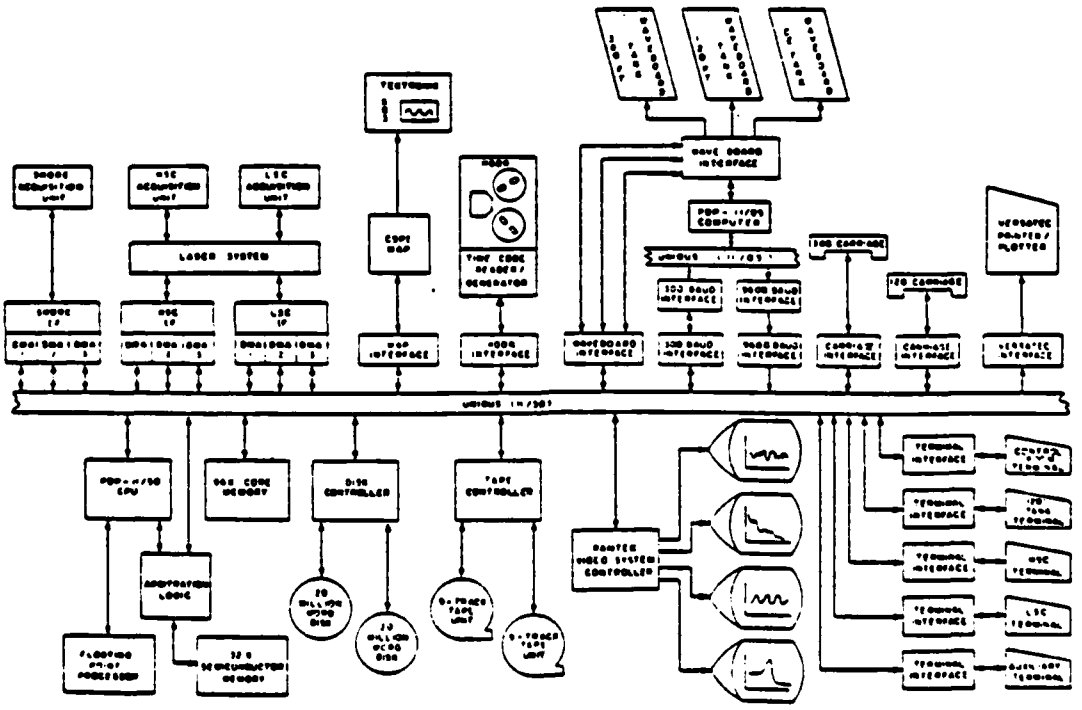
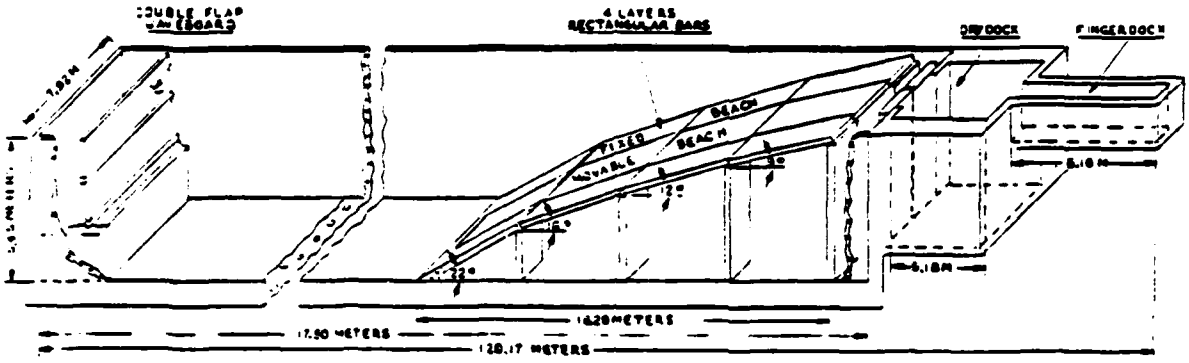
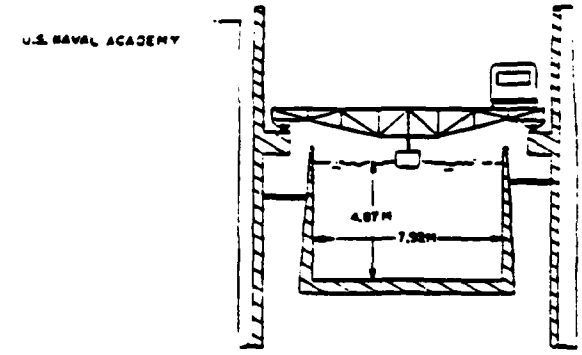


FIGURE 2 380 FOOT TANK



380 FOOT TANK AND WAVEMAKER



DESCRIPTION OF CARRIAGE: 1) high speed - box grider, supported on round way bearings or rulon slippers
2) low speed - supported on round way bearings (towed by high speed carriage)

TYPE OF DRIVE SYSTEM AND TOTAL POWER: twin cables attached to high speed carriage, digital control interface with computer, 2 - 150 kw D.C. motors (400% overload capability)

MAXIMUM CARRIAGE SPEED: low speed carriage - 7.6 m/s (25 fps)
high speed carriage - 14 m/s (45 fps)

OTHER CAPABILITIES: large amplitude planar motion mechanism, computer controlled testing

---

WAVE GENERATION CAPABILITY: regular, irregular and transient water waves, max wave 1m x 10m, wave length 0.6m - 30m

WAVEMAKER TYPE AND EXTENT: dual flap servo-hydraulic control, 7.9m x 2.7m

BEACH TYPE AND LENGTH: 4 layer of rectangular bars, 18.3m

METHOD OF IRREGULAR WAVE GENERATION: computer generated, spectral form specified in frequency domain, generated waves are analyzed and spectrum corrected until desired spectral shape is obtained.

OTHER CAPABILITIES: the "Periodic Irregular Encountered Wave Techniques for Seakeeping Test" is based on irregular wave components which are equally spaced in the encountered frequency domain. This reduces the testing time required to the reciprocal of the frequency resolution of the encountered wave harmonics

---

INSTRUMENTATION : PDP 11/50 in control room, PDP 11/05 for wavemaker control, laser telemetry system between carriage and shore to transmit digital data, t.v., and control channels 15 bit A/D converters on each carriage and on shore, variable reluctance force block for all force measurements, variable torque and thrust dynamometers, Hydronautics multi-T signal conditioners, planing boat and S.E.S. dynamometer, 3 axis submerged model dynamometer open water propeller dynamometers, pitot tube rakes for wake surveys, rudder torque gauges, ultrasonic and resistance wave height gauges, graphic display and/or hard copies available immediately upon completion of test run

MODEL SIZE RANGE: ship model lengths for resistance and propulsion tests 3m - 8m, for seakeeping and maneuvering testing 3m - 5m, ocean structures 1m - 2m in diameter

TESTS PERFORMED: resistance and self-propulsion in calm water and waves, seakeeping tests, open water propeller test, 3-D wake surveys, horizontal planar motion tests, various test of ocean structures, hydrodynamic forces on submerged bodies, foils, etc., capsize and dynamic stability tests, flow visualization

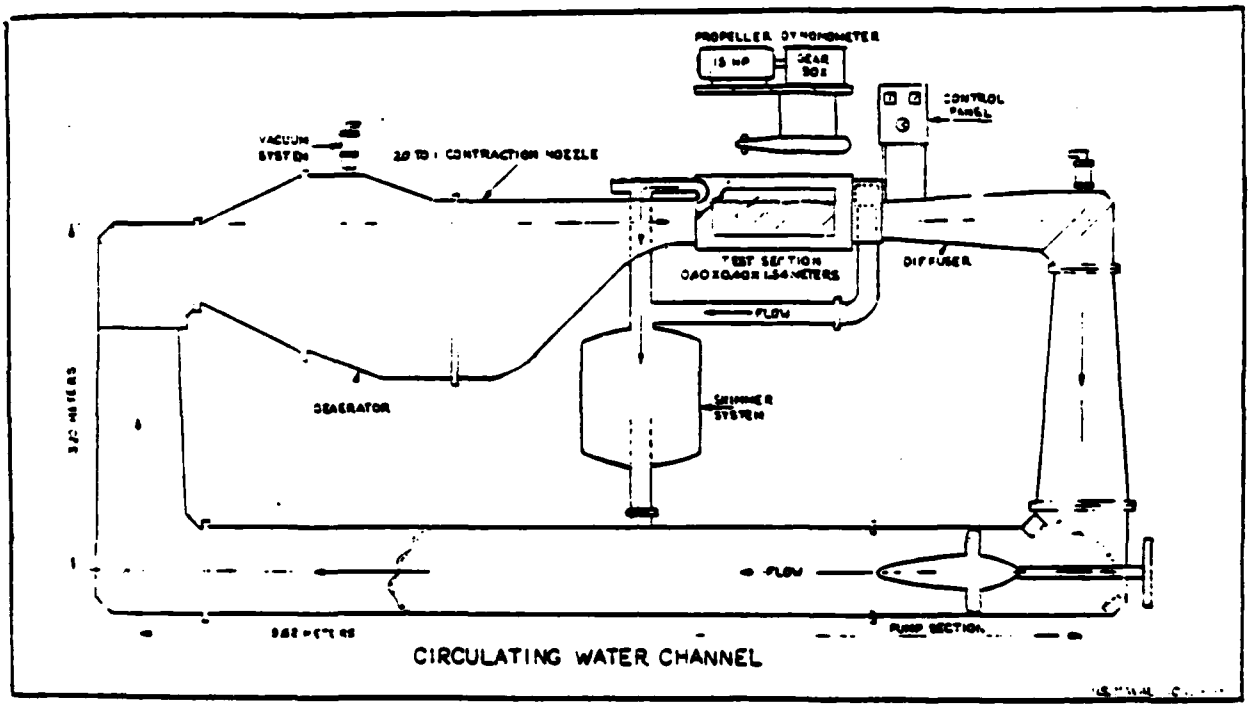
OTHER REMARKS: extensive software developed for standard test data base

---

PUBLISHED DESCRIPTION: proceedings of -

16th American Towing Tank Conference 1971
18th American Towing Tank Conference 1977
19th American Towing Tank Conference 1980

FIGURE 3 CIRCULATING WATER CHANNEL



CIRCULATING WATER CHANNEL

DESCRIPTION OF FACILITY: vertical plane, free surface

TYPE OF DRIVE SYSTEM: 4-bladed axial flow impeller

TOTAL MOTOR POWER: 56kw, 1750 rpm

WORKING SECTION MAX. VELOCITY: 8 m/s

MAX. & MIN. ABS. PRESSURES: 140 kPa, 16 kPa

DIMENSIONS OF WORKING SECTION: 0.4m x 0.4m x 1.54m

INSTRUMENTATION: propeller dynamometer, 3 component balanced

TORQUE AND THRUST DYNAM: Hydronautics varible reluctance mounted in pod

PROPELLER SIZE RANGE: diameters from 130mm - 230mm
typical - 200mm

TESTS PERFORMED: flow visualization, force and pressure distribution on submerged bodies, propeller thrust and torque measurements

---

TABLE 1

COASTAL ENGINEERING TANK (L-SHAPED)

Length	52 feet
Width	48 feet
Water Depth	0.5 to 2 feet
Movable Instrumentation Bridge	
Movable Monorail Hoist System	
Electrohydraulic Piston Type Wavemaker	

STABILITY/BALLASTING TANK

Length	24 feet
Breadth	12 feet
Water Depth	3.5 feet

A key feature of the tow tank operations is the computerized data acquisition and analysis system. Both the 120 foot and 380 foot towing tanks can be operated in any of three modes:

Manual Operation

Operator Interactive Operations

Automated Operation

The latter two operating modes employ a PDP 11-50/PDP 11/34 system. In automated mode, a test has been designed, coded, and stored in the PDP system, and -- after model and dynamometry have been mounted on the appropriate towing carriage -- the entire sequence of events from calibration to the production of "Report Quality" Tables and plots of both model and expanded data (including "off-line" fairing by the test engineer) are executed under computer control. This means that routine tests can be accomplished in a standard manner, quickly and with minimum manpower. In the operator interactive mode, certain subtasks of a test program are automated under the selection and sequencing control of the Test Engineer.

Computer support external to the Hydromechanics Laboratory is and has been strong for experimental as well as purely analytical naval architecture. The academy's extensive time sharing system is accessible via a high speed terminal. The heart of this time sharing system is a Honeywell 6060 Computer main frame. While most of the use of this system is via remote time-shared terminals, batch processing for large programs (like NAVSEA's Ship Hull Characteristics Program) is available at night. Supplementing this general purpose system is one located and operated in Rickover Hall by a Group called CADIG (Computer-Aided Design &

Interactive Graphics). As the name implies, this resource specializes in graphic capabilities utilizing "stand alone" equipment including a large flat-bed plotter, three-dimensional display on a CRT screeen, digitizing tablets, and a numerically controlled milling machine (for small model shaping). The CADIG Group has a Staff to write and maintain software for this equipment and to aid system users.

Outstanding physical support of the Experimental Naval Architectural Program is providided by the Technical Support Department (TSD) of the Division of Engineering and Weapons. Available facilities include a welding shop (gas and electric, aluminum and steel), a small foundry, a sheet metal shop, a machine shop, and a wood shop equipped to handle the specialized crafts involved in making accurate scale models in wood or fiberglass. In addition to being able to fabricate equipment and models of quality, the TSD Staff provides necessary guidance to Midshipmen and Faculty members who want to become involved in the fabrication process.

UNIVERSITY OF MICHIGAN

Development of Bulbous Bows for Slow Speed Vessels

In late 1962, Upper Lakes Shipping LTD of Toronto had the University of Michigan test a bulb designed to reduce the pitching of a new, slow speed, self-unloading ore carrier. The model had been tested for resistance at the Netherlands Ship Model Basin, but no tests were run with a conventional bow. Professor Inui of the University of Tokyo was visiting the University of Michigan at this time. In the late 1950's Inui had developed a method of optimizing bulb for fine-hulled, high speed ships that could provide a reduction of 13% in required power. When a conventional bow suitable for the Great Lakes was designed and tested on the ore carrier, a resistance benefit of approximately 4% at full load and 15% in ballast was obtained. This generated considerable interest with Esso International (now Exxon) which had been doing studies in the Hamburg tank of tankers in ballast. A bulb was designated by the UM Ship Hydrodynamics Laboratory for the "Esso Cristobal" and 1.5 knot speed increase was obtained.

In 1965 Moss and Couch commenced a project to study the properties of protruding bulbs on Series 60 (CB = .80) models with and without fairing the bulb into the hull lines. Three bulb types (B Series, C Series, R Series) were tested, and resistance at ballast, full-load, trim by the stern, and with bulb fairings, were compared against ship speed. The results indicated that optimum shapes were only slightly better than cylindrical bulbs (which are easier to manufacture);

that large protruding bulbs were insensitive to longitudinal position; and that up to a 20% resistance savings could be realized in the ballast condition. Although extensive model testing had been done in other tanks, these results were published in the 1966 SNAME Transactions [Couch and Moss (1966)] as the first systematic information available to the public. The results also clarified the understanding that in addition to reducing wavemaking resistance (including the bow wave), the bulb reduces viscous drag by straightening out the flow and eliminating vortices that curved around the bilge radius.

In 1967-1968 Sharma and Nowacki developed a bulb optimization method which is still used at UM [Sharma & Naegle (1970)] Their approach was to measure the basic wave patterns of a hull without a bulb, and then again with a nominal bulb. Using theoretical considerations, the effects of changing the bulb size and position on the hull were predicted. Curves of constant wave resistance were calculated so that a minimum resistance point and the corresponding optimum size and position were found. This procedure can produce an optimum (cylindrical) bulb design quite easily, and the method is presently widespread.

Development of Twin Rudders for Single Screw Great Lakes Ships

Another Upper Lakes Shipping single-screw ore carrier, also designed in 1965, was to have maximum cargo capacity. In general block coefficients for this type of ship ranged around CB = 0.87, but Professor R. B. Couch designed a buttock flow stern, small bilge radius, and twin rudders with smaller than single rudder chord, that pushed the CB up to 0.92. This ship was built in 1965 and new ore carriers were built that way until the twin screw ore carriers became popular.

Barge Testing

The Ship Hydrodynamics Laboratory has tested more than 400 barge or barge-tug combinations for resistance, and probably more barges for directional stability than any other tank. Having this wealth of data, several attempts have been made to find a way to present it to the interested public. The ideal method would be a set of equations based on a few hull parameters so that the bare hull resistance could be computed with a hand calculator. Moss and Townsend (1969) produced a SNAME T&R Bulletin which gave design suggestions and regression equations for sea-going barges. Swift, Nowacki and Fisher (1973) found equations for Great Lakes bulk carriers. In both papers, the types of barges studied were very limited, that

is, the hull parameters did not vary widely. Since that time, notched barges have become important and their resistance characteristics cannot be predicted by hull parameters alone, so there does not appear to be any way to find valid regression equations for all current barge designs. However, the entire range of test information, including notched barges, is available in SNAME T&R Bulletin 1-42, S. Cohen (1983). Estimates of residuary resistance can be obtained from the tables, as well as some limited information on skegs used for directional stability. In 1980, experiments on the effects of skegs, barge trim, tow rope mass and tow rope length on the directional stability were reported by Latorre, Ashcroft, and Cohen (1980). In the experiments, the barge trajectory during towing was monitored by a light tracker as well as recorded on videotape. These experiments led to the development of a linear time varying computer simulation of the towed barge motion including surge which was used to examine the influence of starting acceleration and tow rope length [Latorre & Bernitsas (1981)]. Latorre and Ashcroft (1981) also published results of 73 barge tests in graphical form with preliminary design suggestions.

Propulsion Work

Although propulsion work is, in a strict sense, outside the realm of resistance and flow, the determination of a correlation allowance depends on full scale trials reduced back to model size through propulsion tests. The Ship Hydrodynamics Laboratory first began propulsion work in 1958 using Kempf and Remmers mechanical dynamometers and replaced them with electric dynamometers in 1960 when a new carriage was installed. Since then a library has been built of over 80 propellers for single screw, twin screw, and Kort nozzle tests. Throughout that time, efforts were made to establish the best C_a values for the tank representing each ship type. In 1978, MARAD certification for tank testing was obtained based on the results for a Sun Ship Company 31000 DWT products carrier. The Ship Hydromechanics Laboratory also participated in the Maritime Administration study with DTMB and Hydronautics [Maritime Administration (1979)] that confirmed that the correlation allowance is negative for very high block coefficient ships.

Full Scale Flow Studies

In 1978 instrumentation was developed for the full scale wake survey of the twin screw "R/V Athena." Twenty-four 5-hole, two 13 hole pitot tubes, and eight 13-tube boundary layer rakes were designed for wake and boundary layer measurements.

One set of pitot tubes was placed ahead of each of the screws, and one was placed behind the starboard strut, the propeller being removed. There was one pizeo-electric pitot tube used to measure time varying pressure. The electronic and mechanical equipment was designed in-house and preliminary research indicated that instead of using water for transmitting the pressure signals through tubes to the transducers, air would be the only feasible method. This was due to the large vertical negative head that developed when the instrumentation was on the deck some 12 feet above the pitot tubes. This novel instrumentation is described in a paper by Troesch, Phelps, and Hackett (1978). Detailed pictures of the installation, and the results are in a DTMB report by Day, Reed, and Hurwitz (1980).

As An Educational Institution

For years beyond a young man's memory there has been an undergraduate-required laboratory course in which resistance and flow experiments are conducted. An EHP test, wake wheel survey, open water test, and SHP test have formed the backbone of this course. In 1980 an elective, graduate level course was introduced in which four experiments, different each year, are given by four faculty members. Recent projects have been bulbous bow optimization, resistance from wave cuts, forces on a moving cylinder, cable strumming frequencies, added mass and damping, and relative ship motions. Although invaluable for the students planning to continue into research, these projects also stress analysis of errors, use of the computer, comparison of theoretical to measured data, and teamwork, which are essential to a well-rounded naval architect. It also gives the faculty a chance to create new experiments which, if effective, can become new teaching aids.

In addition, there are individual student projects, many having to do with sailboat testing and design. Although these reports do not in general become published papers, the range of recent experiments are from full size sailboat resistance comparison to SWATH ship stability tests. Several students have designed new equipment which is used in specialized circumstances.

High Speed Craft

One student project that should be singled out was performed in 1969 by A. Toro. He made an extensive study of the shallow water resistance of a Series 62 planing hull for three L.C.B. positions [Toro (1969)]. A multilever testing apparatus was used to measure the towing force on the propeller shaft centerline for a speed

range of $0.64 < F_\nabla < 3.4$. The 3.5-foot model was tested in deep water and three shallow water depths obtained by a 90-foot adjustable fiberglass false bottom. His results clearly demonstrated that at supercritical speeds (Froude Number based on depth larger than 1.0) residuary resistance falls below that of deep water, representing a power savings. The model and full-scale results in graphical form have subsequently been used by other researchers as verification of theoretical predictions.

Amphibious Vehicles

Some of the work in this field is proprietary and therefore cannot be reported. However, Nowacki et al (1968) tested a family of box-like hull forms with various degrees of streamlining. Seven models were tested and the results compared to earlier tests of bluff bodies. Kilgore (1969) tested vehicles with tracks. Although mainly concerned with propulsion, the resistance of the tracks, skirt deflecting channels and bow fenders are measured and the effect on sinkage and trim noted. Work on this subject is currently going on.

DAVID TAYLOR NAVAL SHIP R&D CENTER

The David Taylor Naval Ship R&D Center (DTNSRDC) has over the years made important contributions to the determination of the viscous resistance of ships as required by the Froude method of using models to predict full-scale ship resistance. After the original Froude method was recast into dimensionless ratios [Granville (1956)], the coefficient of viscous resistance became a function of a length Reynolds number. The dependence of Reynolds number was then relegated to an equivalent flat-plate resistance coefficient or

$$C_v = C_F [R] + C_s$$

Here C_v = viscous resistance coefficient; C_F = flat-plate resistance coefficient; R = length Reynolds number and C_s = separation and form resistance coefficient which is independent of Reynolds number.

Schoenherr (1932) of the Experimental Model Basin (a predecessor of DTNSRDC) developed a logarithmic formula for flat-plate resistance C_F from a von Kármán boundary-layer analysis and from measured data. The Schoenherr line became celebrated and was finally adopted in 1947 by the ATTC as the official friction line for the Froude method. The ITTC followed suit and strangely termed it the 1947 ATTC friction line (probably due to national prejudice at the time). There was much opposition to abandoning the classical friction-plane data of Froude especially from the British.

Complaints from small model testers that the Schoenherr line seemed too low at low Reynolds numbers prompted the ITTC in 1957 to adopt another logarithmic formula which is higher than the Schoenherr line at low Reynolds numbers and agrees with it at high Reynolds numbers. The 1957-ITTC line was now called a correlation line for the Froude method and was considered no longer a flat-plate friction line. Incidentally, the Resistance Committee of the ITTC had a choice of three lines and voted for the one adopted.

Afterwards, Granville (1977) made an analytical study of the turbulent boundary layer and frictional resistance of flat plates at low Reynolds numbers and arrived at a logarithmic formula which agreed with the Schoenherr line at high Reynolds numbers. By great coincidence the Granville formula for flat plates is quite close to the 1957-ITTC correlation line.

Meanwhile dissatisfaction with the existing Froude method of considering the form and separation resistance coefficient invariant with Reynolds number caused Hughes of the NPL in England to propose a viscous-resistance coefficient proportional to the flat-plate resistance coefficient by means of a form factor for

$$C_v = (1 + f)\, C_F\, [R]$$

Aerodynamicists had been using this relation for streamlined bodies, that is, bodies with negligible separation pressure resistance. Hughes proposed the determination of this form factor from the total resistance of models at low Froude numbers where the wavemaking resistance is negligible. Owing to the flow separation on ships it is clear that the Hughes approach is inadequate. Furthermore, it is experimentally difficult to obtain accurate resistance measurements at low Froude numbers which involve low speeds and low resistance. There is also the problem of sufficient turbulence stimulation at such low speeds.

In an effort to eliminate the deficiencies in the Hughes method, Granville (1974) (1975) resurrected an old proposal of Landweber that the form factor relation also required an allowance for the separation resistance or

$$C_v = (1 + \tilde{f})\, C_F\, [R] + \tilde{C}_s$$

This form factor was now dubbed a partial form factor to distinguish it from the Hughes full form factor. The separation resistance coefficient $\tilde{C}_s$ is invariant

with Reynolds number and hence does not have to be determined since in the Froude method only the difference in viscous-resistance coefficient from model to full scale is required.

Granville proposed that the partial form factor, $\bar{f}$, for a particular hull could be calculated from the development of a boundary layer on an equivalent body of revolution representing the wetted hull. There are two radii defined for the equivalent body of revolution, one from the cross-section area of the hull to be used in determination of the pressure distribution and the second from the perimeter of the hull to be used in the boundary-layer calculations so that the correct hull area is accommodated. The partial form factor is to be determined from a simple power-law calculation of both the resistance of the equivalent body of revolution and the resistance of the equivalent flat plate. Since the form factor is based on a quotient of these two resistances, any errors tend to cancel each other. The resulting form factor was then correlated with overall hull geometric factors in order to further simplify practical applications.

Granville (1958) also extended the partial form-factor analysis to rough surfaces. Logarithmic formulas for rough flat plates were also developed for full-scale predictions. This is a more accurate approach than the simple roughness allowances used for full-scale predictions of resistance.

At DTNSRDC there is also a continued effort to determine the viscous resistance from a three-dimensional boundary-layer analysis. To include any Froude-number effect is not feasible at this time since it requires a pressure distribution from wavemaking which is not possible now. In fact, if the wavemaking pressure distribution were known, the wavemaking resistance would also be known.

Consequently, the 3-D boundary-layer analysis has concentrated on the zero Froude-number case for which the pressure distribution can be calculated. Also the zero Froude-number case can be represented by a double model on which convenient measurements may be taken in a wind tunnel. However, this approach eliminates important effects such as the effect of the bow wave on the generation of bilge vortices and the effect of the stern wave on hydrostatic pressure separation.

Even the simpler case of the boundary layer on a double model has problems in its analysis: there is flow separation in the stern; the peculiar hull geometry raises questions about coordinate definition: orthogonal or nonorthogonal,

streamline or fixed, body based or not. Also the cross flows in the boundary layer may change direction across the boundary layer.

The DTNSRDC efforts in 3-D boundary-layer analysis has considered the latest advances in turbulence modeling. Attention has focused on the k-ε method which is proving popular in engineering circles. Here k is the tubulence energy and ε is the rate of turbulence dissipation. Both involve partial differential transport equations. The values of k and ε are then used to calculate the eddy viscosity and consequently the turbulent shear stress. Simpler approaches are also being investigated such as "integral" methods which only involve ordinary differential equations and differential methods based on mixing length and/or eddy viscosity algebraic formulations.

The effect of boundary-layer flow as the inflow to propellers has been the subject of intensive effort. Initial work has centered on the thick axisymmetric boundary layer on the sterns of bodies of revolution. Huang, et al (1979) have performed theoretical and experimental studies on such bodies without the presence of a propeller. Later Huang and Groves (1981) studied the effect of the inflow due to an operating propeller on such axisymmetric boundary layers. More recently, Huang, et al (1983) have extended the investigations to bodies with elliptical cross sections.

DAVIDSON LABORATORY, STEVENS INSTITUTE OF TECHNOLOGY

Dr. K.S.M. Davidson, founder and first director of the Experimental Towing Tank, guided the development of instrumentation and test techniques specifically for "small models" of sailing yachts, ships and marine craft from the time of the Tank's founding in 1935 until his death in 1958. It is appropriate in 1983, twenty-five years after the end of Dr. Davidson's era, to review progress in testing small models in the facility renamed Davidson Laboratory.

Changes in methods of measuring calm water resistance of models 1.2 to 3m in length have been made in the following areas:

- o Instrumentation and data processing.
- o Technique development associated with turbulence stimulation and adapting to models of high-performance craft and unusual marine vessels.

In 1958 model resistance was measured by a coil-spring-and-deadweight balance, using visual averaging of spring deflection. Now resistance is measured by a

leaf spring force gage with a linear variable differential transformer which provides an electrical output proportional to spring deflection. Electronic averaging of signal voltages is done by a tankside digitizer and digital computer.

A key to Dr. Davidson's success in obtaining reliable resistance data with small models was his recognition of the importance of turbulence stimulation. His early work with models of sailing yacht hulls included development of a stimulation technique using a sand strip along the forefoot and leading edge of the fin keel. Presently the Laboratory uses studs for stimulation on yacht and displacement hull models.

Since 1958, numerous high-performance marine vehicles and offshore structures have been model-tested for resistance at the Laboratory. In the offshore category, catamaran ships, semisubmersible platforms, monohulls with large drilling wells amidships, and jackup unit models have been towed to measure resistance at relatively low speeds. Prediction of full-scale resistance from such model tests is believed to be of acceptable accuracy in most cases. However, resistance tests of offshore structures with submerged cylindrical columns and braces pose significant scale-effect problems regardless of model size.

Our models of high-performance craft such as air cushion vehicles, surface effect ships, and SWATH ships generally have been tested at Reynolds numbers at which form and wavemaking drag predominate. Thus, turbulence stimulation in such tests was not a critical necessity. However, satisfactory low-speed resistance data on SWATH models have required the use of a tripwire on the nose of each lower hull and Hama triangles at the leading edge of each strut.

Even with turbulence stimulation, resistance coefficients at very low speeds exhibit scatter and the technique suggested by Prohaska at the Eleventh ITTC has been employed as a fairing aid. (C_{tm}/C_{fm}) is plotted against C_{fm}/F_n^4 to obtain a fair curve through the scatter.

WEBB INSTITUTE OF NAVAL ARCHITECTURE

Hull Roughness Assessment

A special friction plane towing apparatus has been developed to study the effects of surface roughness on turbulent skin friction. Equipment is also available to conduct resistance tests on artificially roughened, submerged bodies of revolution. A hot-wire probe can be used to make mean velocity measurements at any point in the flow. Roughness of various textures have been studied as well as the effects of roughness on the forward half of aft half of an otherwise smooth plate.

Much work on the theoretical boundary layers of two and three dimensional boundary layers over smooth and rough surfaces has been done concurrently with the experimental work as described above. Computer programs for potential flow calculations and integral methods of solution to the turbulent boundary layer growth equations have been developed. While these studies are still undergoing further development and refinement, the effects of size, speed and surface roughness on boundary layer thickness, shape factor and viscous friction can be well predicted. The ultimate goal of these studies is to improve upon Froude's equivalent plank technique by accounting for the effect of particular streamline shaped surface roughness on form factor and separation drag. Also under investigation are means of using this improved knowledge of the flow for predicting hull/propeller interaction and calculating wake and thrust deduction directly.

Hull Form Optimization by Means of a Wake Survey

Progress has been made on the use of wave resistance survey experiments in investigating optimum changes in hull form from a wave energy point of view. This work was supported by the Maritime Administration under the University Research Program. Results are summarized in Ward, et al (1980), (1981), (1982), and (1983). Ward's "XY" wave survey method which involves measuring the wave induced forces on a vertical cylinder was employed. The investigations were carried out on the Mar Ad "Security" Class Mobilization Ships [Kloetzli and Slager (1980)] and involved bow and stern bulbs and/or mid-forebody port and starboard protuberances or combinations. The actual changes were added to the base hull model in the form of clay formed in molds. Many improvements in technique were made over the period. These included computer storage of run data and automated calibration. Two of the experimental challenges were the handling of the small differences between the wave patterns with and without the change or changes, and the precsion of matching run speeds and run conditions. An optimization scheme was developed to predict savings, on either side, of the amount of the change tested and this was found to be successful, even for the small changes represented by stern bulbs, but required the averaging of two sets of run pairs (four combinations) in the latter case.

The foregoing technique and apparatus are now on a working basis and available to industry at Webb Institute and would be at other testing institutions willing to make a reasonable expenditure for the instrumentation involved.

Oscillating Table

An oscillating table facility, acquired with the help of a National Science Foundation grant, has become operational at Webb Institute. The facility can accommodate model tanks 2-feet by 3 feet in plan form. Two degrees of freedom have been provided for -- up to $\pm 30^{\circ}$ of rotation and up to ± 10 inches of translation. Thus, a ship tank model may be oscillated as though the tank were experiencing combined pitch and surge, or combined roll and sway. The design of the facility provides for possible future use with the translation mode of motion shifted 90° in a vertical plane so that heave motions can be modeled.

Utilization of the facility as of date has included a Maritime Administration sponsored project on heat transfer [Rowen and Signell (1983)] in a fluidized bed and the measurement of slosh-induced pressures on a shipboard LPG tank model.

Future use will include an extension of the Maritime Administration sponsored project and a Ship Structure Committee project requiring measurements of slosh-induced forces on internal tank structure.

REFERENCES

Cohen, S. B. (1983) "Tables of Residuary Resistance Coefficient for Barges with and Without Notches," Society of Naval Architects and Marine Engineers T&R Bulletin 1-42.

Compton, R. H (1977) "Experimental Naval Architecture at the U. S. Naval Academy," American Society of Naval Engineers Journal.

Couch, R. B., and Moss, J. L. (1966) "Application of Large Protruding Bulbs to Ships of High Block Coefficient," Transactions, Society of Naval Architects and Marine Engineers.

Day, W., Reed, A., and Hurwitz, R. (1980) "Full Scale Propeller Disk Wake Survey and Boundary Layer Velocity Profile Measurements on the 154-Foot Ship R/V ATHENA," DTNSRDC Report SPD-0833-01.

Granville, P. S. (1956) "The Viscous Resistance of Surface Vessels and the Skin Friction of Flat Plates," Transactions, Society of Naval Architects and Marine Engineers, Vol. 64, pp 209-240.

____. (1958) "The Frictional Resistance and Turbulent Boundary Layer of Rough Surfaces," Journal of Ship Research, Vol. 2, No. 3, pp 52-74.

____. (1974) "A Modified Froude Method for Determining Full-Scale Resistance of Surface Ships from Towed Models," Journal of Ship Research, Vol. 18, No. 4, pp 215-223.

____. (1975) "Partial Form Factors from Equivalent Bodies of Revolution for the Froude Method of Predicting Ship Resistance," Proceedings, First Ship Technology and Research Symposium, Society of Naval Architects and Marine Engineers.

____. (1977) "The Drag and Turbulent Boundary Layer of Flat Plates at Low Reynolds Numbers," Journal of Ship Research, Vol. 21, No. 1, pp 30-39.

Huang, T. T. and Groves, N. C. (1981) "Effective Wake: Theory and Experiment," 13th Symposium on Naval Hydrodynamics, pp 651-673, Shipbuilding Research Association of Japan.

Huang, T. T., Groves, N. C. and Belt, G. S. (1983) "Stern Boundary-Layer Flow on Two Three-Dimensional Bodies Having Elliptical Transverse Cross-Sections," Second Symposium on Numerical and Physical Aspects of Aerodynamic Flows, California State University, Long Beach, CA.

Huang, T. T., Santelli, N. and Belt, G. (1979) "Stern Boundary-Layer Flow on Axisymmetric Bodies," 12th Symposium on Naval Hydrodynamics, pp 127-157, National Academy of Sciences, Washington, DC.

Kilgore, U. (1969) "Hydrodynamic Aspects of Tracked Amphibians," University of Michigan, Department of Naval Architecture and Marine Engineering Report No. 020.

Kloetzli, J. W. and Slager, J. J. (1980) "Resistance and Powering Predictions for U. S. Maritime Administration 'Security' Class Mobilization Ships," (Mar Ad Design C7-S-Ma 134a), Phase III, Hydronautics, Inc.

Latorre, R. and Ashcroft, F. (1981) "Recent Developments in Barge Design, Towing, and Pushing," Marine Technology.

Latorre, R., Ashcroft, F. and Cohen, S. (1980) "Investigation of Barge Towing Performance, Phase I Experiments," Proceedings 19th American Towing Tank Conference, Ann Arbor, MI.

Latorre, R. and Bernitsas, M. (1981) "Influence of Starting Acceleration and Towrope Length on Towed Barge Trajectory," International Shipbuilding Progress, Vol. 28, No. 325.

Maritime Administration. (1979) "Towing Tank Correlation Studies for Large, Full Form Merchant Ships," prepared by Hydronautics for the Office of Commercial Development.

Moss, J. L. and Townsend, C. (1969) "Design Considerations and the Resistance of Large, Towed Seagoing Barges," Society of Naval Architects and Marine Engineers T&R Bulletin 1-29.

Nowacki, H., Moss, J., Snyder, E. and Young B. (1968) "Experiments on the Resistance of a Family of Box-Like Hull Forms for Amphibious Vehicles," University of Michigan, Department of Naval Architecture and Marine Engineering Report No. 006.

Rowen, A. L. and Signell, W. I. (1983) "Performance Characteristics of a Fluidized Bed Operated as an Unfired Heat Exchanger and the Influence of Simulated Ship Motions," Webb Institute Report to the Maritime Administration, Department of Transportation, Mar Ad Contract MA-81-SAC-10065.

Schoenherr, K. E. (1932) "Resistance of Flat Surfaces Moving Through a Fluid," Transactions, Society of Naval Architects and Marine Engineers, Vol. 40, pp 279-313.

Sharma, S. D. and Naegle, J. N. (1970) "Optimization of Bow Bulb Configurations on the Basis of Model Wave Profile Measurements," The University of Michigan, Department of Naval Architecture and Marine Engineering Report No. 104.

Swift, P., Nowacki, H. and Fisher, P. (1973) "Estimation of Great Lakes Bulk Carriers Resistance Based on Model Test Data Regression," Marine Technology.

Toro, A. (1969) "Shallow-Water Performance of a Planing Boat," University of Michigan, Department of Naval Architecture and Marine Engineering Report No. 019.

Troesch, A., Phelps, V. and Hackett, J. (1978) "Full Scale Wake and Boundary Layer Survey Instrumentation Feasibility Study," Univeristy of Michigan, Department of Naval Architecture and Marine Engineering, College of Engineering Report.

Ward, L. W. and Morales, P. J. (1981) "Utilization and Improvements of an Experimental Method to Optimize the Wave Power of Ships," Webb Institute Report to the Maritime Administration, Mar Ad Contract No. MA-79-SAC-00106.

Ward, L. W., Morales, P. J. and Palumbo, E. (1982) "Application of an Experimental Method to Optimize the Wave Power of Ships," Webb Institute Report to the Maritime Administration, Mar Ad Contract No. MA-80-SAC-01079.

____. (1983) "Further Development and Application of an Experimental Method to Optimize the Wave Power of Ships," Webb Institute Report to the Maritime Administration, Mar Ad Contract No. MA-81-SAC-10066.

Ward, L. W. and Sedat, R. D. (1980) "Initial Progress in Development of an Experimental Method to Optimize the Wave Power of Ships," Webb Institute Report to the Maritime Administration, Mar Ad Contract No. DO-A01-78-00-3125.

DISCUSSION

Choung M. Lee
Office of Naval Research

Your progress report on resistance and flow gives an impression that not much progress has been made in the area of ship resistance in the last three years. My recollection is that, even within the limited knowledge of mine, there have been a few interesting research and development works in the resistance and flow area done at David W. Taylor Naval Ship Research and Development Center (DWTNSR&DC). To name a few, the international workshop on wave resistance held at DWTNSR&DC, the investigation on the flow about a transom stern, the investigation of the trip-wire effect on appendage drag and the two projects on appendage drag and wake and separation of flow on three-dimensional bodies which are supported under a NAVSEA special focus program.

I wonder if your final report could contain those interesting investigations conducted in the American Continent which were missing in your present report.



AD-P003 803

WAVE CUT TESTS TO OPTIMIZE HULL FORM CHANGES

By:

L. W. Ward

August 1983

ACKNOWLEDGEMENTS

The author would like to acknowledge the assistance of the faculty, staff and students at Webb Institute. The Office of Maritime Technology of the Maritime Administration is thanked for supporting this important research under the University Research Program.

NOMENCLATURE

A	Centerline Wave Amplitude, Ft.
A_1, A_2	Wave Optimization Factors
$\overline{AB}$	Distance Between Point A and B, Ft.
A,B,C,D	Points, See Figure 1
b	Model Tank Width, Ft.
B	Model Beam, Ft. or Bulb Size Designation
B_1, B_2	Wave Optimization Factors
C	Wave Optimization Factor
C_w	Wave Resistance Coefficient = $R_w/\rho/2SV^2$
D	Wave Optimization Factor
Δ	Model Displacement, Lb.
F_r	Froude Number = $V/\sqrt{gL}$, Non-Dimensional
g	Gravitational Constant, Ft/Sec^2
H	Model Draft, Ft. or Bulb Depth Position (See Figure 2)
I	XY Integral, Ft.
k	Ratio of linear dimension of a hull form variation considered, i.e. a bulb or protuberance, to that used in the model test. Also used as a subscript, thus, 0 would refer to the bare hull test and 1 to the bulb test, and 2 to the protuberance test.
opt	Subscript denoting optimum (best) value of a parameter for a particular bulb or protuberance shape and location.
λ	Scale Ratio
L	Length of Model, Ft.
m	Percentage saving of bare hull wave resistance by use of a bulb or protuberance at some location.
n	Exponent of the bulb or protuberance dimension k to which the wave height is proportional, i.e. n = 2 would assume the wave height to vary with bulb area.
N	Run Number

NOMENCLATURE CONTINUED

P	Protuberance Designation
ρ	Density of Fluid, Slugs/Ft^3
R_w	Wave Resistance, Lbs.
S	Model Wetted Surface, Ft^2
T	Superscript Denoting the Result Includes the Truncation Correction
V	Speed
V_m	Speed of Model, Ft/Sec
x	Coordinate in Direction of Model Travel (See Figure 1)
X	Force on cylinder in x-direction, reduced by calibration to ft. of wave elevation, or bulb station designation.
y	Coordinate perpendicular to direction of model travel (See Figure 1) perpendicular to x.
Y	Force on cylinder in y-direction, reduced by calibration to ft. of wave elevation.
Z	Wave Elevation at Measuring Station, Ft.

SUMMARY

Research was continued in the towing tank at Webb Institute using the established XY wave survey method for determining ship model wave resistance from measurements of the force exerted on a stationary vertical cylinder by the waves produced by the model. As before, the hull form used was the Maritime Administration Security Class Multi-Purpose Mobilization Ship (MMS).

New results using this technique showed, (a) ~~that~~ a Kawasaki-type stern bulb caused a small saving (7% ~~percent~~) of wave energy; (b) ~~that~~ a suggested vertically distributed bow bulb area was not better than the originally designed elliptical distribution; and (c) ~~that~~ a newly developed two-change optimization theory (included in the text) was valid and that the predicted bow bulb-Station 4 protuberance combination was in fact beneficial. The large percentage (about 67% ~~percent~~) saving in wave resistance caused by these additions does not seem to be identifiable by simply comparing the wave signals by eye.

Tests to assess the possible adjustment of the above wave resistance savings to those of wave power by including the effect of average wake values in the propeller disc were made, ~~and~~ it is concluded that such changes were not significant for the present model and bulbs.

INTRODUCTION

The following is a summary of results under the projects (1), (2), (3) and (4)* carried out under the Maritime Administration's University Research Program utilizing a method for assessing ship hull forms from a resistance point of view by an experimental technique of measuring wave resistance in the model tank called the XY Method of Wave Survey. Table 1 shows a summary of this effort. The ultimate objective of these studies is the determination of improved hull forms requiring less power, a question of increasing importance because of continuing high fuel prices. Reports (2), (3) and (4) on the previous studies have been issued and include a discussion of the background of ship wave theory in general and of the XY wave survey method in particular as well as the optimization technique used in analyzing the experiments to deduce the best possible sizes of tested hull form variations from a wave power loss point of view. The XY method is discussed in more detail in References (5) and (6). Only a brief summary of the approach will be included here.

The present study continues the previous investigations of wave-producing qualities of a particular hull, the Mar Ad Multi-Purpose Mobilization Ship, but as redesigned (7), with and without bulbs or other protuberances with the goal of using such assessments in an efficient way to determine optimum size and shape of such hull form changes for a particular Froude number F_r** and loading condition.

---

* Numbers in parentheses denote references listed on Page 78.

** $F_r = V/\sqrt{gL}$ where V = speed of hull, L = length of hull, g = gravitational constant.

TABLE 1

SUMMARY OF WAVE SURVEY RESEARCH AT WEBB INSTITUTE UNDER THE MARITIME ADMINISTRATION UNIVERSITY RESEARCH PROGRAM

DATES FUNDING	MINA NO. CONTRACT NO.	TITLE	MODEL(S)	BULB(S) & LOCATION(S)	F_R'S	LOADS	WAKE?	REPORT AUTHORS	WAVE ANALYSIS ETC
(1) 9/30/78-12/01/79	G-111	"INITIAL PROGRESS IN DEVELOPMENT OF ... (2)"	(A) SERIES 60/.60 C_B (B) MMS-SHORT & LONG HULLS (3)	(A) CIRCULAR (B) ELLIPTICAL AT STATION 0.3	3 DESIGN ±	FULL LOAD	--	MARCH 1980 DNW & RDS REFERENCE (4)	P.D.P. TAPE USED TO TIME SHARING
$32,960	DO-A01-78-00-3125								
(1) 9/29/79-10/31/80	G-136	"UTILIZATION AND IMPROVEMENT OF ... (2)"	MMS-SHORT HULL (3)	ELLIPTICAL FULL AND HALF-SIZE AT STATION 012346 & 2 DRAFTS	3 & 2	FULL LOAD	RUN, NOT ANALYZED	MARCH 1981 DNW & PJM REFERENCE (3)	P.D.P. DISC STORAGE & ANALYSIS, CALIB. AUTOMATED
$33,275	MA-79-SAC-00106								
(1) 9/29/80-81	G-143	"APPLICATION OF ... (2)"	MMS-RE DESIGNED "SECURITY" CLASS (3)	ELLIPTICAL, CIRCULAR & OTHER STATION 0 (& 4)	1 (DESIGN)	FULL LOAD MEDIUM BALLAST LIGHT BALLAST	RUN & ANALYZED AND COMPARED	FEBRUARY 1982 DNW, PJM, & EP REFERENCE (2)	FURTHER AUTO OF CALIB. & SPEED MEASUREMENTS
$30,979	MA-80-SAC-01079								
(1) 9/01/81-12/01/82	G-166	"FURTHER DEVELOPMENT AND APPLICATION OF ... (2)"	AS ABOVE	VARIOUS STATION 0 & STERN BULB & TWO CHANGES	3 DESIGN ±	F, M, L AS ABOVE & FULL LOAD	--	JANUARY 1983 DNW, PJM, & EP	CALC. FOR TWO CHANGES IMPROVED CALIBRATION TECHNIQUES
$18,746	MA-81-SAC-10066								

(1) EXTENDED

(2) "AN EXPERIMENTAL METHOD TO OPTIMIZE THE WAVE POWER OF SHIPS"

(3) MULTI-PURPOSE MOBILIZATION SHIP

The latter variation and especially the question of behavior of the bulbs in light ballast condition was emphasized in the most recent (2) study. The latter will be continued in the present study. Also, investigation of possible wave resistance reduction benefits of a type of stern end bulb as has been proposed by Kawasaki (8) will be examined using the same ("one change") method developed for bow bulbs or protuberances. Finally, a "two-change" theory will be derived and applied to the same hull form, with a bow bulb and forebody protuberance as the two changes, and the optimum combination thus predicted also fitted on the model and a check test run. As before, the goal of the research is the continued improvement of the instrumentation and method of analysis and to demonstrate its potential use in improving the design of ship hull forms and appendages.

The Webb Model Tank, a 93 foot by 10' x 5' rectangular channel, and associated PDP 11 computer data acquisition and Minneapolis Honeywell Visicorder signal conditioning recording system, was used for the present study.

SUMMARY OF THE METHOD AND EXPERIMENTAL APPROACH

The theory and background of the XY wave survey method for obtaining an estimate of the wave making resistance, R_w, of a ship model from the waves produced during a run in a towing tank was originally proposed in Reference (5). This is brought up to date and the currently employed experimental techniques are outlined in detail in References (3) and (4). Only a brief outline will be included here. The analysis involves measuring the energy flux out of control volume ABCD shown in Figure 1. The key result (Equation 18 of Reference (5)) gives the wave resistance R_w as:

$$R_w = \rho g\{I + 1/2\ \overline{AB}\ A^2\}$$

Where:

$$I = \int_{x_B}^{\infty} XY\ dx$$

and X, Y are the x, y components of the force exerted by the model wave system on a long thin vertically-oriented circular cylinder at a distance $y = \overline{AB}$ away from the model centerline converted, by means of calibration, to wave amplitude. The term $\rho g I$ measures the energy flux out of the line BC. That across CD is assumed to be zero. A is the amplitude of the following waves at $x = x_B$ at the point of truncation of the wave signals. The density and gravitation constants are ρ and g, respectively. Any consistent system of units can be used. In the present analysis, the "English" system will be employed, i.e. pounds, feet and seconds, or non-dimensional results will be reported. For the latter purpose, we will use a non-dimensional resistance coefficient C_w:

$$C_w = R_w/(\rho/2)SV_m^2$$

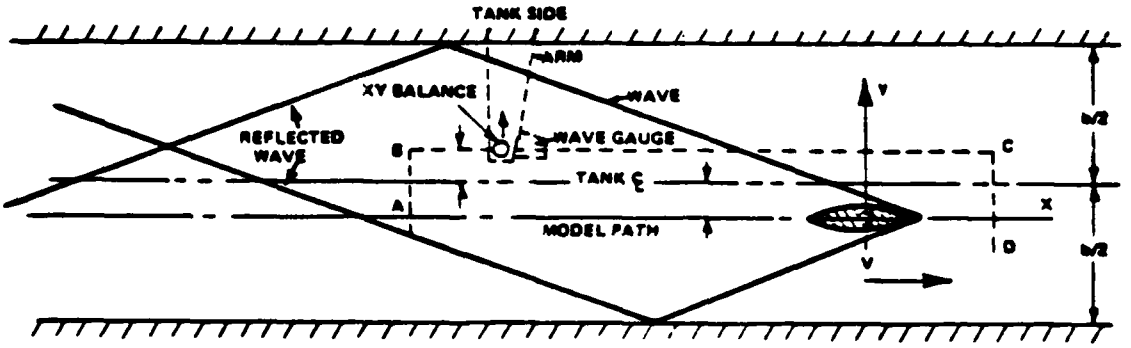


FIGURE 1: XY METHOD GEOMETRY

The term $1/2\ \overline{AB}\ A^2$ measures the energy flux through AB and is a "truncation" addition to the basic XY integration, I, due to the finite length of the record necessitated by avoiding any reflections of the wave pattern from the side walls of the tank.

Details of the force balance used to measure X and Y, the wave gauge used to measure Z, and the calibration procedure are given in References (3), (4) and (5). The signals are recorded visually on a Visicorder tape and are

then sent from the Minneapolis Honeywell amplifiers directly to the PDP 11 digitizing channels for retention on magnetic disc storage for later retrieval and analysis. Calibrations are taken before and after a test series and/or at the beginning or end of a test day. Zeros are taken on all three data channels before each run.

Zeroed and calibrated data are taken for several different model configurations, each run at the same speed. Usually three or four runs are made to obtain two sets of pairs at the same speed. The model variation could be a bow bulb of a specified shape, some other non-bow located protuberance fitted port and starboard as compared with the bare hull, or a combination of these. A simple computer calculation is used to produce the corresponding wave resistance coefficient C_w.

The question now is raised, how best to use these results? One could make a very simple "better or worse" comparison, i.e. is C_{w1} or C_{w2} for the hull with a certain size bulb or protuberance fitted, greater or smaller than the bare hull result C_{w0}? A more quantitative measure would be the percentage savings, m_1 or m_2, of the base hull wave resistance as a result of fitting the bulb or protuberance tested:

$$m_1 = (C_{w0} - C_{w1})/C_{w0}, \quad m_2 = (C_{w0} - C_{w2})/C_{w0}$$

Or, a more analytical optimization approach, as described in the following, can be used.

As discussed in more detail in References (3) and (4), a single change optimization theory based on assumed linearity of the additional bulb wave effect to some bulb size parameter $k^{(n)}$ (i.e. linear dimension (n = 1), area (n = 2) or volume (n = 3)) can be developed to predict the optimum ratio $k_{1\ opt}$ of the best bulb to the bulb tested and the corresponding minimum resistance coefficient $C_{w\ opt}$. The theory shows:

$$k^n_{1\ opt} = A_1/B_1$$

Where: $A_1 = 2C_{w0} - C_{w10}$

$$B_1 = 2(C_{1w} + C_{w0} - C_{w10})$$

and $C_{w1\ opt} = (1 - k^n_{opt})\ C_{w0} + 1/2\ k^n_{opt}\ C_{w10}$

Where C_{w10} is a hypothetical cross wave resistance term based on mixing the XY signals with and without the bulb. Details of the above theory and assumptions are given in References (3) and (4). Challenging problems are the need to carefully match speeds and stack records for the C_{w10} calculation and the basic "zero divided by zero" nature of the equation for $k^n_{1\ opt}$.

The above single change theory can also be applied to a protuberance and the single change optimum $k_{2\ opt}$ and corresponding optimum wave resistance coefficient $C_{w2\ opt}$ derived from a second set of tests. (The bare hull test does not need to be repeated.)

A "two change" optimization theory can be derived in which two variations (i.e. a bow bulb and a forebody protuberance) are made independently and the same assumption of linearity is made with respect to the magnitudes k_1 and k_2 of either. The derivation of this theory is given in Appendix A. The resulting equations, based on results of the

three sets of tests: 0 = bare hull, 1 = bulb or change-1, and 2 = protuberance or change-2 are:

$$k_{1\ opt} = \frac{\begin{vmatrix} A_1 & C \\ A_2 & B_2 \end{vmatrix}}{\begin{vmatrix} B_1 & C \\ C & B_2 \end{vmatrix}}$$

$$k_{2\ opt} = \frac{\begin{vmatrix} B_1 & A_1 \\ C & A_2 \end{vmatrix}}{\begin{vmatrix} B_1 & C \\ C & B_2 \end{vmatrix}}$$

Where: A_1 and B_1 are as defined previously and A_2 and B_2 are as A_1 and B_1 with 2 replacing 1,

and: $C = 2C_{w0} - C_{w10} - C_{w20} + C_{w12}$

If a test is also run with both changes, i.e. 3 = 1 + 2, then C_{w3} can be calculated and we have:

$$C = C_{w3} + C_{w0} - C_{w1} - C_{w2}$$

It can be seen that the above two change optimization formulas will reduce to the single change formulas by setting C = 0.

Reference (3) also describes the use of clay models of the bulbs and protuberances made from plaster molds as a quick and effective means of producing these hull form changes so that runs can be made under essentially identical calibrations. This practice also leads to great advantages where bulb shape changes are also being considered, as these can be easily accomplished using clay.

The bulb-protuberance geometry and locations are defined in Figure 2.

EXPERIMENTS AND RESULTS

General

Experiments were continued in 1982 on a 5.5 foot model of the Mar Ad "Security Class" Mobilization Ship previously tested (7). The model had been adopted from the previous 5.0 foot short hull model of the original Multi-Purpose Mobilization Ship by adding a reduced parallel middle body and changing the scale ratio from 112:1 to 121.8:1. The model particulars and test conditions are given in Table 2. The present tests include three speeds (design speed $\pm$ 5 percent) and three different load conditions from full load to light ballast. Bulbs included a Kawasaki (8) type stern bulb of arbitrary shape, and a new bow bulb with a more vertically distributed sectional area equal to the design elliptical bulb B-1. The latter was an attempt to utilize experience from the previous ballast bulb results in Reference (2) to come up with a better compromise over the range of loadings. The former took advantage of the ongoing research program to look at the latest fad, the stern bulb, from a wave reduction point of view.

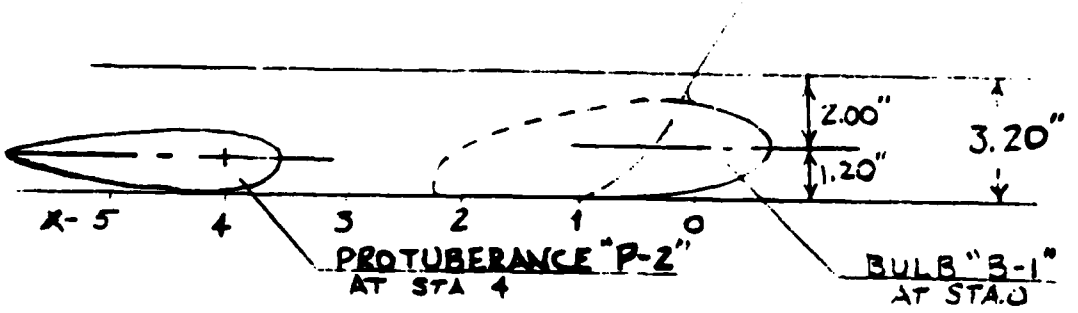


FIGURE 2: BULB AND PROTUBERANCE LOCATIONS

TABLE 2
MODEL PARTICULARS AND TEST CONDITIONS

Maritime Administration "Security" Class Mobilization Ship

	Item	Full Scale	Model*
L =	LBP, Ft.	670.0	5.501
B =	Beam, Ft.	105.5	.866
S =	Wetted Surface, Ft^2	79,681	5.371
V =	Speed, Knots	21.2	3.244 ft/sec
F_r =	Froude Number	.245	.245
Δ -	Full Load Displacement	40,050 LTSW	48.38 lb. FW**
-	Med. Ballast Displacement	33,260 LTSW	40.20 lb. FW**
-	Light Ballast Displacement	25,390 LTSW	30.69 lb. FW**

Draft H (Ft.)	Fwd	⌀	Aft	Fwd	⌀	Aft
				(Inches)		
Full Load	30.0	30.0	30.0	2.96	2.96	2.96
Medium Ballast	22.5	25.0	27.5	2.22	2.46	2.71
Light Ballast	15.5	20.0	25.0	1.48	1.97	2.46

* Scale ratio $\lambda = 121.8$

** With full size elliptical bulb B-1 or equivalent. For no bulb deduct 0.48 lb. For stern bulb add .12 lb.

In addition to the above, bulb protuberance combinations as shown in Figure 2 were run at full load to explore the effect of such combinations and to check out the validity of the proposed two-change theory as well as the effectiveness and practicability of running tests and reducing the data for this more complicated type of optimization.

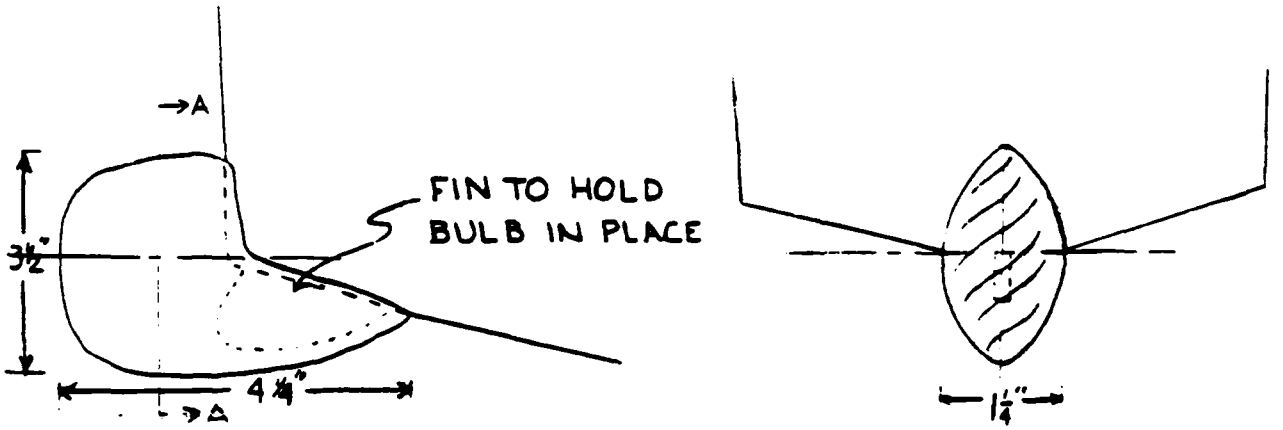
It was planned to carry out all the foregoing tests in the winter of 1982, however, malfunction of the model tank drive system resulted in curtailing the winter series and running the remaining tests, including the ballast bulb variations and a check test on the winter two-change tests, during the summer.

Stern Bulb Tests

Tests were run in the winter of 1982 on a typical Kawasaki type stern end bulb (8) using the one change analysis scheme. While no published drawings of such a bulb were available, Reference (8) indicated that the optimum stern bulb width for a container ship Model SR 138 should be 1 1/2 percent of the waterline length, which would correspond to a 1.0 inch width for the 5.50 foot model. Actually, a 1.25 inch bulb width was adopted. It will be seen that the optimum k value deduced from the experiments was 0.9 thus confirming the advice.

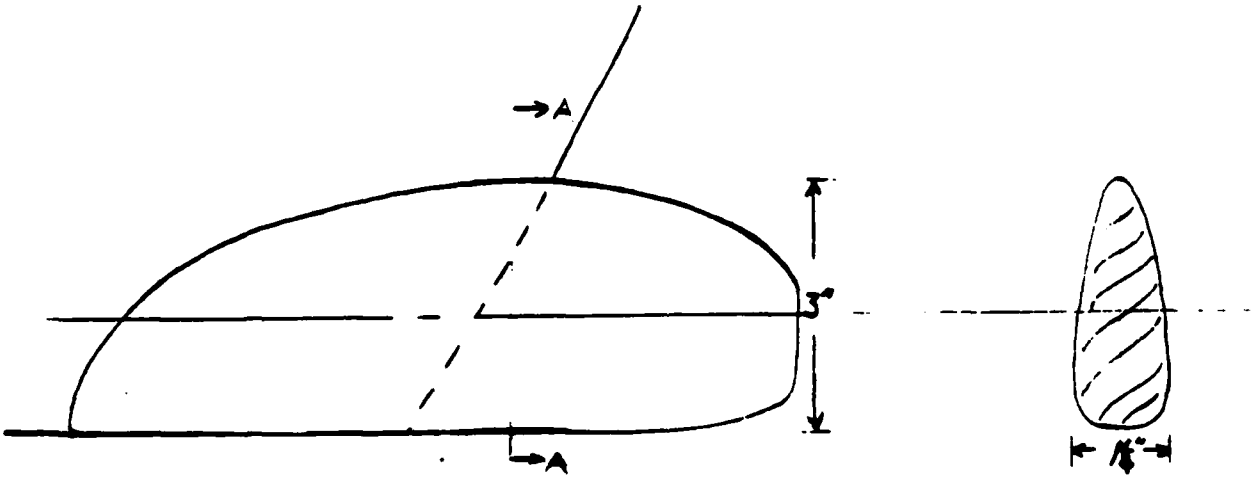
The stern bulb shape and dimensions adopted are shown in Figures 3 and 4 (photos). The profile was based on a sketch in Reference (8) but the other shape characteristics were arbitrary. The bulb itself was made of clay and held on by aid of a thin aluminum fin which was left on for the bare hull tests. Tests were run at the design Froude number F_r = .245 at full load.

Results of the stern bulb tests are shown in Table 3. These tests stretched the accuracy of the one change optimization method way beyond any previous tests due to the very small change in wave pattern involved. As previously, four run combinations were produced by two sets of run pairs and the integrals calculated and corrected to resistance coefficients C_w. These were then averaged and the optimization formulas were applied to the averaged values to produce the results k_{opt} and m_1. The latter indicates that the



PROFILE SECTION A-A

FIGURE 3A : KAWASASKI TYPE STERN BULB
FOR MARAD HULL
(NOT TO SCALE)



PROFILE SECTION A-A

FIGURE 3B : VERTICAL BULB, "VB", FOR
MARAD HULL
(NOT TO SCALE)

saving in wave resistance due to the fitting of the stern bulb was about 6.7 percent of the total bare hull and the former that the optimum stern bulb size should be 91 percent of that fitted. As mentioned before, 91 percent of the 1.25 inch bulb width gives an optimum stern bulb width of 1.13 inches. Thus, the optimum stern bulb width predicted is very close to that recommended in (8), however, the percent saving in resistance for a similar hull is considerably less than that claimed. It should be kept in mind that the present technique deals with the linear wave production only and does not include any other potential savings in non-linear wave or separation phenomena.

TABLE 3

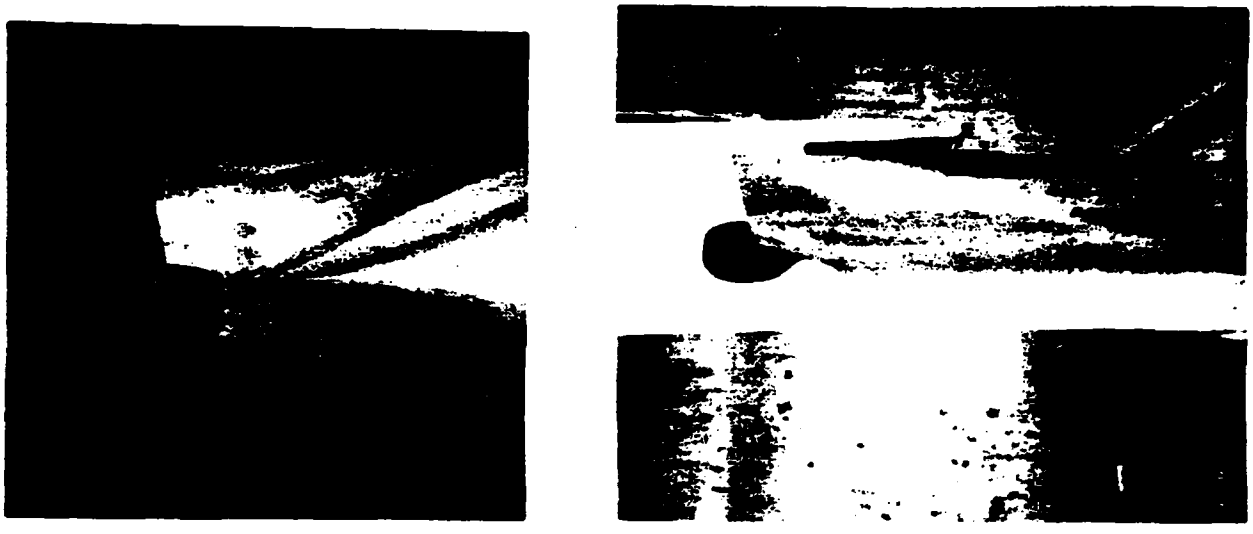
Evaluation of Stern Bulb for Security Class MMS

(No Truncation)

	$\times 10^3$				
{Run Pair}	C_{w0}	C_{w1}	C_{w10}	k_{opt}	m_1%
{29, 25}	.197	.173	.356	1.33	12
{29, 28}	.196	.187	.367	.76	5
{31, 25}	.189	.173	.348	1.05	8
{31, 28}	.188	.187	.357	.52	1
{29, 25; 31, 28}	.193	.180	.357	.91*	6.7

* Calculated from averaged C_w's

FIGURE 4: PHOTOS OF STERN BULB
FITTED ON SECURITY MMS



The foregoing results do not include truncation effects but it is not expected that inclusion of these effects will change the results in any important way for such small changes. The winter 1982 test series was subjected to a partial malfunction of the Minneapolis Honeywell Power Supply during the test period resulting in problems in the calibrations of wave height and of the force components X and Y before and after the test runs. The non-truncated predictions of k_{opt} and m_1 do not depend on calibration, thus affording another reason for their use.

Further Ballast Bulb Tests

The search for a better bulb shape (area distribution) at medium and light ballast, begun in the previous Mar Ad research program (2), was continued. Table 4(c) of Reference (2) seemed to indicate that about half the full elliptical bulb would be optimum at the latter condition. Using clay as before, a vertically

TABLE 4: 1982 TEST RESULTS

FOOTNOTES: (1) (2) (2) (3) (5) (6) (4) (5) (2) (2) (3) (5) (6) (4) (5)

DATE	CONFIG.	F_r	LOAD	RUNS: N_0, N_1 N_0, N_1	$10^3 C_{w_0}$ T	$10^3 C_{w_1}$ T	$10^3 C_{w_{10}}$ T	m_1 % T	(k^n_{opt}) T	$C_{w_{opt}}$ T	m_{opt} % T	$10^3 C_{w_0}$	$10^3 C_{w_1}$	$10^3 C_{w_{10}}$	m_1 %	(k^n_{opt})	$10^3 C_{w_{opt}}$	m_{opt} %
3/02/82	B-2	.245	Full	17, 19 18, 20	----------	----------	----------	NOT EVALUATED	----------	----------	----------	.1659 (7)	.0716 (7)	.1854 (7)	56.8	1.41	.0627 (7)	62.2
"	P-4	"	"	17, 15 18, 16	----------	----------	----------	NOT EVALUATED	----------	----------	----------	.1659 (7)	.1687 (7)	.2992 (7)	-1.7	.46	.1584 (7)	4.5
3/03/82	SB	"	"	29, 25 31, 28	----------	----------	----------	NOT EVALUATED	----------	----------	----------	.193 (7)	.180 (7)	.357 (7)	0.7	.91	.1798 (7)	6.8
7/06/82	7 B-1 + .3 P-4	"	"	15, 5 16, 6	.2158	.0746	.1741	65.4	1.10	.0742	65.6	.2058	.0592	.1495	71.2	1.13	.0577	72.0
"	.3 P-4	"	"	15, 8 16, 10	.2158	.1912	.3935	11.4	1.41	.1889	12.5	.2058	.1803	.3727	12.4	1.46	.1774	13.8
7/07/82	VB-1	"	"	34, 23 35, 25	.2177	.0703	.1237	67.7	.948	.0700	67.8	.2106	.0511	.1004	75.7	.994	.0512	75.7
"	"	"	Medium Ballast	39, 21 40, 22	.2057	.1038	.0206	49.6	.676	.0736	64.2	.1925	.0813	-.0140	57.8	.769	.0391	79.7
"	"	"	Light Ballast	42, 19 43, 20	.1592	.1144	.0954	28.1	.627	.0893	43.9	.1347	.0904	.0473	32.9	.625	.0653	51.5
"	"	.233	Full	37, 27 38, 28	.1749	.0356	.0729	79.6	1.066	.0356	79.6	.1634	.0304	.0575	81.4	.988	.0304	81.4
"	"	.257	"	34, 23 35, 25	.2874	.1376	.2895	52.1	1.063	.1372	52.3	.2478	.0929	.2057	62.5	1.073	.0923	62.8

(1) VB = Vertical Bulb; SB = Stern Bulb, 1 or 2 = Full or Half Size.

(2) $10^3 C_{w_k} = \frac{2000}{F_r^2 S L} (I_k + \overline{AB} A_k^2)$

(3) $10^3 C_{w_{10}} = \frac{2000}{F_r^2 S L} (I_{10} + \overline{AB} A_0 A_1)$

(4) $C_{w_{opt}} = C_{w_0} (1 - k^n_{opt}) + k^n_{opt} C_{w_{10}}$

(5) $m_k = 100 \left(\frac{C_{w_0} - C_{w_k}}{C_{w_0}} \right)$ = % Saving by Type of Bulb Fitted

m_{opt} from $C_{w_k} = C_{w_{opt}}$ = Greastes Possible Savings

(6) Ratio of Best Bulb to Bulb Tested, i.e. 2.0 for B-2 would agree with 1.0 for B-1, assuming n = 2.

(7) To be used relatively only due to calibration problems.

distributed elliptical bulb, "VB", was formed and tested. Figure 5 illustrates this idea as compared with the other variation considered. Table 4 gives these test results in a format similar to those previously run on other bulb variations and reported in Reference (2).

FIGURE 5
BULB AREA VARIATIONS

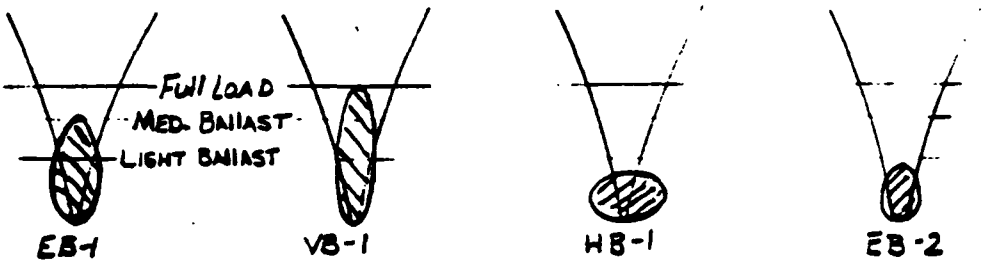


Table 5 also illustrates some other "scenarios" of combined operation as discussed in Reference (2) Predictions are included both with and without truncation. It appears that, depending on the scenario selected, the designed EB is still the best in most cases. The VB idea is competitive with the HB one and the better of the two for some scenarios. It has the additional advantage of not slamming as much should that be a factor.

Sufficient test time was available to investigate the effect of speed variation from the design speed and this was done for the VB at full load. Table 6 summarizes the results and shows that the optimum bulb ratio k is pretty insensitive to speed variation whereas the percentage saving, m, increases at a fairly rapid rate with decreasing speed. This is in agreement with such trends noted in previous Mar Ad research as shown in Figure 7 of Reference (4).

The calibrations taken from the summer 1982 test series were actually quite stable over the two-day test period and give results very compatible with those from the winter 1982 series. This can be seen in Table 4 by comparing C_{w0}'s.

TABLE 5

BALLAST BULB INVESTIGATION SUMMARY INCLUDING NEW SUMMER 1982 VERTICAL BULB

C_w's x 10^{-3}

CODE: [WITH/WITHOUT] TRUNCATION CORRECTION

"Scenarios" Bulb Description	A: Full Load	B: Med. Ballast	C: Lt. Ballast	D: $\frac{2A + B + C}{4}$	E: $\frac{A + B}{2}$	F: $\frac{A + C}{2}$
0 = Bare Hull	.200 / .190	.175 / .153	.120 / .094	.174 / .157	.188 / .172	.160 / .142
VB = Vertical Bulb	.065 / (.046)	.095 / .073	.105 / .082	.083 / .062	.080 / .060	.085 / .064
EB = Elliptical Bulb	(.060) / (.046)	(.060) / (.046)	(.096) / (.075)	(.069) / (.053)	(.060) / (.046)	(.078) / (.061)
HB = Horizontal Bulb	.065 / .057	.066 / .050	.107 / .089	.076 / .063	.066 / .053	.086 / .073

NOTES: (a) Best Bulb Circled Thus ( )

(b) 1981 and 1982 Series Normalized By Making Bare Hull Full Load The Same In Each Case And Equal To That In The 1981 Tests

TABLE 6

EFFECT OF SPEED CHANGES ON VB-1 AT FULL LOAD

(Truncation Included)

Speed Condition	-5%	Design	+5%
F_r	.233	.245	.257
$10^3\ C_{w0}$	.175	.218	.287
$10^3\ C_{w0} \times (.245/F_r)^2$	.194	.218	.260
k_1	1.01	.95	1.05
m_1	79.6	67.7	52.1

In summary, from a strict wave energy point of view, the original elliptical bulb area distribution seems to be the best overall compromise of those investigated, saving 70 percent of the wave energy at full load.

Two-Change Tests

As mentioned previously, it is possible to construct an optimization approach based on the same assumption of linear wave superposition considering two hull form changes simultaneously. Three sets of experimental wave data are needed corresponding to: the bare hull (0), the first change (1) (say a bow bulb) and the second change (2) (say a Station 4 protuberance), and same signal and mixed-signal XY products integrated to predict the optimum values of each change. The method is outlined in the previous section, and the theories given in Appendix A. Great care must be taken to match test speeds. The theory indicates that the two-change values may differ from those predicted by the one-change method applied to each change separately.

Experiments were run on the Mar Ad Model with a bow bulb B-2 (half-size elliptical) and an equal (total) displacement set of Station 4 protuberances P-4. Previous single change tests had

indicated single change optimum values $k_{1\ opt} = 1.40$ and $k_{2\ opt} = .46$, i.e. a combination of a 70 percent full size elliptical bulb and a 23 percent Station 4 protuberance. The two change C_w's without truncation were found to be:

$$C_{w1} = .0716$$
$$C_{w2} = .1687$$
$$C_{w0} = .1659 \quad (\text{all} \times 10^{-3})$$
$$C_{w10} = .1854$$
$$C_{w20} = .2992$$
$$C_{w12} = .1607$$
$$C_{w'12} = .1677$$

The latter check i.e. $C_{w12} \cong C_{w'12}$ gives a good confirmation of the theory. The A's and B's are:

$$A_1 = .1469$$
$$A_2 = .0325$$
$$B_1 = .1042$$
$$B_2 = .0707$$
$$C = .0078 \text{ (or } .0149 \text{ using } I'_{12})$$

These give combined change k_{opts}:

$$k_{1\ opt} = 1.38 \text{ (or } 1.38)$$
$$k_{2\ opt} = .31 \text{ (or } .12)$$

And single change k_{opts}:

$$k'_{1\ opt} = 1.41$$
$$k'_{2\ opt} = .46$$

as given in Table 4.

Incorporating the above two-change optimums, the opt $C_{w\ opt}$ becomes:

$$C_{w3\ opt} = .0597$$

thus, predicting a saving of 64 percent of the bare hull wave resistance $C_{w0} = .1659$. As mentioned previously, because of calibration difficulties, the above C_w's should not be compared quantitatively with those from the previous year's (1981) results or with those from the summer of 1982.

The above predicted optimum combination was actually run in the summer of 1982, reducing the size of the designed bulb and protuberance forms (made of clay) by hand. The resulting net combined wave resistance C_{w3} was found to be:

$$C_{w3} = .0746$$

with $$C_{w0} = .2158$$

thus showing a saving of 65.4 percent of the bare hull wave resistance, very close to that predicted. Moreover, the single change "k_{opt}" value for this combination was found to be 1.10 further confirming the optimum selection.

The above results were also analyzed including truncation corrections. These results and the results without truncation are given in Table 4. The percentage savings predicted without truncation seem always to be higher than those with truncation. The significance of this result, assuming it to be a general one, is not understood at the present time.

It should be noted that most (88 percent) of the bare hull wave resistance saving is due to the bow bulb and only a small amount (12 percent) due to the Station 4 protuberances; however, the latter do seem to have a beneficial effect that could be more important at a different (smaller) Froude number.

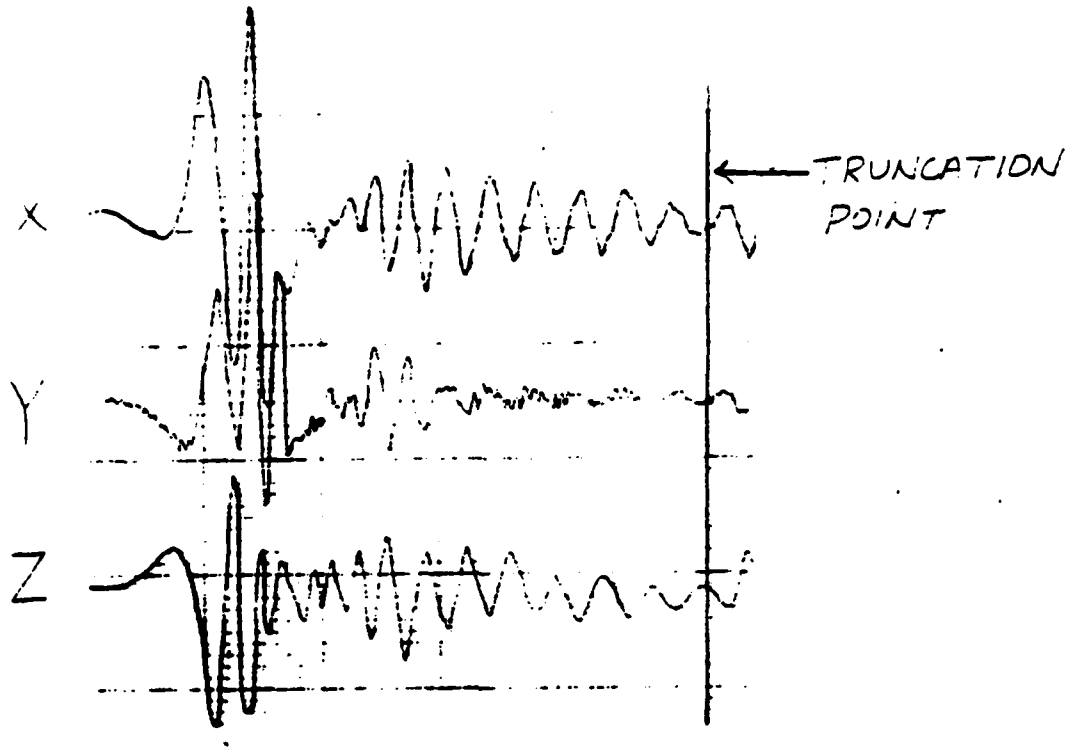
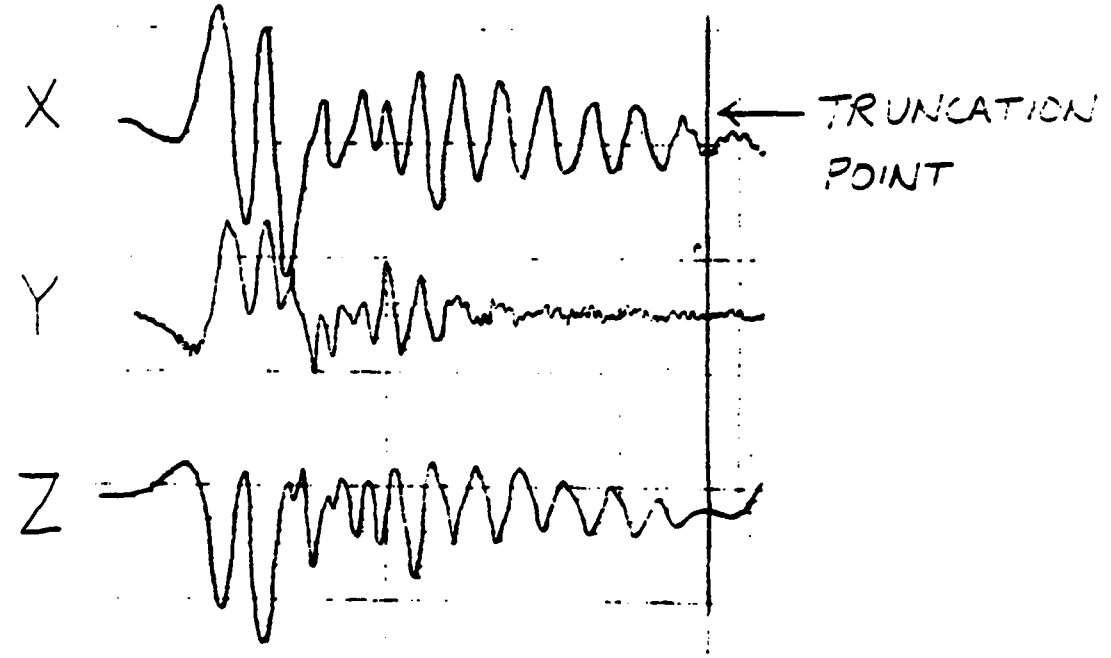


FIGURE 6: COMPARISON OF SIGNALS

A: BARE HULL (RUN EPL014) WAVE RECORDS CORRESPONDING TO $C_{W_0} = 0.2158$



B: OPTIMUM BULB-PROTUBERANCE COMBINATION (RUN EPL005) WAVE RECORDS CORRESPONDING TO $C_{W_0} = 0.0746$

General (Again)

In all of the comparisons involving the above results, including the stern bulb, ballast bulbs and two-change combinations, some from the same week of testing and others as much as a year apart, it should be emphasized that the very nature of the process of deriving optimums, etc., and the repeatability of the data and speed matching needed to assess small changes in wave profiles, will produce differences that might not be the result of real physical cause-effect relationships but could be merely "scatter". At this stage, it is proposed that a difference of 7 percent in any criterion (i.e. a m_1 or percent saving of 66 percent as opposed to 70 percent) not be assumed to prove a trend but one of 10 or 15 percent (60 percent versus 70 percent) be definitely so considered.

The question of the effect, if any, of model size on the foregoing results should be addressed. Wave production is of course a predominantly ideal flow phenomenon. However, the boundary layer thickness is relatively larger for the model than for the ship. This is also true when comparing the smaller model with the larger model. It also grows with distance from bow* to stern for either and has the effect of softening the hull form (i.e. decreasing slopes, etc.) and therefore decreasing its wave producing effectiveness. Thus adopting the foregoing reasoning, it can be argued that the stern bulb tests would be more susceptible to scale effects than those involving the bow bulbs and those involving the Station 4 protuberences somewhere in between. It might be that larger scale wave survey tests on the stern bulb would uncover larger possible savings than the present tests. It would be very surprising, however, if any such important difference due to scale were found in the case of the bow bulb findings.

---

* At the very bow, the boundary layer thickness is zero for all cases.

Finally, having established the value of an analytical experimental method using wave signals to demonstrate a saving of about 2/3 of the bare hull wave resistance, one might wonder if a saving of energy of such a magnitude would be obvious by comparison of the signals themselves. Figure 6 was prepared in an attempt to answer this question. The three signals involved, the XY forces and the Z wave elevation (used for calibration and truncation only) are displayed for: (a) the bare hull and (b) the greatest saving (B-.7 and P-.15) at the same calibration. The signals had to be sketched as the data in the project is available only on a computer disc. We leave it to the reader; if you had seen the wave elevation Z in Figure B in comparison to that in A, would you have concluded that a major saving in wave energy dissipation had occurred? Or if you went further and looked at the X and Y signals and imagined them multiplied (no fair actually doing the multiplication!), would you? An interesting question!

TABLE 7

RESULTS OF EVALUATION OF PREDICTED OPTIMUM BASED ON TWO CHANGES

Froude Number F = .245 Full Load

Change*		1	2	3 = Comb.
Predicted:	k	1.38	0.30	--
2/82	m%	56.8%**	1.7%	64.0%
Tested:	k***	--	1.41**	1.10
7/82 Tests	m%	--	12.5%**	65.9%

* Change 1: Bulb B-2 or EB-1 at Station 0
Change 2: Protuberance B-2 at Station 4 P/S

** Based on changes separately

*** These k-values relate to the changes actually tested i.e. 1.4 B-2 (or 0.7EB-1) and 0.3 B-2 at Station 4.

CONCLUSIONS AND RECOMMENDATIONS

Based on the foregoing results, the following conclusions are drawn and recommendations made:

Application of the now well-established XY wave survey optimization procedure in the Webb Model Tank to the practical problem of searching for an optimum hull form shape can be extended to other cases such as stern bulbs and a bow bulb - forebody protuberance combination in a practical and useful way.

A two-change optimization theory developed to analyze the latter results is shown to be valid.

The Kawasaki stern bulb is shown to have a beneficial effect on reducing wave resistance but smaller (7 percent) than seems to be claimed. This result could be modified by scale effects.

For the Mar Ad "Security Class" Mobilization Ship, the designed elliptical bulb is still the best overall compromise among a series of other shapes tried for combined loadings, now including a vertically distributed area bulb.

The wave energy reductions possible by using hull form changes are quite impressive, about 67 percent. They are not readily identifiable by simple comparison of wave records.

Variations in wave production power as a result of propeller mean wake changes do not seem to be of importance in the present case.

Improvements in stability of test calibration and ease of analysis procedures were also achieved.

It is recommended that the above method be further utilized and applied at Webb and at other model tanks to investigate and assess possible savings in wave power expended by ships under practical operating conditions.

APPENDIX A

TWO-CHANGE THEORY

The XY method is based on a simple integration of the X and Y forces exerted by the waves on a vertically oriented circular cylinder as shown in Figure A-1. We assume that each force component is linearly related to the waves produced by the ship hull with two changes as depicted, and that the waves are a linear superposition of those due to the hull, change-1 (bow bulb illustrated) and change-2 (equal port-starboard protuberances shown). The basic XY integral is:

$$I = \rho g \int_{X_B}^{\infty} X'Y'dx + \text{Trunc.}$$

$$X' = X/C_1 \propto \text{Wave Height}$$

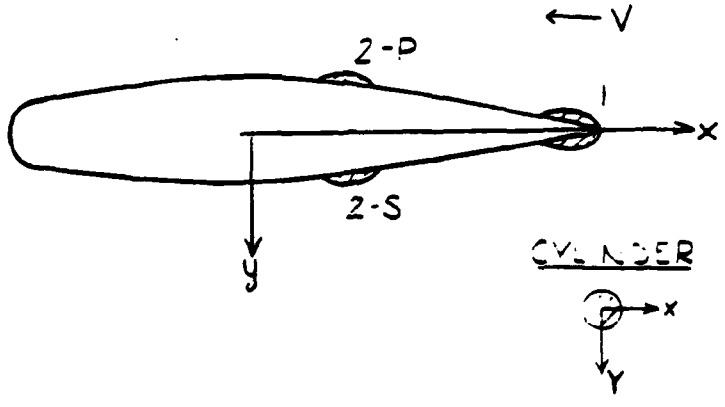


FIGURE A-1: HULL AND TWO CHANGES

The signals are (X only shown):

X_0	Bare Hull Signal
X_1	With Bulb Signal as Tested
X_2	With Protuberance Signal as Tested
X_{1+2}	With Bulb and Protuberance

We introduce control parameters:

k_1	Ratio of Bulb Considered to that Tested
k_2	Ratio of Protuberance Considered to that Tested

The assumed XY signals are:

$$X_{1+2} = X_0 + k_1 (X_1 - X_0) + k_2 (X_2 - X_0)$$

$$Y_{1+2} = Y_0 + k_1 (Y_1 - Y_0) + k_2 (Y_2 - Y_0)$$

The XY integral becomes:

$$I_{1+2} = \rho g \int X_{1+2} \, Y_{1+2} \, dx$$

Combining, we get:

$$I_{1+2} = I_0 + k_1 (I_{10} - 2I_0) + k_2 (I_{20} - 2I_0) +$$

$$k_1 k_2 (2I_0 + I_{10} - I_{20} + I_{12}) + k^2_1 (I_0 + I_1 - I_{10}) +$$

$$k^2_2 (I_0 + I_2 - I_{20})$$

Where: $I_r = \rho g \int X_r \, Y_r \, dx$

$I_{rs} = \rho g \int (X_r \, Y_s + X_s \, Y_r) \, dx$

To optimize, we set:

$$\frac{\delta I_{1+2}}{\delta k_1} = 0$$

$$\frac{\delta I_{1+2}}{\delta k_2} = 0$$

And obtain:

$$B_1 \, k_{1\,opt} + C \, k_{2\,opt} = A_1$$

$$C \, k_{1\,opt} + B_2 \, k_{2\,opt} = A_2$$

Where: $A_{1,2} = 2I_0 - I_{1,20}$

$B_{1,2} = 2(I_0 + I_{1,2} - I_{1,20})$

$C = 2I_0 - I_{10} - I_{20} + I_{12}$

Thus, the two change optimum values are:

$$k_{1\ opt} = \frac{\begin{vmatrix} A_1 & C \\ A_2 & B_2 \end{vmatrix}}{\begin{vmatrix} B_1 & C \\ C & B_2 \end{vmatrix}}$$

$$k_{2\ opt} = \frac{\begin{vmatrix} B_1 & A_1 \\ C & A_2 \end{vmatrix}}{\begin{vmatrix} B_1 & C \\ C & B_2 \end{vmatrix}}$$

For a single change, we set $k_2 = 0$ and obtain:

$$k_{1\ opt} = A_1/B_1 \text{ as before}$$

For C small ($C^2 << B_1B_2$) we have:

$$k_{1\ opt} = k'_{2\ opt} - C/B_1\ k'_{2\ opt}$$
$$k_{2\ opt} = k'_{2\ opt} - C/B_2\ k'_{1\ opt}$$

The evaluation requires three tests to be run:

0 - Bare Hull

1 - Model with Bulb Fitted

2 - Model with Protuberances Fitted

and the corresponding single and mixed integrals: I_0, I_1, I_2, I_{10}, I_{20} and I_{12} to be calculated. If a fourth test: 1 + 2 = 3, i.e. model with both bulb and protuberance fitted, is run and I_3 calculated then I_{12} can be replaced by a predicted I'_{12}:

$$I'_{12} = I_3 - I_0 - I_1 - I_2 + I_{10} + I_{20}$$

and then $C' = I_3 + I_0 - I_1 - I_2$

APPENDIX B:

CALIBRATIONS IN THE SUMMER OF 1982 TESTS

Part of the current research program involves developing good procedures and equipment for obtaining valid calibration factors. During some test periods, in particular that in the winter of 1982 when the Minneapolis Honeywell power supply was subject to intermittent failure as discussed, the calibrations seemed to shift and be subject to interpretation. Accordingly, more care was taken during the summer tests to investigate possible problems and to take data to clarify this question.

The summer 1982 calibration data is summarized in Table B-1. The calibration procedures used are those described in Reference (4). These essentially consist of a static calibration of the wave wire using a known movement, a relative static calibration of the X and Y force balances using a constant weight force in perpendicular directions, and a dynamic calibration of the X signal by analysis of the model runs themselves. The latter has been improved using a new computer analysis of the tail ends of the run signal described in Reference (2). While previously only a few of the latter, usually the bare hull* runs, were analyzed to provide an average Z/X value, in the present case all 27 runs were so analyzed to investigate any time or amplitude based trends and/or daily scatter.

---

*The bare hull runs have larger tail end signal amplitudes since more wave resistance is present.

TABLE B-1

STATIC AND DYNAMIC CALIBRATIONS FOR SUMMER 1982 TESTS

Note: All at F_r = .245, i.e. Same Speed Unless Noted

DATE	TIME	RUN	10^3 C_Z (1)	Y/X (2)	Z/X (3)	10^3 C_X (4)	10^3 C_Y (5)	NOTES
August 6	.	2	.670	1.066	--			"AM" Calibration
"	15:00	5	--	--	.821			
	15:07	6	--	--	.736			
"	15:31	8	--	--	.728			
"	15:40	10	--	--	.625			
"	16:09	14	--	--	.655			
"	16:14	15	--	--	.602			Bare Hull Run
"	16:24	16	--	--	.655			" " "
"		17	.679	1.053	--			"PM" Calibration
August 6	AVERAGE		.675	1.060	.689	.465	.439	
August 7		18	.662	1.026	--			"AM" Calibration
"	13:48	19	--	--	.674			
"	13:52	20	--	--	.638			
"	14:01	21	--	--	.731			
"	14:06	22	--	--	.769			
"	14:16	23	--	--	.786			
"	14:28	25	--	--	.696			
"	14:46	27	--	--	.661			Slower
"	14:50	28	--	--	.612			"
"	14:54	29	--	--	.770			Faster
"	15:00	30	--	--	.807			"
"	15:14	31	--	--	.738			Bare Hull Faster
"	15:19	32	--	--	.713			" " "
"	15:33	34	--	--	1.097			" " "
"	15:38	35	--	--	.723			" " "
"	15:49	37	--	--	.863			Bare Hull Slower
"	15:53	38	--	--	.770			" " "
"	16:06	39	--	--	.806			
"	16:12	40	--	--	.804			
"	16:30	42	--	--	.906			
"	16:34	43	--	--	.964			
"	"	44	.664	1.048	--			"PM" Calibration
August 7	AVERAGE		.663	1.037	.776	.514	.496	
August 6 & 7	AVERAGE		.669	1.049	.754	.504	.481	Used For Analys
August 6	BARE HULL RUN AVERAGE			--	.629			
August 7	" " " "			--	.817			

(1) Ft. Wave Ht. Per Digital Signal Unit. Derived From Static Movement of Wave Wire ±0.50 inches

(2) Derived Statically From Placing Equal Weight Force On Each leg

(3) Derived Dynamically From Computer Program Comparing Amplitudes of Sinusoidal Tail End Portions of Z and X Signals For Each Run

(4) $C_X = C_Z \times Z/X$, Average Values Used

(5) $C_Y = C_X \times Y/Z$, Average Values Used

The results are given in Table B-1 with static calibration runs included in chronological order with the test runs which also serve as dynamic calibration runs as discussed. It can be seen that the former, which were taken before and after each day's test series, are quite stable and essentially give the same values on a given day or between days. The latter are subject to a fair amount of scatter, about $\pm$ 20 percent about a mean of .77. There does not seem to be any definite trend during a particular day. One possibility is that the relationship is not linear with wave height; in that case the set of bare hull runs, for which the wave resistance and therefore the wave amplitude should be larger, should differ in a consistent way from the whole set. It can be seen that this is not the case. Those from August 6 give smaller and those from August 7 give a larger answer. Another possibility is a speed variation. Table B-1 identifies those whose speeds which were slower or faster than the design speed. Again, no trend is evident. It was concluded that the process was one of experimental scatter and an overall average of both days was adopted for use in the analysis.

APPENDIX C:

INTEGRATION OF RUN PAIRS [FROM REFERENCE (3)]

The analysis phase of determining k_{opt}, etc., is challenging. Not only does this require careful matching of pairs of runs with and without the protuberance or bulb in regard to starting points*, run speeds and calibration factors to produce comparable individual XY integrals I_0, I_1 and the mixed integral I_{10}, but the integrals themselves must be calculated accurately using an adequate sampling rate. Figures C-1 and C-2 illustrate the point. In Figure C-1, an actual single run calculation is shown; the XY signals and wave height (Z) signal are given (the latter is needed only for calibration), as are the XY products, which are the integral values, and their running sum which is the integral itself. It is interesting to see what portions of the wave records contribute significantly to the integration. Coincident large XY peaks are very important to this. Furthermore, it is seen that the data sampling rate is just adequate for the calculation in that there are 3-4 data points in the region of the sharpest peaks. Finally, the character of the truncation addition needed at the end of the run can be seen and seems to be in agreement with the assumption of the wave system simplifying to a single plane wave in this region.

---

*Use of the automated data acquisition procedure, where the DC signals starts and stops the process, is a great improvement in this regard.

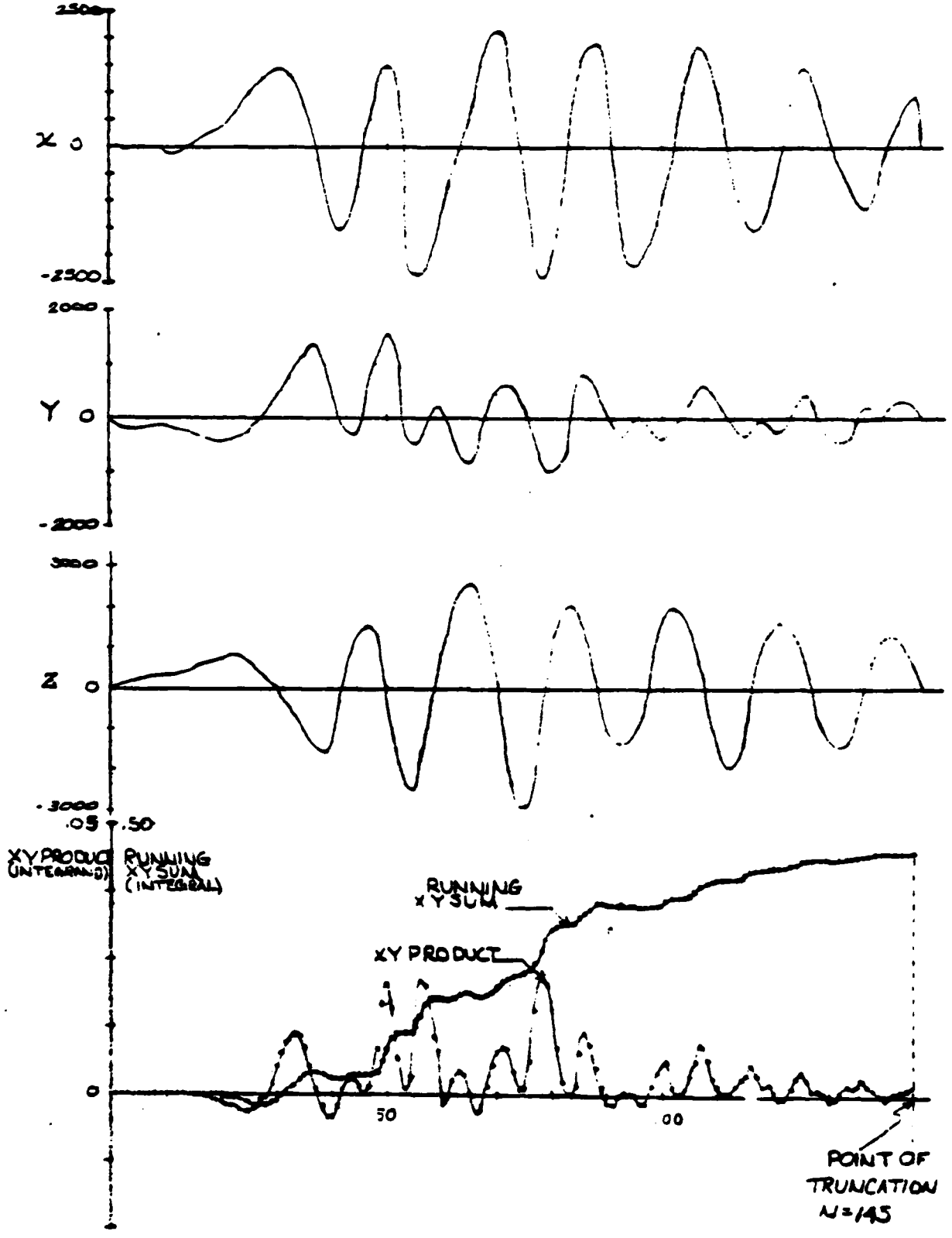


FIG. C-1 : TYPICAL RUN SIGNALS AND INTEGRATION : X, Y, Z, I
RUN # 15

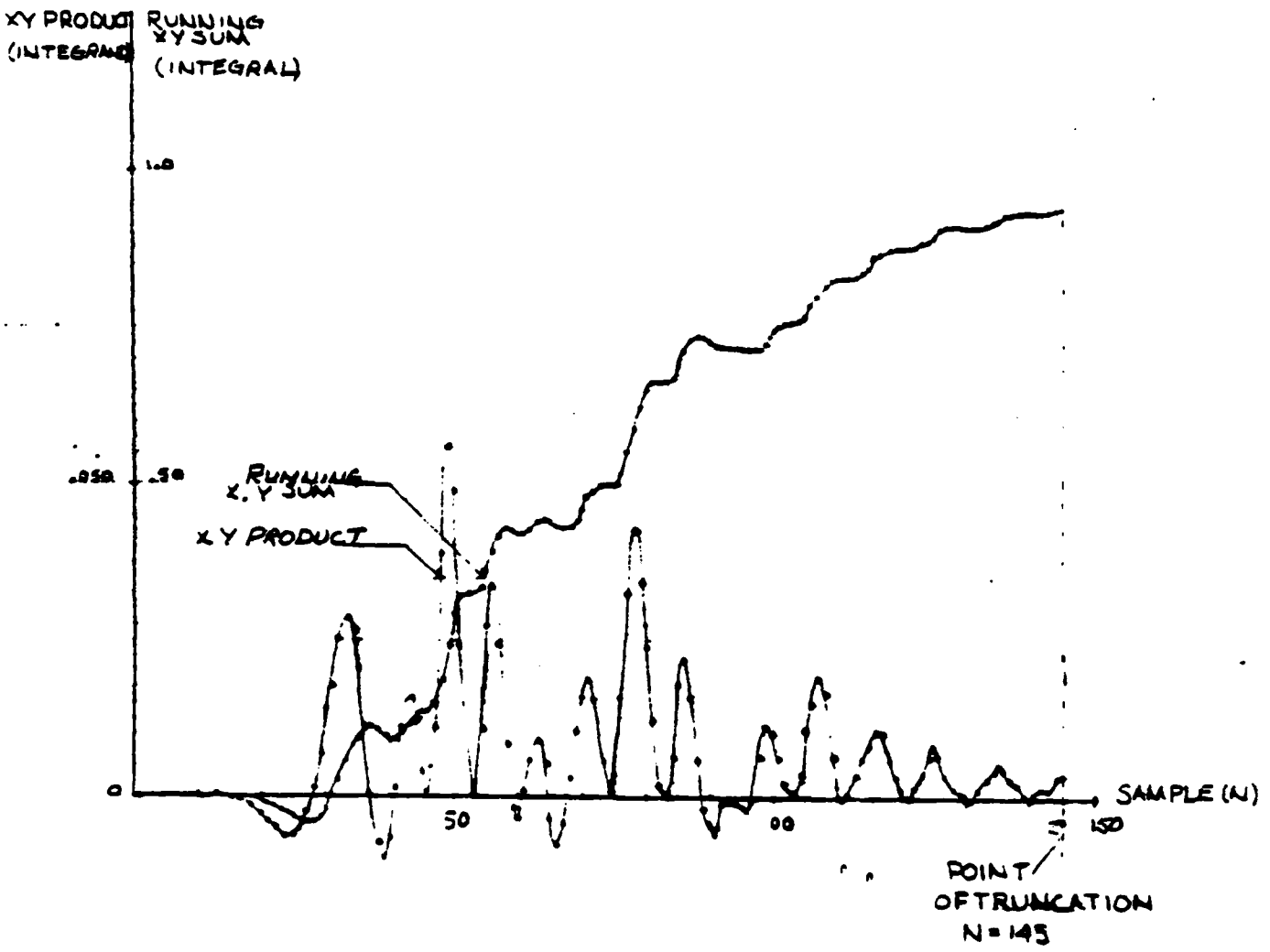


FIG C-2: TYPICAL RUN PAIR INTEGRATION RUNS 4 AND 15

APPENDIX D:

WAKE SURVEY EXPERIMENTS [FROM REFERENCE (2)]

It is possible that savings in wave resistance by addition of bulbs or other hull form changes might be offset (or improved) by changes in the propulsive coefficient due to changes in the nominal wake at the propeller disc, thus, decreasing (or increasing) the net power saving. Such a wake change due to the bulb is expected to be mainly a result of changes in the following wave amplitude at the stern and therefore should be constant over the plane of the propeller disc, except for a minor exponential decay with draft. Thus, in assessing whether any important changes are taking place, it should be sufficient to compare horizontal velocities at propeller hub draft at a sufficient distance either to port or to starboard of the centerline to get away from the boundary layer effects.

Wake assessment experiments as described above were run under the current effort during the summer of 1981 on the Security Class M.M.S. model at the design Froude number at the three different loading conditions used for the wave survey test run the previous winter. Careful attention to the instrumentation, a "CTA" (Constant temperature anemometer hot film probe) and its calibration and cleaning procedure as established for the Webb Model Tank by a previous student thesis gave results that are believed to be consistent and valid for the purpose intended. Also, taking advantage of a calibrated system in place and working another test day was devoted to examining the port-starboard wake profile and time build-up during the run down the tank. Not only are these results interesting in themselves but they show two necessary features of the wake change assessment experiments run during the present investigation:

(a) Port-starboard averaging is necessary to eliminate the effect of any towing eccentricity on the small changes being considered and

(b) Using a lateral distance y to propeller radius R ratio, y/R value of 1.4 to stay outside of the thick boundary layer characteristic of the small 5.5 foot model with a vertical skeg ahead of the propeller. This is clearly shown in Figure D-3.

Figure D-1 shows the calibration curves for the C.T.A. as taken on the morning and afternoon of each test day. The numbers shown are run numbers; they are not related to those for the previous wave survey run numbers but they are consecutive allowing any time dependent or run-length dependent effects, such as the important contamination-cleaning procedure referred to in Reference (7) to be noticed and evaluated.

The wake fractions results obtained by the above procedure are summarized in Table D-1. These are defined as:

$$w = V_m - V_{CTA}/V_m$$

where V_m is the ahead speed of the model and V_{CTA} is the local x-directed velocity measured. Both port and starboard and port-starboard average values are shown for the model with the elliptical bulb EB-1, with the half-size elliptical bulb EB-2 and without any bulb.

It can be seen that there is a small effect of increasing wake with lighter loading but virtually no change due to the bulbs fitted. Other bulb shapes can be assumed to act in the same way. Thus, it is concluded that resistance percentage savings are in effect power percentage savings as well.

During the last test day of the summer 1981 series, the hot film probe constant temperature anemometer (CTA) was used to measure wakes on the 5.501' Mar Ad model (without protuberances). The signals from the CTA were recorded on a brush recorder. The probe was located at the stern of the ship and its horizontal position was varied along a constant depth (probe track) of the axis of the propeller shaft in increments of fractions of propeller radius (y/R). From the brush recorder records, the following was obtained:

1. The average CTA signal, which is proportional to the measured fluid velocity.

2. The "envelope" of the CTA signal, which is a measure of the turbulence. (This is an average of peak to trough values around point C.)

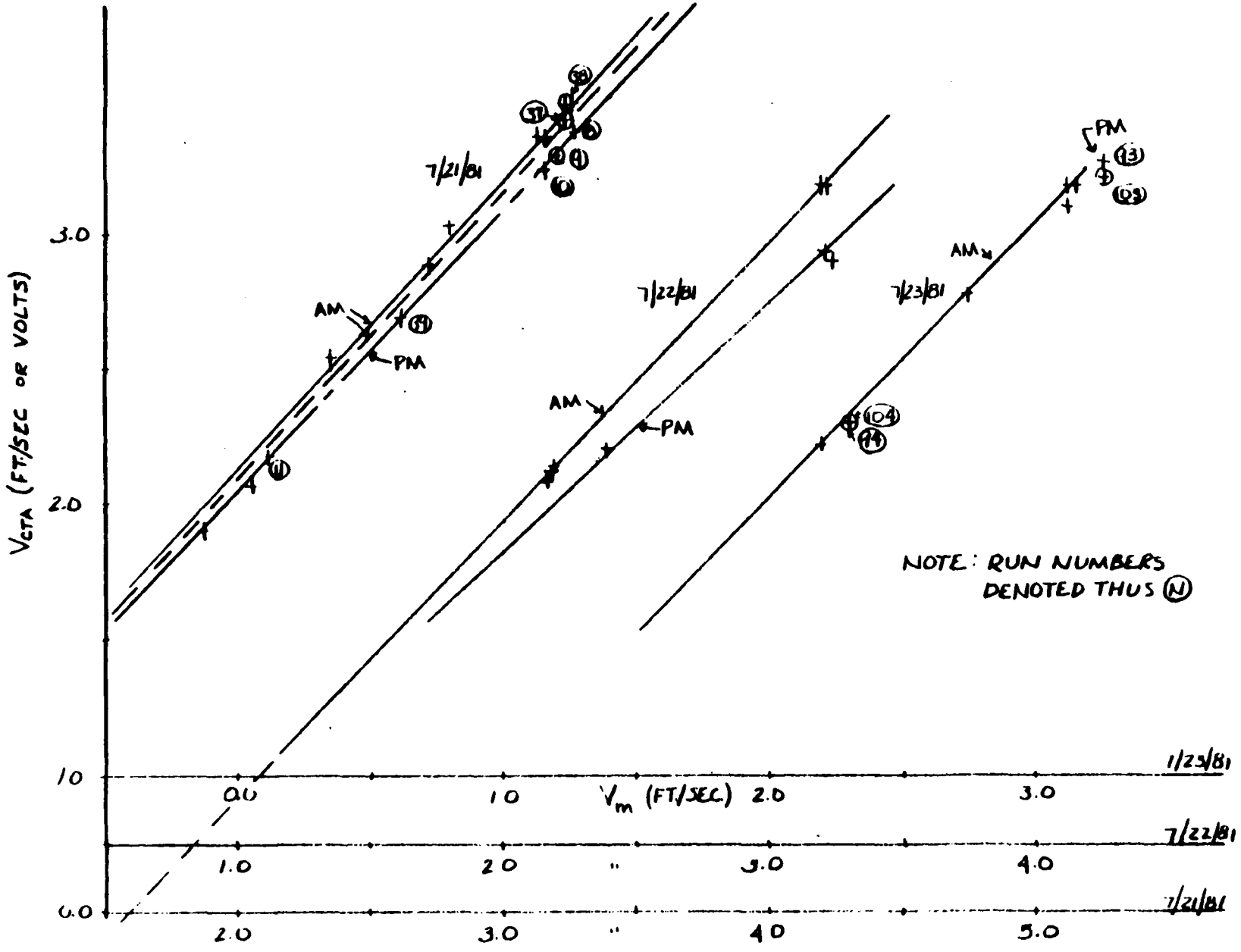


FIGURE D-1: CALIBRATION CURVES FOR C.T.A. WAKE TESTS, PROBE 611

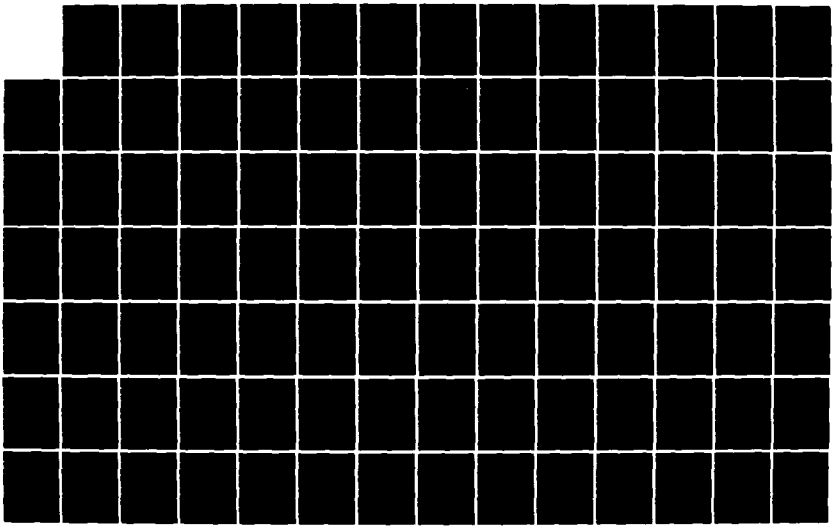
TABLE D-1

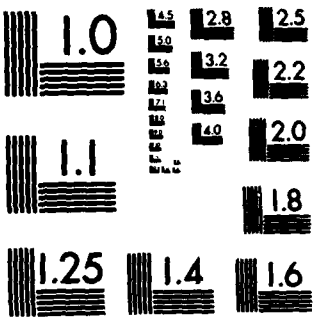
VALUES OF WAKE

@ 1.4 y/R FOR "SECURITY CLASS" MMS

	BARE HULL		EB-2		EB-1	
		P S				
Full Load	P: .10	Runs: 47, 48-45, 46	.09	73, 74-75, 76	.10	47, 48-45,46
	S: .10	Avg: .10	.125	.11	.10	.10
Med. Ballast	P: .10	Runs: 62, 63-60, 61	.10	71, 72-69, 70	.13	49, 50-51
	S: .13	Avg: .12	.14	.12	.12	.125
Light Ballast	P: .12	Runs: 56, 57-58, 59	.11	64, 65-66, 67	.13	54, 55-52, 53
	S: .14	Avg: .13	.13	.12	.11	.12

AD-A144 226 PROCEEDINGS OF THE GENERAL MEETING OF THE AMERICAN 2/1
TOWING TANK CONFERENCE..(U) STEVENS INST OF TECH
HOBOKEN NJ DAVIDSON LAB D SAVITSKY ET AL. AUG 83
UNCLASSIFIED SIT-DL-TR-13029-VOL-1 N00167-83-M-4062 F/G 20/4 NL





MICROCOPY RESOLUTION TEST CHART
NATIONAL BUREAU OF STANDARDS-1963-A

3. The estimated "settling time" (Ts). That is, the estimated time required for the turbulence to reach some state of consistency (no low frequency oscillation).

4. The wake percentage. (Using the measured speed as reference.)

5. The ratio of the CTA envelope to its average = $\frac{\text{No. 2}}{\text{No. 1}}$.

These are tabulated in Table D-2. Table D-3 describes the points on the records marked A-E. The markers on the wall of the tank were used as a distance reference.

The tabulated results in Table D-2 are plotted in Figure D-2. The range for measurements was from 0 to 1.4 y/R fractions of propeller radius on the port side and are reflected on the starboard side. The CTA probe was calibrated so that one of CTA signal closely approximated one foot per second of flow rate. The average speed of the runs tabulated was 3.23 ft./sec. Notice that wake percentage approaches zero on an asymptote as y/R increases and goes to 84.52 percent at y/R = 0. The CTA envelope, which is a measure of the turbulence, reaches a maximum near the point of maximum slope of the percent wake curve.

Figure D-3 shows the foregoing results on the bare hull model as compared with the same model with an elliptical bulb and a longer (24.0 ft.) HSMB model (7) with an elliptical bulb. The results on the same scale model with and without a bulb are practically identical except that the latter shows a port/starboard assymmetry. The differences between the WINA and HSMB results show the effect of model scaling, the longer model having a much thinner wake.

The foregoing results establish (a) that the run time is more than sufficient for the boundary layer to reach steady state and (b) that the small model has a very noticeably thicker boundary layer, thus, requiring measurement of the wave effect on wake at a y/R of at least 1.25 to be outside the region affected by viscosity.

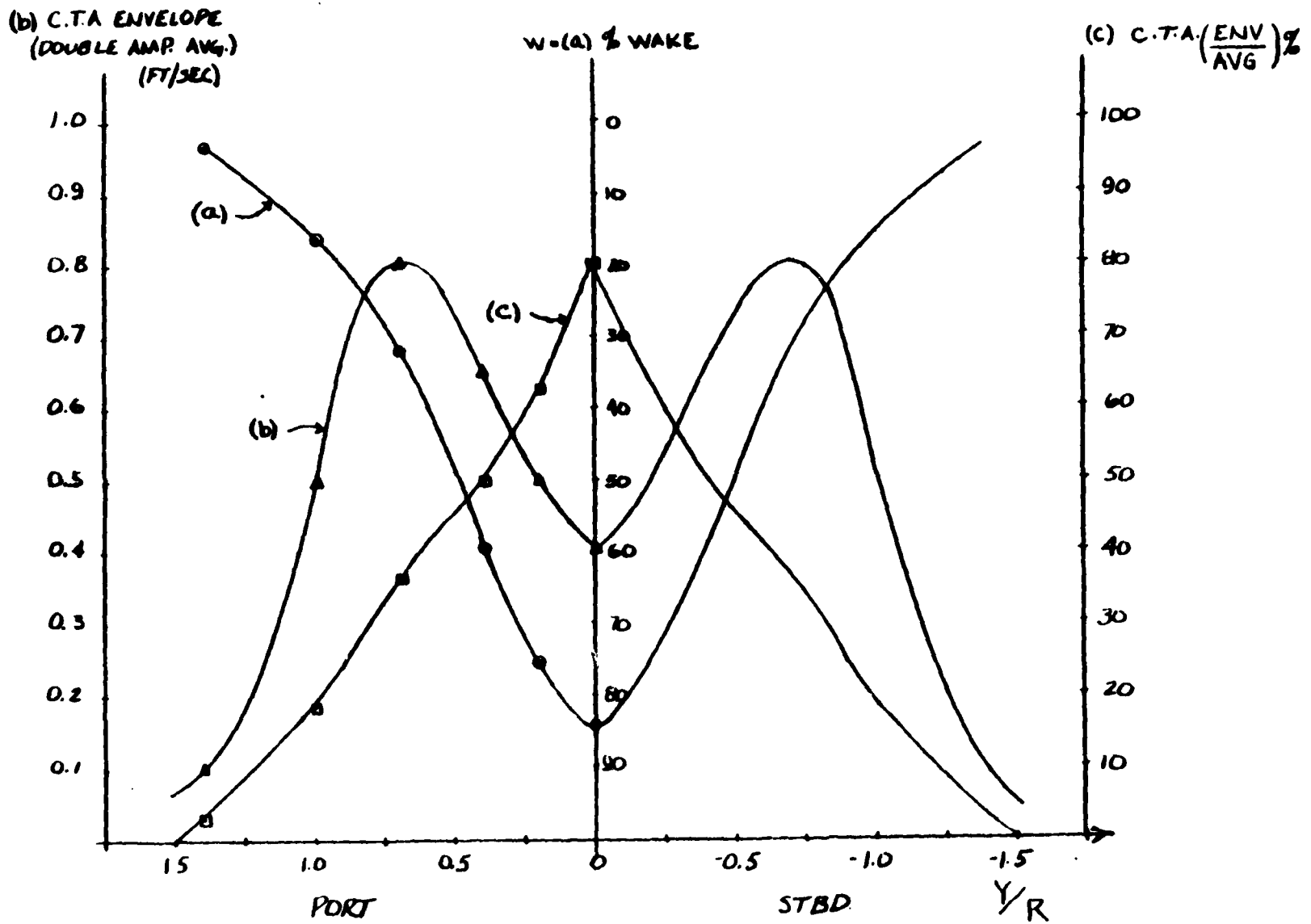


FIGURE D-2: VARIATION OF AVG WAKE AND WAKE FLUCTUATION WITH LATERAL DISTANCE Y/R

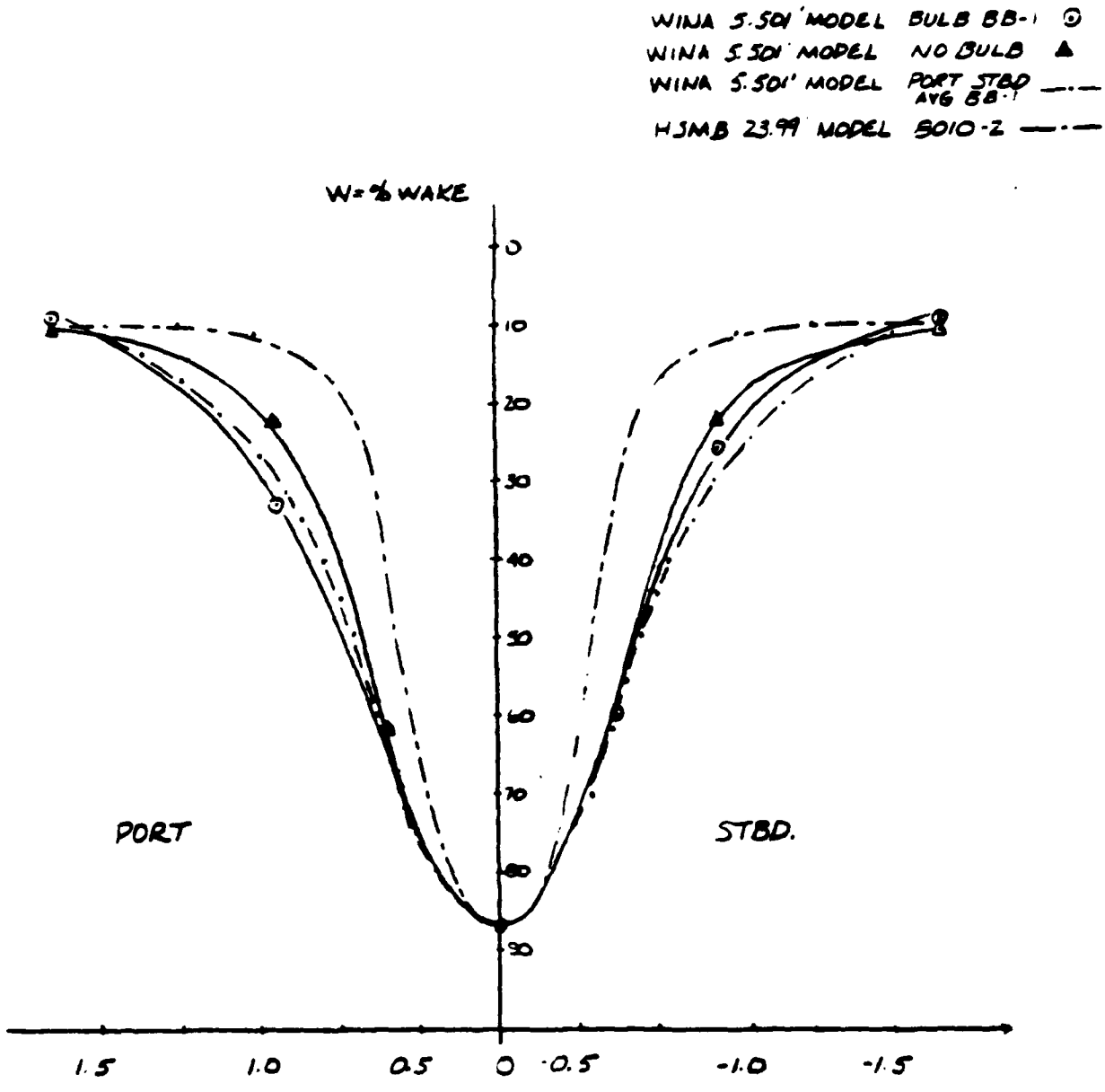


FIGURE D-3: COMPARISON OF WAKE MEASUREMENTS

TABLE D-2

DATA FROM BRUSH RECORDER CHARTS

1 volt = 1 ft/sec

RUN #	y/R	SPEED (ft/sec)	CTA (AVG) (volts)	CTA (ENV) (volts)	T_s (sec)	w - % WAKE	$CTA\frac{(ENV)}{(AVG)}$
2	1.4	3.22	3.10	.1	.64	3.73	.0323
3	1.0	3.24	2.7	.5	.88	16.67	.1852
4	0.7	3.23	2.2	.8	.72	31.89	.3636
5	0.4	3.23	1.3	.65	.72	57.75	.5000
6	0.2	3.23	0.8	.50	1.24	75.23	.6250
7	0.0	3.23	0.5	.4	.70	84.52	.8000
8	no model	3.24	3.25	-	-	-	

TABLE D-3

TEST GEOMETRY

POINT	MARK ON TANK WALL	COMMENTS
A	0	Carriage started
B	3.4	Half way to test region start
C	6.8	Start test region
D	13.5	
E		End of Test Region End of Run

REFERENCES

1. "Further Development and Application of Experimental Means of Assessing and Optimizing for Reducing Wave Production Power of Ships," Webb Institute, Glen Cove, New York, April 17, 1981, Proposal resulting in Mar Ad Contract MA-81-SAC-10066, September 29, 1981.

2. Ward, L. W., Morales, P. J. and Palumbo, E., "Application of an Experimental Method to Optimize the Wave Power of Ships," Webb Institute Report to Mar Ad, Under Contract No. MA-80-SAC-01079, February 1982.

3. Ward, L. W. and Morales, P. J., "Utilization and Improvements of an Experimental Method to Optimize the Wave Power of Ships," Webb Institute Report to Mar Ad, Under Contract No. MA-79-SAC-00106, March 1981.

4. Ward, L. W. and Sedat, R. D., "Initial Progress in Development of an Experimental Method to Optimize the Wave Power of Ships," Webb Institute Report to Mar Ad, Under Contract No. DO A01 78 00 3125, March 1980.

5. Ward, L. W., "Experimental Determination of Ship Wave Resistance from the Wave Pattern," Webb Institute, November 1964 (Sponsored by Bureau of Ships Fundamental Hydrodynamics Research Program).

6. Eggers, K. W. H., Sharma, S. D. and Ward, L. W., "An Assessment of some Experimental Methods for Determining the Wavemaking Characteristics of a Ship Form," SNAME Transactions, 1967.

7. Kloetzli, J. W. and Slager, J. J., "Resistance and Powering Predictions for a U.S. Maritime Administration "Security" Class Mobilization Ships," (Mar Ad Design C7-S-Ma 134a), Phase III, Hydronautics Inc., March 1980.

8. Miyata, H., Tsuchiya, Y., Inui, T. and Adachi, H., "Resistance Reduction by Stern-End Bulb," (First Report), Journal of the Society of Naval Architects of Japan, Volume 148, December 1980.

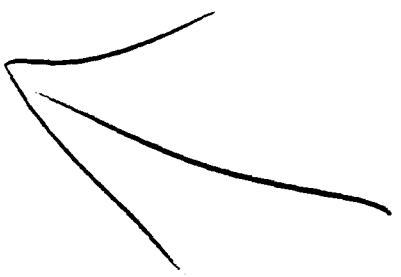
DISCUSSIONS

Grant R. Hagen
Designers and Planners, Inc.

Are wave cut tests applicable to ship hulls in general? Specifically, in instances where a substantial part of the residuary resistance is associated with wave breaking, as for very full form hulls, is it applicable?

C.C. Hsiung
Memorial University of Newfoundland

I would like to comment on the position of proturberances or side-bulbs for the optimal hull forms. In my earlier theoretical study on optimal hull forms (Journal of Ship Research, Vol. 25, No. 2, June 1981), it was found that the side-bulbs usually appeared to be close to the free-surface or at the mid-draft rather than near to the keel as shown in your testing model. May I suggest that in your later experiments, you may adjust the vertical positions of the side-bulbs to check their effectiveness in wave resistance reduction.



AD-P003 804

TOTAL RESISTANCE CALCULATIONS OF APPENDED DESTROYER HULL FORMS

To be presented at
American Towing Tank Conference
at
Stevens Institute of Technology
on
2 August 1983

by
C.H. von Kerczek[1], F. Stern[2],
C.A. Scragg[3] and W. Sandberg[4]

1 Senior Research Scientist, SAI/Annapolis
2 Research Naval Architect, SAI/Annapolis
3 Research Naval Architect, SAI/Annapolis
4 Supervisory Naval Architect, NAVSEA-55W3/Washington, D.C.

SCIENCE APPLICATIONS, INC.

134 Holiday Court, Suite 318
Annapolis, Maryland 21401
(301) 266-0991

1.0 INTRODUCTION

This paper gives the results of using potential flow and boundary layer theories to predict the total drag of fully appended destroyer hull forms. None of the methods used for these predictions are exact. Furthermore, the prediction of the added drag due to the appendages requires a large amount of empirical data. However, by combining the empirical data with calculated flow characteristics, it is hoped that the drag predictions will be improved. This combination also may show more clearly the elements of the empirical drag formulas that are most in need of improvement.

Although neither wave resistance nor boundary layer calculation methods for ships are completely satisfactory, it is time to apply such theories to as many ship hull forms as possible. This will be beneficial both in aiding the design process and the improvement of the calculation methods. Many of the calculation methods do produce useful results for certain classes of ships. The hydrodynamic characteristics of destroyer hull forms seem to be amenable to predictive calculation by virtue of the slenderness of these hulls.

The wave resistance and boundary layer theories used in this study are of the simpler variety. The status of both these theories for ship hulls is reviewed in Bai and McCarthy (1979) and Larsson (1980), respectively. It is shown in these references that simplified wave-resistance and boundary-layer theories are for certain applications as useful as the most sophisticated of these theories. The simpler methods used for this study result in highly efficient and inexpensive computer programs. This is still a major consideration for design studies of hull forms.

Computations of the total resistance of typical appended destroyer hulls have been made in order to assess the capabilities of the theoretically-based drag prediction method.

2.0 COMPUTATIONAL METHOD

The computational method for total drag of appended ship hulls combines potential flow and viscous flow theory with empirical appendage drag coefficient data as shown in Figure 1. This figure is sufficiently detailed to give an overall view of the computational procedure. In this figure

$$C_T(R_n, F_n) = C_{V_S}(R_n) + C_{V_F}(R_n) + C_A(R_n) + C_W(F_n)$$

where

$C_{V_S}(R_n)$ = skin friction (viscous tangential)

$C_{V_F}(R_n)$ = form drag (viscous normal)

$C_A(R_n)$ = appendage drag

$C_W(F_n)$ = wave resistance

R_n = Reynolds number

F_n = Froude number

Complete details of the theories and computational procedures embodied in the method outlined in Figure 1 will be given in a future publication.

The approach to appendage drag is that of Hoerner (1965), in which the appendages are decomposed into elemental shapes (flat plates, cylinders and foils) for which experimental drag coefficients, C_D = Drag/$\frac{1}{2}\rho U^2 A$, are known. Computer programs have been developed by Lasky (1972) which implement Hoerner's method for Naval-type ships and subsequently with improvements by Kirkman, et al. (1979 and 1980). A typical set of Naval ship stern appendages

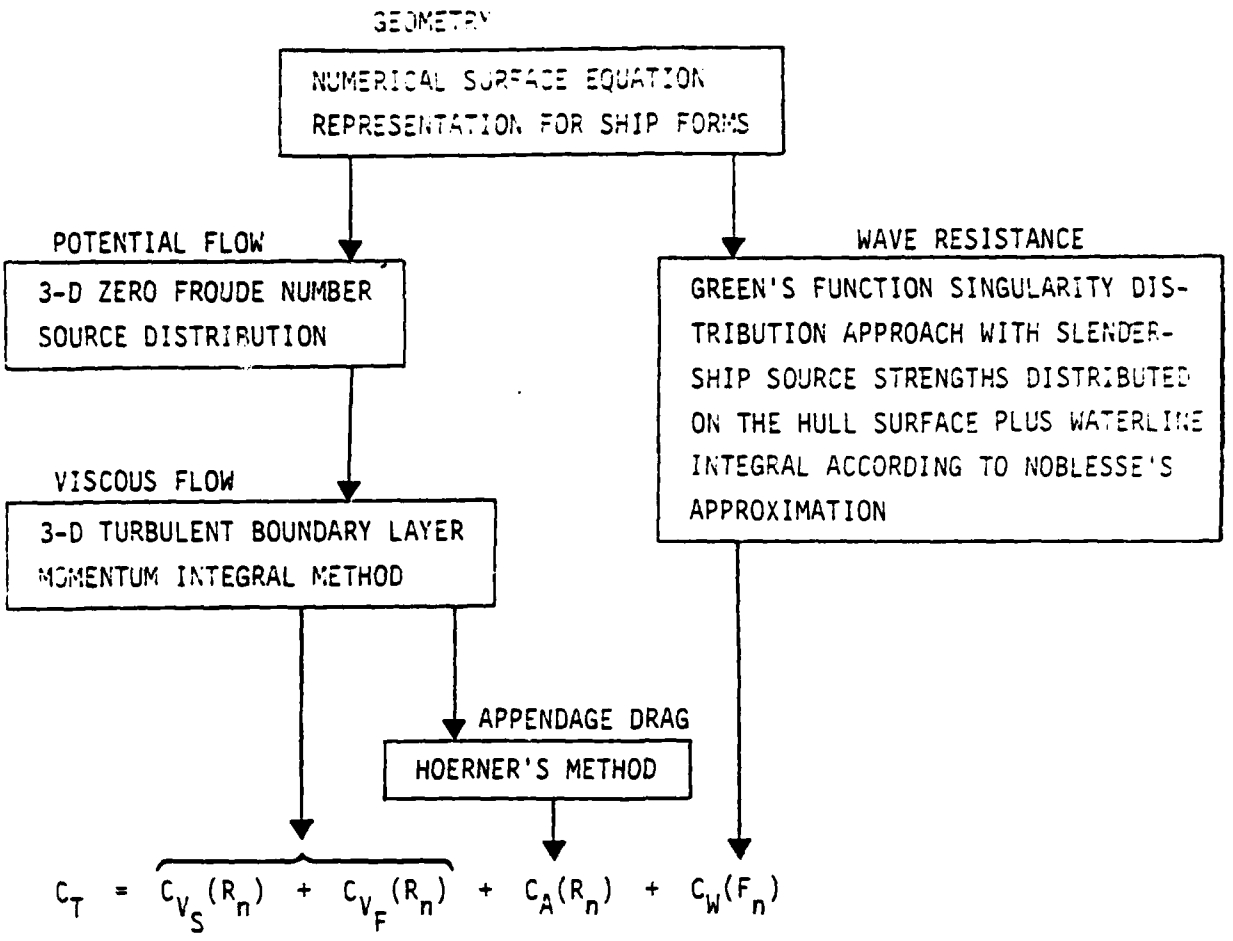


Figure 1. Computational Methods.

(for one propeller shaft) is shown in Figure 2. These appendages can be decomposed into foils with and without interference* and cylinders with and without interference and end drag. Hoerner provides drag coefficient data for such shapes. However, the range of applicability of some of this data for the present circumstances is unknown. A good estimate of the local velocity, U, is doubly important since it determines both the value of R_n and thus the values of $C_D(R_n)$ and the dynamic head, $\frac{1}{2}\rho U^2$. The latter may in fact be the more important since the scale of the drag force is basically set by U^2. Both Lasky and Kirkman use the speed advance, $V_A = \omega(1 - U_S)$, for the fluid velocity on all

* Interference refers to the losses associated with the juncture of an appendage and the hull surface.

appendages where U_S is the ship speed and ω is the average nominal wake fraction in the propeller plane. This is, in fact, a poor estimate of the fluid velocity for most parts of the appendages, particularly for those parts embedded in the ship boundary layer.

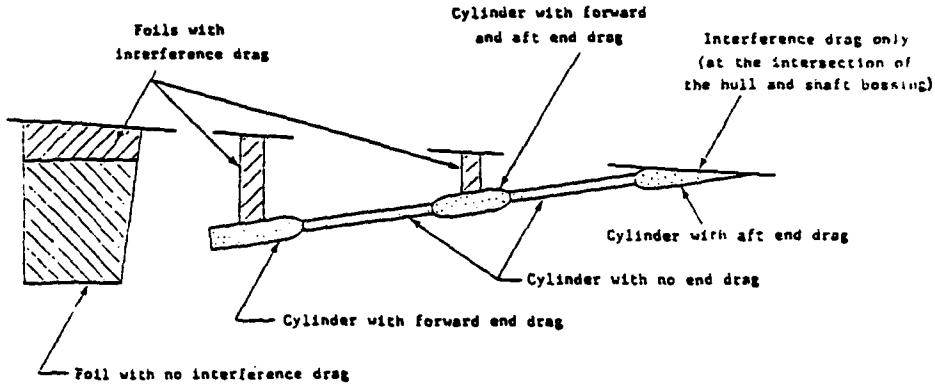


Figure 2. Appendage Decomposition (from Kirkman, et al., 1979)

In the present study the fluid velocity in way of each appendage is determined using the results from the bare hull ship boundary layer calculation. Figure 3 shows a profile view of an appended destroyer hull form with the nominal boundary layer thickness superimposed. It is evident from Figure 3 that substantial portions of the appendages, particularly those parts affected by hull interference, are within the ship boundary layer.

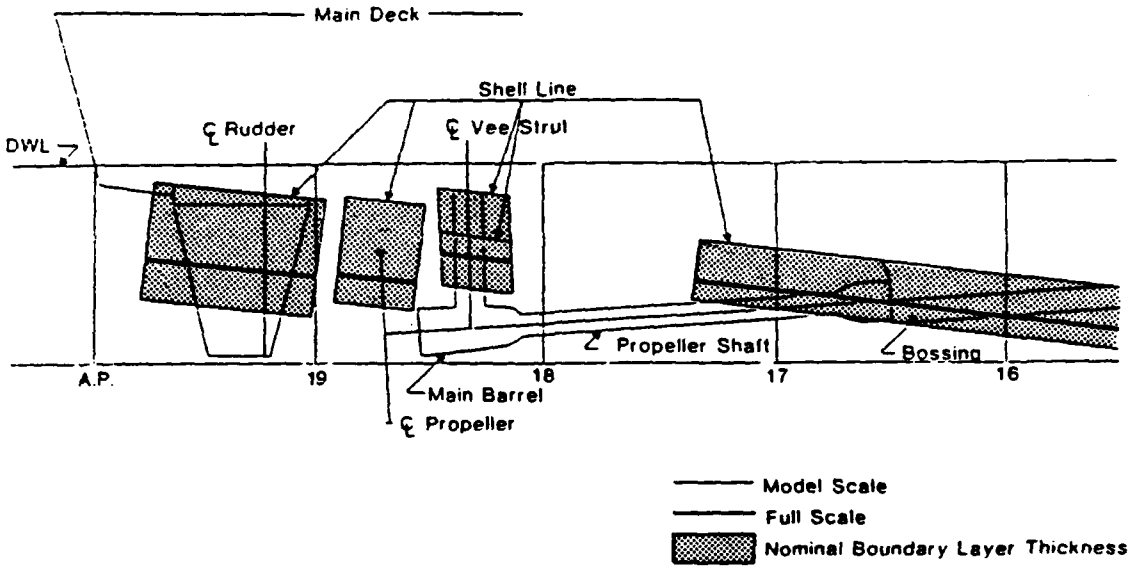


Figure 3. Nominal Boundary Layer Thickness in Way of a Typical Destroyer's Appendages.

3.0 EXAMPLE CALCULATION AND COMPARISON WITH EXPERIMENTAL DATA

3.1 Bare Hull Resistance

Calculations were performed for two typical destroyer hull forms, Hull1 and Hull2. One of the results of the boundary layer calculation is the viscous drag of the hull. Figure 4 shows the skin friction resistance and the total viscous resistance (skin friction plus form drag) for the two hulls. This resistance is compared with the flat plate resistance derived from the 1957 ITTC line. The Reynolds number range calculated corresponds to full scale speed.

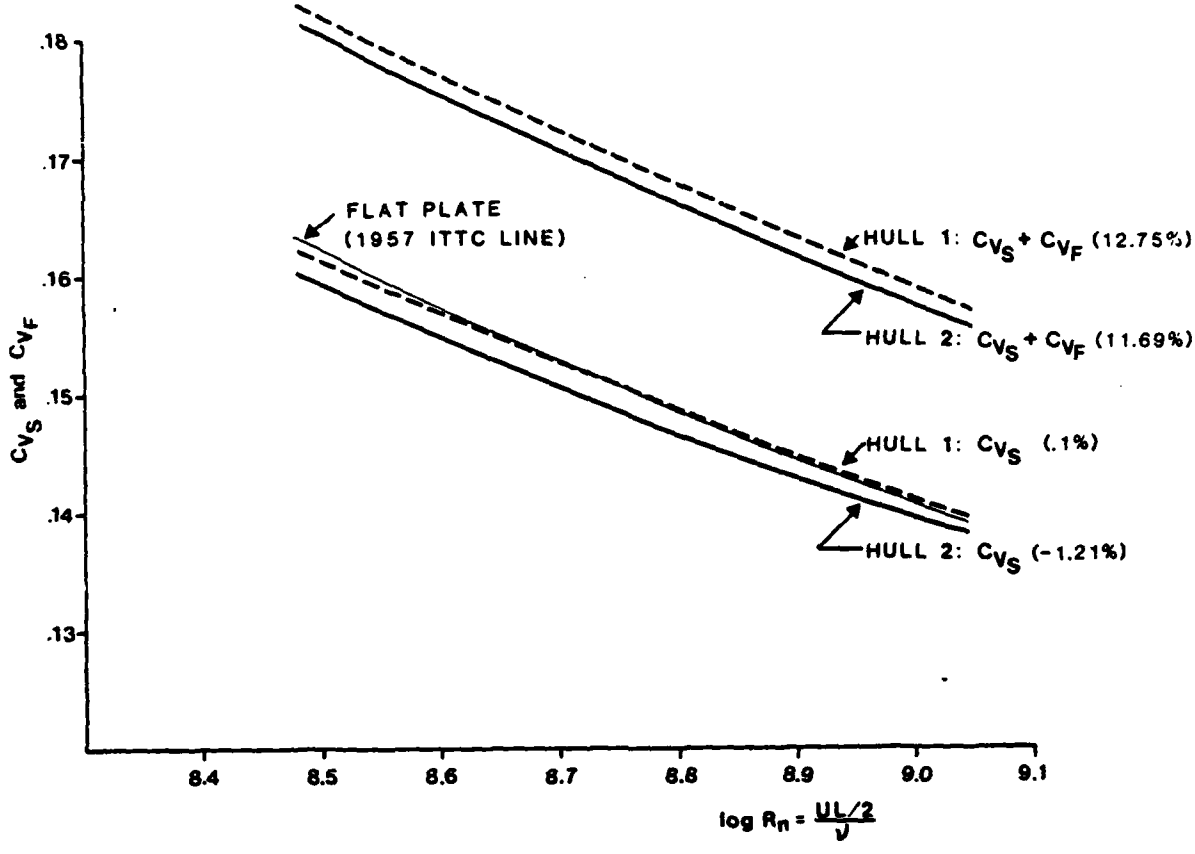


Figure 4. Viscous Resistance Calculation Results for Hull1 and Hull2.

Figure 4 shows that Hull1 has about a 1% higher friction drag. This difference is too small to be considered significant. The difference is probably within the accuracy of the calculations. It is interesting to note that the skin friction resistance for these hulls is not substantially different than the flat plate (zero pressure gradient) resistance. This is due to the cancelling effects of a favorable pressure gradient on the bow sections and an unfavorable pressure gradient on the stern sections of these hulls.

The wave resistance, including the sinkage and trim correction, for both hull forms is shown in Figure 5. Hull2 is seen to have a larger wave resistance than Hull1 at all values of F_n other than between .25 and .325. For values of F_n of about .3, the Hull2 wave resistance is only 59% of the Hull1 value. Both the waterline integral (~ 25% C_W) and the additional resistance due to sinkage and trim (~ 12.5% C_W) were found to have a significant effect on the predicted wave resistance.

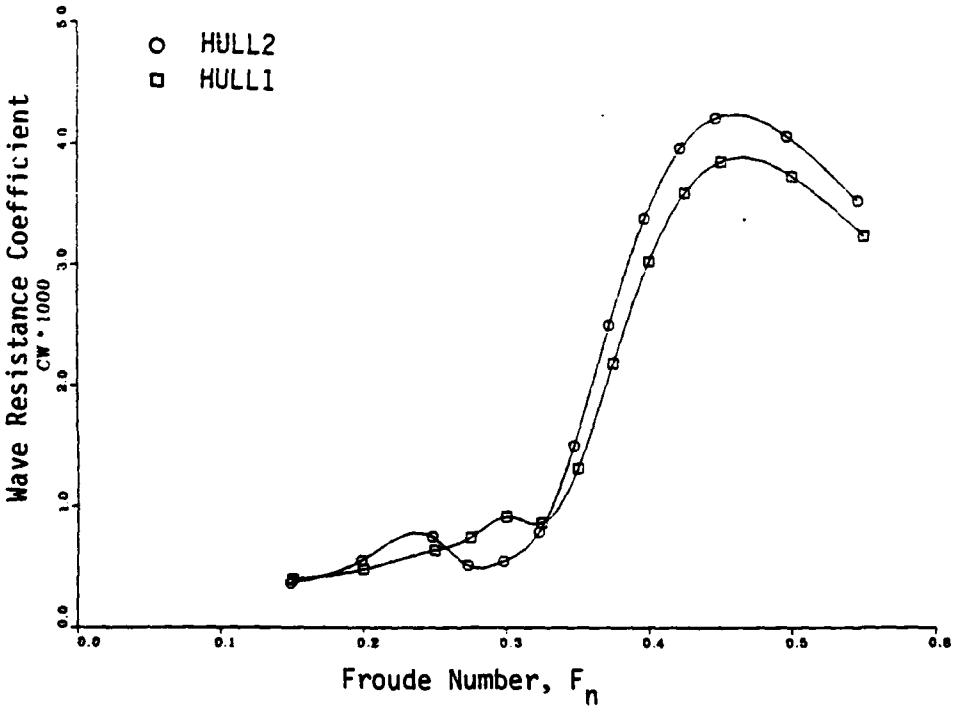


Figure 5. Wave Resistance Coefficient Including Sinkage and Trim Correction. $C_W = R_W/\frac{1}{2}\rho V^2 S$

The total bare hull resistance coefficient, $C_T = C_{V_S} + C_{V_F} + C_W$, is shown in Figure 6. At low speeds, $F_n < .3$, the viscous resistance is much larger than the wave resistance and at high speeds, $F_n > .4$, the opposite is true. Experimental results for these hulls are also shown in Figure 6 for comparison. The calculations are in fair agreement with the experimental results. In particular, the experiments also show a reduction in resistance

for Hull2 relative to Hull1 at moderate F_n ($.25 < F_n < .35$) and an increase at the higher F_n ($> .35$). The experimental value of C_T for Hull2 is lower than Hull1 by a maximum of 14.5% at $F_n = .32$. Similarly, the calculations show a maximum of 17.2% at $F_n = .3$. Figure 6 shows that the magnitude of C_T is also predicted fairly well by the calculations.

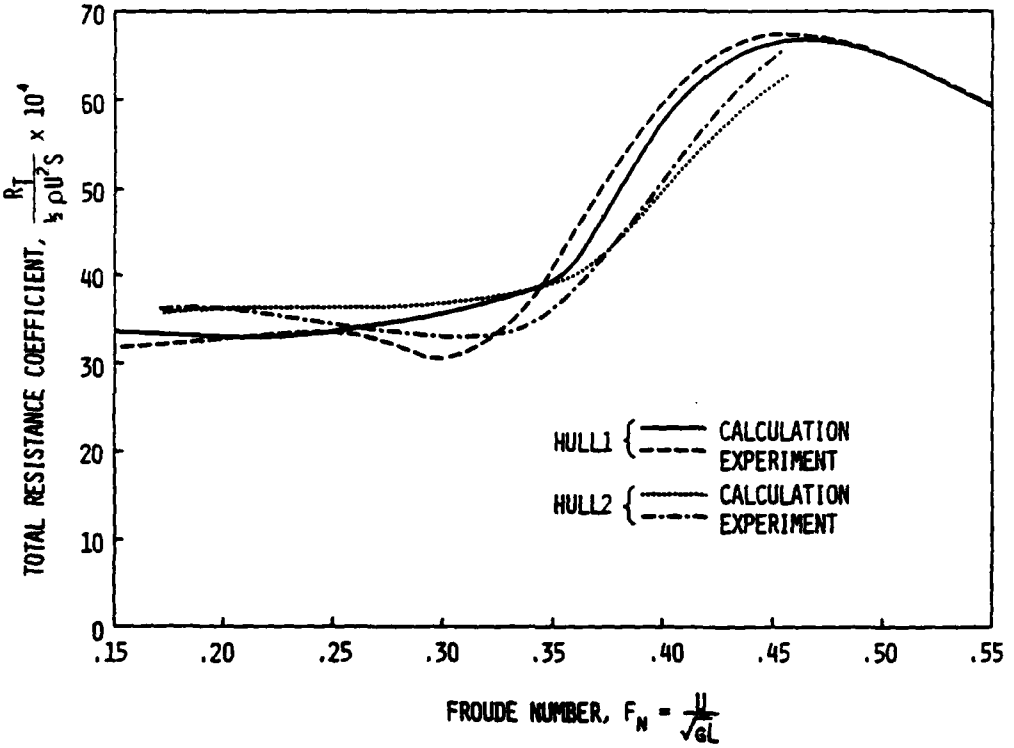


Figure 6. Total Resistance Calculation Results for Hull1 and Hull2.

Appended Hull Resistance

Calculations were also performed of the additional resistance due to certain appendages -- rudders, bilge keels, propeller shafts and support struts -- for a destroyer hull form similar to those used for the bare hull resistance calculations. Computational results were obtained for two values of F_n (.276 and .414) and both for model and full-scale R_n values. Tables 1 and 2 summarize the results and include model-scale experimental data for comparison. Also included are calculations made using the Kirkman procedure

for determining the velocities and flow angles.

	Calculations							
	Model Scale						Full Scale	
	$C_A \times 10^4$ (Experiment)	$C_A \times 10^4$ (with b.l. velocity)	Difference from experimental values (%)	$C_A \times 10^4$ (without b.l. velocity)	Difference from experimental values (%)	% Reduction each appendage due to b.l. velocity	$C_A \times 10^4$ (with b.l. velocity)	$C_A \times 10^4$ (without b.l. velocity)
Rudder	1.3303	1.223	- 8.1	2.542	91.1	51.9	.842	2.053
Bilge Keel	2.4824	1.414	-43.	1.529	-38.4	7.5	.811	.875
Shaft & Strut	3.6158	3.765	4.1	5.752	59.1	34.6	3.973	5.971
Total	7.4285	6.383	-14.1	9.803	32.0	34.9	5.626	8.626

Table 1. Appendage Resistance Result Summary: $F_n = .414$.

	Calculations							
	Model Scale						Full Scale	
	$C_A \times 10^4$ (Experiment)	$C_A \times 10^4$ (with b.l. velocity)	Difference from experimental values (%)	$C_A \times 10^4$ (without b.l. velocity)	Difference from experimental values (%)	% Reduction each appendage due to b.l. velocity	$C_A \times 10^4$ (with b.l. velocity)	$C_A \times 10^4$ (without b.l. velocity)
Rudder	1.126	1.557	38.3	2.984	165.0	47.8	.873	2.107
Bilge Keel	2.706	1.427	-47.3	1.557	-42.5	8.3	.853	.919
Shaft & Strut	4.177	4.196	.5	6.272	50.2	33.1	3.996	6.003
Total	8.009	7.18	-10.4	10.813	35.0	33.6	5.722	9.029

Table 2. Appendage Resistance Result Summary: $F_n = .276$.

From Tables 1 and 2 it is seen that for both values of F_n the results show about a 35% reduction in the total appendage drag prediction by including the boundary layer velocities. Furthermore, the present results are in better agreement with the experimental data: the total appendage drag is underpredicted by about 10% primarily due to the bilge keel component. Kirkman, et al. (1979) shows on the average a 30-40% overestimate as compared to experimental data for 11 test cases. Based on the present results, a much more favorable agreement with experimental data is expected by including the boundary layer velocities.

4.0 CONCLUDING REMARKS

The purpose of this investigation was to develop a fairly complete computational tool to predict the total drag of fully appended destroyer hulls. This has been accomplished in a useful way. However, much remains to be done to validate and improve this computational tool. A basic framework is clearly visible, but the most important aspects need improvement.

The theoretical methods that were incorporated in the drag calculation method are of a simplified variety, but they do give fair results here and are amenable to broader application and improvements.

The items of immediate improvement of the method are the following:

(1) Boundary Layer Method: development of viscous/inviscid interaction method to improve the stern region boundary layer prediction.

(2) Wave Resistance Method: add the additional source strengths due to viscous/inviscid interaction to wave resistance calculations to improve prediction.

(3) Appendage Drag: develop new base and interference drag formulas, using new experimental data, so that incoming boundary layer velocities can be properly used for improved drag predictions.

REFERENCES

Bai, K.J., and J.H. McCarthy (editors), Proceedings of the Workshop on Ship Wave-Resistance Computations, 13-14 November, DTNSRDC, Bethesda, Maryland, 1979.

Hoerner, S.F., Fluid-Dynamic Drag, published by author, 1965.

Kirkman, K.L., D.G. Sanders, and J.J. Slager, "Methodology for Computation of Appendage Resistance (An Interim Report)," NAVSEA Report #3213-79-40, 1979.

Kirkman, K.L., and J.W. Kloetzli, "Scaling Problems of Model Appendages," 19th American Towing Tank Conference, Ann Arbor, 1980.

Larsson, L. (editor), SSPA-ITTC Workshop on Ship Boundary Layers 1980, The Swedish Maritime Research Center (SSPA), Göteborg, Sweden, 1981.

Lasky, M.P., An Investigation of Appendage Drag," DTNSRDC Report, SPD-458-01, 1972.



AD-P003 805

DAVID W. TAYLOR NAVAL SHIP RESEARCH AND DEVELOPMENT CENTER

Bethesda, Maryland 20084

COMPARISONS OF LARGE AND SMALL MODELS FOR THE PREDICTION OF RESISTANCE

by

Steven C. Fisher

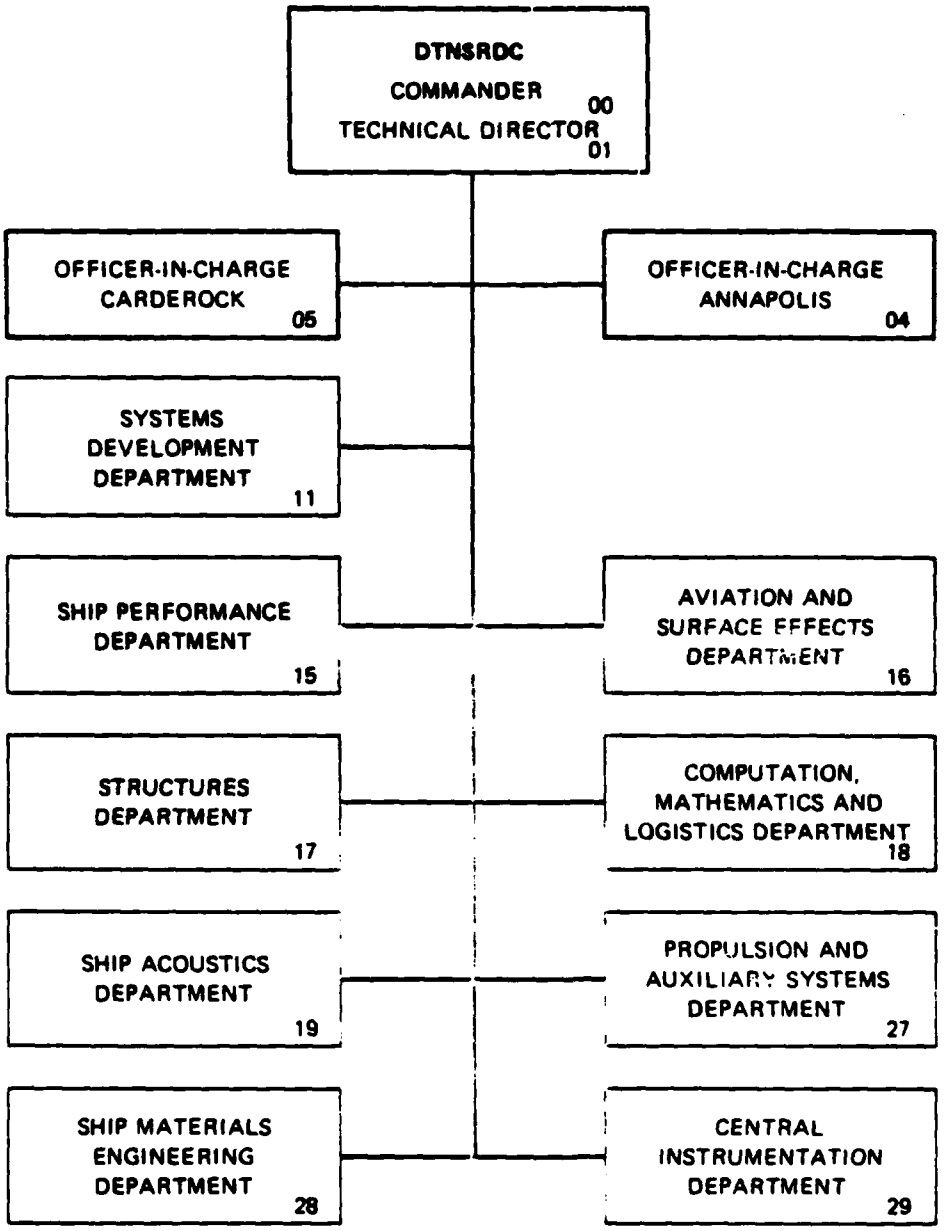
PRESENTED AT THE TWENTIETH AMERICAN TOWING TANK CONFERENCE

AUGUST 2, 1983

COMPARISONS OF LARGE AND SMALL MODELS FOR THE PREDICTION OF RESISTANCE

NDW-DTNSRDC 5602/30 (2-80)
(supersedes 3960/46)

MAJOR DTNSRDC ORGANIZATIONAL COMPONENTS



NOMENCLATURE

		Units*
C_A	Correlation allowance	-
C_B	Block coefficient	-
C_F	Frictional resistance coefficient, $R_F/(\frac{1}{2}\rho SV^2)$	-
C_M	Midships coefficient	-
C_P	Prismatic coefficient	-
C_R	Residuary resistance coefficient, $R_R/(\frac{1}{2}\rho SV^2)$	-
C_{SD}	Stud drag coefficient, $R_{SD}/(\frac{1}{2}\rho SV^2)$	-
C_T	Total resistance coefficient, $R_T/(\frac{1}{2}\rho SV^2)$	-
ΔC_{TM}	Difference in the total resistance coefficient between models with and without studs	-
C_W	Waterplane coefficient	-
C_V	Volumetric coefficient, Volume/L^3	-
F	Longitudinal Center of Floatation	-
$\overline{FB}$	Longitudinal Center of Bouyancy from forward perpendicular	L
F_n	Froude number	-
i_E	Entrance half-angle	-
L	Length	L
R_F	Frictional resistance	ML/T^2
R_R	Residuary resistance	ML/T^2
R_{SD}	Stud drag	ML/T^2
R_T	Total resistance	ML/T^2
S	Wetted surface	L^2
V	Speed	L/T
ρ	Water density	M/L^3

*L = length, T = time, M = mass

ABBREVIATIONS

DL/SIT	Davidson Laboratory of the Stevens Institute of Technology
DTNSRDC	David Taylor Naval Ship Research and Development Center
USNA	United States Naval Academy

SUBSCRIPTS

M	Model
S	Ship

ENGLISH/SI EQUIVALENTS

1 degree (angle)	= 0.01745 rad (radians)
1 foot	= 0.3048 m (meters)
1 foot per second	= 0.3048 m/sec (meters per second)
1 inch	= 25.40 mm (millimeters)
1 knot	= 0.5144 m/s (meters per second)
1 lb (force)	= 4.448 N (Newtons)
1 lb (force) - inch	= 0.1130 N m (Newton-meter)
1 long ton (2240 lbs)	= 1.016 metric tons, or 1016 kilograms
1 horsepower	= 0.746 kW (kilowatts)

ABSTRACT

An investigation was carried out at the David Taylor Naval Ship R&D Center (DTNSRDC) to compare the trends in resistance for similar hull forms between large and small size models. Resistance experiments were conducted with three similar twin screw hull forms having a moderately fine shape (C_B = 0.59). The results of these experiments are presented. The resistance trends obtained with the large and small models show good correlation. However, the full scale resistance predictions with the small and large size models did not compare as well.

INTRODUCTION

An experimental investigation was undertaken at DTNSRDC to determine if the trend in resistance change, due to small changes in hull shape, could be predicted correctly with the use of small size surface ship models.

The model hull size employed typically at DTNSRDC is determined from propulsion experiment requirements. In our experience, model propellers smaller than 0.2 m (8 in) in diameter are inadequate for the modeling of full scale flow conditions. The effect of Reynolds number on the model data becomes too severe, preventing accurate full scale prediction. Thus, the hull model is built to a scale ratio that results in a model propeller diameter of more than 0.2 m (8 in). The resulting model hull lengths vary from 5.5 m (18 ft) to over 9.1m (30 ft). These same hull models are also used for resistance experiments.

Having a large model for resistance experiments has the advantage of obtaining a more accurate geosym of the full scale hull than with the smaller model, with a given manufacturing tolerance, and the difficult

problem of properly stimulating turbulence[1] on the model is also mitigated. However, in terms of time and cost, the use of large models to explore the effect of many minor hull form changes on hull resistance is considered to be not practical. The use of small models in exploring the resistance trends with changes in hull form may provide a solution[2]

Since the early days of ship model testing the issue of model size has been explored extensively. Considerable work has been done comparing resistance experiments with the same model in different towing tanks as well as comparing results obtained with different size models. References 3 through 9 are a sample of the published literature. However, little work has been done to evaluate the effects of model size on the prediction of the trend of resistance due to small changes in hull geometry. Unpublished experiments that have been carried out in the past show that in some cases, trends in resistance are predicted correctly with small models, and in other cases small model resistance trends are not confirmed by the results of large model data. Existing data indicate however, that high block coefficient hulls (C_B >0.65) provide less consistant results, while finer hulls tend to show better correlation between small and large models. Therefore, small models might provide reasonably accurate predictions of resistance trends for relatively fine hull forms.

The purpose of the investigation reported here is to explore the technical merit of the use of small models in predicting the trend in bare hull resistance due to relatively small changes in design geometry; the interest here is not in the absolute values obtained nor in the use of the model data for full scale prediction. It should be noted that,

due to the small sample of data, the results reported here should not be considered conclusive; extensive new experimentation will be required before a general conclusion can be made.

A series of three similar hulls of relatively fine (C_B = 0.59) form were selected for this project. These hull forms have very similar basic hull form parameters and coefficients, yet have significantly different hull form shapes. Two groups of geosyms were built of these hull forms; one group 8.34 m (27.36 ft) long, and one group 1.82 m (5.97 ft) long.

One of the small models was built and its resistance experimentally obtained at the Davidson Laboratory of the Stevens Institute of Technology (DL/SIT). This allowed us to compare the repeatability of our results with one small model to the results of the same model from a model basin with an extensive background in small model experimentation. Additional repeatability experiments were carried out with the small models at DTNSRDC to evaluate the accuracy of the resistance measurements with a 95 percent level of confidence.

The comparison of the small and large model relative resistance prediction and the results from the repeatability experiments with the small models are presented in this report. A comparison of the large and small model predicted resistance values is also included.

EXPERIMENTS

MODELS

Body plans, representing the hull forms used in this investigation, are presented in Figures 1 to 3, and the principal dimensions and hull

form coefficients are presented in Table 1. These hull forms represent modern twin screw ship designs having block coefficients between 0.580 and 0.593, with a length to beam ratio of 6.83. The full scale length of the ships is 262.1 m (860 feet).

The small models, 5385, 5386, and 5387, represent the three design variants A, B, and D respectively. The three models are constructed of wood to a scale ratio of 144, resulting in a model length of 1.83 m (5.97 ft). Models 5385 and 5387 were built at DTNSRDC; Model 5386 was built at DL/SIT. The models have no appendages except for skegs.

The large models, 5368, 5372, and 5382, also represent the three design variants A, B and D, respectively. The three models are constructed of wood to a scale ratio of 31.435, resulting in a model length of 8.34 m (27.36 ft). These models also have no appendages except for skegs.

The A models were ballasted to represent a full scale displacement of 63430 t (62430 L. tons), and an even keel draft of 10.36 m (34.0 ft); the B models were ballasted to represent a full scale displacement of 63430 t (62430 L. tons) and an even keel draft of 10.36 m (34.0 ft); and the D models were ballasted to represent a full scale displacement of 62970 t (61980 L. tons) and an even keel draft of 10.55 m (34.5 ft).

The small models were towed using the planing boat towing bracket on loan from the United States Academy (USNA) model basin. The bracket attaches to the model at one point, and fixes the model in sway, yaw, and roll.

DESCRIPTION OF HULL FORM GEOMETRY

Table 1 shows the principal dimensions and nondimensional coefficients of the three hull forms. A comparison of the basic parameters and nondimensional coefficients shows that there is little difference in these values between the hull forms. There was no change in the length to beam ratio, L/B and a small change in the volumetric coefficient, C_{∇}, of 0.7 percent. The maximum change in the block coefficient was 2.2 percent. The maximum change in the longitudinal center of bouyancy, $\overline{FB}/L$, was 0.9 percent L; the beam to draft ratio, B/T, 1.6 percent; and the longitudinal center of floatation, F, 1.9 percent L. The maximum changes in the prismatic coefficient, C_P, vertical prismatic coefficient, C_{PV}, waterplane coefficient, C_W, midship coefficient, C_M, and wetted surface were between 3.0 and 3.6 percent. The maximum difference in the half angle of entrance, i_E, was 2 degrees.

A comparison of the body plans of hull forms A, B, and D, indicated in Figure 4, shows that there are significant differences in the hull form shapes. Hull form A is U shaped forward and aft, with a transom stern having a waterline width of approximately 40 percent of the maximum beam. The skeg is faired into the hull with a large fillet. Hull form B has a V shaped forebody and afterbody, with virtually no transom immersion. The skeg is faired into the hull to a degree that it might not be considered a separate appendage. Hull form D is U shaped forward, and is very similar to hull form A from station 5 to amidships. Forward of station 5, the sections have the same shape as hull form A but are narrower in beam as a result of the narrower entrance angle. In the afterbody, the shape of hull form D is between that of B and A, but has

no immersed transom, and the skeg is faired into the hull with a much smaller fillet than used with hull form A.

TURBULENCE STIMULATION

Turbulence stimulation was required on the small models to obtain turbulent flow over the hull. Studs were selected for turbulence stimulation because they appeared to provide more consistent resistance data for small models than tripwires and sand strips could.[10] Also, the DL/SIT resistance experiments with the small Model B were performed using studs for turbulence stimulation. Choices of stud size, spacing, and longitudinal location used with the small models were based on the method used by DL/SIT with Model B in order to investigate repeatability.

The studs, 3.2 mm (0.125 in.) dia by 2.5 mm (0.10 in.) high, were spaced 6.4 mm (0.25 in.) apart, and 15 mm (0.6 in.) aft of, and parallel to, the stem line. The longitudinal location was selected using a method by Hughes[11], which uses the entrance half angle to determine the stud longitudinal location.

The studs not only induce turbulence, but also add a drag component to the total measured resistance. This stud parasitic drag component must be subtracted from the measured resistance to obtain the resistance of the hull alone. The method of stud parasitic drag correction used assumes that, at higher speeds, the model without studs has turbulent flow over the entire hull (except in the immediate area of the stem) so that turbulence stimulation is unnecessary. Therefore, the difference in resistance between the model with and without studs at the high speeds is taken as the stud parasitic drag.

No turbulence stimulation was used with the large models because it is not considered necessary with large models of this type hull form. Also, none was used in previous experiments with these large models.

EXPERIMENTAL PROCEDURE

The large models were evaluated in the West Deep Water Basin of DTNSRDC, and the small models were evaluated in the 140 Foot Basin of DTNSRDC. The large and small models were evaluated over a speed range corresponding to 5.1 m/s to 15.4 m/s (10 knots to 30 knots) full scale, or F_n = 0.10 to 0.30. The resistance values were measured using a block gauge, a type of variable reluctance force transducer. A 334 N (75 lb) block gauge was used for the large model experiments, and a 22.2 N (5 lb) block gauge was used for the small model experiments. The large model resistance data was sampled over a period of 5 seconds. The small model resistance data was sampled over a period ranging from 7 to 24 seconds; the longer sampling periods correspond to lower model speeds. Speed on both towing carriages was measured using a toothed wheel with a magnetic pickup.

During the small model tests special attention was paid during the acceleration phase to keep the acceleration of the model constant in order to improve data consistency. No special attempt was made in this respect, during the large model tests.

The repeatability experiments to determine the accuracy of the small model resistance measurements, described in later sections, were performed using three speeds (F_n = 0.18, 0.24, and 0.28), in a random sequence. The models were fitted with studs during these experiments.

The speeds were repeated ten times with the small Model B and six times with the small A and B models. The experiment was repeated two weeks later with Model B repeating the speeds six times.

PRESENTATION OF RESULTS

The measured resistance values for the large and small models are shown Tables 2 to 12. The resistance values for the small Model B form the experiments at DL/SIT are also included. The C_R values, shown in Figures 5 to 11, are calculated from the total resistance, R_{TM}, using the ITTC model-ship correlation line.

To assist in resolving the scatter in the low speed C_R values, a technique is used which is based on a method of data presentation by Prohaska[12]. The data for large and small model B, replotted as C_{TM}/C_{FM} versus F_n^4/C_{FM}, are shown in Figures 12 to 14. Prohaska states that over the range of $F_n = 0.1$ to $F_n = 0.2$, a curve fitted to these points is a relatively straight line for most models. Because of the way the low speed data are compressed, it is much simpler to fair the Prohaska plots than to fair the C_R plots; therefore, the results from faired Prohaska curves are used to assist in fairing the C_R curves. The C_{FM} values are from the ITTC model-ship correlation line.

Curves of total resistance coefficient (C_{TM}) versus Froude number for the small models are shown in Figures 15 to 18. The curves of the difference between the C_{TM} curves of the small models with and without studs, ΔC_{TM}, are also presented in these graphs.

The stud drag coefficient, C_{SD} is considered to be constant with speed, and is calculated by averaging the ΔC_{TM} curves at the high

Froude number range, where the difference in resistance between the models fitted with and without studs is considered to be only due to the drag of the studs. DL/SIT averaged the ΔC_{TM} curve above $F_n = 0.2$ for the small Model B; however, since the ΔC_{TM} values were not found to be constant until somewhat higher Froude numbers were reached, in the present work the ΔC_{TM} curves were averaged above Froude number $F_n = 0.28$.

Figure 19 shows the ratio of R_{TM} (DL/SIT) to R_{TM} (140 Foot Basin) versus Froude number for the small Model B model fitted with studs.

The results of the repeatability experiments with the small models are shown in Table 13. The results are analyzed and presented in terms of the level of confidence[13]. The level of confidence implies that there is a percent probability that the actual resistance value lies within $\pm y$ percent of the average resistance values. The level of confidence used in this repeatability analysis is 95 percent. The maximum excursion from the mean resistance values, as a percent of the mean resistance values, is also given.

A comparison of the large and small model residuary resistance coefficient values, C_R is shown in Figure 20. The comparison is shown in terms of the difference between the large and small model C_R values (C_R (large model) - C_R (small model)) versus Froude number. The C_{FM} values used to determine the C_R values were calculated using the ITTC model-ship correlation line.

To show the relative resistance performance of the models, the full scale predicted resistance curves were normalized by the average of the full scale predicted resistance of the models. The average resistance, $R_{TS}(AVE)$, is defined as:

$$R_{TS}(AVE) = ((R_{TS}(Model\ A) + R_{TS}(Model\ B) + R_{TS}(Model\ D))/3.$$

The large model full scale resistance curves are normalized by the average full scale resistance for the large models, and the small model full scale resistance curves are normalized by the average full scale resistance for the small models. These curves of R_{TS}/R_{TS} (AVE) are shown in Figures 21 and 22 for a correlation allowance of $C_A = 0.0035$ for the large and small models, with the C_{FM} values calculated using the ITTC line.

The predicted relative resistance performances of A, B and D are shown in Figures 23 to 25, respectively. The large model and the small model predictions are plotted together.

Figures 26 to 28 show comparisons of the small model full scale predictions with the large model full scale predictions, presented as R_{TS} (small model)/R_{TS} (large model), versus Froude number. The model data are extrapolated using the Froude method of extrapolation.

DISCUSSION OF RESULTS

SMALL MODEL DATA

At the low Froude numbers, there is noticeable scatter in the small model resistance values, especially when the models are not fitted with studs (Figures 5 to 11). A significant part of this scatter may be attributed to laminar flow in the bow region. If the speeds are low enough, even the use of studs or other turbulence stimulators may not trip the flow from laminar to turbulent. Studs or other turbulence

stimulators do not eliminate laminar flow; however, the use of turbulence stimulators decreases the speed at which laminar flow becomes turbulent[9]. If the flow is not tripped to turbulent flow, the point of natural transition from laminar to turbulent flow may move either upstream or downstream, and may change with time. The location of turbulence inception may also be affected by carriage acceleration. Due to the small size of the model, the area over which the transition point varies can represent a significant percentage of the hull wetted surface. Because the frictional resistance with laminar flow is significantly lower than that for turbulent flow, a change in the location of the flow transition may result in a noticeable change in the total resistance. Since the residuary resistance is calculated by subtracting the frictional resistance for fully turbulent flow from the total resistance, the changes in the total resistance significantly affect the computed residuary resistance. Because the residuary resistance is small relative to the total resistance at these low speeds, the percent change in the residuary resistance can be as great as an order of magnitude larger than the percent change in the total resistance.

The negative C_R values for the unstimulated models are a result of using the ITTC model-ship correlation line for calculating C_F, which assumes that the flow over the entire hull is turbulent; however, because of possible laminar flow existing over part of the hull, the actual frictional resistance must have been lower than that computed using the ITTC model-ship correlation line. Thus, the negative values of C_R appearing in Figure 5 through 11 have no physical significance. It should

be noted that, because the resistance data for the models without studs are used only to determine the stud drag correction, which uses only the resistance data at higher speeds, the C_R scatter and negative C_R values at the lower speeds for the models without studs do not affect the model resistance results used to determine relative resistance. The C_R scatter and negative C_R values for the models with studs may also be due to the studs not inducing fully turbulent flow at very low speeds.

Another reason for the low speed scatter may be that the measured resistance values are small. The block gauge and the instrumentation used may not be able to resolve the resistance with sufficient accuracy at the low speeds. Normally, a block gauge used to measure resistance will have a rating that is between 50 and 100 percent of the maximum measured resistance to ensure that the block gauge will have sufficient sensitivity for accurate low speed measurements. The maximum measured resistance of the small models is 11 percent of the block gauge rating. This means that the sensitivity of the block gauge was less than the norm in resistance experiments. Carriage vibration, speed variation, and acceleration may also have an impact on the meaurements at the lower speeds. These factors may have some impact on the total resistance measurements; as mentioned previously, a small percentage change in the total resistance value may result in a percentage change in the residuary resistance which may be as much as an order of magnitude greater than the total resistance percentage change.

REPEATABILITY

The results of the repeatability experiments for the small models (Table 13) show that over a speed range of F_n = 0.18 to 0.28 the percent range of the mean value with a 95 percent confidence level increased with speed for Model B (initial experiment) from $\pm$0.78 percent at F_n = 0.18 to -1.07 percent at F_n = 0.28, and for Model D from $\pm$0.73 percent at F_n = 0.18 to $\pm$1.20 percent at F_n = 0.28, and decreased with speed for Model B (final experiment) from $\pm$1.35 percent at F_n = 0.18 to $\pm$0.46 percent at F_n = 0.28. The range for Model A decreased from $\pm$0.96 percent at F_n = 0.18 to $\pm$0.79 percent at F_n = 0.24, and then increased to $\pm$1.07 percent at F_n = 0.28.

If the percent range from all four experiments is averaged, as shown in Table 13, there is almost no change in the range with speed ($0.18<F_n<0.28$). If the percent maximum excursions from the mean resistance value are also averaged in this manner, again there is virtually no change in maximum excursion with speed ($0.18<F_n<0.28$). Thus, the repeatability of the small model resistance measurements does not change significantly with speed. This indicates that the flow over the hull is stable and mostly turbulent at and above F_n = 0.18. There were no repeatability experiments performed at speeds below F_n = 0.18; however, the scatter in the C_R curves below F_n = 0.18 indicates that the repeatability decreases significantly. The rapid increase in the scatter of the C_R values of the models with studs below F_n = 0.18 is probably due to flow instability around the model in the region of laminar to turbulent flow transition. The studs may not introduce enough

energy into the flow to establish the flow transition from laminar (at the bow) to turbulent flow at a fixed location. Laminar flow reattachment may also occur. The scatter would have increased at a lower rate with decreasing speed if it was due solely to carriage vibration or block gauge accuracy.

Repeatability experiments were not carried out with the large A, B, and D models. However, a series of repeatability experiments were recently performed on a 6.5 m (large) destroyer model at DTNSRDC. The results of these experiments are used here to illustrate the repeatability of large model data. For this one model four appendage configurations were evaluated; the speeds were repeated 16 times per configuration. The average accuracy of measurement with a 95 percent level of confidence was $\pm$0.68 percent at F_n = 0.26. The average accuracy of measurement with 95 percent confidence level for the small Model B repeating the speeds 16 times (combined initial and repeat experiments) was $\pm$0.64 percent and $\pm$0.63 percent at F_n = 0.24 and 0.28, respectively (the results of the repeatability experiments with models A and D are not included here because of the much smaller sample size). This indicates that the repeatability of the small model resistance values above F_n = 0.18 is comparable to that of large models.

Since the small Model B was evaluated experimentally at both DTNSRDC and DL/SIT the resistance results can be compared directly to determine if the results can be repeated using different facilities and equipment. The faired curve of the DL/SIT resistance data, normalized by the faired R_{TM} data from DTNSRDC is shown in Figure 19. The maximum difference

between the DTNSRDC and the DL/SIT resistance values is 1 percent; therefore, the DL/SIT results have been repeated very well.

RESIDUARY RESISTANCE

As shown in Figure 20, the small model C_R values are less than the large model C_R values by an average of 0.15×10^{-3}. The differences between the large and small model C_R values can be interpreted two ways. One interpretation may be that the large and small model C_R values should be equal, and therefore the small model C_{FM} values should be decreased by an average of 0.15×10^{-3}. These "adjusted" small model C_{FM} values become smaller than the C_{FM} values derived from the ITTC model-ship correlation line, but are larger than the C_{FM} values predicted with the 1947 ATTC friction line.

A study of frictional resistance values of many geosym hull series was conducted by Hinterthan[3]. The residuary resistance coefficient values for the largest model in each geosym series, determined using frictional resistance coefficient values from the ATTC line, were assumed to be correct. By assumig that the large and small model C_R values must be equivalent, the "adjusted" small model C_{FM} values could be calculated. These C_{FM} values, at Reynolds numbers within the range used by small models A, B, and D, generally lie between the ATTC and ITTC lines from models using studs, tripwires or rods for turbulence stimulation. Therefore, the lower "adjusted" C_{FM} values of the small models, obtained in the present experiments, do not seem unreasonable.

The other interpretation of the large and small model C_R differences may be that the C_R values contain components which are Reynolds number

dependent. Therefore, the large and small model C_R values should not be equal. To minimize the differences between the large and small model full scale resistance predictions, the small model C_A value could then be increased by 0.15×10^{-3} over the large model C_A value. Either decreasing the small model C_{FM} values by 0.15×10^{-3} or increasing the small model C_A value by 0.15×10^{-3} results in identical full scale resistance predictions.

Neither interpretation of the differences in the large and small model C_R values is completely satisfactory. A more comprehensive method of resistance decomposition than the Froude method is needed[17,18] before a proper interpretation can be made.

As a matter of convenience, the "adjusted" C_{FM} values, rather than the "adjusted" small model C_A value will be used in the remainder of the paper.

The lower values of small model residuary resistance have also been observed during experiments with a sea control ship (SCS) hull form (published in a report of restricted distribution). This ship has a very fine (C_B<0.50) twin screw hull. The small model SCS (1.86 m long) was evaluated at DL/SIT, and the large model SCS (7.3 m long) was evaluated at DTNSRDC. The models were unappended except for skegs, and the turbulence stimulation method on the small SCS model was identical to that used on models A, B, and D. With the C_{FM} values calculated using the ITTC model-ship correlation line, the small model C_R values calculated using the ITTC model-ship correlation line, the small model C_R values were, on the average, 0.14×10^{-3} lower than the large model C_R values over a speed range of $F_n = 0.23$ to $F_n = 0.31$.

RELATIVE RESISTANCE

The curves of R_{TS}/R_{TS} (AVE) for the small and large models are shown in Figures 21 and 22, respectively. The curves of R_{TS}/R_{TS} (AVE) for the small models using the "adjusted" C_{FM} values by 0.15×10^{-3} changed the relative resistance performances very little; the maximum chagne was 1/2 percent. Since changing the small model C_{FM} values has a negligible effect on the small model relative resistance predictions and the "adjusted" small model C_{FM} values gave the best correlation between the large and small model full scale resistance predictions, the small model R_{TS}/R_{TS} (AVE) predictions are made using the "adjused" C_{FM} values.

The relative resistance values R_{TS}/R_{TS}(AVE, for the large and small A models, Figures 23 to 25, show excellent correlation: less than 1 1/2 percent difference between the relative resistance values above a Froude number of 0.16. The relative resistance values for the large and small B models differ by less than 1 pecent below the Froude number of 0.24 and above the Froude number of 0.28; between $F_n \doteq 0.24$ and 0.28 the difference increases to 3 percent. The relative resistance values for the large and small D models show less than 2 percent difference. Therefore, the relative resistance performances of the small models compares well to the relative resistance performances of the large models.

FULL SCALE EXTRAPOLATION

The small model resistance data are extrapolated to full scale and can be compared with the large model predictions in Figures 26 to 28.

The small model Froude method resistance predictions using the C_{FM} values from the ITTC line are lower than the large model predictions by as much as 9 percent. If the "adjusted" C_{FM} values determined from the large and small model C_R comparisons are used with the small model predictions, the differences between the large and small model predictions are within $\pm$4 percent. The small model resistance predictions are higher than the large model predictions at lower speeds, and lower at the high speeds.

It should be noted that the small model C_{FM} values were decreased (or the C_A value increased) based on the comparison of the large and small model C_R values. With a significantly different hull form, the necessary adjustment to the small model C_{FM} (or C_A) values could be quite different from the one used here. Also, even using "adjusted" C_{FM} values for the small models, the small model predictions differed from the large model predictions by $\pm$4 percent. This type of inaccuracy would not be acceptable for the contract design phase of a new ship design. Because of the small sample (only three small models were tested), no general conclusions should be drawn from this work with respect to the use of small models for absolute resistance prediction.

CONCLUSIONS

The relative resistance predictions with the small models compare well with those of the large models. These results show correlation between the resistance of small and large models for hull forms of block coefficient less than 0.60. For fuller hull forms, where the viscous resistance is a more important component of the total, there would be less confidence in the correlation. Further work is needed to

verify such a conclusion for other fundamentally different hull forms, hull forms of higher block coefficient, and for hull forms having bulbous bows.

The result of the large and small model residuary resistance comparison shows that the small model C_R values are an average of 0.15 x 10^{-3} lower than the large model C_R values. A similar difference in C_R values was also observed with a large and small SCS model. If the small and large model C_R values are assumed to be equal, the "adjusted" small model C_{FM} values lie between the ATTC and ITTC correlation lines. Alternatively, if the C_R values are assumed to be correct, the small models require a larger C_A value in order to minimize the difference between the small and large model full scale resistance predictions.

Even with the aid of large model data to determine the "adjusted" small model C_{FM} values, the small model predictions were only within ± 4 percent of the large model predictions. Thus, using the same (Froude) method for full scale prediction, the small model data provide different results than the large model data for the models reported here. Because of the small sample (three models) general conclusions should not be drawn.

The results of the repeatabilty experiments with these small models indicate that the repeatability of the small model resistance values is comparable to the repeatability of the large model resistance values at the higher speeds. No general conclusions can be drawn due to the small sample investigated.

REFERENCES

1. Todd, F.H., "The Fundamentals of Ship Model Testing", SNAME Transactions, Vol. 59, 1951.

2. Fireman, H., Hough, J., Hoyt, J., and Lones, A., "The Use of Small Models in the Ship Design Process", SNAME Chesapeake Section, October 1982.

3. Hinterthan, W.B., "Report on Geosym Analysis According to the Schoenherr Line", Eleventh ATTC meeting, Washington, D.C., 1957.

4. Gertler, M., and Hancock, C.H., "Comparative Resistance Tests with ATTC Standard Model", DTMB report 1357, July 1959.

5. Lap, A., Van Lammeren, W., and Van Manen, J., "Scale Effect Experiments on Victory Ships and Models", Quarterly Transactions of the Institution of Naval Architects, Volume 97, April 1955.

6. Numata, E., "Correlation Between Resistance of Large and Small Models", Davidson Labortory Note 537, June 1959.

7. Conn, J., Lackenby, H., and Walker, W., "BSRA Resistance Experiments on the LUCY ASHTON", Quarterly Transations of the Institution of Naval Architects, Volume 95, October 1953.

8. Harper, M.S., "Preliminary Report of the Liberty-Ship Series for the American Towing Tank Conference", DTMB Report 615, October 1947.

9. Conn, J., and Ferguson, A., "Results Obtained with a Series of Geometrically Similar Models", RINA Transactions, Volume 110, 1967.

10. Burns, J.A. and Murphy, P.J., "A Hot Film Anemometer Evaluation of Turbulence Stimulators, International Shipbuilding Progress, Vol. 12, 1965.

11. Hughes, G, and Allen, J.P., "Turbulence Stimulation of Ship Models, SNAME Transactions, Vol 59, 1951.

12. Prohaska, C.W., "A Simple Method for the Evaluation of the Form Factor and the Low Speed Wave Resistance", Eleventh International Towing Tank Conference, Tokyo, 1966.

13. Lipson, C., and Sheth, N.H., "Statistical Design and Analysis of Engineering Experiments", McGraw-Hull, 1973.

14. Granville, P.S. "A Modified Froude Method for Determining Full-Scale Resistance of Surface Ships from Towed Models" Journal of Ship Research, Vol. 18, December 1974.

15. Granville, P.S., "Partial Form Factors from Equivalent Bodies of Revolution For the Froude Method of Predicting Ship Resistance", First Ship Technology and Research (STAR) Symposium, SNAME, August 1975.

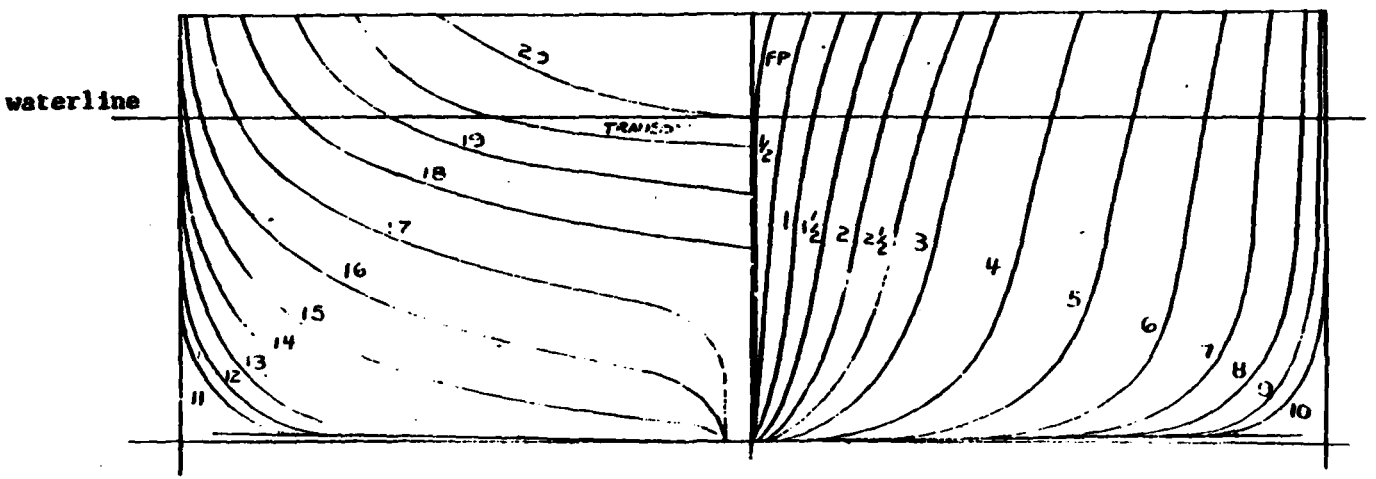


FIGURE 1 - BODY PLAN FOR MODEL A

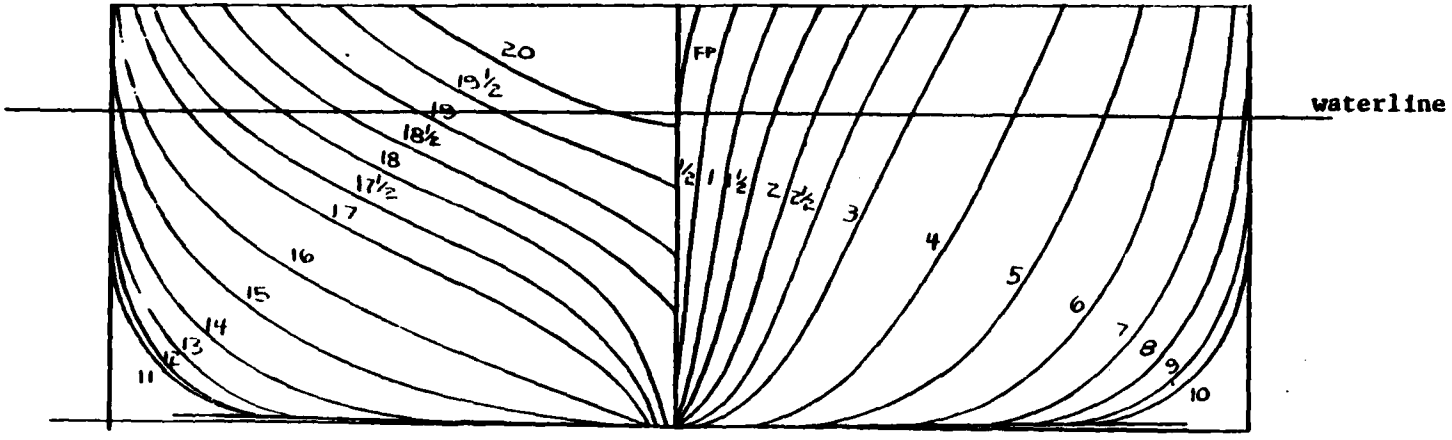


FIGURE 2 - BODY PLAN FOR MODEL B

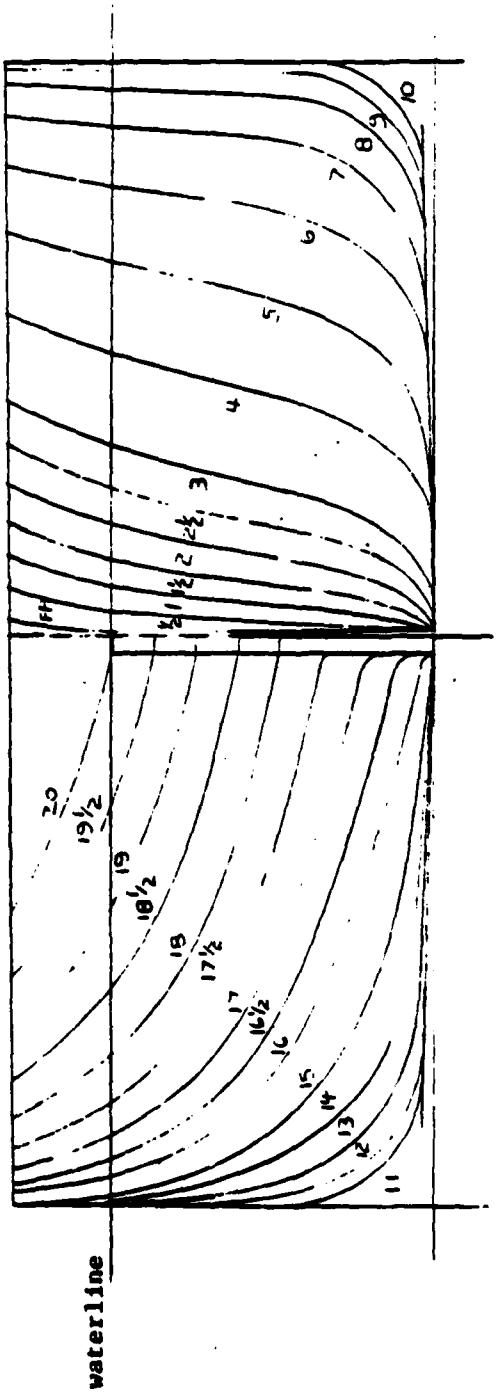


FIGURE 3 - BODY PLAN FOR MODEL D

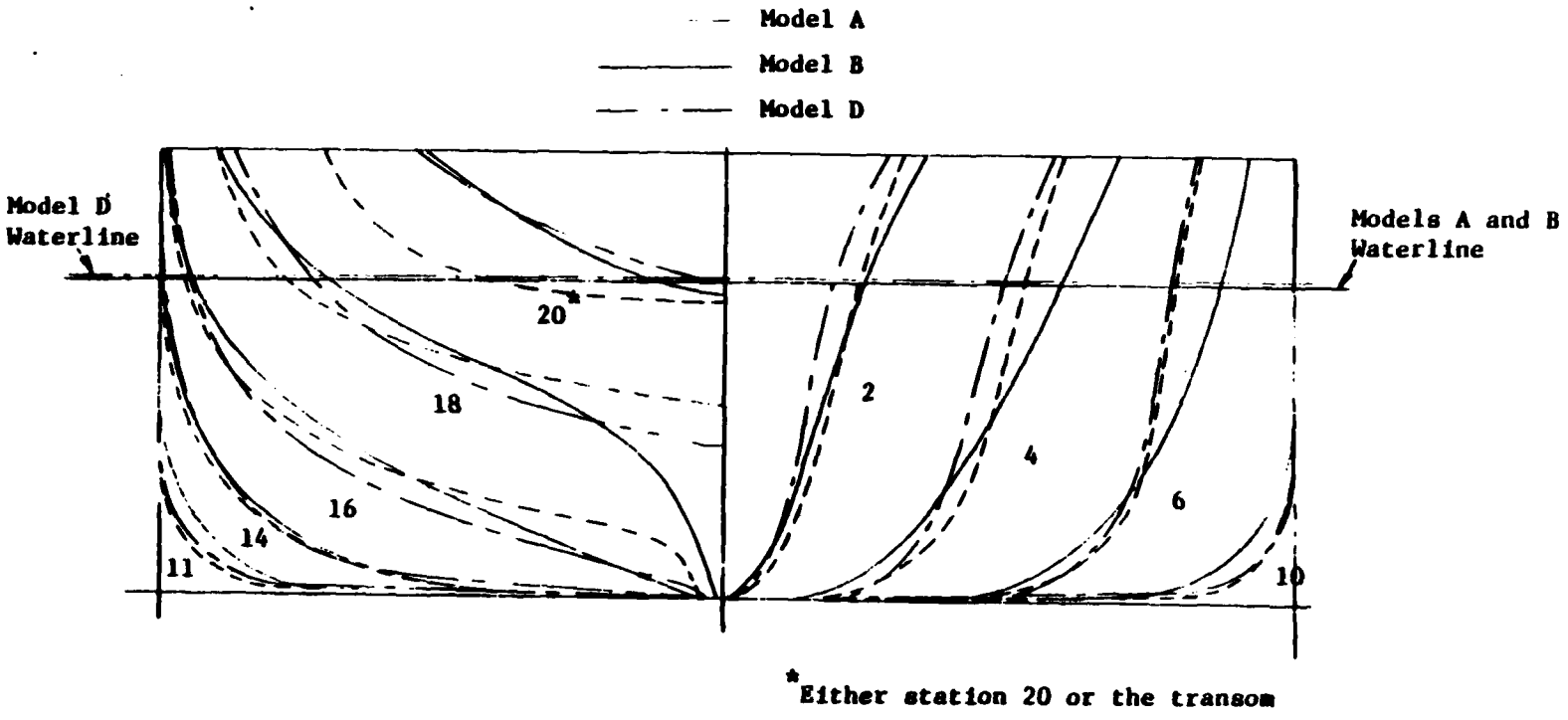


FIGURE 4 - COMPARISON OF BODYPLANS FOR MODELS A, B, AND D

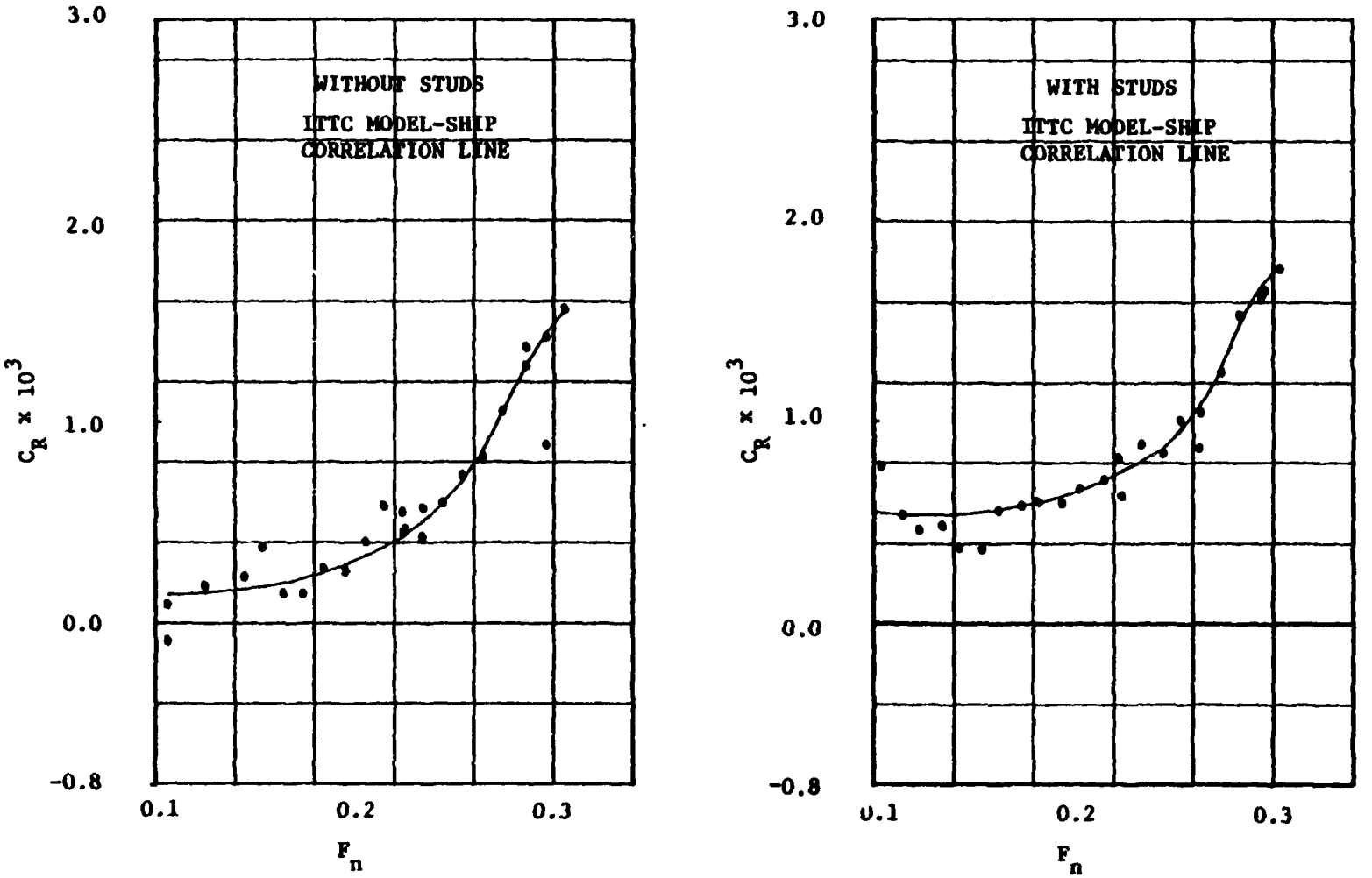


FIGURE 5 - RESIDUARY RESISTANCE COEFFICIENT CURVES FOR THE SMALL MODEL A

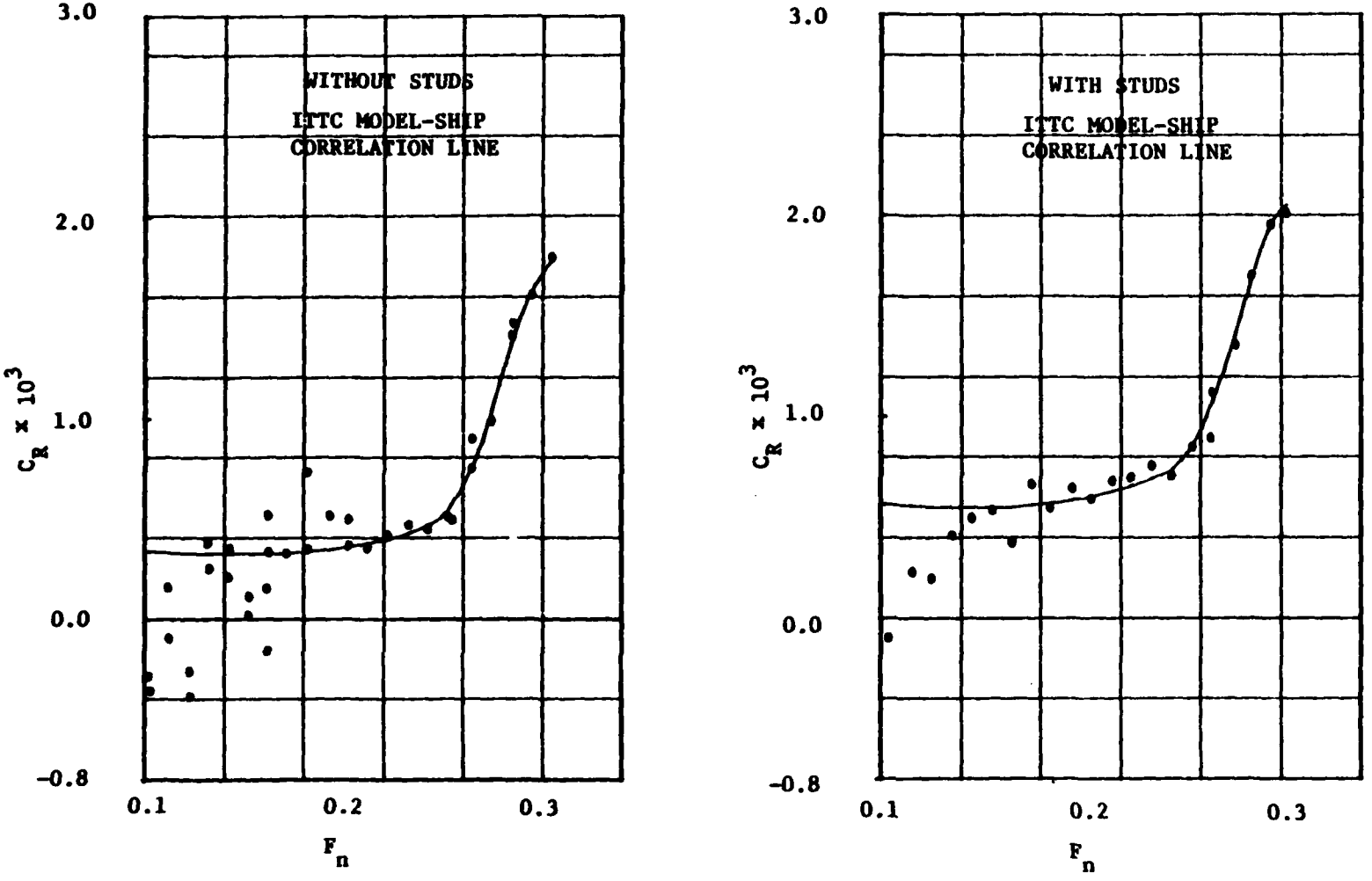


FIGURE 6 - RESIDUARY RESISTANCE COEFFICIENT CURVES FOR THE SMALL MODEL B

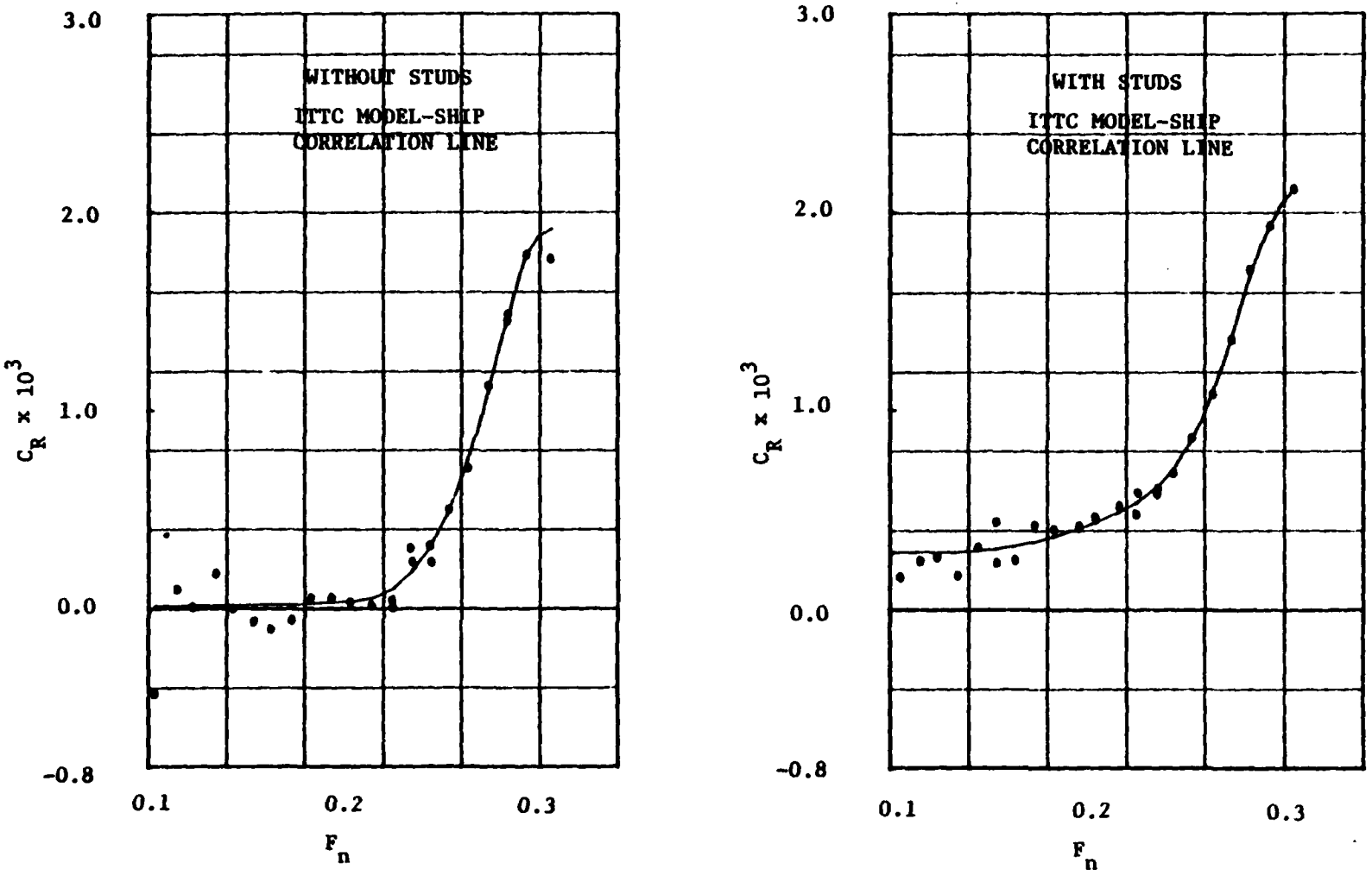


FIGURE 7 - RESIDUARY RESISTANCE COEFFICIENT CURVES FOR THE SMALL MODEL D

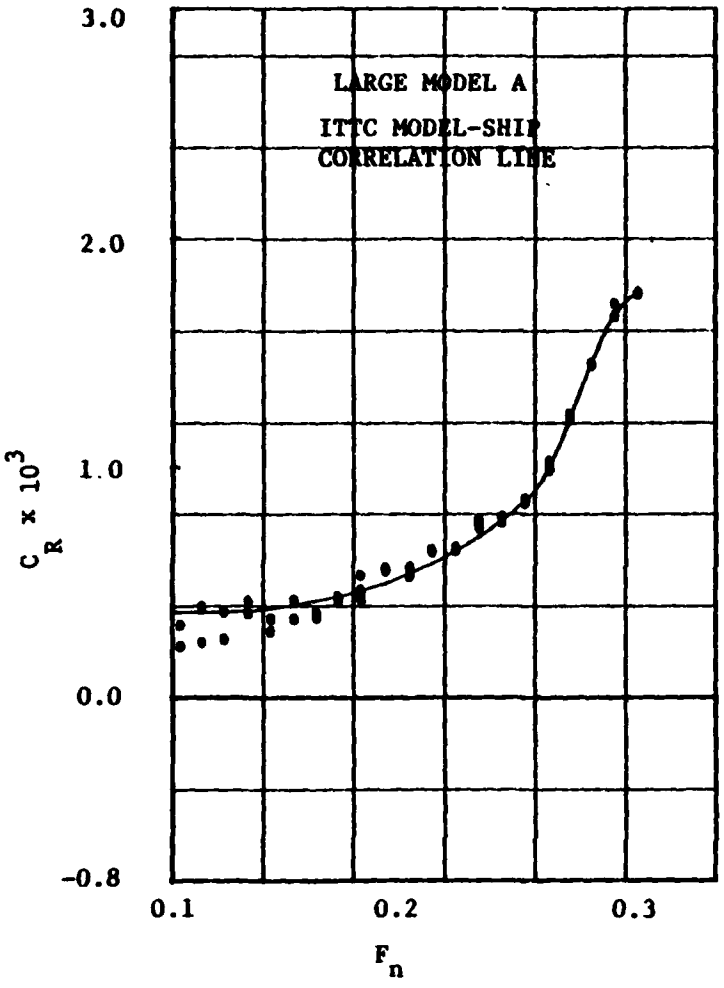


FIGURE 8 - RESIDUARY RESISTANCE COEFFICIENT CURVES FOR THE LARGE MODEL A

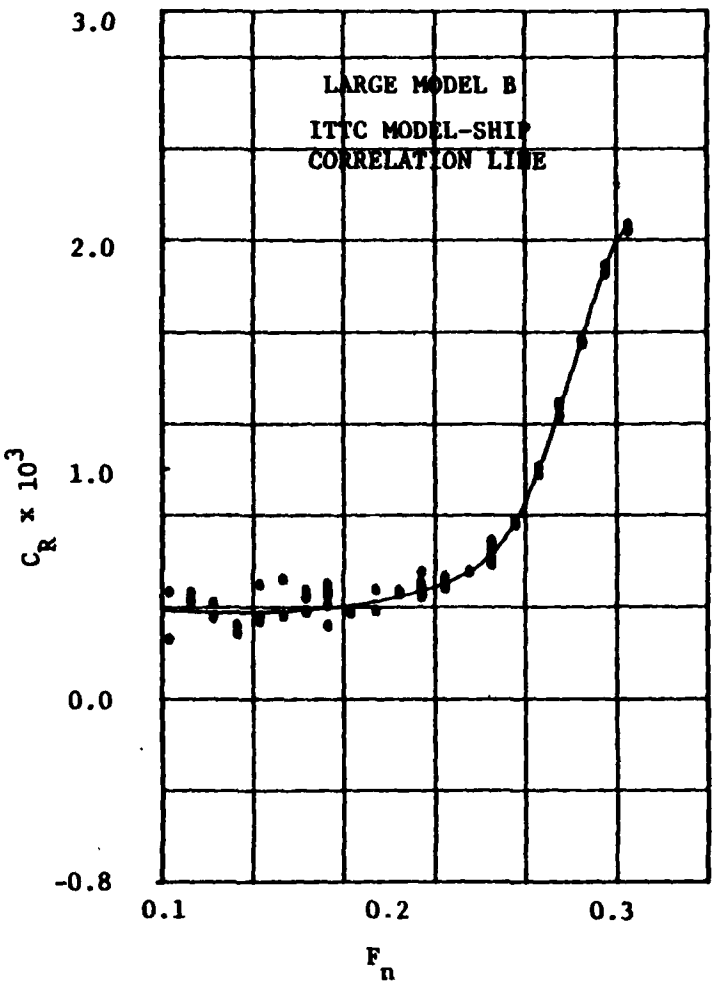


FIGURE 9 - RESIDUARY RESISTANCE COEFFICIENT CURVES FOR THE LARGE MODEL B

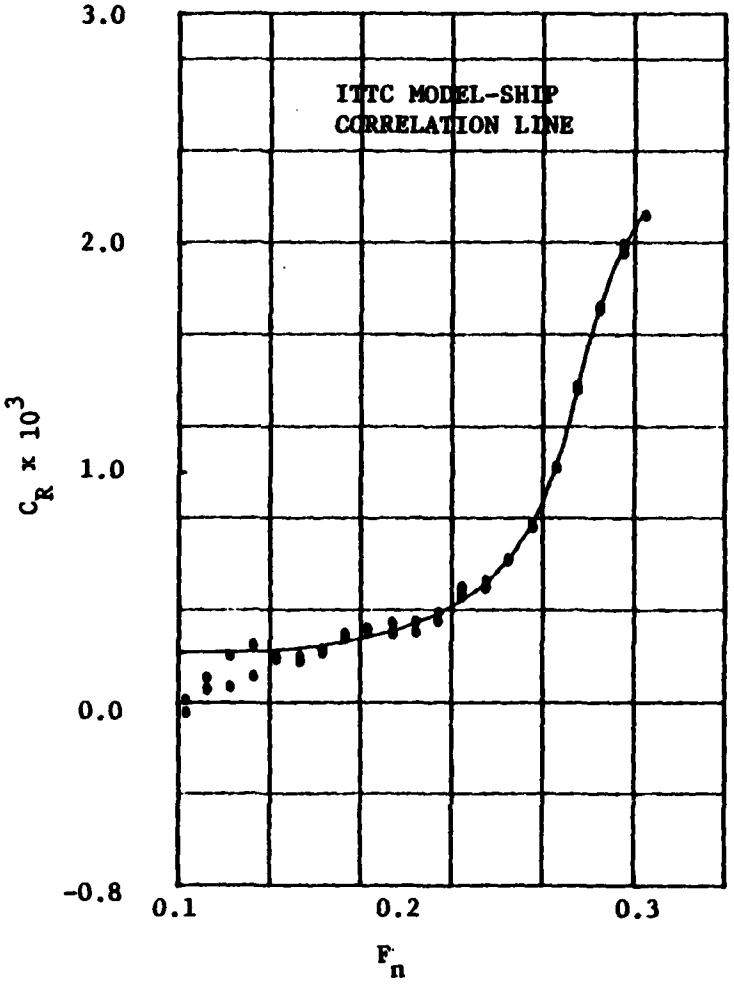


FIGURE 10 - RESIDUARY RESISTANCE COEFFICIENT CURVES FOR THE LARGE MODEL D

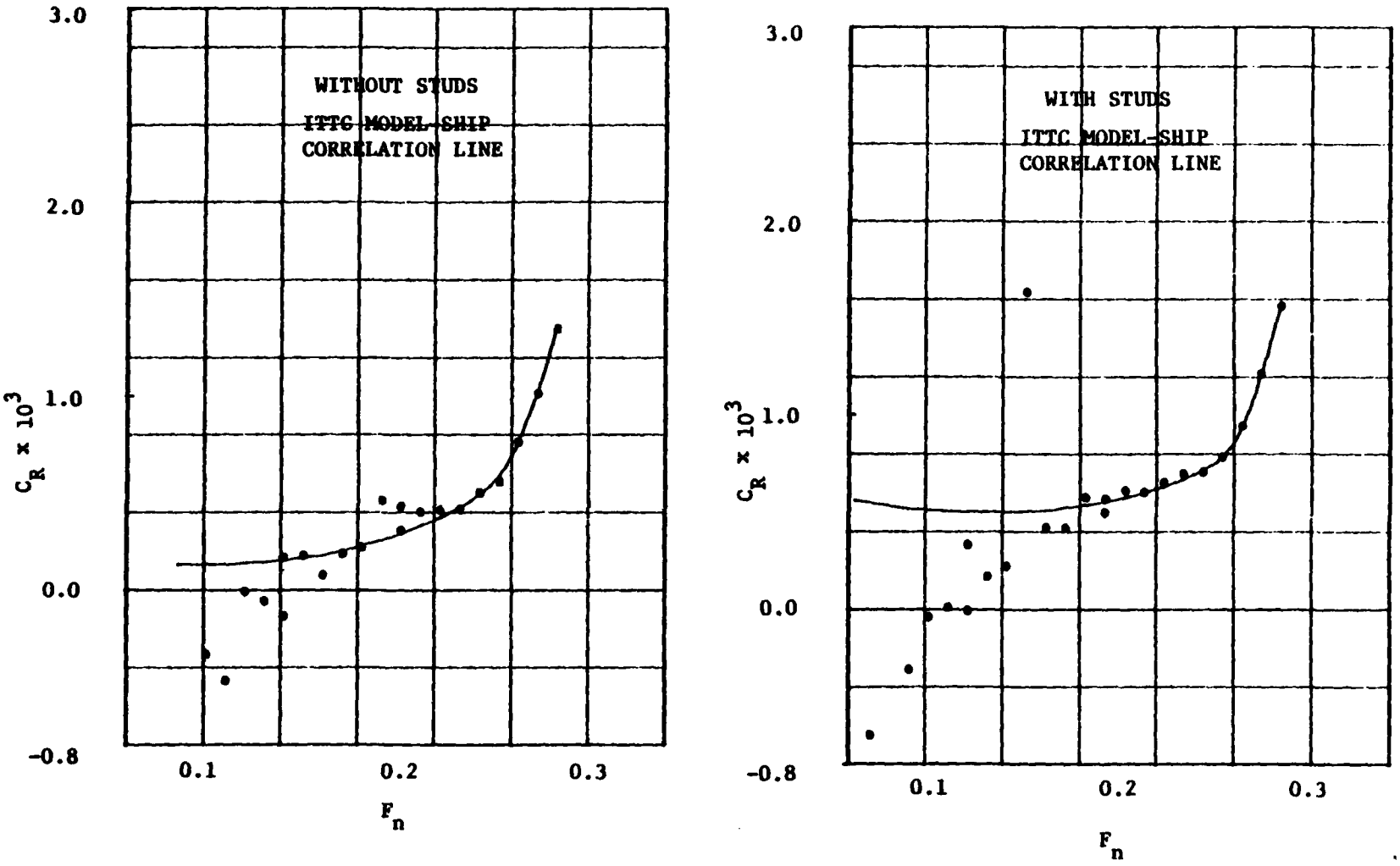
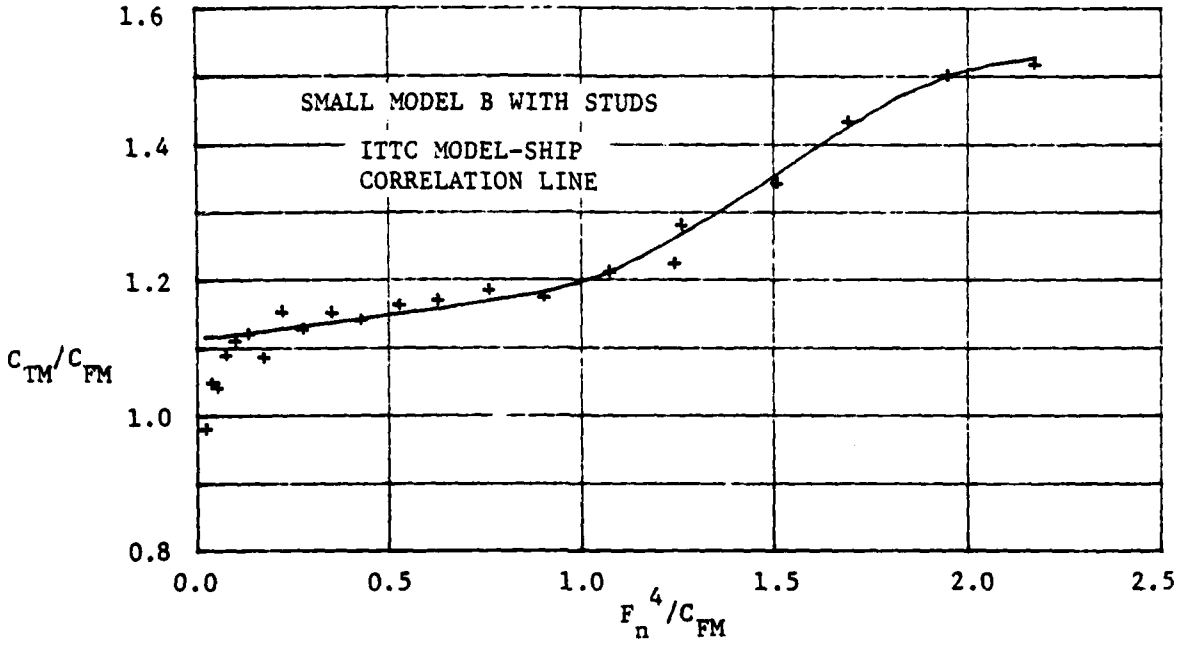


FIGURE 11 - RESIDUARY RESISTANCE COEFFICIENT CURVES FOR THE SMALL MODEL B FROM DL/SIT



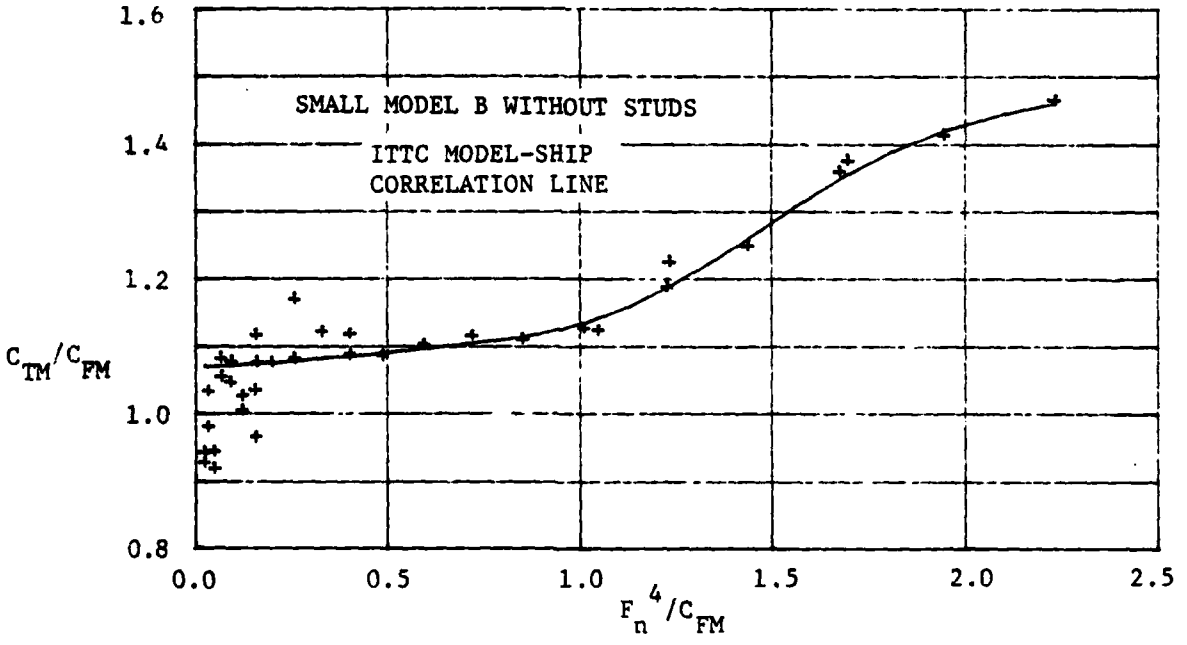


FIGURE 12 - PROHASKA PLOTS FOR THE SMALL MODEL B

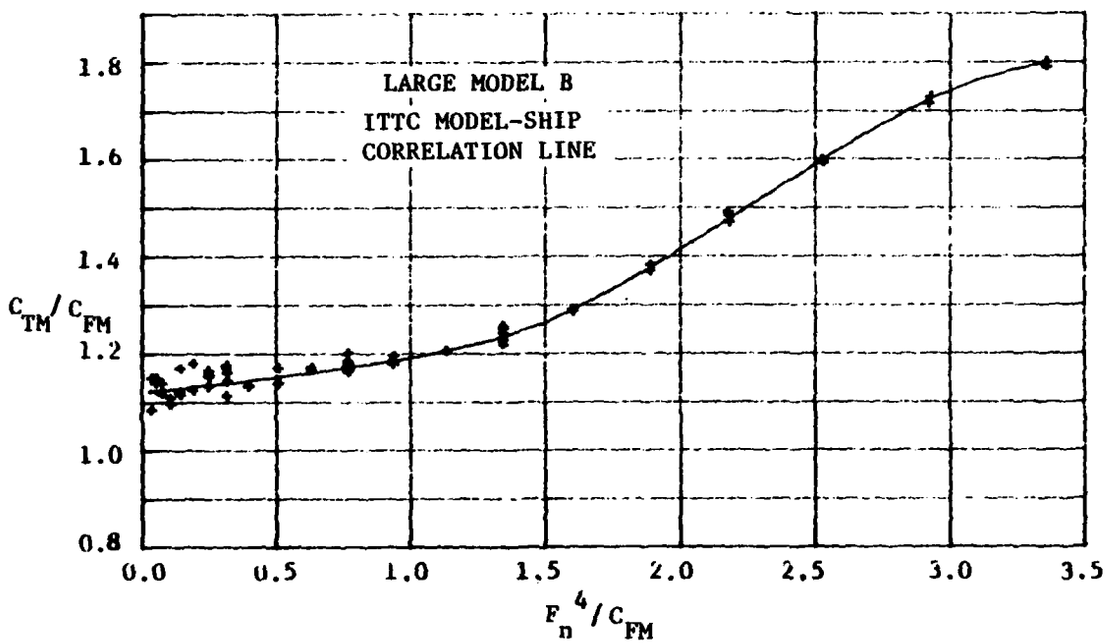
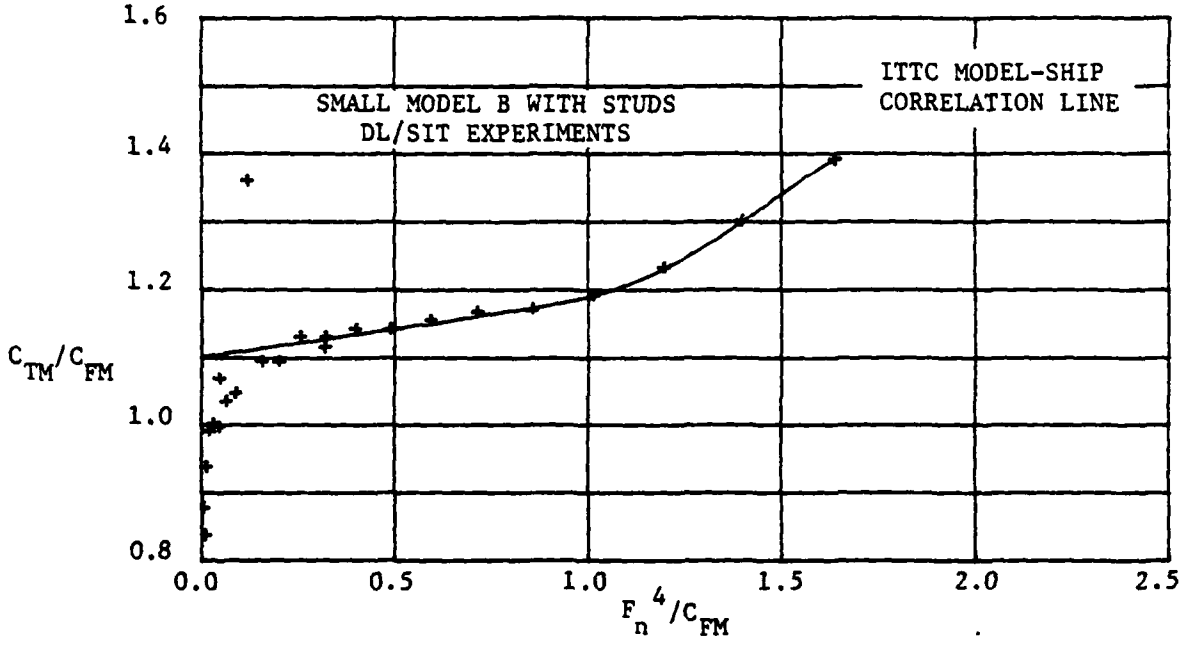


FIGURE 13 - PROHASKA PLOT FOR THE LARGE MODEL B



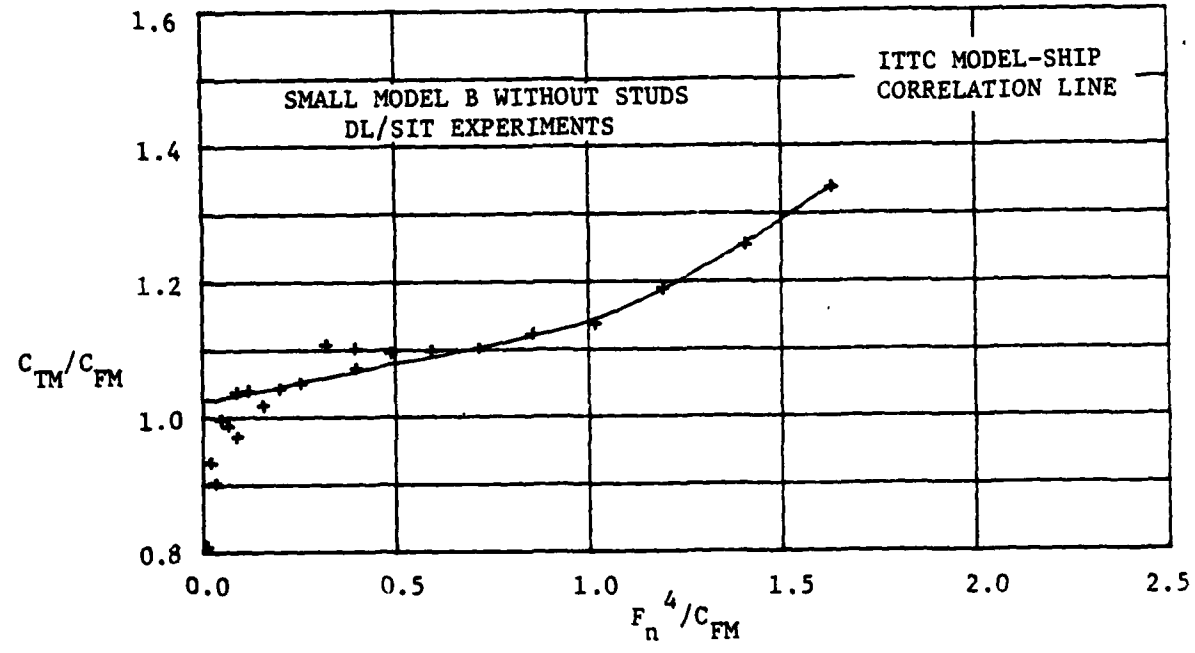


FIGURE 14 - PROHASKA PLOTS FOR THE SMALL MODEL B FROM DL/SIT DATA

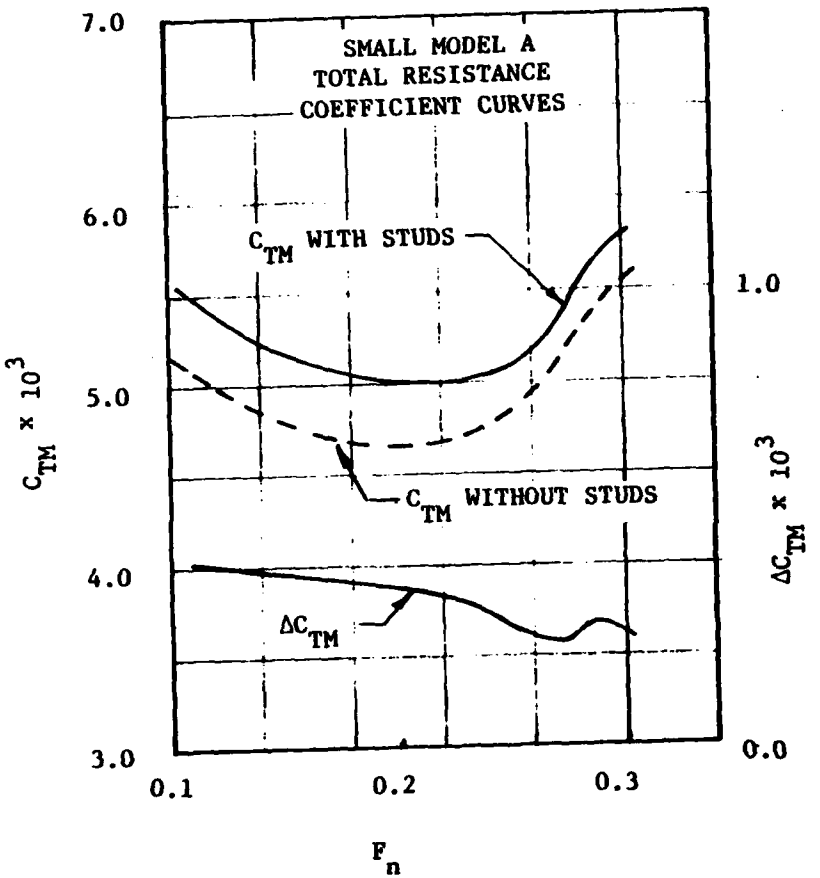


FIGURE 15 - TOTAL RESISTANCE COEFFICIENT CURVES FOR THE SMALL MODEL A

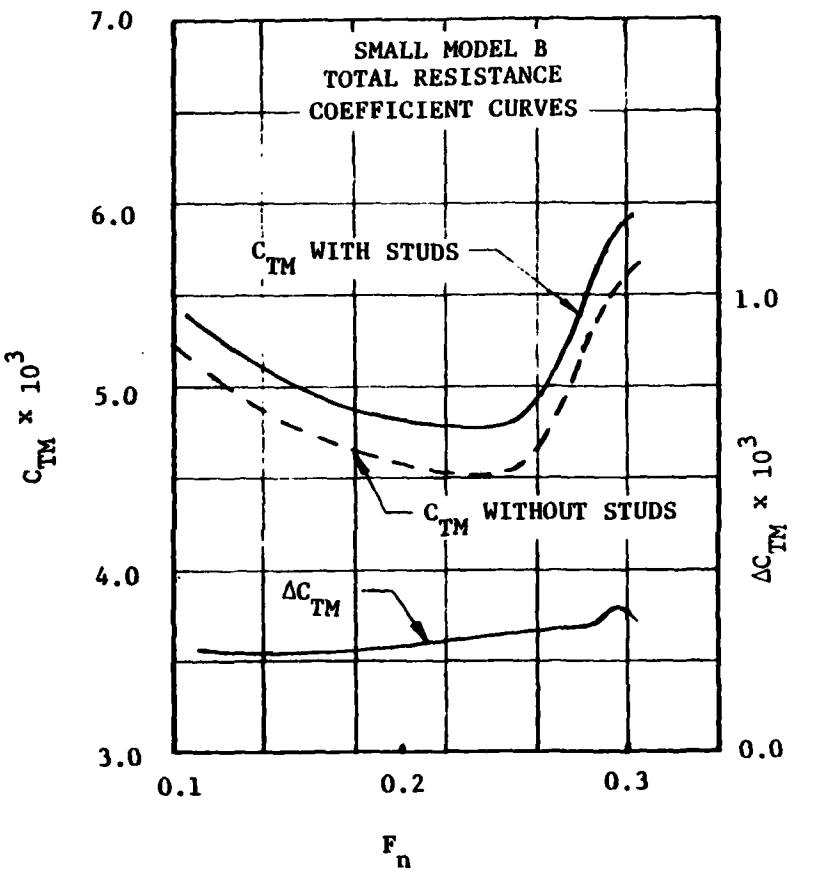


FIGURE 16 - TOTAL RESISTANCE COEFFICIENT CURVES FOR THE SMALL MODEL B

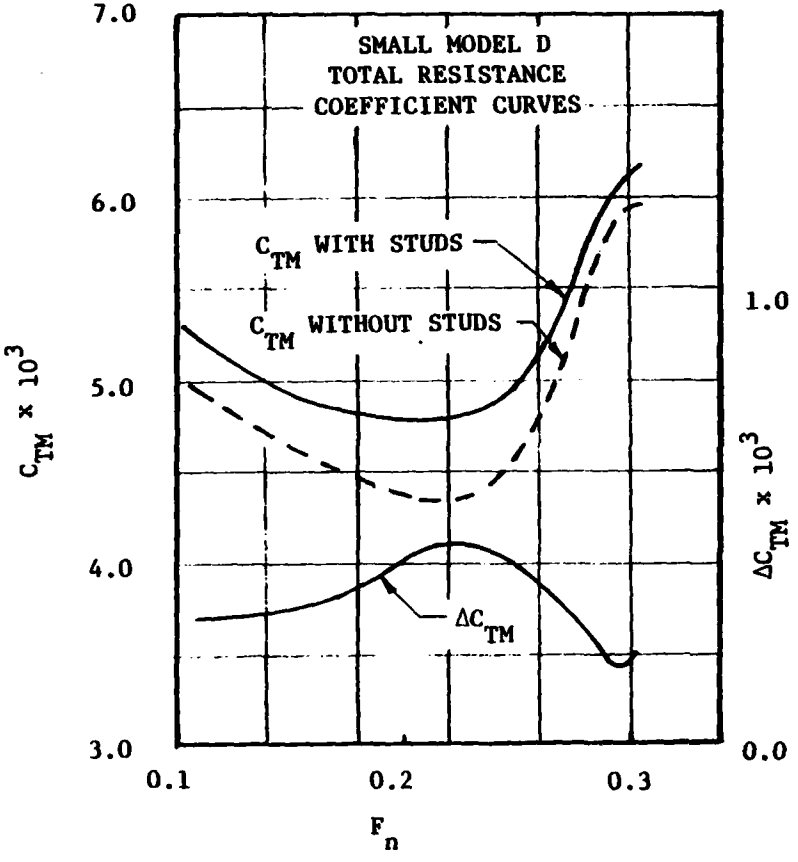


FIGURE 17 - TOTAL RESISTANCE COEFFICIENT CURVES FOR THE SMALL MODEL D

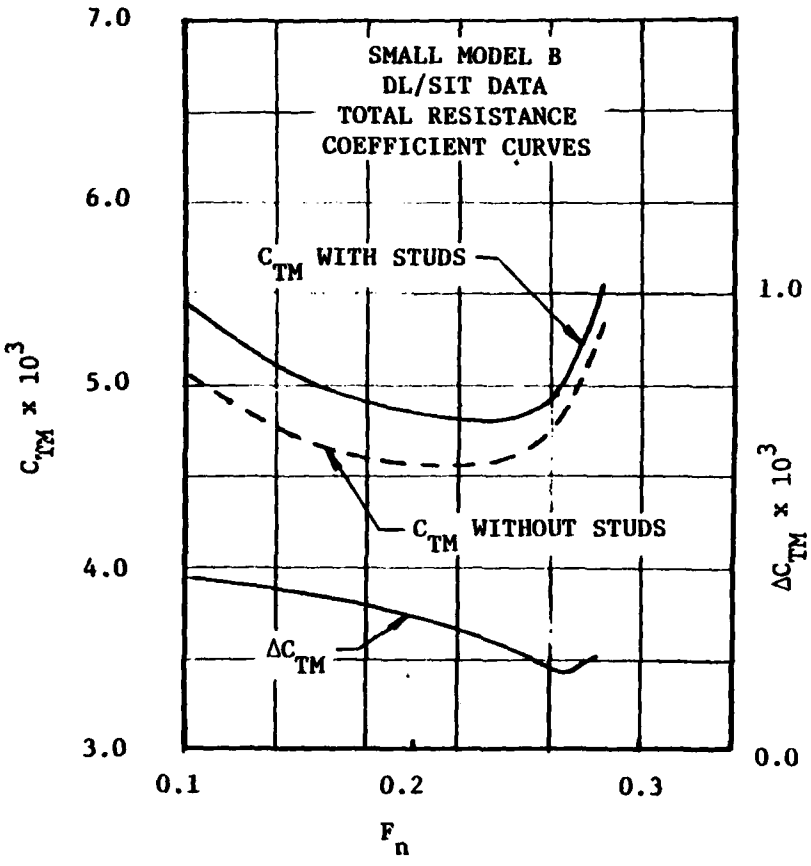


FIGURE 18 - TOTAL RESISTANCE COEFFICIENT CURVES FOR THE SMALL MODEL B FROM DL/SIT

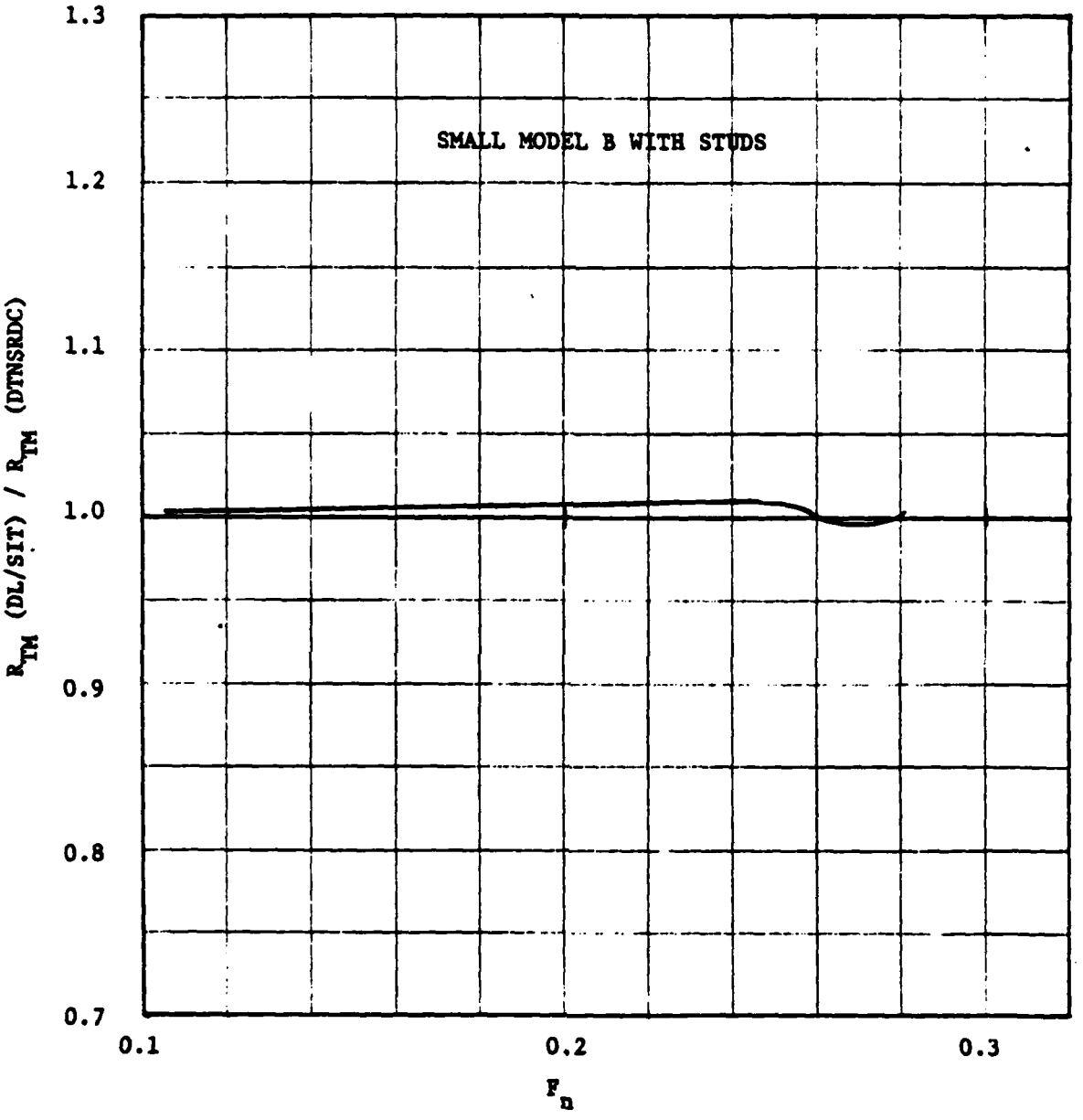


FIGURE 19 - R_{TM} (DL/SIT) / R_{TM} (DTNSRDC) FOR THE SMALL MODEL B

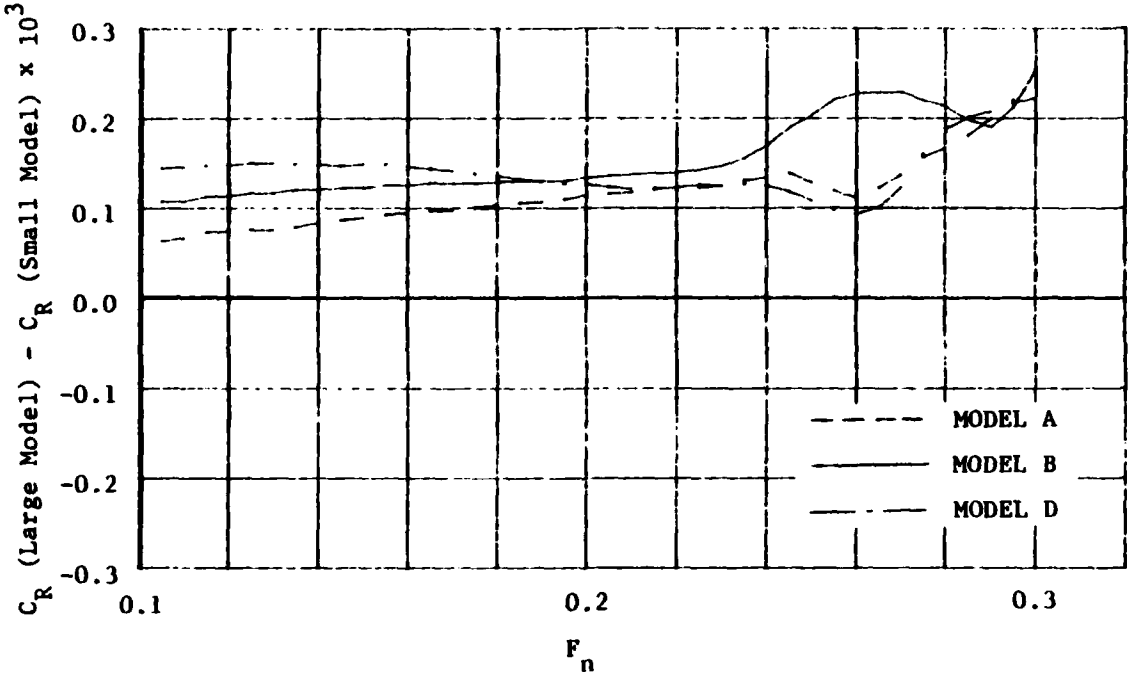


FIGURE 20 - DIFFERENCES BETWEEN THE LARGE AND SMALL MODEL C_R VALUES

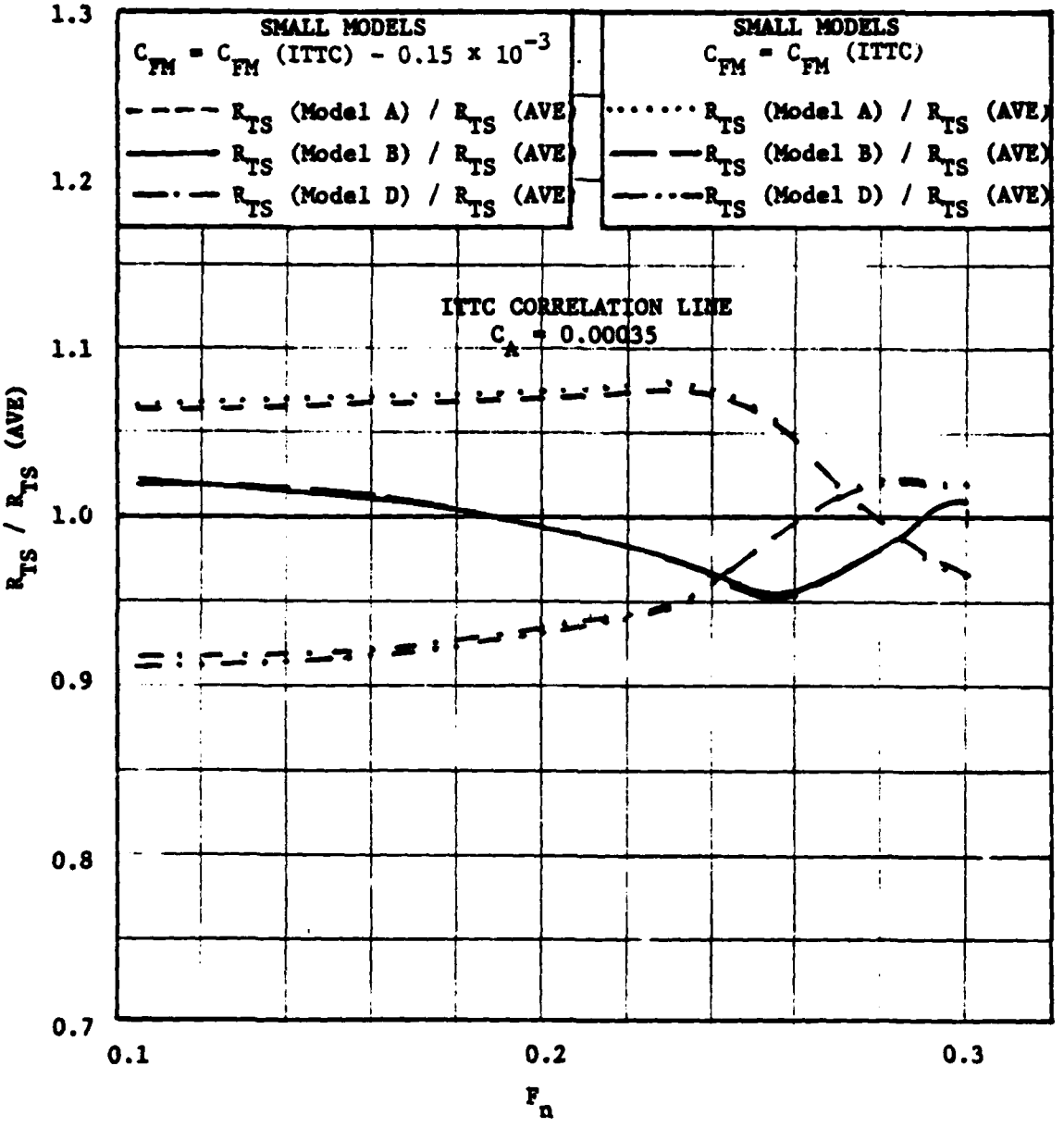


FIGURE 21 - R_{TS} / R_{TS} (AVE) VERSUS FROUDE NUMBER FOR THE SMALL MODELS

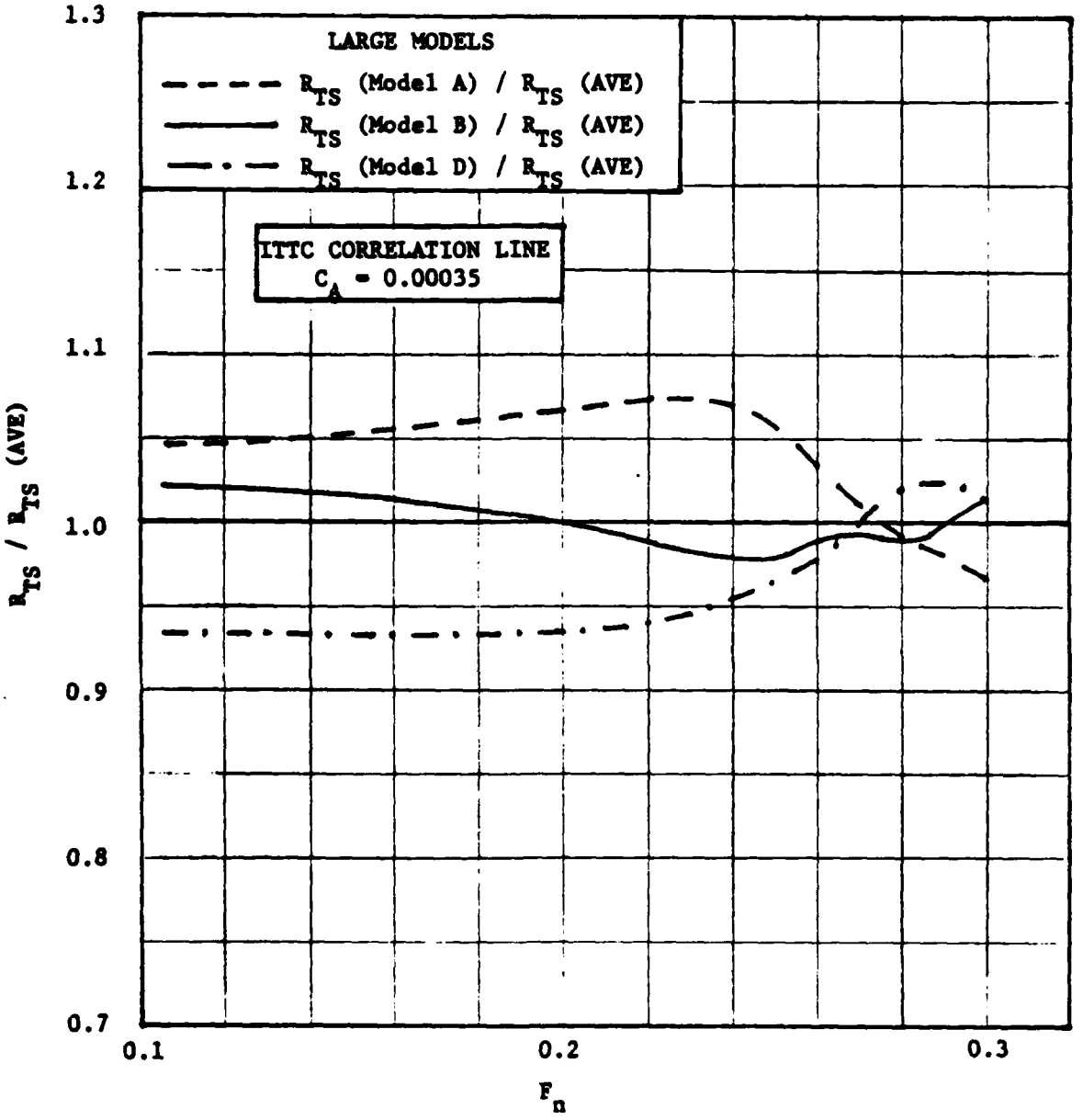


FIGURE 22 - R_{TS} / R_{TS} (AVE) VERSUS FROUDE NUMBER FOR THE LARGE MODELS

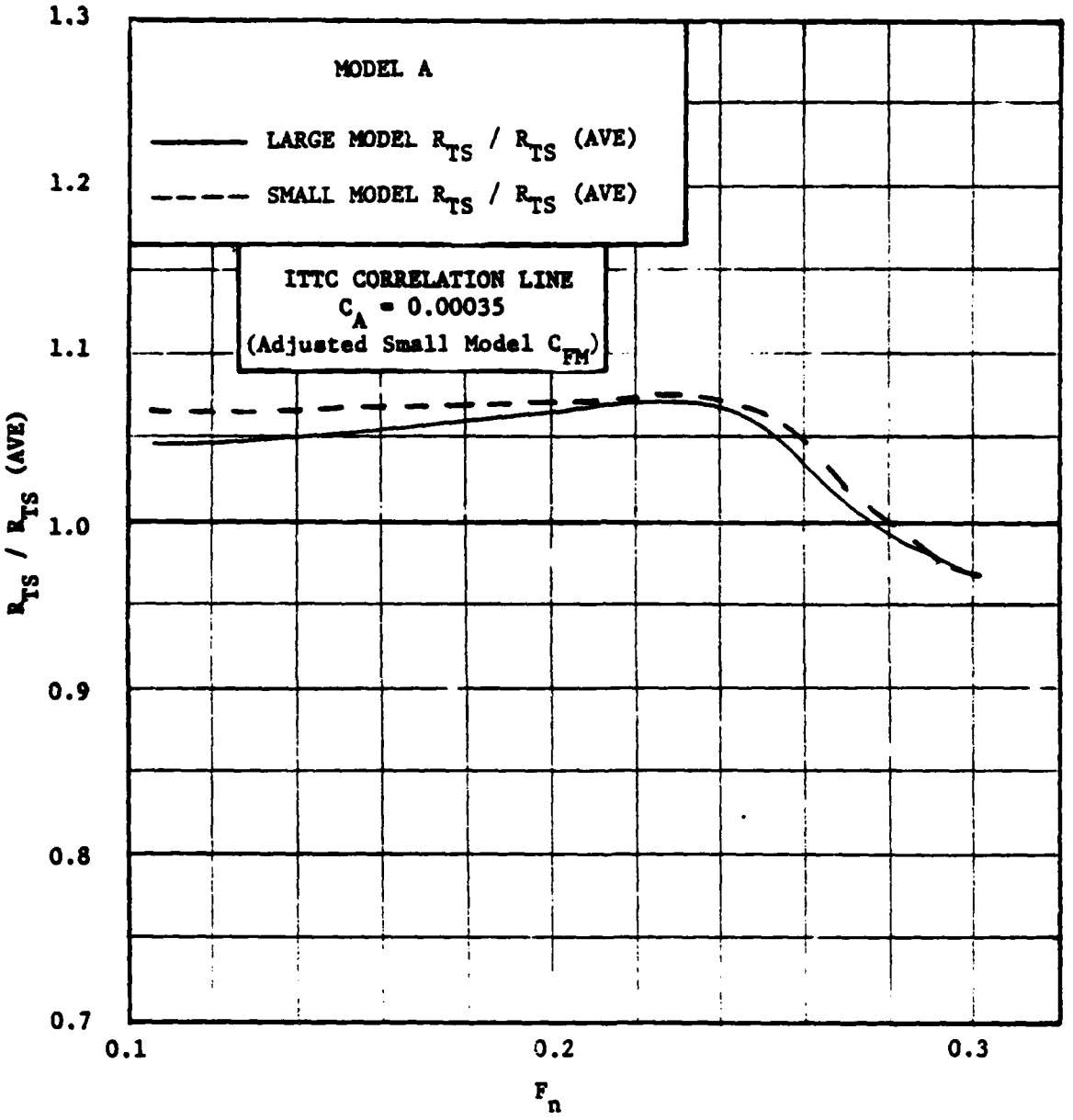


FIGURE 23 - R_{TS} / R_{TS} (AVE) VERSUS FROUDE NUMBER FOR MODEL A

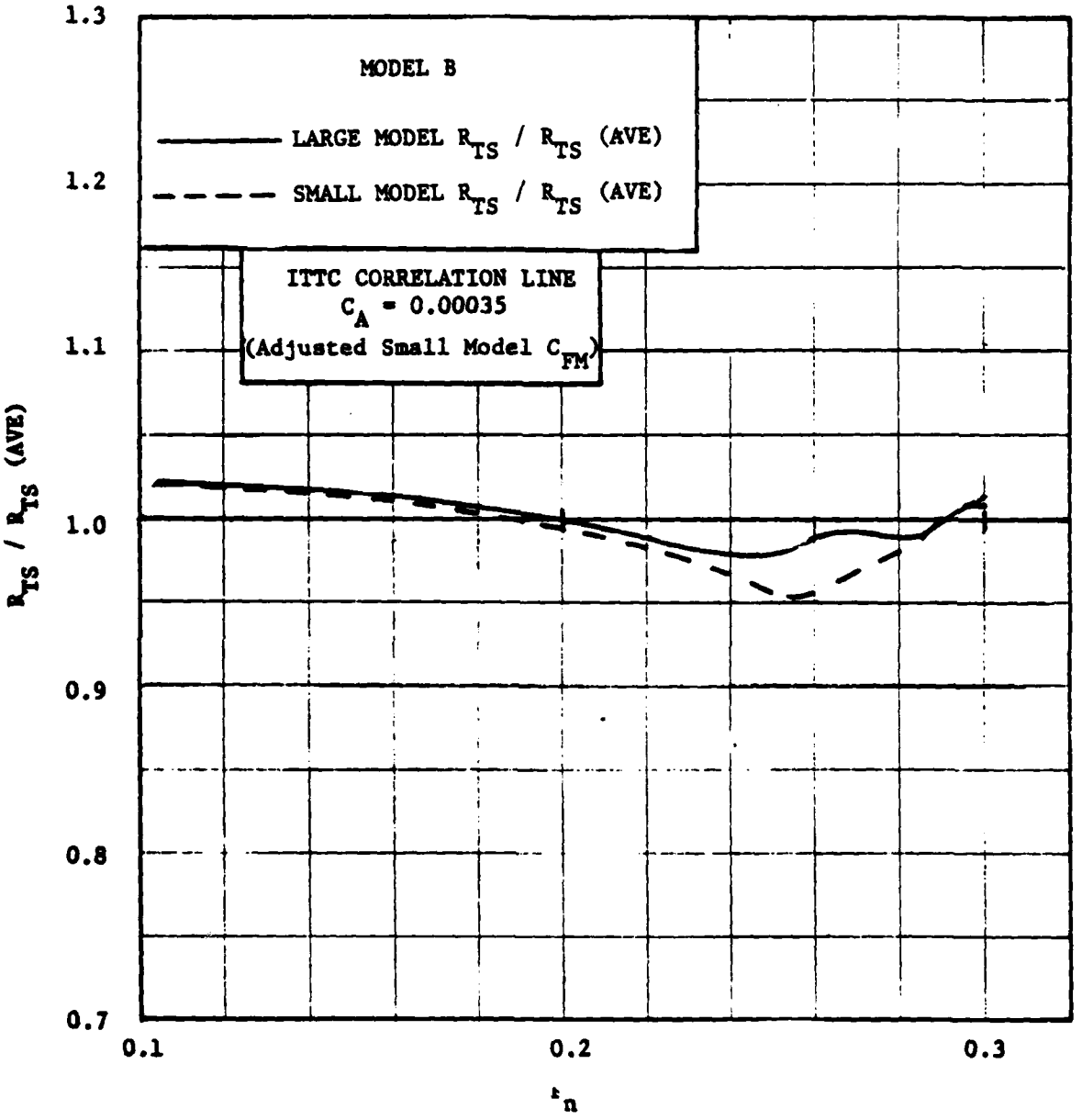


FIGURE 24 - R_{TS} / R_{TS} (AVE) VERSUS FROUDE NUMBER FOR MODEL B

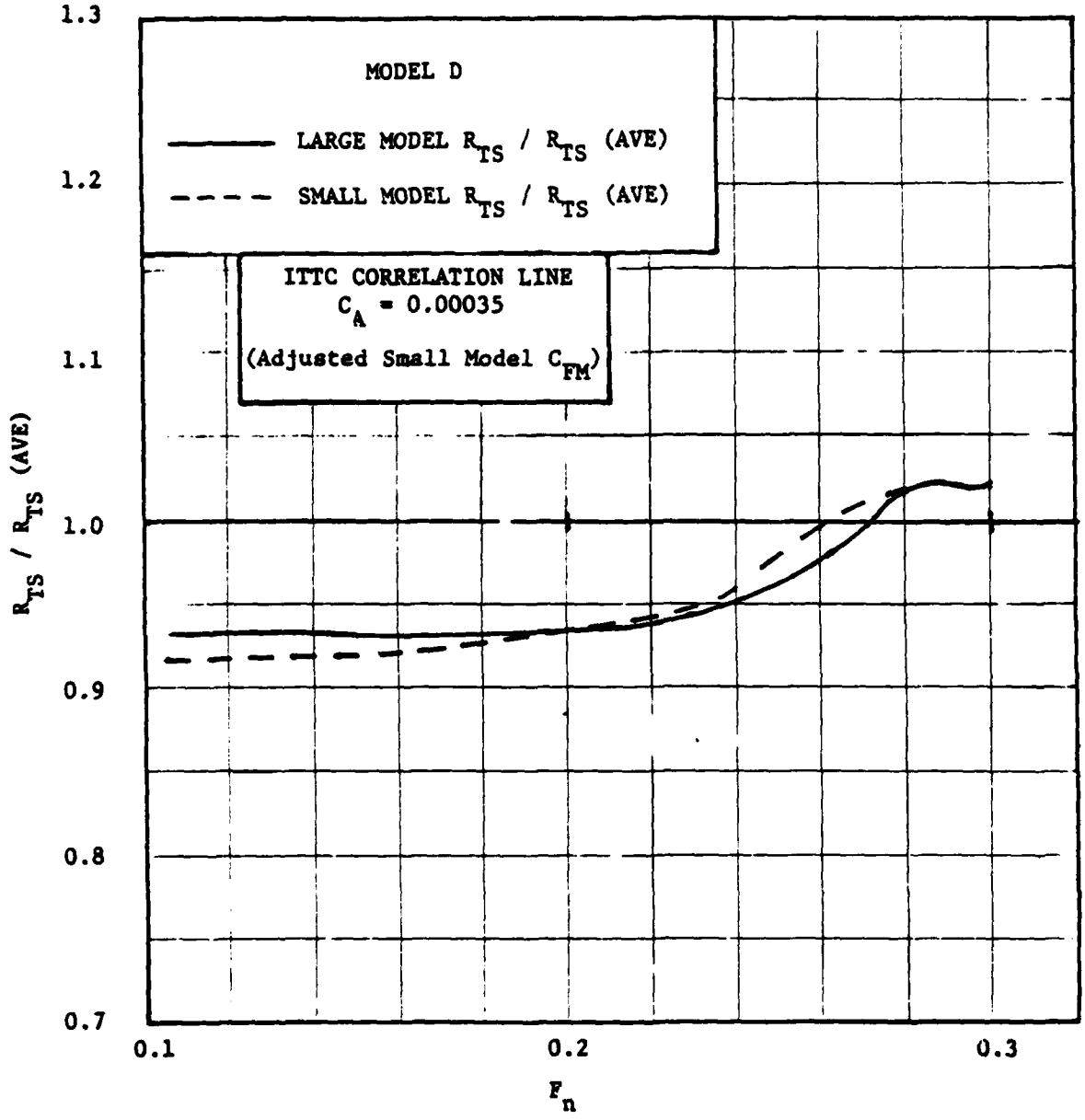


FIGURE 25 - R_{TS} / R_{TS} (AVE) VERSUS FROUDE NUMBER FOR MODEL D

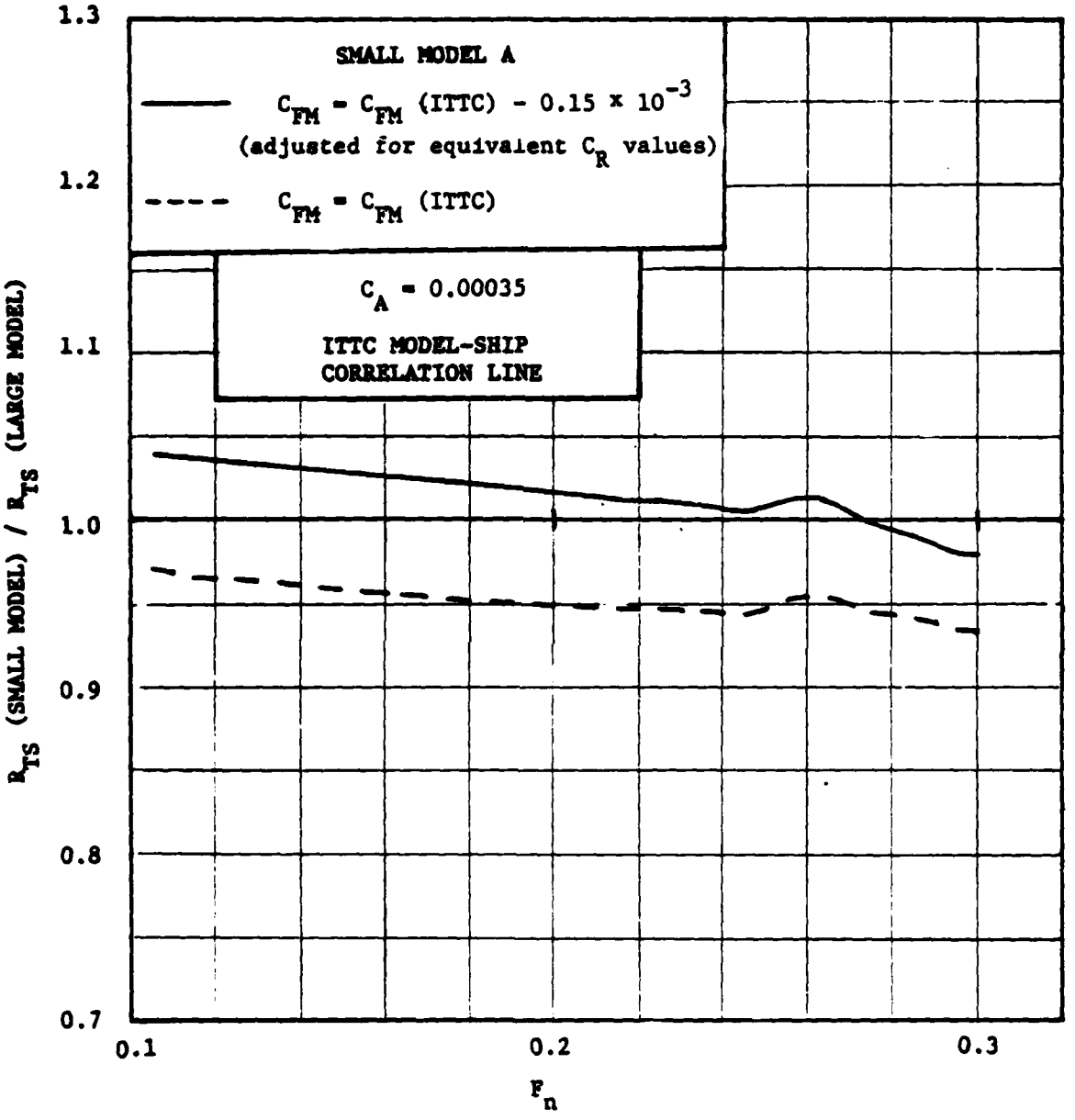


FIGURE 26 - R_{TS} (SMALL MODEL) / R_{TS} (LARGE MODEL) FOR MODEL A

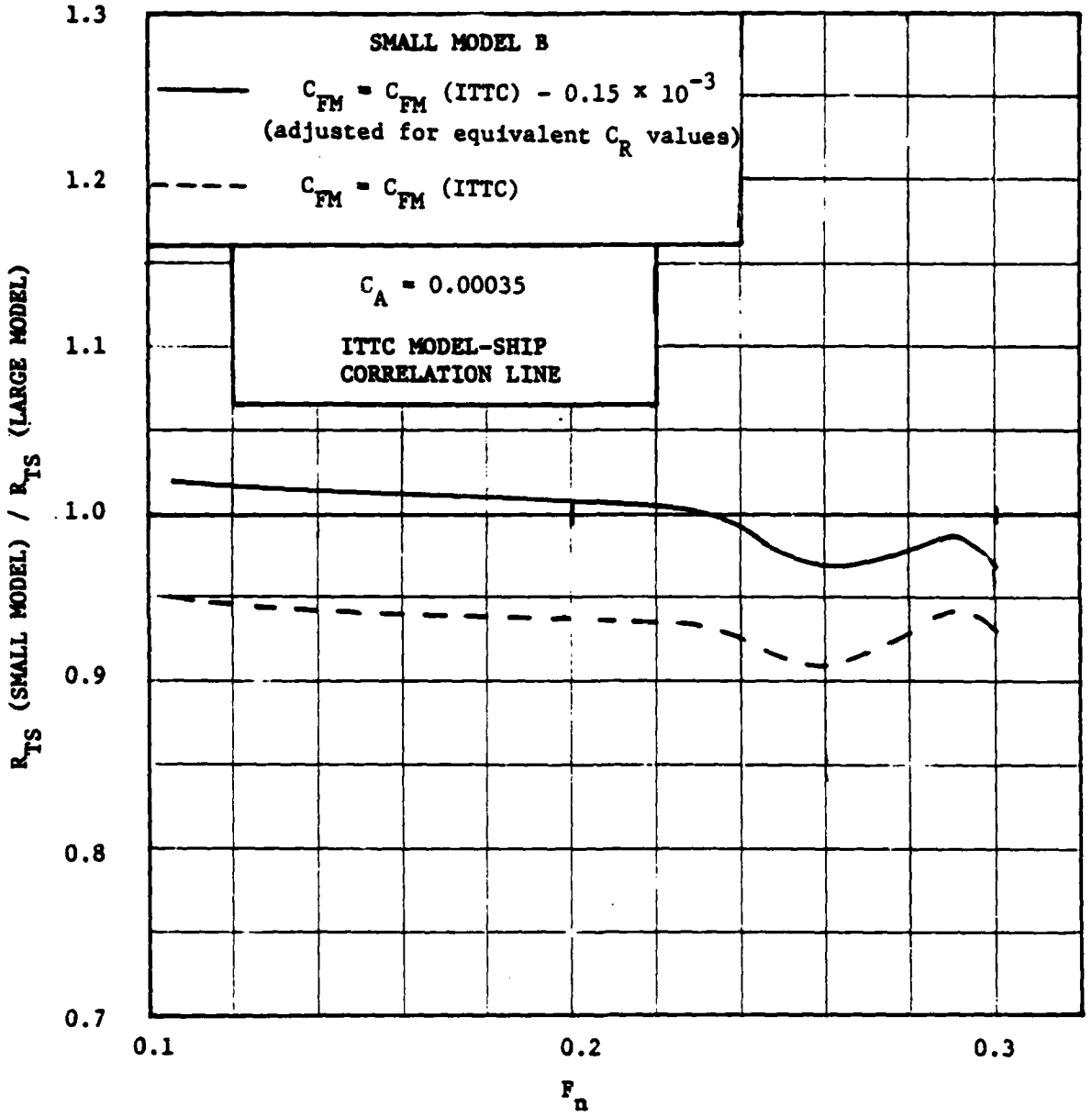


FIGURE 27 - R_{TS} (SMALL MODEL) / R_{TS} (LARGE MODEL) FOR MODEL B

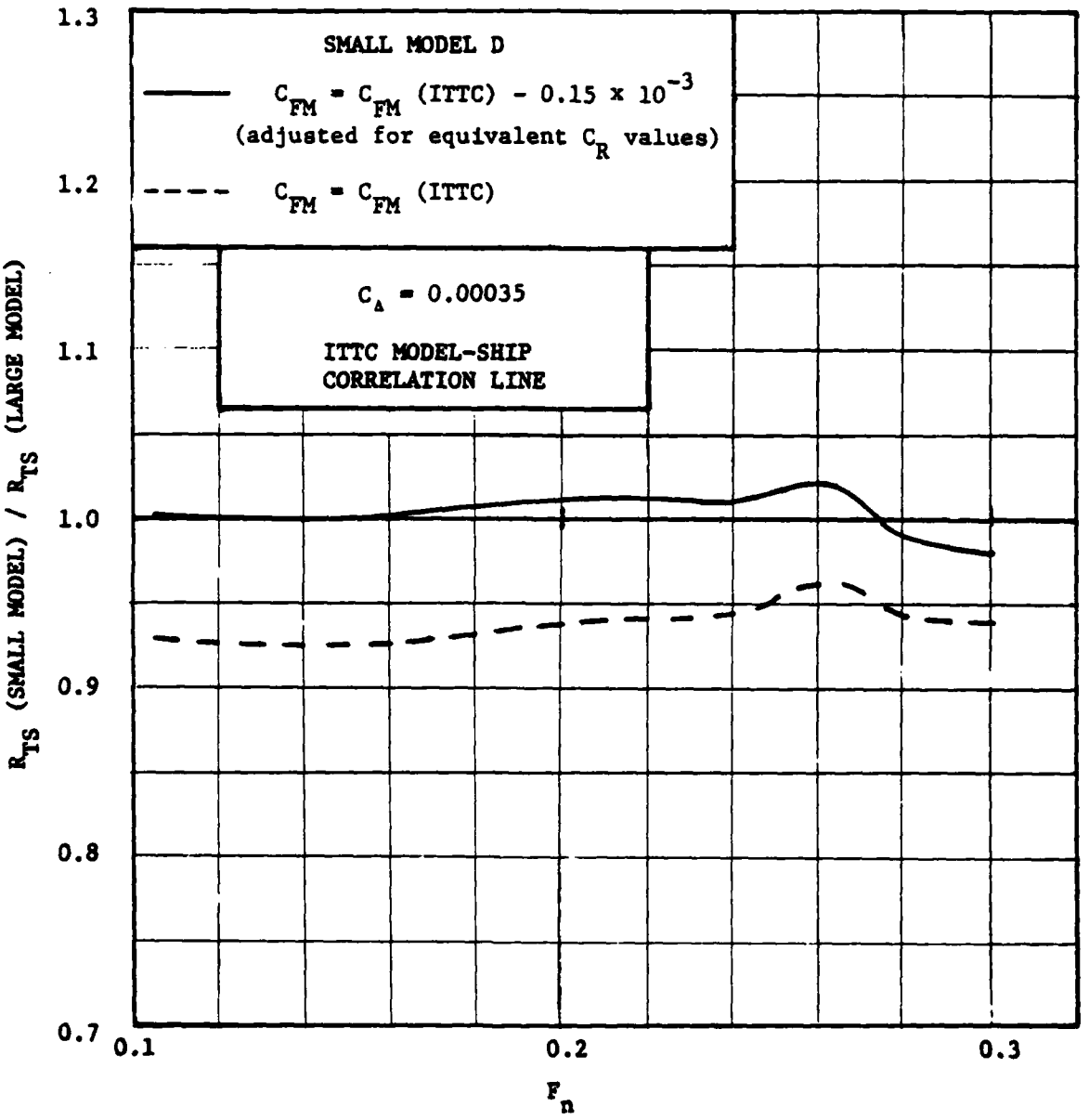


FIGURE 28 - R_{TS} (SMALL MODEL) / R_{TS} (LARGE MODEL) FOR MODEL D

TABLE 1

PRINCIPAL DIMENSIONS OF SHIPS AND MODELS

		SHIP		MODEL λ = 31.435		MODEL λ = 144	
MODEL B							
	LENGTH	262.1 m	(860 ft)	8.34 m	(27.36 ft)	1.82 m	(5.97 ft)
	BEAM	38.4 m	(126 ft)	1.22 m	(4.01 ft)	0.27 m	(0.88 ft)
	DRAFT	10.36 m	(34 ft)	0.33 m	(1.08 ft)	0.072 m	(0.236 ft)
	WETTED SURFACE	10470 m^2	(112700 ft^2)	10.60 m^2	(114.1 ft^2)	0.51 m^2	(5.436 ft^2)
	DISPLACEMENT	63430 t	(62430 L tons)	1985 kg	(4377 lbs)	20.7 kg	(45.6 lbs)
MODEL A							
	LENGTH	262.1 m	(860 ft)	8.34 m	(27.36 ft)	1.82 m	(5.97 ft)
	BEAM	38.4 m	(126 ft)	1.22 m	(4.01 ft)	0.27 m	(0.88 ft)
	DRAFT	10.36 m	(34 ft)	0.33 m	(1.08 ft)	0.072 m	(0.236 ft)
	WETTED SURFACE	10780 m^2	(116050 ft^2)	10.91 m^2	(117.4 ft^2)	0.52 m^2	(5.597 ft^2)
	DISPLACEMENT	63430 t	(62430 L tons)	1985 kg	(4377 lbs)	20.7 kg	(45.6 lbs)
MODEL D							
	LENGTH	262.1 m	(860 ft)	8.34 m	(27.36 ft)	1.82 m	(5.97 ft)
	BEAM	38.4 m	(126 ft)	1.22 m	(4.01 ft)	0.27 m	(0.88 ft)
	DRAFT	10.52 m	(34.5 ft)	0.33 m	(1.10 ft)	0.073 m	(0.240 ft)
	WETTED SURFACE	10620 m^2	(114340 ft^2)	10.75 m^2	(115.7 ft^2)	0.51 m^2	(5.514 ft^2)
	DISPLACEMENT	62970 t	(61980 L tons)	1971 kg	(4345 lbs)	20.5 kg	(45.2 lbs)

TABLE 1 (Continued)

PRINCIPAL DIMENSIONS OF SHIP AND MODELS

NONDIMENSIONAL COEFFICIENTS

	MODEL A	MODEL B	MODEL D	PERCENT MAXIMUM DIFFERENCE
L/B	6.83	6.83	6.83	0.0 %
B/T	3.71	3.71	3.65	1.6 %
C_B	0.593	0.593	0.580	2.2 %
C_M	0.981	0.952	0.962	3.0 %
C_P	0.605	0.623	0.603	3.6 %
C_{PV}	0.808	0.833	0.834	3.2 %
C_W	0.749	0.748	0.723	3.5 %
C_V	3.433×10^{-3}	3.433×10^{-3}	3.408×10^{-3}	0.7 %
F	0.569	0.550	0.566	1.7 % L
$\overline{FB}/L$	0.521	0.524	0.530	0.9 % L
i_E	8.0°	7.5°	6.0°	2.0 degrees

TABLE 2 - UNFAIRED RESISTANCE DATA FOR THE SMALL MODEL A WITHOUT STUDS

ITTC MODEL-SHIP CORRELATION LINE USED FOR CR, CFM VALUES

LENGTH	1.820 M	5.97 FT	DENSITY	997.4 KG/M^3	1.9352 SLUGS/FT^3
WETTED SURFACE	0.520 M^2	5.597 FT^2	KINEMATIC VISCOSITY	0.9307E-6 M^2/S	1.0018E-5 FT^2/S

POINT	FROUDE NUMBER	VS (M/S)	VS (KNOTS)	VM (M/S)	VM (FT/SEC)	RTM (N)	RTM (LBS)	CTM *1000	CR *1000	CFM *1000
1	0.223	11.33	22.03	0.944	3.098	1.080	0.243	4.673	0.553	4.120
2	0.225	11.41	22.18	0.951	3.120	1.074	0.242	4.581	0.467	4.114
3	0.286	14.52	28.22	1.210	3.969	2.008	0.452	5.292	1.372	3.920
4	0.234	11.87	23.07	0.989	3.245	1.180	0.265	4.652	0.570	4.082
5	0.106	5.37	10.44	0.447	1.468	0.255	0.057	4.918	0.092	4.826
6	0.106	5.37	10.44	0.447	1.468	0.246	0.055	4.738	-0.088	4.826
7	0.125	6.32	12.29	0.527	1.729	0.349	0.078	4.843	0.186	4.657
8	0.145	7.35	14.28	0.612	2.009	0.461	0.104	4.740	0.230	4.509
9	0.164	8.33	16.19	0.694	2.277	0.567	0.127	4.537	0.146	4.391
10	0.184	9.34	18.15	0.778	2.553	0.716	0.161	4.561	0.274	4.288
11	0.206	10.43	20.27	0.869	2.851	0.900	0.202	4.596	0.405	4.191
12	0.224	11.38	22.11	0.948	3.110	1.065	0.239	4.570	0.453	4.117
13	0.244	12.38	24.07	1.032	3.386	1.283	0.288	4.645	0.598	4.047
14	0.264	13.39	26.03	1.116	3.661	1.554	0.349	4.812	0.828	3.984
15	0.286	14.52	28.23	1.210	3.970	1.974	0.444	5.199	1.279	3.920
16	0.306	15.49	30.12	1.291	4.236	2.348	0.528	5.431	1.561	3.870
17	0.154	7.80	15.17	0.650	2.133	0.529	0.119	4.830	0.377	4.452
18	0.174	8.83	17.16	0.735	2.413	0.629	0.141	4.484	0.146	4.338
19	0.195	9.90	19.25	0.825	2.708	0.794	0.179	4.495	0.259	4.236
20	0.214	10.87	21.14	0.906	2.973	1.009	0.227	4.738	0.583	4.155
21	0.234	11.86	23.06	0.988	3.243	1.143	0.257	4.510	0.428	4.082
22	0.254	12.87	25.02	1.073	3.519	1.417	0.319	4.749	0.734	4.016
23	0.274	13.90	27.02	1.159	3.801	1.744	0.392	5.010	1.056	3.954
24	0.296	15.02	29.20	1.252	4.107	1.943	0.437	4.782	0.888	3.894
25	0.296	15.01	29.18	1.251	4.104	2.158	0.485	5.318	1.424	3.894

TABLE 3 - UNFAIRED RESISTANCE DATA FOR THE SMALL MODEL A WITH STUDS

ITTC MODEL-SHIP CORRELATION LINE USED FOR CR, CFM VALUES

LENGTH 1.820 M 5.97 FT DENSITY 997.4 KG/M^3 1.9352 SLUGS/FT^3

WETTED SURFACE 0.520 M^2 5.597 FT^2 KINEMATIC VISCOSITY 0.9307E-6 M^2/S 1.0018E-5 FT^2/S

POINT	FROUDE NUMBER	VS (M/S)	VS (KNOTS)	VM (M/S)	VM (FT/SEC)	RTM (N)	RTM (LBS)	CTM *1000	CR *1000	CFM *1000
1	0.104	5.26	10.22	0.438	1.438	0.280	0.063	5.626	0.777	4.848
2	0.123	6.22	12.09	0.518	1.701	0.358	0.081	5.137	0.464	4.673
3	0.143	7.26	14.11	0.605	1.984	0.464	0.104	4.893	0.371	4.521
4	0.163	8.25	16.03	0.687	2.255	0.607	0.137	4.957	0.556	4.400
5	0.183	9.26	18.01	0.772	2.533	0.757	0.170	4.895	0.601	4.295
6	0.203	10.31	20.04	0.859	2.818	0.931	0.209	4.867	0.666	4.201
7	0.225	11.39	22.14	0.949	3.114	1.108	0.249	4.745	0.629	4.116
8	0.245	12.44	24.17	1.036	3.400	1.301	0.306	4.886	0.843	4.043
9	0.263	13.35	25.94	1.112	3.649	1.557	0.350	4.854	0.867	3.986
10	0.283	14.37	27.93	1.198	3.929	2.030	0.456	5.459	1.531	3.928
11	0.304	15.39	29.92	1.283	4.208	2.404	0.540	5.635	1.760	3.875
12	0.115	5.81	11.29	0.484	1.588	0.321	0.072	5.279	0.536	4.744
13	0.134	6.81	13.25	0.568	1.863	0.423	0.095	5.065	0.482	4.583
14	0.155	7.84	15.24	0.653	2.143	0.532	0.120	4.813	0.365	4.448
15	0.174	8.83	17.17	0.736	2.415	0.691	0.155	4.920	0.583	4.337
16	0.195	9.86	19.18	0.822	2.697	0.847	0.190	4.833	0.594	4.239
17	0.216	10.93	21.25	0.911	2.989	1.046	0.235	4.861	0.711	4.151
18	0.234	11.87	23.08	0.989	3.246	1.261	0.284	4.968	0.887	4.081
19	0.254	12.89	25.05	1.074	3.523	1.501	0.337	5.020	1.005	4.015
20	0.274	13.90	27.02	1.159	3.801	1.809	0.407	5.198	1.244	3.954
21	0.294	14.91	28.99	1.243	4.077	2.211	0.497	5.521	1.622	3.899
22	0.223	11.29	21.94	0.941	3.086	1.133	0.255	4.940	0.817	4.124
23	0.264	13.40	26.05	1.117	3.664	1.625	0.365	5.026	1.043	3.983
24	0.284	14.41	28.02	1.201	3.941	2.039	0.459	5.451	1.525	3.926
25	0.296	15.03	29.21	1.252	4.108	2.254	0.507	5.545	1.652	3.893

TABLE 4 - UNFAIRED RESISTANCE DATA FOR THE SMALL MODEL B WITHOUT STUDS

ITTC MODEL-SHIP CORRELATION LINE USED FOR CR, CFM VALUES

LENGTH 1.820 M 5.97 FT — DENSITY 997.4 KG/M^3 1.9352 SLUGS/FT^3

WETTED SURFACE 0.505 M^2 5.436 FT^2 — KINEMATIC VISCOSITY 0.9307E-6 M^2/S 1.0018E-5 FT^2/S

POINT	FROUDE NUMBER	VS (M/S)	VS (KNOTS)	VM (M/S)	VM (FT/SEC)	RTM (N)	RTM (LBS)	CTM *1000	CR *1000	CFM *1000
1	0.112	5.67	11.02	0.472	1.550	0.277	0.062	4.930	0.161	4.769
2	0.112	5.69	11.06	0.474	1.556	0.265	0.060	4.672	-0.093	4.765
3	0.132	6.68	12.99	0.557	1.827	0.389	0.088	4.984	0.382	4.602
4	0.133	6.72	13.06	0.560	1.837	0.383	0.086	4.851	0.254	4.596
5	0.152	7.72	15.00	0.643	2.110	0.467	0.105	4.484	0.021	4.462
6	0.153	7.74	15.04	0.645	2.116	0.479	0.108	4.577	0.118	4.460
7	0.172	8.70	16.91	0.725	2.378	0.620	0.139	4.683	0.332	4.352
8	0.171	8.68	16.87	0.723	2.373	0.166	0.037	1.253	-3.101	4.353
9	0.193	9.80	19.05	0.817	2.680	0.800	0.180	4.762	0.517	4.248
10	0.212	10.76	20.92	0.897	2.942	0.915	0.206	4.520	0.356	4.164
11	0.233	11.81	22.95	0.984	3.228	1.112	0.250	4.560	0.473	4.086
12	0.252	12.80	24.88	1.066	3.499	1.298	0.292	4.533	0.513	4.020
13	0.275	13.92	27.06	1.160	3.806	1.675	0.377	4.943	0.990	3.953
14	0.295	14.96	29.08	1.247	4.090	2.158	0.485	5.513	1.616	3.897
15	0.102	5.18	10.06	0.431	1.415	0.215	0.048	4.586	-0.279	4.866
16	0.103	5.22	10.15	0.435	1.428	0.215	0.048	4.503	-0.353	4.856
17	0.123	6.22	12.09	0.518	1.701	0.299	0.067	4.416	-0.258	4.673
18	0.123	6.25	12.14	0.521	1.708	0.293	0.066	4.288	-0.381	4.669
19	0.143	7.23	14.05	0.602	1.976	0.433	0.097	4.738	0.213	4.525
20	0.143	7.25	14.10	0.604	1.983	0.448	0.101	4.873	0.352	4.522
21	0.162	8.19	15.93	0.683	2.240	0.536	0.120	4.562	0.156	4.406
22	0.162	8.21	15.96	0.684	2.245	0.501	0.113	4.251	-0.153	4.404
23	0.182	9.24	17.95	0.770	2.525	0.750	0.169	5.031	0.733	4.297
24	0.182	9.24	17.97	0.770	2.527	0.694	0.156	4.647	0.351	4.297
25	0.203	10.28	19.98	0.856	2.810	0.869	0.195	4.702	0.499	4.203
26	0.223	11.28	21.93	0.940	3.085	1.012	0.228	4.545	0.421	4.124
27	0.242	12.29	23.89	1.024	3.360	1.189	0.267	4.503	0.450	4.053
28	0.264	13.41	26.06	1.117	3.665	1.488	0.335	4.736	0.753	3.983
29	0.285	14.44	28.07	1.203	3.948	1.946	0.438	5.336	1.412	3.924
30	0.305	15.46	30.05	1.288	4.227	2,373	0.533	5.676	1.804	3.872
31	0.203	10.27	19.97	0.856	2.809	0.844	0.190	4.571	0.367	4.204
32	0.162	8.23	15.99	0.685	2.249	0.582	0.131	4.920	0.517	4.403
33	0.163	8.25	16.03	0.687	2.255	0.564	0.127	4.737	0.337	4.400
34	0.265	13.42	26.09	1.118	3.669	1.538	0.346	4.884	0.902	3.982
35	0.286	14.48	28.15	1.207	3.960	1.980	0.445	5.397	1.476	3.922
36	0.255	12.91	25.09	1.076	3.529	1.314	0.295	4.510	0.496	4.013

TABLE 5 - UNFAIRED RESISTANCE DATA FOR THE SMALL MODEL B WITH STUDS

ITTC MODEL-SHIP CORRELATION LINE USED FOR CR, CFM VALUES

LENGTH 1.820 M 5.97 FT DENSITY 997.4 KG/M^3 1.9352 SLUGS/FT^3

WETTED SURFACE 0.505 M^2 5.436 FT^2 KINEMATIC VISCOSITY 0.9307E-6 M^2/S 1.0018E-5 FT^2/S

POINT	FROUDE NUMBER	VS (M/S)	VS (KNOTS)	VM (M/S)	VM (FT/SEC)	RTM (N)	RTM (LBS)	CTM *1000	CR *1000	CFM *1000
1	0.104	5.27	10.24	0.439	1.440	0.230	0.052	4.749	-0.098	4.847
2	0.125	6.36	12.36	0.530	1.738	0.342	0.077	4.846	0.195	4.652
3	0.146	7.38	14.35	0.615	2.018	0.476	0.107	5.000	0.495	4.505
4	0.166	8.41	16.35	0.701	2.300	0.588	0.132	4.755	0.373	4.382
5	0.185	9.39	18.25	0.782	2.567	0.744	0.167	4.827	0.544	4.283
6	0.206	10.43	20.27	0.869	2.851	0.909	0.204	4.781	0.590	4.191
7	0.225	11.43	22.22	0.953	3.125	1.099	0.247	4.811	0.697	4.113
8	0.246	12.46	24.22	1.038	3.407	1.289	0.290	4.747	0.705	4.042
9	0.265	13.45	26.14	1.121	3.677	1.541	0.347	4.872	0.892	3.980
10	0.285	14.47	28.13	1.206	3.957	2.061	0.463	5.627	1.704	3.922
11	0.303	15.36	29.86	1.280	4.200	2.429	0.546	5.885	2.008	3.876
12	0.116	5.87	11.41	0.489	1.605	0.299	0.067	4.960	0.227	4.733
13	0.136	6.89	13.40	0.575	1.885	0.414	0.093	4.981	0.410	4.571
14	0.156	7.92	15.39	0.660	2.164	0.545	0.123	4.973	0.535	4.439
15	0.176	8.92	17.33	0.743	2.438	0.694	0.156	4.993	0.664	4.329
16	0.196	9.95	19.34	0.829	2.720	0.844	0.190	4.875	0.643	4.232
17	0.216	10.97	21.32	0.914	2.998	1.015	0.228	4.827	0.679	4.148
18	0.236	11.96	23.25	0.997	3.270	1.208	0.272	4.829	0.754	4.075
19	0.256	12.98	25.24	1.082	3.550	1.432	0.322	4.858	0.849	4.008
20	0.278	14.08	27.37	1.173	3.850	1.837	0.413	5.297	1.353	3.944
21	0.295	14.97	29.09	1.247	4.092	2.292	0.515	5.850	1.953	3.896
22	0.266	13.49	26.23	1.124	3.689	1.622	0.365	5.095	1.117	3.978

TABLE 6 - UNFAIRED RESISTANCE DATA FOR THE SMALL MODEL D WITHOUT STUDS

ITTC MODEL-SHIP CORRELATION LINE USED FOR CR, CFM VALUES

LENGTH 1.820 M 5.97 FT — DENSITY 997.4 KG/M^3 1.9352 SLUGS/FT^3

WETTED SURFACE 0.512 M^2 5.514 FT^2 — KINEMATIC VISCOSITY 0.9307E-6 M^2/S 1.0018E-5 FT^2/S

POINT	FROUDE NUMBER	VS (M/S)	VS (KNOTS)	VM (M/S)	VM (FT/SEC)	RTM (N)	RTM (LBS)	CTM *1000	CR *1000	CFM *1000
1	0.103	5.23	10.17	0.436	1.431	0.215	0.048	4.421	-0.433	4.854
2	0.123	6.21	12.08	0.518	1.699	0.321	0.072	4.682	0.007	4.675
3	0.143	7.27	14.13	0.606	1.987	0.423	0.095	4.519	0.000	4.520
4	0.163	8.26	16.06	0.689	2.259	0.520	0.117	4.294	-0.105	4.399
5	0.183	9.28	18.03	0.773	2.536	0.663	0.149	4.345	0.052	4.294
6	0.203	10.31	20.04	0.859	2.818	0.797	0.179	4.230	0.029	4.201
7	0.225	11.39	22.14	0.949	3.114	0.956	0.215	4.154	0.038	4.116
8	0.245	12.41	24.12	1.034	3.392	1.168	0.263	4.276	0.231	4.045
9	0.263	13.35	25.96	1.113	3.651	1.485	0.334	4.695	0.709	3.988
10	0.284	14.38	27.96	1.198	3.932	1.974	0.444	5.360	1.453	3.927
11	0.306	15.51	30.15	1.292	4.240	2.404	0.540	5.634	1.765	3.869
12	0.115	5.81	11.29	0.484	1.588	0.290	0.065	4.839	0.095	4.744
13	0.134	6.82	13.25	0.568	1.864	0.392	0.088	4.758	0.176	4.582
14	0.154	7.83	15.22	0.652	2.140	0.476	0.107	4.383	-0.066	4.449
15	0.174	8.80	17.11	0.734	2.407	0.588	0.132	4.280	-0.060	4.341
16	0.194	9.82	19.09	0.818	2.685	0.735	0.165	4.295	0.052	4.243
17	0.214	10.86	21.11	0.905	2.969	0.872	0.196	4.167	0.011	4.156
18	0.235	11.92	23.18	0.994	3.260	1.087	0.244	4.308	0.231	4.078
19	0.254	12.86	24.99	1.071	3.515	1.323	0.298	4.513	0.497	4.016
20	0.274	13.89	27.00	1.157	3.797	1.737	0.391	5.078	1.123	3.955
21	0.293	14.88	28.92	1.240	4.068	2.232	0.502	5.685	1.783	3.901
22	0.244	12.37	24.04	1.031	3.381	1.183	0.266	4.361	0.313	4.048
23	0.284	14.40	27.98	1.200	3.936	1.990	0.447	5.412	1.485	3.927
24	0.306	15.51	30.15	1.292	4.240	2.404	0.540	5.634	1.765	3.869
25	0.234	11.85	23.04	0.988	3.241	1.093	0.246	4.384	0.301	4.083
26	0.225	11.40	22.17	0.950	3.118	0.950	0.214	4.116	0.001	4.115

TABLE 7 - UNFAIRED RESISTANCE DATA FOR THE SMALL MODEL D WITH STUDS

ITTC MODEL-SHIP CORRELATION LINE USED FOR CR, CFM VALUES

LENGTH 1.820 M 5.97 FT — DENSITY 997.4 KG/M^3 1.9352 SLUGS/FT^3

WETTED SURFACE 0.512 M^2 5.514 FT^2 — KINEMATIC VISCOSITY 0.9307E-6 M^2/S 1.0018E-5 FT^2/S

POINT	FROUDE NUMBER	VS (M/S)	VS (KNOTS)	VM (M/S)	VM (FT/SEC)	RTM (N)	RTM (LBS)	CTM *1000	CR *1000	CFM *1000
1	0.105	5.34	10.37	0.445	1.459	0.252	0.057	4.992	0.160	4.833
2	0.124	6.29	12.23	0.524	1.720	0.346	0.078	4.923	0.261	4.662
3	0.145	7.34	14.27	0.612	2.007	0.461	0.104	4.821	0.310	4.510
4	0.164	8.30	16.13	0.691	2.268	0.567	0.127	4.642	0.247	4.395
5	0.183	9.30	18.07	0.775	2.542	0.719	0.162	4.690	0.399	4.291
6	0.196	9.95	19.33	0.829	2.719	0.816	0.183	4.650	0.418	4.232
7	0.225	11.42	22.20	0.952	3.122	1.062	0.239	4.590	0.476	4.114
8	0.236	11.99	23.30	0.999	3.277	1.193	0.268	4.679	0.606	4.074
9	0.263	12.84	24.96	1.070	3.510	1.426	0.321	4.877	0.860	4.018
10	0.273	13.87	26.95	1.155	3.791	1.812	0.407	5.313	1.357	3.956
11	0.293	14.85	28.87	1.238	4.061	2.282	0.513	5.831	1.929	3.902
12	0.115	5.85	11.37	0.487	1.599	0.302	0.068	4.977	0.241	4.737
13	0.135	6.83	13.27	0.569	1.866	0.392	0.088	4.748	0.167	4.581
14	0.154	7.81	15.19	0.651	2.136	0.529	0.119	4.889	0.438	4.451
15	0.174	8.80	17.10	0.733	2.405	0.654	0.147	4.763	0.422	4.341
16	0.204	10.36	20.14	0.863	2.833	0.887	0.200	4.659	0.463	4.196
17	0.216	10.97	21.33	0.914	3.000	0.996	0.224	4.665	0.517	4.147
18	0.244	12.38	24.07	1.032	3.385	1.286	0.289	4.729	0.682	4.047
19	0.264	13.38	26.01	1.115	3.659	1.610	0.362	5.066	1.082	3.984
20	0.283	14.35	27.90	1.196	3.924	2.061	0.463	5.641	1.712	3.929
21	0.305	15.47	30.07	1.289	4.229	2.541	0.571	5.986	2.115	3.871
22	0.154	7.82	15.19	0.651	2.137	0.508	0.114	4.683	0.232	4.450
23	0.226	11.47	22.30	0.956	3.136	1.096	0.246	4.696	0.586	4.110
24	0.236	11.96	23.24	0.996	3.269	1.180	0.265	4.653	0.577	4.076

TABLE 8 – UNFAIRED RESISTANCE DATA FOR THE LARGE MODEL A

ITTC MODEL-SHIP CORRELATION LINE USED FOR CR, CFM VALUES

LENGTH 8.339 M 27.36 FT DENSITY 997.4 KG/M^3 1.9352 SLUGS/FT^3

WETTED SURFACE 10.907 M^2 117.400 FT^2 KINEMATIC VISCOSITY 0.9307E-6 M^2/S 1.0018E-5 FT^2/S

POINT	FROUDE NUMBER	VS (M/S)	VS (KNOTS)	VM (M/S)	VM (FT/SEC)	RTM (N)	RTM (LBS)	CTM *1000	CR *1000	CFM *1000
1	0.103	5.24	10.19	0.935	3.069	15.771	3.546	3.314	0.220	3.094
2	0.103	5.24	10.19	0.935	3.069	16.212	3.645	3.406	0.312	3.094
3	0.123	6.23	12.11	1.111	3.645	21.850	4.912	3.255	0.252	3.002
4	0.123	6.23	12.11	1.111	3.645	22.643	5.091	3.373	0.371	3.002
5	0.143	7.27	14.13	1.297	4.254	29.339	6.596	3.209	0.285	2.923
6	0.143	7.27	14.14	1.297	4.256	29.868	6.715	3.263	0.340	2.923
7	0.164	8.30	16.13	1.480	4.855	38.150	8.577	3.203	0.345	2.858
8	0.164	8.30	16.13	1.480	4.855	38.414	8.636	3.225	0.367	2.858
9	0.183	9.29	18.06	1.657	5.436	48.194	10.835	3.228	0.424	2.804
10	0.183	9.29	18.06	1.657	5.436	48.811	10.974	3.269	0.465	2.804
11	0.205	10.38	20.17	1.851	6.073	61.850	13.905	3.319	0.566	2.753
12	0.205	10.37	20.17	1.850	6.071	61.057	13.727	3.279	0.526	2.753
13	0.225	11.40	22.17	2.034	6.673	75.683	17.015	3.364	0.654	2.710
14	0.225	11.40	22.16	2.033	6.671	75.331	16.936	3.350	0.640	2.710
15	0.245	12.43	24.16	2.217	7.272	92.423	20.779	3.459	0.787	2.672
16	0.245	12.43	24.16	2.217	7.274	91.806	20.640	3.434	0.762	2.672
17	0.266	13.50	26.23	2.407	7.897	114.450	25.731	3.632	0.996	2.636
18	0.266	13.50	26.23	2.407	7.897	114.185	25.671	3.624	0.987	2.636
19	0.266	13.50	26.23	2.407	7.897	115.419	25.948	3.663	1.027	2.636
20	0.285	14.46	28.10	2.578	8.459	146.785	33.000	4.060	1.453	2.607
21	0.285	14.46	28.11	2.579	8.461	146.696	32.980	4.056	1.449	2.607
22	0.285	14.46	28.10	2.578	8.459	146.785	33.000	4.060	1.453	2.607
23	0.306	15.49	30.11	2.763	9.064	179.912	40.448	4.334	1.756	2.578
24	0.305	15.49	30.10	2.762	9.062	180.089	40.488	4.340	1.762	2.578
25	0.113	5.72	11.12	1.020	3.346	19.471	4.378	3.442	0.394	3.048
26	0.113	5.72	11.12	1.020	3.346	18.590	4.179	3.286	0.239	3.048
27	0.133	6.76	13.13	1.205	3.954	26.256	5.903	3.324	0.363	2.960
28	0.133	6.76	13.14	1.205	3.955	26.696	6.002	3.378	0.417	2.960
29	0.154	7.79	15.15	1.390	4.560	33.921	7.626	3.229	0.340	2.889
30	0.154	7.79	15.15	1.390	4.560	34.802	7.824	3.312	0.424	2.889
31	0.173	8.79	17.08	1.567	5.141	43.436	9.765	3.253	0.422	2.831
32	0.173	8.78	17.07	1.566	5.139	43.612	9.805	3.268	0.437	2.831
33	0.194	9.85	19.14	1.756	5.761	55.859	12.558	3.331	0.554	2.777
34	0.194	9.84	19.13	1.755	5.759	55.947	12.578	3.339	0.561	2.777
35	0.214	10.87	21.12	1.938	6.358	68.899	15.490	3.373	0.641	2.732
36	0.214	10.87	21.12	1.938	6.358	68.723	15.450	3.365	0.633	2.732
37	0.235	11.92	23.18	2.127	6.978	84.758	19.055	3.445	0.755	2.690
38	0.235	11.92	23.18	2.127	6.977	85.022	19.115	3.457	0.766	2.690
39	0.235	11.92	23.18	2.127	6.978	84.317	18.956	3.427	0.737	2.690
40	0.256	12.96	25.19	2.311	7.583	102.115	22.957	3.515	0.861	2.654
41	0.256	12.96	25.18	2.311	7.581	101.586	22.839	3.498	0.844	2.654
42	0.275	13.96	27.13	2.489	8.166	129.340	29.078	3.839	1.217	2.622
43	0.275	13.96	27.13	2.489	8.166	129.868	29.197	3.854	1.232	2.622
44	0.194	9.84	19.13	1.755	5.759	55.771	12.538	3.328	0.551	2.777
45	0.194	9.84	19.12	1.755	5.757	55.947	12.578	3.341	0.563	2.777

TABLE 8 - UNFAIRED RESISTANCE DATA FOR THE LARGE MODEL A (CONTINUED)

ITTC MODEL-SHIP CORRELATION LINE USED FOR CR, CFM VALUES

LENGTH 8.339 M 27.36 FT DENSITY 997.4 KG/M^3 1.9352 SLUGS/FT^3

WETTED SURFACE 10.907 M^2 117.400 FT^2 KINEMATIC VISCOSITY 0.9307E-6 M^2/S 1.0018E-5 FT^2/S

POINT	FROUDE NUMBER	VS (M/S)	VS (KNOTS)	VM (M/S)	VM (FT/SEC)	RTM (N)	RTM (LBS)	CTM *1000	CR *1000	CFM *1000
46	0.235	11.91	23.16	2.125	6.972	84.758	19.055	3.451	0.760	2.691
47	0.235	11.91	23.16	2.125	6.972	85.022	19.115	3.462	0.771	2.691
48	0.295	14.98	29.11	2.671	8.763	167.049	37.556	4.305	1.713	2.592
49	0.295	14.98	29.11	2.671	8.763	164.934	37.081	4.251	1.659	2.592
50	0.183	9.28	18.04	1.655	5.431	49.692	11.172	3.334	0.530	2.805

TABLE 9 - UNFAIRED RESISTANCE DATA FOR THE LARGE MODEL B

ITTC MODEL-SHIP CORRELATION LINE USED FOR CR, CFM VALUES

LENGTH 8.339 M 27.36 FT DENSITY 997.4 KG/M^3 1.9352 SLUGS/FT^3

WETTED SURFACE 10.597 M^2 114.070 FT^2 KINEMATIC VISCOSITY 0.9307E-6 M^2/S 1.0018E-5 FT^2/S

POINT	FROUDE NUMBER	VS (M/S)	VS (KNOTS)	VM (M/S)	VM (FT/SEC)	RTM (N)	RTM (LBS)	CTM *1000	CR *1000	CFM *1000
1	0.103	5.23	10.17	0.933	3.062	16.388	3.684	3.560	0.465	3.095
2	0.103	5.23	10.16	0.933	3.060	15.419	3.466	3.354	0.258	3.096
3	0.122	6.21	12.07	1.108	3.634	21.762	4.893	3.357	0.353	3.004
4	0.123	6.21	12.08	1.108	3.636	22.203	4.992	3.421	0.417	3.004
5	0.143	7.25	14.09	1.293	4.242	30.220	6.794	3.421	0.496	2.925
6	0.143	7.25	14.09	1.293	4.242	28.987	6.517	3.281	0.356	2.925
7	0.143	7.25	14.09	1.293	4.242	28.811	6.477	3.261	0.336	2.925
8	0.163	8.27	16.08	1.476	4.842	37.974	8.537	3.299	0.440	2.860
9	0.163	8.27	16.08	1.476	4.842	38.326	8.616	3.330	0.470	2.860
10	0.183	9.27	18.02	1.654	5.425	45.903	10.320	3.177	0.372	2.805
11	0.183	9.27	18.02	1.654	5.426	45.991	10.340	3.182	0.377	2.805
12	0.204	10.36	20.13	1.847	6.060	57.886	13.014	3.211	0.457	2.754
13	0.204	10.36	20.13	1.847	6.060	58.150	13.073	3.225	0.472	2.754
14	0.225	11.38	22.13	2.030	6.661	69.956	15.728	3.212	0.501	2.711
15	0.225	11.38	22.13	2.030	6.661	70.573	15.866	3.240	0.529	2.711
16	0.225	11.38	22.13	2.030	6.661	69.516	15.629	3.191	0.480	2.711
17	0.245	12.41	24.12	2.213	7.262	85.022	19.115	3.284	0.611	2.673
18	0.245	12.41	24.12	2.213	7.262	84.317	18.956	3.257	0.584	2.673
19	0.266	13.47	26.18	2.402	7.882	110.221	24.780	3.614	0.977	2.637
20	0.266	13.47	26.19	2.403	7.884	111.278	25.018	3.647	1.010	2.637
21	0.285	14.45	28.09	2.577	8.456	145.815	32.782	4.154	1.547	2.607
22	0.285	14.45	28.09	2.577	8.456	146.168	32.861	4.164	1.557	2.607
23	0.285	14.45	28.08	2.577	8.454	146.344	32.901	4.171	1.564	2.607
24	0.163	8.28	16.09	1.476	4.844	37.269	8.379	3.235	0.376	2.859
25	0.163	8.28	16.09	1.476	4.844	38.062	8.557	3.304	0.445	2.859
26	0.305	15.47	30.07	2.759	9.052	185.816	41.775	4.619	2.040	2.579
27	0.305	15.47	30.07	2.759	9.052	186.873	42.013	4.645	2.067	2.579
28	0.113	5.71	11.10	1.018	3.341	19.031	4.279	3.473	0.424	3.048
29	0.113	5.71	11.09	1.018	3.339	19.207	4.318	3.509	0.460	3.049
30	0.133	6.75	13.12	1.204	3.949	25.110	5.645	3.280	0.319	2.961
31	0.133	6.75	13.12	1.204	3.949	24.846	5.586	3.245	0.284	2.961
32	0.153	7.78	15.11	1.387	4.550	33.040	7.428	3.251	0.361	2.890
33	0.153	7.77	15.11	1.386	4.548	34.626	7.785	3.410	0.520	2.890
34	0.173	8.77	17.04	1.563	5.129	42.996	9.666	3.329	0.497	2.832
35	0.173	8.77	17.04	1.563	5.129	42.820	9.627	3.315	0.484	2.832
36	0.194	9.83	19.11	1.754	5.754	51.366	11.548	3.160	0.382	2.778
37	0.194	9.83	19.11	1.754	5.754	52.854	11.885	3.252	0.475	2.778
38	0.214	10.86	21.10	1.936	6.353	63.172	14.202	3.188	0.456	2.732
39	0.214	10.86	21.10	1.936	6.352	62.908	14.143	3.176	0.443	2.732
40	0.235	11.91	23.16	2.125	6.972	77.357	17.391	3.242	0.551	2.691
41	0.235	11.91	23.15	2.124	6.970	77.357	17.391	3.243	0.553	2.691
42	0.255	12.94	25.16	2.309	7.574	96.476	21.690	3.426	0.771	2.654
43	0.255	12.95	25.17	2.309	7.576	96.212	21.630	3.414	0.760	2.654
44	0.275	13.94	27.11	2.487	8.160	127.225	28.603	3.892	1.270	2.622
45	0.275	13.94	27.10	2.487	8.159	127.842	28.741	3.912	1.289	2.622

TABLE 9 - UNFAIRED RESISTANCE DATA FOR THE LARGE MODEL B (CONTINUED)

ITTC MODEL-SHIP CORRELATION LINE USED FOR CR, CFM VALUES

LENGTH 8.339 M 27.36 FT DENSITY 997.4 KG/M^3 1.9352 SLUGS/FT^3

WETTED SURFACE 10.597 M^2 114.070 FT^2 KINEMATIC VISCOSITY 0.9307E-6 M^2/S 1.0018E-5 FT^2/S

POINT	FROUDE NUMBER	VS (M/S)	VS (KNOTS)	VM (M/S)	VM (FT/SEC)	RTM (N)	RTM (LBS)	CTM *1000	CR *1000	CFM *1000
46	0.275	13.95	27.11	2.488	8.162	125.992	28.325	3.852	1.230	2.622
47	0.245	12.41	24.12	2.213	7.262	86.961	19.550	3.359	0.686	2.673
48	0.245	12.42	24.13	2.214	7.265	86.696	19.491	3.346	0.673	2.672
49	0.245	12.41	24.12	2.213	7.262	85.903	19.313	3.318	0.645	2.673
50	0.295	14.97	29.09	2.669	8.757	168.723	37.932	4.482	1.889	2.592
51	0.295	14.96	29.08	2.668	8.753	167.137	37.576	4.444	1.851	2.593
52	0.173	8.77	17.05	1.564	5.132	42.467	9.547	3.284	0.453	2.832
53	0.173	8.77	17.04	1.564	5.131	41.850	9.409	3.238	0.406	2.832
54	0.173	8.77	17.05	1.564	5.132	40.705	9.151	3.148	0.317	2.832
55	0.214	10.85	21.09	1.935	6.350	63.613	14.301	3.213	0.481	2.732
56	0.214	10.85	21.09	1.935	6.350	64.053	14.400	3.236	0.503	2.732
57	0.214	10.85	21.09	1.935	6.350	65.022	14.618	3.285	0.552	2.732
58	0.214	10.86	21.10	1.936	6.353	63.789	14.341	3.219	0.487	2.732

TABLE 10 - UNFAIRED RESISTANCE DATA FOR THE LARGE MODEL D

ITTC MODEL-SHIP CORRELATION LINE USED FOR CR, CFM VALUES

LENGTH 8.339 M 27.36 FT DENSITY 997.4 KG/M^3 1.9352 SLUGS/FT^3

WETTED SURFACE 10.749 M^2 115.700 FT^2 KINEMATIC VISCOSITY 0.9307E-6 M^2/S 1.0018E-5 FT^2/S

POINT	FROUDE NUMBER	VS (M/S)	VS (KNOTS)	VM (M/S)	VM (FT/SEC)	RTM (N)	RTM (LBS)	CTM *1000	CR *1000	CFM *1000
1	0.103	5.24	10.18	0.934	3.065	14.273	3.209	3.051	-0.044	3.095
2	0.103	5.24	10.18	0.934	3.065	14.537	3.268	3.108	0.013	3.095
3	0.123	6.22	12.09	1.109	3.639	20.264	4.556	3.073	0.070	3.003
4	0.123	6.22	12.09	1.109	3.638	21.145	4.754	3.208	0.205	3.003
5	0.143	7.26	14.10	1.294	4.246	28.018	6.299	3.121	0.197	2.924
6	0.143	7.26	14.10	1.294	4.246	27.930	6.279	3.111	0.187	2.924
7	0.163	8.28	16.09	1.477	4.845	35.947	8.082	3.075	0.216	2.859
8	0.163	8.28	16.09	1.477	4.845	36.133	8.121	3.090	0.231	2.859
9	0.183	9.27	18.02	1.654	5.426	45.727	10.280	3.119	0.314	2.805
10	0.183	9.28	18.04	1.655	5.430	45.903	10.320	3.126	0.322	2.805
11	0.204	10.36	20.14	1.848	6.063	56.828	12.776	3.105	0.351	2.754
12	0.204	10.36	20.14	1.848	6.063	55.947	12.578	3.056	0.303	2.754
13	0.225	11.38	22.13	2.031	6.662	70.661	15.886	3.197	0.486	2.711
14	0.225	11.39	22.14	2.031	6.664	70.220	15.787	3.175	0.465	2.711
15	0.245	12.42	24.13	2.214	7.265	86.696	19.491	3.299	0.626	2.672
16	0.245	12.42	24.13	2.214	7.265	86.432	19.432	3.289	0.616	2.672
17	0.266	13.48	26.20	2.404	7.887	113.304	25.473	3.658	1.021	2.637
18	0.266	13.48	26.20	2.404	7.887	113.481	25.513	3.664	1.027	2.637
19	0.285	14.45	28.08	2.576	8.453	154.274	34.684	4.336	1.729	2.607
20	0.285	14.45	28.08	2.577	8.454	153.745	34.565	4.320	1.713	2.607
21	0.305	15.47	30.08	2.760	9.054	191.983	43.162	4.703	2.125	2.579
22	0.305	15.48	30.08	2.760	9.056	191.983	43.162	4.701	2.123	2.578
23	0.113	5.71	11.10	1.018	3.341	17.269	3.882	3.107	0.058	3.048
24	0.113	5.71	11.09	1.018	3.339	17.533	3.942	3.158	0.109	3.049
25	0.133	6.75	13.12	1.204	3.950	23.877	5.368	3.073	0.112	2.961
26	0.133	6.75	13.12	1.204	3.949	24.934	5.606	3.211	0.250	2.961
27	0.153	7.78	15.11	1.387	4.550	31.806	7.151	3.085	0.195	2.890
28	0.153	7.78	15.11	1.387	4.550	31.630	7.111	3.068	0.178	2.890
29	0.173	8.77	17.05	1.564	5.132	41.057	9.231	3.131	0.299	2.832
30	0.173	8.77	17.05	1.564	5.132	40.881	9.191	3.117	0.286	2.832
31	0.194	9.84	19.12	1.755	5.757	50.749	11.409	3.075	0.298	2.777
32	0.194	9.84	19.12	1.755	5.757	51.542	11.588	3.123	0.346	2.777
33	0.214	10.86	21.11	1.937	6.355	62.027	13.945	3.084	0.352	2.732
34	0.214	10.86	21.11	1.937	6.355	62.731	14.103	3.119	0.387	2.732
35	0.235	11.92	23.16	2.125	6.973	77.181	17.352	3.188	0.497	2.691
36	0.235	11.92	23.16	2.125	6.973	77.974	17.530	3.220	0.530	2.691
37	0.255	12.95	25.17	2.310	7.578	97.974	22.026	3.426	0.772	2.654
38	0.256	12.96	25.18	2.311	7.581	97.798	21.987	3.417	0.763	2.654
39	0.275	13.95	27.11	2.488	8.162	132.159	29.712	3.984	1.362	2.622
40	0.275	13.95	27.11	2.488	8.162	132.776	29.851	4.003	1.380	2.622
41	0.225	11.39	22.13	2.030	6.661	70.044	15.747	3.170	0.459	2.711
42	0.225	11.38	22.13	2.030	6.661	70.925	15.945	3.210	0.499	2.711
43	0.225	11.38	22.13	2.031	6.662	71.013	15.965	3.213	0.502	2.711
44	0.295	14.98	29.12	2.672	8.765	174.097	39.141	4.551	1.959	2.592
45	0.295	14.98	29.11	2.671	8.762	175.507	39.458	4.590	1.998	2.592
46	0.295	14.97	29.11	2.671	8.762	175.067	39.358	4.579	1.987	2.592

TABLE 11 - UNFAIRED RESISTANCE DATA FOR THE SMALL MODEL B WITHOUT STUDS FROM THE DL/SIT EXPERIMENTS

ITTC MODEL-SHIP CORRELATION LINE USED FOR CR, CFM VALUES

LENGTH 1.820 M 5.97 FT DENSITY 998.0 KG/M^3 1.9365 SLUGS/FT^3

WETTED SURFACE 0.505 M^2 5.436 FT^2 KINEMATIC VISCOSITY 0.9933E-6 M^2/S 1.0692E-5 FT^2/S

POINT	FROUDE NUMBER	VS (M/S)	VS (KNOTS)	VM (M/S)	VM (FT/SEC)	RTM (N)	RTM (LBS)	CTM *1000	CR *1000	CFM *1000
1	0.061	3.08	5.99	0.257	0.843	0.071	0.016	4.276	-1.282	5.560
2	0.071	3.60	7.00	0.300	0.984	0.089	0.020	3.924	-1.437	5.362
3	0.081	4.11	8.00	0.343	1.125	0.125	0.028	4.203	-0.996	5.199
4	0.091	4.63	8.99	0.386	1.265	0.142	0.032	3.799	-1.263	5.062
5	0.101	5.14	10.00	0.429	1.406	0.214	0.048	4.613	-0.330	4.944
6	0.112	5.65	10.99	0.471	1.546	0.245	0.055	4.372	-0.469	4.841
7	0.122	6.17	11.99	0.514	1.687	0.316	0.071	4.740	-0.009	4.749
8	0.132	6.68	12.99	0.557	1.827	0.360	0.081	4.610	-0.057	4.667
9	0.142	7.19	13.99	0.600	1.967	0.431	0.097	4.763	0.170	4.593
10	0.142	7.20	14.00	0.600	1.969	0.405	0.091	4.459	-0.133	4.592
11	0.152	7.71	14.99	0.643	2.108	0.489	0.110	4.703	0.178	4.526
12	0.162	8.23	16.00	0.686	2.250	0.538	0.121	4.541	0.078	4.463
13	0.172	8.74	16.99	0.728	2.389	0.614	0.138	4.594	0.187	4.407
14	0.182	9.25	17.98	0.771	2.529	0.685	0.154	4.575	0.220	4.355
15	0.193	9.77	18.99	0.814	2.671	0.796	0.179	4.767	0.462	4.305
16	0.203	10.28	19.98	0.856	2.810	0.867	0.195	4.692	0.432	4.260
17	0.203	10.29	19.99	0.857	2.812	0.845	0.190	4.565	0.306	4.260
18	0.213	10.80	21.00	0.900	2.953	0.943	0.212	4.619	0.402	4.217
19	0.223	11.31	21.99	0.943	3.093	1.027	0.231	4.588	0.411	4.177
20	0.233	11.83	23.00	0.986	3.235	1.116	0.251	4.557	0.418	4.139
21	0.243	12.34	23.99	1.028	3.374	1.228	0.276	4.606	0.503	4.103
22	0.254	12.86	24.99	1.071	3.515	1.339	0.301	4.629	0.559	4.070
23	0.263	13.36	25.97	1.113	3.652	1.499	0.337	4.801	0.762	4.038
24	0.274	13.89	27.00	1.157	3.797	1.695	0.381	5.021	1.014	4.007
25	0.284	14.39	27.97	1.199	3.934	1.930	0.434	5.328	1.350	3.978

TABLE 12 - UNFAIRED RESISTANCE DATA FOR THE SMALL MODEL B WITH STUDS FROM THE DL/SIT EXPERIMENTS

ITTC MODEL-SHIP CORRELATION LINE USED FOR CR, CFM VALUES

LENGTH 1.820 M 5.97 FT DENSITY 998.0 KG/M^3 1.9365 SLUGS/FT^3

WETTED SURFACE 0.505 M^2 5.436 FT^2 KINEMATIC VISCOSITY 0.9933E-6 M^2/S 1.0692E-5 FT^2/S

POINT	FROUDE NUMBER	VS (M/S)	VS (KNOTS)	VM (M/S)	VM (FT/SEC)	RTM (N)	RTM (LBS)	CTM *1000	CR -1000	CFM *1000
1	0.061	3.08	5.99	0.257	0.843	0.071	0.016	4.278	-1.282	5.560
2	0.071	3.60	7.00	0.300	0.984	0.107	0.024	4.709	-0.652	5.362
3	0.081	4.11	8.00	0.343	1.125	0.129	0.029	4.353	-0.845	5.199
4	0.091	4.63	8.99	0.386	1.265	0.178	0.040	4.749	-0.313	5.062
5	0.101	5.14	10.00	0.429	1.406	0.227	0.051	4.902	-0.042	4.944
6	0.112	5.65	10.99	0.471	1.546	0.271	0.061	4.849	0.008	4.841
7	0.122	6.17	11.99	0.514	1.686	0.338	0.076	5.080	0.330	4.749
8	0.122	6.17	11.99	0.514	1.687	0.316	0.071	4.740	-0.009	4.749
9	0.132	6.69	13.00	0.557	1.828	0.378	0.085	4.833	0.166	4.666
10	0.142	7.19	13.99	0.600	1.967	0.436	0.098	4.812	0.219	4.593
11	0.152	7.71	14.99	0.643	2.108	0.641	0.144	6.157	1.631	4.526
12	0.162	8.23	15.99	0.685	2.249	0.578	0.130	4.883	0.419	4.464
13	0.172	8.74	16.99	0.728	2.390	0.645	0.145	4.823	0.416	4.407
14	0.183	9.25	17.99	0.771	2.530	0.738	0.166	4.927	0.573	4.354
15	0.193	9.76	18.98	0.814	2.669	0.801	0.180	4.801	0.495	4.306
16	0.193	9.77	19.00	0.814	2.672	0.814	0.183	4.870	0.565	4.305
17	0.203	10.30	20.01	0.858	2.815	0.903	0.203	4.867	0.608	4.259
18	0.213	10.80	20.99	0.900	2.952	0.983	0.221	4.818	0.601	4.217
19	0.223	11.31	21.98	0.942	3.092	1.081	0.243	4.829	0.652	4.177
20	0.233	11.83	22.99	0.985	3.233	1.183	0.266	4.835	0.696	4.139
21	0.243	12.34	23.99	1.028	3.374	1.281	0.288	4.807	0.703	4.103
22	0.253	12.85	24.97	1.070	3.512	1.401	0.315	4.852	0.782	4.070
23	0.264	13.37	25.99	1.114	3.655	1.557	0.350	4.978	0.940	4.038
24	0.274	13.87	26.96	1.156	3.792	1.757	0.395	5.219	1.211	4.008
25	0.284	14.40	28.00	1.200	3.938	2.010	0.452	5.538	1.560	3.978

TABLE 13

RESULTS FROM THE SMALL MODEL REPEATABILITY EXPERIMENTS

95% Confidence Level

Froude Number	0.18	0.24	0.28
	Range of Mean	Range of Mean	Range of Mean
Model A	± 0.96 %	± 0.79 %	± 1.07 %
Model B* (Initial Experiment)	± 0.78 %	± 0.87 %	± 1.07 %
Model D	± 0.73 %	± 1.05 %	± 1.20 %
Model B (Final Experiment)	± 1.35 %	± 0.57 %	± 0.46 %
AVERAGE VALUES	± 0.96 %	± 0.82 %	± 0.95 %
Model B (16 points - initial + final expts)	± 0.90 %	± 0.64 %	± 0.63 %

*Only the first six points (resistance values) were used

Froude Number	0.18	0.24	0.28
	Maximum Excursion from Mean	Maximum Excursion from Mean	Maximum Excursion from Mean
Model A	3.1 %	2.5 %	3.0 %
Model B	2.8 %	3.1 %	2.2%
Model D	2.6 %	3.4 %	3.5 %
AVERAGE VALUES	2.8 %	3.0 %	2.9 %

Maximum excursion from the mean is the maximum difference in the resistance values from the mean resistance value / mean resistance value.

DTNSRDC ISSUES THREE TYPES OF REPORTS

1. DTNSRDC REPORTS, A FORMAL SERIES, CONTAIN INFORMATION OF PERMANENT TECHNICAL VALUE. THEY CARRY A CONSECUTIVE NUMERICAL IDENTIFICATION REGARDLESS OF THEIR CLASSIFICATION OR THE ORIGINATING DEPARTMENT.

2. DEPARTMENTAL REPORTS, A SEMIFORMAL SERIES, CONTAIN INFORMATION OF A PRELIMINARY, TEMPORARY, OR PROPRIETARY NATURE OR OF LIMITED INTEREST OR SIGNIFICANCE. THEY CARRY A DEPARTMENTAL ALPHANUMERICAL IDENTIFICATION.

3. TECHNICAL MEMORANDA, AN INFORMAL SERIES, CONTAIN TECHNICAL DOCUMENTATION OF LIMITED USE AND INTEREST. THEY ARE PRIMARILY WORKING PAPERS INTENDED FOR INTERNAL USE. THEY CARRY AN IDENTIFYING NUMBER WHICH INDICATES THEIR TYPE AND THE NUMERICAL CODE OF THE ORIGINATING DEPARTMENT. ANY DISTRIBUTION OUTSIDE DTNSRDC MUST BE APPROVED BY THE HEAD OF THE ORIGINATING DEPARTMENT ON A CASE-BY-CASE BASIS.

Dup

MIXING-LENGTH FORMULATIONS FOR TURBULENT BOUNDARY LAYERS OVER ARBITRARILY ROUGH SURFACES

By

Paul S. Granville
David W. Taylor Naval Ship R&D Center
Bethesda, Maryland 20084

(Resistance and Flow)

20th American Towing Tank Conference
Davidson Laboratory
Stevens Institute of Technology
Hoboken, New Jersey 07030

August 1983

NOTATION

A = slope of logarithmic velocity law, $A = 1/\kappa$

B_1 = intercept of logarithmic velocity law in Reynolds-number mode

$B_{1,s}$ = value of B_1 for smooth surfaces

B_r = intercept of logarithmic velocity law in relative-roughness mode

$\hat{B}_r$ = value of B_r for fully rough regime

I_1, I_2 = integrals defined by Equation (26)

k = roughness height

$k_1, k_2, \ldots$ = other roughness lengths

k^* = roughness Reynolds number, $k^* = u_\tau k/\nu$

ℓ = mixing length

ℓ^* = nondimensional mixing length, $\ell^* = u_\tau \ell/\nu$

ℓ^*_w = value of ℓ^* at the wall

M = modification function

T = roughness texture, $T = k/k_1, k_1/k_2, \ldots$

u = streamwise velocity component

u^* = nondimensional u, $u^* = u/u_\tau$

u_τ = shear velocity, $u_\tau = \sqrt{\tau_w/\rho}$

y = normal distance from wall

y^* = nondimensional y, $y^* = u_\tau y/\nu$

y_L = laminar sublayer thickness

y_L^* = nondimensional y_L, $y_L^* = u_\tau y_L/\nu$

ΔB = drag characterization, $\Delta B = B_1 - B_{1,s}$

Δy^* = Rotta II shift

κ = von Kármán constant

λ = length factor in modification function

λ^* = nondimensional λ, $\lambda^* = u_\tau \lambda / \nu$

λ^*_h = λ^* for hyperbolic tangent modification function

λ^*_s = λ^*_v for smooth surfaces

λ_v = λ^* for van Driest modification function

ν = kinematic viscosity of fluid

ν_t = turbulent eddy viscosity

τ = shearing stress

τ_l = laminar shearing stress

τ_t = turbulent shearing stress

τ_w = wall shearing stress

ABSTRACT

The drag characterizations for arbitrarily rough surfaces are correlated with the van Driest mixing-length formulation and with the Rotta mixing-length formulation.

INTRODUCTION

The development of turbulent boundary layers over arbitrarily rough surfaces may be predicted by mixing length formulations close to the boundary wall. Existing calculation methods for smooth surfaces using the Prandtl-van Driest wall mixing length may be adapted to arbitrarily rough surfaces. Such are the method of Patankar and Spalding[1], the method of Cebeci and Smith[2] or its subsequent modification by Nituch et al.[3] and the method of Huang et al.[4]

Wall mixing lengths or rather the associated eddy viscosities are also required for heat or mass transfer methods using turbulent Prandtl numbers or turbulent Schmidt numbers to predict the turbulent diffusivities of heat or mass.[5] Furthermore, mixing lengths or eddy viscosities near the wall may be required as boundary conditions to the k-ε transport equations for predictions of the development of turbulent boundary layers.[6] In general, the mixing length increases with distance away from the wall until a limiting value is reached which is compatible to the mixing length for the outer region.

Initially in 1950, Rotta[7] considered the Prandtl wall mixing length for turbulent shear stress to apply only outside the laminar sublayer and was able to correlate the laminar sublayer thickness with the roughness drag characterization. However, subsequent turbulence measurements showed that turbulent shear stresses start at the wall. The concept of a purely laminar sublayer was discarded and the laminar sublayer was renamed the viscous sublayer. For smooth surfaces the van Driest modification to the Prandtl wall mixing-length formulation provided a turbulent shear stress which started at the wall. Rotta[8] then adapted the van Driest-Prandtl mixing length to rough surfaces by shifting the position of the reference wall an appropriate distance. Rotta presented the numerical results in graphical form for two well-known roughnesses: the Nikuradse sand-grain roughness and the Colebrook-White engineering roughness. Later Cebeci and Smith[2] provided an analytical fit to the wall shift for the sand-grain roughness which was then used by Cebeci and Chang[9] for calculations of turbulent boundary layers over rough surfaces.

For arbitrarily rough surfaces the van Driest factor is correlated in this paper with roughness drag characterization until a limiting value of zero is reached. This is considered to represent the beginning of the fully rough regime. Then for the fully rough regime, the mixing length is considered to assume an initial value at the wall in accordance with Rotta's original (1950) analysis.

For purposes of comparison the second Rotta analysis of a wall shift is generalized to produce numerical results for the drag characterization of arbitrary roughness.

In an appendix an explicit conversion of mixing-lengths to eddy viscosities is derived.

CHARACTERIZATION OF ROUGHNESS DRAG

A brief review is presented of pertient features of the velocity similarity laws and the associated drag characterizations of rough surfaces.

Close to the wall the logarithmic velocity law for an arbitrarily rough surface defined by a sufficient number of length factors k, k_1, k_2, ... is given in what may be called the Reynolds-number mode as

$$\frac{u}{u_\tau} = A \ln y^* + B_1 [k^*, T] \qquad (1)$$

and in what may be called the relative-roughness mode as

$$\frac{u}{u_\tau} = A \ln \frac{y}{k} + B_r [k^*, T] \qquad (2)$$

where

$$B_r = B_1 + A \ln k^* \qquad (3)$$

Here u = Streamwise Velocity Component

u_τ = Shear Velocity $u_\tau = \sqrt{\tau_w/\rho}$

τ_w = Wall Shear Stress

ρ = Density of Fluid

$y^* = u_\tau y/\nu$

y = Normal Distance from Wall

ν = Kinematic Viscosity of Fluid

T = Texture of Roughness Configuration, $T = \underline{k}, \underline{k_1}, \ldots$
$\quad\quad\quad

As defined ΔB is always negative for rough surfaces. Nikuradse[10] used the B_r--characterization while Hama[11] preferred the ΔB (actually $-\Delta B$) characterization.

To experimentally determine a characterization for a specific arbitrarily rough surface, there are various procedures available. The direct procedure requires velocity measurements close to the wall to define a logarthmic law as well as the measurement of the wall shear stress. Simpler, indirect procedures may be used such as involving the total drag of a flat plate[12] or the torque of a rotating disk.[13]

MIXING LENGTH THEORY

According to the Prandtl mixing length theory, the turbulent shear stress τ_t is related to the velocity gradient by

$$\frac{\tau_t}{\rho} = \ell^2 \left(\frac{du}{dy}\right)^2 \qquad (7)$$

where ℓ is the mixing length which, in general, is not constant but a function of its position in the flow field.

The total shear stress τ at a point in the flow is the sum of laminar τ_ℓ and turbulent τ_t shear stresses or

$$\frac{\tau}{\rho} = \nu \frac{du}{dy} + \ell^2 \left(\frac{du}{dy}\right)^2 \qquad (8)$$

where

$$\frac{\tau_\ell}{\rho} = \nu \frac{du}{dy}$$, the Newton Law of Viscosity.

For a shear layer with zero longtiudinal pressure gradient, $\tau \equiv \tau_w$ close to the wall. The nondimensionally

$$\ell^{*2} \left(\frac{du^*}{dy^*}\right)^2 + \frac{du^*}{dy^*} = 1 \qquad (9)$$

where ℓ^* is a nondimensional mixing length, $\ell^* = u_\tau \ell/\nu$, and u^* is a nondimensional velocity, $u^* = u/u_\tau$.

Solving for du^*/dy^* as a quadratic expression and integrating from the wall, $y^* = 0$ and $u^* = 0$, results in a velocity profile

$$u^* = \int_0^{y^*} \frac{2}{1 + \sqrt{1 + (2\ell^*)^2}} \, dy^* \tag{10}$$

Close to the wall Prandtl proposed a linear variation of mixing length with distance from the wall

$$\ell^* = \kappa y^* \tag{11}$$

where κ is the von Kármán constant. Use of this relation, in Equation (10), leads to a logarthmic velocity law with $A = 1/\kappa$. However, an erroneous value of B_1 results. Furthermore, in so far as the logarthmic velocity law does not hold right up to the wall, so does the Prandtl wall mixing length. To remedy this, a modification function M ($\ell^* = M\kappa y^*$) is needed as a function of y^* and λ^* where λ^* is an additional nondimensional length, $\lambda^* = u_\tau \lambda/\nu$. Furthermore, M should equal zero at $y^* = 0$ and equal unity at $y^* \to \infty$.

For smooth surfaces van Driest proposed [14] a M such that

$$M = 1 - \exp\left(-y^*/\lambda_v^*\right) \tag{12}$$

where λ_v^* is the λ^* associated with van Driest.

Other modification functions may be formulated as for example the hyperbolic tangent function alluded to by Patel[15]

$$M = \sqrt{\tanh\left(y^*/\lambda^*_h\right)^2} \tag{13}$$

where λ^*_h is the λ^* used here.

EXISTING MIXING-LENGTH METHODS FOR ROUGH SURFACES

Some pertinent existing mixing-length methods for rough surfaces are now critically examined.

ROTTA I

An extension of the Prandtl wall mixing length to rough surfaces was initially proposed by Rotta which assumed a laminar sublayer thickness that would decrease with roughness or

$$\ell^* = \kappa(y^* - y_L^*) \tag{14}$$

where y_L is the laminar sublayer thickness and $y_L^* = u_\tau y_L/\nu$. The introduction of this ℓ^* in Equation (10) resulted in an integration in elementary functions and a relation between y_L^* and B_1

$$y_L^* = B_1 + \frac{1}{\kappa}(1-\ell n\, 4\kappa) \tag{15}$$

With increasing roughness the laminar sublayer finally vanishes, $y_L^* = 0$, and $B_1 = -\frac{1}{\kappa}(1-\ell n\, 4\kappa)$. This is now considered to be the beginning of the fully rough regime.

For the fully rough regime Rotta assumed an initial mixing length ℓ_w^* at the wall where $y_L^* = 0$ or

$$\ell^* = \ell_w^* + \kappa y^* \tag{16}$$

The use of this mixing length for the fully rough regime into the velocity profile, Equation (10), results in an analytical solution.

$$u^* = \frac{1}{\kappa \ell^*}\left(1/2 - \sqrt{\ell^{*2} + 1/4}\right) - \frac{1}{\kappa \ell^*_w}\left(1/2 - \sqrt{\ell_w^{*2} + 1/4}\right)$$

$$+ \frac{1}{\kappa} \ell n \left(\frac{\ell^* + \sqrt{\ell^{*2} + 1/4}}{\ell^*_w + \sqrt{\ell^*_w + 1/4}} \right) \qquad (17)$$

At higher values of y^*, this relation reduces to the usual log law, Equation (1) so that

$$B_1 = \frac{1}{\kappa}\left(\ell n\, 4\kappa - 1\right) - \frac{1}{\kappa \ell_w^*}\left(1/2 - \sqrt{\ell_w^{*2} + 1/4}\right) \qquad (18)$$

$$- \frac{1}{\kappa} \ell n \left(2\, \ell^*_w + 2 \sqrt{\ell_w^{*2} + 1/4} \right)$$

This relates B_1 and ℓ_w^* and hence the velocity profile, Equation (10), is a function of y^* and B_1.

Rotta II

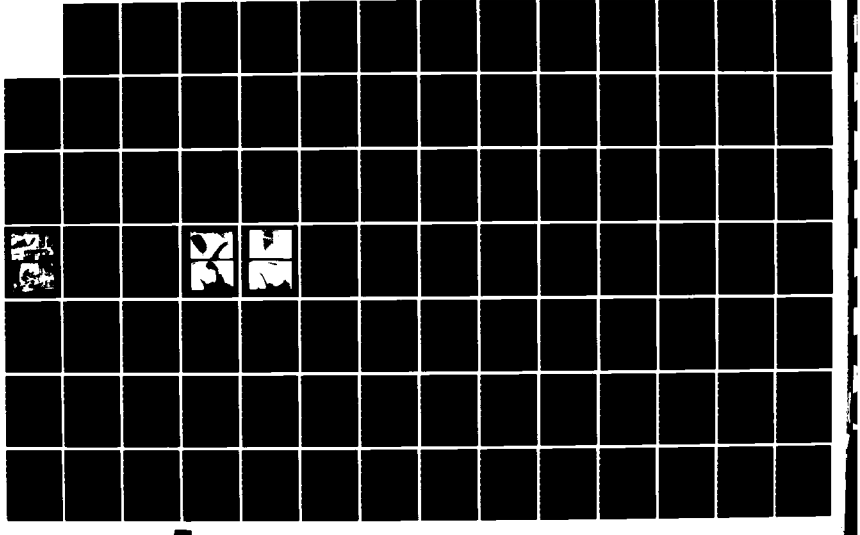
Rotta [8] seems to have abandoned the laminar sublayer approach in analyzing rough surfaces after the whole concept of a purely laminar flow next to the wall became untenable. Since there are turbulent stresses even in the laminar sublayer, the sublayer has been renamed the viscous sublayer.

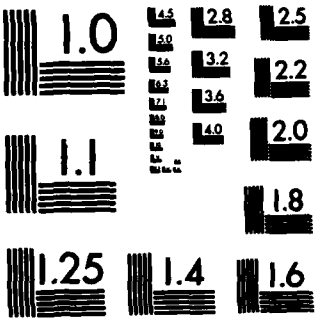
Rotta extended the van Driest formulation for smooth surfaces to rough surfaces by adding a length Δy to the y coordinate such that

$$\ell^* = \kappa(y^* + \Delta y^*) \left\{ 1 - \exp\left[-(y^* + \Delta y^*)/\lambda^*_s \right] \right\} \qquad (19)$$

AD-A144 226 PROCEEDINGS OF THE GENERAL MEETING OF THE AMERICAN TOWING TANK CONFERENCE.. (U) STEVENS INST OF TECH HOBOKEN NJ DAVIDSON LAB D SAVITSKY ET AL. AUG 83 3/7

UNCLASSIFIED SIT-DL-TR-13029-VOL-1 N00167-83-M-4062 F/G 20/4 NL





MICROCOPY RESOLUTION TEST CHART
NATIONAL BUREAU OF STANDARDS-1963-A

where λ^*_s is the value of λ^*_v for smooth surfaces. When this mixing length is incorporated into the velocity profile, Equation (10), and related to the logarithmic law, Equation (1), Δy^* becomes a function of $B_1[k^*, T]$. Instead of solving the general case of $\Delta y^* = f[B_1]$, Rotta solved $\Delta y^* = f[k^*]$ for the Nikuradse sand-grain roughness and $\Delta y^* = f[k^*]$ for the Colebrook-White engineering roughness and presented the results graphically. Cebeci and Smith[2] fitted the results for the Nikuradse sand-grain roughness to an empirical formula. Subsequently Chang and Cebeci[9] used this formula in boundary-layer calculations.

The Rotta formulation leads to an initial value of ℓ^*, ℓ^*_w, at the wall at $y^* = 0$ or

$$\ell^*_w = \kappa \Delta y^* \left[1-\exp\left(-\Delta y^*/\lambda^*_s\right)\right] \tag{20}$$

Hence $\ell^*_w = f[B_1] = f[k^*,T]$ for all roughness regimes.

Having a non-zero mixing length and consequently a turbulent shear stress at the wall may be considered objectionable for the regime of intermediate roughness where there is still a substantial viscous sublayer.

Dahm

Dahm[16] proposed a differential equation for the mixing lengths of rough surfaces based on empirical considerations which for zero mass injection becomes

$$\frac{d\ell^*}{dy^*} = \frac{0.4y^* - (\ell^* - \ell^*_w)}{11.83} \tag{21}$$

It may be of interest to solve this equation as a linear differential equation to

$$\ell^* = 0.4y^* + \ell^*_w + (0.4)\,(11.83)\left(\frac{1}{e^{y^*/11.83}} - 1\right) \tag{22}$$

It is to be noted that this formula resembles that of Rotta, Equation (16), for the fully rough regime ($\kappa = 0.4$; also at $y^* = 0$, $\ell^* = \ell^*_w$). In actual use, values of ℓ^*_w would have to be correlated with drag characterization B_1.

PROPOSED NEAR-WALL MIXING LENGTHS FOR ROUGH SURFACES

General

Equating the velocity profiles from mixing lengths, Equation (10), and the logarithmic law, Equation (1), produces

$$B_1 = \int_0^{\tilde{y}^*} \frac{2}{1 + \sqrt{1 + (2\ell^*)^2}}\, dy^* - \frac{1}{\kappa} \ell n\, \tilde{y}^* \tag{23}$$

and with $\ell n\, \tilde{y}^* = \int_1^{\tilde{y}^*} \frac{dy^*}{y^*}$ (24)

$$B_1 = \int_0^1 \frac{2}{1 + \sqrt{1+(2\ell^*)^2}}\, dy^* + \int_1^{\tilde{y}^*} \left[\frac{2}{1+\sqrt{1+2(\ell^*)^2}} - \frac{1}{\kappa y^*} \right] dy^* \tag{25}$$

or

$$B_1 = I_1 + I_2 \tag{26}$$

where $\tilde{y}^*$ is a sufficiently large value of y^* so that the second integrand of Equation (25), I_2, becomes negligible.

Intermediate Roughness Regime

With the Prandtl-van Driest mixing length

$$\ell^* = \kappa y^* \left[1-\exp(-y^*/\lambda^*_v) \right] \qquad (27)$$

In Equation (25), the van Driest factor λ^*_v becomes a function of B_1 and hence a function of roughness factors, k^* and T or $\lambda^*_v = f[B_1] = f[k^*,T]$.

Numerically then λ^*_v from the preceeding decreases with a decreasing of B_1 until the limit $\lambda^*_v = 0$ is reached. Then $\ell^* = \kappa y^*$.

The range of λ^*_v from its smooth value of λ^*_s to its limit 0 may be considered to cover the intermediate roughness regime at $\lambda^*_s > \lambda^*_v > 0$.

Fully Rough Regime

The original Rotta I proposal of an initial mixing length ℓ^*_w at the wall for the fully rough regime is now considered appropriate for the fully rough regime. Accordingly Equations (11), (17), and (18) apply.

Generalized Rotta II

In order to make comparisons the Rotta II method of an additional length Δy^* is now generalized. The Rotta II mixing length for rough surfaces Equation (19) is substituted into Equations (23) or (25) for B_1 so that Δy^* becomes a function of B_1 or $\Delta y^* = f[B_1] = f[k^*,T]$.

NUMERICAL RESULTS

In determining B_1 from an integration of mixing lengths by means of Equation (25), it is necessary to specify a limiting value of $\bar{y}^*$ so that the integrand of I_2 becomes practically zero. As an example, the integrand dI_2/dy^* is plotted in Figure 1 for the smooth case $\lambda_v^* = 26$ and for the case of the beginning of the fully rough regime $\lambda_v^* = 0$ with $\kappa = 0.4$. To compensate for the logarithmic abscissa, the ordinate is multiplied by y^* so that the area under the curve represents the integral I_2. Then $dI_2/dy^* = y^* (dI_2/dy^*)(d\ell ny^*/dy^*)$. Here a value of $y^* = 200$ seems sufficiently large.

In Figure 2 the van Driest factor λ_v^* is correlated with drag characterization B_1 for the intermediate roughness regime by means of Equation (25). This accommodates any arbitrary roughness. The limiting value is $B_1 = -1.325$ for $\lambda_v^* = 0$. Smaller values of B_1 are then in the fully rough regime.

The wall mixing length ℓ^*_w for the fully rough regime is plotted against drag characterization B_1 in Figure 3 in accordance with the Rotta I relation, Equation (18).

In Figures 4 and 5 the Rotta factor Δy^* is plotted against drag characterization B_1, as a result of solving Equations (19) and (25). This correlation applies to any arbitrary rough surface and consequently includes the Nikuradse sand-grain roughness and the Colebrook-White roughness.

A comparison is shown in Figure 6 for the mixing length ℓ^*_w at the wall as a function of roughness characterization B_1. It should be noted that the Rotta II formulation has values of ℓ^*_w in the intermediate roughness regime in accordance with Equation (20). On the other hand, the van Driest formulation has a zero value. For the fully rough regime the Rotta I values are compared to the Rotta II values of ℓ^*_w.

A comparison of the variation of mixing lengths ℓ^* with normal distance y^* is displayed in Figure 7 for various formulations on the basis of equal values of B_1. The smooth case is shown for a van Driest factor of 26. As an example of the intermediate roughness regime a comparison is shown between the van Driest and Rotta II formulations for $B_1 = 2$. It is to be noted that the Rotta II value of the mixing length is larger close to the wall. This is a result of having an initial value ℓ^*_w at the wall. Mixing lengths at the border between the intermediate roughness and fully rough regimes are also compared. Here $\lambda^*_v = 0$ and $B_1 = -1.325$. For the fully rough regime an example comparison is shown for $B_1 = -6$. It is to be further noted that for large values of y^* all the values of ℓ^* tend to converge to the original Prandtl wall mixing length of $\ell^* = \kappa y^*$ as to be expected.

SUMMARY

For arbitrarily rough surfaces two procedures have been developed.

First there is the extension of the Prandtl-van Driest formulation, Equation (12), to the intermediate roughness regime. Here the van Driest factor λ^*_v is correlated with drag characterization B_1 in Figure 2. For the fully rough regime, the Rotta I procedure is to be used as given by Equations (16) and (18) which is plotted in Figure 3 as ℓ^*_w against B_1.

Secondly, there is the Rotta II correlation, Equation (19), developed for arbitrarily rough surfaces. Figure 4 correlates Δy^* with B_1 for the intermediate roughness regime and Figure 5 for the fully rough regime.

Conceptually the first procedure which has no wall mixing length for the intermediate roughness regime seems more acceptable.

APPENDIX

CONVERSION OF MIXING LENGTHS TO EDDY VISCOSITIES

The concept of eddy viscosity ν_t (more properly eddy kinematic viscosity) was originally proposed during the last century by Boussinesq for turbulent flows as an analogy to the usual viscosity for laminar flows or

$$\frac{\tau_t}{\rho} = \nu_t \frac{du}{dy} \tag{A1}$$

Equating this to the turbulent shear stress given in terms of mixing lengths, Equation (7), produces the well known expression

$$\nu_t = \ell^2 \frac{du}{dy} \tag{A2}$$

It is to be noted that eddy viscosity unlike laminar viscosity is not a property of the fluid but depends on its position in the flow.

For sundry reasons it may be more desirable to relate eddy viscosity ν_t to mixing length without the presence of velocity gradient du/dy.

In general, shear stress τ has laminar and turbulent contributions such that

$$\frac{\tau}{\rho} = (\nu + \nu_t) \frac{du}{dy} \tag{A3}$$

Close to the wall $\tau = \tau_w$ and nondimensionally then

$$\frac{du^*}{dy^*} = \frac{1}{1 + \frac{\nu_t}{\nu}} \tag{A4}$$

Also from Equation (10)

$$\frac{du^*}{dy^*} = \frac{2}{1+\sqrt{1+(2\ell^*)^2}} \tag{A5}$$

Equating the two expressions for $\frac{du^*}{dy^*}$ results in

$$\frac{\nu_t}{\nu} = 1/2 \sqrt{1 + (2\ell^*)^2} - 1/2 \tag{A6}$$

This is the desired relation for converting mixing lengths to eddy viscosities.

At large values of ℓ^*, $\frac{\nu_t}{\nu} \to \ell^* \to \kappa y^*$ or $\nu_t \to u_\tau \ell \to \kappa u_\tau y$

For the van Driest formulation for arbitrarily rough surfaces, Figure 8 shows the variation of eddy viscosity ratio ν_t/ν with normal distance y^*. The smooth case is shown as well as the case for the boundary between the intermediate and fully rough regimes. Also an example of the fully rough regime is shown for $B_1 = -6$. At large values of y^*, $\frac{\nu_t}{\nu} \to \kappa y^*$

It is to be noted that the increase of ν_t/ν with y^* presented here applies only to the boundary-layer region next to the wall. A limiting value is reached which corresponds to outer-region values such as given by Cebeci and Smith[2].

REFERENCES

1. Patankar, S.V. and D.B. Spalding, "Heat and Mass Transfer in Boundary Layers," C.R.C. Press, Cleveland, Ohio (1968).

2. Cebeci, T. and A.M.O. Smith, "Analysis of Turbulent Boundary Layers," Academic Press, N.Y. (1974).

3. Nituch, M.J., S.S. Sjolander and M.R. Head, "An Improved Version of Cebeci-Smith Eddy-Viscosity Model," Aeronautical Quarterly, Vol. 29, Pt. 3, pp. 207-225 (Aug 1978).

4. Huang, T.T., N. Santelli and G. Belt, "Stern Boundary-Layer on Axisymmetric Bodies," 12th Symposium on Naval Hydrodynamics, National Academy of Sciences, Washington, D.C. (1979).

5. Sideman, S. and W.V. Pinczewski, "Turbulent Heat and Mass Transfer at Interfaces: Transport Models and Mechanisms," in "Topics in Transport Phenomena," C. Gutfinger, ed., pp. 47-207, Hemisphere Publishing Corporation, Washington, D.C. (1975).

6. Arora, R., K.K. Kuo and M.K. Razdan, "Near-Wall Treatment for Turbulent Boundary-Layer Computations," AIAA Journal, Vol. 20, No. 11, pp. 1481-1482 (Nov 1982).

7. Rotta, J., "Das in Wandnähe gültige Geschwindigkeitsgesetz turbulenter Strömungen," Ingenieur-Archiv, Vol. 18, pp. 277-280 (1950).

8. Rotta, J., "Turbulent Boundary Layers in Incompressible Flow," in "Progress in Aeronautical Sciences," Vol. 2, A. Ferri, D. Küchemann and L.H.G. Sterne, eds., pp. 1-219, Pergamon Press, N.Y. (1962).

9. Cebeci, T. and K.C. Chang, "Calculation of Incompressible Rough-Wall Boundary-Layer Flows," AIAA Journal, Vol. 16, No. 7, pp. 730-735 (Jul 1978).

10. Nikuradse, J., "Laws of Flow in Rough Pipes," NACA TM 1292 (Nov 1950) (Translation from VDI-Forschungsheft 361, Jul/Aug 1933).

11. Hama, F.R., "Boundary-Layer Characteristics for Smooth and Rough Surfaces," Transactions, Society of Naval Architects and Marine Engineers, Vol. 62, pp. 333-358 (1954)

12. Granville, P.S., "The Frictional Resistance and Turbulent Boundary Layer of Rough Surfaces," Journal of Ship Research, Vol. 2, No. 3, pp. 52-74 (Dec 1958).

13. Granville, P.S., "Drag-Characterization Method for Arbitrarily Rough Surfaces by Means of Rotating Disks," Journal of Fluids Engineeing, Vol. 104, No. 3, pp. 373-374 (Sep 1982).

14. van Driest, E.R., "On Turbulent Flow Near A Wall," Journal of Aeronautical Sciences, Vol. 23, pp. 1007-1011, 1036 (1956).

15. Patel, V.C., "A Unified View of the Law of the Wall Using Mixing-Length Theory," Aeronautical Quarterly, Vol. 24, Pt. 1, pp. 55-70 (Feb 1973).

16. Dahm, T., Personal Communication to T.C. Lin and R.J. Bywater, "Turbulence Models for High-Speed Rough-Wall Boundary Layers," AIAA Journal, Vol. 20, No. 3, pp. 325-333 (Mar 1982).

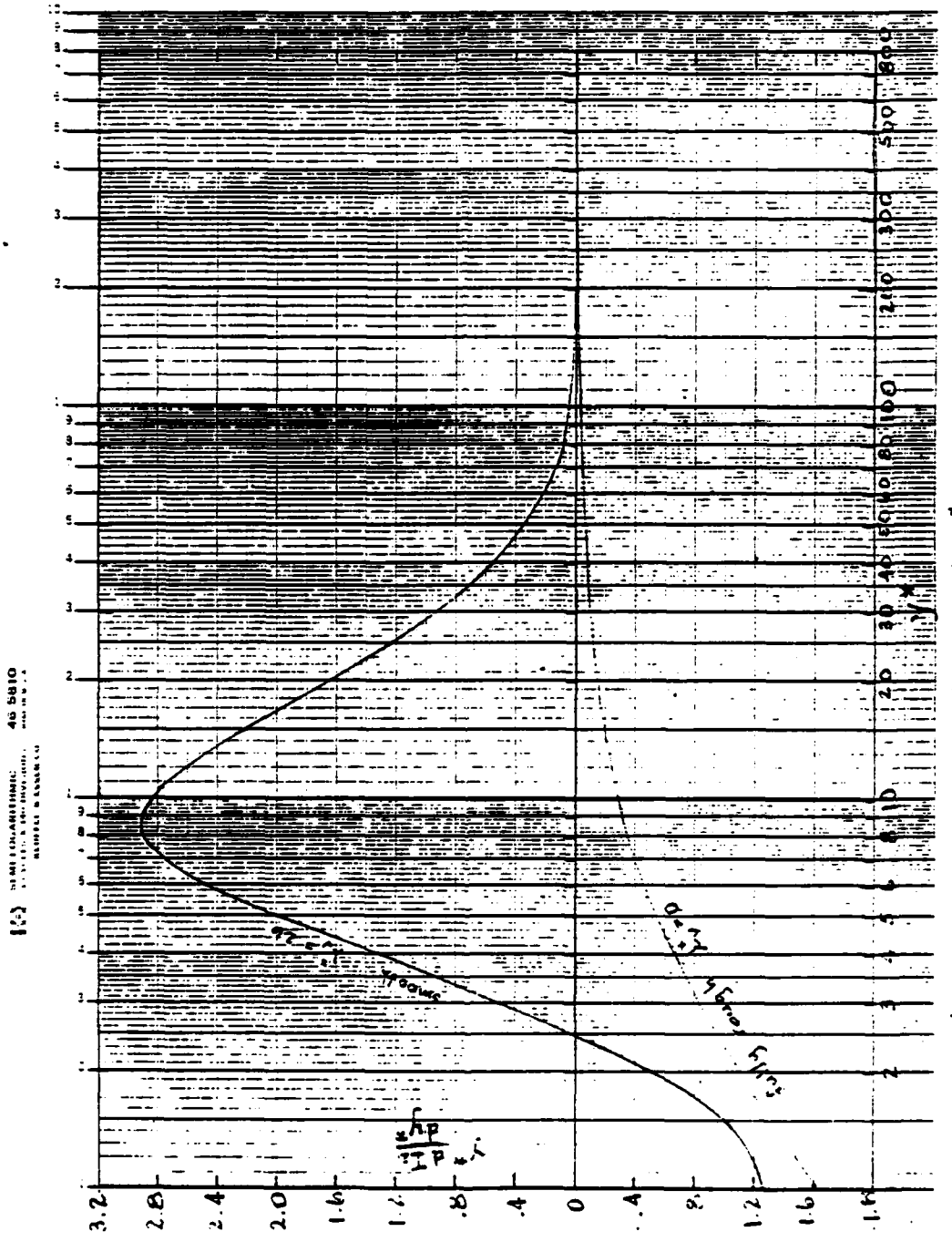
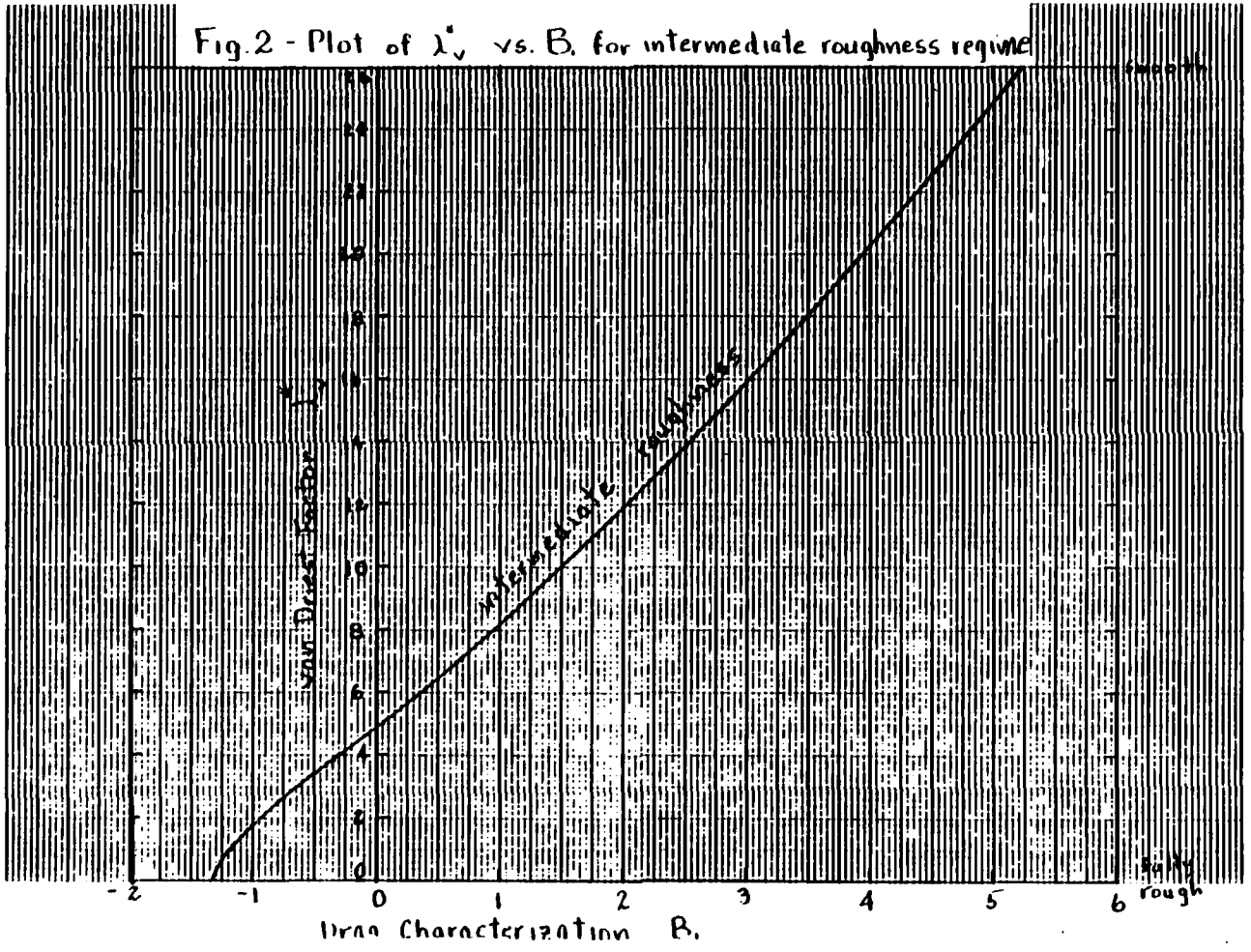


Fig. 1 - Variation of integrand $dI_2/d\gamma^*$ with γ^*


Fig. 2 - Plot of λ_v^* vs. B. for intermediate roughness regime
smooth
Intermediate roughness
Van Driest Factor
Drag Characterization B.
-2
-1
0
1
2
3
4
5
6
fairly rough

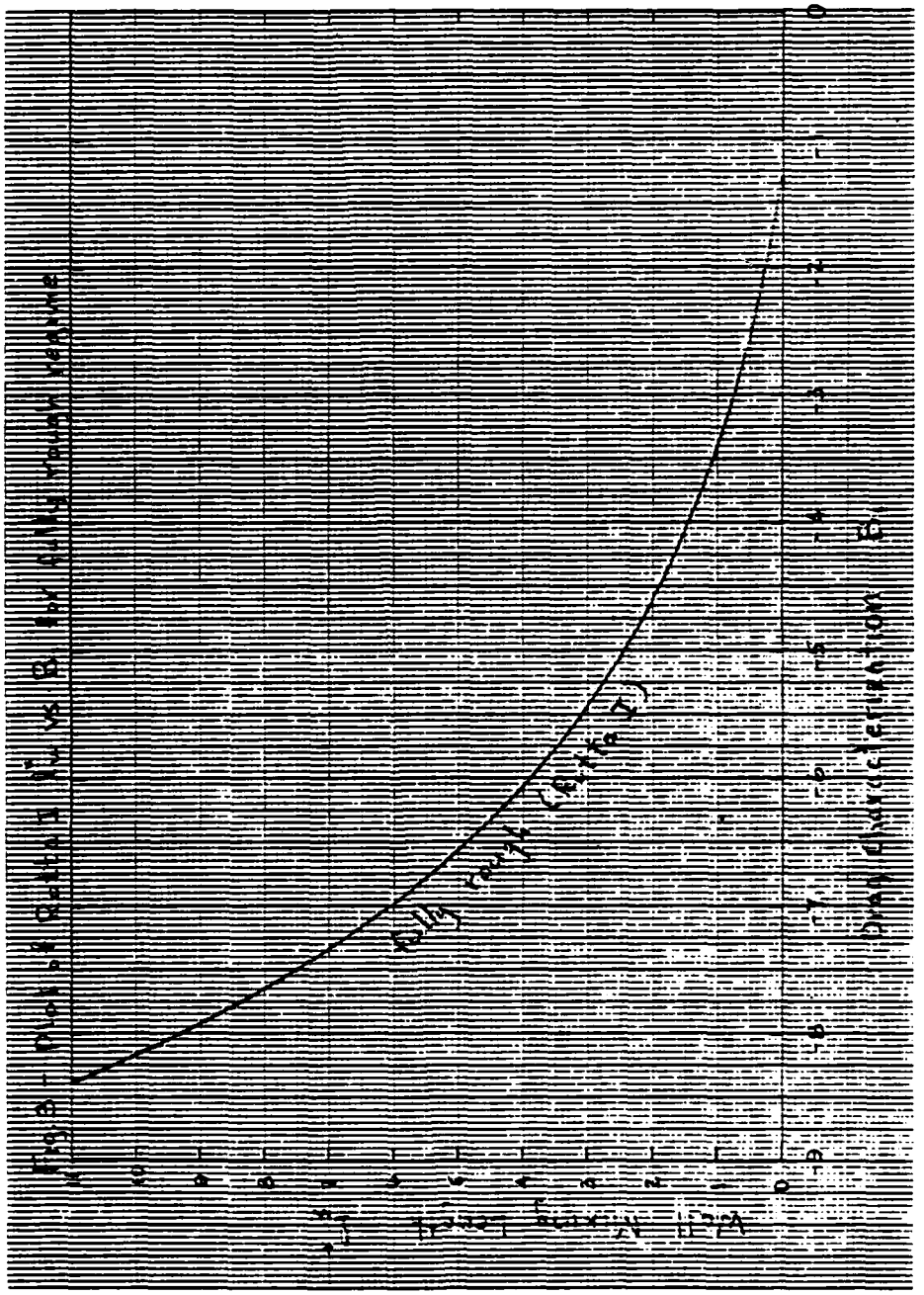
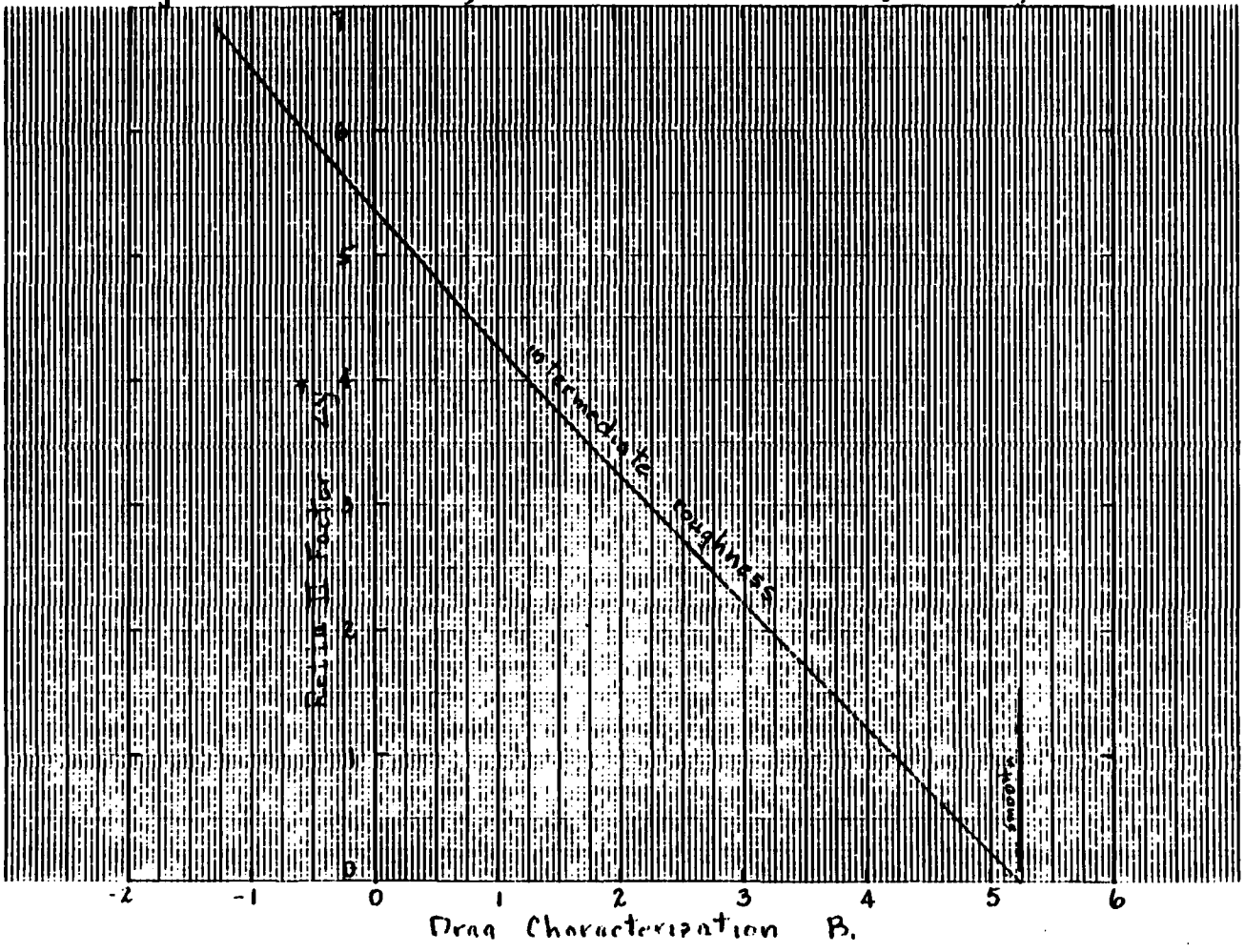


Fig. 4 - Correlation of Δy^+ with B, for intermediate roughness regime



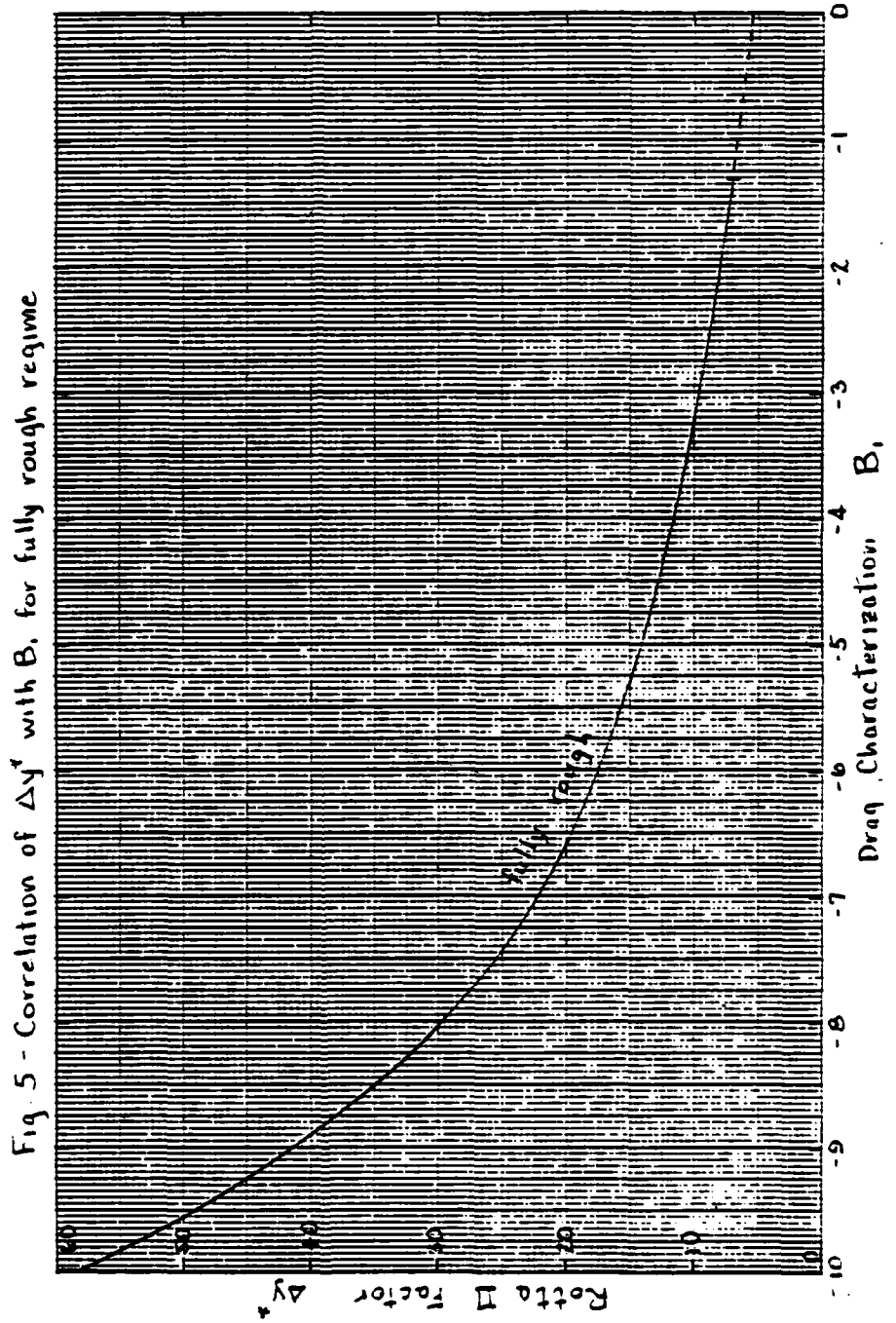


Fig 5 - Correlation of Δy^+ with B_1 for fully rough regime

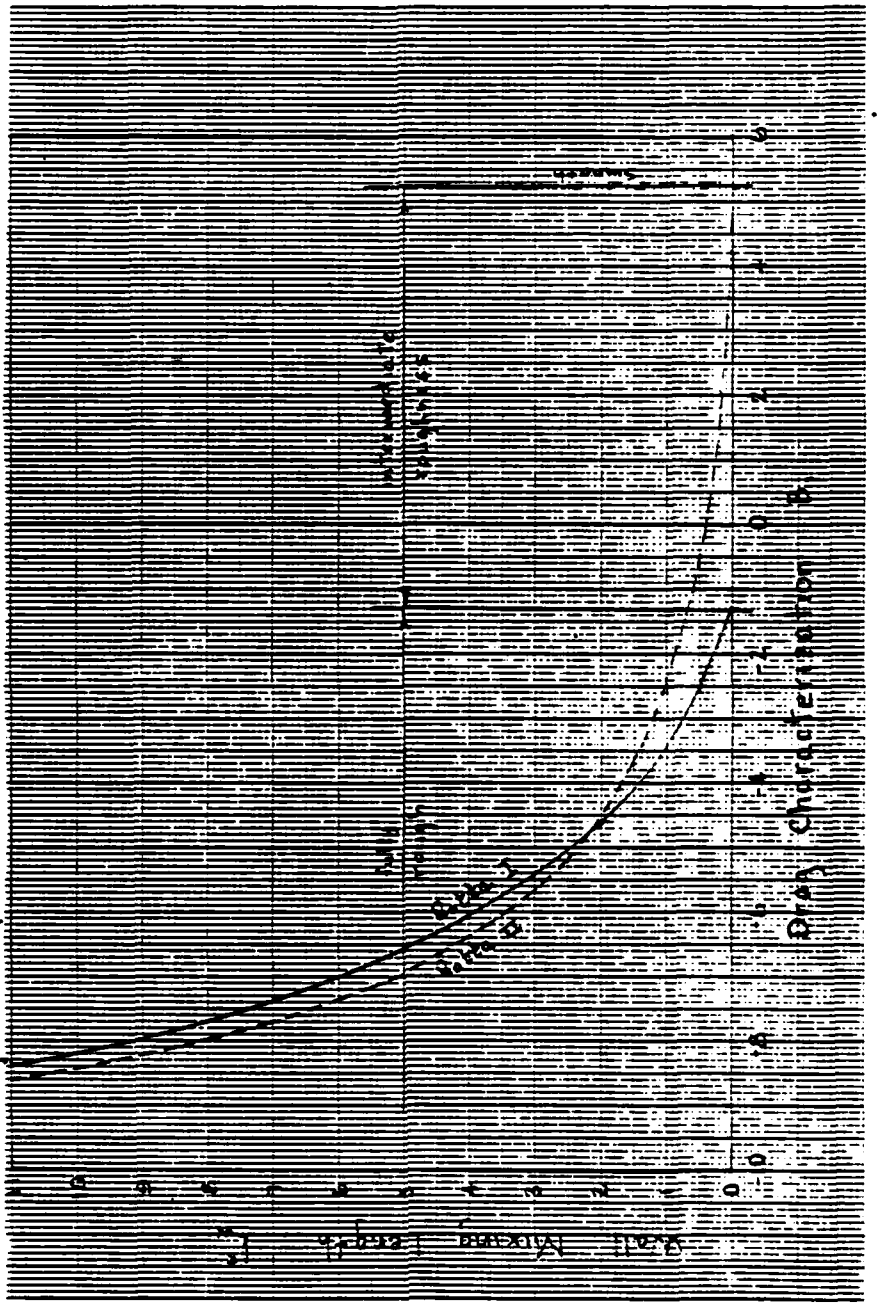


Fig. 6 - Comparison of Rotta I & Rotta II ℓ'_w's

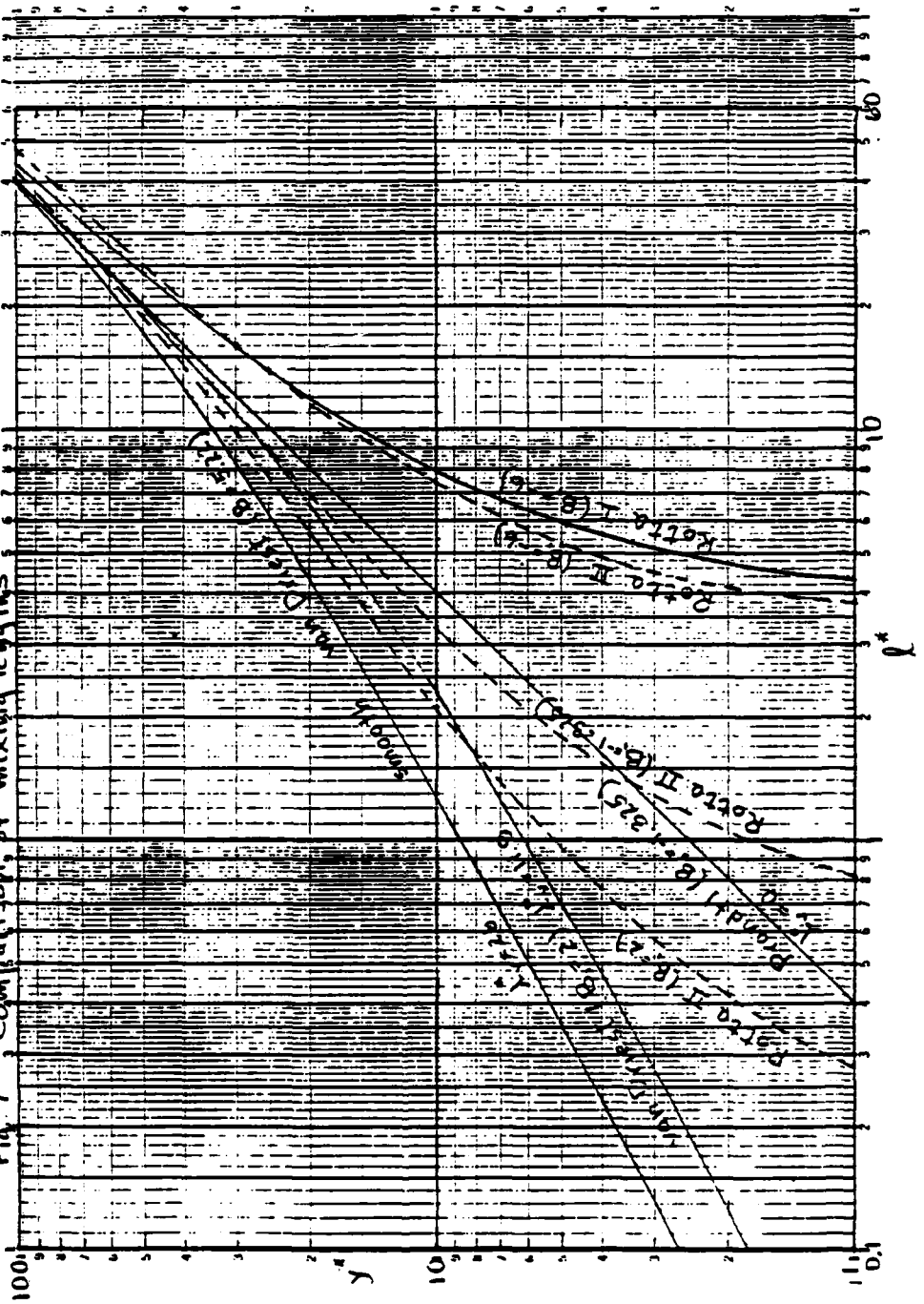
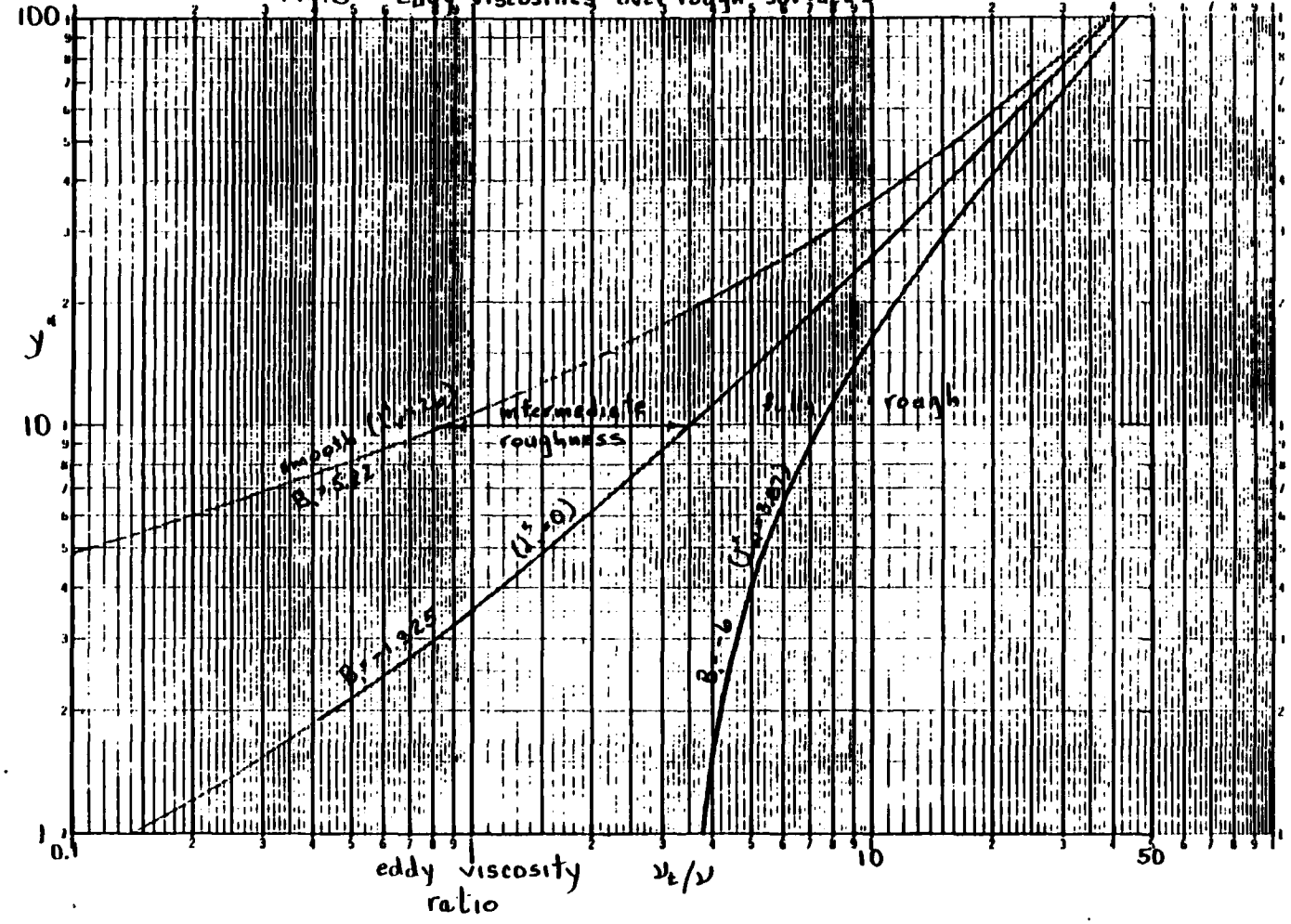


Fig. 7 - Comparison of mixing lengths

Fig. 8 - Eddy viscosities over rough surfaces



REPORTS OF THE

PROPULSION

COMMITTEE

PROPULSION COMMITTEE REPORT

Twentieth Meeting of the
American Towing Tank Conference

Davidson Laboratory
Stevens Institute of Technology
Hoboken, New Jersey

2 August 1983

FOREWORD

The report of the Propulsion Committee of the Twentieth American Towing Tank Conference is presented as contributions from individual members. Although work in the area of ship model propulsion experiments has been somewhat limited by the low level of commercial shipbuilding experience in recent years, several special topics have been investigated by ATTC members. In addition, the ongoing work of the Performance Committee of the International Towing Tank Conference is reported.

Specific contributions to this report include:

- "Activities of the ITTC Performance Committee," authored by Dr. Wen-Chin Lin of DTNSRDC,
- "A Comparison of Two Propellers for the Acoustic Research Ship CFAV Quest," authored by Messrs J.L. Kennedy, L.J. Leggat and N.C. Sponagle, DREA,
- "Comparative Performance of Stock and Design Propellers Derived from Propulsion Experiments," authored by Messrs. Gabor Karafiath and Charles J. Wilson, DTNSRDC, and
- "Problems Associated with the Evaluation of Combined Waterjet-Propeller Performance," authored by Professor Armin Troesch.

Ship-model correlation issues addressed by the ITTC Performance Committee include trial measurement methods, model experimental techniques form factors and scale effects on propeller performance. In the current session of the Performance Committee new methods and results from using the 1978 ITTC Performance Prediction Methods are addressed. The report discusses specific areas being investigated and identifies committee members to whom contributions from the ATTC community may be addressed.

Propellers which are to be used in acoustic research have very stringent design requirements with respect to cavitation and powering performance. Rarely is the designer or the experimenter priviledged enough to receive full scale information as "feed-back" to the design or scaling process. Messrs Kennedy, Leggat and Sponagle have generously shared their experience with the community. Their contribution will add to the proceedings with valuable documentation of this demanding propeller design.

Messrs Karafiath and Wilson have addressed the issue of using "stock" propellers for powering predictions of surface ships. Predictions are made using the propeller-hull interaction coefficients from the stock propeller propulsion experiments combined with open-water characteristics of the design propeller. The results are compared with experimental data from design propeller propulsion experiments. Conclusions are made regarding the suitability of such a process. The guidance provided will improve propulsion predictions from future experiments.

Finally, an unusual propulsion problem is addressed by Professor Troesch in the discussion of tankery problems associated with model testing a combined waterjet-propeller propulsion system. Critical areas of the actual model configuration are discussed and conclusions are drawn concerning the modeling procedure.

Although limited in number, the significance of each contribution is worthy of careful consideration by the membership of American Towing Tank Conference. Discussion and additional contributions are welcomed.

ACTIVITIES OF THE ITTC PERFORMANCE COMMITTEE

Dr. Wen-Chin Lin
David W. Taylor Naval Ship R&D Center

The Performance Committee of the 17th International Towing Tank Conference (ITTC), appointed by the 16th ITTC in September 1981, consists of the following members:

Dr. H. Tanibayashi, Chairman (MHI, Japan)
Dr. W. C. Lin, Secretary (DTNSRDC, U.S.A.)
Mr. D. Bailey (NMI, U.K.)
Dr. G. Collatz (HSVA, West Germany)
Dr. B. Della Loggia (CETENA, Italy)
Mr. T. Holtrop (MARIN, Netherlands)
Mr. T. Munk (DSRL, Denmark)
Mr. B. Nizery (IRCN, France)
Dr. K. Varsamov (BSHC, Bulgaria)

In accordance with the guidance of the general conference, the Performance Committee formulated a technical plan of investigation on the basis of recommendations of the 16th ITTC pertaining to ship performance. Advice was sought among the ITTC member organizations, concerning all relevant topics that had been identified, to determine their order of priority. As a result, twelve subject areas were selected as the most critical and relevant to the Committee's work. Table 1 presents these twelve subject areas, the relationship of each area to the recommendations of the 16th ITTC, and the leading investigators of the respective fields.

Steady progress has been made by committee members in performing investigations in their respective subject areas. Suitably scheduled meetings have been fully attended by the members to review such progress. Table 2 presents a tentative table of contents to document a planned report of committee work.

Member organizations of the ATTC who wish to contribute to specific items on Table 2 are invited to communicate with the appropriate committee members (see the subject area assignment in Table 1) for the purpose of incorporating such contributions into the committee report.

Table 1 - Tasks For the 17th ITTC Performance Committee

	Subject Area	16th ITTC Comm. Recommendations		Reporters	
		Perform.	Propeller	Lead	Assist
1.	Form Factor	No. 1		Munk	
2.	Assessment of the shaft rate of rotation on the basis of power identity	No. 1		Tanibayashi	
3.	Trial and Model Data for Fine Hull Ships	No. 4 No. 5		Tanibayashi	All Members
4.	Twin-Screw Ships	No. 6		Lin	All Members
5.	Scale Effect on Propeller Performance and on Propulsive Coefficient	No. 7		Collatz	Lin Della Loggia
6.	Resistance and Power Increase due to Hull and Propeller Roughness	No. 8		Della Loggia	Varsamov
7.	Recent Alternative Procedure for Powering Performance Prediction	No. 9		Holtrop	Munk Collatz
8.	Quantification of Factors Affecting Service Margin	No. 10		Nizery	Collatz
9.	Propulsion in Shallow Water	No. 11		Holtrop	Tanibayashi
10.	Prediction of Effective Wake and Various Propulsive Coefficients		No. 1	Varsamov	
11.	Criteria for Propulsor and Hull Design Optimization		No. 6	Munk	
12.	Propulsor Performance in Waves		No. 8	Nizery	

Table 2 - Tentative Table of Contents to Document a Planned Report of Committee Work

I. General

1. Membership and Meetings
2. Recommendations of the 16th ITTC

II. Review of Ship Performance Research of Interest to the ITTC

1. Introduction
2. Factors Affecting Model-Ship Correlations
   - 2.1 Full-Scale Resistance
     - 2.11 Form Factor
     - 2.12 Roughness
     - 2.13 Appendage Resistance
     - 2.14 Flow Separation
   - 2.2 Scale and Roughness Effects on Propeller Characteristics
   - 2.3 Scale Effect on Propulsion Factors
   - 2.4 Model Testing
   - 2.5 Full-Scale Measurements
     - 2.51 Thrust Measurements (full scale)
     - 2.52 Measured-Mile Trials
     - 2.53 Correction for Wind and Current
3. Performance Prediction Method
   - 3.1 Extension of Computer Program
   - 3.2 Results from Trial Analysis of Five Single-Screw Ships
   - 3.3 Results from Trial Analysis of Twin-Screw Ships
   - 3.4 Results from Trial Analysis of Good Trial Data
   - 3.5 Subjects for Further Investigation
4. High-Speed Craft
5. Hull-Propulsor Optimization
6. Service Performance of Ships
   - 6.1 Effect of Fouling and Surface Deterioration of Hull and Propeller
   - 6.2 Effect of Wind and Current
   - 6.3 Service Performance Analysis
   - 6.4 Sea Margin Determination
7. Performance of Ships in Restricted Water
8. Acknowledgment
9. Nomenclature
10. References

III. Recommendations of the Committee

Appendix

AD-P003 806

A COMPARISON OF TWO PROPELLERS FOR THE ACOUSTIC RESEARCH SHIP CFAV QUEST

by

J.L. KENNEDY, L.J. LEGGAT AND N.C. SPONAGLE

ABSTRACT

CFAV QUEST is a specially designed quiet ship used for underwater acoustics research at the Defence Research Establishment Atlantic. A new set of highly skewed propellers was designed in 1979 to meet new acoustic requirements. Model test results on these propellers were presented at the 1980 ATTC.

In 1981, full scale trials were carried out on CFAV QUEST with both the original and the new set of propellers. Propulsion trials were conducted on a measured mile course with the propeller shafts instrumented using strain gauges. A set of propeller viewing trials, covering the measurement of cavitation inception and cavitation patterns on the propellers, were also carried out. The development of the cavitation on the blades was photographed and the acoustic performance of the propellers was evaluated.

This paper presents results obtained in these trials. A comparison of the two propellers shows that the new propellers exhibit superior cavitation and acoustic performance. Cavitation inception speeds were raised and the amount of cavitation at any given speed was reduced. This was accomplished at no cost in propulsive performance

1. INTRODUCTION

The Canadian Forces Auxiliary Vessel (CFAV) QUEST was conceived and designed as an open ocean acoustic research vessel. To be effective in this area of research QUEST required low levels of self and radiated noise. The original propellers were designed to be free of cavitation at low speeds, however the cavitation inception speed of these propellers was below seven knots and this limited QUEST's quiet operating speed range. Also, advances in sonar technology produced a requirement that QUEST's radiated noise levels be reduced at speeds above seven knots. A project was therefore initiated to design a new set of propellers which would delay cavitation inception to speeds well above seven knots, and minimize the extent of cavitation at any speed. A new set of propellers was designed and model tested to meet the new, more stringent, acoustic requirements. In 1981, full scale trials were carried out on QUEST with both the old and the new set of propellers. Three types of trials were carried out for each set. These were, propulsion trials, radiated noise trials and cavitation viewing trials, which included cavitation inception and cavitation pattern measurement. The purpose of this paper is to outline the procedures used and to present some of the results obtained on these trials.

2. BACKGROUND

The general characteristics of QUEST's hull are shown in Figure 1. The ship has twin screws and twin rudders and the propeller shafts are supported on streamlined bossings. The main propulsion machinery consists of a diesel electric system with two main diesel generators. To mitigate the two major sources of ship noise; the main machinery, for both propulsion and ship services, and the propellers; the acoustic design included special arrangements for mounting the machinery, the provision of acoustic bulkheads and the design of propellers which were to be cavitation free at low speeds. These procedures were shown[1] to be very effective in reducing the ship noise levels at low speeds. During quiet operations at speeds up to seven knots, propulsive power and ship service power can be provided by a gas turbine driven generator which is mounted in a separate accoustically isolated compartment. Because the cavitation inception speed on the original propellers was below seven knots, the maximum quiet operating speed was limited by propeller cavitation rather than by the power available from the gas turbine.

To reach a new propeller design, the Defence Research Establishment Atlantic (DREA) entered into a joint propeller design and model test program with the Netherlands Ship Model Basin (NSMB). The propeller design procedure used has been presented[2] previously in some detail together with the model test predictions.

As part of the pre-design testing at NSMB, a wake survey in the propeller plane was conducted on a 1/10 scale model at a ship speed of 16 knots. The three orthogonal velocity components were measured; Figure 2 shows the axial velocity components at three radii. This figure clearly demonstrates the large axial velocity deficit behind the shaft bossing and in the boundary layer on the hull. The large angle of attack variations which the propeller blades experience as they pass through this wake peak promote cavitation inception.

The portside original propeller, referred to as 5349, mounted on QUEST, is shown in Figure 3. The blades have little skew and thus line up with the wake peak behind the bossing. This is an undesirable feature as it accentuates the unsteady loading on the blades. The blades shown have been marked to assist in locating cavitation on the blade during cavitation viewing trials. Figure 4 shows the new portside propeller, referred to as 5363, mounted on QUEST. In addition to other features, skew was adopted for this propeller in order to delay cavitation inception and also to smooth out the cavity volume accelerations which occur as the blade passes through the wake peak. As the acoustic source strength is proportional to the cavitation volume acceleration, reduction of these fluctuations in the wake peak result in reductions in the radiated noise levels.

The results of comparative model tests on both sets of propellers showed that, for the full power case, an increase in ship speed of about 0.2 kt could be achieved with the new propellers. Also the cavitation inception speeds on the new propeller were substantially higher than those on the old propeller. For tip vortex cavitation the increase was 2 kt and for sheet cavitation the increase was over 7 kt. Correspondingly, the radiated noise tests showed that the noise characteristics of the new propellers would be superior to those of the old propellers.

3. PROPULSION TRIALS

The objectives of the full scale propulsion trials were, first to ensure that the new propellers provided the necessary ship speed, second to compare the performance of the two propellers and third to investigate the correlation between model predictions and full scale measurements for the ship. The procedure used was to conduct normal standardization trials for the two propellers with the minimum time delay between them.

The principal parameters which were determined included the shaft power and revolution rate as a function of the ship speed. The shaft torques were measured on both shafts using four-arm-active strain gauge bridges. The output from these was processed and transmitted to a receiver unit mounted close to the shaft. The particular system used was one that is commercially available. The revolution rate was measured using a toothed wheel fixed to the shaft and a magnetic pickup which monitored the passage of the teeth.

The propulsion data which was obtained from the propeller shafts was processed by a microprocessor controlled data acquisition system. The system sampled the required measurements of torque and revolution rate and processed them into engineering units. Other relevant shipboard data were also handled by this system which could sample at a rate of 20 times per second. The mean and standard deviations of all calculated quantities were displayed dynamically on the operator's terminal as the trials progressed, providing the operator with a clear indication of any irregularities in the data as they were collected. The raw data for any run were recorded on magnetic tape and the averaged values, for a completed run, were displayed on the operator's terminal and on a line printer. The right hand side of Figure 5 shows schematically the set up of the shaft instrumentation and data acquisition system.

Ideally, the trials should have been conducted immediately before and after a docking to change the propellers. Due to the many scientific demands which were placed on QUEST, this was not possible. The trials with the 5349 propellers were conducted in June 1981, the ship was docked to exchange the propellers in August 1981, and the trials with the 5363 propellers were conducted in September 1981. The ship's hull condition was not expected to have altered significantly between the two trials dates and the hull was not cleaned during the docking period.

For the purpose of comparing trials results with model test predictions, it was necessary to modify the "new ship" model test prediction to give an "after service" prediction which would reflect the condition of QUEST at the time of the trials. Hull roughness is an important factor which can have a large effect on ship propulsion. No hull roughness measurements were available from the docking in August 1981, however mesurements taken in March 1982 with a BSRA Hull Roughness Analyser showed an average roughness of 380 microns. In the absence of any previous data, this was taken to be the roughness at the time of the trials.

In order to estimate the effect of hull roughness on the delivered power, the trials prediction formula for (1+x) given by Scott[3] was utilized. The effect of the hull roughness is taken to be proportional to the ratio of (1+x) for the trials condition to (1+x) for a new ship. The latter was calculated for an assumed roughness of 150 microns. Thus the effective power for the trials prediction is given by

$$P_{ET} = P_{EN} \frac{(1+x)_T}{(1+x)_N}$$

The new ship prediction, P_{EN}, was obtained from the model tests at the NSMB using the ITTC friction line with a form factor of (1+k) = 1.30 and a model-ship correlation factor of C_A = 0.00058. The delivered power and revolution rate were calculated from this trials prediction using a wake scaling correlation factor of 1.0005 and correcting the propeller characteristics according to the ITTC'78 method.[4]

Propulsion data for the 5349 propeller are presented in Figure 6. The results shown are the mean values of two pairs of reciprocal runs at each speed, except at the lowest speed where only one pair was available. The delivered power data were corrected for the prevailing wind by using the method of Isherwood.[5] Figure 7 presents the data for the 5363 propeller for which two pairs of reciprocal runs were available at all speeds. On trials, the 5363 propeller provided a top speed of 14.6 kt at 141.5 r.p.m. compared to 14.5 kt at 135.4 r.p.m. for the 5349 propeller. At this condition the new propellers absorbed about 6 per cent less power than the old propellers. The full power condition was not achieved with the new propellers due to a limit on the allowable revolution rate.

Throughout the speed range measured there was a consistent reduction in delivered power between the new and old propellers. This reduction is most significant at low speeds, and at 8 kt the new propellers absorb about 14 per cent less power than the old propellers. Such an improvement is more than that predicted by the model test results and may be due to the physical condition of the propellers. Hundley[6] has shown that considerable improvements can be made to a ship's overall powering performance by having a propeller maintained at its designed condition. In these trials the 5363 propeller was new whereas the 5349 propeller had seen several years of use.

The shaft revolution rate on the new propellers was from 3 to 5 rpm higher than on the old propeller at the same ship speed. This does not give rise to any great problems as the required ship speeds can be met with the allowable revolution rates.

The model predictions for power agree well with the trials data in both cases. However there is a consistent trend for the prediction method to overestimate the power at the higher speeds. This is most apparent in the results with propeller 5363. The results are, however, well within the confidence limit which one can place on the present use of Scott's prediction method. The correlation for shaft revolution rate is very good for the 5349 propeller. For the 5363 propeller, the trials values of revolution rate are higher than the prediction by between 1 and 3 rpm. This is considered to be within the limits of confidence of such prediction methods.

4. CAVITATION VIEWING TRIALS

A series of propeller viewing trials were carried out in conjunction with the propulsion trials described in the previous section. These were performed to ensure that the necessary improvements in cavitation were achieved. Also these trials provided the opportunity for comparing the model prediction of cavitation inception with the full scale observations.

Such trials require viewing ports in the hull above the propeller. A total of six viewing ports were installed in QUEST above the port propeller. The layout of the viewing ports relative to the propellers and the transverse frames is shown in Figure 8. The ports are distributed such that both the face and back of each blade can be viewed. The propellers are outward turning and, because of the inclination of the shaft, face cavitation would most probably occur on the inboard side when the blade was coming up. This could be viewed and illuminated from ports A and B. Model tests showed that back cavitation occurred in an arc from the wake peak, behind the bossing, to a position more than 30° past top-dead-centre. This could be viewed from ports C and D, however it is clear from Figure 8 that these ports offer a very restricted view. Following a recommendation made by the NSMB, ports X and Y were therefore fitted to be used with a prism for viewing the blades.

The design of the viewing ports was taken from a DTNSRDC design for a 9 inch diameter viewing port. Prisms, machined from solid slabs of clear acrylic plastic, were manufactured to fit inside the ports as shown in Figure 9. To use these prisms, the interface between the prism and the glass must be filled with a layer of water, or any other transparent liquid whose refractive index closely matches that of the glass and plastic. The water layer is sealed in place by the O-ring around the base of the prism. Excess water is expelled through vents which are located out of the direct view of the observer. Optimum viewing was achieved with the viewing face of the prism cut at 45°. This arrangement, using a prism in port X, proved to be invaluable for cavitation viewing and photography as a clear view of the back of the blades could be obtained with very little distortion.

To allow for the accurate determination of the extent of cavitation, a series of grid lines were applied to the blades by a brush electroplating process. Lines were marked on at 0.6, 0.7, 0.8 and 0.9 of the full blade radius and at 1/4 and 1/2 of the blade section chords. These lines can be seen clearly in Figures 3 and 4.

Cavitation viewing and photography requires the use of strobe lights to freeze the motion of the propeller and, as the cavitation state can vary greatly with the position of the blades, it is necessary to be able to freeze the motion with the blades in any position. A strobe control system was therefore developed which was able to meet those needs. The system was based on the use of a 360 tooth wheel fixed to the propeller shaft. By controlling the pulses from a magnetic pickup which monitors the passing of each tooth, it was possible to locate the observed position of the blade to within one degree. Figure 5 shows schematically the set up of the lighting and photographing system.

The system was remotely controlled by the cavitation observer using a hand held unit. For cavitation inception studies, low power strobe lights were used and the camera was disabled. The observer could freeze the propeller in any angular position or allow the observed image to rotate, forward or back, at a rate of 1 degree per revolution. When photographing the cavitation it was normal to take a series of photographs showing the development of the cavitation as the propeller rotated. For this case, high power strobe lights were used and photographs were taken with the observed image moving 3 degrees between frames. A 35 mm camera with the capability of taking 250 frames in sequence was used. This allowed for the recording of the cavitation state through two complete revolutions of the propeller.

In determining the cavitation inception points, the shaft revolution rates were gradually increased until cavitation was first observed. At inception the cavitation can be intermittent, depending on the motions at the stern of the ship. By varying the ship speed about the inception point, the inception speed can be obtained to within ±2 r.p.m. The cavitation inception trials were conducted during long straight runs because any variations in rudder angles were observed to influence the cavitation adversely.

A variety of cavitation types were observed on the two propellers. Table 1 presents the cavitation inception speeds for both sets of propellers and for both model and full scale. The model values were obtained from the NSMB's cavitation diagrams[2] with the ship operating line obtained from the full scale propulsion trials.

TABLE 1

CAVITATION INCEPTION SPEEDS (kt)

PROPELLER	5349		5363	
	MODEL	FULL SCALE	MODEL	FULL SCALE
Tip Vortex	7.3	5.9	9.6	8.9
Back Sheet	7.0	5.9	14.7	10.0
Back Cloud		10.5		
Hub Vortex (Intermittent)		14.4		

The model test for the 5349 propeller did not specify the inception speed for back cloud cavitation however it was observed on the model at the predicted full power condition. No face cavitation was observed on either propeller.

Table 1 shows a great improvement in the cavitation performance of the 5363 propeller over the 5349 propeller. QUEST's cavitation free speed range was improved by 3 kt to 8.9 kt. Also there was no evidence of the sheet cavitation breaking down into cloud cavitation, nor was there any hub vortex cavitation on the 5363 propeller. The requirements to delay cavitation inception to speeds above 7 kt, and to reduce the amount of cavitation thereafter were therefore met.

A comparison of the model and full scale inception speeds shows that the model test results gave higher inception speed predictions than were obtained on the trials. The agreement for tip vortex cavitation is fair, considering that the model test data has to be scaled to account for the large differences in Reynolds' number between the model and full scale. For the 5349 propeller, which is straight bladed, there is fair agreement between the predicted and observed inception speeds for sheet cavitation. This is not true for the highly skewed 5363 propeller.

A qualitative explanation of why such large differences occur on highly skewed propellers has been provided by Greeley and Kerwin[7]. Sheet cavitation is brought about by a suction peak close to the leading edge of the blade. This suction peak can be reduced if a long region of laminar separation forms behind it. The length of the laminar separation region is influenced by the local Reynolds' number and the leading edge sweep angle. At the low Reynolds' numbers of the model test, the suction peaks on the highly skewed propellers could have been reduced to the point where sheet cavitation was inhibited. On the straight bladed propellers such suction peak reductions would be considerably less. In the model test program, roughness was applied to the blade leading edges, however it appears that this was not sufficient to overcome the differences in Reynolds' number.

At all speeds where cavitation was observed, the extent of cavitation on the 5349 propeller was greater than on the 5363 propeller. Comparative photographs taken at approximately the full power conditions show the main features of the cavitation on both propellers. Small differences in the construction of the individual propeller blades led to differences in the amount of cavitation on them, as did motions in the stern of the ship during the trials. The photographs presented in Figures 10 to 13 represent the average cavitation state on the propellers at approximately 14.7 kt.

Figure 10 shows propeller 5349 with blade number 3 in the wake peak experiencing the maximum amount of cavitation. A well developed sheet cavity can be seen on the propeller, extending from the X = 0.75 radius to the blade tip. At radii greater than X = 0.85 the flow over the blade separates, producing cloud cavitation which is clearly visible extending from the trailing edge of the sheet cavity downstream. Vortex cavitation can be observed at the blade tip.

Figure 11 shows propeller 5363 with blade number 5 in a similar location, at which the maximum amount of cavitation was observed. By comparison with the above observations, there is very little cavitation on the 5363 propeller. The cavitation, which can be observed extending from the X = 0.9 radius to the tip, was a mixture of sheet and leading edge vortex cavitation. As Greeley and Kerwin[7] have pointed out, the appearance of leading edge vortices is a feature which is associated with the swept back shape of highly skewed propellers. This cavitation does not extend far in the chordwise direction, nor does the cavity break down to give cloud cavitation.

Figures 12 and 13 show the same blades rotated a further 24° beyond those of Figures 10 and 11. In this position, the 5363 propeller again exhibits substantially less cavitation than the 5349 propeller. On the latter there is extensive sheet cavitation, which breaks down into cloud cavitation and extends well downstream of the trailing edge. On the 5363 propeller there is no sheet or cloud cavitation. A thick tip vortex cavity, which extends far downstream, can be seen on the 5349 propeller. By comparison, the tip vortex cavitation on the 5363 propeller is both finer and less extensive.

The development of the cavities as the propeller rotates, shows another notable difference between the two propellers. The sheet cavity on the old propeller remains isolated on the blade and persists to angles more than 72° after the wake peak, as can be seen on blade 2 in Figure 10. By comparison, the cavitation on the new propeller blade flows smoothly into the tip vortex. The latter condition is a desirable feature as the cavities then collapse off the blade reducing the possibility of blade erosion.

The improvements in cavitation performance reflect the attention that was paid to solving the problems posed by the large wake deficit. The 5349 propeller was not designed to handle the large velocity fluctuations in the wake of the propeller bossing.[6] On the other hand, the 5363 propeller was designed specifically to handle these fluctuations by the use of blade sections with the wider cavitation buckets and by the application of skew.

5. RADIATED NOISE TRIALS

The objective in designing a new set of propellers for QUEST was to reduce the radiated noise levels. The radiated noise levels were measured with both sets of propellers to verify that such reductions were achieved.

In conducting such trials, QUEST made long straight runs over a range which is instrumented with hydrophones. The procedure used is similar to that used on standardization trials although the instrumented range is relatively short by comparison. Reciprocal runs were made at constant shaft revolution rate so that the effects of winds and currents could be averaged out. Ambient noise measurements with all ships far removed from the range were made at various times during the trials to ensure that the quiet operating condition results were not contaminated by high background noise levels.

The relevant parameter which should be examined in comparing the noise levels of the two propellers is the noise reduction, ΔL_s, defined by

$$\Delta L_s \approx 20 \log \left(\frac{P_1}{P_2}\right)$$

where P_1 is the sound pressure for the 5349 propeller and P_2 is the sound pressure for the 5363 propeller. The noise reduction, in octave bands, as a function of frequency is shown in Figure 14. These data were obtained from runs at an estimated speed of 14.7 kt, which was slightly faster than was achieved on the measured mile. Substantial noise reductions were achieved across the whole frequency spectrum. The largest reductions being in the low frequency region where the influence of reducing the cavity volume accelerations from the old to the new propeller are most strongly felt. The noise reductions at higher frequencies reflect the reduction in the amount of cavitation present on the new propeller relative to the old propeller. Similar noise reductions to those shown in Figure 14 were observed at all the speeds tested.

The procedure for comparing the two propellers was to conduct trials on both propellers at the same shaft revolution rate, except for the 14.7 kt case. This procedure resulted in different ship speeds, as can be seen from the results of the propulsion trials. In order to compare the radiated noise levels at a fixed ship speed, the noise levels were interpolated, using smooth curves, to corresponding ship speeds. The results so derived are presented in Figure 15 for the 2 kHz octave band.

At the lowest speed tested, the 5349 propeller had both sheet and tip vortex cavitation present and the 5363 propeller had none. The amount of cavitation on the 5349 propeller grew progressively with ship speed and the noise levels generally follow that trend. The slight dip in noise reduction at 7 kt is not significant considering the scatter in the original data at such low speeds. The noise reduction leveled off once tip vortex cavitation began on the 5363 propeller. The inception of sheet cavitation on the 5363 propeller could be expected to lower the noise reduction still further, however this event is followed closely by the inception of cloud cavitation on the 5349 propeller. This trade-off continues to about 12.5 kt at which point the noise reduction lowers rapidly. This is due to the still increasing noise production of the 5363 propeller, while the noise production of the 5349 propeller levels off. The rise in the noise reduction to the 14.7 kt condition is attributed to the inception of hub vortex cavitation on the 5349 propeller at 14.4 kt.

5. CONCLUDING REMARKS

The objectives of performing the new propeller design for CFAV QUEST were to reduce the radiated noise levels and ensure cavitation inception speeds in excess of 7 kt. These aims were met with the new propeller. QUEST's cavitation free speed range was improved by 3 kt and the new propellers are substantially quieter than the old ones. This improvement in acoustic performance with the use of the new propeller was accompanied by a small improvement in propulsive performance at all speeds. With the new propellers, QUEST's ability to conduct underwater acoustics research has been significantly enhanced.

The essential difference between the two propellers was that the new propeller was designed to handle the deep axial wake behind the bossing. Most of the gains in cavitation performance are attributable to the new propeller being adapted to this wake.

The application of large skew on the new propeller has led to some interesting results. The sheet cavitation inception speed in the model test is much higher than was observed on full scale. These results are believed to be due to the formation of regions of laminar separation together with a leading edge vortex. These effects are very scale dependent and the application of roughness strips to overcome such scale effects did not appear to be effective in this case. It remains to be seen if some other technique can be used to identify sheet and leading edge vortex cavitation in the model testing of highly skewed propellers.

Good correlation was achieved between model prediction and full scale trials data for ship powering when the effect of hull roughness was taken into account. Although the correlation for shaft revolution rate was not as good for the new propeller as for the old, the results are within the limits of confidence of the methods used.

NOTATION

C_A	Model-ship correlation allowance
P_1	Sound pressure - 5349 propeller
P_2	Sound pressure - 5363 propeller
P_D	Delivered power
P_{EN}	Effective power for "new ship" conditions
P_{ET}	Effective power for "after service" conditions
V	Ship speed
V_x	Axial wake velocity component
X	Dimensionless radius
(1+k)	Form factor
$(1+x)_N$	Ratio of apparent P_{EN} to effective power predicted by ITTC line
$(1+x)_T$	Ratio of apparent P_{ET} to effective power predicted by ITTC line
ΔL_s	Noise reduction

REFERENCES

1. Collier, A.J., George, A.J., "Acoustic Features of CFAV QUEST" IN, OCEANS'81. pp 1038-1043. IEEE, 1981.

2. Leggat, L.J., Kennedy, J.L., Ligtelijn, J.Th., "Propeller Design Studies for the Acoustic Research Ship CFAV QUEST" ATTC 19th General Meeting. Proceedings. Ann Arbor Science Pub. Inc. 1981.

3. Scott, J.R., "A Method of Predicting Trial Performance of Twin Screw Merchant Ships" RINA Trans, 1973, pp. 175-186.

4. International Towing Tank Conference, 15th. The Hugue, Sept 1978. Proceedings. N.S.M.B. Wageningen.

5. Isherwood, R.M., "Wind Resistance of Merchant Ships", RINA Trans, 1972, pp. 327-338.

6. Hundley, L.L., "The Effects of Fouling on the Powering Characteristics of U.S. Navy Surface Combatants." ATTC 19th General Meeting. Proceedings. Ann Arbor Science Pub. Inc. 1981.

7. Greeley, D.S., Kerwin, J.E., "Numerical Methods for Propeller Design and Analysis in Steady Flow", S.N.A.M.E. Annual Meeting, S.N.A.M.E. New York, 1982.

8. Straszack, J.S.C., "Propeller Design for N.R.E. Vessel" National Research Council of Canada, Division of Mechanical Engineering, Report No. MB 261 May 1964.

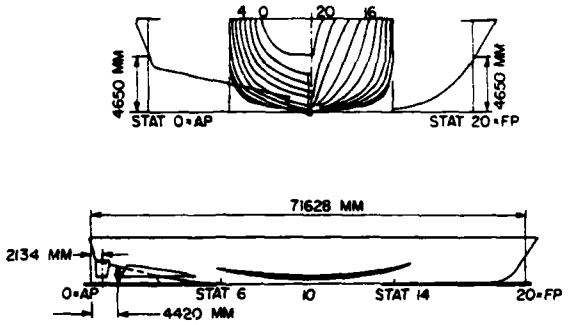


FIGURE 1: BODY PLAN, CONTOURS, AND APPENDAGE ARRANGEMENT FOR QUEST

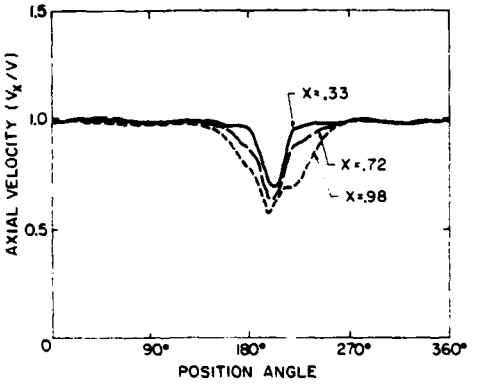


FIGURE 2: AXIAL WAKE DISTRIBUTION IN PORT PROPELLER PLANE



FIGURE 3: PROPELLER 5349 MOUNTED ON CFAV QUEST



FIGURE 4: PROPELLER 5363 MOUNTED ON CFAV QUEST

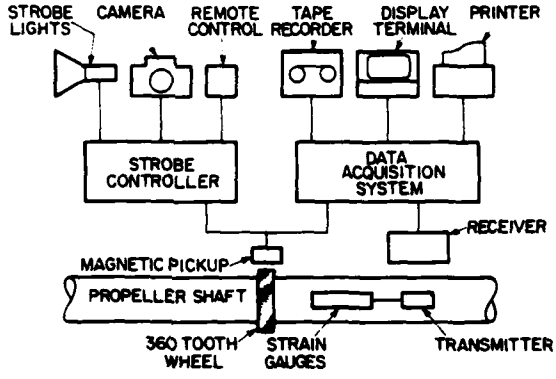


FIGURE 5: PROPELLER SHAFT INSTRUMENTATION FOR PROPULSION AND CAVITATION TRIALS

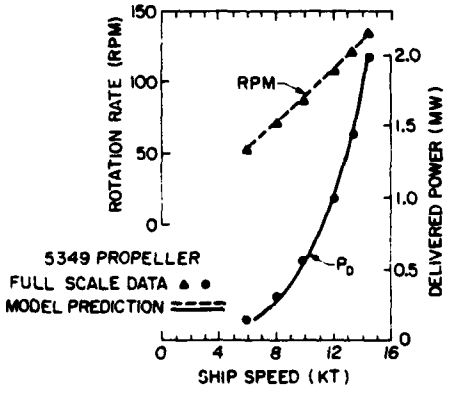


FIGURE 6: CORRELATION OF MODEL AND FULL SCALE PROPULSION DATA FOR PROPELLER 5349

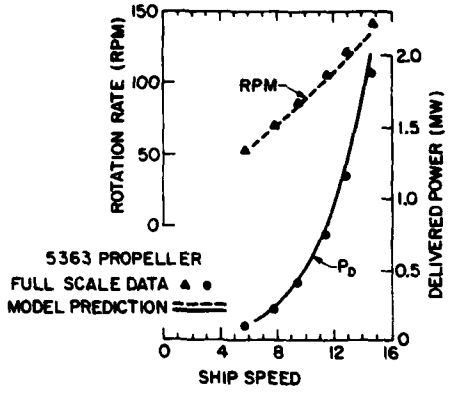


FIGURE 7: CORRELATION OF MODEL AND FULL SCALE PROPULSION DATA FOR PROPELLER 5363

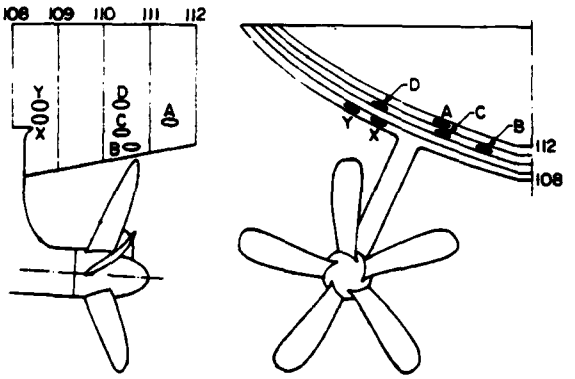


FIGURE 8: ARRANGEMENT OF VIEWING PORTS ON QUEST

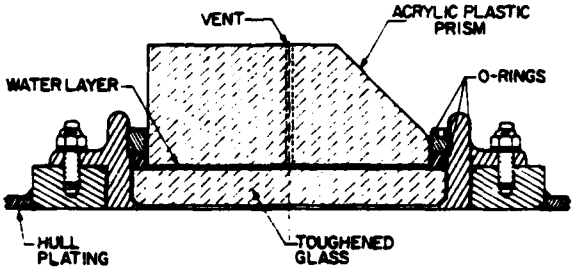


FIGURE 9: SECTION THROUGH VIEWING PORT WITH PRISM



FIGURE 10: PROPELLER 5349, 14.7 KNOTS, IN WAKE PEAK

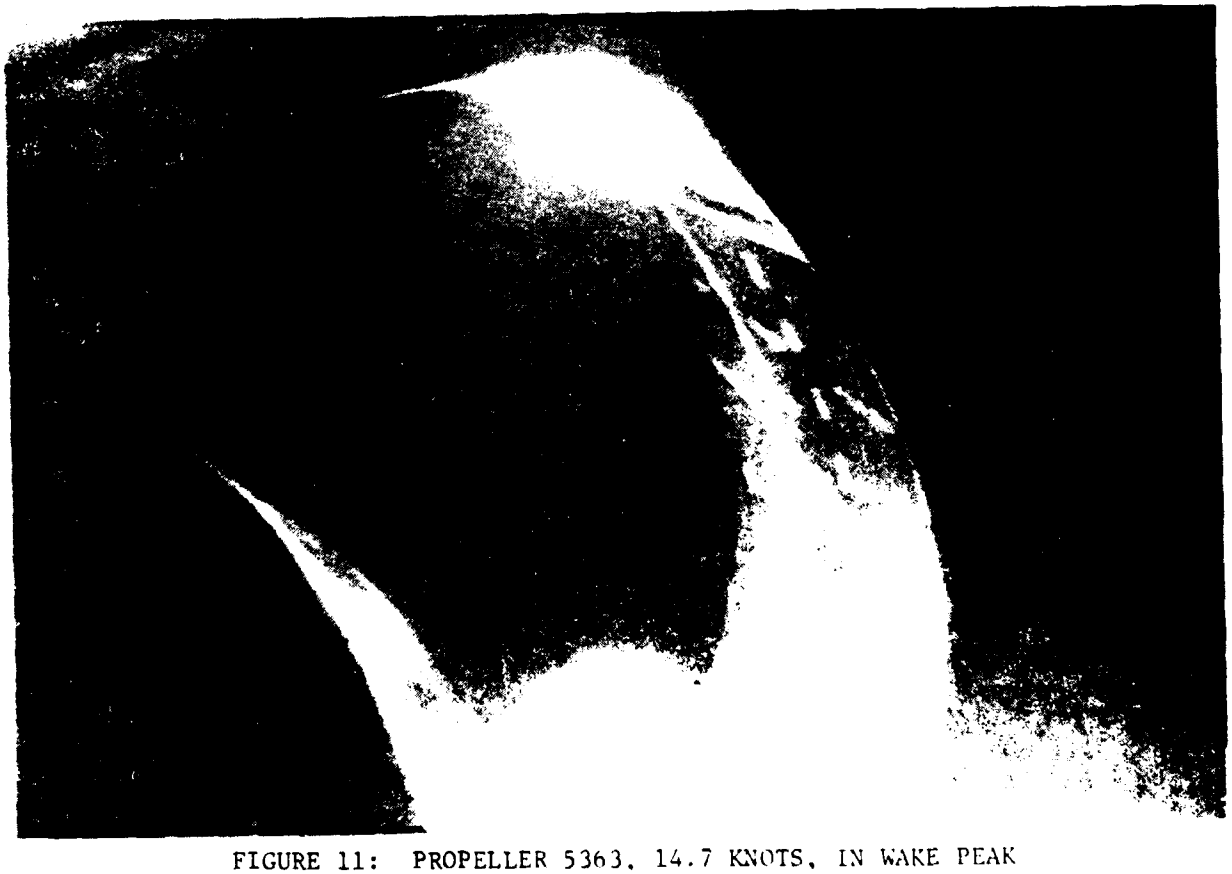


FIGURE 11: PROPELLER 5363, 14.7 KNOTS, IN WAKE PEAK



FIGURE 12: PROPELLER 5349, 14.6 KNOTS, 24° AFTER WAKE PEAK



FIGURE 13: PROPELLER 5363, 14.7 KNOTS, 24° AFTER WAKE PEAK

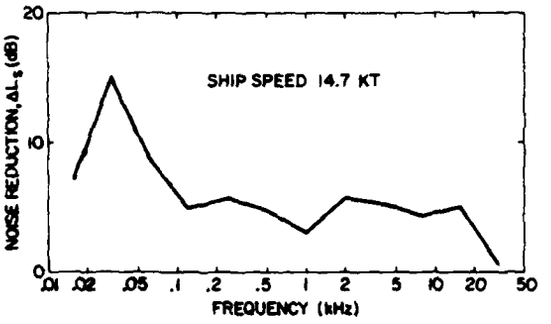


FIGURE 14: NOISE REDUCTION BETWEEN PROPELLERS 5349 AND 5363 AT 14.7 KNOTS

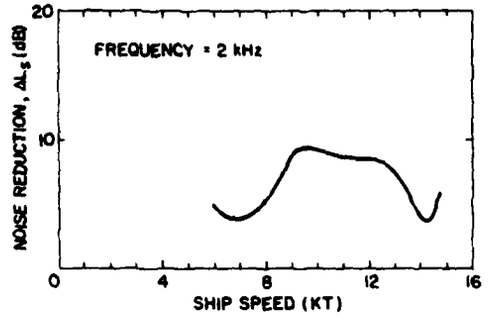


FIGURE 15: NOISE REDUCTION BETWEEN PROPELLERS 5349 AND 5363 AT 2 kHz

AD-P003 807

COMPARATIVE PERFORMANCE OF STOCK AND DESIGN PROPELLERS DERIVED FROM PROPULSION EXPERIMENTS

by

Gabor Karafiath

and

Charles J. Wilson

Presented at 1983 American Towing Tank Conference
Stevens Institute of Technology
Hoboken, New Jersey

AUGUST 1983

NOTATION

The notation contained herein conforms with the ITTC notation as presented in British Research Association Technical Memorandum 500, May 1976, with the following additions noted below.

Subscripts:

Stock - refers to the stock propeller

Design - refers to the design propeller

ADMINISTRATIVE INFORMATION

Funds for this work were provided by the Naval Material Command (NAVMAT) through the Energy Research and Development Office (ERD) of the David Taylor Naval Ship R&D Center (DTNSRDC), Code 2705, and engineering support was provided by ORI, Inc. under contract N00600-81-D-F269.

BACKGROUND

It has been the practice for many years at towing tanks to conduct propulsion experiments with propellers selected from the stock of propellers available at the particular facility. The purpose of this type of experiment is to predict the magnitude of the interaction effects between the hull, its appendages and the propeller, for use as one of the major inputs to the propeller design process and to obtain an estimate of the power and speed for a new ship design. To this end an estimate is made of the primary dimensions of the proposed propeller design to assist in selecting a stock propeller. In the past it has been considered satisfactory to select a stock propeller which is in reasonable agreement on propeller diameter, with propeller pitch as a secondary consideration, and, finally, with some thought being given to reasonable values of blade area ratio and number of blades. The justification for the propulsion experiment with stock propellers selected by such a procedure was based on the assumptions that thrust deduction and wake factors, hence hull efficiency, and relative rotative efficiency were largely independent of pitch ratio, blade area ratio and other propeller parameters as long as the diameters of the stock and design propellers were similar.

In the past it has been considered a reasonable practice at many tanks to use the open water efficiency for a design propeller with the interaction coefficients derived from the stock propeller propulsion experiments to predict the powering performance of the hull fitted with the design propeller. Experience at DTNSRDC prior to 1970 showed that results using this technique were reasonably accurate as long as the stock propellers were selected with certain limitations in mind. Experiments reported by Taylor[1] indicate that hull-propeller tip clearance is of

---

[1] References are listed on page 233.

paramount importance in affecting changes in the propulsion interaction coefficients for a given hull. With this in mind, the critical dimension for stock propellers is the diameter. The scale of the hull model was usually based on the diameter of the stock model propeller which was selected from an estimate of the diameter of the ship propeller made either by the sponsor or by the staff of DTNSRDC. The mean pitch ratio was the next critical item in stock propeller selection. The number of blades, blade area ratio and hub/diameter ratio were considered of lesser importance. The experience at the National Physical Laboratory, as described in Reference 2, was that the interaction coefficients may usually be assumed to be independent of mean pitch ratio and blade area ratio provided that the diameters of the stock and design propellers are identical and that the propeller blade loading and behind propeller efficiency for both the stock and design propellers is reasonably close to the optimum condition. Reference 2 states that the reliability of assuming that the propulsive components, other than open water efficiency, are the same for design and stock propellers may be checked by using series propeller charts to compare the loading conditions for the two propellers. It should be noted that the radial pitch distribution of the propellers considered in References 1 and 2 was either constant or the variations were comparatively small, such as in the 4-bladed Troost B Series.

Cavitation and vibration problems became signficant with propellers of conventional design as the speed and power of ships increased in the post World War II years. These problems led to the development of the highly skewed propeller and to rather radical changes of pitch distribution to unload the propeller at the tips with the objective of reducing tip erosion. The work on skewed propellers at DTNSRDC in the late 1960's resulted in a number of experimental designs and full

scale designs as reported in Reference 3 which was published in 1971. A comparison of the powering performance for a conventional and a highly skewed propeller designed for the same ship is presented in Reference 4. It may be noted from Table 3 of Reference 4 that the propulsion interaction coefficients derived from model experiments with the two propeller designs were identical in this particular comparison.

Coincidental with the development of the highly skewed propeller was the increased use of the controllable and reversible pitch propeller dictated by the interest of the U.S. Navy in the marinized gas turbine as a prime mover for high speed combatant ships. The more recent propeller designs at DTNSRDC for combatant ships are unloaded significantly at both the tips and the hub. The net result is that the stock propellers chosen in recent years are not very close, by past standards, in skew or pitch distribution to the design propellers. In addition, the scanty supply of recent propellers which may be used as stock propellers has led to selections which had sizeable differences in mean pitch ratio from the design values.

REVIEW OF HISTORICAL DATA BASE

The records at the Center were searched to determine which hull models had been fitted with both stock and design propellers for propulsion experiments from 1960 to the present. The emphasis in the search was placed first on high speed single and twin screw combatant ships, but was later expanded to include other hull forms as the number of samples of high speed surface combatant ships in the data base for the period from 1973, when the accurate prediction of propulsion interaction coefficients with stock propellers first started to become a problem, was not as great as desired.

PRESENTATION OF DATA

The data retrieved from the historical data base available at the Center for this report are presented in Figures 1 through 19. Each figure lists the hull and propeller model numbers used in the propulsion experiments of interest for the particular model. Propeller dimensions such as diameter, pitch, number of blades, etc., are given for both stock and design propellers to permit comparisons of the various parameters. Plots of pitch distribution and total rake, defined as the combination of skew induced rake and rake added in the design process to achieve a desired tip position, are compared for stock and design propellers. The difference in longitudinal tip positions for the stock and design propellers, defined as the difference in hub lengths from the forward face of the hub to the propeller axis of rotation ± the difference in total rake is also shown. The propulsion coefficients for the stock and design propellers are listed for purposes of comparison at two ship speeds for combatant ships and at one speed for naval auxiliaries. Also listed are values of estimated η_D and $\Delta\eta_D$

where η_D Stock = η_O Stock X η_H Stock X η_R Stock

η_D Design = η_O Design X η_H Design X η_R Design

η_D Estimate = ηO Design X η_H Stock X η_R Stock

and,

$$\Delta\eta_D = \eta_D \text{ Estimate} - \eta_D \text{ Design}$$

Finally, where applicable, notes are listed for differences in displacement, trim, appendages, etc., between stock and design propeller experiments. If no comments are noted it should be assumed that experimental conditions were identical for stock and design propellers.

The quantity $\Delta\eta_D$ defined above is a measure of the accuracy of powering predictions based on stock propeller powering experiments with an assumed error free

estimate of the design propeller performance. Setting $\Delta\eta_D$ equal to zero one can also derive the expression

$$\frac{\eta_D \text{ Stock}}{\eta_D \text{ Design}} = \frac{\eta_O \text{ Stock}}{\eta_O \text{ Design}}$$

to represent the case where the predicted power based on stock propeller powering experiments has no error.

DISCUSSION OF HISTORIC DATA

Ideally it should be possible to pick a stock propeller, if the stock of propellers was unlimited, such that all the propulsion coefficients from the stock propeller experiments would agree with those from the design propeller experiments within experimental accuracy. As mentioned in previous sections of this report there are a number of reasons why such ideal conditions are rarely met including the finite number of stock propellers available at the Center. It was found, rather typically, in the course of this project that individual coefficients such as thrust deduction and wake factors, hull and relative rotative efficiencies varied in more random fashion than the incremental propulsive efficiency ($\Delta\eta_D$). This trend for the values of increased propulsive efficiency to vary less than its individual components has been noted on many occasions in the past. It is generally attributed to the fact that the experimental values for η_D are derived from the resistance and self-propulsion experiments only. To compute certain of the individual components such as wake factor, for example, it is necessary to include the results from the open water propeller experiments on both the stock and design propellers which adds additional sets of experimental accuracies to consider. For this reason the primary emphasis in this project has been placed on variations of propulsive efficiency ($\Delta\eta_D$) rather than on individual components.

Considering the possible variations in Δn_D due to experimental accuracy alone it was decided at the beginning of the investigation that a difference of ± 1 1/2 percentage points would probably be reasonable and ± 2 percentage points was tolerable. It is admitted that the above limits are controversial as most sponsors would like limits on the order of ± 1/2 percentage point.

It should be noted that the accuracies for model experiments for surface ships at DTNSRDC for model speeds above 2 knots are ± 1 1/2 percent for effective power and ± 2 1/2 percent for shaft power measurements. A variation of ± 1 percentage point in the values of the interaction coefficients from one set of experiments to another for the same hull and propeller at a given condition of loading is considered normal. It is for this reason that it is critical to repeat the experiments with the stock propeller in the same time period as the design propeller using the same dynamometers if a precise comparison is desired. It should be also noted that appendage changes are made on occasion between the original experiments with the stock propeller and those with the design propeller. In such cases it is particularly important to repeat the stock propeller experiments with the altered appendages. Regrettably this procedure was not always followed due to the limitations of time and money.

With regard to accuracy, if one were to perform an experiment specifically designed to explore the effect of changing propeller geometry on the interaction coefficients then that experiment would be designed so that many propellers of different systematic design would be tested on one model at a limited number of speeds with a statistically significant number of repeat points. The confidence level from such an experiment would be very high and based on past experience it is expected that a 1 percent difference in delivered power would be significant at the 90 percent confidence level.

ANALYSIS OF DATA

As mentioned before, historical practice for selecting stock propellers is to consider the following variables tested in the order of their importance:

1. Match the anticipated design propeller diameter,
2. Match the anticipated design propeller pitch ratio, and
3. Match blade area and number of blades.

In reviewing Figures 1 through 19, it is possible to observe that there are a number of older models where the stock propeller is noticeably different from the design propeller in either diameter, rake or hub length to the vertical axis of revolution which affects tip position.

The clearances between the propeller, particularly at the tips, and the hull of the ship, and its appendages, are considered to be of prime interest in affecting the interaction coefficients. Generally, for a single screw ship a decrease in diameter usually results in an increase in thrust deduction factor $(1 - t)$, and wake factor $(1 - \omega)$, although the increase in wake factor will normally be smaller than that for thrust deduction factor. For twin screw ships the same trends should be anticipated except the change in thrust deduction factor will usually be smaller than for single screw and the change in wake factor may be quite small or insignificant. For a decrease in propeller diameter, then, an increase in hull efficiency, η_H, should be anticipated.

In the more recent propeller models listed on Figures 1 through 19 the differences between stock and design propellers is in skew and pitch distribution. Specifically, design trends regarding blade skew which may induce rake, and pitch distribution have undergone quite radical changes in the last 15 years. It is believed by the propeller designers at the Center that both of these parameters affect the interaction coefficients although the individual contributions of skew

and pitch distribution are difficult to quantify separately as current propeller designs normally incorporate both. Differences in propeller blade shape, area ratio and thickness are thought to affect the interaction coefficients to a lesser degree than those parameters previously commented on. Figures 20 and 21 show a typical skewed and a typical non-skewed propeller

EFFECTS OF VARYING PROPELLER DIAMETER

Examples of performance where stock and design propeller diameters are different are presented in Figures 8, 11, 13, 16, 17, and 18 for Models 4858-1, 5324, 5279-1, 4870, 4773, and 4554, respectively. A plot of $\Delta\eta_D$ against the ratio of stock to design propeller diameters is presented in Figure 22. The solid spots of Figure 22 and succeeding figures represent single screw ships and the open spots represent twin screw ships. It may be noted that the comparison between design and stock propeller performance is generally poor when the diameters are different with only one exception, Model 4858-1. Examination of the individual propulsion efficiency components shows the major contributor to the poor comparison is $\Delta\eta_R$, the difference in the relative rotative efficiencies for design and stock propellers. A plot of $\Delta\eta_R$ against diameter ratio, included in Figure 23, indicates that $\Delta\eta_R \cong \Delta\eta_D$ when diameter changes. It would appear, then, that every effort should be made to assure that the stock propeller diameter is identical, or very nearly identical to that for the design propeller, as even a 4 percent difference in diameter degrades the predictions from the stock propeller to a significant degree.

EFFECTS OF VARYING PITCH RATIO

A plot of $\Delta\eta_D$ against pitch ratio at 0.7 radius ratio for design and stock propellers is presented in Figure 24. The experience derived from DTNSRDC experiments agrees in general with that from Reference 2 in that variations in pitch

ratio are not as important as changes in diameter. From Figure 24 it may be seen that a variation of at least ± 15 percent in pitch ratio between stock and design propellers is quite acceptable.

Figures 1, 3 and 24 also show the effect of using controllable pitch stock propellers set at an off-design pitch as was done for Models 5401 and 5340. In each case the original design-stock propeller comparison was made with the stock propellers set at an off-design pitch which approximated the pitch for the design propellers. The agreement between stock and design coefficients was quite poor. Note in Figure 1 that $\Delta\eta_D$ is + 0.033 for the 10 knot speed and + 0.063 for the 16 knot speed for the off-design pitch ratio setting of 1.813 contrasted to -0.010 at 10 knots and + 0.024 at 16 knots when the stock propellers are set at the design pitch ratio of 1.511. The same trend is apparent in Figure 3 where the values of $\Delta\eta_D$ are quite small for the design pitch ratio setting of 1.54 on the stock propellers and unacceptably large for the off-design pitch setting. Figure 24 shows the effects on the propulsion coefficients of operating at pitch settings off the design pitch value for Model 5340 when fitted with stock propellers 4660 and 4661. In both cases, Model 5340 and 5401, a better prediction was obtained when the stock propeller was operated at its design pitch then at off-design pitch even though the off-design pitch was a much better match to the design propeller pitch.

Note that there are significant changes in both η_R and particularly in η_H as well as the anticipated major change in η_O as the pitch ratio is changed to the off-design value. The same trend for significant changes in the component efficiencies may be noted in the data presented in Figure 1. For Model 5401, fitted with stock propellers 4740A, 4741A, the greatest change is in η_R for the two off-design pitch settings. The small difference in displacement and trim between

stock and design propeller experiments is not considered significant as far as effects on the propulsion coefficients are concerned. It should be noted, however, that the design propellers for Model 5401 have button shape type fairwaters while the stock propellers have streamlined fairwaters. This difference has a measurable effect on thrust deduction factor and $\Delta\eta_D$. For Model 5340 all propellers fitted have the same button shape fairwaters.

EFFECT OF PROPELLER EFFICIENCY

As mentioned earlier, a perfect prediction occurs when the ratio η_O Stock/η_O Design equals the ratio η_D Stock/η_D Design. An estimate of η_O Stock/η_O Design can be made prior to choosing a stock propeller. The usefulness of this ratio is shown in Figures 25 and 26. Notice that when the off-design pitch stock propeller tests are excluded all the predictions fall within ± 4.0 percent η_D for the cases where η_O Stock/η_O Design is greater than 0.98. It is also important to note that the models where the stock propeller varied more than 3 percent from the design propeller diameter (see Figure 22) and showed poor $\Delta\eta_D$ also had low, 0.93 to 0.98, values of η_O Stock/η_O Design. By contrast, Model 4858-1 which had good $\Delta\eta_D$ independent of the extreme D Stock/D Design diameter ratios also had high ratios of η_O Stock/η_O Design ranging from 0.97 to 1.04.

EFFECTS OF VARYING OTHER PROPELLER PARAMETERS

Plots of the effects of varying the number of blades, blade thickness, projected area ratio, expanded area ratio, skew, and longitudinal tip position on $\Delta\eta_D$ have been examined and are shown in Figures 27 through 32. The correlation for any of these parameters by itself is not very meaningful. Undoubtedly certain of the parameters, such as blade thickness, for example, do affect propulsion

performance but it has not been possible in this study to ascertain the significance of the individual parameters. Part of the problem is that each time propellers are designed it is the rule to find changes in some of the above parameters as well as in camber, chord length and pitch distribution. The use of the regression analysis for the data in this report is ruled out by the limited number of samples.

GENERAL COMMENTS

If the samples where there were diameter changes or off-design pitch settings are removed from the population of data, the use of the stock propeller for predicting the performance of the design propeller is justified. The accuracy of the prediction is improved as the open water efficiency of the stock propelller exceeds that of the design propeller. It is not apparent that skew, pitch distribution and blade thickness effects on propulsion performance coefficients are large enough to be discerned at the present time.

Plots were also prepared of $\Delta(1 - t)$ and $\Delta(1 - \omega t)$ versus $\Delta\eta_D$, however, even when the diameter variations and off-design pitch stock propeller cases were deleted the data did not show any significant trends and therefore the plots are not included.

RECOMMENDATIONS FOR THE SELECTION AND USE OF STOCK PROPELLERS

The diameter of available propellers should be considered of primary importance in selecting a stock propeller. If precise identity with the proposed design diameter is not possible with existing propellers it is recommended that a stock propeller with the correct diameter be built for the project.

Adjustable pitch propellers should be set only at their design pitch when being used for stock propellers. There is sufficient evidence to indicate that

setting a propeller at a pitch other than design affects not only the propeller efficiency but relative rotative efficiency as well. The effects of a difference in pitch ratio between the stock and design propellers is distinctly secondary to that for diameter and off-design pitch settings.

Differences in skew, blade thickness, pitch distribution, etc., should be kept to a minimum but their individual effects are difficult to identify and are probably smaller than the diameter effect and off-design pitch effect.

Propulsion experiments should be run as a check with the stock propellers at any time the hull model, appendages, loading conditions, or design propellers have changed to establish possible differences with different dynamometers or experimental set-ups.

The open water efficiency of a stock propeller should be checked prior to use to ensure that the performance of the stock propeller will not be markedly inferior to that anticipated for the design propeller.

SUMMARY

It has been the practice at DTNSRDC and other towing tanks to use the results of experiments with stock propellers fitted to a hull model to make preliminary predictions of the powering performance of the hull, and to provide propulsion coefficients to be used in the propeller design process. At times selected stock propulsion coefficients have been used with the propeller efficiency of the design propeller to provide a more precise estimate of the powering performance of the hull when fitted with the design propeller. The purpose of this report has been to investigate problems which have arisen in the selection and use of stock propellers with the objectives of comparing the propulsion coefficients derived from experiments with stock and design propellers and recommending changes to existing practices if practicable.

Data from experiments with 19 hull forms representing destroyers, frigates, and various naval auxiliaries were retrieved from the records at DTNSRDC. Some of the hulls had more than one design propeller(s) fitted, so it is possible in certain samples to compare the stock propeller performance to several design propellers and that of one design propeller to another.

The reasons for variations of propeller performance in the behind condition are conjectural. Variations in diameter, pitch ratio and distribution, skew, rake, blade thickness, mean width and area ratios all probably affect propulsion performance to some degree. The current investigation, due in part to the limited number of samples, is successful only in identifying what are considered to be major contributions to the variations in performance.

Differences in diameter between stock and design propellers appear to be the major contributor to poor predictions of performance. In 5 of the 6 samples available with different diameter propellers the difference in predicted propulsive efficiency using the values of η_H and η_R from the stock propellers with the propeller efficiency η_O from the design propeller experiments, compared to the propulsive efficiency from the design propeller experiments, $(\Delta\eta_D)$, exceeded the tolerable limits of ± 2 percentage points by a sizeable margin. It was found that this difference was due for the most part to the differences in the values of η_R for the stock and design propeller experiments such that $\Delta\eta_D \equiv \Delta\eta_R$. The reason for this change in η_R is not apparent at this time, so the recommendation is to avoid stock propellers where diameter is an obvious problem. If necessary a new stock propeller should be built to avoid this problem.

Another obvious problem is the practice of using a stock adjustable pitch propeller at an off-design pitch with the thought of approximating the design pitch

of the design propeller. Plots of propulsion coefficients derived from experiments at several pitch settings indicate that there may be substantial changes in η_R, particularly at the higher pitch settings, as well as the anticipated changes in η_O. Comparisons of performance with the stock and design propellers set at their respective design pitches agreed within tolerable limits. This should not be too surprising as previous experience has shown that propulsion performance is not affected significantly unless the pitch changes are sizeable (20 percent or greater).

It is suggested that the open water performance of prospective stock propellers be compared to the applicable Troost Series charts. There is a tendency for poor performing propellers in open water to be even less effective behind hulls such that the other propulsion coefficient elements, η_H and/or η_R may be affected to a degree that makes a tolerable prediction of design propeller performance unlikely.

If there is a trend for other propeller parameters such as skew, blade thickness, etc. to affect propeller performance behind the hull it is not readily apparent from the limited number of samples available.

It is strongly urged that a curtailed experiment with the stock propeller fitted be conducted whenever there are changes to the hull, appendages or design propellers which required additional propulsion experiments. The purpose of the check experiments with the stock propeller is to determine changes due to instrumentation.

REFERENCES

1. Taylor, D.W., "The Speed and Power of Ships". United States Government Printing Office, (1943).

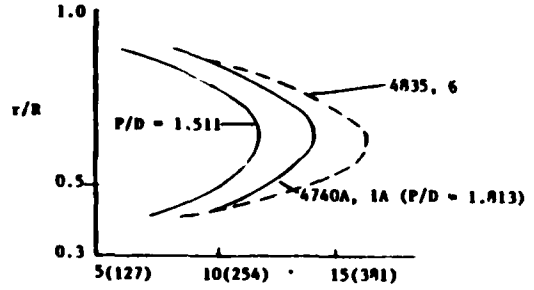
2. Bowden, B.S., "The Use of Stock Screws for Propulsion Experiments". National Physical Laboratory Ship Division Report 146, (Oct 1970).

3. Cumming, R.A., W.B. Morgan, and R.J. Boswell, "Highly Skewed Propellers". Transactions, The Society of Naval Architects and Marine Engineers, Vol. 80, (1972).

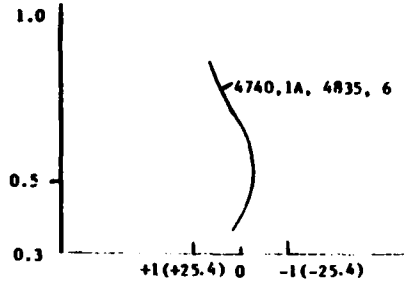
4. Boswell, R.J. and G.G. Cox, "Design and Model Evaluation of a Highly Skewed Propeller for a Cargo Ship", Marine Technology, (Jan 1974).

MODEL 5401 PROPELLERS 4740A, 4741A (STOCK CP SET AT TOW PITCH RATIOS); 4835, 4836 (DESIGN CP)

PROPELLER NO.	DIAMETER INCHES (MM)	PITCH INCHES (MM)	P/D	NUMBER OF BLADES	HUB DIAMETER INCHES (MM)	MEAN WIDTH RATIO	t/c at 0.7 R	PROJECTED AREA RATIO	EXPANDED AREA RATIO	SKEW AT TIP DEGREES	HUB LENGTH TO AXIS INCHES (MM)	TOTAL RAKE AT TIP INCHES (MM)
4835, 6	7.623 (193.6)	15.653 (397.5)	2.053	5	2.287 (58.09)	0.338	0.932	0.559	0.716	25	1.155 (29.34)	0.57 (14.5)
4740A, 1A	7.623 (193.6)	11.518 (292.5)	1.511	5	2.250 (57.15)	0.336	.0446	0.590	0.725	25	1.250 (31.75)	0.43 (10.9)
4740A, 1A	7.623 (193.6)	13.820 (351.0)	1.813*	5	2.250 (57.15)	0.336	.0446	0.590	0.725	25	1.250 (31.75)	0.43 (10.9)



PITCH - INCHES (MM)



TOTAL RAKE - INCHES (MM)

COMPARISON OF PERFORMANCE AT 10 AND 16 KNOTS

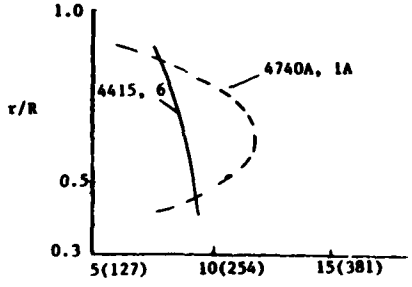
PROP. NOS.	DESIGNATION	P/D	V_S KNOTS	η_D	η_Φ	η_H	η_R	1-t	$1-w_T$	$1-w_Q$	η_DEST	$\Delta\eta_D$
4740A, 1A	STOCK CP	1.813	10	.615	.725	.940	.905	.940	1.000	.925		
4835, 6	DESIGN CP	2.053	10	.590	.655	.905	1.000	.875	.970	.970	.557	-.033
4740A, 1A	STOCK CP	1.511	10	.615	.670	.955	.960	.945	.990	.965		
4835, 6	DESIGN CP	2.053	10	.590	.655	.905	1.000	.875	.970	.970	.600	+.010
4740A, 1A	STOCK CP	1.813	16	.585	.700	.895	.930	.885	.990	.930		
4835, 6	DESIGN CP	2.053	16	.575	.615	.920	1.000	.860	.935	.955	.512	-.063
4740A, 1A	STOCK CP	1.511	16	.600	.670	.905	.990	.890	.985	.980		
4835, 6	DESIGN CP	2.053	16	.575	.615	.920	1.010	.860	.935	.955	.551	-.024

NOTE: STOCK PROPELLER EXPERIMENTS CONDUCTED AT CONDITIONS EQUIVALENT TO 1005 TONS (1021 METRIC TONS), EVEN KEEL
DESIGN PROPELLER EXPERIMENTS CONDUCTED AT CONDITIONS EQUIVALENT TO 1030 TONS (1043 METRIC TONS), 1.1 FT. (.335 M) BY STERN
*SET AT OFF-DESIGN PITCH

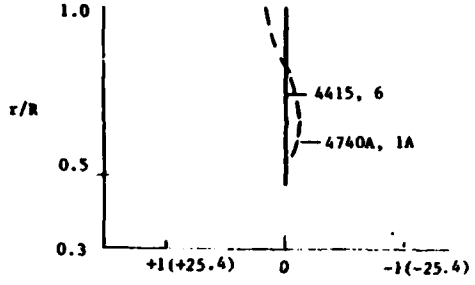
Figure 1 - Propulsion Performance Coefficients and Propeller Information for Twin Screw Model 5401 Fitted with Stock Propellers 4740A, 4741A, and Design Propellers 4835, 4836

MODEL 5367 PROPELLERS 4415, 4416, (STOCK FP); 4740A, 4741A (DESIGN CP)

PROPELLER NO.	DIAMETER INCHES (MM)	PITCH INCHES (MM)	P/D	NUMBER OF BLADES	HUB DIAMETER INCHES (MM)	MEAN WIDTH RATIO	t/c at 0.7R	PROJECTED AREA RATIO	EXPANDED AREA RATIO	SKEW AT TIP DEGREES	HUB LENGTH TO AXIS INCHES (MM)	TOTAL RAKE AT TIP INCHES (MM)
4415, 6	7.623 (193.6)	8.755 (222.4)	1.148	5	1.545 (39.2)	.302	.0420	.672	.785	0	--	0
4740A,1A	7.623 (193.6)	11.518 (292.6)	1.511	5	2.250 (57.1)	.336	.0446	.590	.725	25	1.250 (31.75)	+0.43 (10.9)



PITCH - INCHES (MM)



TOTAL RAKE-INCHES (MM)

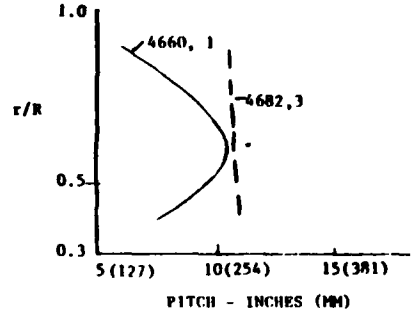
COMPARISON OF PROPELLERS AT 14 AND 22 KNOTS

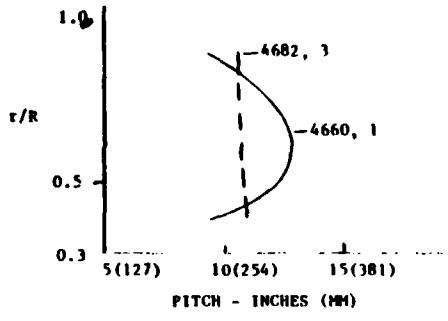
PROP. NOS.	DESIGNATION	P/D	V_S KNOTS	η_D	η_θ	η_H	η_R	1-t	$1-w_T$	$1-w_Q$	η_{DEST}	$\Delta\eta_D$
4415, 6	STOCK CP	1.148	14	.635	.700	.920	.985	.870	.945	.935	--	--
4740A,1A	DESIGN CP	1.511	14	.650	.670	1.010	.960	.920	.915	.885	.607	-.043
4415, 6	STOCK CP	1.148	22	.615	.685	.890	1.005	.840	.945	.950	--	--
4740A,1A	DESIGN CP	1.511	22	.635	.665	.975	.980	.885	.965	.955	.595	-.040

Figure 2 - Propulsion Performance Coefficients and Propeller Information for Twin Screw Model 5367 Fitted with Stock Propellers 4415, 4416, and Design Propellers 4740A, 4741A

MODEL 5340 PROPELLERS 4660, 4661 (STOCK CP SET AT TWO PITCH RATIOS); 4682, [illegible] (DESIGN CP)

PROPELLER NO.	DIAMETER INCHES (MM)	PITCH INCHES (MM)	P/D	NUMBER OF BLADES	HUB DIAMETER INCHES (MM)	MEAN WIDTH RATIO	t/c at 0.7R	PROJECTED AREA RATIO	EXPANDED AREA RATIO	SKEW AT TIP DEGREES	HUB LENGTH TO AXIS INCHES (MM)	TOTAL RAKE AT TIP INCHES (MM)
4660, 1	8.218 (208.7)	12.655 (321.4)	1.540	5	2.316 (58.8)	.328	.0359	.591	.730	21.88	0.905 (22.99)	0
4682, 3	8.218 (208.7)	10.667 (270.9)	1.298	4	2.316 (58.8)	.439	.0344	.647	.783	0	1.017 (25.83)	0





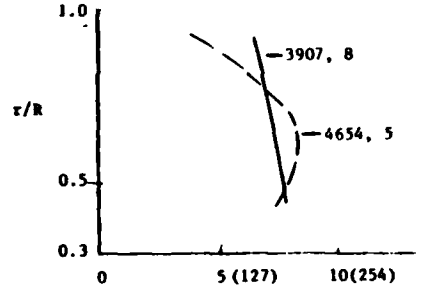
COMPARISON AT 20 AND 34 KNOTS

PROP. NOS.	DESIGNATION	P/D	V_S KNOTS	η_D	η_θ	η_H	η_R	1-t	$1-w_T$	$1-w_Q$	η_DEST	$\Delta\eta_D$
4660,1	STOCK CP	1.200	20	.605	.640	.945	1.000	.888	.940	.940	--	--
4682,3	DESIGN CP	1.298	20	.680	.750	.920	.985	.885	.965	.955	.709	+.029
4660,1	STOCK CP	1.540	20	.662	.748	.900	.985	.873	.970	.960	--	--
4682,3	DESIGN CP	1.298	20	.680	.750	.920	.985	.885	.965	.955	.665	-.015
4660,1	STOCK CP	1.200	34	.618	.640	.940	1.028	.896	.953	.963	--	--
4682,3	DESIGN CP	1.298	34	.655	.750	.885	.985	.885	1.000	.990	.725	+.070
4660,1	STOCK CP	1.540	34	.651	.748	.882	.988	.873	.990	.984	--	--
4682,3	DESIGN CP	1.298	34	.655	.750	.885	.985	.885	1.000	.990	.654	-.001

Figure 3 - Propulsion Performance Coefficients and Propeller Information for Twin Screw Model 5340 Fitted with Stock Propellers 4660, 4661, and Design Propellers 4682, 4683

MODEL 5335 PROPELLERS 3907, 3908 (STOCK FP SET AT ONE PITCH RATIO); 4654, 4655 (DESIGN FP)

PROPELLER NO.	DIAMETER INCHES (MM)	PITCH INCHES (MM)	P/D	NUMBER OF BLADES	HUB DIAMETER INCHES (MM)	MEAN WIDTH RATIO	t/c at 0.7R	PROJECTED AREA RATIO	EXPANDED AREA RATIO	SKEW AT TIP DEGREES	HUB LENGTH TO AXIS INCHES (MM)	TOTAL RAKE AT TIP INCHES (MM)
3907, 8	7.399 (187.9)	7.046 (179.0)	.952	5	1.508 (38.3)	.358	.0328	.765	.823	0	1.145 (29.08)	0
4654, 5	7.399 (187.9)	7.458 (189.4)	1.008	5	1.508 (38.3)	.375	.0274	.315	.950	.535	1.145 (29.08)	+0.58 (14.7)



PITCH - INCHES (MM)

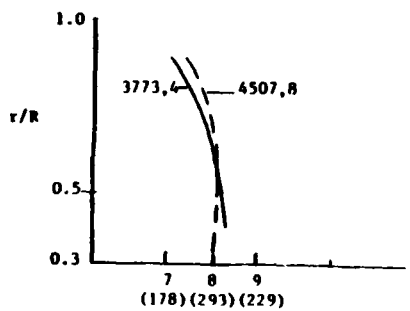
PROPELLER COMPARISON AT 22 AND 30 KNOTS

PROP. NOS.	DESIGNATION	P/D	V_S KNOTS	η_D	η_Θ	η_H	η_R	1-t	$1-w_T$	$1-w_Q$	η_DEST	$\Delta\eta_D$
3907, 8	STOCK FP	.952	22	.59	.65	.95	.95	.94	.99	.97	--	--
4654, 5	DESIGN FP	1.008	22	.60	.64	.96	.98	.93	.97	.96	.58	-.02
3907, 8	STOCK FP	.952	30	.58	.65	.93	.95	.95	1.02	.99	--	--
4654, 5	DESIGN FP	1.008	30	.60	.64	.95	.99	.94	.99	.98	.565	-.035

Figure 4 - Propulsion Performance Coefficients and Propeller Information for Twin Screw Model 5335 Fitted with Stock Propellers 3907, 3908, and Design Propellers 4654, 4655

MODEL 5201 PROPELLERS 3773, 3774 (STOCK FP);4507, 4508 (DESIGN FP)

PROPELLER NO.	DIAMETER INCHES (MM)	PITCH INCHES (MM)	P/D	NUMBER OF BLADES	HUB DIAMETER INCHES (MM)	MEAN WIDTH RATIO	t/c at 0.7R	PROJECTED AREA RATIO	EXPANDED AREA RATIO	SKEW AT TIP DEGREES	HUB LENGTH TO AXIS INCHES (MM)	TOTAL RAKE AT TIP INCHES (MM)
3773, 4	7.480 (190.0)	7.832 (198.9)	1.047	5	1.545 (39.2)	.324	.0343	.675	.816	0	1.680 (42.7)	0
4507, 8	7.480 (190.0)	7.758 (202.1)	1.064	5	1.496 (38.0)	.275	.0451	.580	.701	0	1.101 (28.0)	0



PTICH - INCHES (MM)

COMPARISON AT 22 AND 32 KNOTS

PROP. NOS.	DESIGNATION	P/D	V_S KNOTS	η_D	η_O	η_H	η_R	1-t	$1-w_T$	$1-w_Q$	η_DEST	$\Delta\eta_D$
3773, 4	STOCK FP	1.047	22	.660	.695	.955	.990	.915	.955	.950	--	--
4507, 8	DESIGN FP	1.064	22	.660	.715	.925	.995	.890	.960	.960	.676	+.016
3773, 4	STOCK FP	1.047	32	.635	.685	.940	.980	.930	.985	.975	--	--
4507, 8	DESIGN FP	1.064	32	.660	.705	.940	1.000	.915	.975	.975	.649	-.011

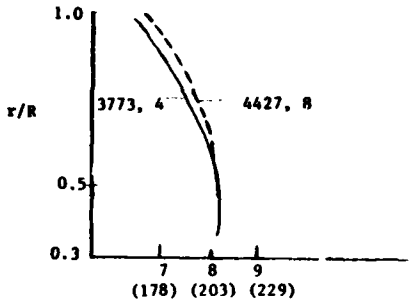
COMMENTS: DESIGN PROPS. CLOSER TO HULL (DIFF. IN HUB LENGTHS TO PROP. AXIS)
(1.68" STOCK, 1.10" DESIGN)

Figure 5 - Propulsion Performance Coefficients and Propeller Information for Twin Screw Model 5201 Fitted with Stock Propellers 3773, 3774, and Design Propellers 4507, 4508

MODEL 5047 PROPELLERS 3773, 3774 (STOCK FP); 4427, 4428 (DESIGN FP)

PROPELLER NO.	DIAMETER INCHES (MM)	PITCH INCHES (MM)	P/D	NUMBER OF BLADES	HUB DIAMETER INCHES (MM)	MEAN WIDTH RATIO	t/c at 0.7R	PROJECTED AREA RATIO	EXPANDED AREA RATIO	SKEW AT TIP DEGREES	HUB LENGTH TO AXIS INCHES (MM)	TOTAL RAKE AT TIP INCHES (MM)
3773, 4	7.480 (190.0)	7.832 (198.9)	1.047	5	1.545 (39.2)	.324	.0343	.675	.816	0	1.680 (42.67)	0
4427, 8	7.480 (190.0)	8.026 (203.9)	1.073	5	1.545 (39.2)	.322	.0343	.672	.813	0	1.680 (42.67)	0

NOTE: APPENDAGES ALTERED



COMPARISON OF PERFORMANCE AT 22 AND 30 KNOTS

PROP. NOS.	DESIGNATION	P/D	V_S KNOTS	η_D	η_Θ	η_H	η_R	1-t	$1-w_T$	$1-w_Q$	η_DEST	$\Delta\eta_D$
3773, 4	STOCK FP	1.047	22	.660	.735	.935	.955	.915	.975	.960	--	--
4427, 8	DESIGN FP	1.073	22	.660	.720	.945	.970	.920	.960	.970	.643	-.017
3773, 4	STOCK FP	1.047	30	.650	.730	.925	.955	.915	.985	.970	--	--
4427, 8	DESIGN FP	1.073	30	.650	.710	.940	.970	.925	.970	.980	.627	-.023

Figure 6 - Propulsion Performance Coefficients and Propeller Information for Twin Screw Model 5047 Fitted with Stock Propellers 3773, 3774, and Design Propellers 4427, 4428

MODEL 4997 PROPELLERS 1716, 1717 (STOCK FP); 4253, 4254 (DESIGN FP)

PROPELLER NO.	DIAMETER INCHES (MM)	PITCH INCHES (MM)	P/D	NUMBER OF BLADES	HUB DIAMETER INCHES (MM)	MEAN WIDTH RATIO	t/c at 0.7R	PROJECTED AREA RATIO	EXPANDED AREA RATIO	SKEW AT TIP DEGREES	HUB LENGTH TO AXIS INCHES (MM)	TOTAL RAKE AT TIP INCHES (MM)
1716, 7	8.80 (223.5)	8.622 (219.0)	.980	4	1.49 (3.78)	.22		.397	.471	6	0.85 (21.59)	+0.73 (18.5)
4253, 4	8.590 (218.1)	9.964 (253.0)	1.160	4	1.500* (3.81)	.238	.0470	.390	.486	0	--	0

COMPARISON OF PERFORMANCE 20 KNOTS

PROP. NOS.	DESIGNATION	P/D	V_S KNOTS	η_D	η_O	η_H	η_R	1-t	$1-w_T$	$1-w_Q$	η_DEST	$\Delta\eta_D$
1716, 7	STOCK FP	.980	20	.690	.750	.930	.985	.837	.900	.905	--	--
4253, 4	DESIGN FP	1.160	20	.683	.723	.900	1.050	.820	.910	.935	.662	+.021

COMMENTS - STOCK PROP. D IS LARGER THAN DESIGN PROP. D

STOCK PROP. D HAS RAKE +95° DESIGN PROP. RAKE IS 0°

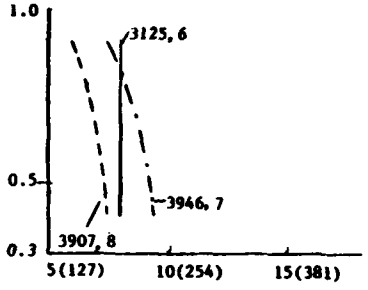
∴ SHOULD COMPENSATE FOR CHANGES IN IT AND $1-w_T$ (ΔD EFFECTS VS RAKE EFFECTS)

* HUBS BUILT UP

Figure 7 - Propulsion Performance Coefficients and Propeller Information for Twin Screw Model 4997 Fitted with Stock Propellers 1716, 1717, and Design Propellers 4253, 4254

MODEL 4858-1 PROPELLERS 3125, 3126 (STOCK FP); 3907, 3908, 3946, 3947 (DESIGN FP)

PROPELLER NO.	DIAMETER INCHES (MM)	PITCH INCHES (MM)	P/D	NUMBER OF BLADES	HUB DIAMETER INCHES (MM)	MEAN WIDTH RATIO	t/c at 0.7R	PROJECTED AREA RATIO	EXPANDED AREA RATIO	SKEW AT TIP DEGREES	HUB LENGTH TO AXIS INCHES (MM)	TOTAL RAKE AT TIP INCHES (MM)
3125, 6	7.48 (190.0)	8.076 (205.1)	1.080	4	1.545 (39.2)	.430	.0262	.747	.911	0	1.680 (42.7)	0
3907, 8	7.399 (187.9)	7.046 (179.0)	.952	5	1.508 (38.3)	.358	.0328	.765	.823	0	1.145 (29.1)	0
3946, 7	7.795 (198.0)	8.765 (222.6)	1.124	6	1.508 (38.3)	.336	.0306	.853	1 035	0	1.145 (29.1)	0



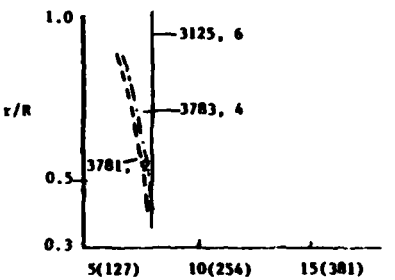
COMPARISON OF PERFORMANCE AT 20 AND 30 KNOTS

PROP. NOS.	DESIGNATION	P/D	V_S KNOTS	η_D	η_Θ	η_H	η_R	1-t	$1-w_T$	$1-w_Q$	η_DEST	$\Delta\eta_D$
3125, 6	STOCK FP	1.080	20	.644	.682	.982	.958	.920	.930	.917	--	--
3907, 8	DESIGN FP I	.952	20	.612	.652	.976	.962	.920	.940	.920	.613	+.001
3125, 6	STOCK FP	1.080	20	.644	.682	.982	.958	.920	.940	.920	--	--
3946, 7	DESIGN FP II	1.124	20	.640	.668	.982	.972	.918	.935	.922	.628	-.012
3907, 8	DESIGN FP I	.952	20	.612	.652	.976	.962	.920	.940	.920	--	--
3946, 7	DESIGN FP II	1.124	20	.640	.668	.982	.972	.918	.935	.922	.627	-.013
3125, 6	STOCK FP	1.080	30	.660	.678	.960	1.008	.917	.948	.948	--	--
3907, 8	DESIGN FP I	.952	30	.615	.648	.965	.983	.917	.950	.938	.627	+.012
3125, 6	STOCK FP	1.080	30	.660	.678	.960	1.008	--	--	--	--	--
3946, 7	DESIGN FP III	1.124	30	.637	.668	.968	.983	.918	.948	.938	.646	+.009
3907, 8	DESIGN FP I	.952	30	.615	.648	.965	.983	.917	.950	.938	--	--
3946, 7	DESIGN FP II	1.124	30	.637	.668	.968	.983	.918	.948	.938	.634	-.003

Figure 8 - Propulsion Performance Coefficients and Propeller Information for Twin Screw Model 4858-1 Fitted with Stock Propellers 3125, 3126, Design Propellers 3907, 3908, and 3946, 3947

MODEL 4702 PROPELLER 3125, 3126 (STOCK FP); 3781, 3782, 3783, 3784 (DESIGN FP)

PROPELLER NO.	DIAMETER INCHES (MM)	PITCH INCHES (MM)	P/D	NUMBER OF BLADES	HUB DIAMETER INCHES (MM)	MEAN WIDTH RATIO	t/c at 0.7R	PROJECTED AREA RATIO	EXPANDED AREA RATIO	SKEW AT TIP DEGREES	HUB LENGTH TO AXIS INCHES (MM)	TOTAL RAKE AT TIP INCHES (MM)
3125, 6	7.48 (190.0)	8.076 (205.1)	1.080	4	1.545 (39.2)	.430	.0262	.747	.911	0	1.680 (42.7)	0
3781, 2	7.399 (187.7)	7.378 (187.4)	.997	5	1.545 (39.2)	.395	.0275	.829	.988	0	1.680 (42.7)	0
3783, 4	7.135 (181.2)	7.832 (198.9)	1.047	5	1.545 (39.2)	.324	.0274	.675	.816	0	1.680 (42.7)	0



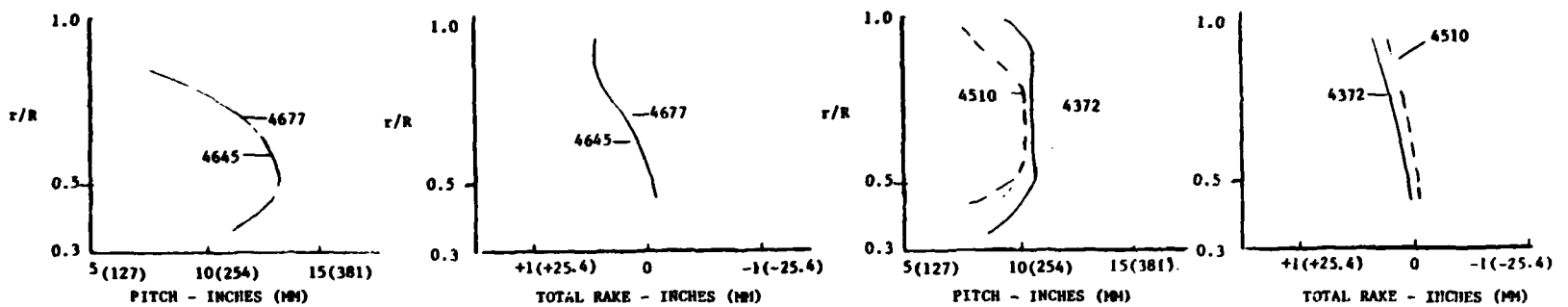
COMPARISON OF PERFORMANCE AT 20 AND 30 KNOTS

PROP. NOS.	DESIGNATION	P/D	V_S KNOTS	η_D	η_B	η_H	η_R	1-t	$1-w_T$	$1-w_Q$	η_DEST	$\Delta\eta_D$
3125, 6	STOCK FP	1.080	20	.648	.683	.957	.997	.892	.932	.932	--	--
3781, 2	DESIGN FP I	.997	20	.604	.662	.945	.967	.900	.952	.935	.632	+.028
3125, 6	STOCK FP	1.080	20	.648	.683	.957	.997	.892	.932	.932	--	--
3783, 4	DESIGN FP II	1.069	20	.620	.710	.928	.940	.900	.968	.940	.677	+.057
3781, 2	DESIGN FP I	.997	20	.604	.662	.945	.967	.900	.952	.935	--	--
3783, 4	DESIGN FP II	1.069	20	.620	.710	.928	.940	.900	.968	.940	.649	+.020
3125, 6	STOCK FP	1.080	30	.642	.672	.952	1.008	.908	.955	.952	--	--
3781, 2	DESIGN FP I	.997	30	.602	.663	.938	.968	.913	.976	.954	.916	+.034
3125, 6	STOCK FP	1.080	30	--	.672	.952	1.008	.908	.955	.952	--	--
3783, 4	DESIGN FP II	1.069	30	.610	.703	.922	.942	.912	.990	.957	.675	+.065
3781, 2	DESIGN FP I	.997	30	.602	.663	.938	.968	.913	.976	.954	--	--
3783, 4	DESIGN FP II	1.069	30	.610	.703	.922	.942	.912	.990	.957	.638	+.029

Figure 9 - Propulsion Performance Coefficients and Propeller Information for Twin Screw Model 4702 Fitted with Stock Propellers 3125, 3126, and Design Propellers 3781, 3782, and 3783, 3784

MODEL 5326 PROPELLERS 4327A, 4510 (STOCK CP); 4645, 4677 (DESIGN FP)

PROPELLER NO.	DIAMETER INCHES (MM)	PITCH INCHES (MM)	P/D	NUMBER OF BLADES	HUB DIAMETER INCHES (MM)	MEAN WIDTH RATIO	t/c at 0.7R	PROJECTED AREA RATIO	EXPANDED AREA RATIO	SKEW AT TIP DEGREES	HUB LENGTH TO AXIS INCHES (MM)	TOTAL RAKE AT TIP INCHES (MM)
4372A	10.800 (274.3)	10.569 (268.4)	.979	7	3.300 (83.8)	.173	.0895	.513	.600	30	1.716 (43.59)	+.85 (21.5)
4510	10.800 (274.3)	10.165 (258.2)	.941	7	2.827 (71.8)	.176	.0912	.539	.620	45	1.032 (26.21)	+.48 (12.1)
4645	9.812 (249.2)	12.265 (311.5)	1.250	7	2.320 (58.9)	.211	.0910	.590	.754	45	1.394 (35.41)	+1.13 (28.7)
4677	9.812 (249.2)	12.265 (311.5)	1.250	7	2.320 (58.9)	.216	.0716	.590	.771	45	1.394 (35.41)	+1.13 (28.7)



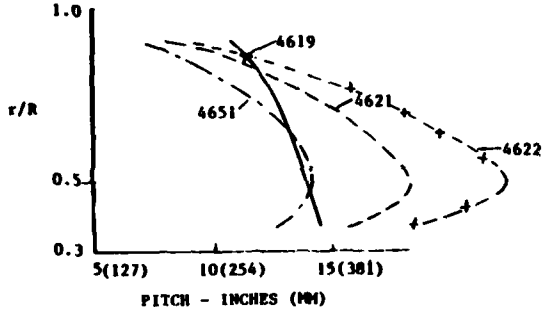
COMPARISON OF PERFORMANCE AT 20 KNOTS

PROP. NOS.	DESIGNATION	P/D	V_S KNOTS	η_D	η_O	η_H	η_R	1-t	$1-w_T$	$1-w_Q$	η_{DEST}	$\Delta\eta_D$
4645	DESIGN FP I	1.250	20	.75	.65	1.10	1.05	.86	.78	.82		
4677	DESIGN FP II	1.250	20	.77	.65	1.13	1.05	.88	.78	.81	.751	-.019
4372A	STOCK CP I	.979	20	.72	.67	1.07	1.01	.83	.77	.77		
4510	STOCK CP II	.941	20	.70	.63	1.09	1.01	.81	.74	.75	.681	-.019

Figure 10 - Propulsion Performance Coefficients and Propeller Information for Single Screw Model 5326 Fitted with Stock Propeller 4372A, Stock Propeller 4510, Design Propeller 4645, and Design Propeller 4677

MODEL 5324 PROPELLERS 4619, 4621, 4651, 4622 (DESIGN FP)

PROPELLER NO.	DIAMETER INCHES (MM)	PITCH INCHES (MM)	P/D	NUMBER OF BLADES	HUB DIAMETER INCHES (MM)	MEAN WIDTH RATIO	t/c at 0.7R	PROJECTED AREA RATIO	EXPANDED AREA RATIO	SKEW AT TIP DEGREES	HUB LENGTH TO AXIS INCHES (MM)	TOTAL RAKE AT TIP INCHES (MM)
4619	12.798 (325.0)	12.900 (327.7)	1.008	5	2.773 (70.4)	.351	.0298	.751	.875	0	1.751 (44.5)	0
4621	12.798 (325.0)	15.319 (389.1)	1.197	5	2.773 (70.4)	.345	.0349	.696	.860	53.5	1.751 (44.5)	0
4651	12.798 (325.0)	12.490 (317.2)	.976	5	2.773 (70.4)	.347	.0279	.728	.864	53.5	1.751 (44.5)	0
4622	12.798 (325.0)	18.020 (457.7)	1.408	5	2.773 (70.4)	.345	.0375	.657	.860	53.5	1.751 (44.5)	0



COMPARISON OF PERFORMANCE AT 20 KNOTS

PROP. NOS.	DESIGNATION	P/D	V_S KNOTS	η_D	η_Θ	η_H	η_R	1-t	$1-w_T$	$1-w_Q$	η_DEST	$\Delta\eta_D$
4619	DESIGN I	1.008	20	.620	.650	.95	1.00	.890	.940	.940	.618	--
4651	DESIGN VI	.976	20	.620	.650	.98	.97	.920	.940	.930		
4621	DESIGN III	1.197	20	.670	.650	1.01	1.02	.920	.910	.920	.670	--
4622	DESIGN IV	1.408	20	.670	.650	1.01	1.02	.920	.910	.930		

Figure 11 - Propulsion Performance Coefficients and Propeller Information for Single Screw Model 5324 Fitted with a Series of Design Propellers Numbers 4619, 4621, 4622, and 4651

MODEL 5298 PROPELLERS 4354 (STOCK MICHIGAN WHEEL); 4575 (DESIGN CP)

PROPELLER NO.	DIAMETER INCHES (MM)	PITCH INCHES (MM)	P/D	NUMBER OF BLADES	HUB DIAMETER INCHES (MM)	MEAN WIDTH RATIO	t/c at 0.7R	PROJECTED AREA RATIO	EXPANDED AREA RATIO	SKEW AT TIP DEGREES	HUB LENGTH TO AXIS INCHES (MM)	TOTAL RAKE AT TIP INCHES (MM)
4354	10.000 (254.0)	11.000 (279.4)	1.110	3						0	1.18 (30.0)	0
4575	9.846 (250.0)	11.746 (298.3)	1.193	5	2.954 (75.03)	.292	.0444		.729	11.62	0.90 (22.86)	

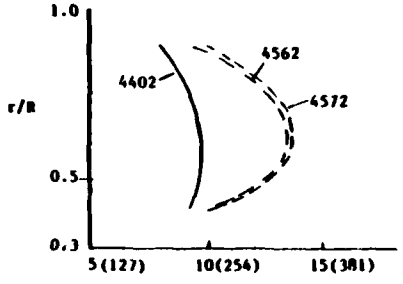
COMPARISON OF PERFORMANCE AT 20 AND 26 KNOTS

PROP. NOS.	DESIGNATION	P/D	V_s KNOTS	η_D	η_θ	η_H	η_R	1-t	$1-w_T$	$1-w_Q$	η_DEST	$\Delta\eta_D$
4354	STOCK	1.116	20	.625	.700	.935	.955	.910	.980			
4575	DESIGN CP	1.193	20	.630	.710	.940	.950	.900	.950		.624	+.004
4354	STOCK	1.116	26	.600	.680	.905	.970	.890	.985			
4575	DESIGN CP	1.193	26	.620	.700	.920	.970	.880	.950		.614	-.006

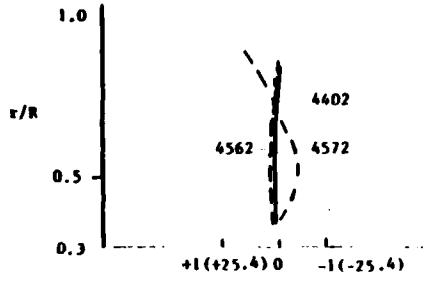
Figure 12 - Propulsion Performance Coefficients and Propeller Information for Single Screw Model 5298 Fitted with Stock Propeller 4354 and Design Propeller 4575

MODEL 5279, 5279-1 PROPELLERS 4402 (STOCK CP); 4562, 4572 (DESIGN CP)

PROPELLER NO.	DIAMETER INCHES (MM)	PITCH INCHES (MM)	P/D	NUMBER OF BLADES	HUB DIAMETER INCHES (MM)	MEAN WIDTH RATIO	t/c at 0.7R	PROJECTED AREA RATIO	EXPANDED AREA RATIO	SKEW AT TIP DEGREES	HUB LENGTH TO AXIS INCHES (MM)	TOTAL RAKE AT TIP INCHES (MM)
4402	9.224 (234.2)	9.787 (248.5)	1.061	5	2.665 (67.7)	.356	.0300	.719	.816	2.5	1.307 (3.32)	+.08 (2.0)
4562	9.512 (241.6)	13.222 (335.9)	1.390	5	2.748 (69.9)	.369	.0301	.693	.835	2.5	1.348 (3.42)	+.08 (2.0)
4572	9.512 (241.6)	13.555 (344.3)	1.425	5	2.748 (69.9)	.328	.0378	.597	.729	25	1.213 (3.08)	+.069 (17.5)



PITCH - INCHES (MM)



TOTAL RAKE - INCHES (MM)

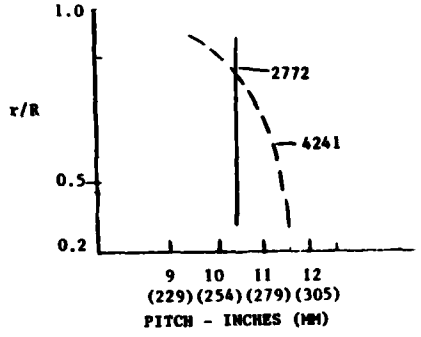
COMPARISON OF PERFORMANCE AT 22 AND 32 KNOTS

PROP. NOS.	DESIGNATION	P/D	V_S KNOTS	η_D	η_O	η_H	η_R	1-t	$1-w_T$	$1-w_Q$	η_DEST	$\Delta\eta_D$
4402	STOCK CP	1.061	22	.615	.680	.925	.975	.890	.960	.955		
4562	DESIGN CP I	1.390	22	.645	.695	.945	.985	.930	.985	.980	.627	-.018
4402	STOCK CP	1.061	32	.585	.655	.915	.975	.895	.975	.965		
4562	DESIGN CP I	1.390	32	.640	.670	.940	1.010	.930	.990	.995	.598	-.042
4402	STOCK CP	1.061	22	.615	.680	.925	.975	.890	.960	.955		
4572	DESIGN CP II	1.425	22	.700	.715	.970	1.005	.925	.955	.960	.645	-.055
4402	STOCK CP	1.061	32	.585	.655	.915	.975	.895	.975	.965		
4572	DESIGN CP II	1.425	32	.635	.690	.940	.980	.925	.985	.975	.615	-.020
4562	DESIGN CP I	1.390	22	.645	.695	.945	.985	.930	.985	.980		
4572	DESIGN CP II	1.425	22	.700	.715	.970	1.005	.925	.955	.960	.645	-.015
4562	DESIGN CP I	1.390	32	.640	.670	.940	1.010	.930	.990	.995		
4572	DESIGN CP II	1.425	32	.635	.690	.940	.980	.925	.985	.975	.655	-.005

Figure 13 - Propulsion Performance Coefficients and Propeller Information for Single Screw Model 5279 Fitted with Stock Propeller 4402, Design Propeller 4562 and Design Propeller 4572

MODEL 5004 PROPELLERS 2772 (STOCK FP); 4241 (DESIGN FP)

PROPELLER NO.	DIAMETER INCHES (MM)	PITCH INCHES (MM)	P/D	NUMBER OF BLADES	HUB DIAMETER INCHES (MM)	MEAN WIDTH RATIO	t/c at 0.7R	PROJECTED AREA RATIO	EXPANDED AREA RATIO	SKEW AT TIP DEGREES	HUB LENGTH TO AXIS INCHES (MM)	TOTAL RAKE AT TIP INCHES (MM)
2772	8.750 (222.2)	10.430 (264.9)	1.192	4	2.040 (51.8)	.300	--	.490	.617	7.5	0.785 (19.94)	+0.78 (19.8)
4241	8.750 (222.2)	10.859 (275.8)	1.241	4	1.750 (44.5)	.370	0.318	.590	.753	0	1.200 (30.48)	+ .77 (19.6)



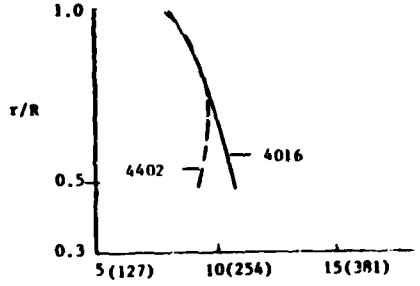
COMPARISON OF PERFORMANCE AT 20 KNOTS

PROP. NOS.	DESIGNATION	P/D	V_S KNOTS	η_D	η_O	η_H	η_R	1-t	$1-W_T$	$1-W_Q$	η_{DEST}	$\Delta\eta_D$	DISP-TONS S.W.
2772	STOCK FP	1.192	20	.720	.710	1.005	1.015	.920	.915	.930	--	--	18500
4241	DESIGN FP	1.241	20	.690	.665	1.000	1.030	.900	.900	.915	.678	-.012	18500
2772	STOCK FP	1.192	20	.730	.720	1.010	1.010	.895	.890	.895	--	--	13000
4241	DESIGN FP	1.241	20	.700	.680	1.020	1.015	.885	.870	.880	.694	- .006	13000

Figure 14 - Propulsion Performance Coefficients and Propeller Information for Single Screw Model 5004 Fitted with Stock Propeller 2772, and Design Propeller 4241

MODEL 4989 PROPELLERS 4016 (STOCK FP); 4402 (DESIGN CP)

PROPELLER NO.	DIAMETER INCHES (MM)	PITCH INCHES (MM)	P/D	NUMBER OF BLADES	HUB DIAMETER INCHES (MM)	MEAN WIDTH RATIO	t/c at 0.7R	PROJECTED AREA RATIO	EXPANDED AREA RATIO	SKEW AT TIP DEGREES	HUB LENGTH TO AXIS INCHES (MM)	TOTAL RAKE AT TIP INCHES (MM)
4016	9.224 (234.2)	9.661 (245.3)	1.047	5	1.830 (46.4)	.349	.0298	.743	.890	0	1.281 (32.54)	0
4402	9.224 (234.2)	9.787 (248.5)	1.061	5	2.665 (67.7)	.356	.0300	.719	.816	2.5	1.307 (33.20)	+ .08 (2.03)



COMPARISON OF PERFORMANCE AT 20 and 28 KNOTS

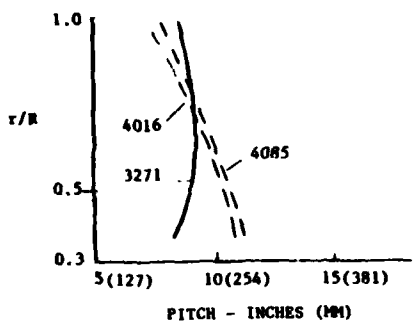
PROP. NOS.	DESIGNATION	P/D	V_S KNOTS	η_D	η_θ	η_H	η_R	1-t	$1-w_T$	$1-w_Q$	η_DEST	$\Delta\eta_D$
4016	STOCK FP	1.047	20	.630	.680	.960	.970	.930	.970	.950	--	--
4402	DESIGN CP	1.061	20	.610	.655	.945	.980	.915	.965	.960	.610	0
4016	STOCK FP	1.047	28	.620	.675	.950	.970	.935	.980	.955	--	--
4402	DESIGN CP	1.061	28	.615	.655	.950	.990	.930	.975	.970	.604	-.011

Figure 15 - Propulsion Performance Coefficients and Propeller Information for Single Screw Model 4989 Fitted with Stock Propeller 4016, and Design Propeller 4402

MODEL 4870 (ALSO 4881-1) PROPELLERS 3271 (STOCK FP); 4016, 4085 (DESIGN CP)

PROPELLER NO.	DIAMETER INCHES (MM)	PITCH INCHES (MM)	P/D	NUMBER OF BLADES	HUB DIAMETER INCHES (MM)	MEAN WIDTH RATIO	t/c at 0.7R	PROJECTED AREA RATIO	EXPANDED AREA RATIO	SKEW AT TIP DEGREES	HUB LENGTH TO AXIS INCHES (MM)	TOTAL RAKE AT TIP INCHES (MM)
3271	8.853 (224.9)	9.341 (237.2)	1.055	5	1.830 (46.5)	.359	.0282	.768	.933	2	0.989 (25.12)	+0.48 (12.1)
4016	9.224 (234.2)	9.661 (245.3)	1.047	5	1.830 (46.5)	.349	.0298	.743	.890	0	1.281 (32.54)	0
4085	9.224 (234.2)	9.797 (248.8)	1.062	5	2.665 (67.7)	.356	.0285	.719	.816	3		0

MODELS 4870 AND 4881-1 ARE IDENTICAL ACCORDING TO RUTH GOLDBERG RECORDS



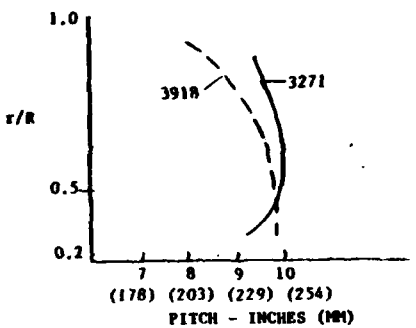
COMPARISON OF PERFORMANCE AT 27 KNOTS

PROP. NOS.	DESIGNATION	P/D	V_S KNOTS	η_D	η_Q	η_H	η_R	1-t	$1-w_T$	$1-w_Q$	η_DEST	$\Delta\eta_D$	MODELS
3271	STOCK CP	1.055	27	.621	.633	.979	1.001	.914	.934	.934			4870
4016	DESIGN CP I	1.047	27	.619	.680	.948	.960	.927	.978	.954	.666	+.047	4881-1
3271	STOCK CP	1.055	27	.621	.633	.979	1.001	.914	.934	.934			4870
4085	DESIGN CP II	1.062	27	.598	.681	.920	.955	.894	.972	.950	.667	+.069	4870
4016	DESIGN CP I	1.047	27	.619	.680	.948	.960	.927	.978	.954			4881-1
4085	DESIGN CP II	1.062	27	.598	.691	.920	.955	.894	.972	.950	.620	+.022	4870

Figure 16 - Propulsion Performance Coefficients and Propeller Information for Single Screw Models 4870 and 4881-1 Fitted with Stock Propeller 3271, Design Propeller 4016, and Design Propeller 4085

MODEL 4773 PROPELLERS 3271 (STOCK FP); 3918 (DESIGN FP)

PROPELLER NO.	DIAMETER INCHES (MM)	PITCH INCHES (MM)	P/D	NUMBER OF BLADES	HUB DIAMETER INCHES (MM)	MEAN WIDTH RATIO	t/c at 0.7R	PROJECTED AREA RATIO	EXPANDED AREA RATIO	SKEW AT TIP DEGREES	HUB LENGTH TO AXIS INCHES (MM)	TOTAL RAKE AT TIP INCHES (MM)
3271	8.853 (224.9)	9.341 (237.3)	1.055	5	1.830 (46.5)	.359	.0282	.768	.933	2	0.989 (25.12)	+0.48 (12.1)
3918	9.032 (229.4)	8.956 (227.5)	.992	5	1.830 (46.5)	.298	.0398	.642	.764	0	0.989 (25.12)	0



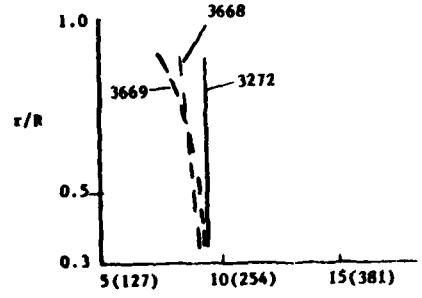
COMPARISON OF PERFORMANCE AT 26 KNOTS

PROP. NOS.	DESIGNATION	P/D	V_S KNOTS	η_D	η_O	η_H	η_R	1-t	$1-w_T$	$1-w_Q$	η_DEST	$\Delta\eta_D$
3271	STOCK FP	1.055	26	.607	.612	.959	1.034	.904	.943	.965		
3918	DESIGN FP	.992	26	.627	.653	.960	1.000	.918	.954	.954	.648	+.021

Figure 17 - Propulsion Performance Coefficients and Propeller Information for Single Screw Model 4773 Fitted with Stock Propeller 3271, and Design Propeller 3918

MODEL 4554 PROPELLERS 3272 (STOCK FP); 3668, 3669 (DESIGN FP)

PROPELLER NO.	DIAMETER INCHES (MM)	PITCH INCHES (MM)	P/D	NUMBER OF BLADES	HUB DIAMETER INCHES (MM)	MEAN WIDTH RATIO	t/c at 0.7R	PROJECTED AREA RATIO	EXPANDED AREA RATIO	SKEW AT TIP DEGREES	HUB LENGTH TO AXIS INCHES (MM)	TOTAL RAKE AT TIP INCHES (MM)
3272	8.855 (244.9)	9.386 (238.4)	1.060	5	1.830 (46.5)	.301	.0407	.545	.661	3	1.30 (33.0)	0
3668	9.298 (236.1)	8.726 (221.6)	.938	5	1.992 (50.6)	.255	.0460	.594	.697	0	1.218 (30.9)	0
3669	9.224 (234.2)	8.726 (221.6)	.946	5	1.942 (49.3)	.300	.0410	.655	.770	0	1.218 (30.9)	0



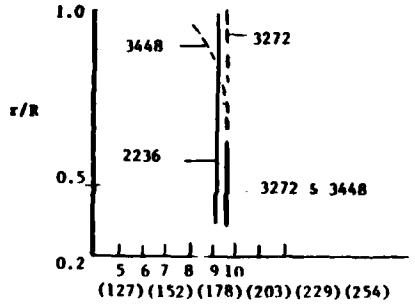
COMPARISON OF PERFORMANCE AT 22 KNOTS

PROP. NOS.	DESIGNATION	P/D	V_S KNOTS	η_D	η_Θ	η_H	η_R	1-t	$1-w_T$	$1-w_Q$	η_DEST	$\Delta\eta_D$
3272	STOCK FP	1.060	22	.651	.639	1.008	1.022	.959	.944	.959		
3668	DESIGN FP I	.938	22	.645	.660	.998	.979	.930	.932	.917	.680	+.035
3272	STOCK FP	1.060	22	.651	.639	1.008	1.022	.959	.944	.959		
3669	DESIGN FP II	.946	22	.627	.641	.989	.989	.927	.937	.930	.660	+.033
3668	DESIGN FP I	.938	22	.645	.660	.998	.979	.930	.932	.917		
3669	DESIGN FP II	.946	22	.627	.641	.989	.989	.927	.937	.930	.626	-.001

Figure 18 - Propulsion Performance Coefficients and Propeller Information for Single Screw Model 4554 Fitted with Stock Propeller 3272, Design Propeller 3668, and Design Propeller 3669

MODEL 4360, 4360-1 PROPELLERS 2236, (STOCK FP); 3272, 3448 (DESIGN FP)

PROPELLER NO.	DIAMETER INCHES (MM)	PITCH INCHES (MM)	P/D	NUMBER OF BLADES	HUB DIAMETER INCHES (MM)	MEAN WIDTH RATIO	t/c at 0.7R	PROJECTED AREA RATIO	EXPANDED AREA RATIO	SKEW AT TIP DEGREES	HUB LENGTH TO AXIS INCHES (MM)	TOTAL RAKE AT TIP INCHES (MM)
2236	8.671 (220.2)	9.055 (230.0)	1.034	4	1.760 (44.7)	.248		.526	.634	2	1.35 (34.3)	0
3272	8.855 (224.9)	9.386 (238.4)	1.060	5	1.830 (46.5)	.301	.0282	.545	.661	1	1.30 (33.0)	0
3448	8.855 (224.9)	9.333 (237.1)	1.054	5	1.830 (46.5)	.304	.0407	.644	.780	0	1.30 (33.0)	0



COMPARISON OF PERFORMANCE AT 25 KNOTS

PROP. NOS.	DESIGNATION	P/D	V_S KNOTS	η_D	η_Θ	η_H	η_R	1-t	$1-w_T$	$1-w_Q$	η_DEST	$\Delta\eta_D$	MODEL
2236	STOCK FP	1.034	25	.672	.700	.978	.981	.955	.976	.970			4360
3272	DESIGN FP I	1.060	25	.638	.656	.958	1.015	.941	.922	.922	.629	-.009	4360-1
2236	STOCK FP	1.034	25	.672	.700	.978	.981	.955	.976	.970			4360
3448	DESIGN FP II	1.054	25	.619	.644	.952	1.009	.921	.967	.967	.618	-.001	4360-1
3272	DESIGN FP I	1.060	25	.638	.656	.958	1.015	.941	.922	.922			4360-1
3448	DESIGN FP II	1.054	25	.619	.644	.952	1.009	.921	.967	.967	.626	+.007	4360-1

Figure 19 - Propulsion Performance Coefficients and Propeller Information for Single Screw Model 4360 Fitted with Stock Propeller 2236, Design Propeller 3272, and Design Propeller 3448

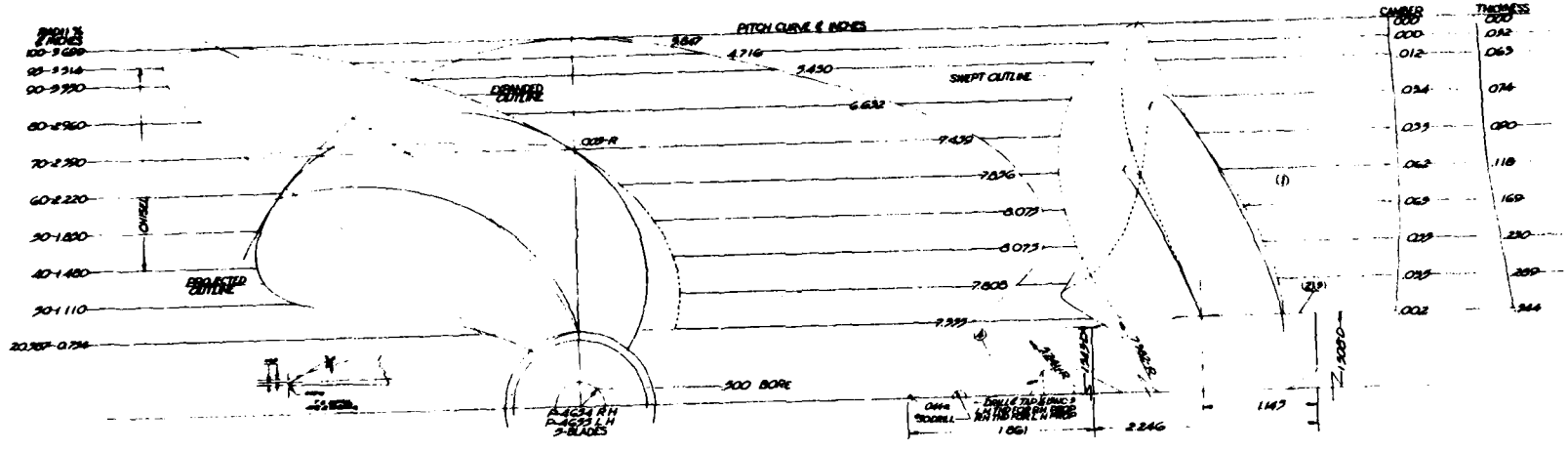


Figure 20 - Drawings of Propellers 4654 and 4655 Representing Typical Recent Design and Skew and Variable Pitch Distribution

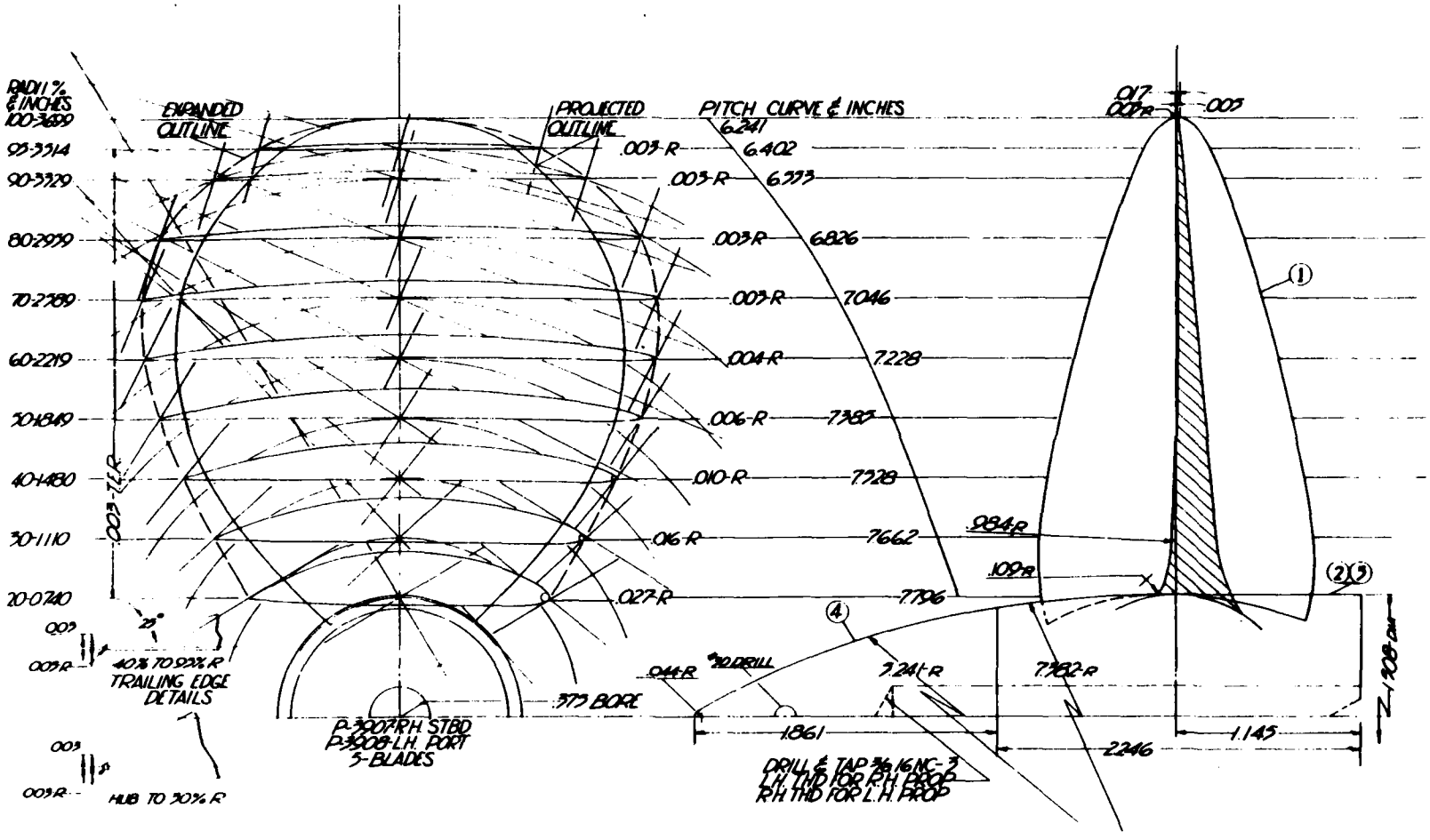


Figure 21 - Drawings of Propellers 3907 and 3908 Representing Typical Older Design without Skew and Relatively Constant Pitch Distribution

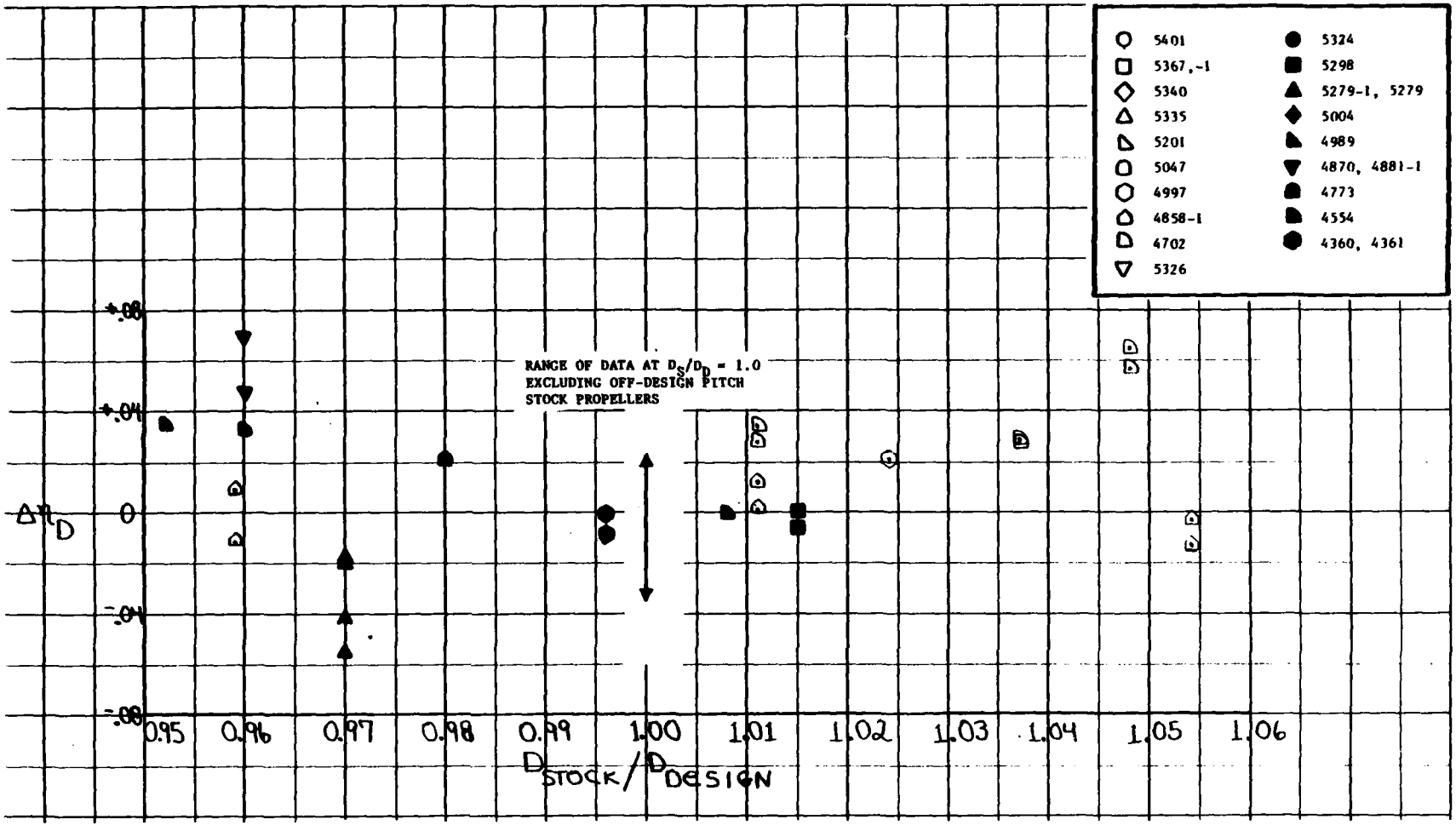


Figure 22 - Effect of Varying Propeller Diameter on $\Delta\eta_D$

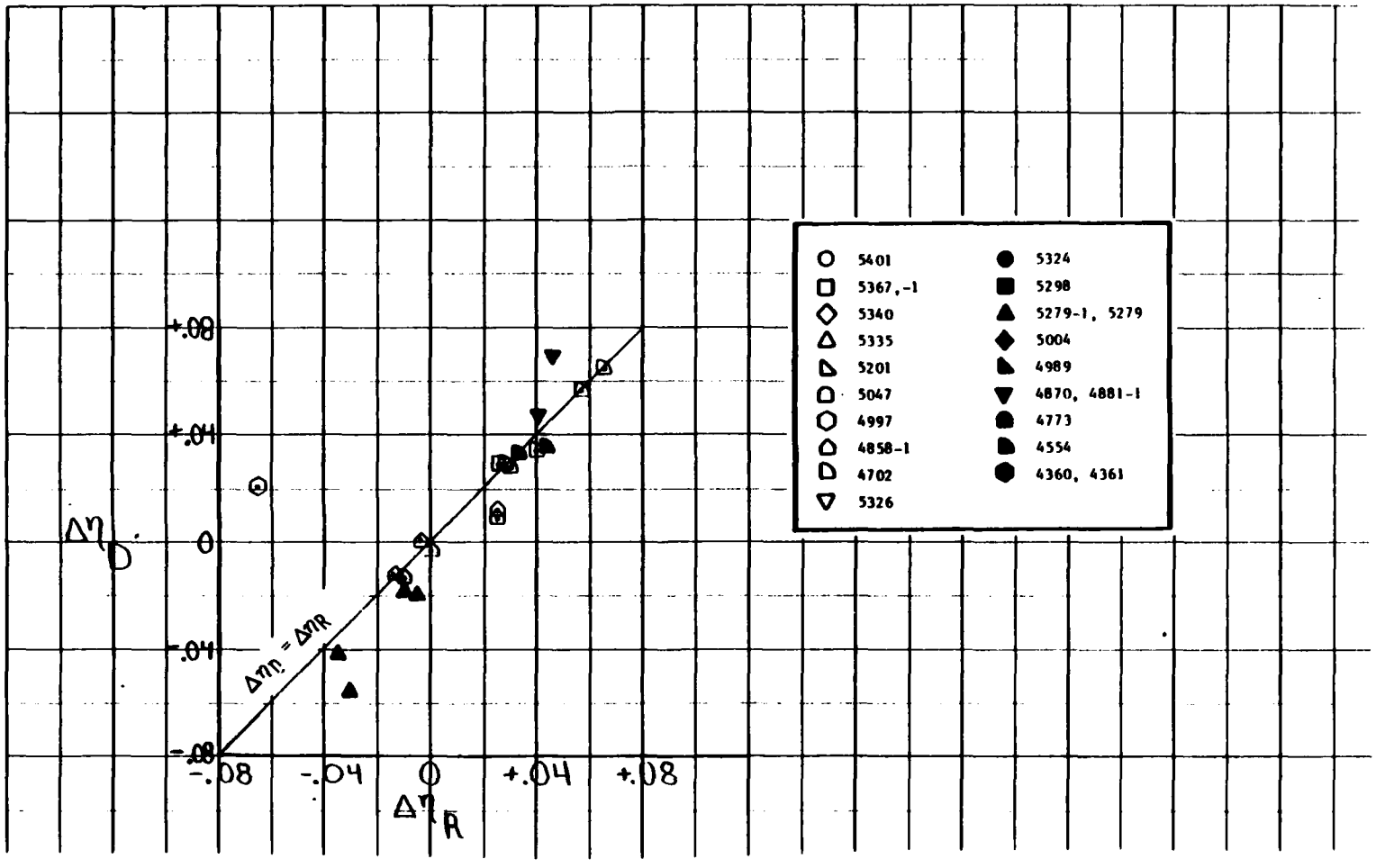


Figure 23 - $\Delta\eta_D$ versus $\Delta\eta_R$ for Cases with Variation Between Stock and Design Propeller Diameters

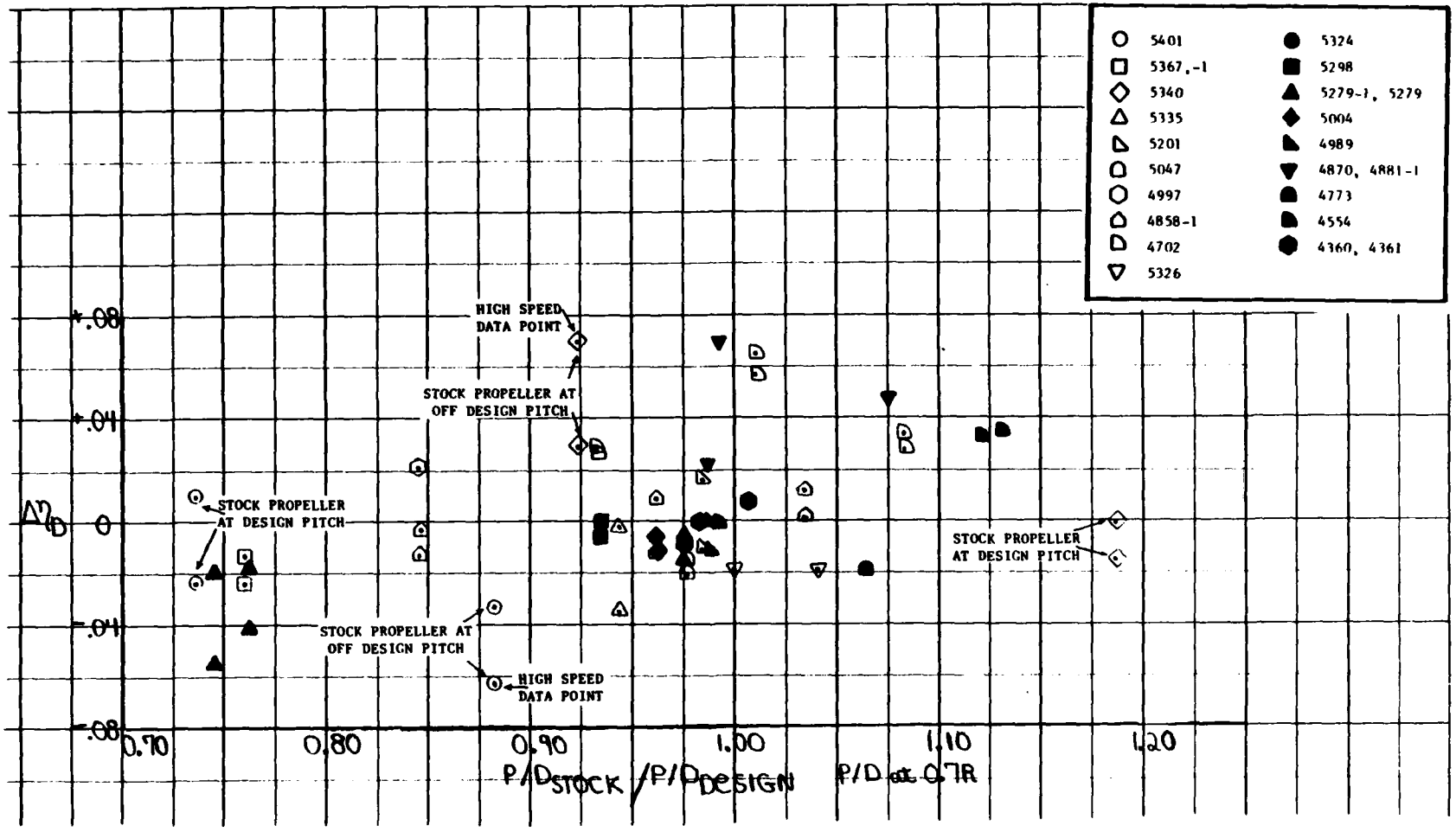


Figure 24 - Effect of Propeller Pitch-to-Diameter Ratio on Δn_D

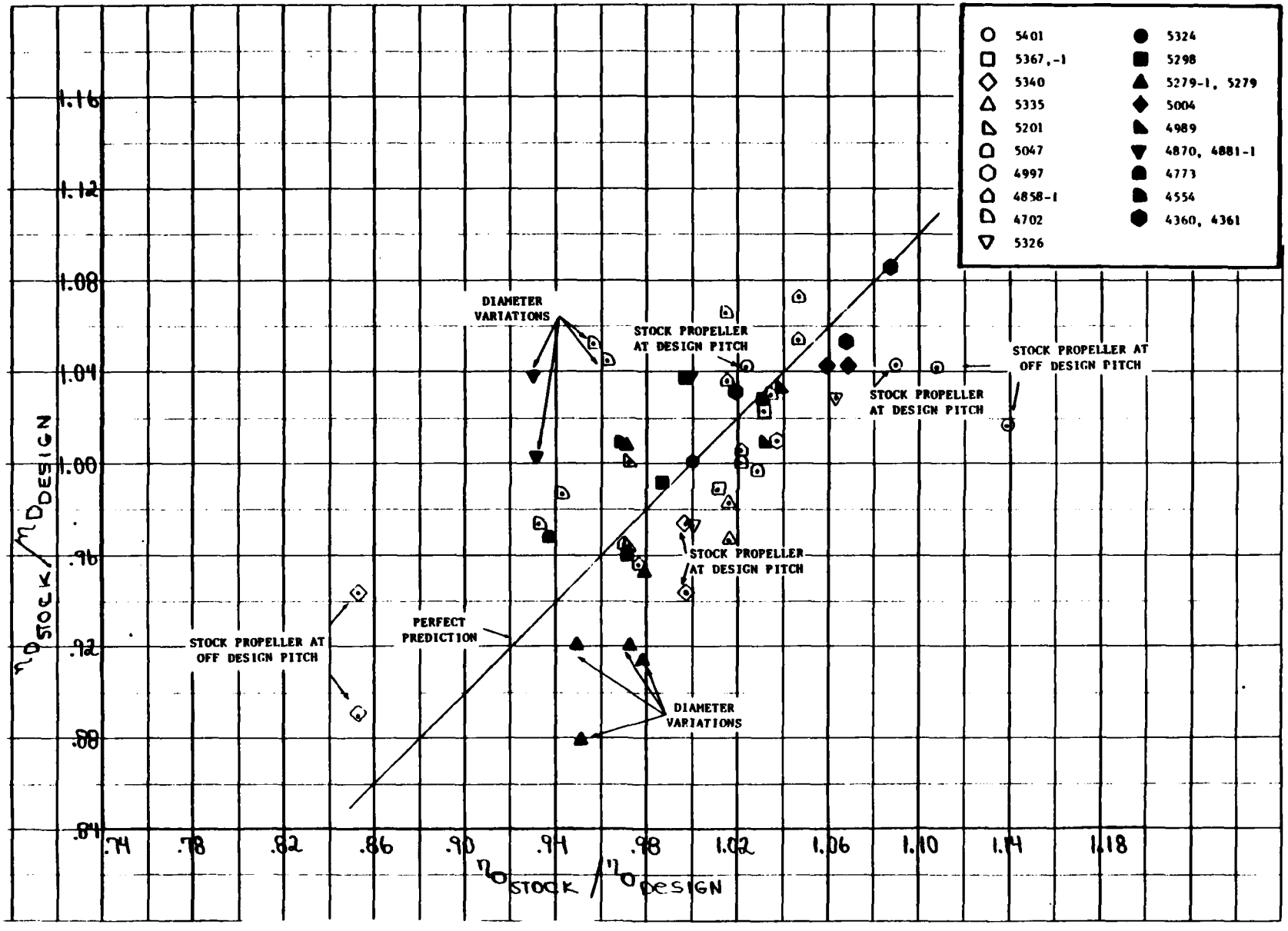


Figure 25 - Comparison of η_D Stock/η_D Design to the Ratio η_O Stock/η_O Design

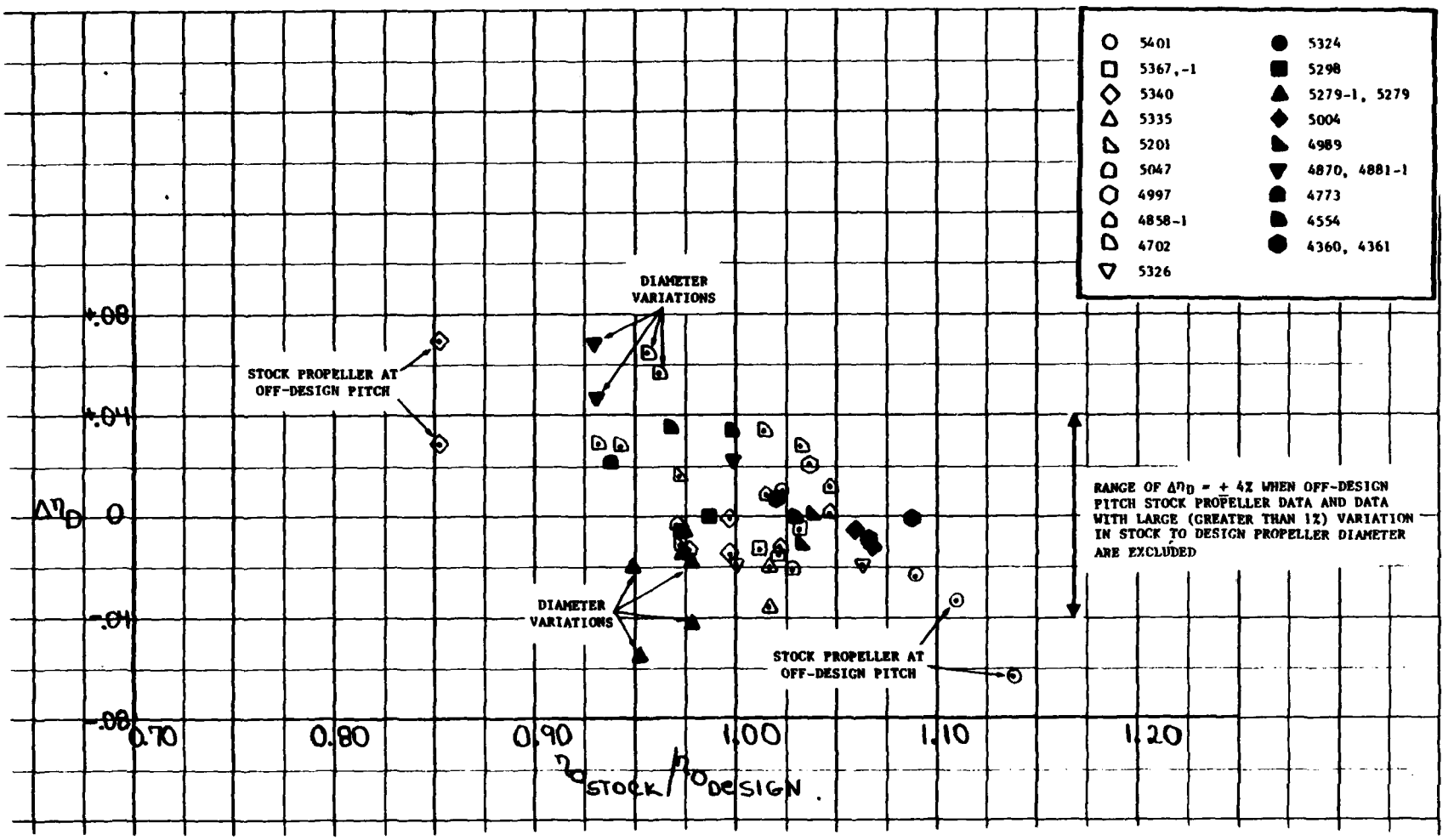


Figure 26 - Effect of Propeller Open Water Efficiency on $\Delta\eta_D$

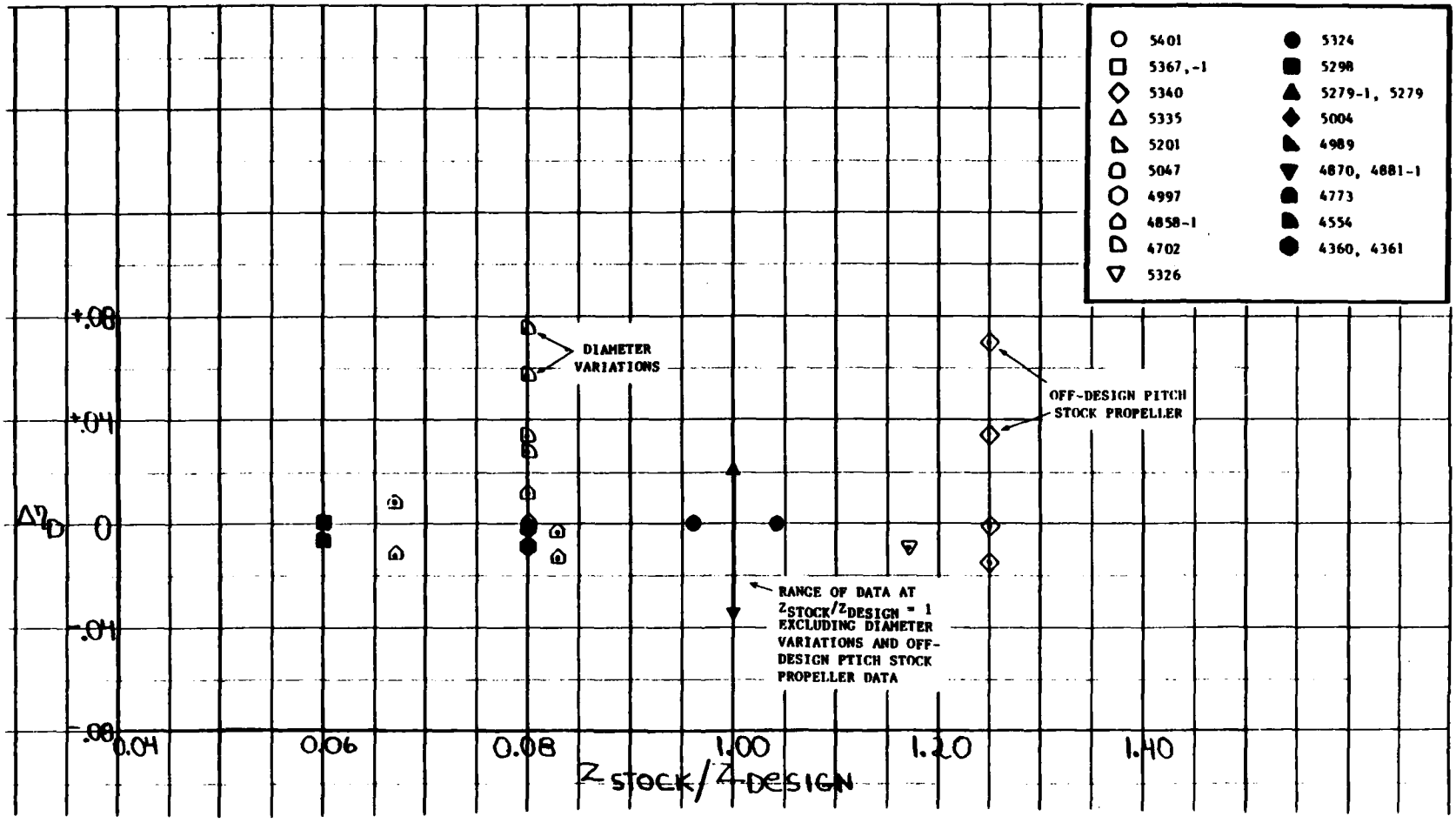


Figure 27 - Effect of Number of Propeller Blades on $\Delta\eta_D$

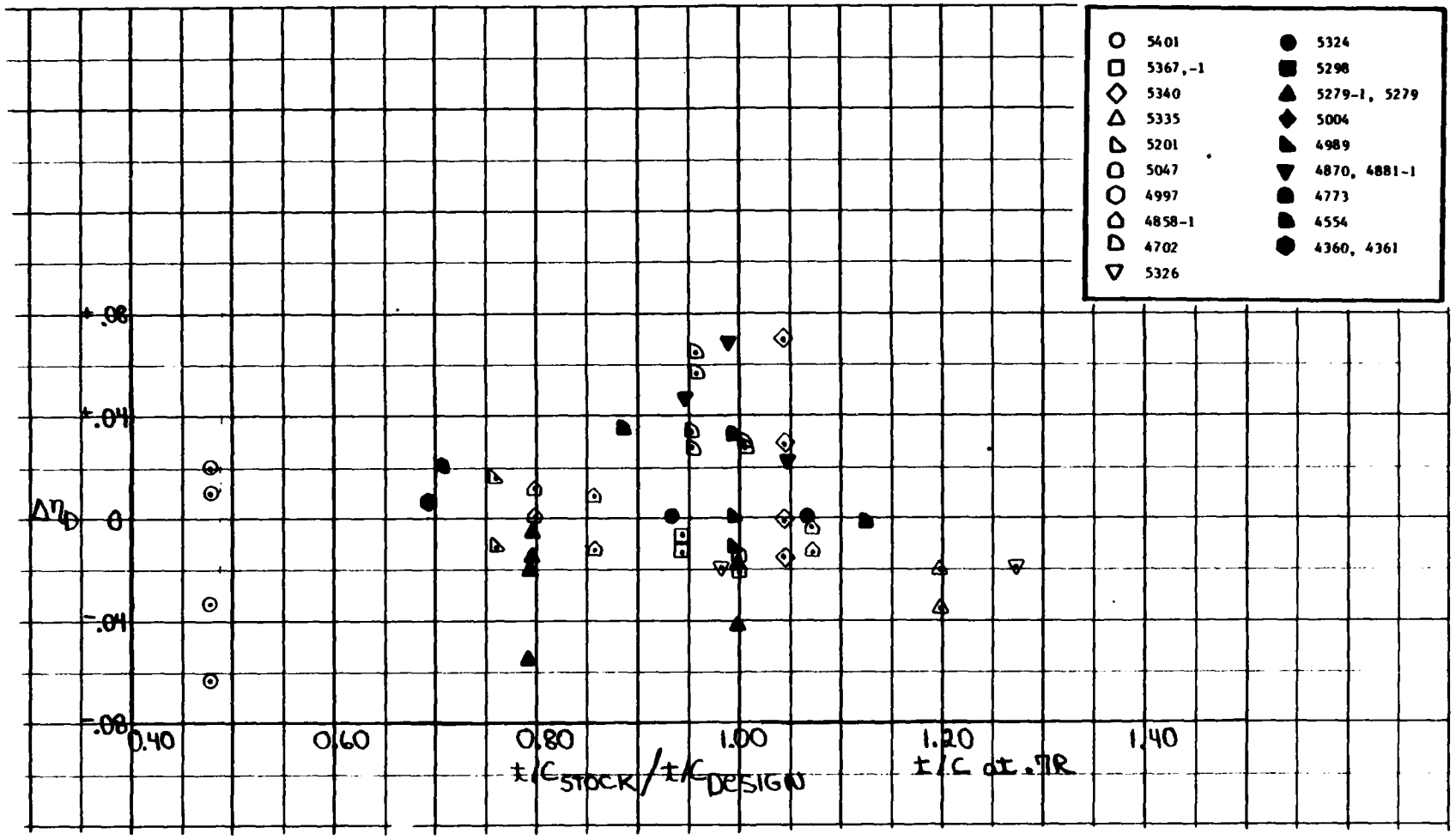


Figure 28 - Effect of Propeller Thickness-to-Chord Ratio on $\Delta\eta_D$

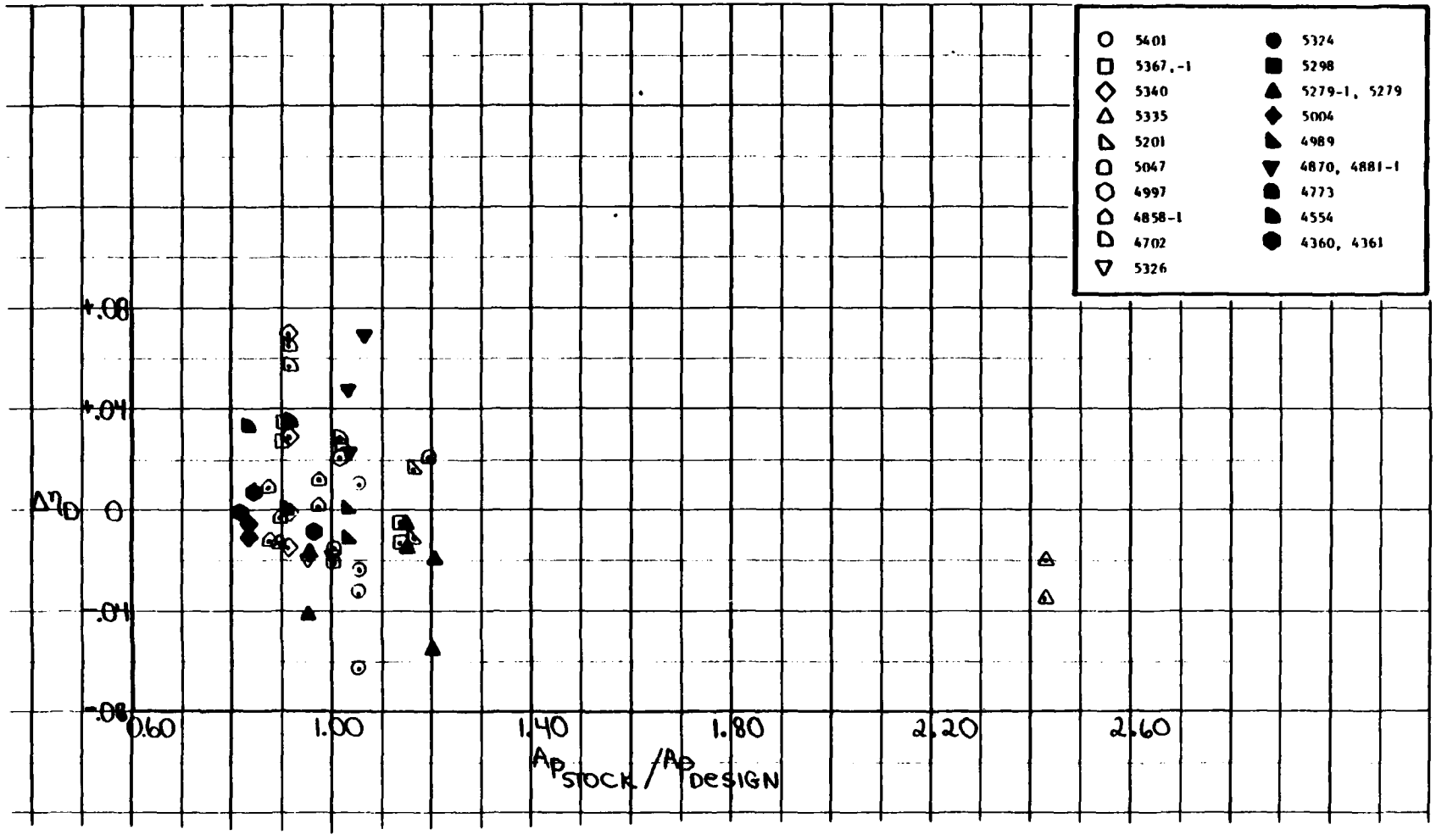


Figure 29 - Effect of Propeller Projected Area Ratio on $\Delta\eta_D$

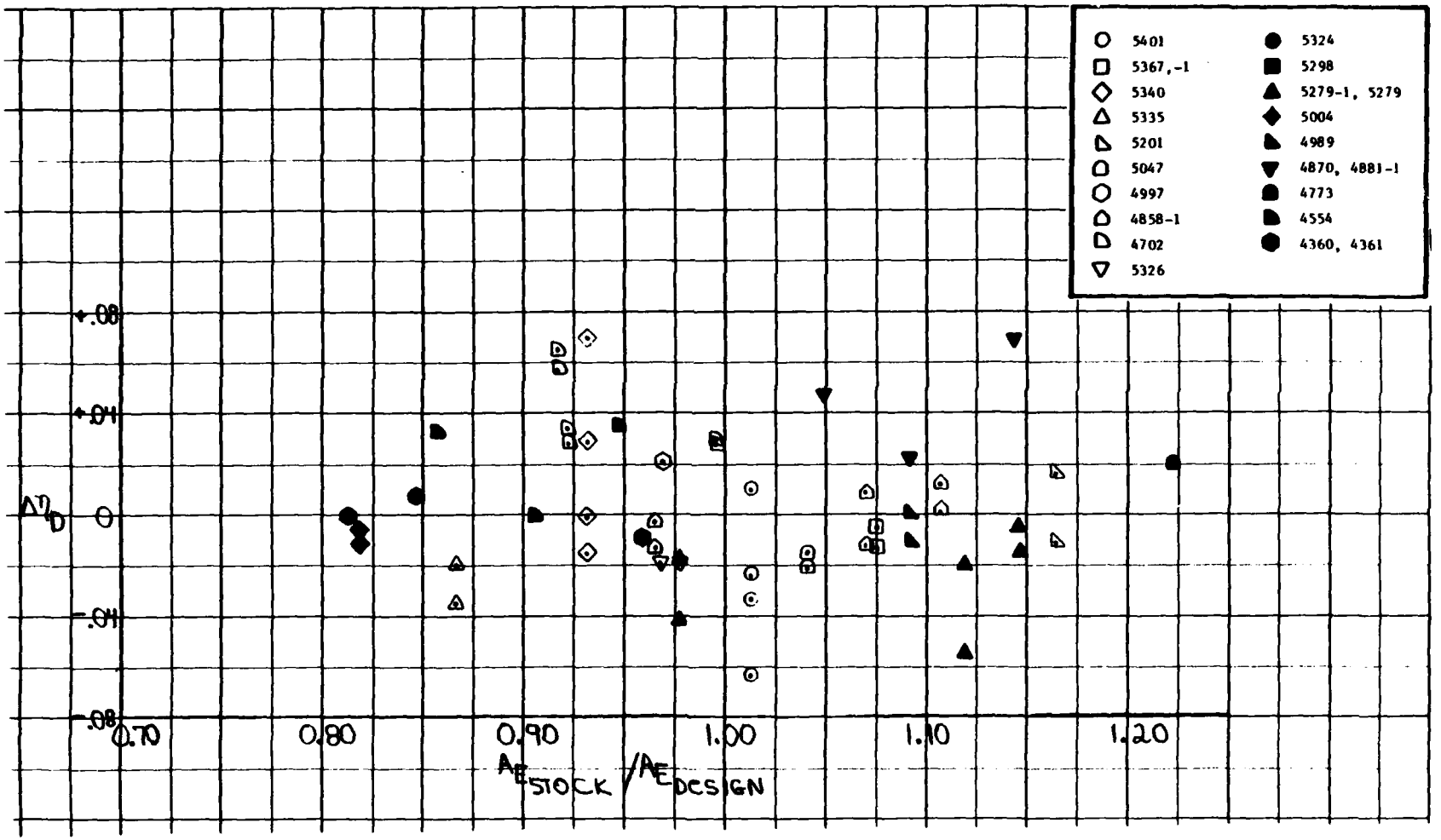


Figure 30 - Effect of Propeller Expanded Area Ratio on $\Delta\eta_D$

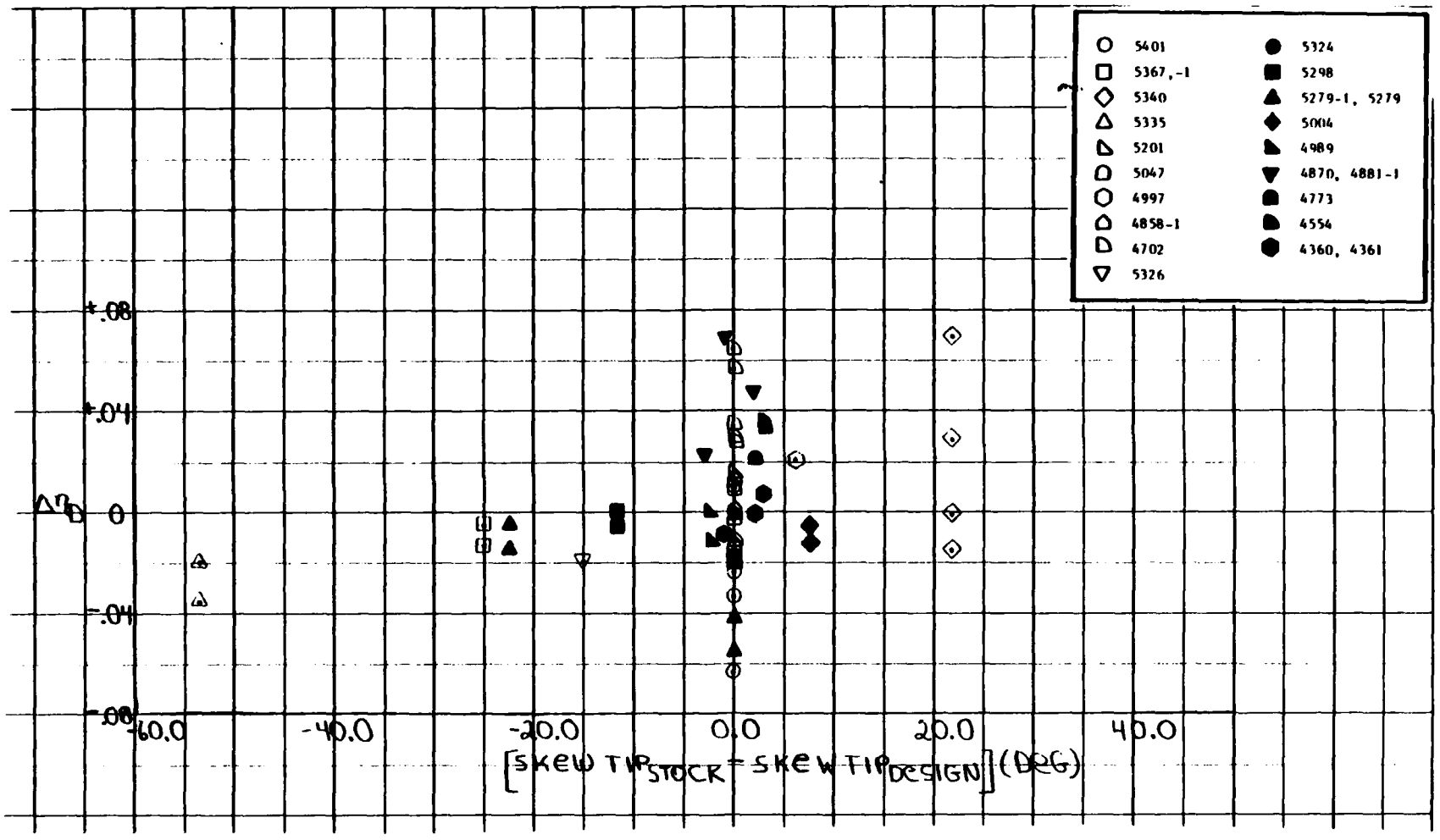


Figure 31 - Effect of Propeller Skew on $\Delta\eta_D$

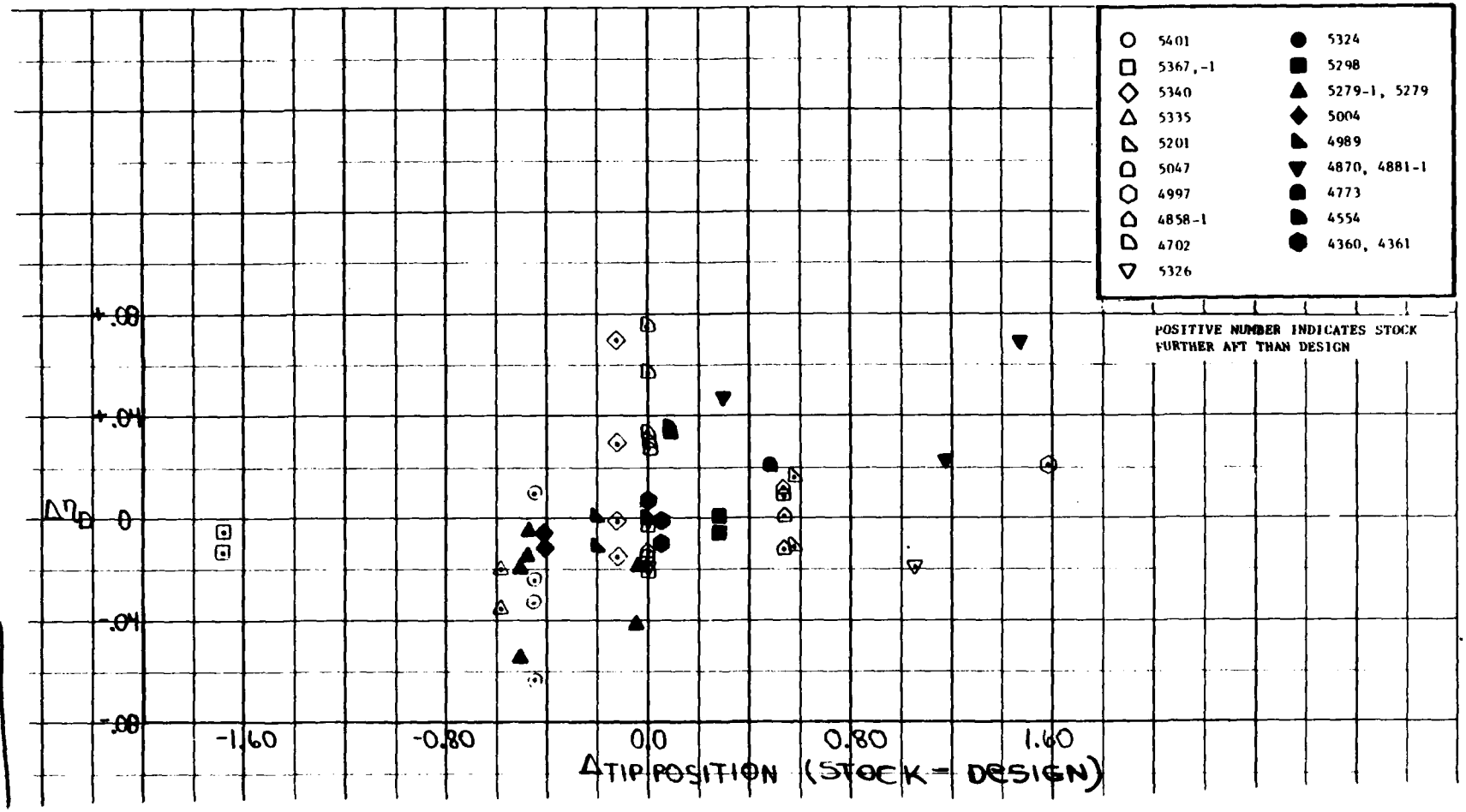
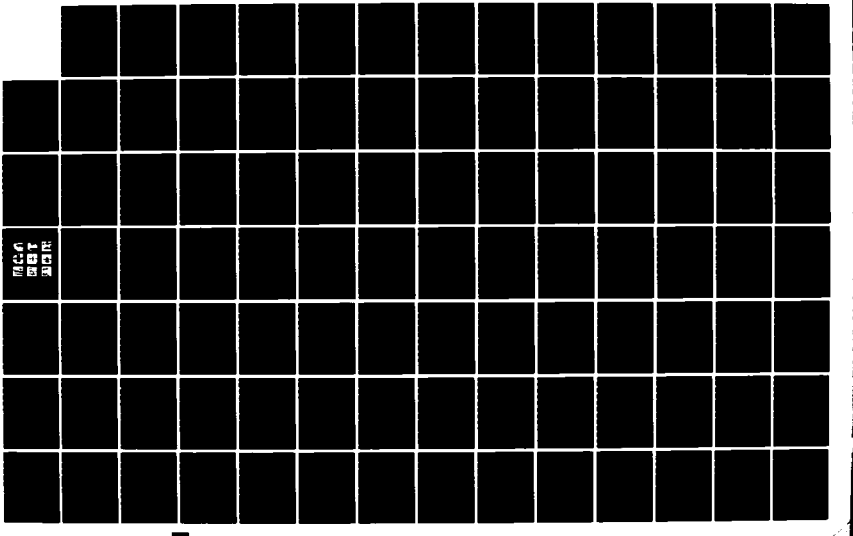
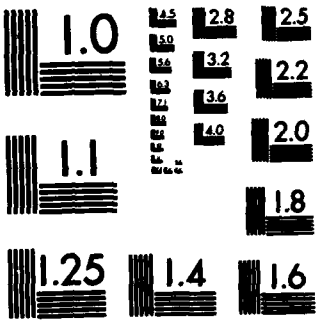


Figure 32 - Effect of Propeller Longitudinal Tip Position on $\Delta\eta_D$

AD-A144 226 PROCEEDINGS OF THE GENERAL MEETING OF THE AMERICAN 4/7
TOWING TANK CONFERENCE..(U) STEVENS INST OF TECH
HOBOKEN NJ DAVIDSON LAB D SAVITSKY ET AL. AUG 83
UNCLASSIFIED SIT-DL-TR-13029-VOL-1 N00167-83-M-4062 F/G 20/4 NL





MICROCOPY RESOLUTION TEST CHART
NATIONAL BUREAU OF STANDARDS-1963-A

RECENT ACTIVITIES OF THE ITTC PROPELLER COMMITTEE

by

Terry Brockett
DTNSRDC

In its report[1] presented to the 16th ITTC at Leningrad, USSR, during September 1981, the Propeller Committee identifies the central problem with conventional propellers to be cavitation and vibration resulting from operation in the ship's wake. The Committee also notes the growing importance of (1) interactions between the propulsor and the vessel and (2) propulsor performance in transitory modes of operation. That Committee Report presents surveys of eight areas of current interest:

1. Effective Wake: The effective wake can be defined as the velocity at the propeller minus the potential flow self-induced velocity component. Hence it is the design onset speed for use with a potential flow model of the flow field. Procedures for deriving and utilizing the effective wake are presented in the Committee Report. Analytical and experimental methods are described and a review of instrumentation suitable for undertaking the required measurements is given. Scaling of the effective wake is also considered. Concern is expressed relative to the complicated and incomplete experimental procedures for defining effective wake from tests at model scale. It is noted that analytic procedures are incomplete because of inadequate treatment of circumferentially nonuniform flow. The Committee concludes that this topic would be important for some years to come.

2. Propeller Induced Vibrations: Vibration due to propeller operation in a nonuniform wake field may arise from excitation transmitted both through the shaft and via the pressure field created on the hull by the rotating propeller. Cavitating and noncavitating propulsors are of concern. This topic has long been of concern to the ITTC. Since much is known about shaft-transmitted excitation, only the pressure field excitation is considered, with emphasis on a cavitating propeller. The main problem is the prediction of the instantaneous cavity volume. Some general guidance for reducing the level of excitation by improved hull shape and appendages for wake modification, by propeller parameters (especially skew and tip unloading) for reduced propeller response and design selection (e.g., clearance increases, air layer, and isolation) are described. Guidance is also discussed relative to allowable

levels of hull pressure values, surface forces, shaft bearing forces, and wake nonuniformity. These criteria are based on replies to a questionnaire developed by the Committee.

3. Prediction Techniques for Single Blade Loads: The Committee concludes that available information indicates that theoretical and experimental methods are available for predicting single-blade forces and moments with sufficient accuracy for a wake that is accurately defined. Hence further surveys in the area will not be required for some time.

4. Real Fluid Effects: Extensive consideration of real-fluid effects was presented to the 15th ITTC by the Propeller, Cavitation, and Performance Committees. The minimum Reynolds number for a lack of difficult scaling problems was estimated by these Committees to be a local value at 0.75 radius of from 2.5 to 4 x 10^5. Differences were noted in open water and propulsion evaluations relative to Reynolds number effects. The 16th ITTC Propeller Committee surveyed how various establishments considered real fluid effects during propeller model testing and analysis by means of a questionnaire. The results of the survey were that the majority of responses stated their criteria were to have a local Reynolds number of at least 4 to 5 x 10^5 for open-water tests and at least a value of 1 to 2 x 10^5 for propulsion evaluations. Wide variations were quoted for the minimum Reynolds number for cavitation evaluation and for evaluation of duct loads. Surface roughness criteria and turbulence stimulation use were less clearly settled relative to a consensus of their importance and effect. The Committee concludes that the real fluid effects on the propulsive characteristics of a propeller are reasonably well understood and taken into consideration during experimental evaluations.

5. Propeller and Thruster Slipstreams: The Committee considered two zones of the slipstream behind an operating propeller: (1) near the propeller where there is a discrete vortex sheet behind each blade, and (2) a far downstream location where a free shear flow exists and the flow is more like a rotating turbulent jet with a maximum radius greater than that of the propeller. The two regions are not well defined. Methods of specifying the vortex sheet are described and analytical results presented. Experimental measurements of both circumferential average and local values of the induced velocity field are discussed. Measured data for the far wake region are described and noted to be unstable but generally similar between model and full scale. Further investigation in these areas is recommended.

6. Propeller and Thruster Interaction: The growth in ocean engineering has led to unconventional marine structures either powered by a multiple arrangement of propulsors or towed by tugs. The interaction between the propulsors, the propulsors and structure, and the towing tugs and structures are described in the Committee Report. Of particular concern is the propeller slipstream interaction at large distances downstream (e.g., up to 100 propeller diameters). The interactions on these unconventional marine structures are not well understood and may be subject to significant scale effect. The Committee concludes that adequate guidance relative to these interactions is not available.

7. Propellers in Transitory Modes of Operation: Increasing use of simulators for predicting the transitory motion of ships, submersibles, and other floating bodies creates a need for propeller performance data undergoing these modes of operation. The Committee surveyed the degree of simulation carried out for propeller performance and the need for further information required for the simulation. The Committee finds the methods of propulsor performance prediction are mostly based on quasi-steady assumptions and four-quadrant open-water propeller data. The survey indicates that the propeller data furnished for use in improved definition for the effects of simulations are inadequate from the technical point of view. In particular, lateral forces, cavitation, air drawing, wake, and interaction coefficients are needed. However, it is not known whether or not improvements in the quality of the propeller data will significantly improve the simulations.

8. Energy Saving Propulsors - Problems with Designing and Testing: Since the cost of fuel oil may be as much as 40 to 50 percent of the total ship operating cost, energy saving propulsors are becoming an important research theme. The Committee identifies problems associated with design and testing of such propulsors. Improvement in the efficiency of conventional propellers may be obtained with reduced loading coefficients arising from large-diameter, slow-turning propulsors. The use of other concepts such as ducted, tandem, and contrarotating propulsors and reaction fins are also discussed. Significant problems may arise relative to predicting the performance of these devices especially with regard to interaction coefficients, integration with the hull, model test techniques/scaling to prototype, and other relevant problems (e.g., vibratory forces).

The Report of the 16th ITTC Propeller Committe also contained recommendations for topics to be addressed by the 17th ITTC Propeller Committee. These recommendations have been modified and increased to form the eight areas of interest currently being addressed:

1. Effective Wake: The state-of-the-art review is to continue. Two three-dimensional aspects are recognized: the nonuniform wake and the propeller. Specific interest is the analytical prediction of wake.
2. Propeller Cavitation: Two areas are to be addressed: (1) means of reducing noise and (2) prediction methods of unsteady cavitation and its effect. The unsteady effects may be restricted to no more than twice blade frequency.
3. Pressure Distribution on Propeller Blades: A previously obtained survey of procedures employed by various organizations to compute pressure distributions will be analyzed. In addition, comparative calculations of pressure distribution about a large model propeller (diameter of 0.95 m) operating over a range of advance coefficients in uniform flow will be analyzed and correlated with experimental data[2] obtained at a local Reynolds number of 1.9×10^6 at 0.75R. Separation of flow over the blades occurred during the experimental determination of the pressure but it appears to have only a local effect.
4. Methods for Design of Nonconventional Propulsion Devices: A survey of the approaches to design of novel propulsors (such as ducted, contrarotating, tandem, preswirl vanes, vertical axis) will be assembled. As much as possible, details of differences will be avoided.
5. Methods and Parameters Used for Propulsion Optimization: Emphasis is on criterion for selecting propulsor number, type, rpm, diameter, blade area, load distribution, etc., to minimize the shaft horsepower full-scale.
6. Transitory Modes: This area is a continuation of the review of propulsor performance in transitory modes such as crash back, lateral motion, periodic cavitation, air drawing, variable wake, and variable interaction coefficients. Special attention will be given to high-skew and controllable-pitch propellers.
7. Propulsors in Waves: The performance of propulsors in waves will be addressed. Areas of interest are excitation forces, propulsive coefficients, strength, relevant hydrodynamic model, and prediction capability.
8. Propeller Vortex System and Viscous Effects: The review of the specification of the vortex system shed by the lifting blades of a propulsor will be continued. Viscous effects are included both as they are responsible for creation

of the shed vortex sheet and as they create blade drag in conjunction with the boundary layer development over the surface. A survey of anomalous viscous effects occurring on the blades of lifting surfaces will be prepared.

A single unified report containing information on these topics is being prepared by the present Committee and will be submitted to the full conference for presentation in Göteborg, Sweden, in September 1984. As is customary, individual members are preparing first drafts of information in a particular area with final integration and approval by all members of the Committee. The final draft is expected to be about 15,000 words long. Organization and effective presentation of the material is a matter of concern to the Committee.

References:

1. Proceedings of Sixteenth International Towing Tank Conference, Leningrad, September 1981.
2. Namimatsu, M., "Experiments for MP 282 Large Model Propeller," IHI Ship Model Basin Report 450-0, Yokohama, about 1979.

REPORTS OF THE

CAVITATION

COMMITTEE

CAVITATION COMMITTEE

SUMMARY REPORT

20th American Towing Tank Conference

by

Blaine R. Parkin, Chairman

Since the report of the 19th American Towing Tank Conference (ATTC) at The University of Michigan in 1980, cavitation research has remained active. The object of this research has always been to enhance the fidelity with which laboratory experiments can be made to model the cavitation to be expected in full scale applications of marine and other hydraulic machinery. This brings to the fore such questions as scaling of inception, erosion, noise, ventilation and unsteady cavitation.

All of these topics were considered by the 19th ATTC Cavitation Committee by giving comprehensive reviews of some and limiting others to presentation of specific new results of interest to the towing tank and water tunnel community. In all cases, this community is seeking to learn how to use its hydrodynamic research facilities most effectively in its work to predict full-scale cavitation performance. In this report, the 19th ATTC Cavitation Committee pointed out again that laboratory work definitely needs the supporting data obtained from full-scale trials for correlation of results. This continues to be true today and although some progress is being made in this regard the difficulties and expense of sea trials makes the accumulation of full scale data a slow process.

For the 20th ATTC, the Cavitation Committee has not tried to arrive at any general conclusions with respect to research needs or overviews of progress since the 19th ATTC. Instead, we have chosen to concentrate

our efforts on a few specific topics of interest to the hydrodynamic testing community in the realms of cavitation inception and cavity flows.

For cavitation inception, members of the committee have prepared a report comparing methods for microbubble measurement and techniques for measuring cavitation susceptibility. In a closely related work, we are given results of new research on design problems of venturi cavitation susceptibility meters. Finally, new inception research results on the practical problem of isolated roughness effects in the presence of pressure gradients are given. All of these topics can be seen to be of importance for the interpretation of laboratory and full scale inception data.

In the realm of cavity flows, one of the committee reports involves a predominantly theoretical analysis of a free streamline approach to both wake flows and separation bubbles without cavitation and to steady and unsteady cavity flows past foils and propellers with partial cavitation. Considerations of tunnel wall effects on these flows are also discussed. In a new departure for this committee, its final contribution concerns the computational hydrodynamics of cavity flows applied to marine propellers. This recent numerical approach includes nonlinear effects of foil and cavity thickness in steady two-dimensional flow.

AD-P003 808

CAVITATION INCEPTION

A Review-Progress Since 19th ATTC

by

Young T. Shen

David Taylor Naval Ship Research and Development Center

and

Frank B. Peterson

Naval Sea Systems Command

20th American Towing Conference
Stevens Institute of Technology
Hoboken, New Jersey
August 1983

INTRODUCTION

Most heavily loaded hydrofoils or propellers will develop tip vortex and surface cavitation at high speed. The occurrence of cavitation leads to undesirable changes in hydrodynamic performance, noise generation, and physical damage from vibration and erosion. Therefore, the ability to predict the occurrence of cavitation becomes an important engineering problem. Because of the complexity of physical processes involved with cavitation inception, the prediction of cavitation performance has relied heavily on model experiments and extrapolation of the results to full scale.

It has often been observed that cavitation takes a variety of forms which may differ from facility to facility with a similar model or even the same model. The test results of the ITTC (International Towing Tank Conference) standard headform is a good example. Tests on this flat-faced ellipsoidal body were carried out in many different laboratories throughout the world. Measured cavitation inception indices on this single headform ranged dramatically from 0.3 to 0.6 (Acosta, 1979).* Even the appearance of the cavitation varied, some forms looking totally dissimilar from one another (see Figure 1). These apparently chaotic results were clearly pointed out by Johnsson (1969). Recently, the experimental observation of cavitation in an orifice and a venturi by Oba et al. (1983) showed similar variation in cavitation inception index and cavity appearances.

The well known series of photographs (Figure 1) provides an impetus on cavitation research activities. Acosta and Parkin (1974) in the 17th ATTC (American Towing Tank Conference) cavitation inception review paper showed

---

*See reference at end of paper.

that fluid viscosity and free-stream nuclei distribution are responsible for producing the various appearances of the cavitation on a single test model. For many tests both of these subjects are intimately linked.

In the decade of the 1960's, numerous studies of the effect of air content on cavitation inception were carried out. They showed that a gross increase in the air content will decrease the cavitation inception speed. This effect was attributed to the existence of cavitation nuclei, i.e., the impurities in water which prevent the water from supporting the amount of tension computed for a pure, homogeneous water. A qualitative relationship between the presence of cavitation nuclei and the appearance of cavitation has been observed experimentally and computed theoretically (see review papers by Acosta and Parkin 1980, Arndt 1981). It is recognized that quantitative prediction of such relationship depends on the ability to obtain measurements of cavitation nuclei such as size distribution and concentration. Knowledge of the nuclei population with respect to size and kind is needed to relate the bubble dynamics to cavitation and the appearance observed in cavitation testing.

Several types of instruments had been developed and adapted to measure "nucleating sources" in a liquid, including acoustic methods, holographic and photographic methods, and light scattering methods. The principle of operation and the accuracy of measurements associated with each method were summarized by Morgan (1972). A few series of instrument comparison tests were made in the decade of the 1970's to evaluate the merits of each measuring technique (Peterson et al. 1981). Of the many methods applied to nuclei measurements, two optical techniques, light scattering and holography, have received more attention among cavitation researchers. Significant improvements on these measuring techniques have been made in the last three years.

One result of this review is our recognition of an increase in the use of recently developed nuclei measuring instrument along with cavitation inception measurements. The influence of free-stream nuclei on cavitation has been more clearly identified and differentiation between active and nonactive nuclei have received greater attention. Research activities have also continued on "nuclei and scaling relationship" over the last three years.

With the recent successful development of instruments for nuclei measurements and the improved understanding on the influence of nuclei on cavitation inception, the need to control the nuclei concentration and size distribution in laboratories during model cavitation tests has become an interesting subject. Nucleation control appears to be an idea whose time is rapidly approaching.

In addition to the free-stream nuclei, viscosity also plays a major role on scaling problems. With the recent advances in cavitation research, the possibility of "solving" these laboratory testing problems has stimulated more work to make this possibility more of a practical reality. The concept of using roughness elements (Kuiper 1979) to simulate a high Reynolds number prototype cavitation condition has received special attention among cavitation researchers in the last few years as noted by the number of published papers and reports on this subject.

NUCLEI

From the full scale investigation on the container ship "SYDNEY EXPRESS" and the comparison with oceanographic investigations, Weitendorf (1979) found that in the sea a great number of cavitation nuclei are always present. Recently, the U.S. Navy made measurements of the cavitation susceptibility of the water off the coast of Florida. The cavitation susceptibility was measured by a venturi, microbubbles by a light-scattering device, and particulates by

a Coulter counter, and correlated with standard oceanographic measurements. The preliminary results seem to confirm the previous observation that the ocean is full of cavitation nuclei. Experiments by Medwin (1977, 1979) in coastal waters indicate that bubbles with radii between 15 and 200 μm are present to depths of order 40 m.

Mechanisms for bubble generation and persistence in the ocean have been investigated by many researchers (see Isay (1981) pp. 58 to 67) and recently by Mulhearn (1981) theoretically along with experimental observations. His results suggest that the larger bubbles (radius > 60 μm) may be generated continuously by decaying matter on the sea floor, but that smaller ones (radius < 60 μm) persist indefinitely, once formed, because of surfactant coating and attachment to particles. Following the crevice model of Harvey, Yount et al. (1982) proposed a "skins of varying-permeability" model to show the existence of stable gas nuclei. The stability is provided by elastic skins or membranes consisting of surface active molecules.

Using a different approach from the aforementioned mechanism, Cha (1981) provides a different mechanism for the existence of permanent microbubble nuclei. His mathematical model on the equilibrium of cavitation nuclei in liquid-gas solutions showed that a gas vapor can persist in a liquid-gas solution. As pointed out by Plesset, should Cha's finding be sustained, such bubbles could serve as sites for the initiation of cavitation. As a remark, different mechanisms had been studied previously. For example, the stability of bubbles in water tunnels by rectified diffusion due to turbulent pressure fluctuations was studied by Ripkin and Killen (1962).

In a cavitation tunnel free gas bubbles are generated by the impeller, by sharp corners in the circuit and by the cavitating device in the test section

(Kuiper 1981, Ling et al. 1982). The mechanics of bubble generation are quite different between the ocean and laboratories. To characterize the nuclei distribution in laboratories, Gates and Billet (1980) measured the nuclei distribution in two Caltech water tunnels and one ARL tunnel. Katz (1981) and Ooi (1982), and Katz et al. (1983) provided further information on the influence of various flow parameters on nuclei distributions at Caltech facilities, and Ling et al. (1982) and Gowing (1983) at DTNSRDC facilities. Significant variations in nuclei spectra at different facilities and flow conditions were measured.

Recent works by Wetzel et al. (1983) and Barral (1983) showed a promising result that there is a subtle, albeit definitive relationship, between the level of dissolved gas and the nuclei population in a given facility. On a log-log plot the measured nuclei size spectra from several facilities shift up and down as a function of the level of dissolved gas. The total nuclei density is seen to vary orderly with total air content. If this relationship could be further verified, a given facility could be calibrated for nuclei size distribution as a function of dissolved gas, allowing rather simple monitoring of the nuclei content via the measurement of dissolved gas by the use of van Slyke meter.

The need to establish standards for required nuclei spectral in test facilities has been well recognized (Peterson et al. 1981). Because the true role of nuclei and their characteristics had not been fully established at either model or full scale conditions, a required spectral distribution has not been recommended either by ATTC or ITTC. With the increasing trend of using nuclei measurement as part of cavitation experiments, the demand for standard spectra will be intensified.

NUCLEI AND CAVITATION INCEPTION

One of the significant advancements in the past few years in cavitation research was the use of nuclei measurements and flow visualization along with cavitation observation. The influence of free stream nuclei and the intimate relationship between nuclei and viscous effect on cavitation inception was brought out by Gates and Billet (1980) on headforms and van der Meulen and Ye (1982) on a NACA foil.

For a hemispherical headform tested in a facility of low gas bubble concentration, Gates and Billet showed that the nuclei passing through the minimum pressure region experience tension as much as half an atmosphere. The cavitation does not appear in this minimum pressure region but at a location further downstream. For the same model tested in a facility of high gas bubbles, the nuclei passing through the minimum pressure region cannot withstand substantial tension, and the inception of travelling bubbles begins in the minimum pressure region. The measured cavitation inception index in the facility of high gas bubble concentration is thus much higher than in the facility of low gas bubble concentration. The variation in cavitation inception index, various forms of cavitation, and variation in inception location on headforms experienced at different test facilites and flow conditions are now better understood relative to the nuclei concentrations and boundary layer properties on the models.

Holl and Carroll (1981) presented experimental observations of various types of limited cavitation on several headforms. They observed that in most cases, the measured cavitation inception index of travelling bubbles was found to decrease with an increase in freestream speed. However, in some cases the opposite trend was observed. At a DTNSRDC facility, Brockett reported an increasing trend in cavitation index with speed for travelling cavitation.

Ling et al. (1982) and Carroll (1981) showed that the critical bubble radius decreases with an increase in free-stream speed. Based on the theory of bubble dynamics, the cavitation index should increase with an increase in free-stream speed. This kind of inconsistency had been noticed in the past.

Gates and Billet speculated that at the high free-stream velocities the static tunnel pressure is high at inception and, hence, one might expect fewer free-stream bubbles to be present. The measurements by van der Meulen and Ye (1982) indicated that the number of bubble population is lower at high speeds than in low speed (Table 7). This series of experiments support the speculation by Gates and Billet. Experimental observations clearly show that travelling cavitation is very sensitive to changes in free-stream nuclei.

Ooi (1981, 1982) recently studied scale effects on cavitation inception in submerged jets. The measured inception index was independent of the exit velocity for a constant size jet. However, when the flow was seeded with bubbles, the inception number showed a linear increase with velocity within the test range of 10 to 30 m/s, and this dependency increased with increased number of seeded nuclei. This experimental observation is in agreement with the theory of bubble dynamics. The present study points out the importance of simultaneous measurements of cavitation and bubble population. Cavitation observations by Henry et al. (1980) and Le Goff and Lecoffre (1982) indicated the same trend, i.e., the scale effect disappears when a suitable quantity of cavitation nuclei are introduced into the flow.

As pointed out previously, the theoretically computed critical bubble radius decreases with an increase in free-stream speed. Holl and Carroll (1981) analyzed the measured data from four investigators. All the data are collapsed into a trend as predicted by the theory of bubble dynamics. For an increase in the

tunnel velocity from 20 to 70 feet per second, the average value of critical radius decreased by two orders of magnitude. Thus testing speed is shown to influence significantly the amount of active bubble population. Additionally, the effect of free-stream bubbles on cavitation inception requires that the bubble has to be exposed to a low pressure for a sufficient time (Ling et al. 1982, Katz 1981). Gates and Billet (1980) studied two geometrically similar models of 25.4 mm body (1 in.) and 50.8 mm body (2 in.) Travelling bubble events were rare on the 25.4 mm body even though free-stream conditions were similar to those during the 50.8 mm body tests. This experimental result seems to support the previous theoretical calculations that bubble cavitation is influenced by the model size. Further studies are required to quantify the true role of nuclei in cavitation inception. It seems that required nuclei spectra may have to depend on tunnel speed, model size and type of cavitation.

Another important conclusion from Gates and Billet (1980) is that micro-bubbles are more important to cavitation than the other types of cavitation nuclei. On the other hand, Weitendorf (1979) made a cavitation observation from the container ship "SYDNEY EXPRESS." Nuclei spectra were measured by a laser light-scattering device. Weitendorf suggested that some of these suspended particles with diameters below 20 μm act as pore nuclei at the cavitation process, into which the liquid evaporates if the pressure is reduced. By the use of filter to vary the amount of particulates, Kuiper (1981) found noticeable change in cavitation inception characteristics from his model tests. It seems that differentiation between particulates and bubbles on cavitation inception is still of some controversy.

Godefory et al. (1981) and Oldenziel et al. (1982) studied experimentally the influence of nuclei on cavitation of a valve. The free gas content was

controlled by microbubble injection systems and the mean bubble size and bubble concentration measured by holography, acoustic doppler and light scattering. The tensile strength of the liquid was measured by venturis. The significant results obtained from this series of tests are that they were able to distinguish between "nonactive" and "active" nuclei. The concentration of active cavitation nuclei is several orders of magnitude lower than the conentration of all non-active suspended in the liquid, even if artificial gas nuclei are injected. This system may offer a possibility to identify the roles of particulates and bubbles.

Latorre (1981, 1982) also used the theory of bubble dynamics to relate the growth of nuclei in propeller tip vortex inception. His mathematically simulated model seemed to give qualitative agreement with experimental observation. Quantitatively, the influence of air content on tip vortex cavitation inception is still unclear with some experiments showing positive contribution and some experiments showing weak dependency. Kuiper (1981) showed that measured tip vortex cavitation inception indices on model propellers tested in a depressurized tank differ noticeably with and without the use of electrolysis. Measurements by Platzer and Souders at DTNSRDC showed only a weak dependency of tip vortex cavitation on the variation of air content. This kind of inconsistency is often found in experimental measurements. One possible explanation is that the nuclei population in a depressurized tank is very low. With the use of electrolysis, nuclei population is increased by an order of magnitude (see Figures 5.7 and 5.8 of Kuiper 1981). On the other hand, at DTNSRDC 36-in. water tunnel, due to the existence of relatively long legs of resorbor, the nuclei population does not vary significantly with air content (Ling et al. 1982). This speculation points to the importance of measuring nuclei population

in cavitation experiments. The influence of free stream nuclei on vortex cavitation requires further investigation. This is an area that requires further studies.

Le Goff and Lecoffre (1982) gave an interesting paper presenting the main steps in the ten-year research program by NEYRTEC of France concerning the influence of nuclei on cavitation. They proposed a scaling law for developed bubble cavitation where the concentration of nuclei is λ^3 times that of the prototype, λ being the prototype-to-model scale ratio. If the experiments are done at different speeds, a further condition is to be placed on the critical pressure of the microbubbles. If the model is too small, the influence of bubbles having insufficient residence time must be corrected.

The role of microbubbles on cavitation inception was investigated theoretically by Ling et al. (1982). A new set of parameters based on bubble dynamics was used to parameterize the cavitation inception. They showed that cavitation of large-scale, high-speed prototype is largely independent of the size distribution of the available microbubbles, whereas small scale models operating at low speed can cavitate only when a narrow band of microbubble size is available. This theoretical work related the nuclei size distribution to the scaling problem of travelling bubble type cavitation inception.

VISCOUS EFFECT

According to Weitendorf (1982), the travelling bubble type of cavitation was rarely observed in full scale propellers. All full scale cavitation observations have revealed attached type sheet cavitation.

Cavitation inception on six headforms was investigated by Huang (1981). Travelling bubble cavitation was observed on headforms with natural flow transition. Attached type ring cavitation starting at a separation point was

observed on headforms with laminar separation. Holl and Carroll (1981) investigated experimentally the mechanisms of formation of various types of cavitation. They found that the travelling bubble cavitation and travelling patch cavitation are very sensitive to nuclei content. Fixed patch and attached band bubble ring cavitation are mostly due to boundary layer effects and are insensitive to the air content.

Recently, the subject of attached bubble ring cavitation was studied theoretically by Parkin (1981a, 1981b, 1982) on a hemispherical headform. Gaseous growth as well as vaporous growth is found to be associated with the onset of bubble-ring cavitation. Parkin then provided the sequence of events of cavitation bubble growth. The inception criterion was subsequently derived. Onset of bubble-ring cavitation is shown practically independent of air content provided the dissolved air concentration of the water is sufficient to support air diffusion into the bubble. This is a well observed experimental fact. Parkin's theory also shows the existence of a lowest speed and cavitation number at which "bubble-ring" cavitation can exist. This phenomenon is also well observed in experiments that at low speed the cavitation on headform is of the travelling bubble type; however, as the tunnel speed is increased to a critical speed, the cavitation changes to ring-bubble or fixed patch cavitation. Using this asymptotic theory, Parkin found that the cavitation number at inception is less than the magnitude of the pressure coefficient at the laminar separation point. The predicted onset of bubble ring cavitation agrees well with experimental data measured by Holl and Carroll. Most remarkably, Parkin has successfully derived this theory based upon first principles.

A hydrofoil under the pitching oscillation was investigated by Shen and Peterson (1978, 1980). The occurrence of leading edge sheet cavitation was

measured. The delay in cavitation inception at a given reduced frequency and cavitation number was measured and correctly predicted when the inception angles were compared with the steady flow condition. However, the measured angles at cavitation inception, in all cases studied, are higher than the the theory predicted. The same problem was recently studied by Stern (1982). His nonlinear potential flow theory predicted a similar result as given by Shen and Peterson.

It has been well documented that a leading edge sheet cavitation in model testing does not occur if the flow is laminar. Consequently, the measured cavitation inception angle is higher than the potential flow theory predicted (see, for example, Shen 1982). The same phenomenon was observed in unsteady flow condition by Shen and Peterson, and Stern (1982). Whether the role played by viscous effect in unsteady cavitation inception is the same as in steady flow condition remains to be investigated.

The existence of high intensity pressure fluctuations in a laminar separation zone has been measured. The influence of pressure fluctuations on cavitation inception has been well documented. Recently, Katz (1981) provided a more intensive measurement of pressure fluctuations in a separated zone. This report provides an important information on response time of bubbles versus spectra of pressure fluctuations. The rates of cavitation events are correlated with the nuclei population. Ooi (1982) provided additional measurements of pressure fluctuations in a submerged jet.

The attempts to produce "high-Reynolds-number" cavitation phenomena in tests of model propellers continue to receive high attention (see Huang 1983). This work was originated at the Netherlands Ship Model Basin. Kuiper (1981, 1982) used a strip of 60 μm carborundum irregular particles about 1 mm from the

leading edge of propeller blades to stimulate the boundary layer on a propeller model and showed the reduction of viscous effects on propeller cavitation.

Shen (1982) used a uniformly distributed roughness, consisting of spherical glass beads of 90 μm covering the first 1.5 percent of the chord length on both the upper and lower surface of a cambered foil to simulate the high Reynolds number cavitation phenomenon. The measured cavitation inception index was found to agree well with the theoretically predicted minimum pressure coefficient. Similar results were also obtained by Huang and Belt (1983) on headform models. Experimental investigation by van der Meulen and Ye (1982) on NACA 4412 foil showed that a scale effect exists on the model. However, if the surface roughness is applied, the scale effect disappears completely in one case studied.

Microbubble measurement plus flow visualization by van der Meulen and Ye clearly show that the application of leading edge roughness is capable of not only reducing viscous effects but also providing needed nuclei. The use of roughness to simulate high Reynolds number cavitation condition is a very promising tool. However, experimental observations by Shen (1982) showed that the leading edge roughness could also produce an undesired pressure disturbance near the minimum pressure location that might cause early cavitation on the roughness elements. The zero lift angle in fully wetted condition was found to change noticeably. This fact must be included in comparing model test results with and without the application of surface roughness.

The influence of roughness size on cavitation inception has been studied recently by Billet et al. (1982) and Holl et al. (1983). The cavitation inception number is expressed in terms of relative roughness height, Reynolds number, and the mean pressure coefficient. In the case of the existence of

pressure gradient, Clauser's equilibrium boundary layer shape factor is included.

In a full scale propeller, the relative boundary layer thickness is thin. A full scale propeller is thus more prone to cavitation caused by a local roughness. However, the pressure distributions and the three-dimensional boundary layer properties of the propellers are often not available or, if available, not accurately determined. In this respect, the attention is called to a recent report by Jessup (1982) who measured pressure distributions on two controllable pitch propellers in uniform and inclined flows. The theoretically computed pressure field was found to differ noticeably from experimental measurements. More activity in this area is expected, and the influence of roughness on propeller cavitation will remain an important issue for the next few years.

CAVITATION SUSCEPTIBILITY

The results given by indirect method of cavitation nuclei measurements, such as light scattering or holography, always show very large amounts of nuclei (Peterson et al. 1975) - more than 1000 per cm^3 in the range of diameters above 1 μm. Godefroy et al. (1981) distinguished between the nuclei as "nonactive" and "active" and based experimental observations on cavitation bodies show that the number of vapor bubbles is limited in 1 - 10 active nuclei per cm^3. This observation has led to the development of totally different type of instruments to measure the impurities in water, namely the tensile strength of water at which the weakest nuclei explodes and is termed cavitation susceptibility.

Oldenziel (1975, 1979) has developed a cavitation susceptibility instrument. Following the approach of Oldenziel, Lecoffre and Bonnin (1979) also developed a venturi system at NEYRTEC for cavitation susceptibility measurement. The

test fluid is made to pass through a venturi nozzle in such a way that the pressure is lowered to a value sufficient to make nuclei grow explosively, then collapse. The occurrence of vapor bubbles is detected by acoustic signal. The event rate is related to the concentration, and the amplitude of the acoustic signal is related to the size of a microbubble at a given pressure.

A recent instrument comparison with venturis, laser light scattering and holography was completed (Godefroy et al. 1981, Oldenziel 1982). A summary of bubble concentration measurements for the five measuring systems is given in Godefroy et al. (Table 5). In most cases, the agreement between the venturis of Oldenziel and Lecoffre is within a factor of 2. On the other hand, the comparison between venturi system and optical system is inconclusive.

The cavitation susceptibility study by Le Goff and Lecoffre (1982) indicated that the active nuclei correspond to equivalent bubble sizes of less than 2 μm in diameter. On the other hand, the resolution of an optical device based on laser light scattering limits the ability to measure the nuclei size to 5 μm diameter and larger. The experimental results by Le Goff and Lecoffre seem to indicate that the nuclei measured by the indirect method (optical instruments) are inadequate to measure the whole active nuclei population. They concluded that using a direct method, such as a venturi, is the only way to measure the nuclei content in full scale conditions at the laboratories. This new system appears to be very promising for cavitation research.

Recently, the U.S. Navy had made ocean cavitation susceptibility measurements. The venturi used in this sea trip was made by NEYRTEC with the throat diameter of 2 mm. The cavitation nuclei are detected by a hydrophone. At a given ambient pressure, the measured flow rate was very repeatable when cavitation inception occurred. Once cavitation inception was detected, a slight

increase in the flow rate resulted in a significant increase in cavitation event rates. The occurrence of bubble cavitation was very random. Single bursting and multiple bursting were randomly detected by the hydrophone. Occasionally, attached type surface cavitation also was detected. Reduction of flow rate was very effective to eliminate surface cavitation.

Based on this cavitation susceptibility studies, the critical pressure, i.e., the tensile strength of the weakest nuclei in ocean water exploded in the venturi throat was obtained. The preliminary result seems to indicate that the measured critical pressure is very close to vapor pressure. More definite value has to wait until the completion of post calibration of instruments. A significant increase in cavitation events with a slight increase in the flow rate seems to indicate that the ocean is full of active nuclei.

As a remark, the use of a venturi for cavitation susceptibility measurement is not new. Crump (1949, 1951) used a venturi to determine the critical pressure for the inception of cavitation as a function of the air content in fresh water and sea water. By lowering the air content, the ability to sustain a substantial degree of tensile stress was demonstrated experimentally. However, the concept introduced by Oldenziel of using a venturi to measure bubble concentration and size distribution is a positive contribution. This device may offer a possibility to identify "active" nuclei from bubbles and particulates.

NUCLEATION CONTROL

Measurements by Weitendorf and Keller (1978) and Weitendorf (1979) have shown that the ocean is full of nuclei. Their investigation on the container ship "SYDNEY EXPRESS" revealed the large influence of the free gas content of the test water on the propeller cavitation and hereby excited pressure fluctuations. Lecoffre and Bonnin stress that nuclei influence almost all

cavitation types (1979). Experiments on ship propellers by Kuiper (1982) in the laboratory show the influence of scale effects on cavitation not only near inception but also with developed cavitation.

With recent success in the development of instruments for nuclei measurements and the physical understanding on the influence of nuclei on cavitation, the need to control the nuclei distribution in laboratories during model cavitation tests is gaining more attention. Electrolysis has been used extensively in many laboratories to vary the nuclei content of the water. Kuiper (1979, 1982) showed that, with bubble seeding, cavitation inception and cavity patterns on model propellers compare more favorably with the full scale data. The procedures to generate nuclei and the difficulties of applying electrolysis in high speed water tunnels are well discussed by Kuiper in his dissertation (1981).

Van der Meulen and Ye (1982) used wires to seed nuclei. The wires were located ahead of the model. The problem of generating excessive vorticity which may affect model cavitation was detected. Otherwise, this technique is very effective.

Roughness distribution around the leading edge of the foil is found to be an effective device to produce nuclei and reduce the scale effect (Shen 1982, van der Meulen and Ye 1982, Kuiper 1981). However, care must be exercised to select the proper sand size to avoid undesirable modification of local pressure distribution and premature cavitation induced by the local roughness height (Holl et al. 1983).

Oldenziel (1982) has developed a system for bubble injection by use of a bubble filter. This system is based on the relative motion of bubbles due to the gravity field. Water jets in air penetrate the liquid surface and generate several small gas bubbles in the size range of below 40 μm. The injection of a small amount of soap increases the number of bubbles.

NEYRTEC (Le Goff and Lecoffre 1982) has developed a system for artificial nucleation by a so-called "expansion method." A tank is almost filled with water having a high dissolved gas content. The pressure in the tank is kept at high value. If bubbles are wanted, water is injected from the tank into the water tunnel through very small holes. The bubbles produced had an average diameter of 50 μm.

Nucleation control appears to be an idea whose time is rapidly approaching. One of the design concerns of a new large cavitation channel to be built at DTNSRDC is the requirement of nucleation control. The possibility of injecting highly saturated water into the tunnel upstream of the test section is being considered. The requirement of nucleation control specified in this newly designed large cavitation channel clearly demonstrates the progress in recent years on the subject of "nuclei and cavitation inception."

MEASUREMENT OF NUCLEI

Continued development of practical and reliable instruments for nuclei measurements were noticed in the last three years. Among the many devices adapted and tested in laboratories for nuclei measurements, holography and light scattering have become more favored than the others.

A workshop on the scattered light technique for cavitation nuclei determination was held in Fraunhofer Institut fur Hydroakaustik (Baiter 1981). The problems associated with light scattered technique encountered in the last few years were discussed. Three questions have come to the fore which have not sufficiently been taken into account in the past: statistical data analysis, discrimination of different kinds of scattering objects (in particular bubbles and solid particles), and light intensity distribution in the control volume.

The possible source of error associated with partial crossing between the scatterers and the control volume was studied by Yungkurth (1982) and Avellan and Resch (1983). A criteria to design the control volume in terms of total nuclei concentration and acceptable probability of coincidence and side effects was given in these reports.

The problem associated with nonuniform light intensity distribution in the control volume was investigated by Davis (1983) and Gowing (1983) using the matrix inversion technique (see Holve and Self 1978) with weighting functions to simulate the nonuniformity in the light intensity distribution. The ability to use this method to correct the nonuniformity in light intensity distribution is demonstrated by the fact that the difference in measured cavitation nuclei between light scattering and holography at CIT water tunnel as discussed previously is reasonably simulated by Davis and Billet.

One of the disadvantages associated with the laser light scattering device as pointed out by Peterson et al. (1975) is that it is unable to differentiate between bubbles and solid particles. Keller applied and tested a method at the Delft Hydraulics Laboratory (Godefroy 1981) by subtracting distributions obtained at high pressure from those of low pressure. This method proved quite successful. However, recently a more rigorous method of using dual detectors to differentiate particles from bubbles was developed by Billet and Yungkurth (1982). The method is based on the observation that the microbubbles, being spherical, will cause symmetric light scattering, whereas the particles are, in general, randomly shaped and, therefore, will scatter light randomly. Their experimental results confirm that discrimination can be obtained with an accuracy as high as 95%.

Gowing and Ling (1980) have developed a means of sizing bubbles and particulates by detecting the amount of incoherent light scattered. This method utilized the specular reflections of bubbles to differentiate them from the nonspecular reflections of particles. The instrument uses a Koehler lamp as a light source. According to Gowing and Ling, an incandescent light source has the advantage over a laser light source because there is no diffraction at the edges of the control volume; consequently, the intensity of light across the breadth of the beam is more uniform. Because of the use of an ordinary white light as the light source, the ability to penetrate distance through water has not been well explored yet. The system has been used to date, only in a bypass channel of a 2-in. pipe to the main test section. The advantages of this device are that it can provide real time data analysis, high statistical accuracy, differentiation of particles from bubbles. The instrument is simple, inexpensive, and easy to set-up. With further improvements on calibration, this incoherent light scattering technique would be an attractive candidate as a general purpose instrument.

In the area of photography as pointed out by Peterson, data analysis of this method is very tedious and time consuming. Efforts are being made at Physikalisches Institut of the University of Gottingen (Haussmann 1978 and Haussmann and Lauterborn 1980) to develop automatic scanning and evaluation of holographic records of cavitation bubbles. This technique could be used to make holographic measurement of cavitation nuclei more efficient.

The need to obtain adequate correlation between laboratory and field conditions for cavitation tests motivated the development of an underwater holocamera at Caltech (Katz 1979, Acosta et al. 1983). This holographic system is designed for use either in the laboratory or the ocean up to the depth of 30 meters (100 ft). The device had been successfully tested in the Caltech

Low Turbulence Water Tunnel jointly with the white light scattering device (Katz et al. 1983). The results presented so far suggest that reliable measurements of nuclei size spectra by holography and light scattering are possible now.

Acoustic methods for determination of bubble sizes have been used for many years. For example, Schiebe and Killen (1971) used the acoustic tone burst attenuation technique and tried to measure the bubble size distribution in water. The problem with all these active acoustic techniques is that a relatively small structural reflection causes a great amount of noise in the detected signal.

Medwin (1979), with an improved theory, was able to achieve a bubble density resolution at 600 μm diamter, 0.5 bubbles/m^3, and at 40 μm diameter, 200 bubbles/m^3, respectively. However, at bubble sizes smaller than 40 μm diameter, the ability to produce the required high acoustic frequencies limits the application of this method.

Jansen (see Godefroy 1981) has developed an acoustic instrument "ultrasonic doppler scatterometer" to measure the bubble concentration and the flow velocity in cavitation studies. The advantage of this system is that it measures continuously and simultaneously the bubble concentration and velocity without obstructing the flow. The disadvantage is that it does not measure the size distribution. Furthermore, the system requires complicated calibration. This system had been compared with holographic and laser light scattering devices and was found to be a promising tool in cavitation studies.

Oba et al. (1981) has developed a new Coulter counter system to measure nuclei directly without adding any salt in water. The system can measure the nuclei size ranges from 8 μm to 100 μm. The water sample is collected in a

small schield box. Fluid, passing through the ruby orifice of 0.2 mm in diameter and 0.15 mm in length, generates voltage pulses proportional to the volume of nuclei. The application of this system was compared favorably with the existing data obtained from other sources.

ACKNOWLEDGMENTS

The work described in this paper was funded under the David W. Taylor Naval Research and Development Center's Independent Research Program, Program Element 61152N, Project Number ZR 000 01. The authors would like to acknowledge the benefit of discussion with T.T. Huang.

REFERENCES

Acosta, A.J. and Parkin, B.R., (1974) "Cavitation Inception - A Selective Review," 17th American Towing Tank Conference.

Acosta, A.J. and Parkin, B.R., (1980) "Report of the ATTC Cavitation Inception Committee," 19th American Towing Tank Conference.

Acosta, A.J. et al., (1983) "Microbubbles and Cavitation," California Institute of Technology, Report No. E261.2.

Arakeri, V.H. and Acosta, A., (1981) "Viscous Effects in the Inception of Cavitation," J. of Fluid Eng., Vol. 103, pp. 280-286.

Arndt, R.E., (1981) "Cavitation in Fluid Machinery and Hydraulic Structures," Annual Review of Fluids Mechanics, Vol. 13, pp. 273-328.

Baiter, H.J., (1981) "Workshop on the Scattered Light Technique for Cavitation Nuclei Determination," Fraunhofer - Institut fur Hydroakaustik, Ottobrunn, Germany.

Barral, L., (1983) "A Critical Examination of the Influence of Dissolved Gas on the Cavitation Process in Turbulent Shear Flows," M.S. thesis in Fluids Mechanics, University of Minnesota.

Billet, M.L. and Holl, J.W., (1981) "Scale Effects on Various Types of Limited Cavitation," J. of Fluids Eng., Vol. 103, pp. 405-

Billet, M.L. and Gates, E.M., (1981) "A Comparison of Two Optical Techniques for Measuring Cavitation Nuclei," J. of Fluids Eng., Vol. 130, No. 1, pp. 8-13.

Billet, M.L., Holl, J.W. and Parkin, B.R., (1982) "Scale Effects on Cavitating Flows Due to Surface Roughness and Laminar Separation," AIAA Journal 82-4115.

Billet, M.L., and Yungkurth, C.B., (1982) "Light Scattering System: Analysis and Calibration," Measurements in Polyphase Flows, ASME, pp. 97-102.

Carroll, H., (1981) "Observation of the Effects of Boundary Layer and Nuclei on Cavitation of Axisymmetric Bodies," ARL Tech. Memo. 81-60, Penn State University.

Cha, Y.S., (1981) "On the Equilibrium of Cavitation Nuclei in Liquid-Gas Solutions," J. of Fluids Engineering, Vol. 103, pp. 425-431.

Crump, S., (1949) "Determination of Critical Pressures for the Inception of Cavitation in Fresh and Sea Water as Influenced by Air Content of the Water," DTMB Report 575.

Crump, S., (1951) "Critical Pressures for the Inception of Cavitation in a Large-Scale Numachi Nozzle as Influenced by the Air Content of the Water," DTMB Report 770.

Davis, R.J. and Billet, M.L., (1983) "Light Scattering System: Probe Volume Statistical Analysis," Cavitation and Multiphase Flow Forum, Houston,

Gates, E.M. and Billet, M.L., (1980) "Cavitation Nuclei and Inception," 10th IAHR Symposium, Tokyo, pp. 3-25.

Godefroy, H.W. et al., (1981) "Comparison of Measuring and Control Methods of the Water Quality with Respect to Cavitation Behavior," Delft Hydraulic Laboratory.

Gowing, S., (1983) "Measurements of Microbubbles in the DTNSRDC 12-Inch and 36-Inch Water Tunnels with a Light Scattering Microbubble Detector, DTNSRDC Report.

Gowing, S. and Ling, S.C., (1980) "Measurements of Microbubbles in a Water Tunnel," 19th American Towing Tank Conference.

Haussmann, G., (1979) "Determination of Bubble Size Spectra by Digital Processing of Holograms," Proc. First International Conf. on Cavitation and Inhomogeneities in Underwater Acoustics, Gottingen, pp. 219-224.

Haussmann, G. and Lauterborn, W., (1980) "Particle Analysis by Digital Processing of Three Dimensional Hologram Reconstructions," The Society of Photo-Optical Instrumentation Seminar, Beilingham, Washington, Vol. 210.

Henry, P. et al., (1980) "Effects a'Echelle en Cavitation," 10th IAHR Symposium, Tokyo, pp. 103-114.

Holl, J.W. and Carroll, J.A., (1981) "Observations of the Various Types of Limited Cavitation on Axisymmetric Bodies," J. of Fluid Engineering, Vol. 103, pp. 415-424.

Holl J.W. et al., (1983) "The Influence of Pressure Gradient on Desinent Cavitation Produced by the Separated Flow from an Isolated Triangular Surface Protrusion," 20th American Towing Tank Conference, Hoboken, New Jersey.

Huang, T.T. and Belt, G., (1983) "The Effects of Boundary-Layer Turbulence Stimulation on Cavitation Inception," DTNSRDC Report.

Huang, T.T., (1981) "Cavitation Inception Observation on Six Axisymmetric Headforms," J. of Fluids Eng., Vol. 103, pp. 273-279.

Huang, T.T., (1983) "Turbulence Stimulators to Reduce Scale Effects on Cavitation Inception," 1983 Cavitation Committee Report.

Isay, W.H., (1981) "Cavitation," Schiffarhts-Verlag Hansa, C. Schroedter & Co., Hamburg.

Jessup, S.D., (1982) "Measurement of the Pressure Distribution on Two Model Propellers," DTNSRDC Report 82/035.

Johnsson, C.A., (1969) "Cavitation Inception on Headforms, Further Tests," 12th International Towing Tank Conference, Rome, pp. 381-392.

Katz, J., (1981) "Cavitation Inception in Separated Flows," California Institute of Technology, Report No. 183-5.

Katz, J. et al., (1983) "A Comparative Study Between Holographic and Light-Scattering Techniques of Microbubble Detection," IUTAM Symposium, Measuring Technique in Gas-Liquid Two-Phase Flows, Nancy, France.

Keller, A.P., (1972) "The Influence of the Cavitation Nucleus Spectrum on Cavitation Inception, Investigated with a Scattered Light Counting Method," J. of Basic Eng., pp. 917-925.

Keller, A.P. and Weitendorf, E.A., (1978) "A Determination of the Free Air Content and Velocity in Front of the "SYDNEY EXPRESS" Propeller in Connection with Pressure Fluctuation Measurements," 12th Symposium on Naval Hydrodynamics, Washington, D.C.

Kuiper, G., (1979) "Some Experiments with Distinguished Types of Cavitation on Ship Propellers," ASME International Symposium on Cavitation Inception, New York, pp. 171-182.

Kuiper, G., (1981) "Cavitation Inception on Ship Propeller Models," Ph.D. dissertation, Netherlands Ship Model Basin.

Kuiper, G., (1982) "Some Experiments with Specific Types of Cavitation on Ship Propellers," J. of Fluids Engineering, Vol. 104, pp. 105-114.

Latorre, R., (1981) "Propeller Tip Vortex Cavitation Noise Inception," Propeller 81 Symposium, Virginia.

Latorre R., (1982) "T.V.C. Noise Envelope - An Approach to Tip Vortex Cavitation Noise Scaling," Journal of Ship Research, Vol. 26.

Lecoffre, Y. and Bonnin, J., (1979) "Cavitation Tests and Nucleation Control," ASME International Symposium on Cavitation Inception, New York, pp. 141-146.

Le Goff, J.P. and Lecoffre, Y., (1982) "Nuclei and Cavitation," 14th Symposium on Naval Hydrodynamics.

Medwin, H., (1979) "Acoustical Bubble Spectrometry at Sea," Proc. First International Conference on Cavitation and Inhomogeneities in Underwater Acoustics, Gottingen, pp. 187-193.

Morgan, W., (1972) "Air Content and Nuclei Measurement," Appendix 1, Report of the Cavitation Committee, Proc. 13th ITTC, Berlin/Hamburg.

Mulhearn, P.J., (1981) "Distribution of Microbubbles in Coastal Waters," Journal of Geophysical Research, Vol. 86, pp. 6429-6434.

Oba, R. et al., (1981) "Cavitation Nuclei Measurements by a Newly Made Coulter Counter Without Adding Salt in Water," Rep. Inst. High Speed Mech., Tohoku Univ., Vol. 43, No. 340.

Oba, R. and Ito, Y., (1983) "Cavitation Aspects in a Venturi ("Johnson Effects" in a Low Turbulent Flow)," Inst. High Speed Mech., Tohoku Univ., Vol. 46.

Oldenziel, D.M., (1979) "Bubble Cavitation in Relation to Liquid Quality," Ph.D. thesis, Tech. Univ. Twente, Delft Hydraulics Lab. Publication No. 211.

Oldenziel, D.M., (1982) "A Set of Instruments Useful for Liquid Quality Control During Cavitation Research," J. of Fluids Eng., Vol. 104, pp. 443-450.

Oldenziel, D.M., (1982) "A New Instrument in Cavitation Research: The Cavitation Susceptibility Meter," J. of Fluids Eng., Vol. 104, pp. 136-142.

Oldenziel, D.M. et al., (1982) "Comparison of Instruments for the Detection of Bubbles and Particles in Water During Cavitation Studies," 11th IAHR, Amsterdam, The Netherlands.

Ooi, K.K., (1981) "Scale Effects on Cavitation Inception in Submerged Jets," California Institute of Technology Rep. No. 183-6.

Ooi, K.K., (1982) "Lagrangian Pressure Fluctuations in a Jet," Cavitation and Polyphase Flow Forum - 1982 ASME, St. Louis, Missouri.

Peterson, F. et al., (1981) "81 ITTC Cavitation Committee Report."

Peterson, F. et al., (1975) "Comparative Measruements of Bubble and Particulate Spectra by Three Optical Methods," Appendix 1, Report of Cavitation Committe, Proc. 14 ITTC, Ottawa.

Parkin, B., (1981a) "A Possible Criterion for Cavitation Inception on Hemispherical Headforms," J. of Fluids Eng., Vol. 103, pp. 577-582.

Parkin, B., (1981b) "The Initiation of Gaseous Microbubble Growth in Laminar Separation Bubbles," J. of Fluid Eng., Vol. 103, pp. 543-550.

Parkin, B., (1982) "The Onset of Bubble-Ring Cavitation on Hemispherical Headforms," J. of Fluids Eng., Vol. 104, pp. 115-122.

Ripkin, J.R. and Killen, A.P., (1962) "Gas Bubbles: Their Occurrence, Measurement, and Influence in Cavitation Testing," Proc. IAHR Symposium, Sendai, Japan.

Schiebe, F.R. and Killen, J.M., (1971) "An Evaluation of Techniques for Measuring Gas Bubble Size Distribution in Cavitation Research," St. Anthony Falls Hydraulic Lab, Univ. of Minn., Report 120.

Shen, Y.T., (1982) "Cavitation - Free Buckets of YS-920 and NACA 66 (MOD) Foil Section," DTNSRDC Report SPD-1049-01.

Shen, Y.T. and Peterson, F., (1978) "Unsteady Cavitation on an Oscillating Hydrofoil," 12th Symposium on Naval Hydrodynamics, Washington, D.C.

Shen, Y.T. and Peterson, F.B., (1980) "The Influence of Hydrofoil Oscillation on Boundary Layer Transition and Cavitation Noise," 13th Symposium on Naval Hydrodynamics, Tokyo.

Stern, F., (1982) "Comparison of Computational and Experimental Unsteady Sheet Cavitation," 14th Symposium on Naval Hydrodynamics, Ann Arbor, Michigan.

Weitendorf, E.A., (1979) "Complementing Discussion Contribution to the Papers of H. Medwin, P. Schippers, and A. Lovik," Proc. First International Conference on Cavitation and Inhomogeneities in Underwater Acoustics, Gottingen.

Weitendorf, E.A., (1979) "Conclusions from Full-Scale and Model Investigations of the Free Air Content and of the Propeller-Excited Hull Pressure Amplitudes Due to Cavitation," International Symposium on Cavitation Inception, ASME.

Weitendorf, E.A., (1982) "Complementing Discussion Contribution to the Paper of Le Goff and Lecoffre," 14th Symposium on Naval Hydrodynamics, Ann Arbor, Michigan.

Wetzel, J.M. et al., (1983) "Evaluation of Overall Hydrodynamic Performance of the Large Cavitation Channel," Final Report on Phase A-2, prepared for SSV&K/DMJM, University of Minnesota.

Yount, D.E. et al., (1982) "A Microscopic Study of Gas Cavitation Nuclei," Cavitation and Polyphase Flow Forum - 1982 ASME, St. Louis, Missouri.

Yungkurth, C.B., (1982) "A Light-Scattering System to Measure Cavitation Nuclei: Analysis and Calibration," ARL T.M. 82-204, Penn State University.

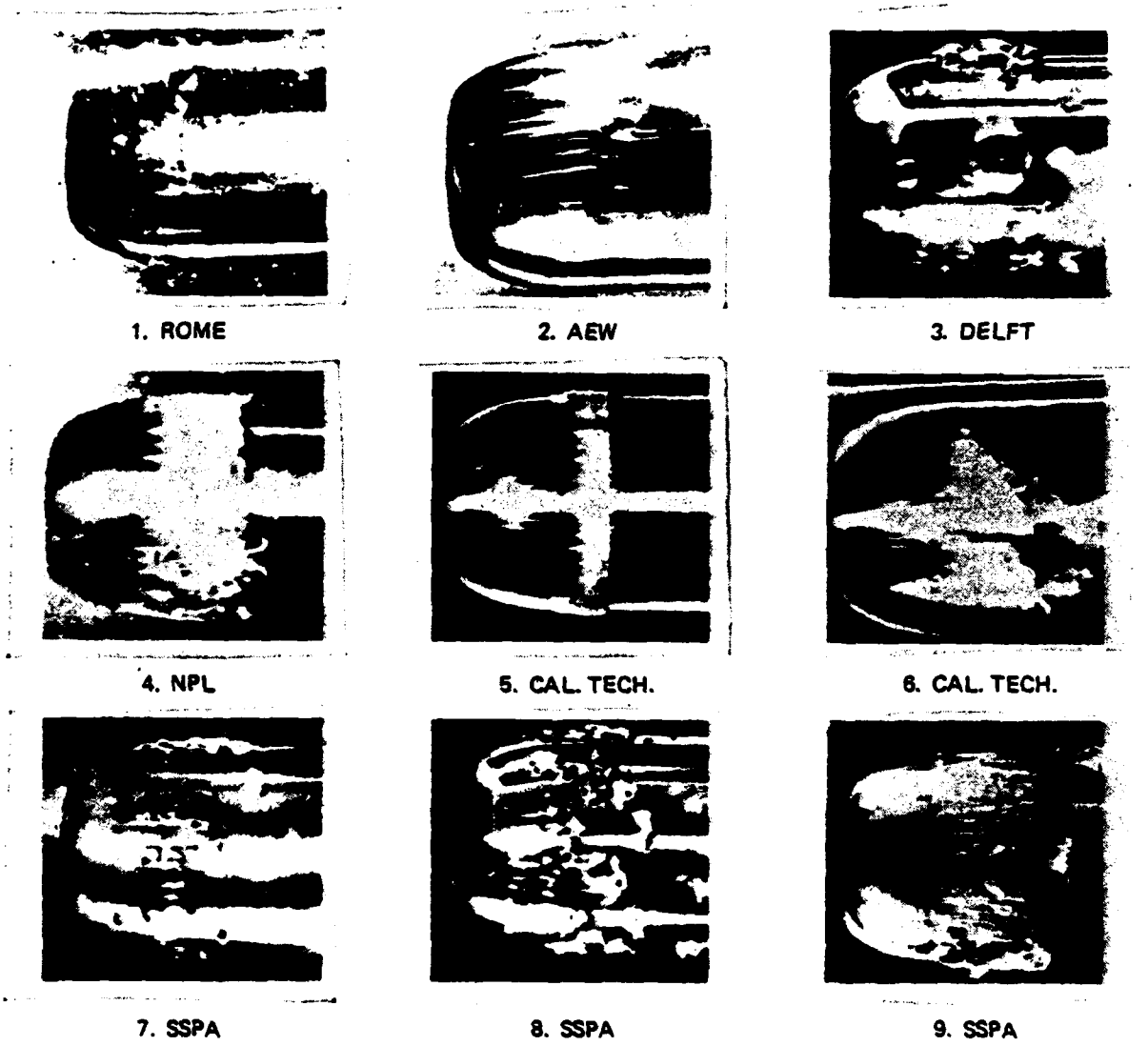


Figure 1 - Incipient Cavitation on the ITTC Headform in Various Facilities (Johnsson 1969)

AD-P003 809

ON THE DESIGN OF CAVITATION SUSCEPTIBILITY METERS (C.S.M.'s)

by Luca d'Agostino and A. J. Acosta
California Institute of Technology

for presentation at

the 20th American Towing Tank Conference
1983

Abstract

The observation of cavitation in C.S.M.'s at the throat of a Venturi tube provides an ideally simple and direct method to monitor the liquid quality in terms of the concentration of unstable nuclei as a function of the applied tension. In the previous work of Oldenziel and Lecoffre, the use of C.S.M.'s was limited to the measurement of the tensile strength of the weakest nuclei present in the liquid. The purpose of the current research is to extend this application to determine the concentration of unstable cavitation nuclei as a function of the applied tension over a wide range so that the nuclei number distribution can be derived. Various approximations are made to construct a simplified but still representative physical model of C.S.M.'s; these factors included the liquid sample initial conditions and properties, critical tension and concentration of cavitation nuclei (i.e. liquid quality) and required accuracy and range of the nuclei concentration measurement. The overall performance of C.S.M.'s is described in terms of a set of dependent parameters including the volume flux, velocity and pressure at the throat and at the exit (these are fluid mechanical parameters); the throat volume, diameter and length, and exit diameter (geometrical parameters); cavitation rate and bubble response time (cavitation parameters); error due to the interference of more than one nucleus simultaneously present in the cavitation region and error due

to the finite time duration of the observation (statistical parameters); nuclei concentration measurement, sample volume and sampling time (measuring process parameters in general). The relative dependence of these parameters is investigated. A simple quasi one-dimensional model is used to analyze the flow. Viscous effects in the venturi tube are estimated by matching an axisymmetric boundary layer with an ideal flow solution in order to demonstrate the presence of a potential core in the throat section where cavitation is to occur. The dynamics of a spherical bubble growing and travelling in a semi-infinite pipe are used to deduce both the critical tension and the response time of cavitation nuclei. The occurrence of nuclei in the cavitation region and the observation of cavitation events are treated as stochastic processes of Poisson's type in space and time, respectively. On the basis of the assumed nuclei number distribution, the expected errors due to nuclei interference and to finite observation time are thus related to the volume of the cavitation region and to the duration of the observation itself.

Finally, it is shown that these parameters can be organized into a functional network, leading to a systematic representation of the C.S.M. design problem.

The most important deductions are that:

(1) the pressure in the cavitation region is an extremely sensitive parameter and cannot be directly measured with the necessary accuracy. It is therefore proposed to deduce the pressure from the potential core velocity at the throat obtained by using a L.D.V.;

(2) the volume of the cavitation region must be reduced as much as possible in order to increase the applied tension without incurring in

large errors due to nuclei interference;

(3) the time response of cavitation nuclei imposes a lower bound for the length of the cavitation region.

Preliminary tests of a prototype venturi made of acrylic plastic showed that the flow in the inlet can sustain, without separation, the very steep and large contraction suggested by design considerations, but that it is extremely sensitive to separation in the diffuser section following the test volume.

INTRODUCTION

Early studies have shown [5] that the maximum tensile strength that liquids can sustain is considerably reduced by the presence of weak spots, generically called "nuclei". Although their nature has not yet been fully understood, it has been recognized that small gas bubbles, certain types of solid impurities, and gas pockets contained inside crevices and cracks of a liquid-solid interface are nuclei, since they act as preferred points for the onset of liquid rupture.

The presence of nuclei is considerably important in many flows of technical interest, where they are responsible for originating or variously modifying the occurrence of cavitation, a generally undesired phenomenon which severely limits the performances of hydraulic operating machinery. In this respect the number of nuclei which become unstable at a given level of tension is therefore a fundamental parameter in the attempt both to predict the onset of cavitation and to deduce scaling laws capable of extending the results obtained from model tests to full-scale operation.

The effect of the presence of nuclei in liquids is not limited to cavitation. Inhomogeneities and, in particular, micro-bubbles, considerably change the optical and acoustical properties of liquids in a way which also depends in general on their concentration and size distribution [6]. Such phenomena, as well as cavitation, are of great practical importance in many technological applications of underwater acoustics and optics.

Therefore significant efforts have been made in developing methods to detect nuclei contained within liquids, whose effects usually dominate the ones due to the nuclei localized at the flow boundaries.

Some methods, such as photography or holography, which produce a recorded image of a sample volume in the liquid, allow one to detect nuclei whose size is larger than about 10 μm. They also can discriminate between bubbles and particles, but have the disadvantage that results are not immediately and continuously available because the analysis of the obtained data requires a considerable time.

Other methods, based upon optical or acoustical radiation scattered by the nuclei, can operate continuously providing results which are readily available, but do not allow one to distinguish readily between bubbles and particles. For satisfactory operation, a careful calibration using a liquid sample of known characteristics is needed. Non uniform illumination and finite size of the scattering volume may also generate systematic errors which are difficult to take into account. Besides, when particles are prevalent, considerable uncertainty is introduced by the fact that both their shape and index of refraction are unknown.

Bubbles in liquids can also be detected from the large attenuation experienced by acoustical radiation which resonates with the bubble natural frequency of volume oscillation. Detection systems based on this concept do not require long times for data analysis, but are unable to detect particles and need comparatively large and homogeneous sample volumes.

For the purpose of cavitation research, a common disadvantage of all the above methods is that only size distribution and concentration of the nuclei are measured. The value of the critical tension that makes each nucleus unstable, as required for cavitation studies, must therefore be deduced indirectly from size measurements, which can be done only in the case of micro-bubbles. Solid particles, when detected and recognized, can be included or not in the measurement of nuclei concentration, but no information is provided about their critical tension, yet it is known that only part of the solid particulates are active as cavitation nuclei.

To overcome these difficulties, cavitation events occurring in a known pressure field can be detected and counted. When applied to bodies of standardized form and size, this method has indeed the advantage of providing a direct measurement. However, since many nuclei are simultaneously exposed to the tension, the response of the weakest ones inevitably dominates the flow, so that only cavitation susceptibility evaluations can be obtained.

Recently Oldenziel, [1], [2], [3], [4], proposed a new instrument, the Cavitation Susceptibility Meter (C.S.M.), in which the internal flow of a liquid through a glass venturi is used to induce cavitation at the throat and bubbles are detected optically. The C.S.M. developed by Lecoffre at Neyrtec, [13], is based on the same principle, but it utilizes a stainless steel

venturi, where cavitation bubbles are counted by recording the noise generated by their collapse in the diffuser downstream the throat section.

Various methods to monitor the cavitation nuclei population of water samples, including the above two C.S.M.'s, have been recently compared together at Delft Hydraulics Laboratory [4]. The results confirm that C.S.M.'s can reliably measure the critical tension of the weakest nuclei and their concentration up to a maximum of the order of 10 cm^{-3}, after which the venturi throat becomes saturated with bubbles and the flow chokes. Reportedly the Neyrtec system can also measure the nuclei critical pressure in the range 0 bar to -2 bar without incurring in saturation, provided that the concentration of unstable nuclei does not exceed about 1 cm^{-3}. Nevertheless such low values of the pressure correspond to bubbles having an equilibrium radius between .1 and 1 μm, whose concentration in most water samples is expected to be considerably larger than 1 cm^{-3}. Therefore it appears that, during operation in these conditions, several unstable nuclei are simultaneously present in the cavitation region of the C.S.M. When this happens, the pressure in the throat increases significantly with respect to its nominal steady state non-cavitating value. The C.S.M. is then partially saturated and the actual range over which reliable measurements of both the nuclei critical tension and concentration are possible is significantly reduced.

Yet, when compared to other techniques, C.S.M.'s seem to have several attractive features:

(i) they provide a direct measure of both the nuclei critical tension and concentration, thus eliminating the problem of the uncertain behaviour of particles as cavitation nuclei;

(ii) data analysis only requires a comparatively short time, so that the measure can be carried out in an almost continuous way;

(iii) there is no limitation on the size of the smallest detectable nuclei.

On the other hand, successful operation of C.S.M.'s is severely limited by the nuclei concentration compared to the other techniques mentioned. But, because the C.S.M. is such a promising device in cavitation research, we have concerned ourselves in the present paper with all of the various considerations necessary for a reliable measurement to be made. We present these thoughts here in the hope that they will be useful since there is little discussion of these considerations in the literature.

C.S.M. OPERATION ANALYSIS

General Approach

The configuration of the axisymmetric C.S.M. venturi pipe considered in the present study is shown in Fig. 1. The flow originates from the far field on the left (subscript o), representing the sampled liquid, to the exhaust region on the right (subscript ex). Both the upstream and downstream conditions are supposed to be time-independent. A volume flux Q(t) of liquid flows with axial velocity u(x,r,t) and radial velocity v(x,r,t) through the duct of local radius B(x) and cross-sectional area $A(x) = \pi B^2(x)$, divided in five segments: a cylindrical inlet (subscript i), a contraction (subscript c), a cylindrical throat (subscript t), a diffuser inlet (subscript di) and a conical diffuser (subscript de). The length L of each segment of the duct is shown in the same figure; contraction area ratio is: $C_r = A_t / A_i$ and the

diffuser area ratio (expansion ratio) is: $C_e = A_{ex} / A_t$.

The main parameters used to describe the overall performance of C.S.M.'s are shown in the block diagram of Fig. 2. The existence of functional relations between two parameters is indicated by arrows connecting the two corresponding blocks. The nature of these relations will be discussed in detail later.

Some of the parameters in the diagram represent given data, some can be considered as independent requirements and some as resulting or dependent factors. However, the subdivision in such categories is somewhat arbitrary, since it depends on the view point chosen to approach the whole problem of C.S.M. design. The one implicitly adopted in most of the present analysis can be summarized as follows:

-first it is assumed that the sample initial conditions and properties are given;

-second a nuclei number distribution (i.e. the liquid quality) of the sample is postulated, which is generally representative of typical water samples of technological interest;

- finally a set of conditions on the remaining dependent parameters is deduced for the measurement of unstable nuclei concentration to be possible over the assigned or assumed nuclei radius range with the required precision.

This point of view is particularly useful for design orientation. On the other hand, for performance assessment of a given design, the obtainable precision in the measurement of unstable nuclei concentration over a certain radius range is the result of the specific C.S.M. geometry which can be

analyzed with the methods contained herein.

Liquid Quality and Critical Tension

In cavitation research literature the liquid quality of a sample is usually expressed by means of the nuclei number distribution: $N(R_o) = - dn/dR_o$, where $n(R_o)$ is the number concentration of nuclei whose equilibrium radius is not smaller than R_o. The nuclei number distributions of water samples of technological interest spread in practice over a very large range. Here, for simplicity, we assume: $N(R_o) = K_{dis} / R_o^3$, where $K_{dis} = 10^{-4}$ to 10^{-3} m^{-1} (typically $K_{dis} = 10^{-3}$ m^{-1}), which is in the average representative of the data reported in the literature in the radius range 10 to 100 μm. Thus it follows that

$$n(R_o) = \frac{K_{dis}}{2R_o^2} \quad . \tag{1}$$

In order to relate the nuclei number distribution to the corresponding critical pressure, we make the hypothesis that all the nuclei consist of equilibrium gas bubbles, for which the critical tension with respect to dynamic stability, [5], is expressed by:

$$(p_v - p)_{cr} = 4 \frac{S}{3 R_o} \left[3 \left(1 + \frac{p_o - p_v}{2 S / R_o} \right) \right]^{-\frac{3}{2}} \tag{2}$$

where p_o and R_o are the equilibrium pressure and radius of the bubble, p_v is the vapor pressure and S the surface tension (see Fig. 3). The corresponding "critical" velocity at the venturi throat deduced from ideal, incompressible, steady flow calculations is shown is Fig. 4. Similarly, the exhaust pressure coefficient $C_{pex} = (p_{ex}-p_v)/(p_o-p_v)$ is plotted in Fig. 5 for the case $p_o = 1$

bar and various expansion ratios. When the equilibrium pressure p_o increases, the C_{pex} curves shift to the left in the diagram.

Note that the critical tensions of bubbles in the size range of interest (say 10 to 100 μm) are quite small. Also note, on the other hand, that, on the same range, the radius of marginally stable bubbles (critical radius) is a very sensitive function of the applied tension. These facts have several important (and unfortunate) consequences for the design of C.S.M.'s. The first is that it is virtually impossible to measure these small pressures at the throat because of inadequate sensitivity and, if done intrusively, separation or cavitation may be induced. The second is that the throat pressure must be evaluated accurately to avoid large errors in the determination of the nuclei number distribution. A third consequence has to do with the problem of regulating the flow by varying the exhaust pressure. The curves of Fig. 5 deduced for p_o = 1 bar show that very low sensitivity is obtained, unless diffusers with a very small expansion ratio are used. Besides, due to the shift of the curves to the left when the equilibrium pressure p_o increases, the same sensitivity cannot be achieved thoughout the radius range of interest with the same diffuser geometry which can be analyzed with the methods contained herein.

Saturation and Throat Section Volume

As pointed out briefly in the introduction, the problem of saturation poses a significant limiation to the operation of C.S.M.'s. It also introduces a systematic error, since the unsteady pressure perturbations do to the presence of a growing or collapsing bubble in the cavitation region of the C.S.M. can prevent the normal growth of other neighbouring nuclei.

To control such an error the probability of finding more than one unstable nucleus in the low pressure volume, V_{lp}, of the C.S.M. must be minimized. When the nuclei concentration is uniform, the occurrence of m unstable nuclei in V_{lp} is expected to follow the Poisson distribution:

$$Pr(m) = \frac{N_{ub}^{m}}{m!} e^{-N_{ub}} \tag{3}$$

where $N_{ub} = n(R_o)\ V_{lp}$ is the average number of unstable nuclei in V_{lp}. Therefore the cumulative probability of observing two or more unstable nuclei in V_{lp} (bubble interference probability, see Fig. 6) is:

$$\beta = 1 - Pr(0) - Pr(1) = - (1 + N_{ub})\ e^{-N_{ub}} \tag{4}$$

It is now possible to express the low pressure volume of the C.S.M. as a function of the equilibrium bubble radius and of the bubble interference probability. The results of Fig. 7 show that, in the radius range 10 to 100 μm, if the error is to be reduced to an acceptable level, the volume of the cavitation region of the C.S.M. should not exceed about 50 mm^3.

Bubble Dynamic Response and Throat Section Geometry

The problem of the response of an isolated bubble in the throat of the C.S.M. is now addressed. The solution of such a problem in terms of the detection time, T_{det}, and detection length, L_{det} (respectively defined as the time and the length necessary for the bubble to grow to a detectable radius size, R_{det}), will be used to estimate the minimum length of the low pressure volume, thus completing the geometrical definition of this component.

A number of assumptions are made in order to construct a simplified set of equations which nevertheless models the interactions between the bubble and the liquid. First the flow is supposed to be one-dimensional, ideal, incompressible and the relative motion of the bubble with respect to the liquid is neglected. The bubble, moving along the centerline of the duct with instantaneous position $x_b(t)$, remains spherical and its radius R(t) is determined by the Rayleigh-Plesset equation [7]:

$$p_v - p_b = \rho \left[R \frac{d^2R}{dt^2} + \frac{3}{2} \left(\frac{dR}{dt} \right)^2 \right] - p_g \left(\frac{R_o}{R} \right)^3 + 2 \frac{S}{R} \tag{5}$$

where S is the surface tension and diffusive and thermal effects are neglected (p_v and p_g are constant). Here p_b is the external pressure driving the bubble volume changes and it is assumed to be about equal to the pressure of the liquid in the proximity of the bubble. Then, from the continuity and unsteady Bernoulli's equations for the flow upstream (subscript u) and downstream (subscript d) the bubble:

$$Q_u - Q_b + 2 \pi R^2 \frac{dR}{dt} = 0 \tag{6}$$

$$Q_d - Q_b - 2 \pi R^2 \frac{dR}{dt} = 0 \tag{7}$$

$$- I_u \frac{dQ_u}{dt} + \frac{p_o - p_b}{\rho} - \frac{1}{2} \frac{Q_b^2}{A_b^2} = 0 \tag{8}$$

$$- I_d \frac{dQ_d}{dt} + \frac{p_b - p_{ex}}{\rho} + \frac{1}{2} \frac{Q_b^2}{A_b^2} - \frac{Q_d^2}{A_d^2} = 0 \tag{9}$$

where $A_b = A(x_b)$, p_o and p_{ex} are constant and:

$$I_u \simeq \int_{x_1}^{x_b} \frac{dx}{A(x)} \quad ; \quad I_d \simeq \int_{x_b}^{x_6} \frac{dx}{A(x)} \tag{10}$$

Equations (6) through (9) are then transformed by introducing perturbation quantities with respect to the steady state solution and linearized for small changes in the volume fluxes. Finally, if $I_u \simeq X_b / A_b = u_t\ t / A_t << I_u + I_d$, which is essentially equivalent to consider the dynamics of a bubble entering a semi-infinite pipe of constant cross-sectional area A_t, the perturbation and Rayleigh-Plesset equations can be reduced to the following 2nd order differential equation for the bubble radius R(t):

$$\frac{2\ \pi\ \rho\ u_t}{A_t}\left[2\ t\ R^2\ \frac{d^2R}{dt^2} + 4\ t\ R\left(\frac{dR}{dt}\right)^2 + R^2\ \frac{dR}{dt}\right] + \rho\ R\ \frac{d^2R}{dt^2} + \frac{3}{2}\ \rho\left(\frac{dR}{dt}\right)^2 + \tag{11}$$

$$- p_v - p_g\left(\frac{R_o}{R}\right)^3 + 2\ \frac{S}{R} + p_t = 0$$

where p_t and u_t are the steady state pressure and velocity at the throat. The detection time, T_{det}, and detection length, L_{det}, computed for a detection radius R_{det} = 150 μm. and a throat diameter D_t = 1 mm by numerically integrating the above equation, are shown in Fig. 8 and Fig. 9. The maximum in the results separates two regimes: in the lower radius range the inertial effects of the displaced liquid dominate, while in the upper one the effect of bubble gas content prevails, therefore accelerating the bubble dynamic response. Note that, in the radius range of interest, the detection length is almost independent of the equilibrium bubble pressure and that the length of the throat section should not be shorter than 5 to 10 mm. Also note that the solution of the above equation depends on A_t, the throat cross-sectional area. Therefore, if the low pressure volume is initially fixed in order to properly

limit the bubble interaction probability, some iteration on the throat diameter may be required to completely define the geometry of the C.S.M. low pressure volume.

Cavitation Rate and Unstable Nuclei Concentration Measurement

Once the throat cross-sectional area has been determined, the volume flux: $q = u_t A_t$ and the mean cavitation event rate $\nu_c = Q\, n(R_o)$ can be computed. Results shown in Fig. 10 and Fig. 11 for a throat diameter Dt = 1 mm indicate that, in the radius range from 10 to 100 μm, as many as a few hundreds of cavitation events per second are to be expected.

For a given pressure at the throat, the corresponding concentration of unstable nuclei can be estimated from the count of the cavitation bubbles observed during the sampling time. In steady state conditions, if the liquid quality of the sample is constant, the occurrence of m cavitation events in the time interval T_s (sampling time) is expected to follow the Poisson distribution with parameter $\xi = \nu_c T_s$, equal to the average number of events in the same time. Since T_s can be conveniently measured, the problem of extimating ν_c now reduces to the estimation of ξ.

It is known from the theory of probability distributions, [11], that the best estimator of the Poisson parameter is the observed frequnecy m, whose variance is: V[m] = ξ and (1 - α) confidence limits are given by:

$$\xi_1 = \frac{1}{2}\,\chi^2_{\alpha/2}(2m) \;;\quad \xi_2 = \frac{1}{2}\,\chi^2_{\alpha/2}(2m + 2) \qquad (12)$$

where $\chi^2_p(q)$ is the p-percentile of the χ^2 distribution with q degrees of freedom (see Fig. 12). Thus, one way to assess the relative indetermination in the

estimate of ξ consists in normalizing the confidence interval with respect to the corresponding observed frequency (see Fig. 13, where $\alpha = .20$). Another less rigorous method uses the estimated root mean square (r.m.s.) error of the observed frequency $\sqrt{\bar{m}} \simeq \sqrt{V[m]}$ instead of the confidence interval. The results of this second case are presented in Fig. 14 and comparison with Fig. 13 shows that the two methods are essentially equivalent for large observed frequencies ($m > 30$), apart from a scaling factor. Indeed the agreement could be made closer by simply adjusting the confidence level $1 - \alpha$. Because of its simplicity, the second method is used here. Then, if ε is the estimated r.m.s. relative error in the measurement of ν_c (or any other linearly related quantity, like $n(R_o)$ and $N(R_o)$), the necessary sampling time: $T_s = 1 / \nu_c \varepsilon^2$ and liquid volume: $V_s = Q T_s$ are plotted in Fig. 15, 16 and 17. From them it appears that the liquid sample volume and sampling time required for one single measurement of unstable nuclei concentration of acceptable precision are at most of the order of 10 dm^3 and 10 sec respectively. Of course, the overall sampling time and volume of the liquid necessary for the evaluation of the nuclei number distribution will depend on the total choice of number of points where the measurement of the unstable nuclei concentration is carried out.

Viscous Effects and Separation

It was previously mentioned that one of the most difficult problems of C.S.M.'s consists in measuring the throat pressure with the required precision. Since direct measurements are virtually impossible, indirect methods must be used. Most naturally the throat pressure may be deduced from velocity measurements by using Bernoulli's equation. An unavoidable problem associated

with this technique is that the throat pressure, being inherently small compared to the total and kinetic pressures, is expressed as the difference of two almost equal quantities. Thus, relative errors in the evaluation of such quantities lead to a larger relative error for the throat pressure.

In existing C.S.M.'s, [1], [2], [3], [4], the velocity measurement was carried out in the inlet section of the duct, upstream of the contraction. This method appears to be rather unsatisfactory for various reasons. First, any intrinsic error in the measurement of the upstream velocity or due to inaccurate estimate of boundary layer effects is amplified proportionally to the contraction ratio when the throat velocity is derived from continuity arguments. This limitation is particularly severe since in C.S.M.'s the contraction ratio should be as large as possible in order not to appreciably affect the condition of the sampled liquid during its flow in the inlet section. Morover, it is generally necessary to make the inlet section longer, which also is likely to affect the conditions of the sampled liquid, especially when a second venturi of smaller contraction ratio is used to monitor the velocity.

These difficulties are overcome if the velocity measurement is carried out at the throat. In consideration of the various requirements and limitations involved, the use of a laser Doppler velocimeter (L.D.V.) presently seems to be the best solution. But, for the pressure to be deduced from velocity measurements, the presence of a potential core at the C.S.M. throat must be demonstrated. Viscous effects have therefore been estimated by matching an axisymmetric boundary layer, [10], with the quasi one-dimensional ideal flow solution based on the duct geometry, [8], [9]. The duct radius B(x) has been assumed to be continuous with continuous first and second derivatives, as

required by fluid mechanical considerations to avoid separation. In the contraction and diffuser inlet sections B(x) was supposed to have sinusoidal second derivative. The inlet and throat sections were taken to be cylindrical and the diffuser exit section to be conical, of given semi-aperture angle. The length of each section has also been specified in terms of the inlet duct radius.

The results of such boundary layer calculations obtained for a prototype venturi made of acrylic plastic with Reynolds number based on the inlet radius and average velocity $Re_i = 700$ (the lowest expected value during operation) are summarized in Fig. 18 through 22. The geometrical characteristics of the above prototype venturi are: $L_i = 11.4$ mm, $L_c = 10.4$ mm, $L_t = 7.7$ mm, $L_{di} = 3$ mm, $L_{de} = 6.6$ mm, $\beta_d = .80$ deg, $D_t = 1$ mm, $C_r = 100$, $D_{ex} / D_t = 1.23$ and the duct shape profile is shown in Fig. 18, where the scales on the two axes are different. The boundary layer displacement and momentum thicknesses plotted in Fig. 19 (normalized with respect to the inlet radius) and in Fig. 20 (normalized with respect to the local duct radius) clearly demonstrate the presence of a potential core in the throat section of the C.S.M. In Fig. 21 the pressure coefficients at the centerline, C_{pcl}, and at the boundary layer edge, C_{ped}, are shown as functions of the axial coordinate of the duct. Here the pressure is normalized with respect to the inlet pressure and velocity. Note the very steep pressure drop in the contraction and the milder recovery in the diffuser.

Two kinds of problems may be expected in the venturi as a consequence of viscous effects. If the contraction is too steep, Taylor-Görtler instability may develop, and, if too large negative pressure gradients are present, flow separation may occur at the contraction inlet, at the throat inlet or in the

diffuser. Preliminary tests on the prototype venturi of Fig. 18 showed no evidence of any of the above mentioned phenomena, with the exception of intermittent rotating separation in the diffuser, a problem reported by Oldenziel as well [1]. In view of this, the boundary layer correlation parameter $\lambda = \theta^2 U'/\nu$ (where θ is the momentum thickness, U' is the streamwise derivative of the boundary layer edge velocity and ν is the kinematic viscosity) and the Stratford laminar boundary layer separation criterion, S_c, [12] have been plotted in Fig. 22. Separation is predicted when $\lambda = -.09$ or $S_c = 0$. The two methods agree well with each other and also with the observed location of separation in the prototype venturi, thus indicating that less steep diffusers should be used.

SUMMARY AND CONCLUSIONS

The operation of C.S.M.'s has been analyzed in order to investigate the possibility of extending their use to determine the concentration of unstable cavitation nuclei in a liquid as a function of the applied tension, from which the nuclei number distribution can be deduced.

By means of various assumptions and approximations, a simplified model has been derived which adequately represents the operation of C.S.M.'s in terms of a limited number of relevant parameters. The investigation of their mutual relations led to a functional description of C.S.M. operation which enables one to address the problem of their design in a systematic and organic way.

The above model has been applied to simulate C.S.M. operation for the case of a typical nuclei number distribution in water. The results can be

summarized as follows:

a) the pressure in the C.S.M. cavitation region is an extremely sensitive parameter and cannot be measured directly with the necessary accuracy;

b) the indirect measurement of the pressure in the cavitation region is best accomplished by the measurement of the potential core velocity at the C.S.M. throat by means of a L.D.V.;

c) the existence of a potential core at the throat has been demonstrated by estimating boundary layer effects;

d) for the specific nuclei number distribution considered, the errors and limitations due to saturation can be reduced by appropriately decreasing the volume of the cavitation region;

e) the time response of the cavitating nuclei imposes a lower bound for the length of the C.S.M. throat section;

f) the flow can sustain without separation or fluid mechanical instabilitites the very large and steep contraction suggested by design considerations, but is extremely sensitive to separation in the diffuser;

g) in the case of the nuclei number distribution used as an example, it appears that C.S.M.'s can be designed which are capable of detecting gas bubbles having an equilibrium radius larger than about 10 μm within the errors typical of other alternative techniques currently available;

h) due to the considerable complexity of the phenomena involved, the interpretation of the data obtained from C.S.M.'s requires a careful analysis.

ACKNOWLEDGEMENT

The authors would like to thank Carol Kirsch for her help in organizing this manuscript. This work was supported by Naval Sea Systems Command General Hydromechanics Research Program Administered by the David Taylor Naval Ship Research and Development Center under Contract No. N00014-75-C-0378.

REFERENCES

1. Oldenziel, D. M., "A new instrument in cavitation research: the cavitation susceptibility meter", ASME Journal of Fluids Engineering, 104, June 1982, pp. 136-142.

2. Oldenziel, D. M., Jansen, R. H. J., Keller, A. P., Lecoffre, Y., and van Renesse, R. L., "Comparison of instruments for detection of particles and bubbles in water during cavitation studies", Proceedings of Symposium on Operating Problems of Pump Stations and Power Plants, IAHR, Amsterdam, September 1982.

3. Oldenziel, D. M., "Utility of available instruments during cavitation tests", Proceedings of Symposium on Operating Problems of Pump Stations and Power Plants, IAHR, Amsterdam, September 1982.

4. Godefroy, H. W. H. E., Jansen, R. H. J., Keller, A. P., and van Renesse, R. L., "Comparison of measuring and control methods of the water quality with respect to cavitation behaviour", Delft Hydraulics Laboratory Publication, January 1981.

5. Knapp, R. T., Daly, J. W. and Hammit, F. G., "Cavitation", McGraw Hill, 1970.

6. van Wijngaarden, L., 1972, "One-dimensional flow of liquids containing small gas bubbles", Ann. Rev. Fluid Mech., Vol. 4, pp.369-396.

7. Plesset, M.S. and Prosperetti, A., "Bubble dynamics and cavitation", Ann. Rev. Fluid Mech., 1977, Vol. 9, 145-85.

8. Chmielewski, G. E., "Boundary layer consideration in the design of aerodynamic contractions", J. of Aircraft, Vol. 11, No. 8, August 1974, pp. 435-438.

9. Mikhail, M. N., "Optimum design of wind tunnel contractions", AIAA Journal, Vol. 17, No. 5, May 1978, pp. 471-477.

10. White, F. M., "Viscous fluid flow", Mc Graw Hill, 1974.

11. Brownlee, K. A., "Statistical theory and methodology in science and engineering", John Wiley & Sons, 1960.

12. Stratford, B. S., "Flow in laminar boundary layer near separation", Aeronautical Research Council, R&M 3002, November 1954.

13. Le Goff, J. P. and Lecoffre, Y., "Nuclei and cavitation", 14th. Symposium on Naval Hydrodynamics, National Academy Press, 1983, pp. 215-242.

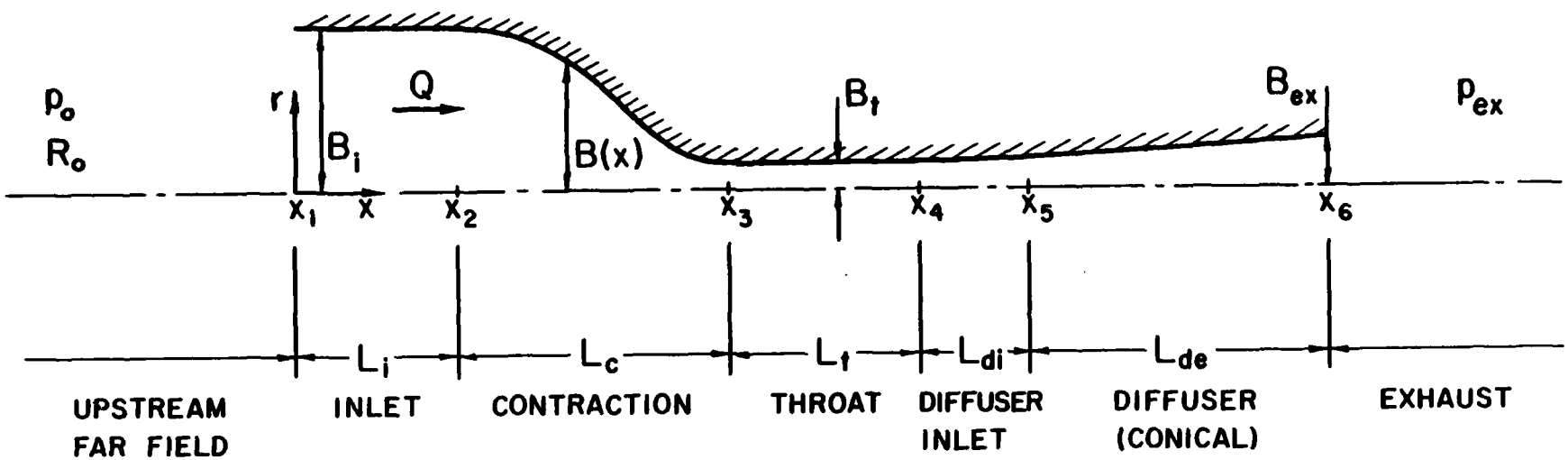


Figure 1. Axisymmetric duct geometry and nomenclature.

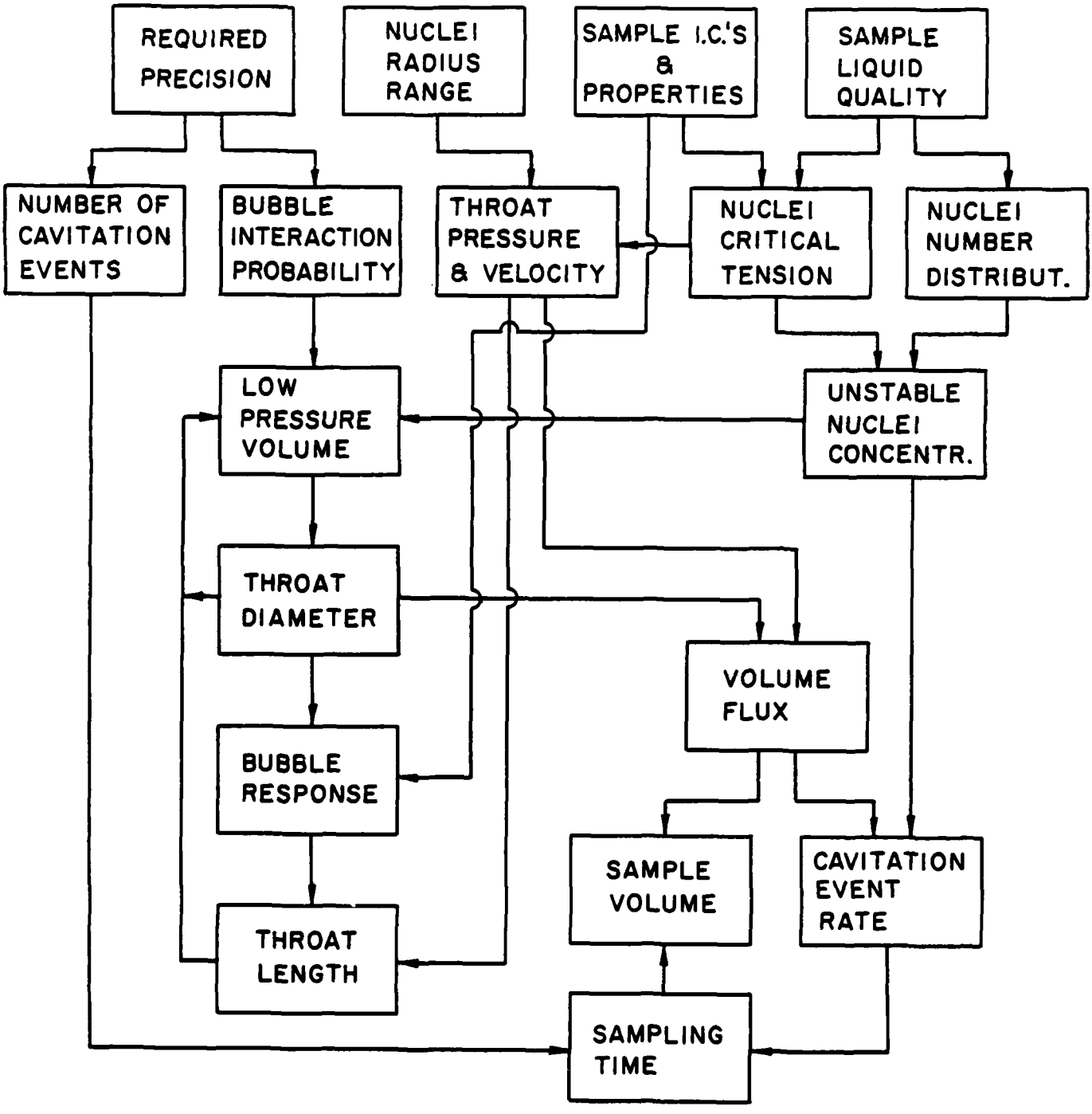


Figure 2. Block diagram showing the main parameters of C.S.R.'s and their mutual relations.

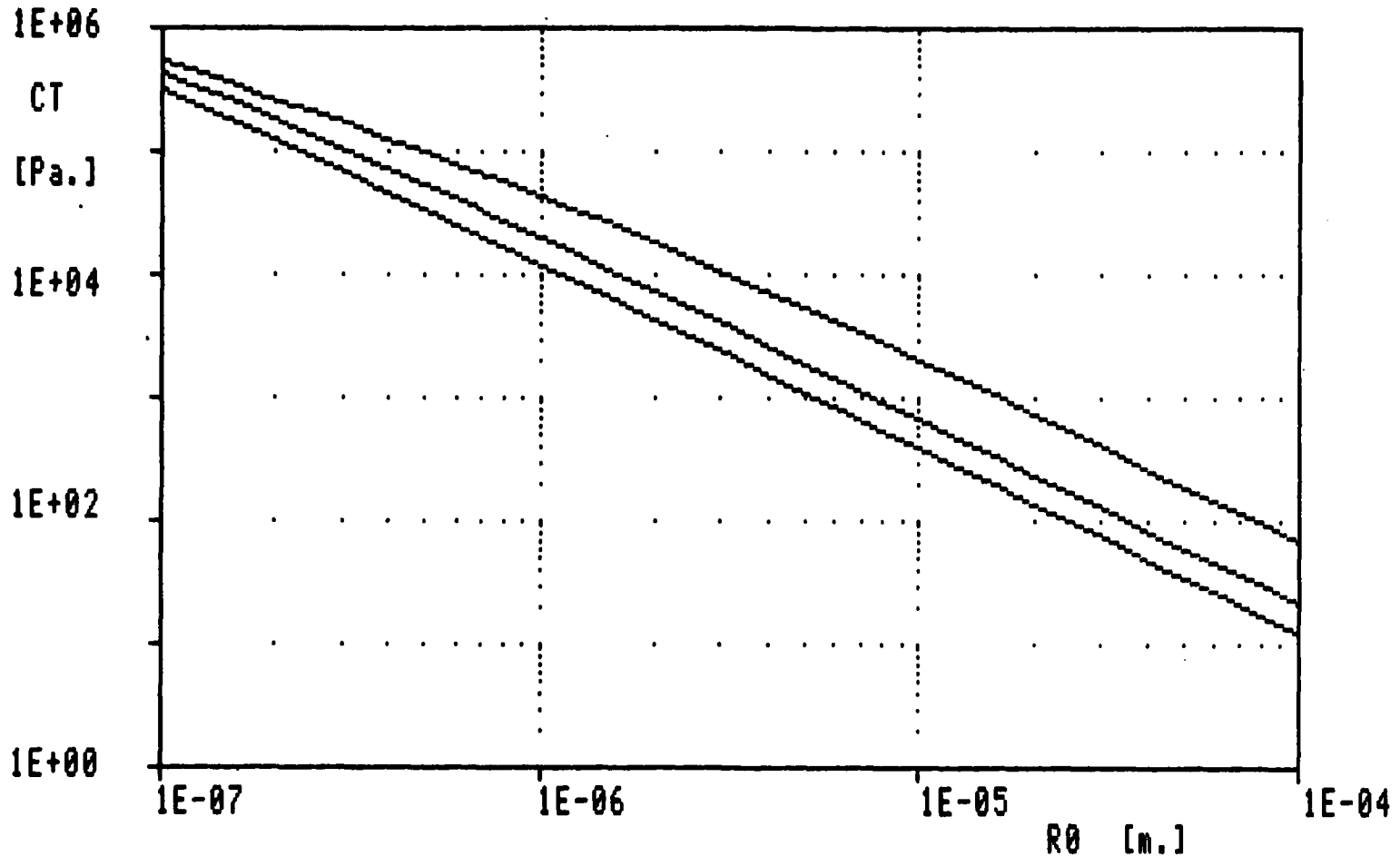
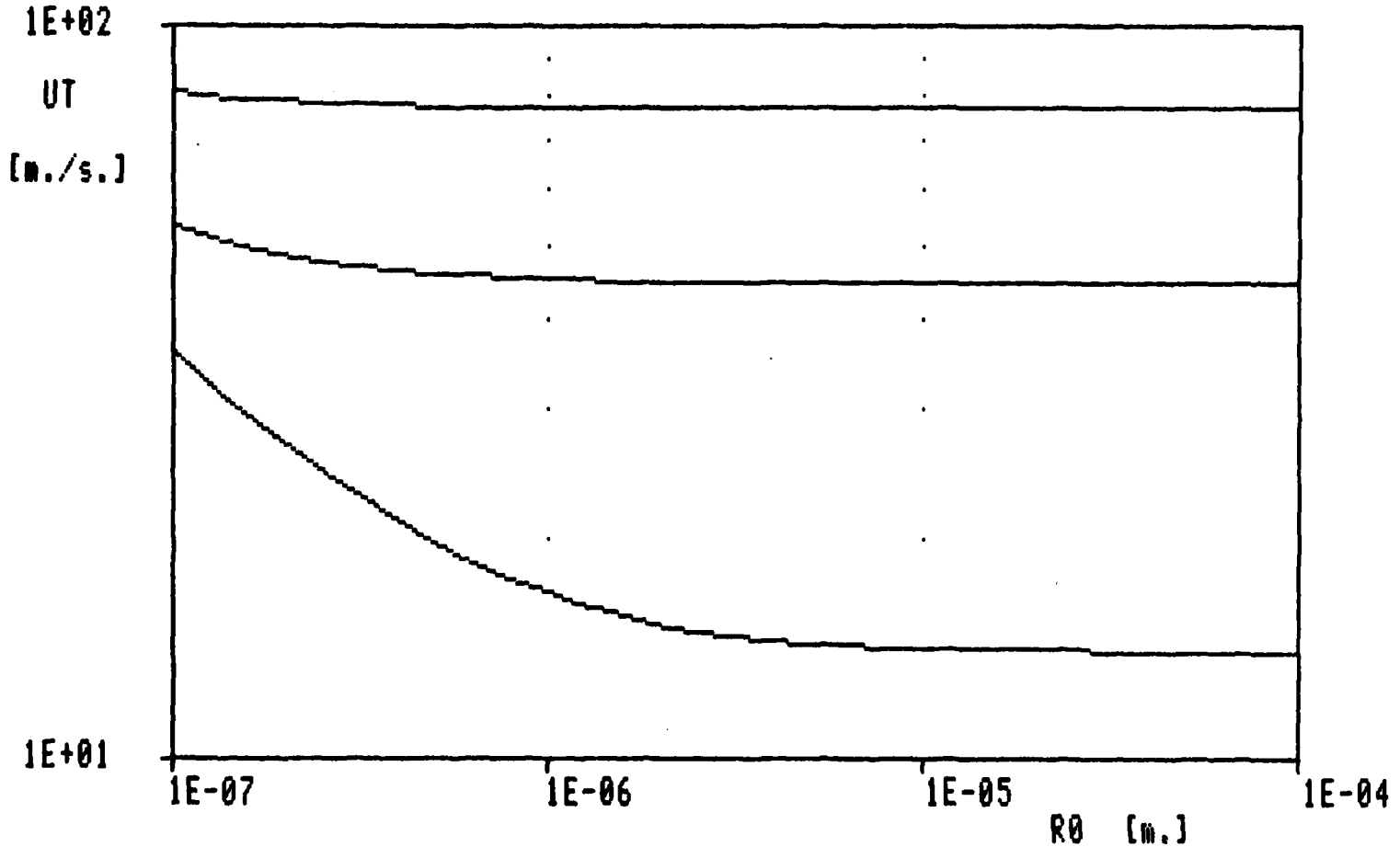
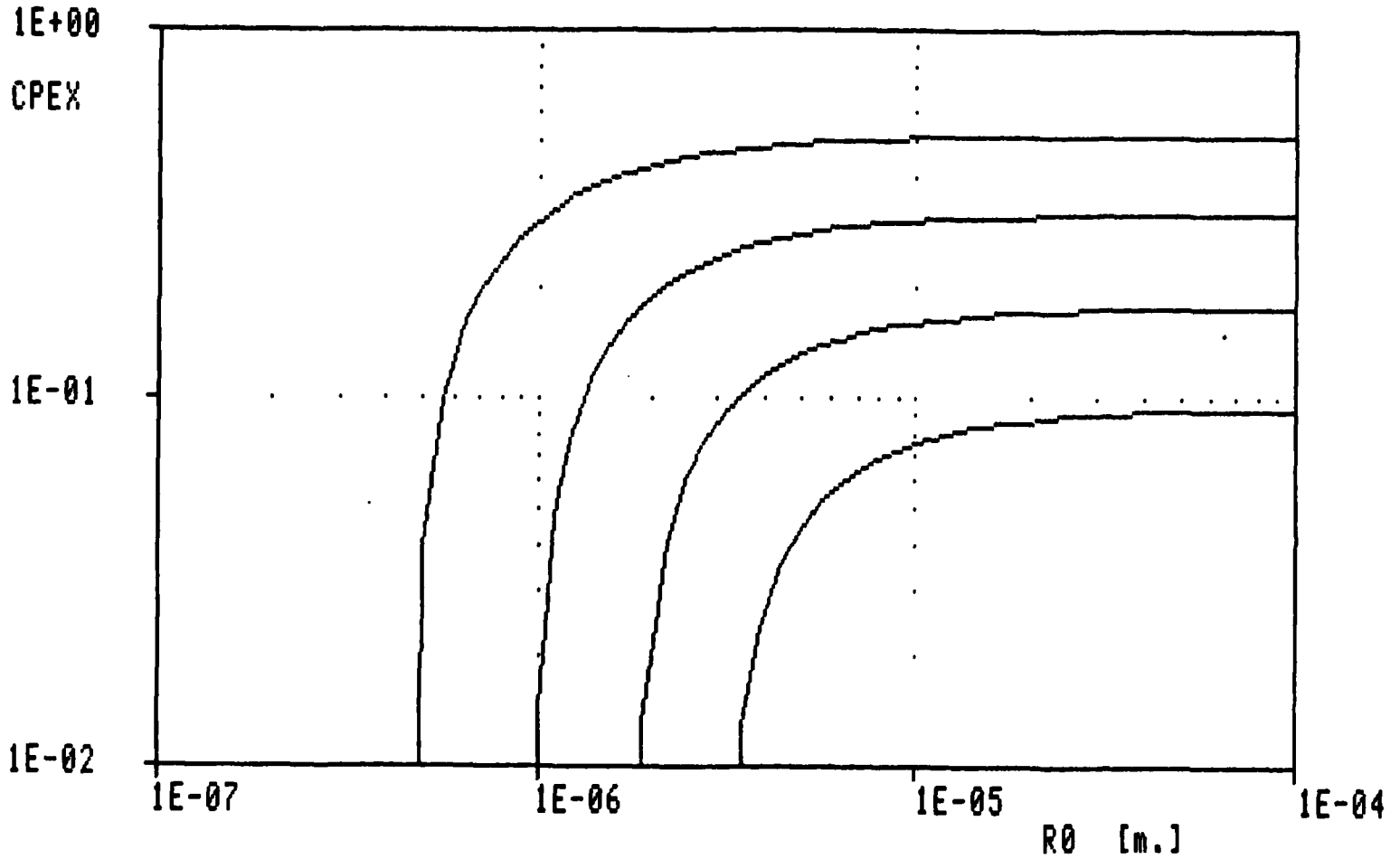


Figure 3. Critical tension, $(p_v - p)_{cr}$ [CT], of isolated spherical bubbles in an unbounded liquid as function of their static equilibrium radius, R_o [R0], at various equilibrium pressures: p_o = 1 bar (upper curve), p_o = 10 bar (intermediate curve) and p_o = 30 bar (lower curve) for water – air at T = 20 °C (surface tension S = .073 N/m and vapor pressure p_v = 1919 Pa).



CRITICAL THROAT VELOCITY, UT, V/S EQUILIBRIUM RADIUS, R0

Figure 4. Throat velocity, u_t [UT], v/s bubble equilibrium radius, R_o [R0], at various equilibrium pressures: p_o = 1 bar (lower curve), p_o = 10 bar (intermediate curve) and p_o = 30 bar (upper curve) for S = .073 N/m (surface tension), p_v = 1919 Pa (vapor pressure) and ρ = 1000 kg/m^3 (liquid density).



EXHAUST PRESSURE COEFFICIENT, CPEX, V/S EQUILIBRIUM BUBBLE RADIUS, R0

Figure 5. Exhaust pressure coefficient, C_{pex} [CPEX], v/s bubble equilibrium radius, R_o [RO], at p_o = 1 bar and for exhaust to throat diameter ratio: D_{ex}/D_t = 1.025, 1.050, 1.100 and 1.200 from the lower to the upper curve respectively. Here: $C_{pex} = (p_{ex} - p_v)/(p_o - p_v)$, where p_{ex} is the exhaust pressure. The curves shift to the left at higher values of p_o.

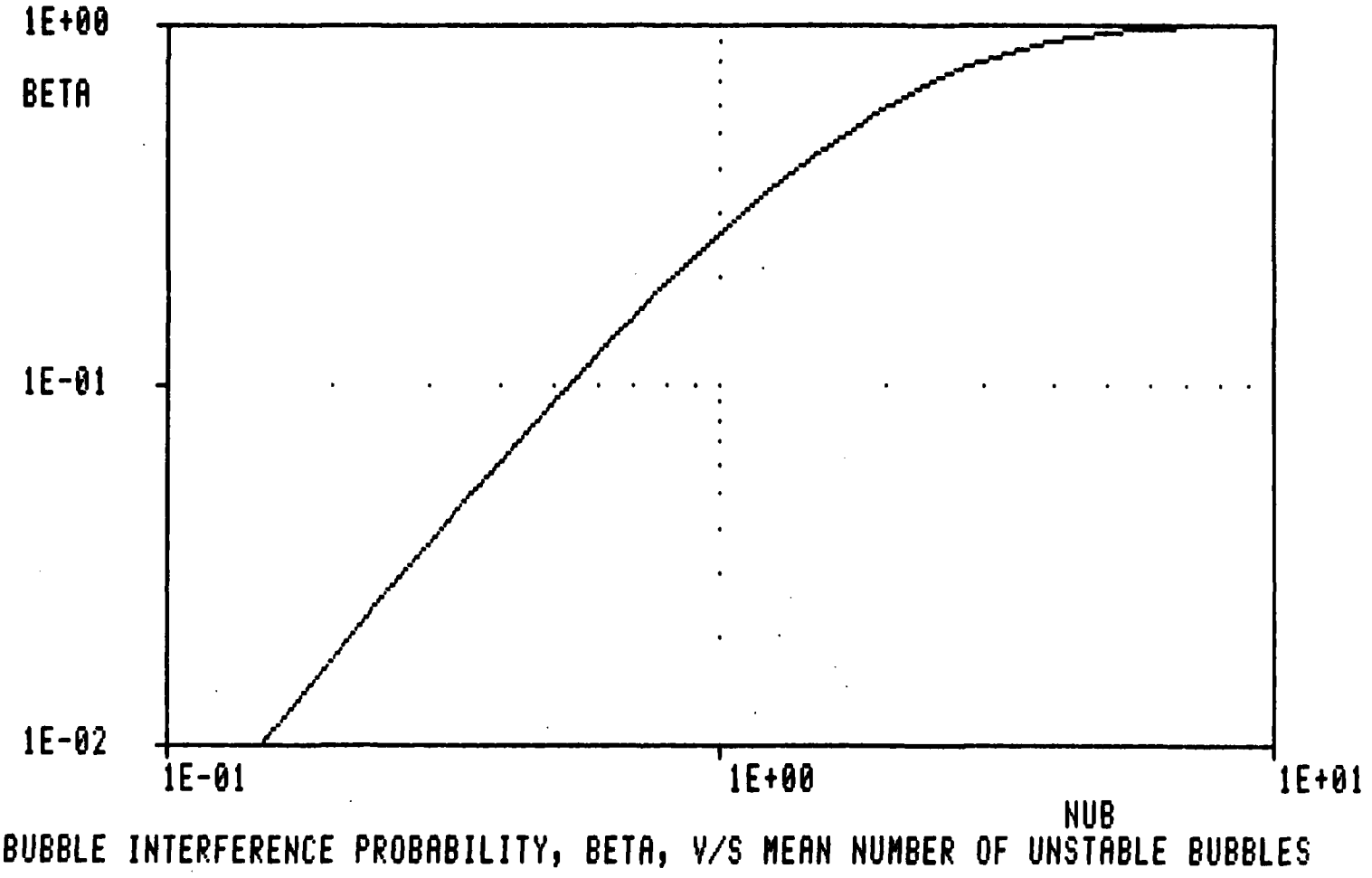


Figure 6. Bubble interference probability, β [BETA], i.e probability of finding more than one bubble in the cavitation region of the duct, v/s the average number of unstable bubbles in the same region, N_{ub} [NUB]. Such probabilities are calculated assuming that the occurrence of cavitation nuclei in a given volume is represented by a Poisson process.

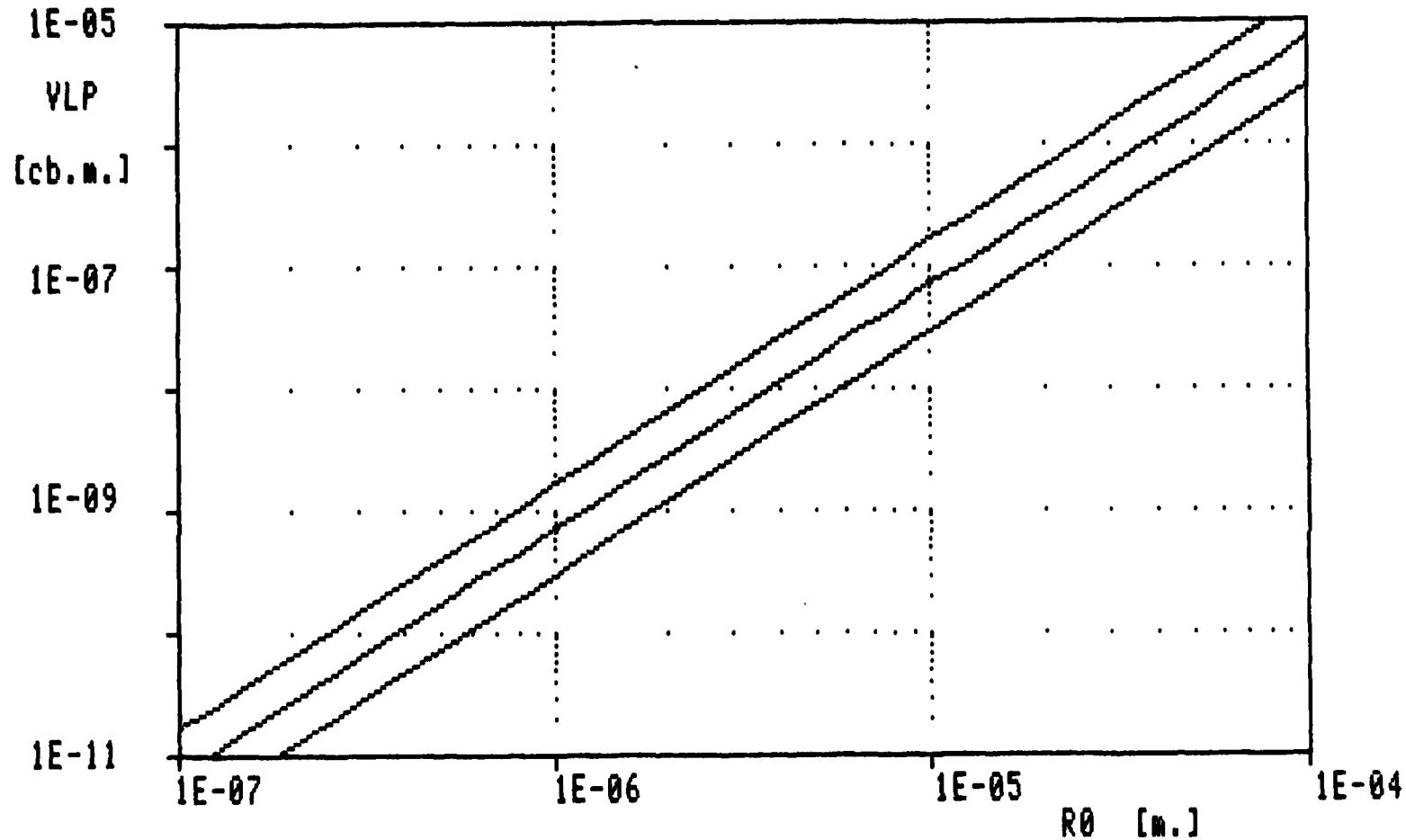
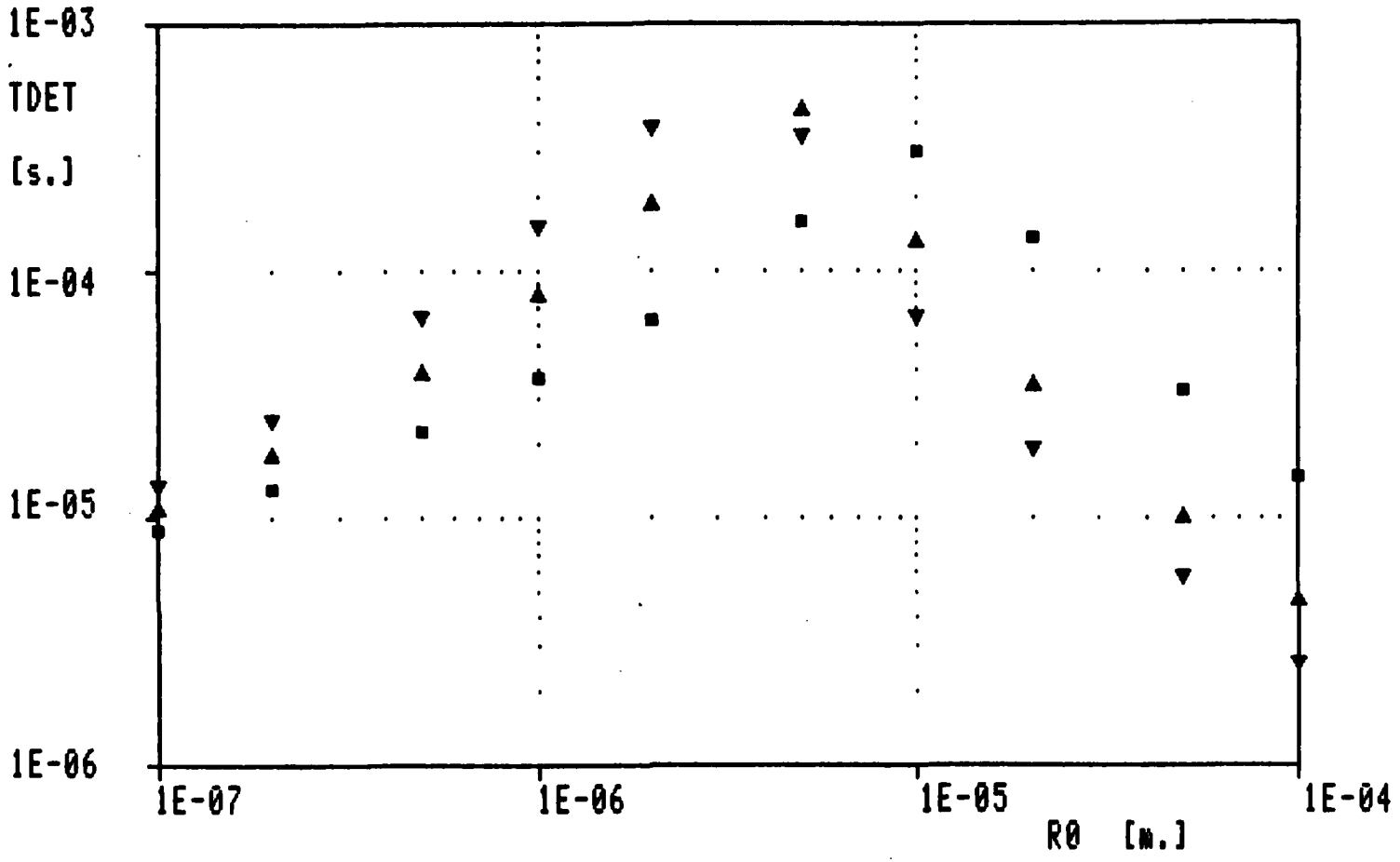
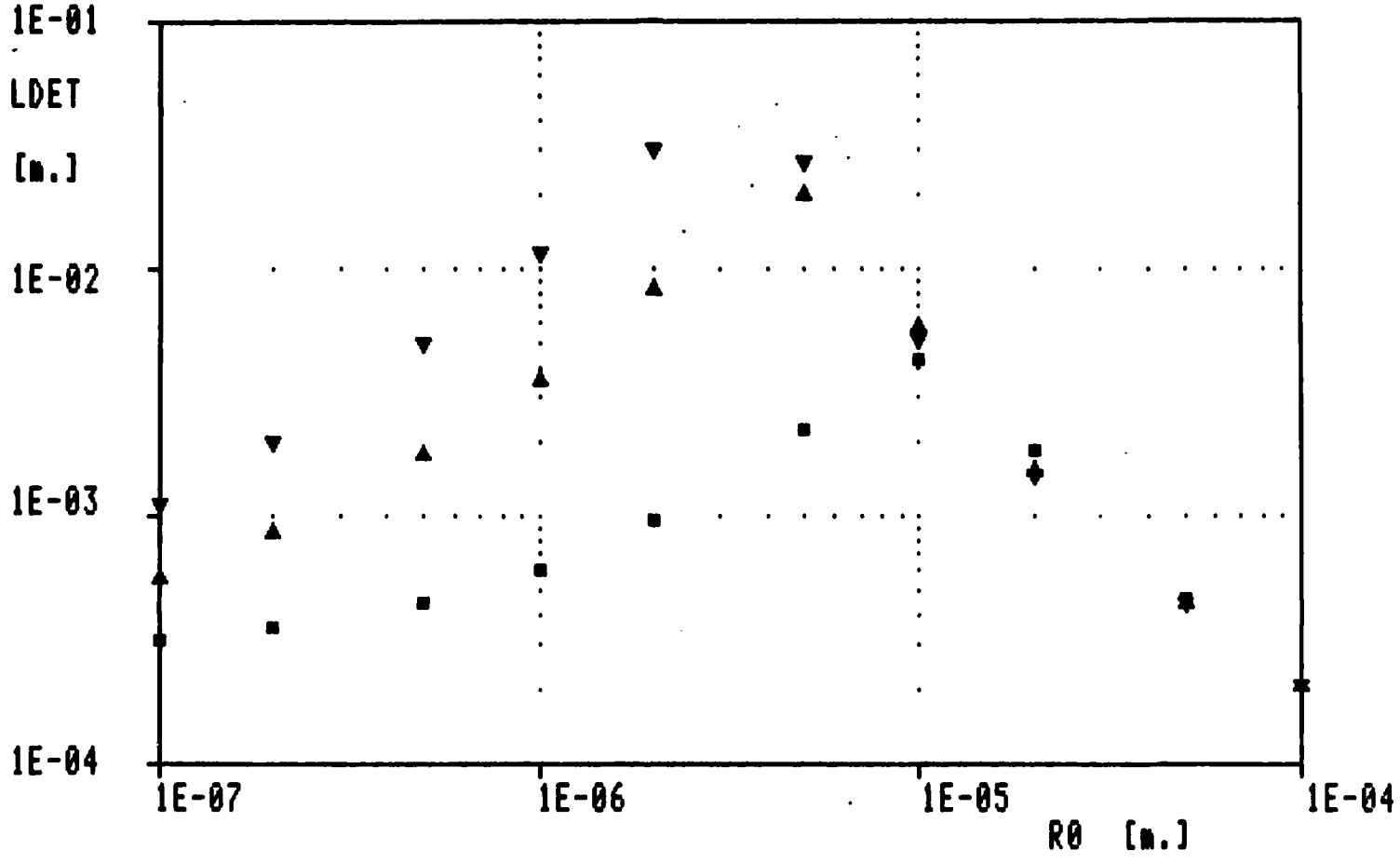


Figure 7. *Low pressure volume of the duct,* V_{lp} [VLP], v/s bubble equilibrium radius, R_o [R0], for K_{dis} = .001 1/m (nuclei number distribution parameter) and various average numbers of unstable bubles in such a volume: N_{ub} = .1486 (lower curve), .3554 (intermediate curve), and .8244 (upper curve). The corresponding values of the bubble interference probability are: β = .01, .05 and .20.



DETECTION TIME, TDET, V/S EQUILIBRIUM BUBBLE RADIUS, R0

Figure 8. Bubble detection time, T_{det} [TDET], i.e. time necessary for a bubble to reach a detectable radius size, R_{det}, v/s equilibrium bubble radius, R_o [R0], for various bubble equilibrium pressures: p_o = 1 bar (squares), 10 bar (upward triangles) and 30 bar (downward triangles). Here: R_{det} = .150 mm, p_v = 1919 Pa (vapor pressure), S = .073 N/m (surface tension), ρ = 1000 kg/m^3 (liquid denisty) and D_t = 1 mm (throat diameter). The data are obtained from the numerical solution of the unsteady one-dimensional ideal flow generated by the growth of a single spherical bubble in a semi-infinite cylindrical duct, whose unperturbed steady pressure is equal to the bubble critical pressure.



DETECTION LENGTH, LDET, V/S EQUILIBRIUM BUBBLE RADIUS, R0

Figure 9. Bubble detection length, L_{det} [LDET], i.e. length necessary for a bubble to reach a detectable radius size, R_{det}, v/s equilibrium bubble radius R_o [R0], for various bubble equilibrium pressures: p_o = 1 bar (squares), 10 bar (upward triangles) and 30 bar (downward triangles). Here: R_{det} = 150 μm, p_v = 1919 Pa (vapor pressure), S = .073 N/m (surface tension), ρ = 1000 kg/m^3 (liquid density) and D_t = 1 mm (throat diameter). The data are obtained from the numerical solution of the unsteady one-dimensional ideal flow generated by the growth of a single spherical bubble in a semi-infinite cylindrical duct, whose unperturbed steady pressure is equal to the bubble

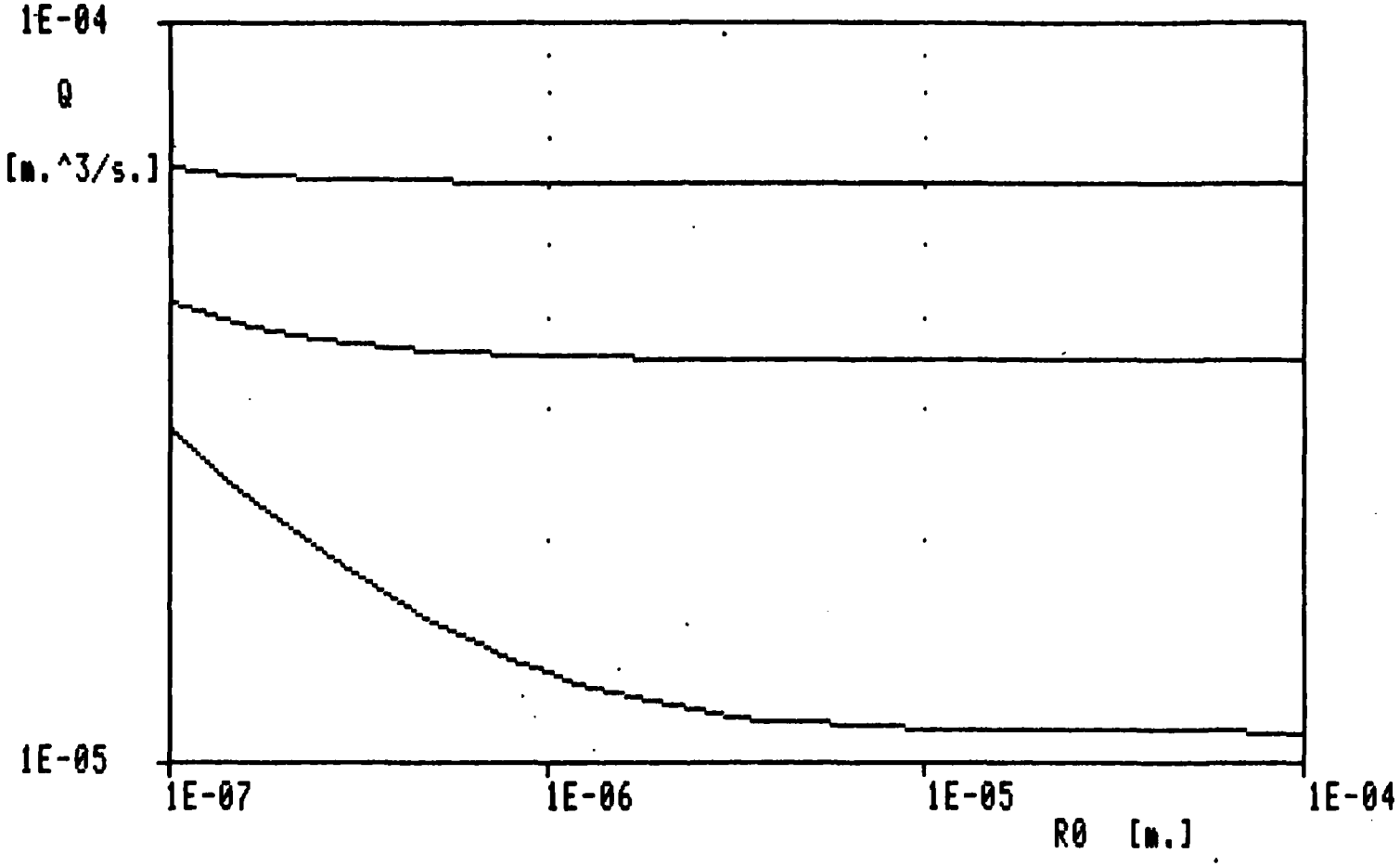
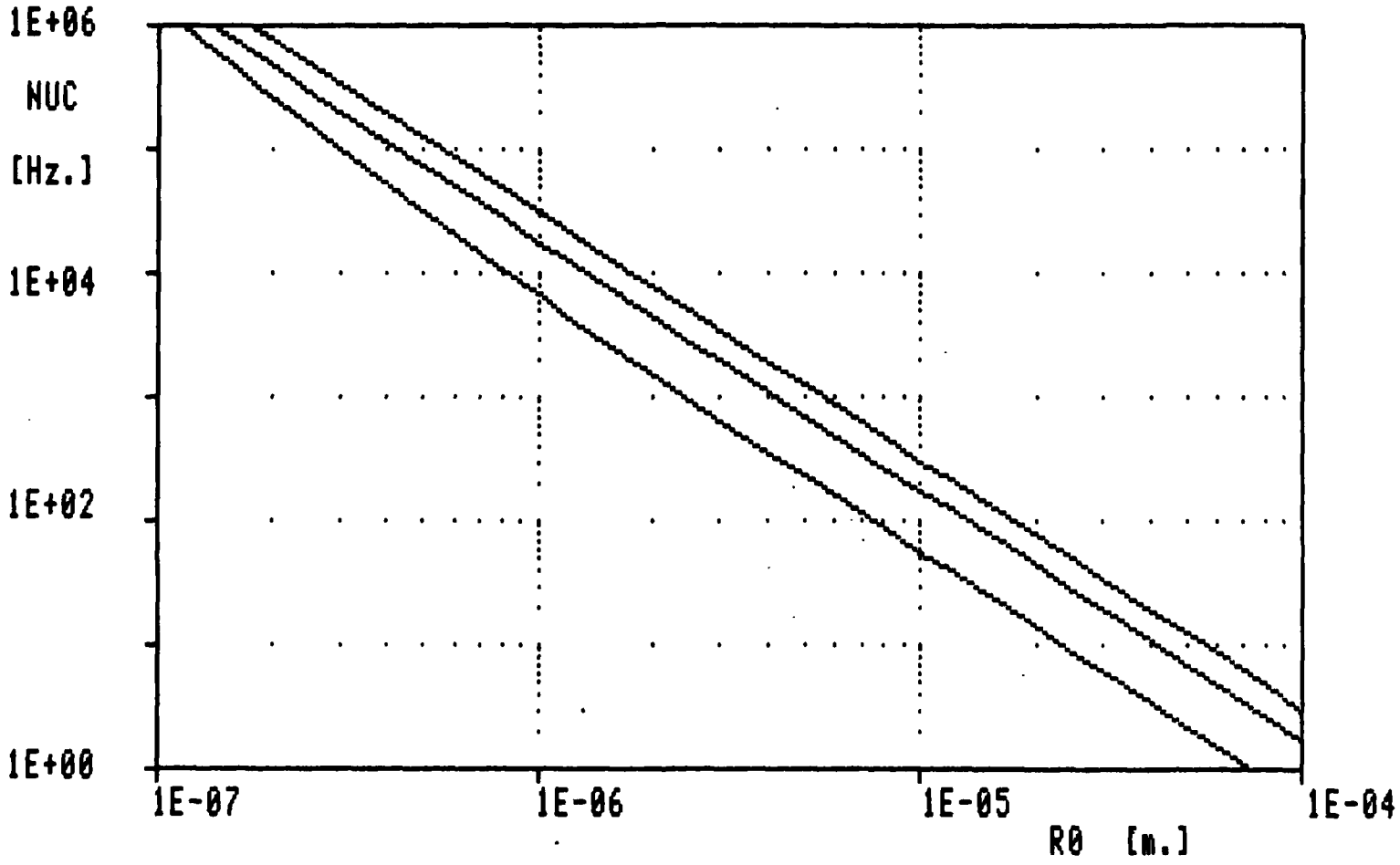


Figure 10. Volume flow rate, Q, v/s equilibrium bubble radius, R_o [R0], at various equilibrium pressures: p_o = 1 bar (lower curve), p_o = 10 bar (intermediate curve) and p_o = 30 bar (upper curve) for S = .073 N/m (surface tension), p_v = 1919 Pa (vapor pressure), ρ = 1000 kg/m^3 (liquid denisty) and D_t = 1 mm (throat diameter).



MEAN CAVITATION EVENT RATE, NUC, V/S BUBBLE EQUILIBRIUM RADIUS, R0

Figure 11. Mean cavitation event rate, ν_0 [NUC], v/s bubble equilibrium radius, R_0 [R0], for various bubble equilibrium pressures: p_o = 1 bar (lower curve), 18 bar (intermediate curve) and 30 bar (upper curve). Here: D_t = 1 mm (throat diameter), p_v = 1919 Pa (vapor pressure), S = .073 N/m (surface tension), ρ = 1000 kg/m^3 (liquid density) and K_{dis} = .001 1/m (nuclei number distribution parameter).

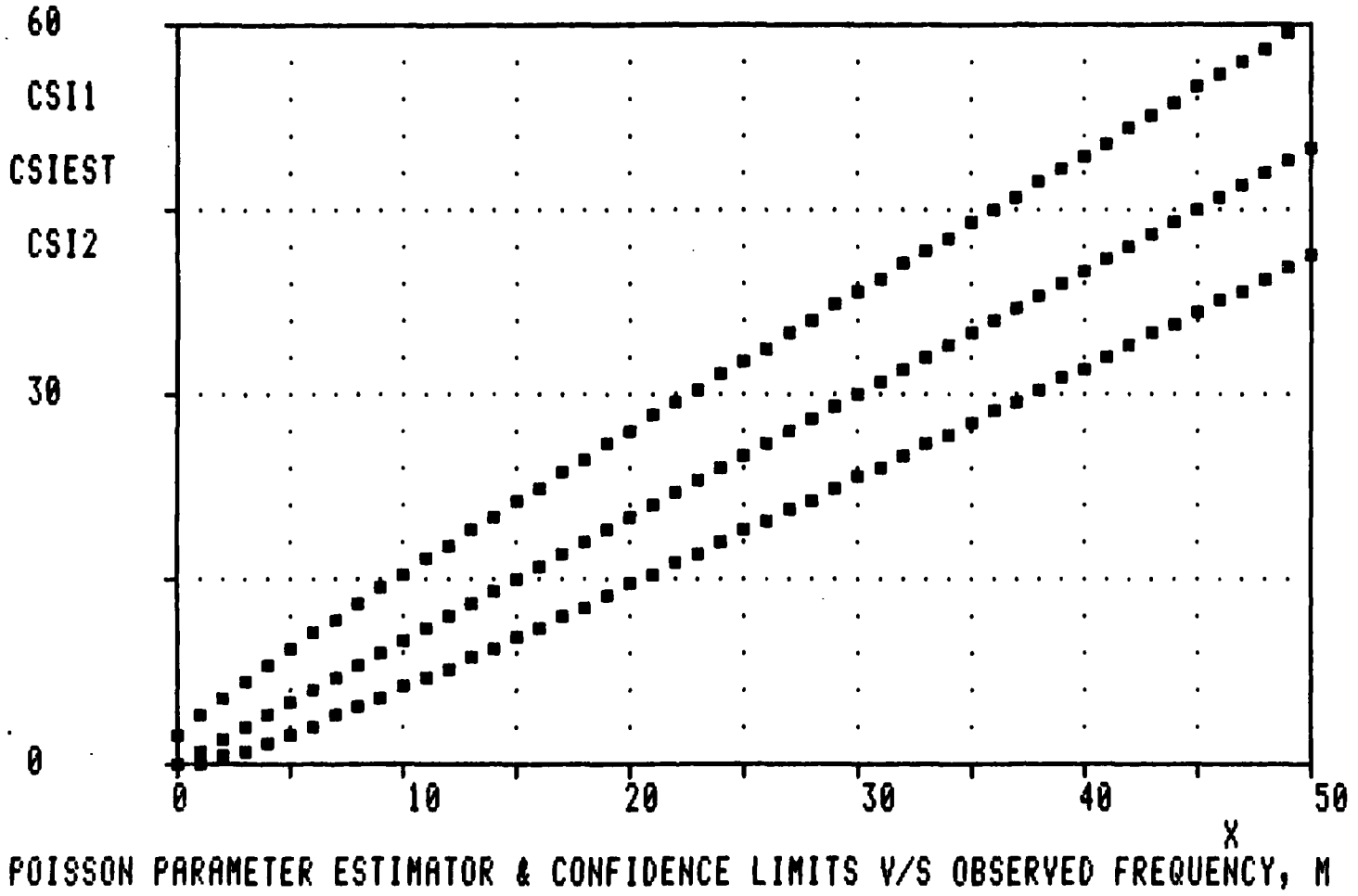


Figure 12. Poisson's distribution parameter estimator, ξ_{est} [CSIEST], and confidence limits, ξ_1 [CSI1] and ξ_2 [CSI2], v/s sample statistical frequence, m [M]. Here the confidence level is: $1 - \alpha = .8$.

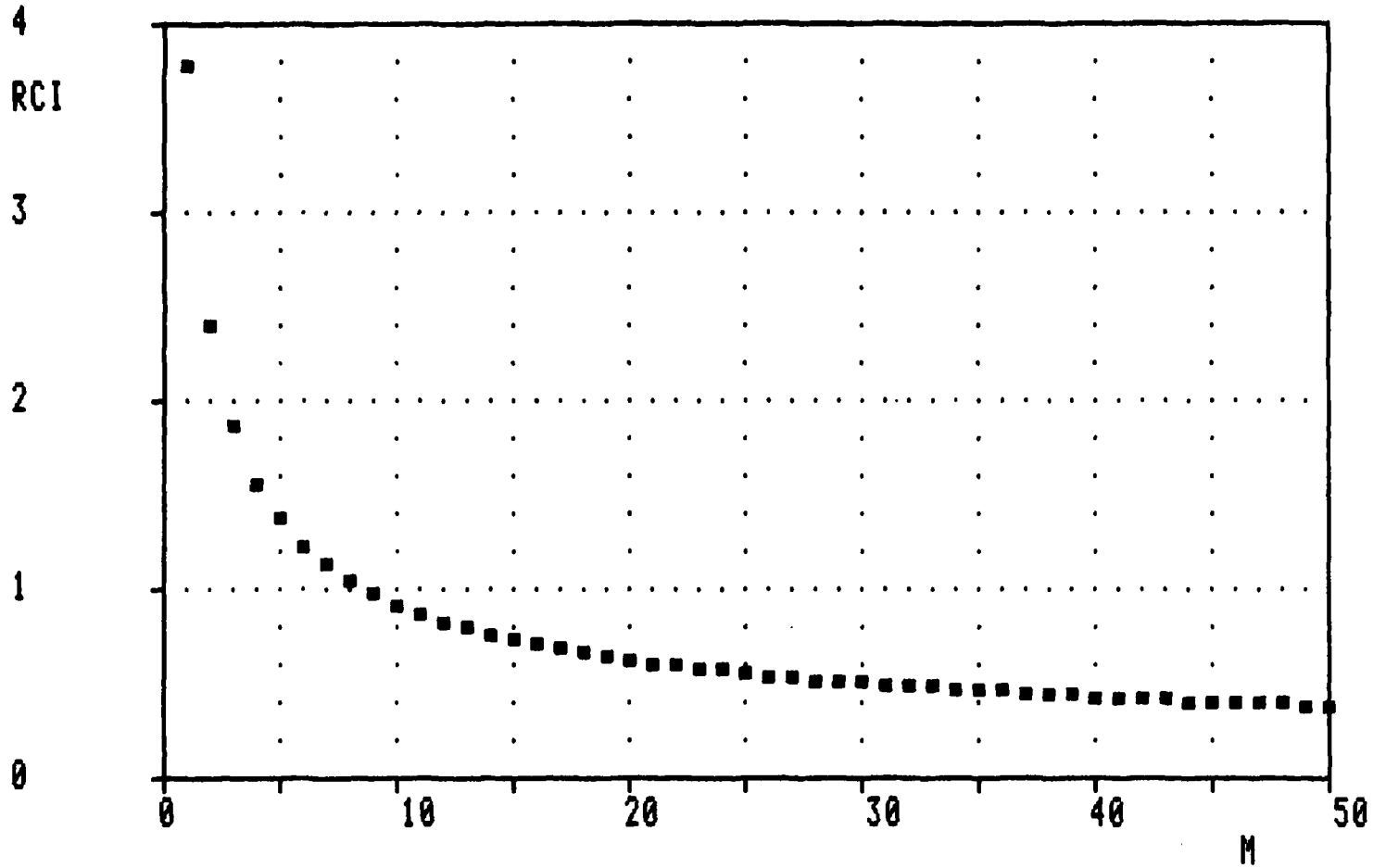


Figure 13. Poisson's distribution parameter relative confidence interval, $(\xi_2 - \xi_1)/m$ [RCI], v/s sample statistical frequency, m [M]. Here the confidence level is: $1 - \alpha = .8$ and the confidence interval is normalized w.r.t. the sample frequency.

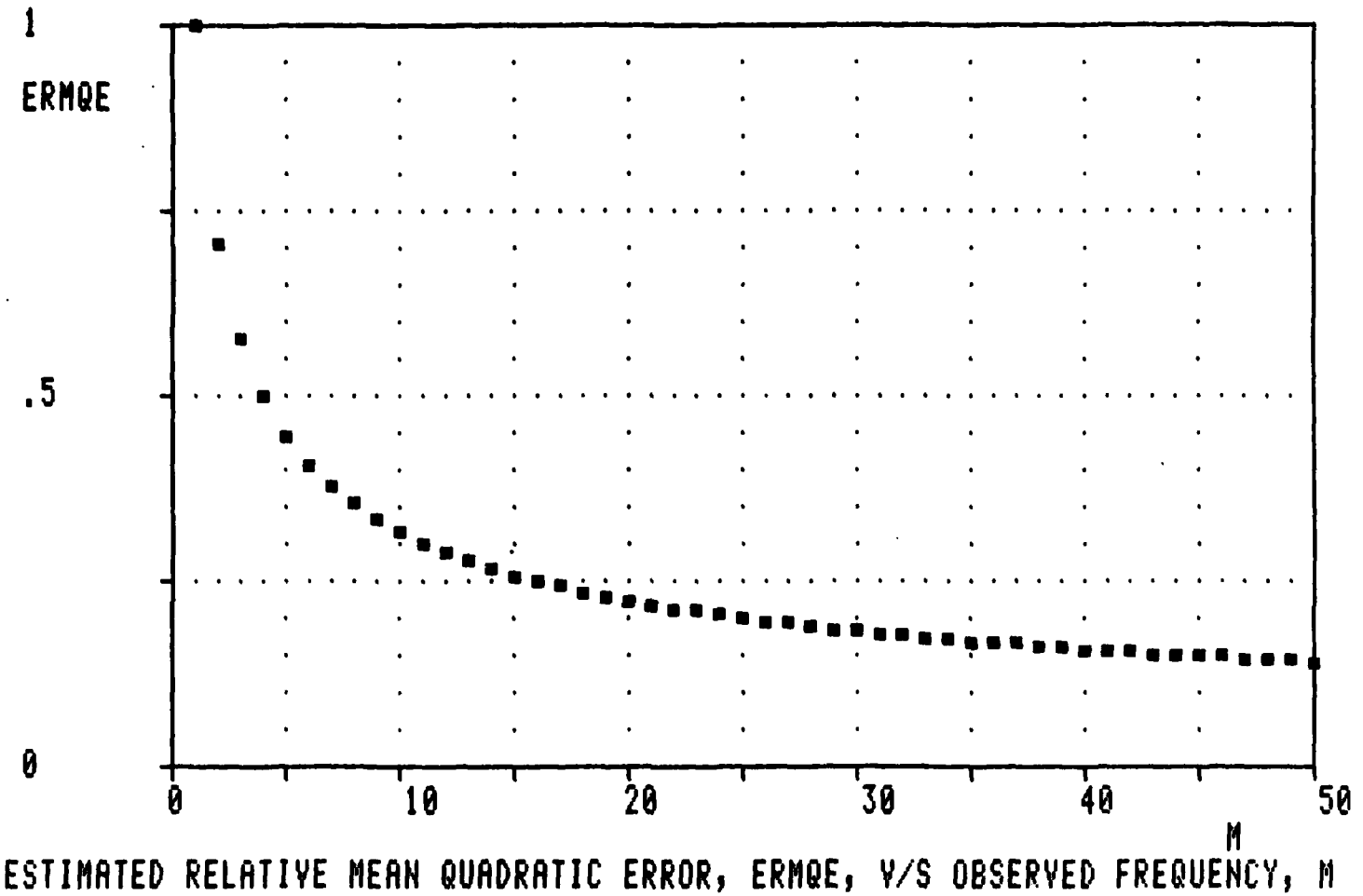


Figure 14. Poisson's distribution parameter estimated relative mean quadratic error, ε [ERMQE], v/s sample statistical frequency m [M]. Here the best estimator of the Poisson's distribution parameter (the sample frequency) is used to both evaluate the r.m.s. error and to normalize it.

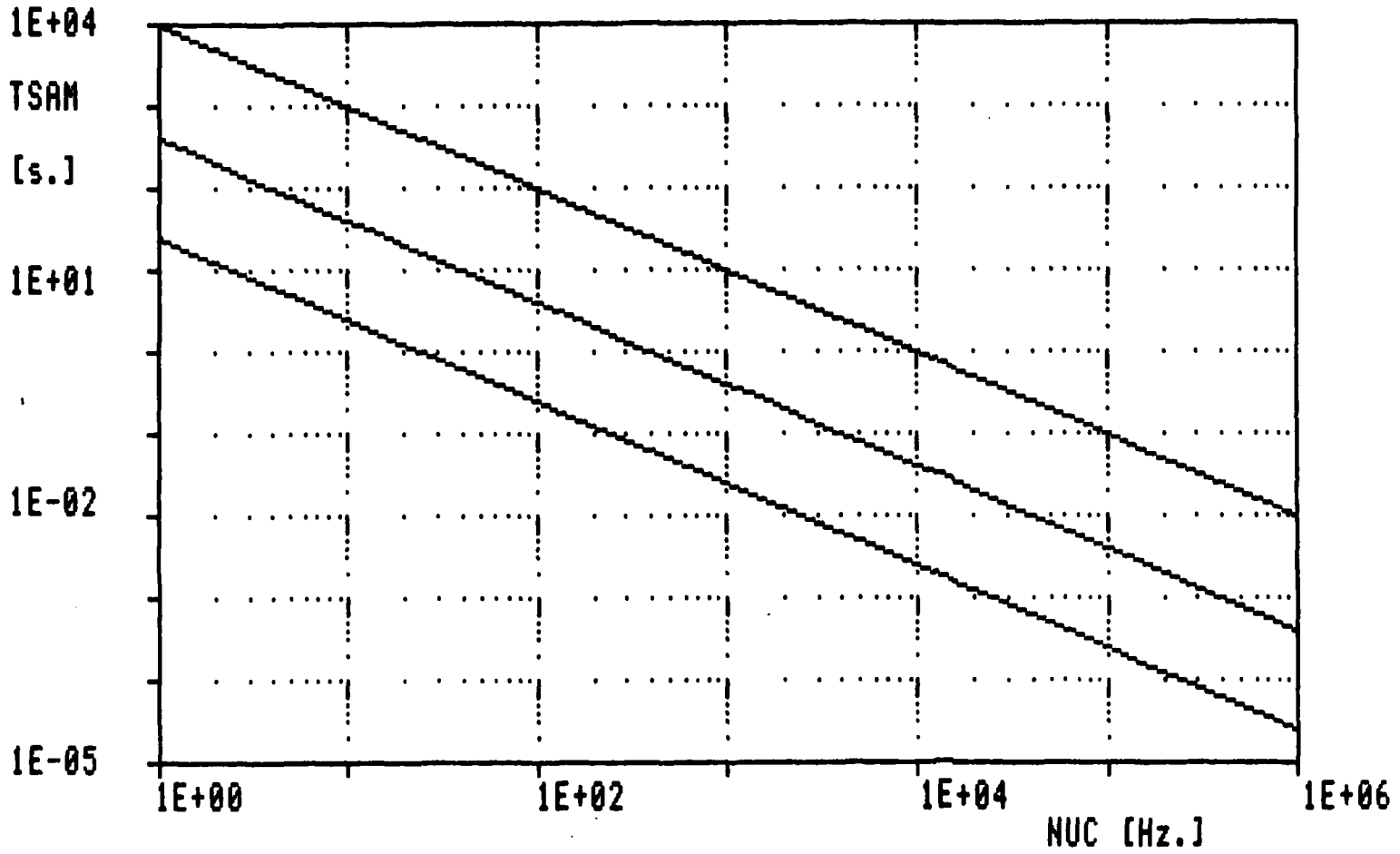


Figure 15. Sampling time, T_s [TSAM], v/s average cavitation event rate, ν_c [NUC], for various values of the relative estimated r.m.s. error: $\varepsilon = 0.1$ (upper curve), .05 (intermediate curve) and .20 (lower curve).

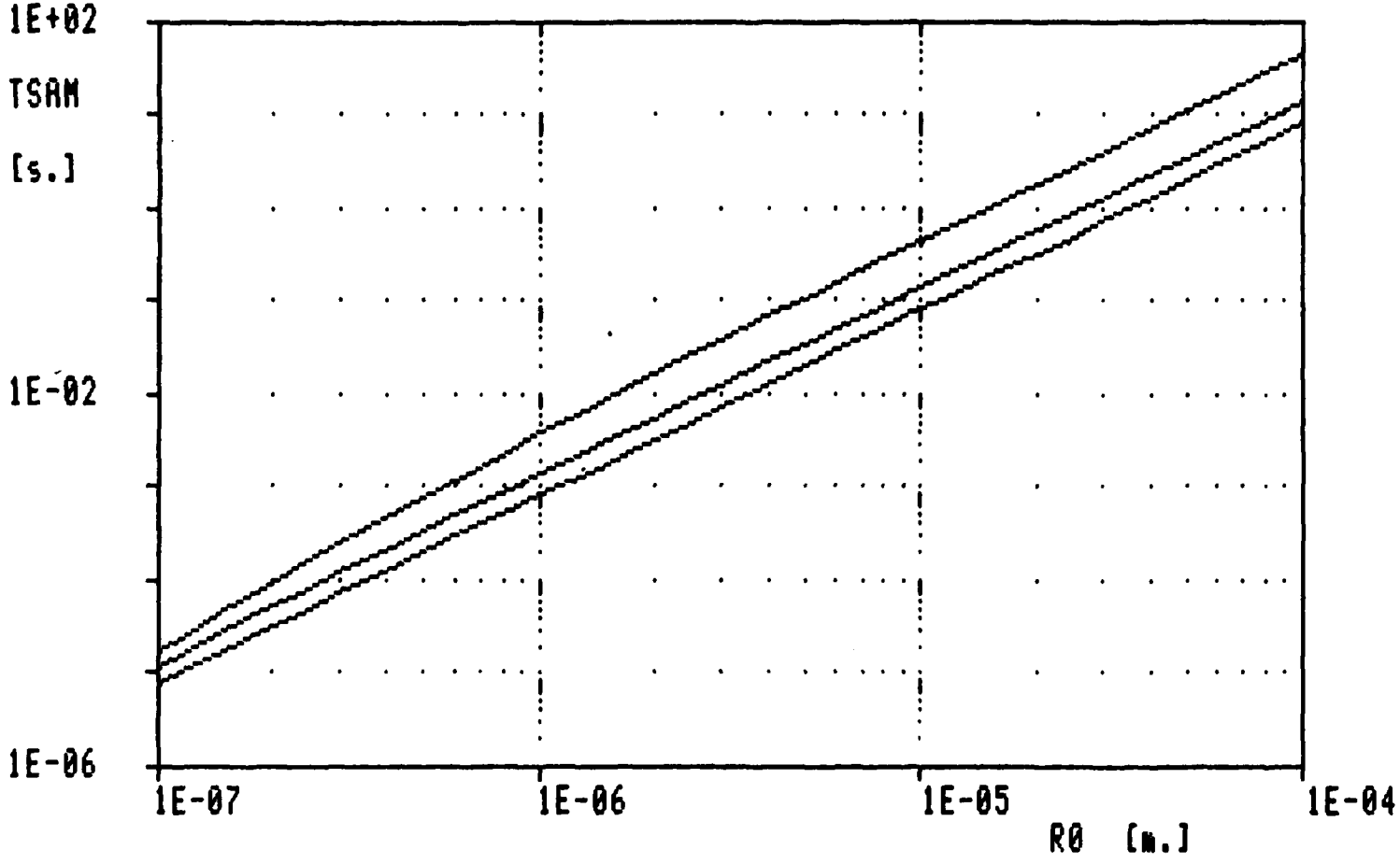


Figure 16. Sampling time T_s [TSAM], v/s bubble equilibrium radius, R_o [RO], for various values of the bubble equilibrium pressure: p_o = 1 bar (upper curve), 10 bar (intermediate curve) and 30 bar (lower curve). Here: ε = .20 (estimated relative r.m.s. error in the measure of the cavitation event rate), D_t = .001 m (throat diameter), p_v = 1919 Pa (vapor pressure), S = .073 N/m (surface tension), ρ = 1000 kg/m^3 (liquid density) and K_{dis} = .001 1/m (nuclei number distribution parameter).

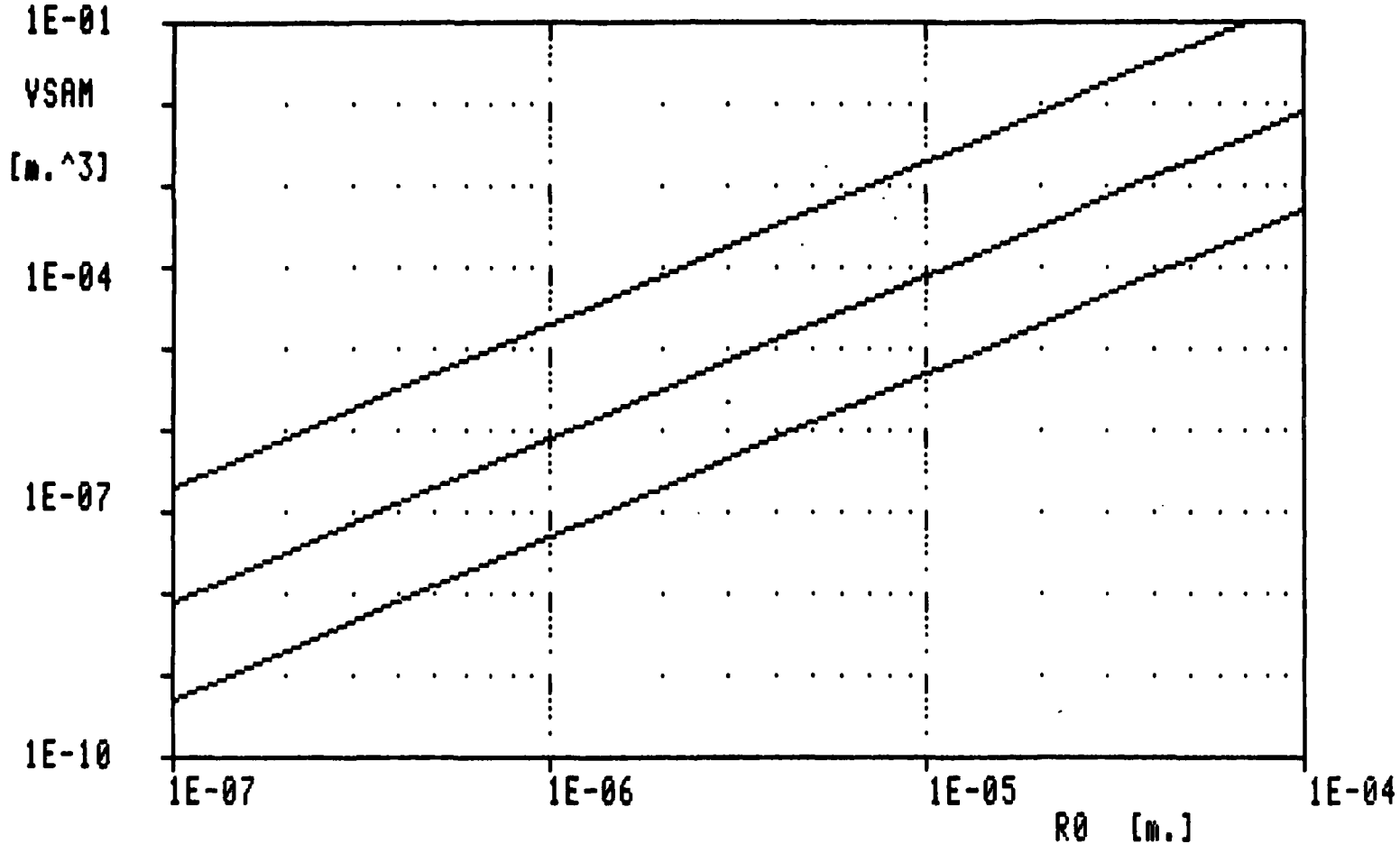
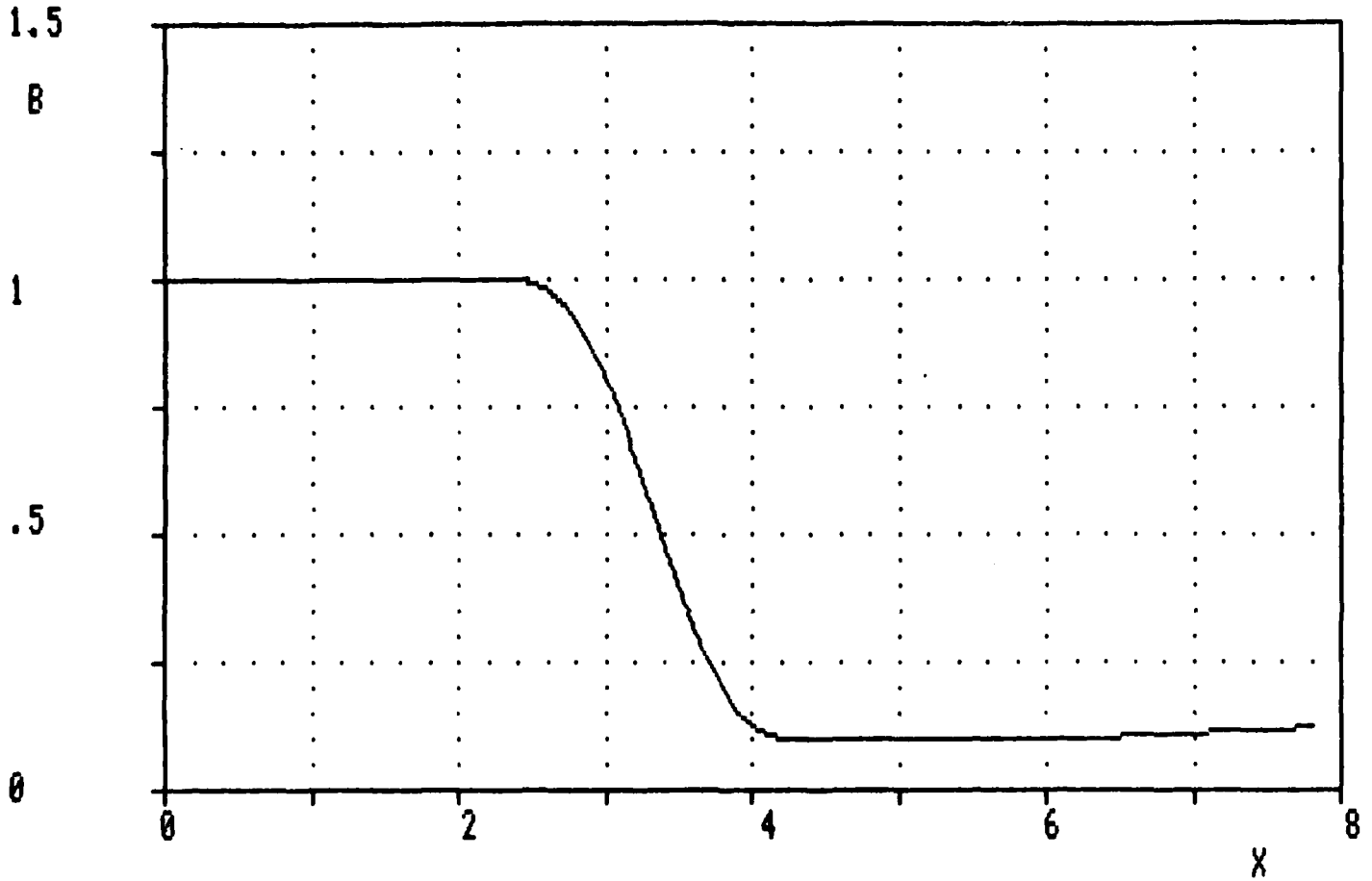


Figure 17. Liquid sample volume, V_s [VSAM], v/s bubble equilibrium radius, R_o [RO], for various values of the estimated relative r.m.s. error in the measure of the cavitation event rate: ε = .01 (upper curve), 0.85 (intermediate curve) and .28 (lower curve). Here: K_{dis} = .001 1/m (nuclei number distribution parameter).



C.S.M. PROTOTYPE VENTURI DUCT RADIUS, B(X), V/S AXIAL COORDINATE, X

Figure 18. Duct shape of prototype C.S.M. venturi in normalized coordinates X (axial) and B (radial) with: C_r = 100 (contraction ratio), L_i = 2.278 (normalized inlet length), L_c = 2.076 (normalized contaction length), L_t = 1.544 (normalized throat length), L_{di} = .597 (normalized diffuser inlet length), L_{de} = 1.327 (normalized conical 1.327 diffuser length) and β_d = .803 deg (diffuser semi-aperature angle). Lengths are normalized w.r.t. the duct inlet radius, B_i = 5 mm.

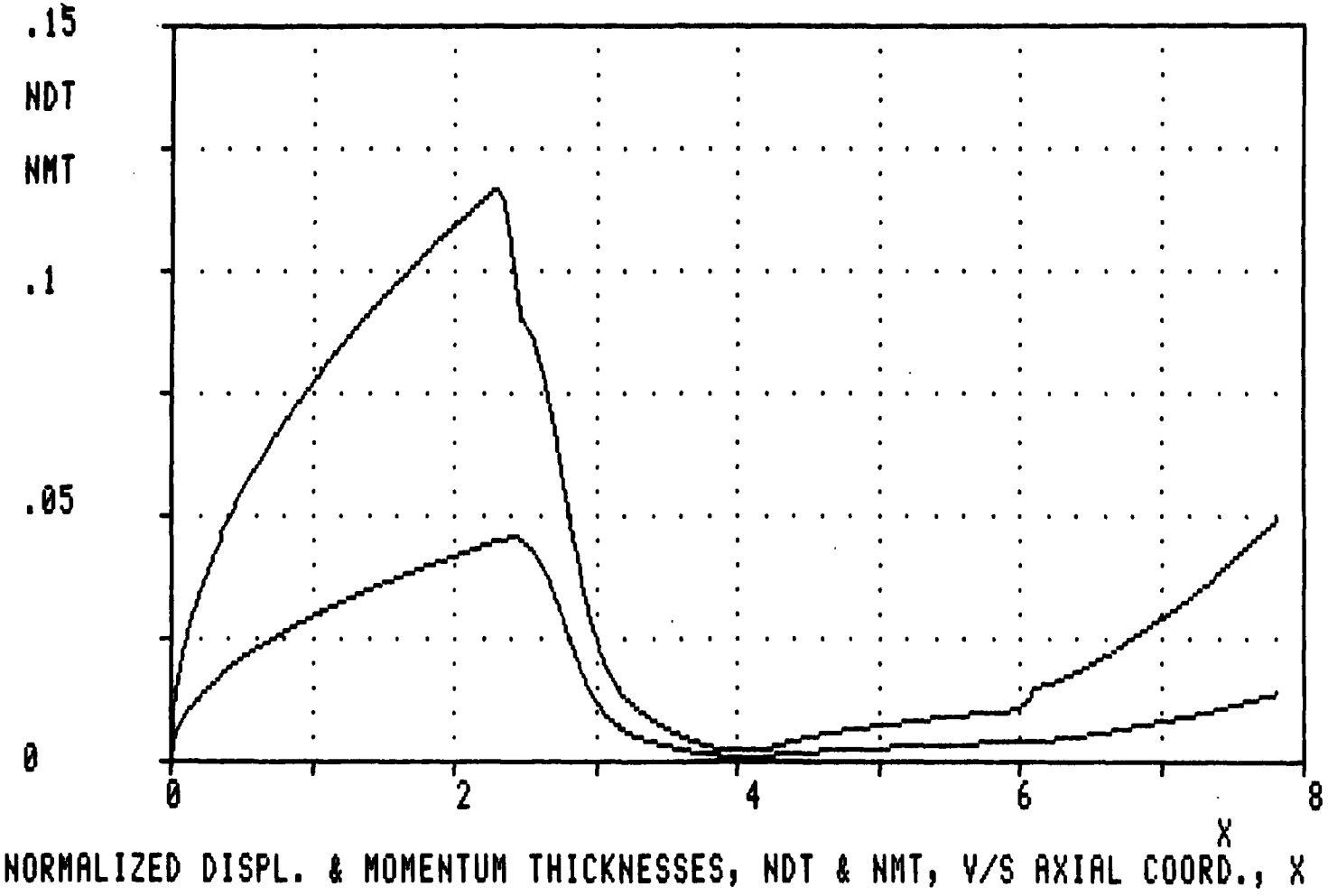


Figure 19. Normalized displacement thickness, NDT (upper curve), and momentum thickness, NMT (lower curve), v/s normalized axial coordinate, X, in the laminar C.S.M. venturi of Fig. 18. The Reynolds number at the inlet, based on the volume average velocity and duct radius, is: $Re_1 = 700$. Boundary layer calculations are based on a quasi one-dimensional model of the flow in the duct.

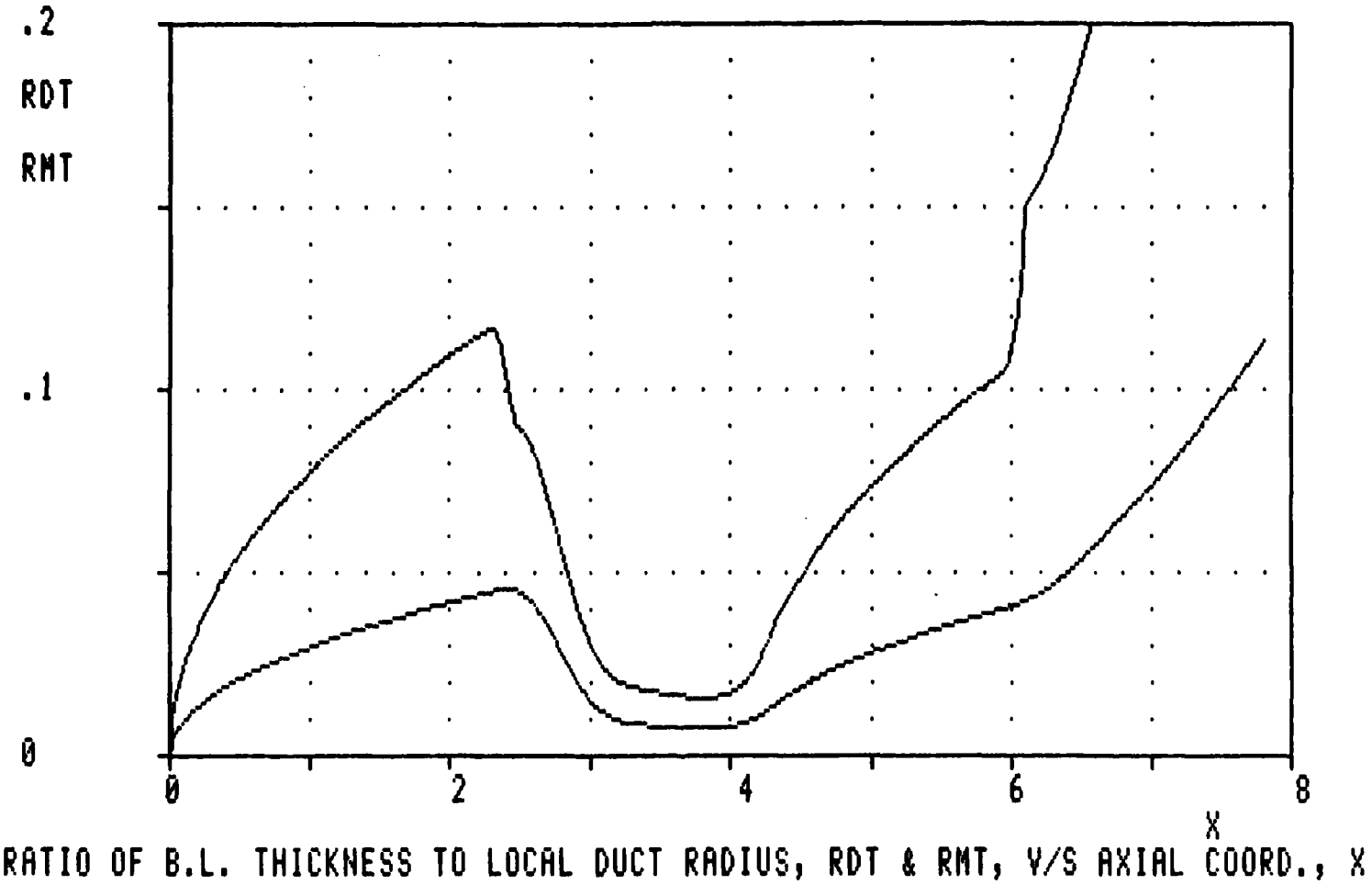


Figure 20. Relative displacement thickness, RDT (upper curve), and momentum thickness, RMT (lower curve), v/s normalized axial coordinate, X, in the laminar C.S.M venturi of Fig. 18. The Reynolds number at the inlet, based on the volume average velocity and the duct radius is: Re_i = 700 and the boundary layer thicknesses are expressed as fractions of the local duct radius. Boundary layer computations are based on a quasi one- dimensional model of the flow in the duct.

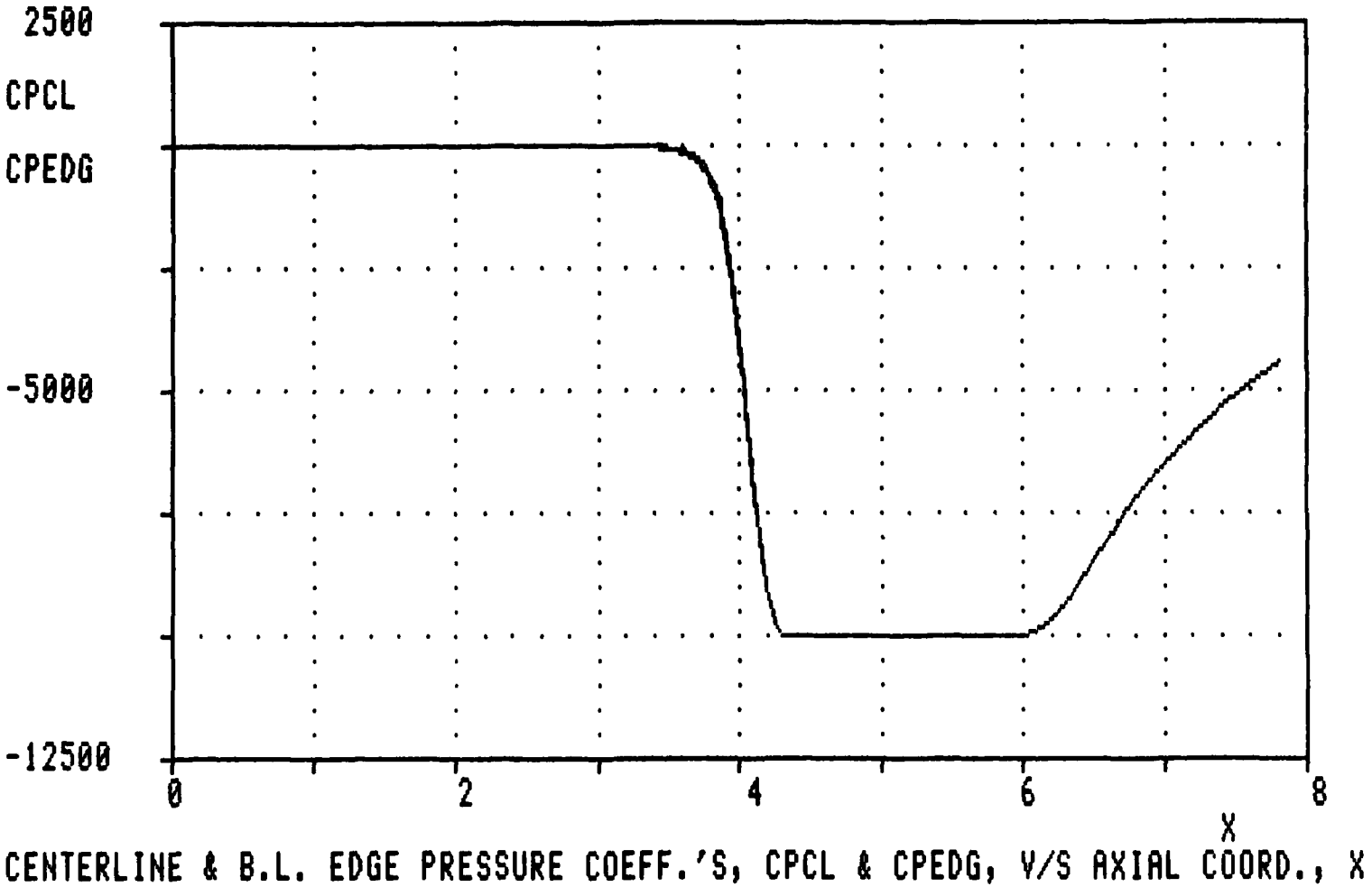
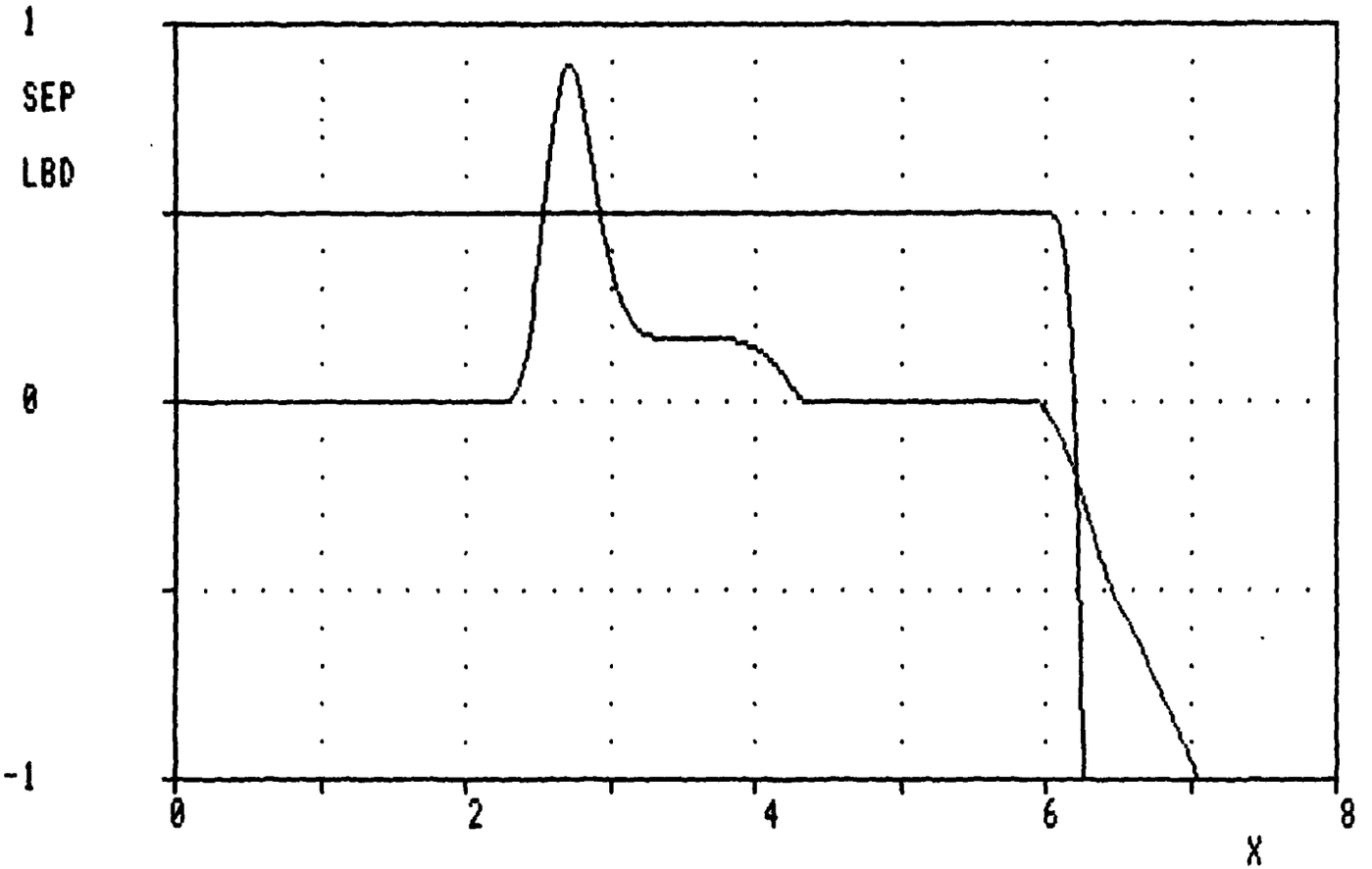


Figure 21. Centerline pressure coefficient, C_{pcl} [CPCL] (lower curve, essentially collapsed on the upper one), and boundary layer edge pressure coefficient C_{ped} [CPEDG] (upper curve), v/s normalized axial coordinate, X, for the C.S.M. Venturi of Fig. 18. Here the pressure is normalized w.r.t. the conditions at the duct inlet and computations are based on a quasi one-dimensional model of the flow.



SEPARATION & CORRELATION PARAMETERS, SEP & LBD, V/S AXIAL COORD., X

Figure 22. Stratford's laminar separation parameter, S_c [SEP] (upper curve), and Thwaites' shear and shape correlation parameter λ [LBD] (lower curve), v/s normalized axial coordinate, X , for the C.S.M. venturi of Fig. 18. Here Stratford's laminar separation equation is rearranged so that separation is predicted when SEP goes through zero or $\lambda = -.09$. Boundary layer computations are based on a quasi one-dimensional model of the flow in the duct.

AD-P003 810

The Influence of Pressure Gradient on Desinent Cavitation Produced by the Separated Flow from an Isolated Triangular Surface Protrusion[1]

by

J. William Holl[2], Michael L. Billet[3], and Masaru Tada[4]

Applied Research Laboratory of The Pennsylvania State University

ABSTRACT

An experimental investigation was conducted to study the desinent cavitation characteristics of various sizes of two-dimensional triangular protrusions in a turbulent boundary layer for favorable, zero, and unfavorable pressure gradients. Eight roughness heights (h) were employed in the studies ranging from 0.01 to 0.30 inches. The relative height (h/δ) varied from 0.026 to 2.53. Desinent cavitation numbers (σ_d) were obtained visually over a velocity range of 30 to 60 fps at an average total air content of 3.7 ppm (mole basis). The data for zero pressure gradient were in fair agreement with data obtained for the same protrusion shape by Holl (1958). The cavitation number (σ_d) was correlated with relative height, (h/δ), Reynolds Number ($U\delta/\nu$), and Clauser's (1954) equilibrium boundary layer shape factor (G) which includes the effect of pressure gradient. The data show that σ_d increases with pressure gradient. This result was not expected since it appears to contradict the trends implied by the so-called characteristic velocity theory developed by Holl (1958).

---

[1]Paper presented at the 20th American Towing Tank Conference; Davidson Laboratory, Stevens Institute of Technology, Castle Point Station, Hoboken, New Jersey, August 2-4, 1983.

[2]Professor of Aerospace Engineering

[3]Senior Research Associate

[4]Former graduate student in the Department of Aerospace Engineering.

[1] INTRODUCTION

Systematic investigations of the limited cavitation characteristics of isolated surface irregularities were conducted at ARL/PSU in the 1950's and reported in the doctoral work of Holl in 1958 [1]* and [2]. In 1966, Benson [3] reported on tests conducted with isolated asperities at DTMB. Subsequently, investigations were conducted at MIT on distributed roughness and reported in the doctoral work of Arndt in 1967 [4] and [5]. Later, these investigations were augmented by additional studies at ARL/PSU and were reported by Arndt, Holl, Bohn and Bechtel [6] together with the earlier investigations. These investigations were all conducted under essentially flat plate conditions, i.e., $\frac{dP}{dx} = 0$.

The results of the aforementioned flat plate studies for isolated protrusions were employed by Billet, Holl, and Parkin [7] to analyze a cavitation scale effect on families of hydrofoils and hemispherical headforms. The results suggested that it would be prudent to investigate the effect of pressure gradient on the limited cavitation characteristics of an isolated surface protrusion. Consequently, the present investigataion was conducted to satisfy this need. A two-dimensional irregularity with a triangular cross section similar to that employed by Holl [1] was studied in the 4.5 inch x 20 inch water tunnel at ARL/PSU for various values of pressure gradient, velocity, and relative roughness height. A detailed description of this investigation is given in Reference [8].

---

*Numbers in brackets refer to documents in the list of references.

[2] DESCRIPTION OF THE INVESTIGATION

2.1 Test Arrangement

The tests were conducted in the 4.5 inch x 20 inch water tunnel at ARL/PSU. The characteristics of this facility have been described by Lehman [9]. Major features of the test setup are shown in Figure 1. The test arrangement utilized the two walls of the rectangular test section which were 20 inches in width and 4.5 inches apart. A curved wall was installed on one side of the test section to produce various pressure gradients in the test section. The triangular protrusions were inserted in various slots along the opposite wall which was flat. The curved wall made of plexiglass consisted of a hydrofoil with a 20 inch span and 17 inch chord. The cross section of the hydrofoil was one-half of a symmetrical hydrofoil section. Details of the curved wall are shown in Figure 2. In order to measure the velocity profile at each location on the flat wall, i.e. the wall opposite to the curved wall, seven holes were drilled in the curved wall for the insertion of a total head tube.. These seven locations are designated STA. I, II, III, IV, V, VI and VII as shown in Figure 3.

2.2 Triangular Protrusions

The triangular protrusions were made of plexiglass. The cross section was a 45° triangle with the vertical side towards the incoming flow as shown in Figure 1. This is the same cross-section as that employed by Holl [1]. The span of each protrusion was 4 inches and slots were machined in a flat wall at the seven stations shown in Figure 3. When a slot was tested at any given station, such as Station 1 in Figure 3, the remaining slots were filled with small plexiglass plates. Eight roughness heights (h) were employed in the tests; namely, 0.01, 0.02, 0.03, 0.05, 0.07, 0.10, 0.15, and 0.30 inches and were mounted on the flat wall one at a time for each experiment. The

roughness locations shown in Figure 3 correspond to the leading edge of the total head tube which was inserted into the flow through the seven holes in the curved wall shown in Figure 2.

2.3 Measurement of the Velocity at Infinity

The wall pressure (P_∞') 6.4 inches upstream of the curved wall together with the pressure in the settling section (P_o) was used to find a nominal velocity at infinity (U_∞'). However, the measuring station at 6.4 inches was influenced by the curved wall so that it was not possible to determine the actual velocity at infinity (U_∞) by measurement. This was determined by an application of the Douglas-Neumann method which indicated that $U_\infty'/U_\infty = 0.9833$.

2.4 Measurement of the Pressure Distribution on the Flat Wall

The pressure distribution along the flat wall was measured by static pressure taps located between the measuring stations along the wall. The data were expressed in coefficient form, i.e.

$$C_p = \frac{P - P_\infty}{\frac{1}{2} \rho U_\infty^2} \quad . \tag{1}$$

These data are shown by the open circular symbols in Figure 4.

The velocity at the edge of the boundary layer (U) was measured by a total head tube as described in the next section. These data are shown in Figure 5. The wall pressure coefficient was calculated by the relation

$$C_p = 1 - \left(\frac{U}{U_\infty}\right)^2 \quad . \tag{2}$$

These values of C_p shown by the open triangular symbols in Figure 4 are in good agreement with C_p obtained by wall pressure taps.

The theoretical pressure distribution on the wall as obtained by the Douglas-Neumann (DN) computer program is shown by the solid circular symbols in Figure 4.

2.5 Determination of Velocity Profile Characteristics

The velocity profiles were measured by traversing the boundary layer with a probe which was fabricated from a tube of rectangular cross section with an external size of 0.018 inch x 0.083 inch. A traversing device allowed the positioning of the total head tube within 0.001 inch. The edge of the boundary layer was attained when the total pressure became constant. The measured values of boundary layer thickness (δ) are compared with values determined by the method of E. Truckenbrodt [10] in Figure 6. It was necessary to shift the origin of the theoretical calculation in order to agree with the measured data.

The velocity profile data were not obtained sufficiently close to the wall to determine momentum thickness (θ), displacement thickness (δ^*), boundary layer shape parameter ($H = \delta^*/\theta$) and wall shear stress (τ_w). Thus, δ^*, θ, and H were determined by the Truckenbrodt method [10] and τ_w was determined from the Ludwieg-Tillmann [11] relation

$$\frac{\tau_w}{\frac{1}{2}\rho U^2} = 0.246 \times 10^{-0.678H} \left(\frac{U\theta}{\nu}\right)^{-0.268} \qquad (3)$$

where U is the velocity at the edge of the boundary layer.

Measured values of δ together with calculated values of δ^*, θ, and H are given in Table 1. The wall shear stress, pressure gradient and the parameters β, Π and G are given in Table 2. All data are shown for a nominal velocity (U_∞) of 40 fps. Experimental values of δ were scaled to 40 fps by the equation

$$\delta = 0.37 \times \left(\frac{UX}{\nu}\right)^{-0.2} . \qquad (4)$$

2.6 Cavitation Experiments

There was not sufficient time available to conduct cavitation experiments at all seven stations so that three representative stations were selected for the experiments. These were Station I ($dP/dx < 0$), Station IV ($dP/dx \approx 0$) and Station VII ($dP/dx > 0$).

During the experiments the total gas content was maintained at approximately 4 moles of air per million moles of water (ppm). The mean value for all tests was 3.7 ppm. The gas content was determined by a Van Slyke apparatus.

The primary purpose of the cavitation experiments was to determine the limited cavitation number (σ_ℓ) defined as

$$\sigma_\ell = \frac{P_{\infty\ell} - P_v}{\frac{1}{2} \rho U_\infty^2} \quad . \tag{5}$$

This cavitation number can be determined experimentally by either the inception or desinence procedure. The desinence procedure was employed in this investigation. Thus $\sigma_\ell = \sigma_d$ where σ_d is the desinent cavitation number given by

$$\sigma_d = \frac{P_{\infty d} - P_v}{\frac{1}{2} \rho U_\infty^2} \quad . \tag{6}$$

The desinence procedure consists of holding the velocity constant and increasing the pressure until the cavitation disappears.

A strobe light was used to aid in visually observing cavitation. When cavitation occurred along the top edge of the triangular protrusion, which appeared as luminous streaks originating several inches downstream of the protrusion, another type of cavitation appeared at both ends of the protrusion. These two types of cavitation joined together downstream.

Special care was taken to see that the cavitation caused by the ends was not mistaken for that caused by the top edge of the triangular protrusion.

Desinent cavitation was defined as the absence of cavitation at the top edge of the protrusion for less than 30 seconds. Throughout the experiment, the observations were done by the same person. The pressure was lowered and raised seven times for each velocity setting. The desinent cavitation number was based on the average pressure obtained from those seven readings. The gas content and temperature was measured before and after each run.

As indicated in a subsequent section σ_d was correlated with several parameters which were characteristic of the flow. Two parameters which included the pressure gradient effects were employed in this analysis. These were the Coles' [12] wake parameter Π and Clauser's [13] shape parameter G. The parameter G is defined as

$$G = \left(1 - \frac{1}{H}\right)\sqrt{\frac{2}{C_f}} \tag{7}$$

where $H = \delta^*/\theta$ and $C_f = \tau_w/1/2\ \rho\ U^2$. The values of G tabulated in Table 2 were calculated by Nash's [14] approximation

$$G \simeq 6.1\sqrt{\beta + 1.81} - 1.7 \quad . \tag{8}$$

Cole's wake parameter was approximated by the relation

$$\Pi \simeq 0.8\ (\beta + 0.5)^{0.75} \tag{9}$$

where

$$\beta = \frac{\delta^*}{\tau_w}\frac{dP}{dx} \quad . \tag{10}$$

In establishing a correlation for the cavitation number it is prudent to calculate the cavitation number under essentially flat plate conditions ($\sigma_{\ell fp}$), i.e. the wall pressure (P) and velocity at the edge of the boundary layer (U) become the "local" infinity condition in the equation for cavitation number. Thus we have

$$\frac{P_\infty - P_v}{\frac{1}{2}\rho U_\infty^2} = -\frac{P - P_\infty}{\frac{1}{2}\rho U_\infty^2} + \frac{P - P_v}{\frac{1}{2}\rho U_\infty^2} \tag{11}$$

or

$$\sigma_\ell = -C_p + \left(\frac{U}{U_\infty}\right)^2 \left(\frac{P - P_v}{\frac{1}{2}\rho U^2}\right) \tag{12}$$

or

$$\sigma_\ell = -C_p + (1 - C_p)\,\sigma_{\ell fp} \tag{13}$$

which is the superposition equation developed by Holl [1]. Solving for $\sigma_{\ell fp}$ yields

$$\sigma_{\ell fp} = \frac{\sigma_\ell + C_p}{1 - C_p} \tag{14}$$

Thus in the experiment, σ_ℓ was determined by the desinence procedure, C_p was determined from Figure 4 and $\sigma_{\ell fp}$ was then calculated from Equation (14).

[3] RESULTS OF THE CAVITATION TESTS

The major results of the cavitation experiments are shown in Figures 7-10. The data from Station IV ($dP/dx \approx 0$) are compared with the characteristic velocity theory in Figure 7. The same data are compared with the earlier results of Holl [1] in Figure 8. The cavitation number for all three stations are shown in Figure 9 as a function of relative height (h/δ). A power-law correlation is shown in Figure 10 for all of the data at the three stations.

Referring to Figure 7, $\sigma_{\ell fp}$ is shown as a function of h/δ for various velocities. These data were obtained at Station IV where $dP/dx \approx 0$. They display a strong dependence upon the relative height (h/δ) and are in fair agreement with the characteristic velocity theory (CVT) developed by Holl [1], [15]. This theory assumes that if one knows σ for the case $\delta = 0$ one can correct σ by the proper choice of a characteristic velocity (U_c). This leads to

$$\sigma_{\ell fp} = \left(\frac{U_c}{U}\right)^2 \sigma_{\ell fp}' \tag{15}$$

where $\sigma_{\ell fp}'$ corresponds to the case $\delta = 0$. Assuming that U_c^2 is the average of the square of the velocity profile over the height of the protrusion (h) and employing power-law type velocity profiles, i.e. $u/U = (Y/\delta)^{1/m}$, we can write

$$\sigma_{\ell fp} = \frac{1}{H}\left(\frac{h}{\delta}\right)^{2/m} \sigma_{\ell fp}' \text{ for } h/\delta \leq 1 \tag{16}$$

and

$$\sigma_{\ell fp} = \left[1 - \frac{\delta}{h}\left(1 - \frac{1}{H}\right)\right]\sigma_{\ell fp}' \text{ for } h/\delta \geq 1 \tag{17}$$

where $H = \delta^*/\theta = m+2/m$. The cavitation number $\sigma_{\ell fp}'$ has been determined by J. W. Holl and C. B. Baker at ARL/PSU by testing a family of sharp edged flat plates in a uniform stream. The data were correlated reasonably well by the equation

$$\sigma_{\ell fp}' = 0.0214\ Re_h^{0.424} \tag{18}$$

where h is one-half the height of the flat plates which was taken to be equivalent to the roughness height when $\delta \approx 0$. Re_h is the Reynolds number Uh/ν.

The data from the present investigation for Station IV where $dP/dx = 0$ are compared with that of Holl [1] in Figure 8. The Holl data were obtained at a much higher gas content and were thus corrected to the average gas content of this program, i.e. 3.7 ppm, by a procedure described by Tada [8]. The Holl data are higher than the present data at smaller values of h/δ and display a smaller exponent on h/δ than does the present data. We find that for constant Reynolds number

$$\sigma_{\ell fp} = \text{constant} \left(\frac{h}{\delta}\right)^{0.4} \quad \text{(Holl - 1958)} \tag{19}$$

and

$$\sigma_{\ell fp} = \text{constant} \left(\frac{h}{\delta}\right)^{0.53} \quad \text{(present study)} \quad . \tag{20}$$

Perhaps these differences are due to gas content effects.

The cavitation data for all three of the measuring stations are shown in Figure 9. The data from Station IV ($dP/dx \approx 0$) and Station I ($dP/dx < 0$) are fairly close together. However the data for Station VII ($dP/dx > 0$) where we have an adverse pressure gradient are significantly higher. This was an unexpected result since as indicated by Equation (15), the CVT would predict a decrease in $\sigma_{\ell fp}$ due to the smaller value of U_c produced by the less uniform

velocity profile characteristic of the adverse pressure gradient. However, the experimental data may contain significant effects related to the separating flow over the protrusion which are not adequately accounted for in the CVT.

Cavitation data for the zero-pressure gradient case were successfully correlated by Arndt, Holl, Bohn and Bechtel [6] with relative height (h/δ) and Reynolds number ($U\delta/\nu$) using a power-law equation. In this program it was necessary to include a shape parameter to account for pressure gradient effects. Both the G parameter of Clauser and Cole's wake parameter Π were employed. It was determined that by using G one obtains a somewhat better correlation. The results are shown in Figure 10 where the data are correlated by the relation

$$\sigma_{\ell fp} = 0.0143 \left(\frac{h}{\delta}\right)^{0.53} \left(\frac{U\delta}{\nu}\right)^{0.20} G^{1.25} \quad . \tag{21}$$

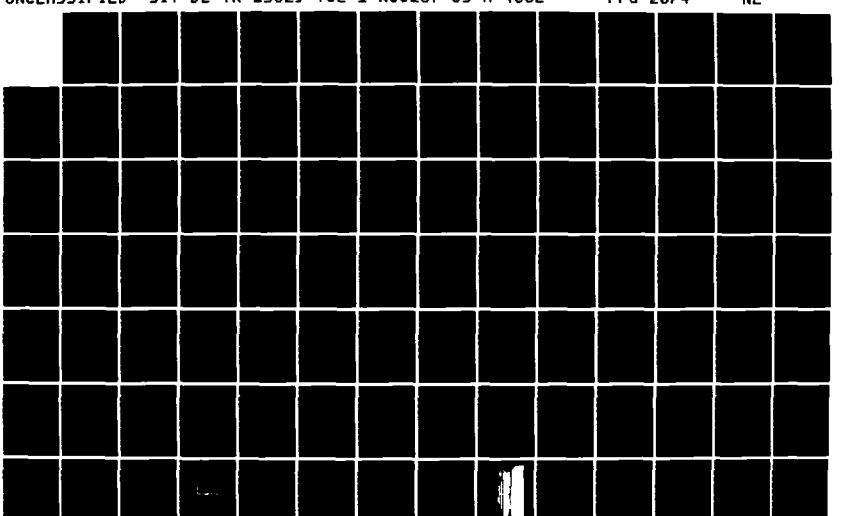
The relation appears to be a reasonable correlation for these data.

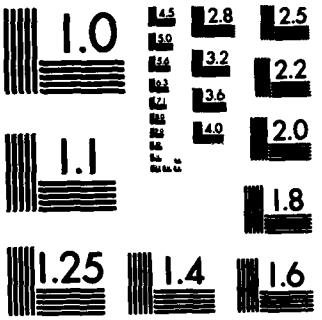
[4] ACKNOWLEDGMENT

This investigation was sponsored by the Naval Sea Systems Command Code 63R-31 which is administered by Dr. Thomas E. Peirce.

AD-A144 226 PROCEEDINGS OF THE GENERAL MEETING OF THE AMERICAN TOWING TANK CONFERENCE..(U) STEVENS INST OF TECH HOBOKEN NJ DAVIDSON LAB D SAVITSKY ET AL. AUG 83 5/7

UNCLASSIFIED SIT-DL-TR-13029-VOL-1 N00167-83-M-4062 F/G 20/4 NL





MICROCOPY RESOLUTION TEST CHART
NATIONAL BUREAU OF STANDARDS-1963-A

[5] REFERENCES

[1] Holl, J. W., "The Effect of Surface Irregularities on Incipient Cavitation," Ph.D. Thesis, The Pennsylvania State University, State College, PA, June 1958.

[2] Holl, J. W., "The Inception of Cavitation on Isolated Surface Irregularities," Journal of Basic Engineering, Trans. ASME, Vol. 82, 1960, pp. 169-183.

[3] Benson, B. W., "Cavitataion Inception on Three-Dimensional Roughness Elements," David Taylor Model Basin, Report No. 2104, May 1966.

[4] Arndt, R. E. A., "Cavitation Near Surfaces of Distributed Roughness," Ph.D. Dissertation, Department of Civil Engineering, Massachusetts Institute of Technology, June 1967.

[5] Arndt, R. E. A., and Ippen, A. T., "Rough Surface Effects on Cavitation Inception," Trans. ASME, Journal of Basic Engineering, Vol. 90, pp. 249-261, 1968.

[6] Arndt, R. E. A., Holl, J. W., Bohn, J. C., and Bechtel, W. T., "Influence of Surface Irregularities on Cavitation Performance," Journal of Ship Research, Vol. 23, No. 3, September 1979.

[7] Billet, M. L., Holl, J. W., and Parkin, B. R., "Scale Effects on Cavitating Flows Due to Surface Roughness and Laminar Separation," AIAA Journal, Vol. 20, pp. 632-637, May 1982.

[8] Tada, M., "Effect of Pressure Gradient on Cavitation Inception From an Isolated Surface Roughness," Master of Science Thesis, Department of Aerospace Engineering, The Pennsylvania State University, May 1983.

[9] Lehman, A. F., "The Garfield Thomas Water Tunnel," ORL Report No. NOrd 16597-56, The Pennsylvania State University, 1957.

[10] Truckenbrodt, E., "A Method of Quadrature for Calculation of the Laminar and Turbulent Boundary Layer in Case of Plane and Rotationally Symmetrical Flow," NACA TM 1379, May 1955.

[11] Ludwieg, H. and Tillmann, W., Untersuchunger uber die Wandschubspannung in Turbulenten Reibungasschichten. Ing.-Arch. 17, 288-299 (1949); summary of both paper ZAMM 29, 15-16 (1949). Eng. trans. in NACA TM 1285, 1955.

[12] Coles, D. E., "The Law of the Wake in the Turbulent Boundary Layer," Journal of Fluid Mechanics, Vol. 1, pp. 191-226, July 1966.

[13] Clauser, F. H., "The Turbulent Boundary Layer," Advances in Applied Mech., Vol. 4, pp. 1-51. 1956.

[14] Nash, J. F., National Physics Laboratory, Aeronautical Report 1137, England, 1965.

[15] Holl, J. W., "The Estimation of the Effect of Surface Irregularities on the Inception of Cavitation," Proceedings of Symposium on Cavitation in Fluid Machinery, ASME, 1965.

TABLE 1

BOUNDARY LAYER PARAMETERS AT EACH STATION

STA	$\frac{x}{c}$	δ (inches)	δ^* (inches)	θ (inches)	H
I	0.10	0.124	0.0122	0.0091	1.34
II	0.25	0.156	0.0148	0.0111	1.33
III	0.33	0.162	0.0162	0.0123	1.32
IV	0.41	0.167	0.0183	0.0137	1.335
V	0.51	0.183	0.0213	0.0159	1.34
VI	0.65	0.233	0.0270	0.0197	1.37
VII	0.80	0.374	0.0354	0.0255	1.39

These parameters correspond to U_∞ = 40fps

TABLE 2

SHAPE FACTOR (G) AND WAKE PARAMETER (Π) AT EACH STATION

STA	$\frac{x}{c}$	δ^* (inches)	τ_w (lb/ft^2)	dp/dx (lb/ft^3)	β	Π	G
I	0.10	0.0122	3.366	-584.2	-0.176	0.344	6.100
II	0.25	0.0148	3.508	-438.2	-0.154	0.361	6.150
III	0.33	0.0162	3.537	-219.1	-0.084	0.414	6.314
IV	0.41	0.0183	3.381	- 58.4	-0.026	0.457	6.448
V	0.51	0.0213	3.209	+146.1	+0.081	0.532	6.688
VI	0.65	0.0270	2.811	+321.3	+0.257	0.649	7.070
VII	0.80	0.0354	2.401	+438.2	+0.538	0.823	7.647

The shape factor (G), wake parameter (Π) and Clauser's equilibrium parameter (β) were calculated by using Equations (8), (9) and (10), respectively. Data are for U_∞ = 40 fps.

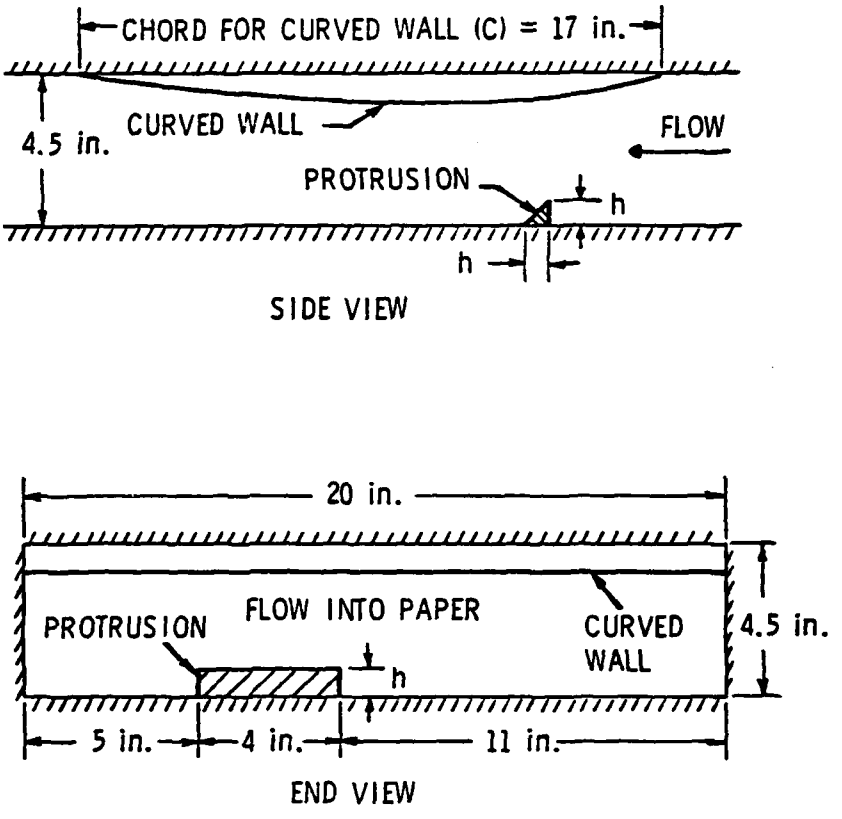
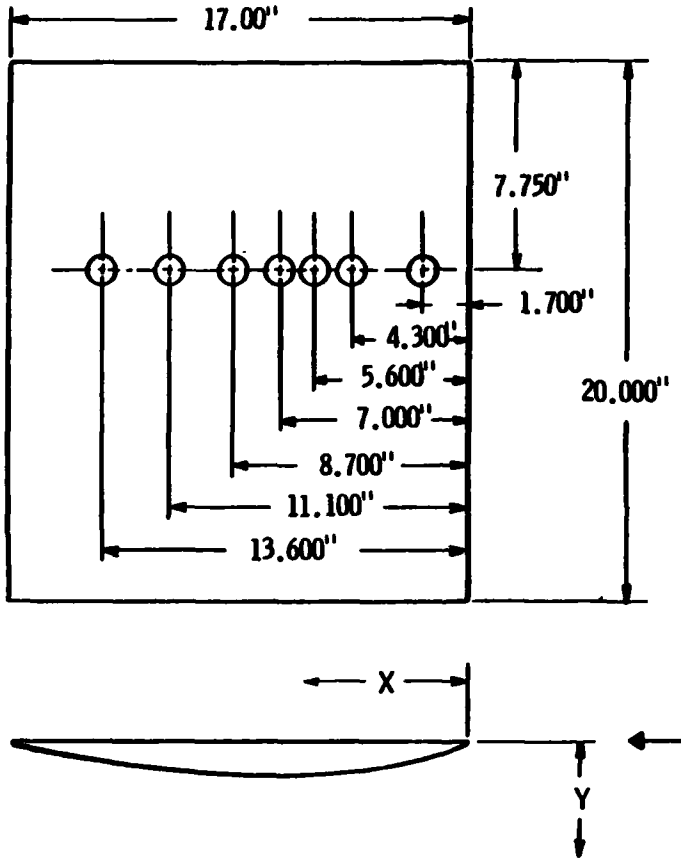


Figure 1. Test Section Arrangement in the 4.5 inch x 20 inch Water Tunnel.



X (in.)	Y (in.)
0	0
0.213	0.128
0.425	0.190
0.850	0.283
1.275	0.355
1.700	0.414
2.550	0.509
3.400	0.577
5.100	0.657
6.800	0.680
8.500	0.660
10.200	0.603
11.900	0.508
13.600	0.376
15.300	0.212
16.150	0.116
17.000	0

Figure 2. Details of the Curved Wall.

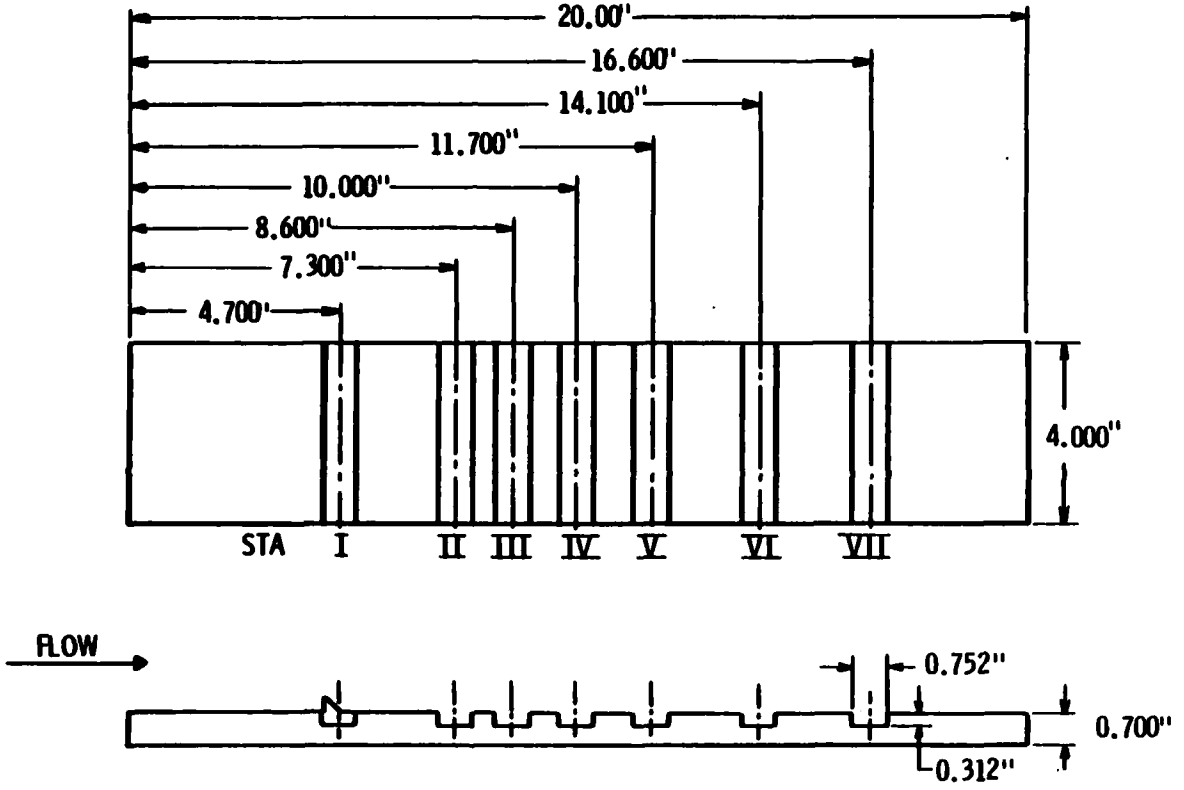


Figure 3. Test Stations for the Triangular Protrusions.

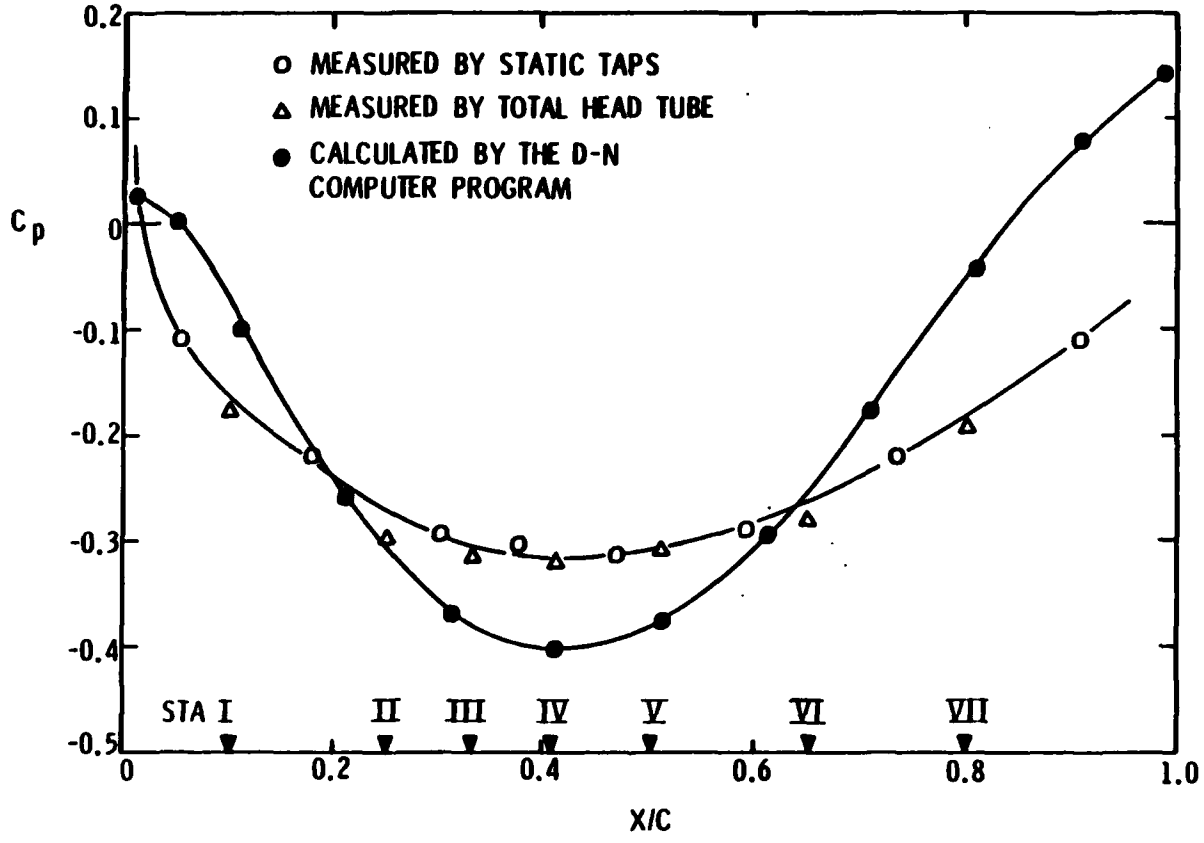


Figure 4. Pressure Coefficient on the Flat Wall in the Test Section.

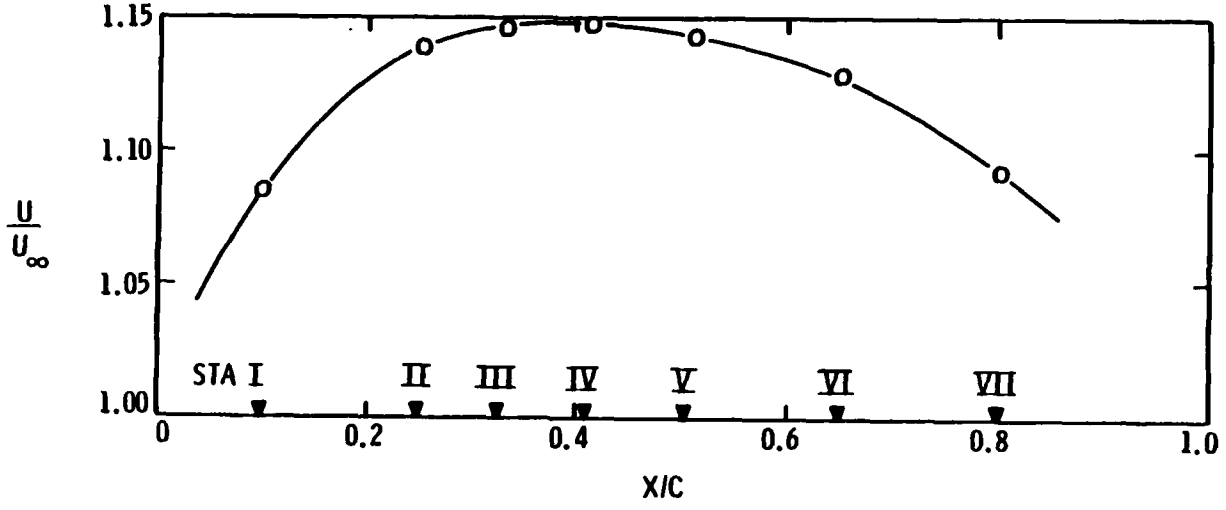


Figure 5. Velocity at the Edge of the Boundary Layer on the Flat Wall in the Test Section.

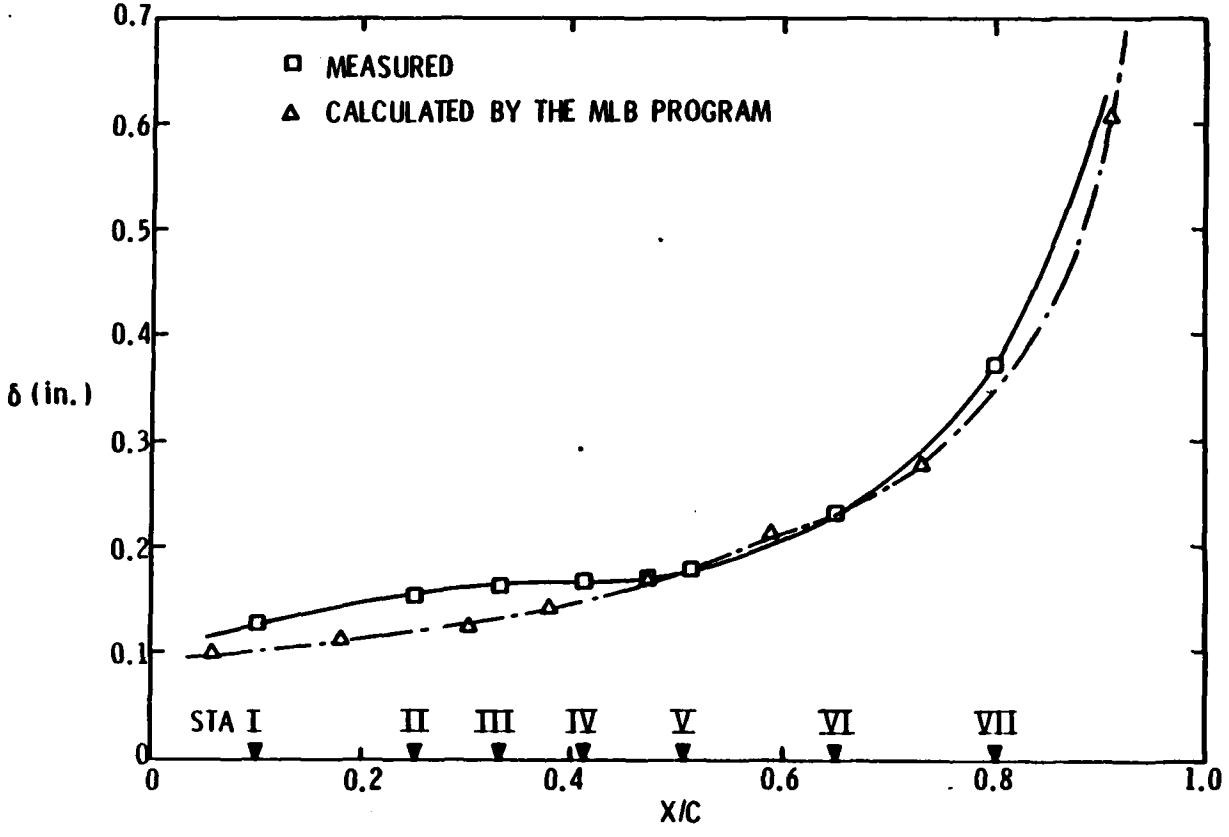


Figure 6. Boundary Layer Thickness on the Flat Wall in the Test Section.

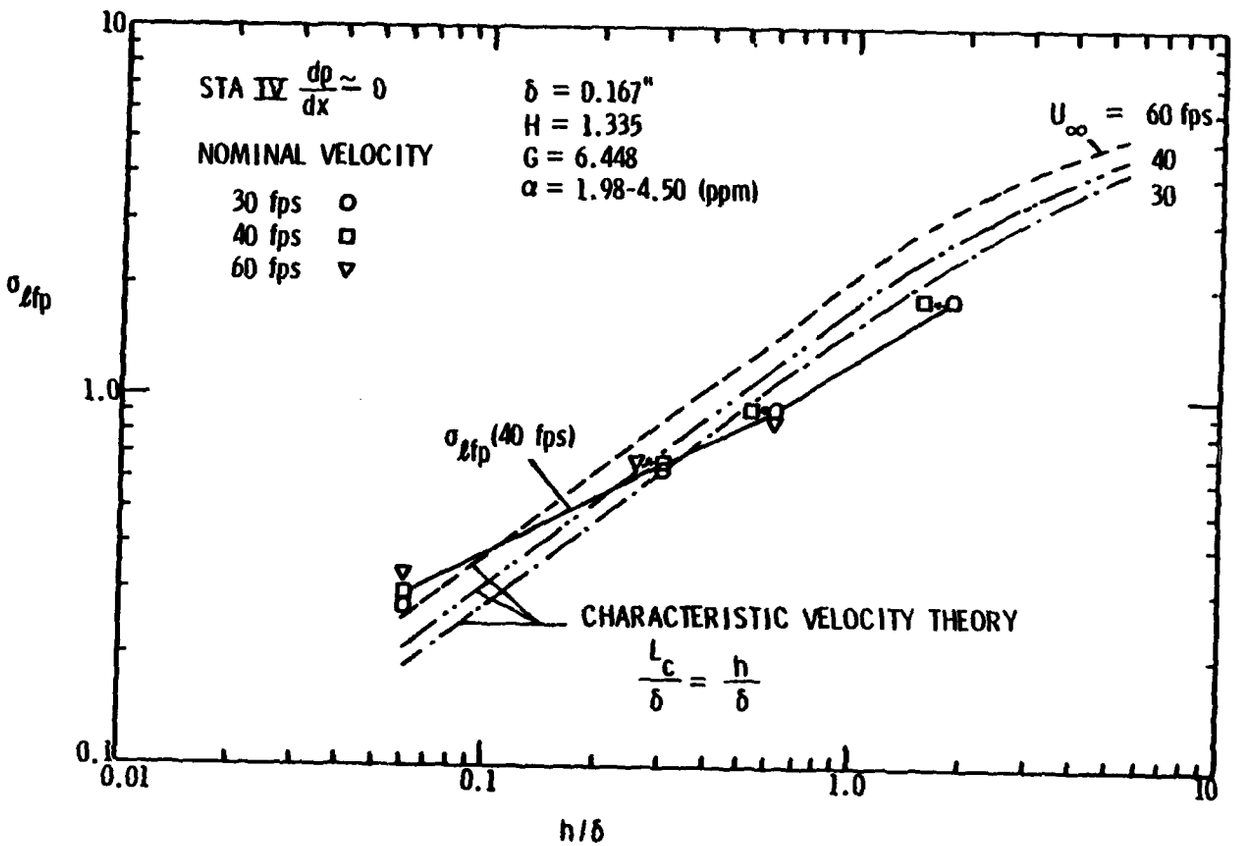


Figure 7. Variation of Cavitation Number with Relative Height $\left(\frac{dP}{dx} \simeq 0\right)$.

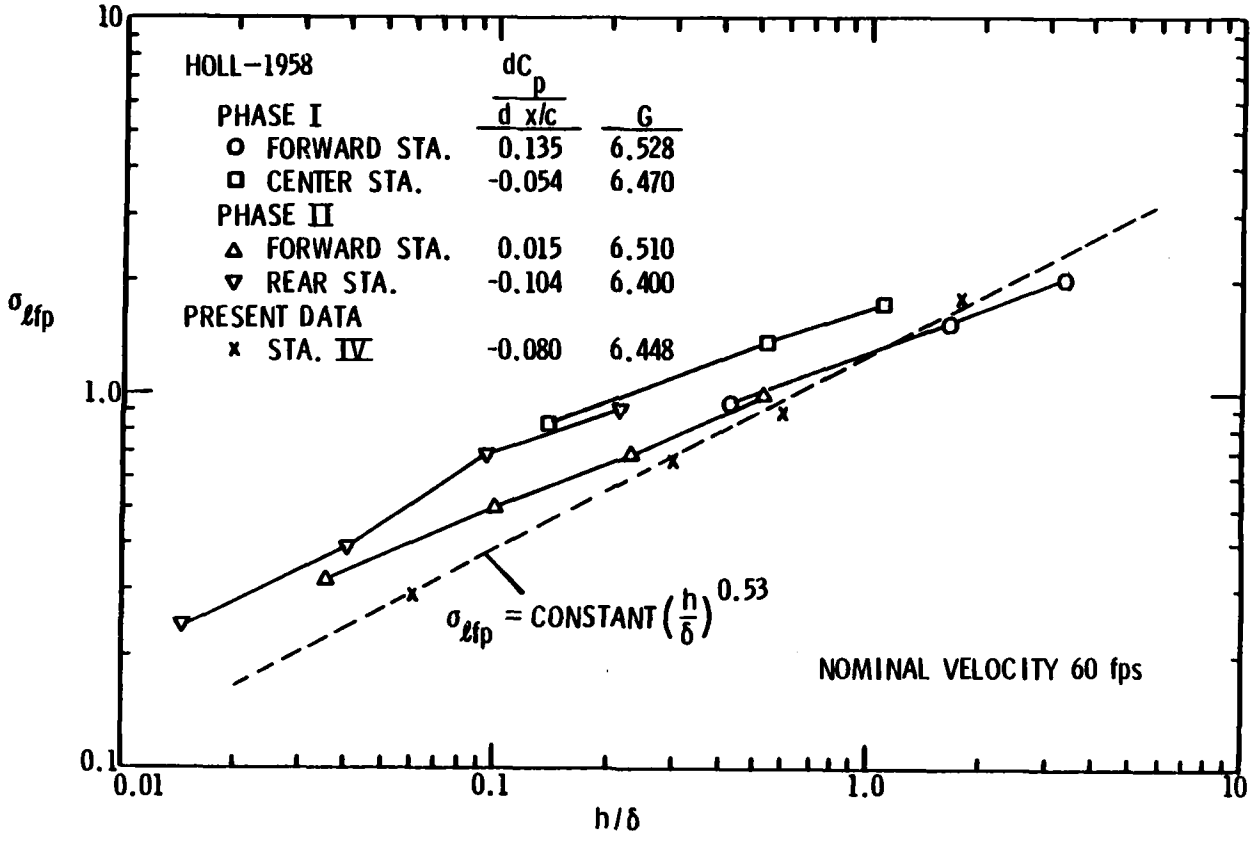


Figure 8. Comparison of $\sigma_{\ell fp}$ versus $\frac{h}{\delta}$ with that of Ref. [1].
Corrected to α of 3.7 ppm $\left(\frac{dP}{dx} \simeq 0\right)$.

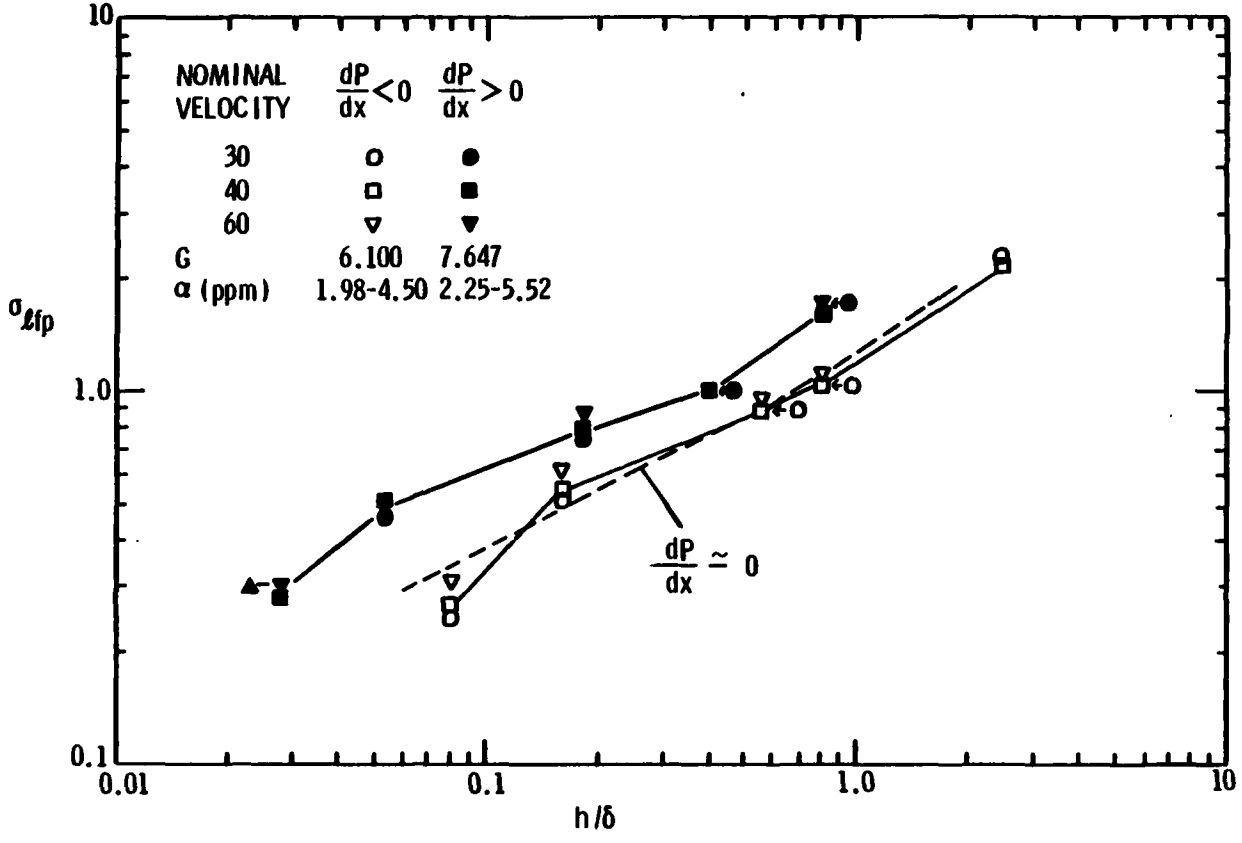


Figure 9. Variation of Cavitation Number with Relative Height for Finite Pressure Gradients.

	h/δ	$U_\infty \delta/\nu$	G
● $\frac{dP}{dx} \simeq 0$	0.058–1.790	43.400–86.800	6.448
△ $\frac{dP}{dx} < 0$	0.070–2.526	32.200–64.400	6.100
▲ $\frac{dP}{dx} > 0$	0.026–0.837	97.200–194.400	7.647

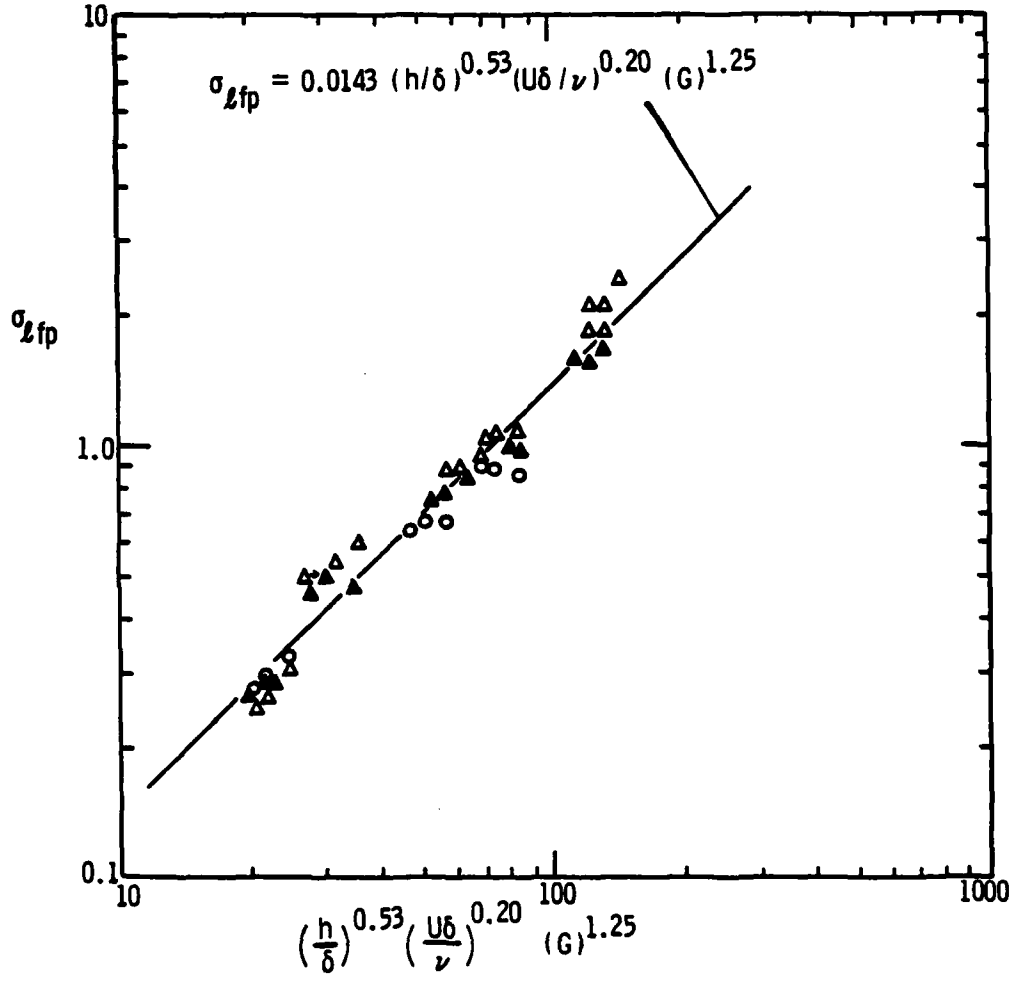


Figure 10. Power Law Cavitation Number Correlation for an Isolated Triangular Roughness (Present Investigation).

AD-P003 811

SOME APPLICATIONS OF FREE STREAMLINE THEORY

BY

C. C. HSU
Tracor Hydronautics

ABSTRACT

Applications are made of free streamline theory to flows involving wakes and separation bubbles. Results for two-dimensional flows past backward-facing step and normal plate in a solid wall channel are given and compared with existing experimental data. Some results for flow past airfoil section with leading edge separations are also given.

1.0 INTRODUCTION

Free streamline theory, in its classical form, deals with flows past objects which are bounded in part by separated regions throughout which the pressure is more or less constant. These flows involve a rich variety of physical phenomena, of both viscous and inviscid nature.

For separated flow, the outer flow corresponds to the potential flow about a cavity at constant pressure. In such a flow, the length of cavity as well as the drag depends on the pressure within the cavity. It has been a long standing problem to understand how the pressure and drag is in fact determined. In a recent paper Tulin and Hsu (1980) suggested a simple viscous modeling and provides the necessary closure of the problem. In brief, the pressure is determined by the matching of outer potential and inner viscous flows, where the matching is accomplished by requiring that the drag in the inner and outer flows are identical.

In this report, results for flows past two-dimensional backward facing step and normal plate in a channel are given and compared with existing experimental data. Some results for flow past foils with leading edge separation or partial cavitation are also given.

2.0 MATCHING OF INNER AND OUTER FLOWS

The drag for the inner viscous flow, based on the momentum integral equation, can be approximated by (for details see Tulin and Hsu (1980)):

$$C_D = 2\lambda \left(\frac{\ell}{D}\right) C_S \ (1 + \sigma)^{\frac{H+2}{2}} \qquad (1)$$

where C_D = drag coefficient
C_P = pressure coefficient
C_S = friction coefficient on the dividing streamline
D = length dimension of the body
H = boundary layer form parameter
ℓ = length of separation region (or cavity)
σ = cavitation number = $- C_p$
λ = a parameter equals 1 for a single sided cavity and 2 for a two sided cavity.

In general, the value of boundary layer parameters C_S and H are depended on flow conditions. In the present discussions, it is assumed that the Reynolds numbers are sufficiently high and the flows are fully turbulent and the values of C_S and H are taken to be constant. The value of length ℓ are depended on body shapes and external boundaries and can be expressed, for various flow conditions, in the form:

$$\frac{\ell}{D} = K \frac{\sigma^2}{C_D} \qquad (2)$$

Substituting (2) into (1) then gives

$$K = \sigma^2 / \left[2\lambda \ C_S \ (1 + \sigma)^{\frac{H+2}{2}}\right] \qquad (3)$$

Equation (2) may also be expressed as

$$K = \left(\frac{C_D}{\sigma^2}\right) \left(\frac{\ell}{D}\right) \tag{4}$$

The values of C_D and ℓ/D in Equation (4) for a given σ can of course be calculated by free streamline theories. The precise relationships between D_D, ℓ/D and σ generally depend on the cavity closure models. In the following, the external potential flow calculations are all based on single spiral termination model.

The matching of inner viscous and external potential flow is accomplished by requiring

$$K = \sigma^2 / \left[2\lambda\, C_S\, (1 + \sigma)^{\frac{H + 2}{2}}\right] \text{ (viscous flow approximations)}$$

$$= \left(\frac{C_D}{\sigma^2}\right) \left(\frac{\ell}{D}\right) \quad \text{(potential flow calculations)}$$

3.0 SOME APPLICATIONS

3.1 Flow Past A Backward Facing Step

The potential flow past a two-dimensional backward-facing step of height D in a solid wall channel of width H, with the aid of conformal mapping, can be analyzed by the free streamline theory, the solution can be shown to be

$$\frac{D}{H} = \frac{\sigma}{2}\left(1 - e^{-\frac{\pi \ell}{2H}}\right) \tag{5}$$

$$C_D = \sigma \tag{6}$$

The value of K based on Equation (3) with the values:

$$\lambda = 1$$

$$C_S = .013$$

$$H = 2.70$$

for viscous flow and Equation (4) with the values of C_D, ℓ/D and σ given by Equations (5) and (6) for various D/H are shown in Figure 1. The intersection of the two curves determine the approximated base pressure coefficient (σ) in the separated region. The extents of separated region for various D/H are given in Figure 2. Also shown in Figure 2 are the experimental data of Badri Narayanan (1974) and Kuehn (1980). The results are in fairly good agreement.

3.2 Flow Past A Normal Plate

The solutions for flow past a normal plate of height D may be approximated by

$$\frac{\ell}{D} \approx \frac{16}{\pi + 4} \left(\frac{1 + \sigma}{\sigma^2}\right) \tag{7}$$

$$C_D \approx 0.88 \ (1 + \sigma) \tag{8}$$

The effects of solid channel wall on the flow can be estimated by Hsu's simple wall correction rule (1980).

The value of K with the values:

$$\lambda = 2$$
$$C_S = 0.011$$
$$H = 2.70$$

for viscous flow and based on potential flow calculations for various D/H are given in Figure 3. The base pressure coefficients (σ) and the length of the separated region for various D/H are shown in Figures 4 and 5 respectively. In these figures experimental data of Arie and Rouse (1956), Roshko and Lau (1965) and Smits (1982) (all with stabilized split plates) are also given. The present calculations seem to be in qualitatively agreement with the existing data.

3.3 Leading Edge Separation on Foils

The potential flows past foils with partial cavitation may be estimated by the method suggested by Tulin and Hsu (1977). The values of K based on this approach for NACA64A006 section and based on Equation (3) with the values:

$$\lambda = 1$$
$$C_S = 0.011$$
$$H = 2.7$$

for viscous flow are shown in Figure 6. The pressure coefficients in the separated region and reattachment lengths, calculated by the matching principle together with the experimental data of McCullough and Gault (1949) are given in Figure 7. The calculations seem to be in very good agreement with data.

4.0 CONCLUDING REMARKS

Although all the calculations presented in the present paper are approximated in nature, the proposed theoretical approaches are in qualitative agreement with existing data. The separated flows are seen to be sensitive to the presence of the bounding surfaces such as tunnel walls. The values of C_S and H may not remain constant if wall spacings (H/D) are small. However with some further refinements it may be possible to predict flow characteristics involving separations.

REFERENCES

Arie, M. and Rouse, H. (1956) "Experiments on Two-Dimensional Flow Over A Normal Wall," J. of Fluid Mechanics, Vol. 1, pp. 129-141.

Badri Narayanan, N. A., Khadgi, Y. N., and Wiswanath, P. R. (1974) "Similarities in Pressure Distribution in Separated Flow Behind Backward-Facing Steps," Aeronautical Quarterly, Vol. 25, Part 4, pp. 305-312.

Hsu, C. C. (1980) "On Wall Effects in Cavity Flows," Proc. of 19th ATTC.

Kuehn, D. M. (1980) "Effect of Adverse Pressure Gradient on the Incompressible Reattaching Flow Over a Rearward-Facing Step," AIAA Journal, Vol. 18, No. 3, pp. 343-344.

McCullough, G. B. and Gault, D. E. (1949) "Boundary Layer and Stalling Characteristics of NACA 64A006 Airforce Section" NACA TN 1923.

Roshko, A. and Lau, J. C. (1965) "Some Observations on Transition and Reattachment of a Free Shear Layer in Incompressible Flow," Proc. of the 1965 Heat Transfer and Fluid Mechanics Inst., PP157-167.

Smits, A. J. (1982) "Scaling Parameters for a Time-Averaged Separation Bubbles," ASME J. Fluid Engineering, Vol. 104, No. 2, pp. 178-184.

Tulin, M. P. and Hsu, C. C. (1977) "The Theory of Leading Edge Cavitation on Lifting Surfaces With Thickness," Proc. of Symp. Hydrodynamics of Ship and Offshore Propulsion Systems.

Tulin, M. P. and Hsu, C. C. (1980) "New Applications of Cavity Flow Theory," 13th Symp. on Naval Hydrodynamics, pp. 107-131.

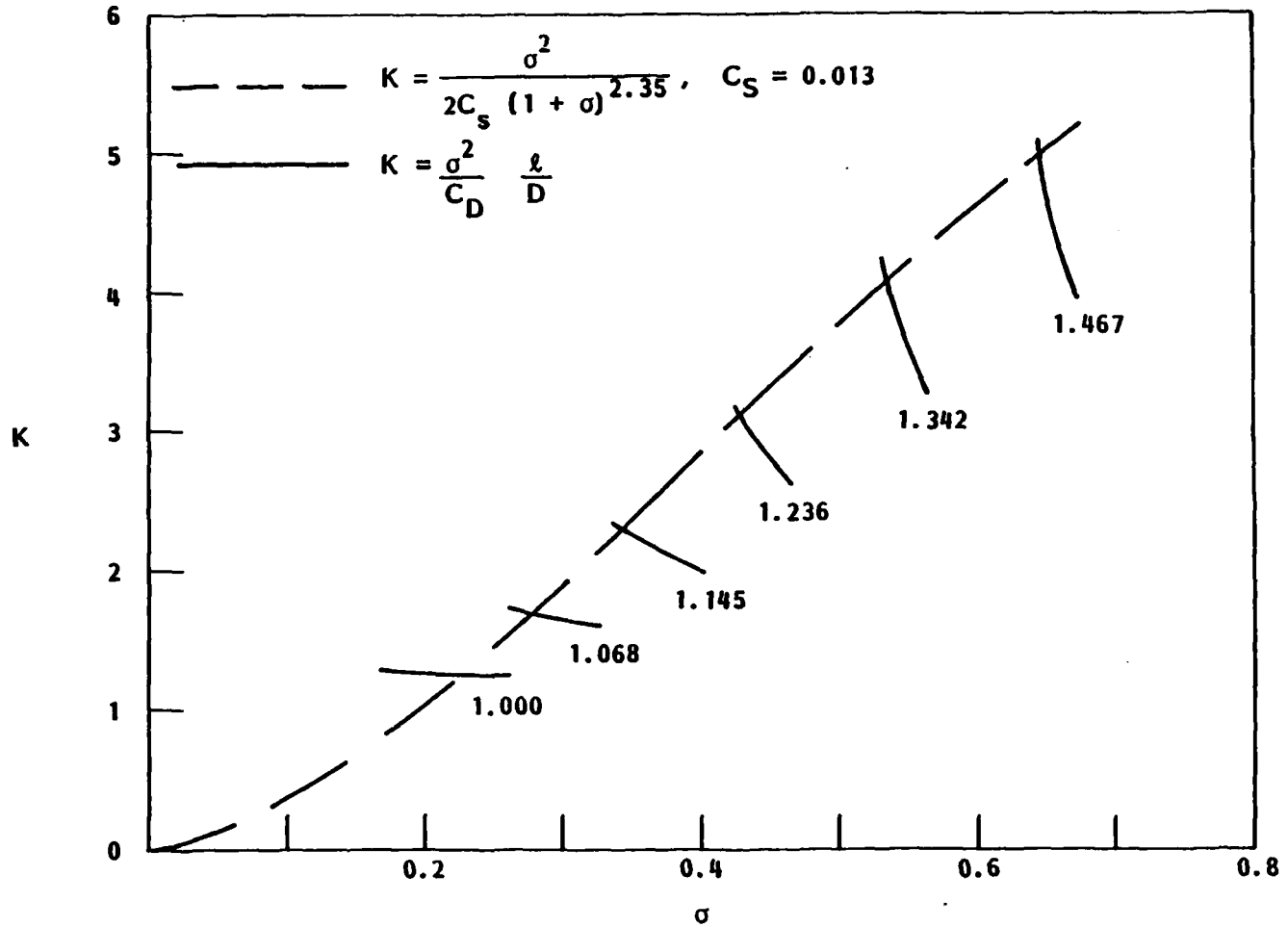


FIGURE 1 - MATCHING OF INNER AND OUTER FLOW OVER A STEP

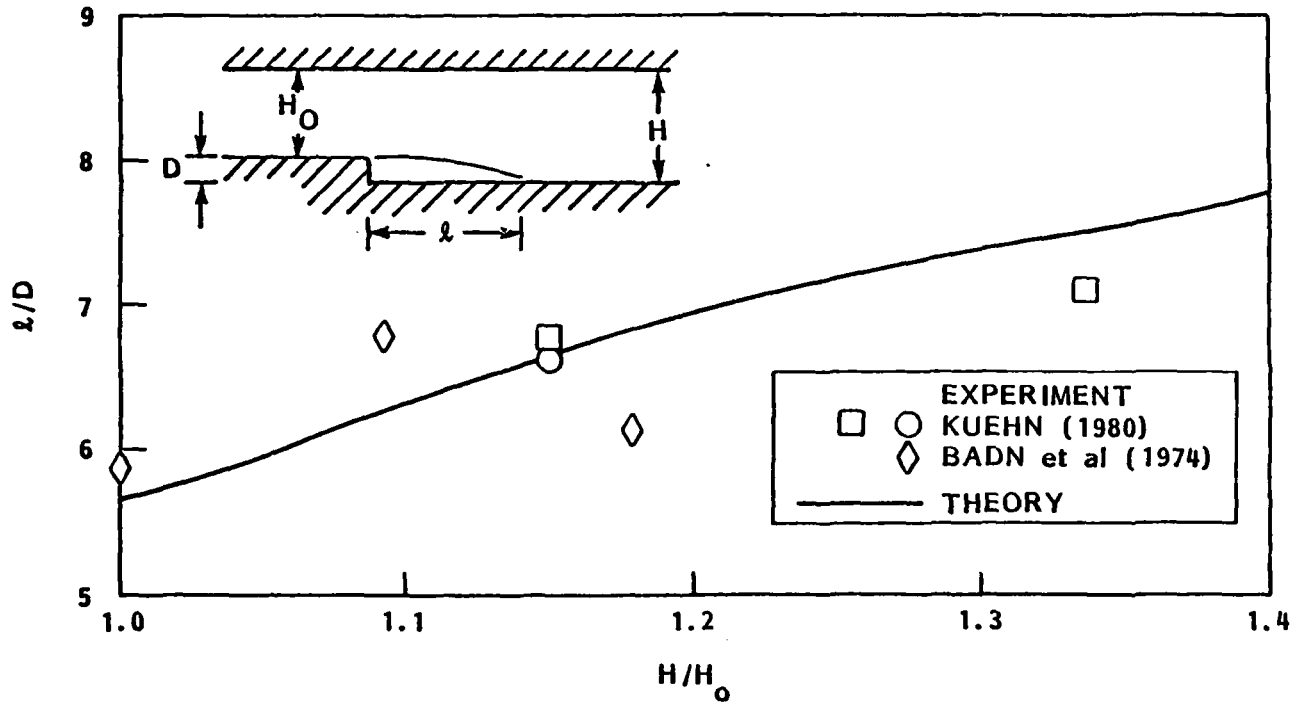


FIGURE 2 - DISTANCE TO REATTACHMENT VERSUS BLOCK RATIO

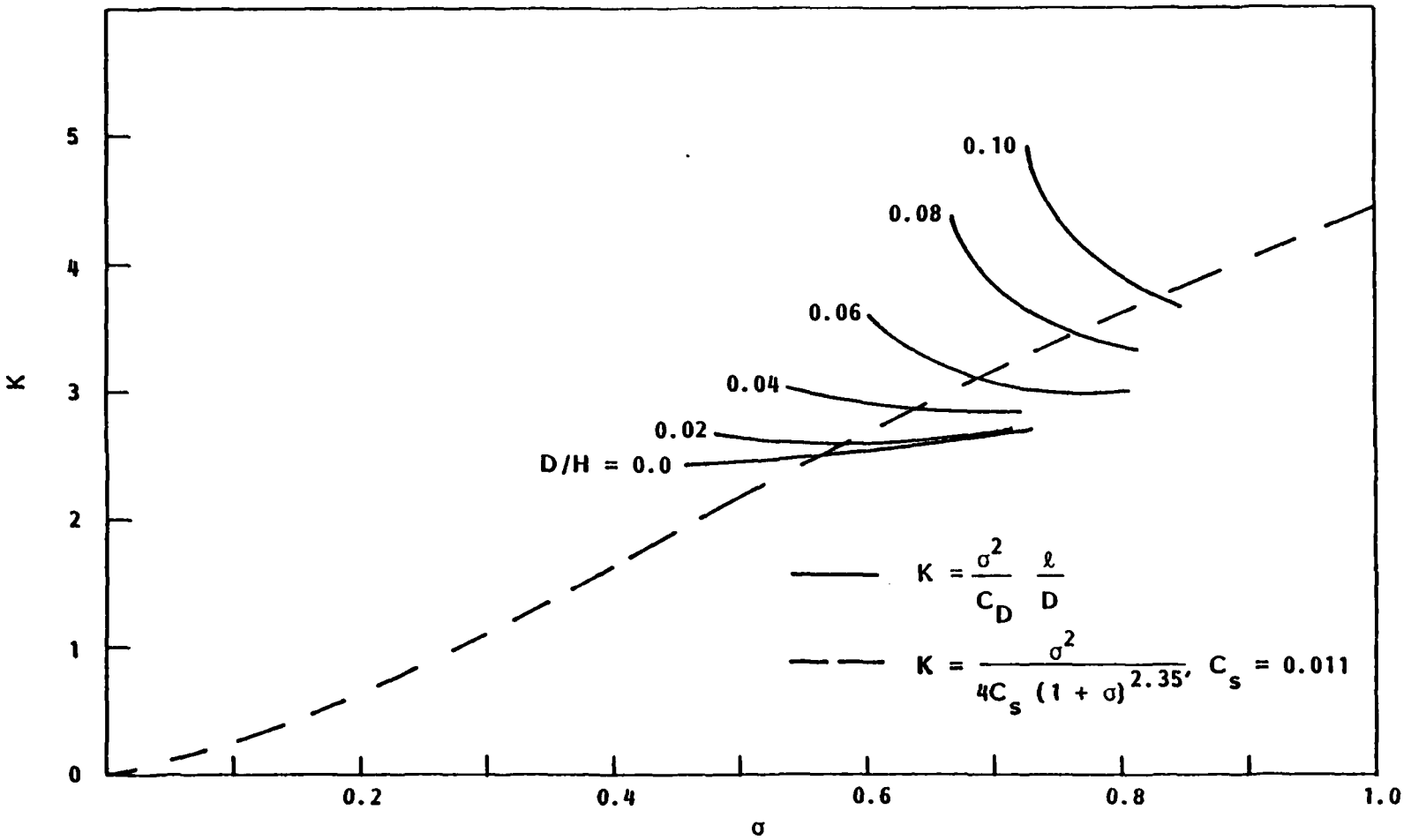


FIGURE 3 - MATCHING OF INNER AND OUTER FLOWS PAST A NORMAL PLATE

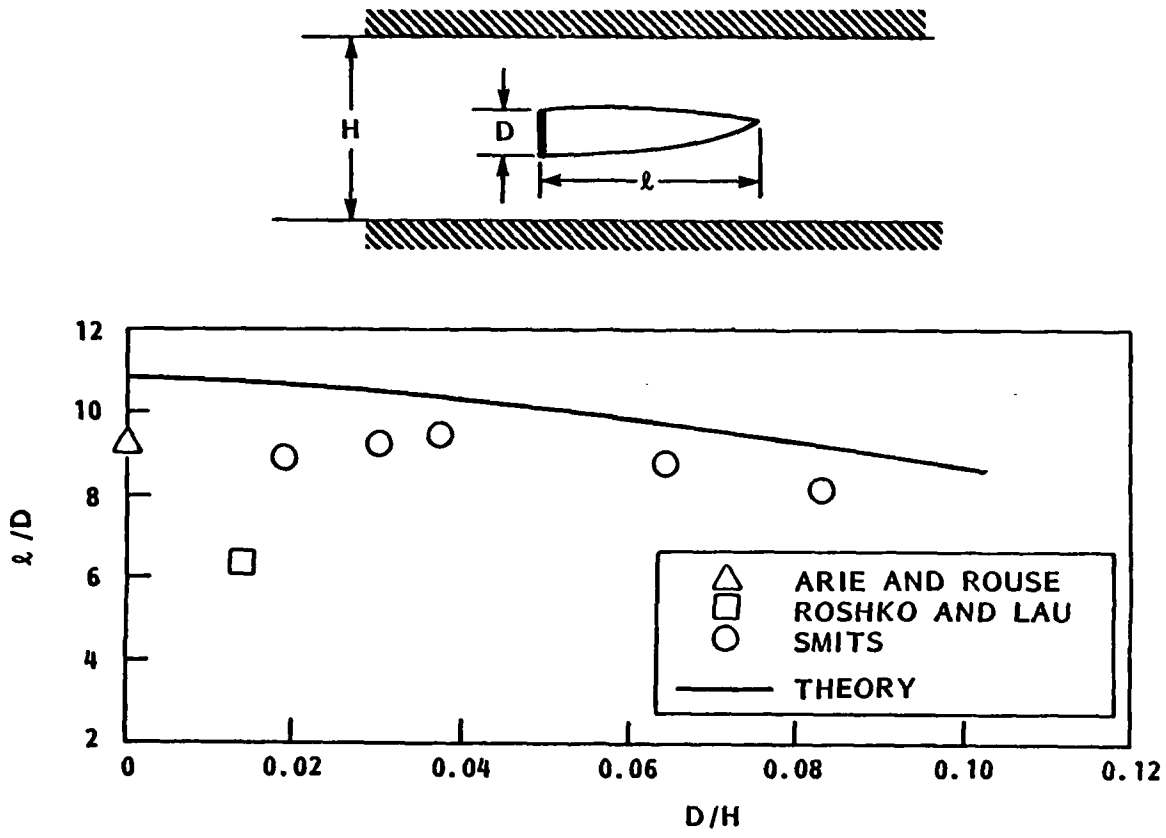


FIGURE 4 - DISTANCE TO REATTACHEMENT VERSUS BLOCKAGE RATIO

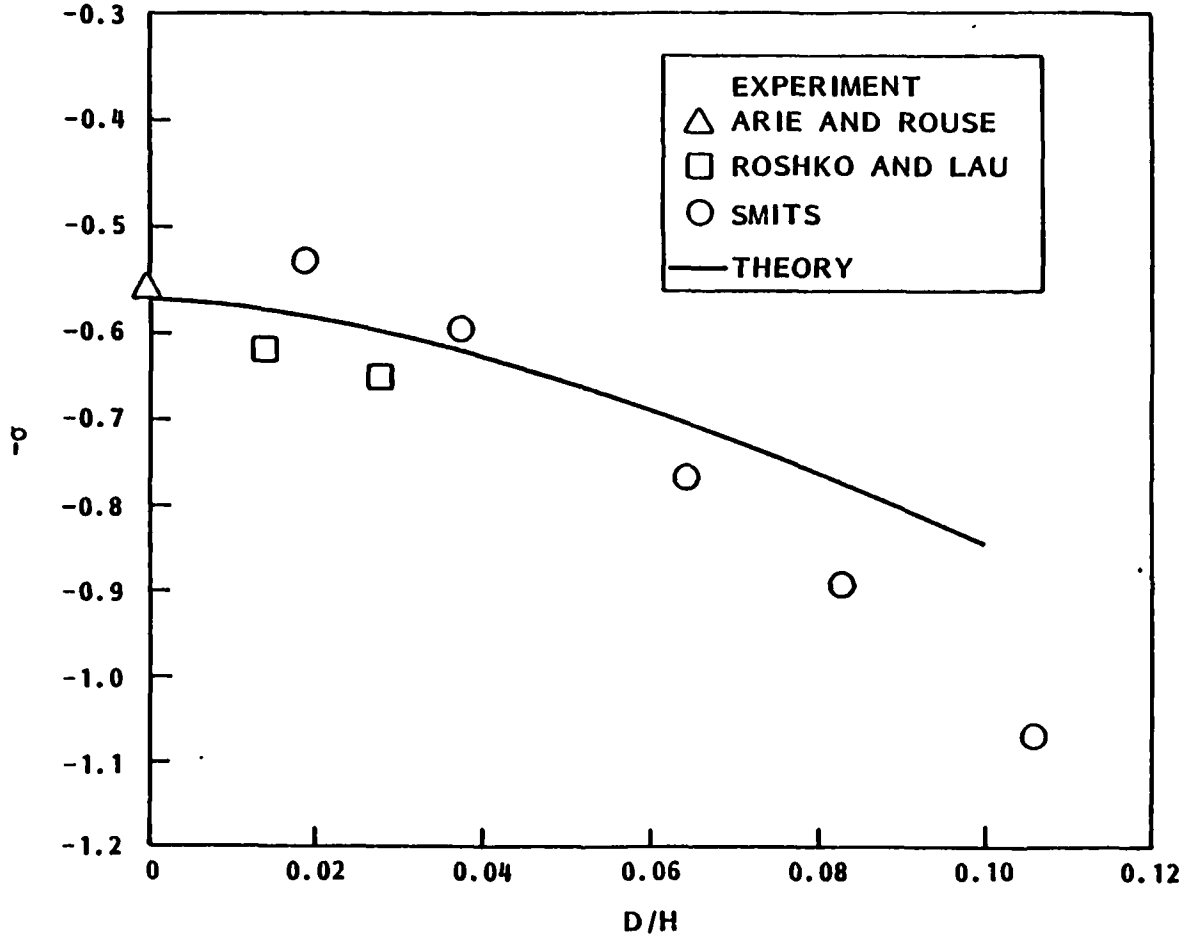


FIGURE 5 - BASE PRESSURE COEFFICIENT VERSUS BLOCKAGE RATIO

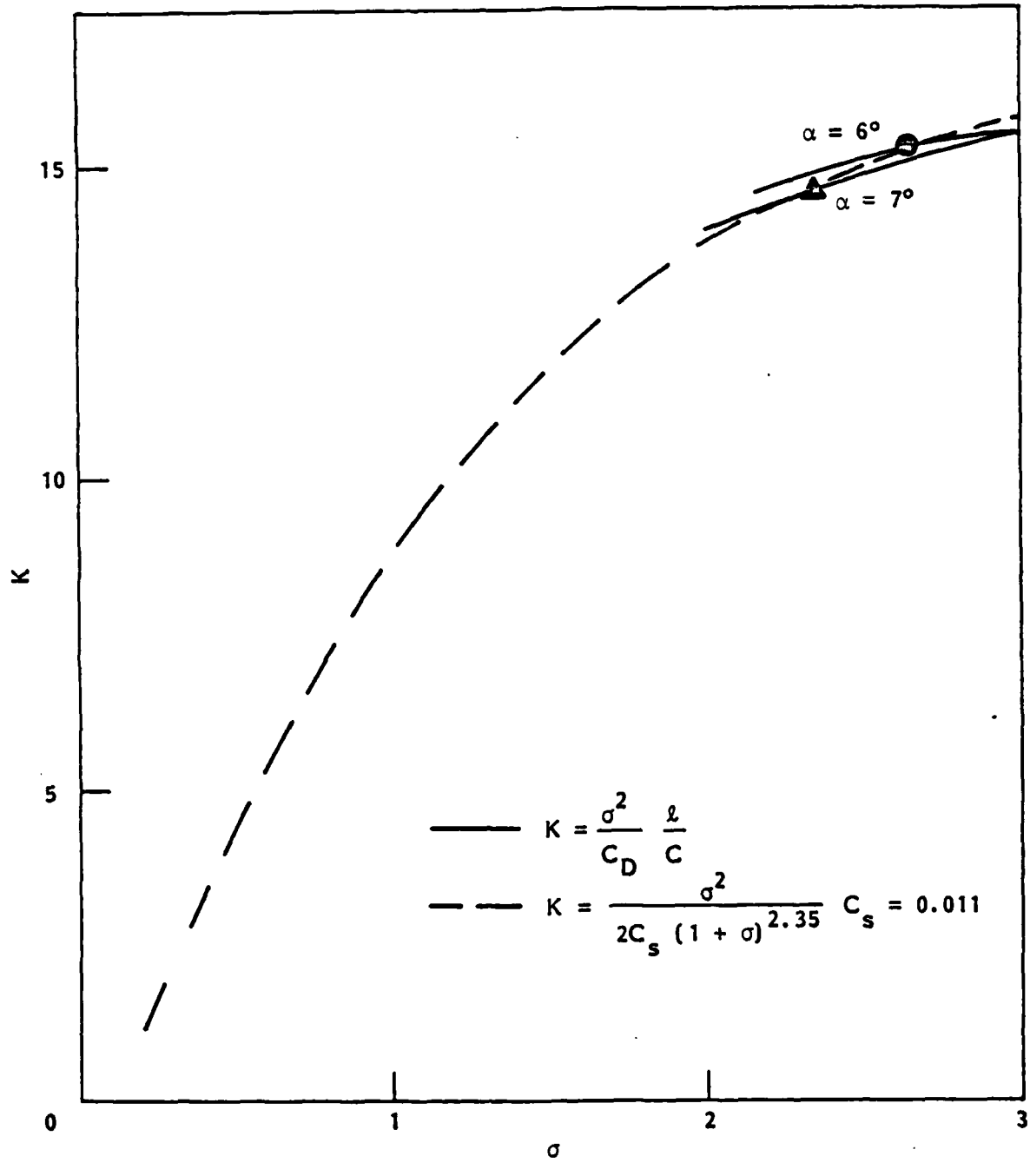


FIGURE 6 - MATCHING OF INNER AND OUTER FLOWS PAST A NACA 64 A 006 FOIL

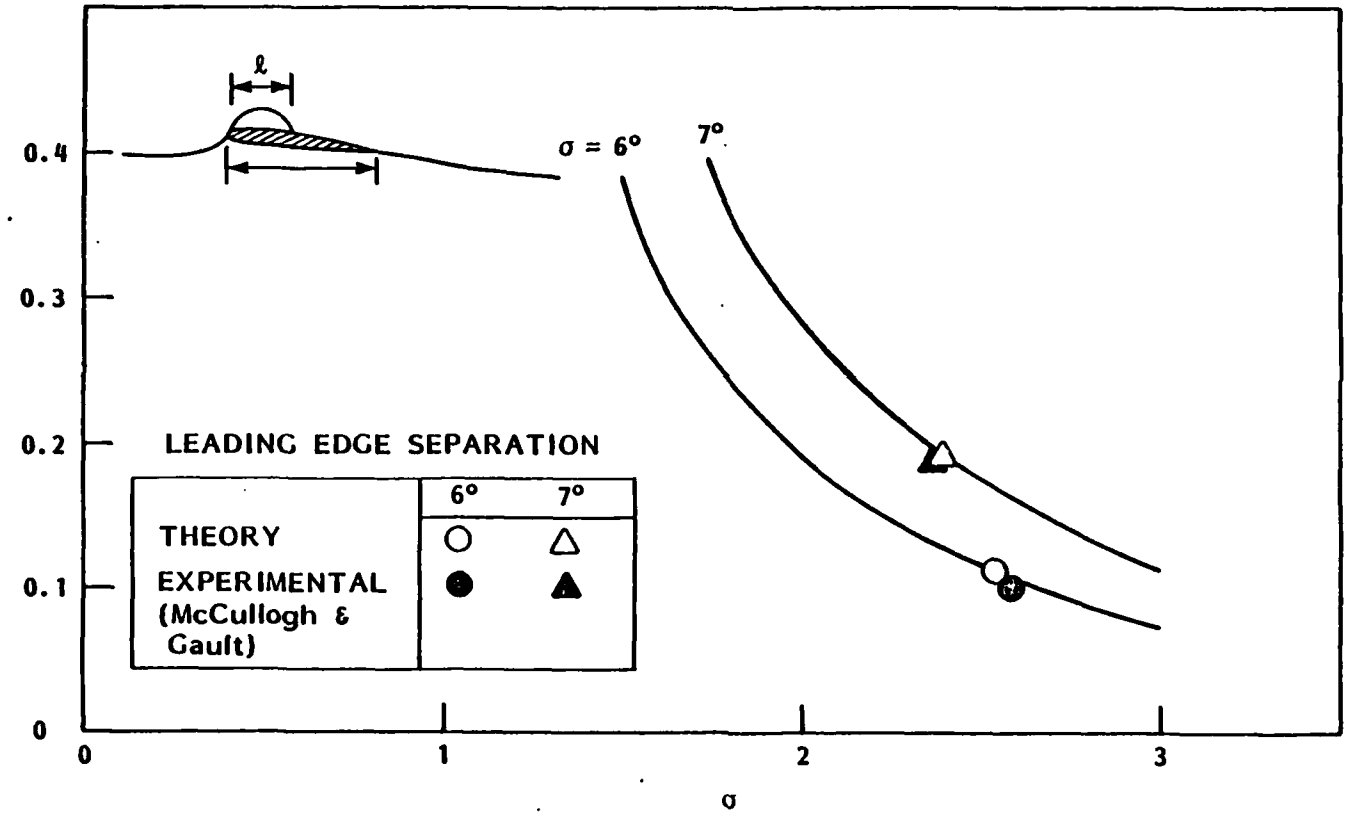


FIGURE 7 - CAVITY LENGTH-CHORD RATIO VERSUS CAVITATION NUMBER

NUMERICAL SOLUTIONS OF LIFTING SURFACE SHEET CAVITATION

A REVIEW OF RESEARCH AT M.I.T.

AD-P003 812

Robert J. Van Houten [1]
Justin E. Kerwin [1]
James S. Uhlman [2]

July 1983

The preparation of this review was supported by the Office of Naval Research Contract N00014-82-K-0198

For presentation at the 20th American Towing Tank Conference (ATTC), 2-4 August 1983, Davidson Laboratory, Stevens Institute of Technology, Hoboken, New Jersey.

1. Department of Ocean Engineering, MIT, Cambridge, MA.
2. Gould, Inc. Ocean Systems Division, Middleton, R.I.

INTRODUCTION

The theoretical investigation of cavitating flows about marine lifting surfaces has progressed very quickly in the last thirty years. This period of rapid advance can be said to have begun with the introduction by Tulin [1] in 1953 of the linearized theory for steady two-dimensional supercavitating flow at zero cavitation number. This work was soon followed by that of Tulin [2], Acosta [3] and Geurst [4,5], who introduced linearized theories for steady two-dimensional partially cavitating and super cavitating flows at finite cavitation number. Further analytic work has been done (for example [6],[7],[8]), but it was the advent of the high speed computer and associated numerical techniques that has been the major factor that has allowed the analysis of cavitating flows to become as extensive as it is presently. It is to this numerical aspect, specifically the numerical techniques that have been employed at MIT in the analysis of cavitating flows, that this review is directed.

When one endeavors to write a review of the numerical methods in use in a particular field one must define what one means by a numerical method. Computers are used in virtually all aspects of theoretical work, from evaluating the transcendental functions that may arise in an analytic solution to computational approaches that don't even require an explicit mathematical

formulation of the problem. In this review the numerical techniques that are described stem from an approach wherein the fundamental problem is recast in the form of coupled integral equations, which are attacked directly by techniques which are exact in some appropriate limit.

The first section of this overview contains a review of linear methods used in analyzing cavitating planar hydrofoils. The second section discusses the application of these methods to marine propellers. The third section discusses a recent numerical technique for the solution of the exact nonlinear 2-D steady cavitating hydrofoil problem. The work described herein was supported largely by the United States Maritime Administration and the U.S. Navy.

I. DEVELOPMENT OF LINEAR METHODS FOR PLANAR HYDROFOILS

Perhaps the earliest of the numerical methods employed at MIT in the analysis of cavitating flows was that of Widnall [9]. She formulated the linear integral equations for an oscillating super cavitating hydrofoil of finite span and solved them by expressing the unknowns as series of modes with unknown coefficients. This procedure resulted in a set of simultaneous linear algebraic equations for the unknowns, which could then be determined by computer solution of the matrix equation. She assigned the cavity lengths a priori and demonstrated that for long cavities the lift coefficients were insensitive to the assumed cavity length.

Golden [10] obtained a numerical solution of a two-dimensional cavitating hydrofoil of zero thickness in steady flow, for both the partial- and super-cavitating regimes. Assuming that the foil and cavity were slender, he linearized the kinematic and dynamic boundary conditions, and represented the foil and cavity as a source and vortex distribution on an axis parallel to the onset flow. The boundary value problem was then posed as a set of coupled integral equations, one of which satisfied flow tangency on the wetted portions of the foil and the other satisfying pressure constancy over the cavitated region. A Kutta condition was imposed at the trailing edge of the foil, where the vorticity was assumed to be zero. A final condition on the flow was obtained from a closure condition which required that the net

source strength be zero.

An important contribution of Golden's work was his development of an iterative method for determining cavity length at a given cavitation number. The cavity was assumed to start at the leading edge of the foil. In order to pose the boundary value problem, the length of the cavity had to be specified. The cavitation number corresponding to that length could then be solved for. The computed value of the cavitation number was then compared with the actual cavitation number, and the length adjusted. This procedure was iterated until the two values of cavitation number agreed.

In order to obtain a numerical solution, Golden represented the continuous singularity distributions as a finite number of elements in each of which the singularity strength was constant. The only exception to this was made at the foil trailing edge where the vorticity was taken to be a linear function, going to zero at the trailing edge. The length of the elements in the cavitated region was allowed to differ from that of the elements in the fully wetted region, and, in the case of supercavitation, the element length behind the foil could differ from that on the foil. At the leading edge of the cavity, the trailing edge of the cavity, and the trailing edge of the foil, half-size elements were used. Control points were empirically chosen within each element so as to give the best agreement with the theory of Geurst for the case of a flat plate. The agreement obtained was

in general acceptable when 20 to 30 elements were used over the foil chord.

Jiang and Leehey [11] extended the work of Golden to unsteady flow. They considered 3-D as well as 2-D hydrofoils, but restricted their attention to supercavitating foils. Their 3-D results were compared with experimental observations. Although unsteady effects were considered in formulating the dynamic boundary condition the form of the closure condition used was that appropriate for steady flow --that the net source strength is zero at all times.

Jiang and Leehey utilized a source/vortex lattice to represent the hydrofoil and its cavity. Each chordwise strip was discretized into a number of equal length elements, with the exception of the first two elements which were one-half that length. Following James [12], a line vortex was placed at the quarter-chord position of each element, and a tangency control point was placed at the three-quarter chord position. Line sources and pressure control points were given the opposite positions, with the source at the three-quarter chord point and the control point at the quarter chord point. This procedure was used because each boundary condition contains a local contribution from one distribution, and a principal value integral of the other distribution. The only exception to this procedure was made at the leading edge, where the first source and pressure control point positions were switched. In general,

this discretization was a successful one since it simplified the calculation of influence coefficients, and, for a given number of elements, proved to be more accurate than the method of Golden when compared with the steady results of Geurst.

Jiang and Leehey solved the unsteady flow problem as an initial value problem, starting with a steady solution. An initial estimate of cavity length was made at each time step in order to solve for a cavitation number, which could be compared with the actual cavitation number. The assumed cavity length was then adjusted and the process iterated. Kelvin's condition was satisfied by shedding vorticity into the wake at each time step, and the wake was made force-free by convecting wake vorticity at the speed of the onset flow.

Van Houten [13] extended the unsteady theory of Jiang and Leehey to the case of a partially cavitating foil. This work was restricted to foils of high aspect ratio, and the effect of aspect ratio on the volume velocity of the cavity was investigated. It is well-known that in incompressible 2-D flow, the volume velocity of the cavity must be zero. Otherwise, infinitely large pressure terms make the dynamic boundary condition impossible to satisfy. What is not so clear is the allowable volume velocity at large but finite aspect ratio. This subject has been addressed by several authors, who have reached somewhat different conclusions. Tulin [14] considered foils of moderate aspect ratios, where the product of the reduced

frequency and the natural log of the aspect ratio is of order one, and concluded that unsteady effects are felt exclusively in the cavity closure condition, so that there is no dependence on aspect ratio. In other words, Tulin found that the terms which are infinite in the 2-D case are negligible at moderate aspect ratios. Peters, Goodman, and Breslin [15] concluded that for high aspect ratios, the volume velocity varies inversely as at least the square of the aspect ratio. Although it might be argued that "high" aspect ratios do not overlap "moderate" aspect ratios, the conclusions of these two investigators do not appear to be compatible.

Van Houten obtained the inner solution of the high aspect ratio problem by numerical procedures similar to those of Jiang and Leehey. The cavity was assumed to start at the leading edge of the foil, and the cavity length was allowed to vary from zero to several chord lengths within the oscillation cycle. The correct unsteady form of the closure condition was used. The inner problem was assumed to be two-dimensional except for the requirement that the solution match with the outer solution at a distance of many chord lengths from the foil. This outer solution was taken to be a line source distribution, the strength of which was known after obtaining the inner solution at various spanwise positions. Once the outer solution was obtained, the inner solution was again found, and the procedure iterated until convergence. It was found that most of the 3-D effects could be accounted for in the initial inner solution by taking the arbitrary constant in the

2-D source potential to be minus the natural log of the span of the foil.

Van Houten followed Jiang and Leehey in using alternating discrete sources and vortices, but spaced them differently. The singularities were placed at equal intervals in a transformed coordinate system which was obtained from a Glauert type transformation wherein the element spacing is a maximum at the trailing edge and a minimum at the leading edge. This spacing was used in order to obtain good resolution in calculating small cavities. The spacing of singularities was identical at all time steps, and the cavity was assumed to encompass an integer number of discrete elements. At each time step trial cavity lengths were tested until the actual cavitation number lay between those calculated for adjacent cavity termination points. An interpolation formula was then applied to the calculated singularity strengths. This method allows one to invert a reasonable number of matrices before solving the initial value problem, and thereby avoid solving simultaneus equations at each time step.

An example of the resulting cavity profiles on a flat plate in a gust is given in figure 1. This shows the typical slow cavity growth and rapid collapse which is found experimentally. The cavity termination passes smoothly over the trailing edge of the foil. Figure 2 shows that the cavity length variations are

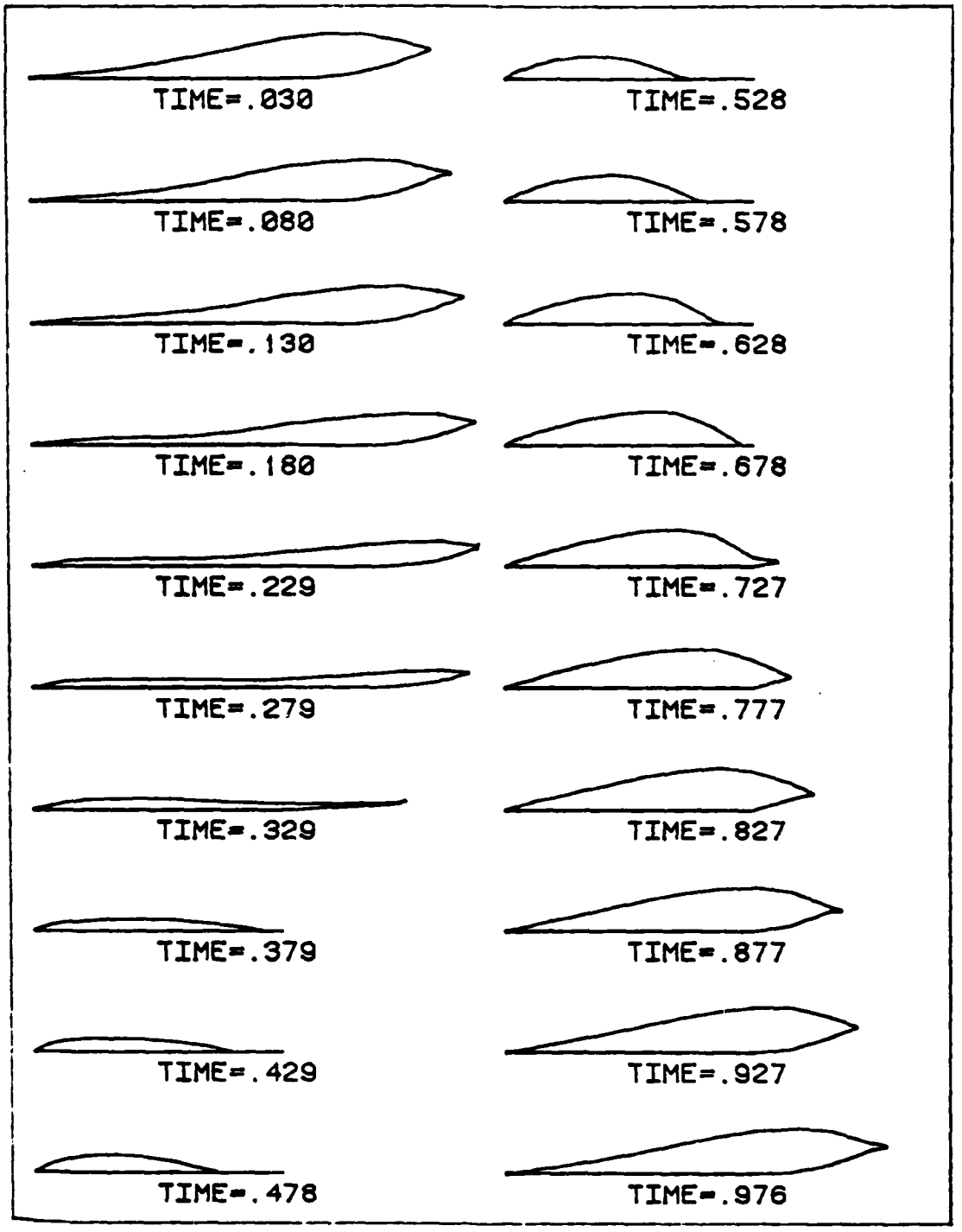


FIGURE 1 CAVITY PROFILES VS TIME
VERTICAL GUST, ALPHA=0-.1, SIGMA=.25, AR=10, K=1

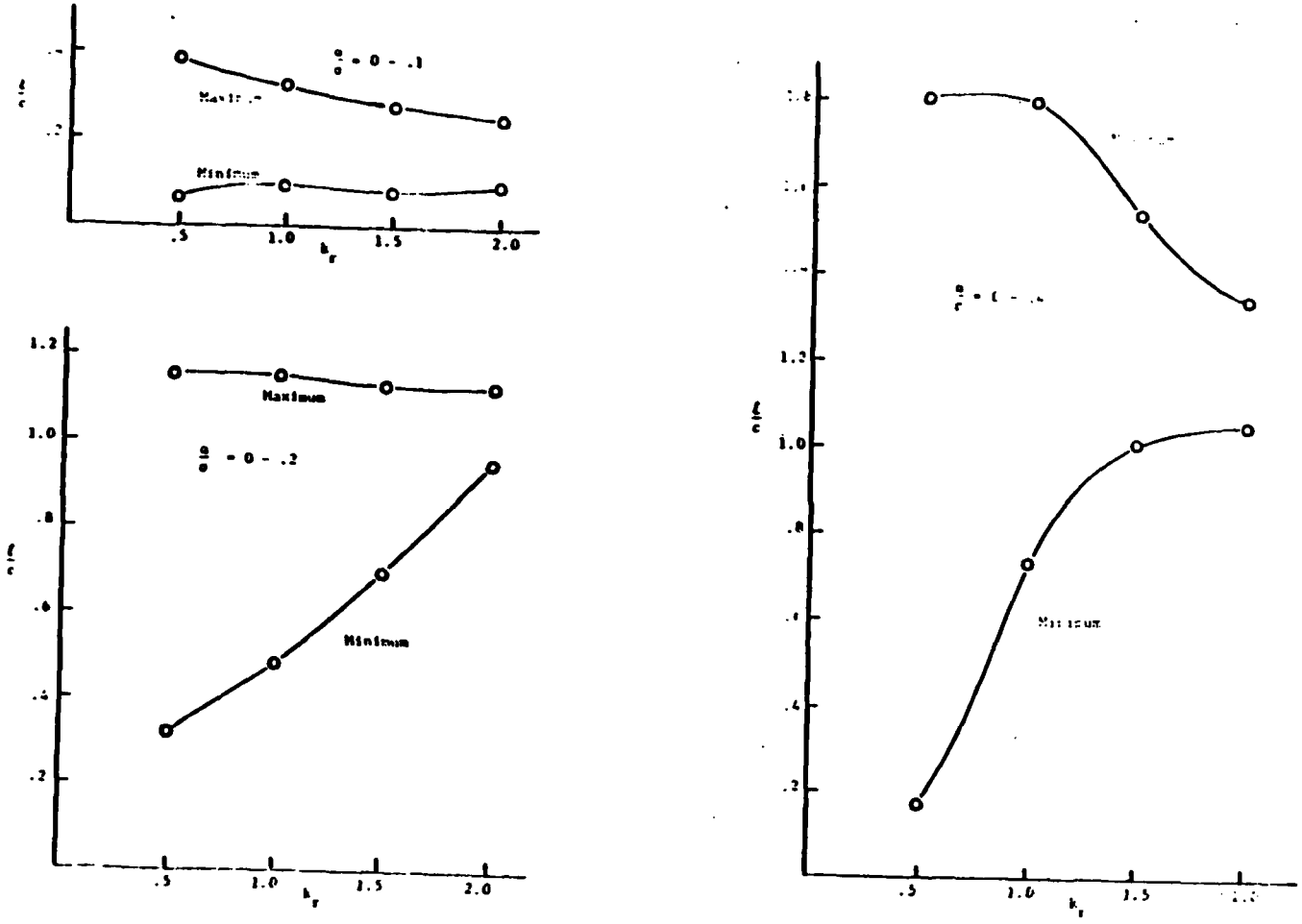


Figure 2 Maximum and minimum cavity lengths vs. reduced wavenumber for flat plate in gust.

reduced significantly by an increase in reduced frequency, and figures 3 and 4 show the effect of aspect ratio on the cavity volume and length variations. These latter results indicate that although aspect ratio plays a significant role in determining volume velocity, it does not have the importance indicated by the results of Peters, Goodman, and Breslin. The reason for this disagreement has not been resolved.

Van Houten and Sayre [16] extended the numerical method to account for the presence of cavity gas. It was assumed that a constant mass of gas existed in the cavity at all times, and that it behaved according to the polytropic gas law. The cavity length was iterated at each time step until this gas law was satisfied. This model predicted that cavity gas can have a sizeable effect on the variability of cavity length and volume.

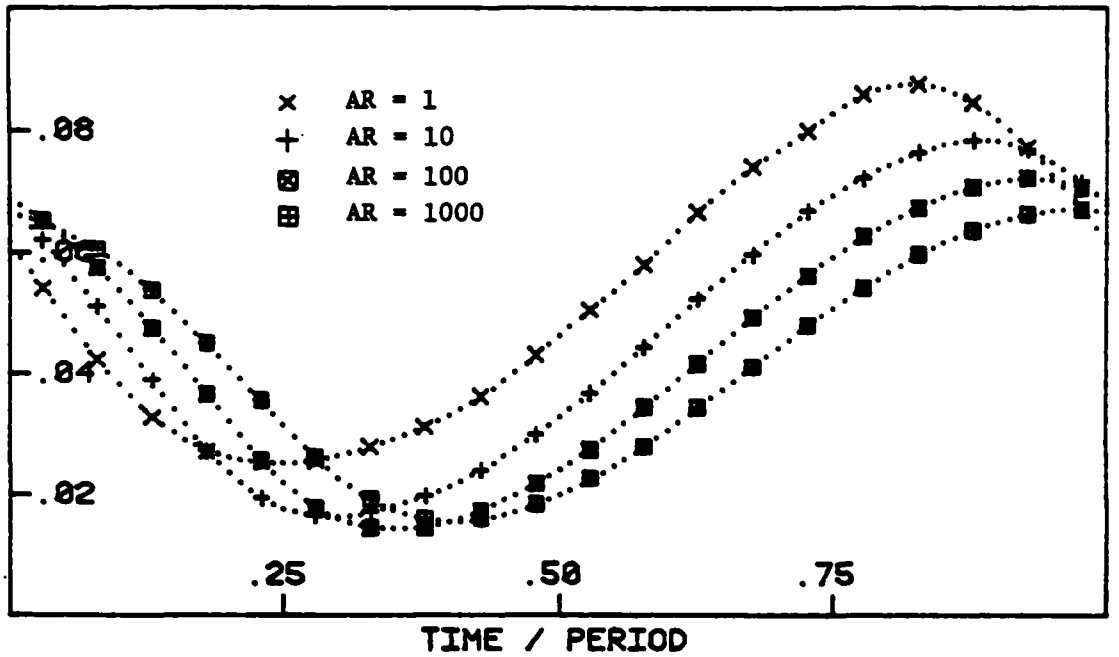


FIGURE 3 Cavity volume vs time for four values of aspect ratio. (Flat plate in gust, α = 0-.1, σ = .5, k_r = 1)

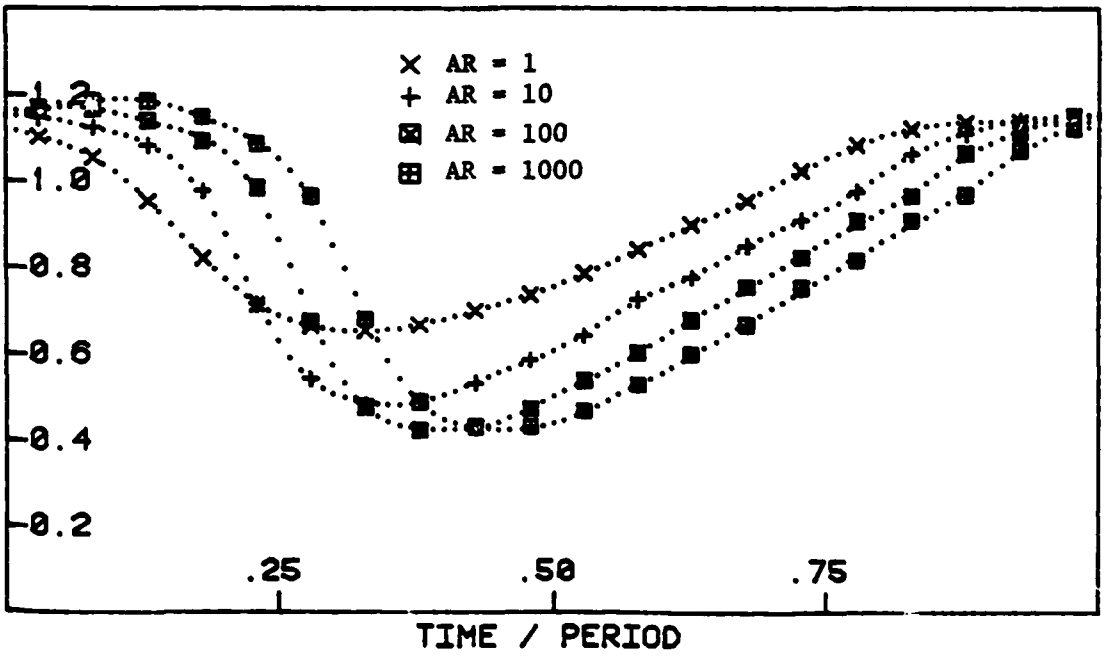


FIGURE 4 Cavity length vs time for four values of aspect ratio. (Flat plate in gust, α = 0-.1, σ = .5, k_r = 1)

2. APPLICATION OF LINEAR THEORY TO UNSTEADY PROPELLER SHEET CAVITATION

The numerical method of solution of the high aspect ratio unsteady cavitating hydrofoil problem was extended to the case of a propeller operating in a non-uniform wake field by Lee [17]. This was done by combining the method of solution for a non-cavitating propeller developed by Kerwin and Lee [18] with the cavity solution developed by Van Houten [13].

As in the case of a planar hydrofoil, a time-domain solution was necessary due to the non-linear effect of the changing cavity length. It was in anticipation of this that the non-cavitating propeller program of Kerwin and Lee [18] was formulated in the time domain. In the propeller case, the time step was determined from a prescribed propeller rotational increment. Starting from a suitably devised initial condition, the propeller was rotated in discrete time steps through several propeller revolutions until a periodic solution was obtained. The number of time steps per revolution determined the number of harmonics of loading and cavity volume velocity which could ultimately be derived from the time record. It was found that sixty time steps were sufficient to resolve at least up to the twice blade rate harmonic of the fluctuating force and cavity volume.

While conceptually similar, the propeller problem is made much more difficult due to the complicated geometry of the blade and its trailing vortex wake and due to the presence of multiple

blades. The former was the main motivation for using a lattice of discrete line vortex and source elements to represent the continuous singularity distributions. Once the geometrical problem of defining an arbitrary blade and wake surface was worked out, propellers with extreme skew, rake and radial pitch variation could be accommodated as easily as more conventional designs.

The presence of multiple blades was treated in an iterative way as developed for the non-cavitating case in [18]. The boundary value problem was solved on a single "key" blade, while the singularity strengths on the other blades were presumed to be known. An estimate of their strengths was obtained from the key blade solutions obtained at previous time steps where the key blade occupied the current position of each of the other blades. This estimate was not very good until the key blade completed at least one revolution. Since several revolutions had to be computed anyway, this did not add significantly to the computational effort required.

The arrangement of line singularities used in [17] is shown in figure 5. The key blade is divided into nine chordwise panels as shown. Within each panel, ten line source and vortex elements are arranged in a manner similar to that used by Van Houten [13], and the same arrangement of control points for the dynamic and kinematic boundary conditions is employed.

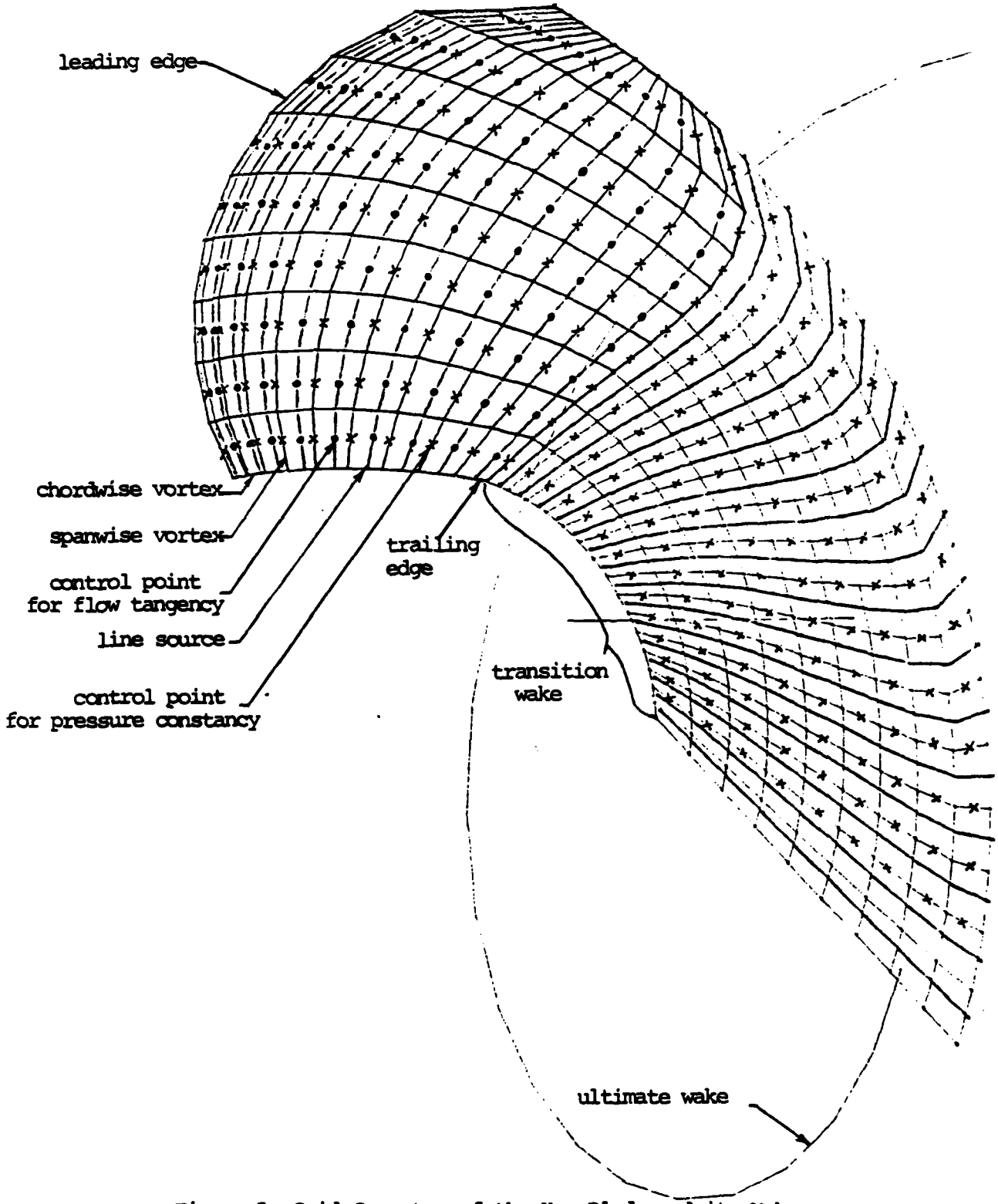


Figure 5 Grid Geometry of the Key Blade and its Wake

Downstream of the blade is a transition wake region which contains the trailing and shed vorticity associated with the unsteady loading, and a set of radially oriented cavity source lines. Beyond the transition wake is the ultimate wake which consists of a single concentrated helical tip vortex and a concentrated hub vortex (the latter not shown in figure 5). The strengths of the ultimate wake hub and tip vortex are determined from the circumferential mean loading, and are therefore independent of time.

While provision was originally made for the vortices in the transition wake to split at the mid-radius and to deform continuously into the ultimate hub and tip vortex, this feature is presently suppressed and figure 5 shows the vorticity rolling up abruptly at the beginning of the ultimate wake. It is expected that this wake representation will eventually be replaced by a more realistic model similar to that developed by Greeley and Kerwin [19].

The source lines on the blade represent both blade thickness and the presence of the cavity. The former is known and presumed independent of time. The cavity sources are non-zero only in the region of the blade covered by the sheet cavity, and the boundary of the latter region must be determined by iteration. The sources in the transition wake would be non-zero only if the cavity were found to extend beyond the trailing edge.

The arrangement of singularities on the other blades is similar, except that fewer elements are used in order to reduce storage and computer time.

Once the geometrical arrangement of the singularities is determined, the solution process can begin. The first step in his process is to solve the steady, non-cavitating boundary value problem. This can be done very quickly by setting all of the inflow wake velocities to their circumferential mean values, and by setting the loading on the other blades equal to that on the key blade. Starting with this as an initial condition, the non-cavitating unsteady solution is next obtained. This is accomplished by time-stepping the propeller through three revolutions, at which point a reasonably periodic loading is obtained.

The cavity solution process now begins, using the non-cavitating unsteady loading just obtained as an initial guess at each time step. In those cases in which the cavity disappears completely during a significant portion of a propeller revolution, it is expedient to start the cavity solution at a time step somewhat before inception.

The steps in the cavity solution are shown pictorially in figure 6. The correct cavity length, and the resulting strengths of the sources and vortices, are found separately for each chordwise

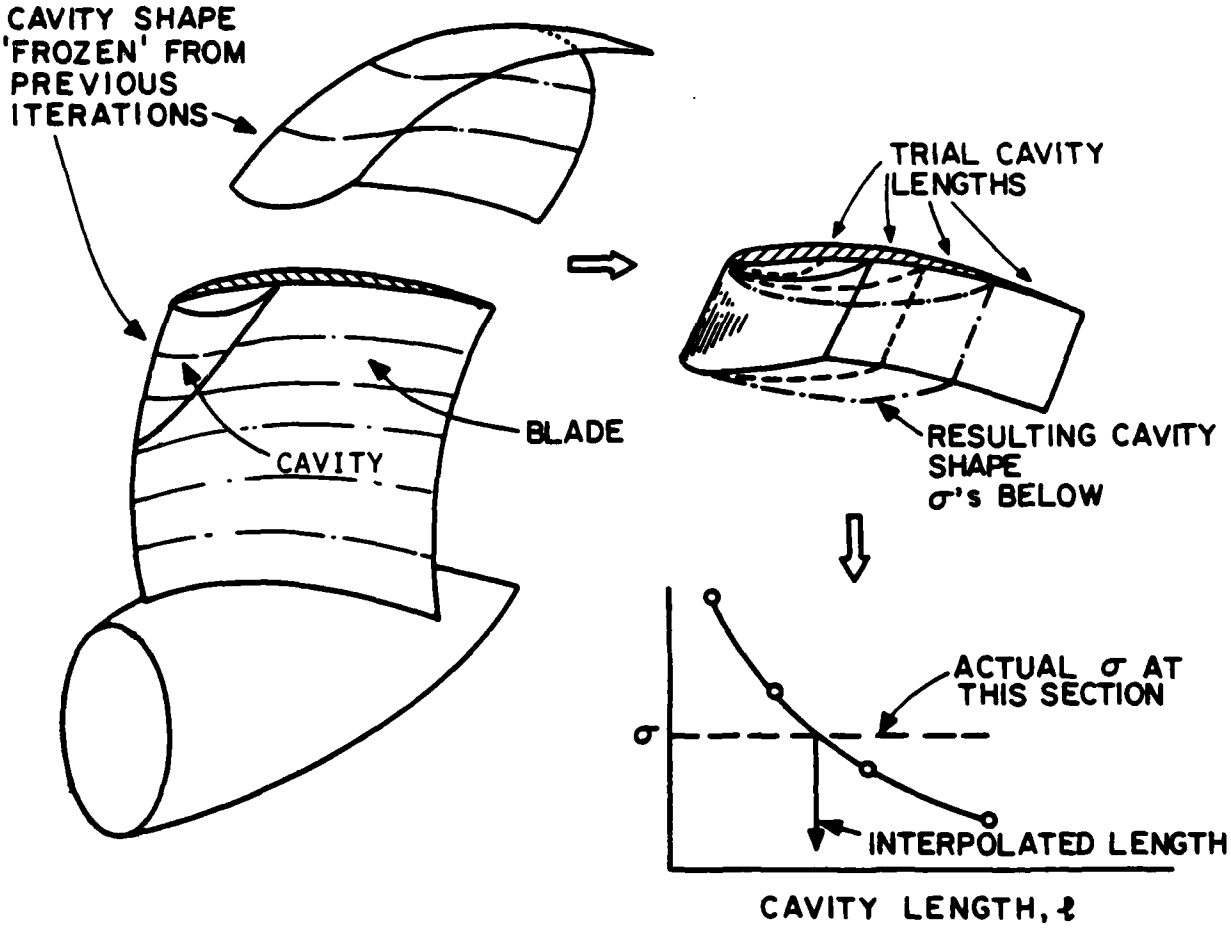


Figure 6 Pictorial of iterative solution for three-dimensional cavity.

panel. Following the work of Van Houten [13], the boundary value problem is solved for several trial cavity lengths, and the resulting non-dimensional cavity pressure is obtained for each trial. The correct length and the resulting singularity strengths is then obtained by linear interpolation. The influence of the other chordwise panels, as well as the other blades, is obtained from the known singularity strengths obtained earlier in the solution process.

This is accomplished by adding yet one more level of iteration. At the first time step, the cavity solution is first obtained for the innermost chordwise panel, assuming that there is no cavitation elsewhere. The cavity obtained for this panel is then frozen, and a solution is obtained for the next panel, allowing for the presence of the cavitation just obtained for the preceding panel. The process is then repeated out to the tip, back to the hub and out again until a converged solution is obtained. Each of these individual panel solutions requires the iteration on cavity length described earlier.

The propeller is then advanced by one angular increment, and the entire process is repeated. However, rather than starting from an assumed condition of zero cavitation, the cavity on all chordwise strips except the one that is being worked on is initialized to the converged value from the preceding time step. Since the extent of cavitation does not change greatly in one time step, the convergence of the process is very rapid.

The cavity solution is carried out typically for two additional complete propeller revolutions. Thus a total of five propeller revolutions are computed, the first three being without cavitation.

A graphical representation of a typical solution is shown in figure 7. The propeller and wake field is from Wilson et.al.[20]. Integration of the cavity ordinates yields total cavity volume, whose time history is shown plotted in figure 8.

One of the principal objectives in obtaining a solution of the unsteady propeller cavitation problem is to permit the computation of vibratory exciting forces on the ship hull. An essential step in this process is the computation of the free-space potential field induced by the moving time varying singularities representing the propeller. This can readily be accomplished once the solution for the singularities is obtained, and the procedure, together with some examples, was briefly described by Kerwin [21].

The combination of the numerical procedure for solving the unsteady propeller cavitation problem developed at MIT with the procedure for computing hull excitation forces developed at the Davidson Laboratory was presented by Breslin, Kerwin, Van Houten and Johnsson in [22].

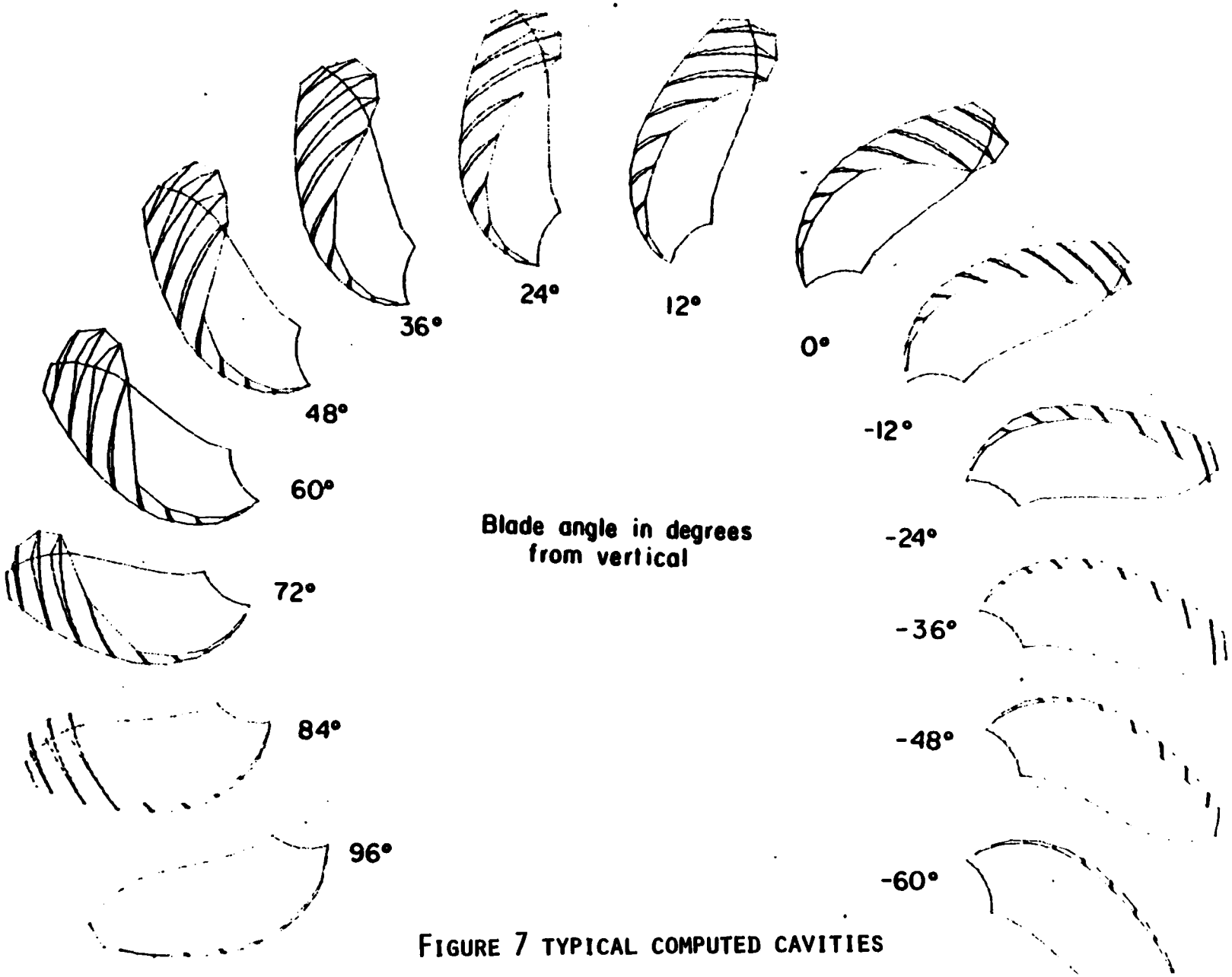


FIGURE 7 TYPICAL COMPUTED CAVITIES

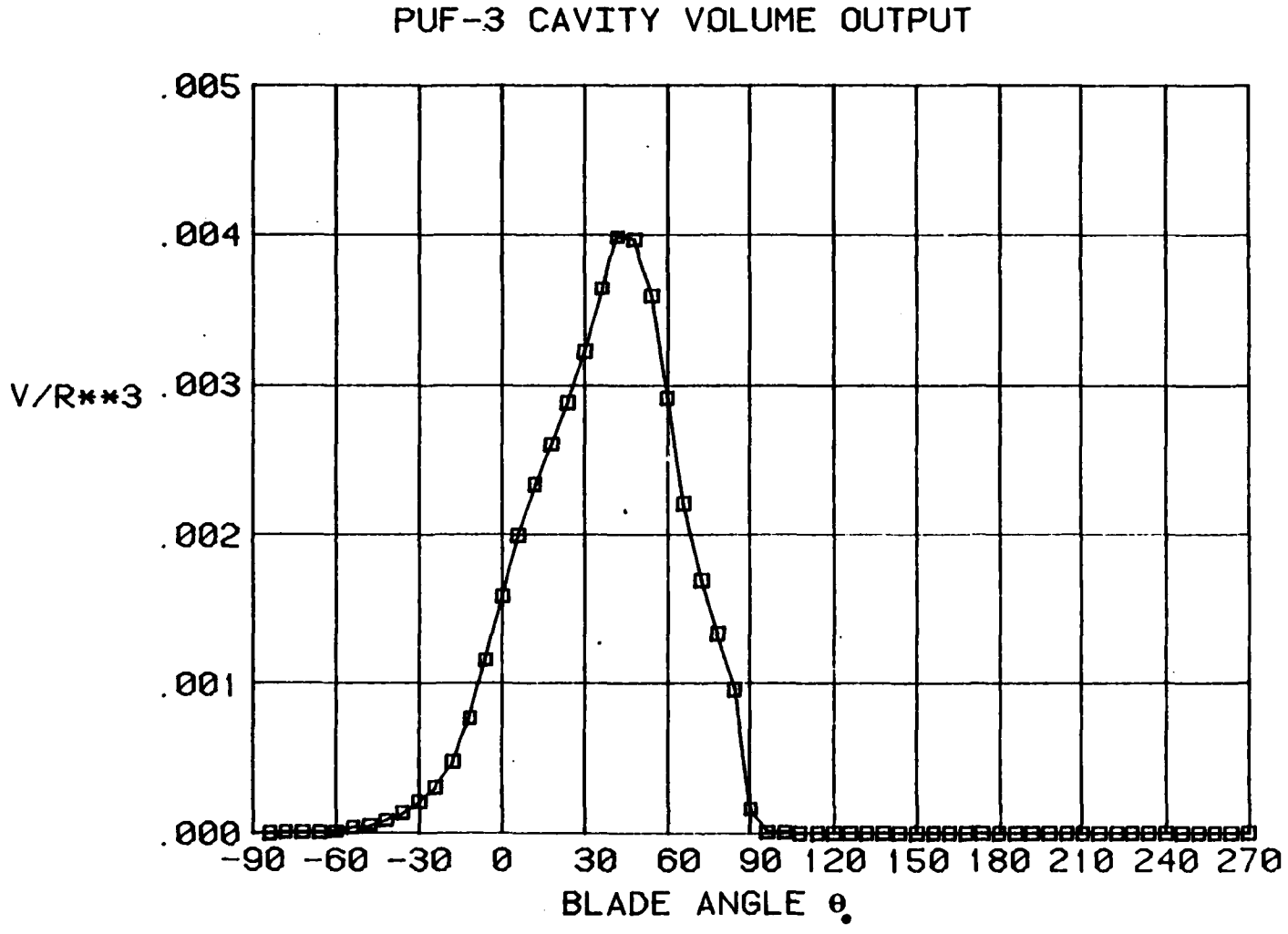


FIGURE 8 TYPICAL NON-DIMENSIONAL CAVITY VOLUME FOR A SINGLE BLADE.

3. A NONLINEAR METHOD FOR STEADY, 2-D HYDROFOILS

All of the methods previously described involved linearizing the cavity boundary value problem. The analysis procedures for planar hydrofoils were linearized with respect to angle of attack, camber, and thickness. In the propeller analysis method the singularity distributions are placed on the mean surface of the blades, and an exact tangency condition is applied, so this method incorporates some nonlinear effects. However, it is still linearized with respect to blade and cavity thickness.

It has been suggested by Tulin and Hsu [23] that the presence of finite section leading edge radius has a major influence on global cavity characteristics. Their results indicated that an increase in section thickness, with a resulting increase in leading edge radius, tended to greatly reduce cavity volumes. This effect was so strong that it appeared that even the relatively thin tip sections of marine propellers would have much smaller cavities than would be predicted on the basis of linear theory.

An investigation into this effect was carried out by Uhlman [24]. He solved the steady nonlinear partially cavitating two-dimensional hydrofoil problem by using a piecewise constant vorticity distribution on the foil-cavity boundary. Starting with a given cavity length and an assumed cavity shape, the unknown

vorticity distribution was determined by satisfying a kinematic boundary condition on the wetted portions of the foil boundary and a dynamic boundary condition on the surface of the cavity. The kinematic boundary condition on the cavity surface was then employed to generate a new cavity shape. The problem was then reformulated using the new position of the cavity and the problem was solved again. This procedure was repeated until both boundary conditions were satisfied to the desired degree of accuracy.

By taking the square root of Bernoulli's equation, the dynamic boundary condition on the cavity was made linear with respect to the vorticity distribution and the unknown $\sqrt{1+\sigma}$, where σ represents the cavitation number. Since the kinematic boundary condition is also linear with respect to the vorticity, the boundary value problem for each assumed cavity shape could be approximated by a set of linear algebraic equations.

An additional condition imposed on the flow was a Kutta condition at the foil trailing edge. A closure condition of zero net source strength, as employed in linear theories, is inappropriate in an exact nonlinear approach. Instead, a cavity termination model must be adopted. In Uhlman's work a modified Riabouchinsky cavity termination model was used.

Typical results are presented in figures 9 and 10. Figure 9 shows the final converged cavity shape for a cavity of 50% of the chord length on an NACA 16-006 section at 4 degrees angle of attack.

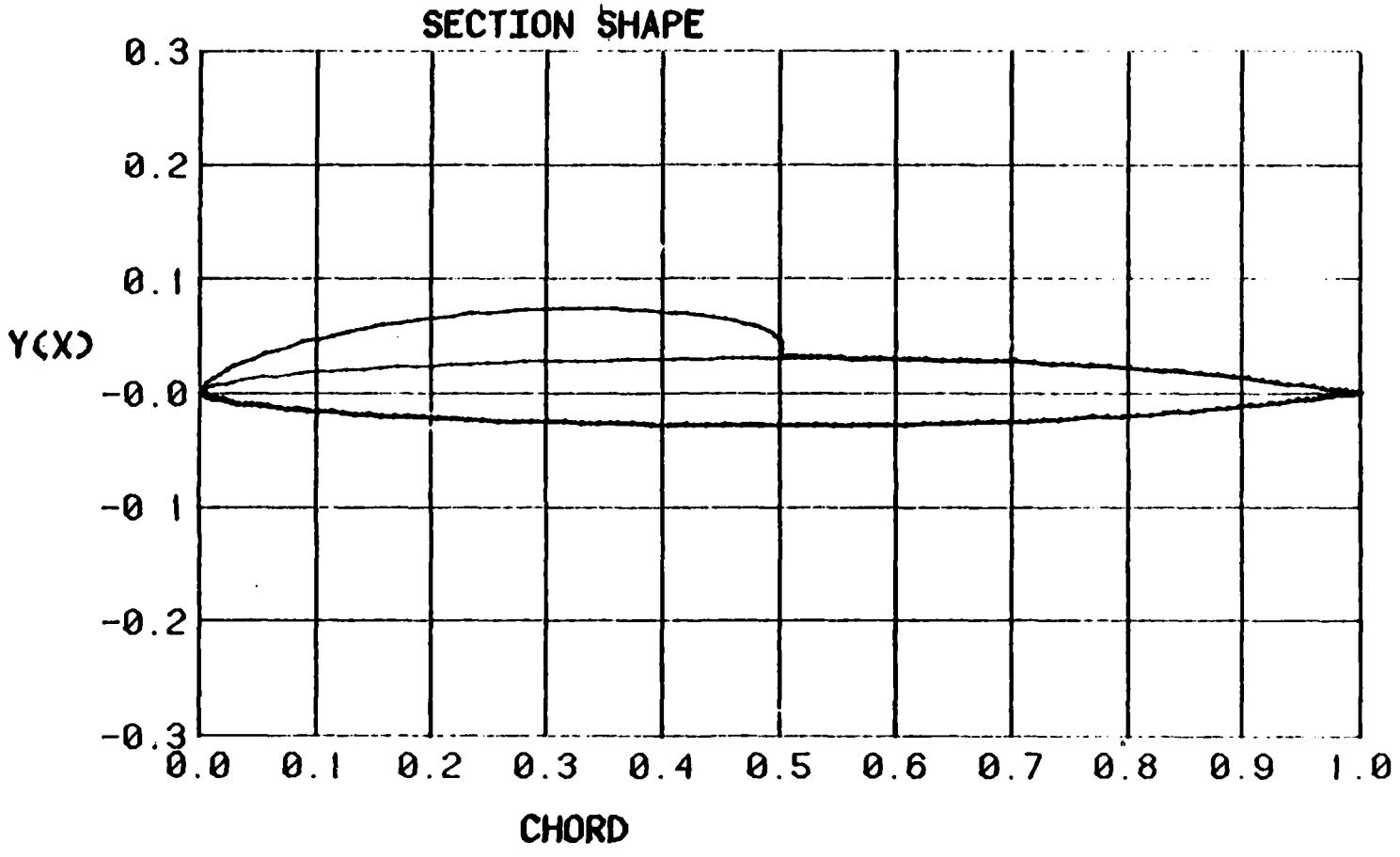


Figure 9

Cavitating NACA 16-006 Section
$\alpha = 4°$, $\ell/c = 0.50$
final cavity shape after 15 iterations

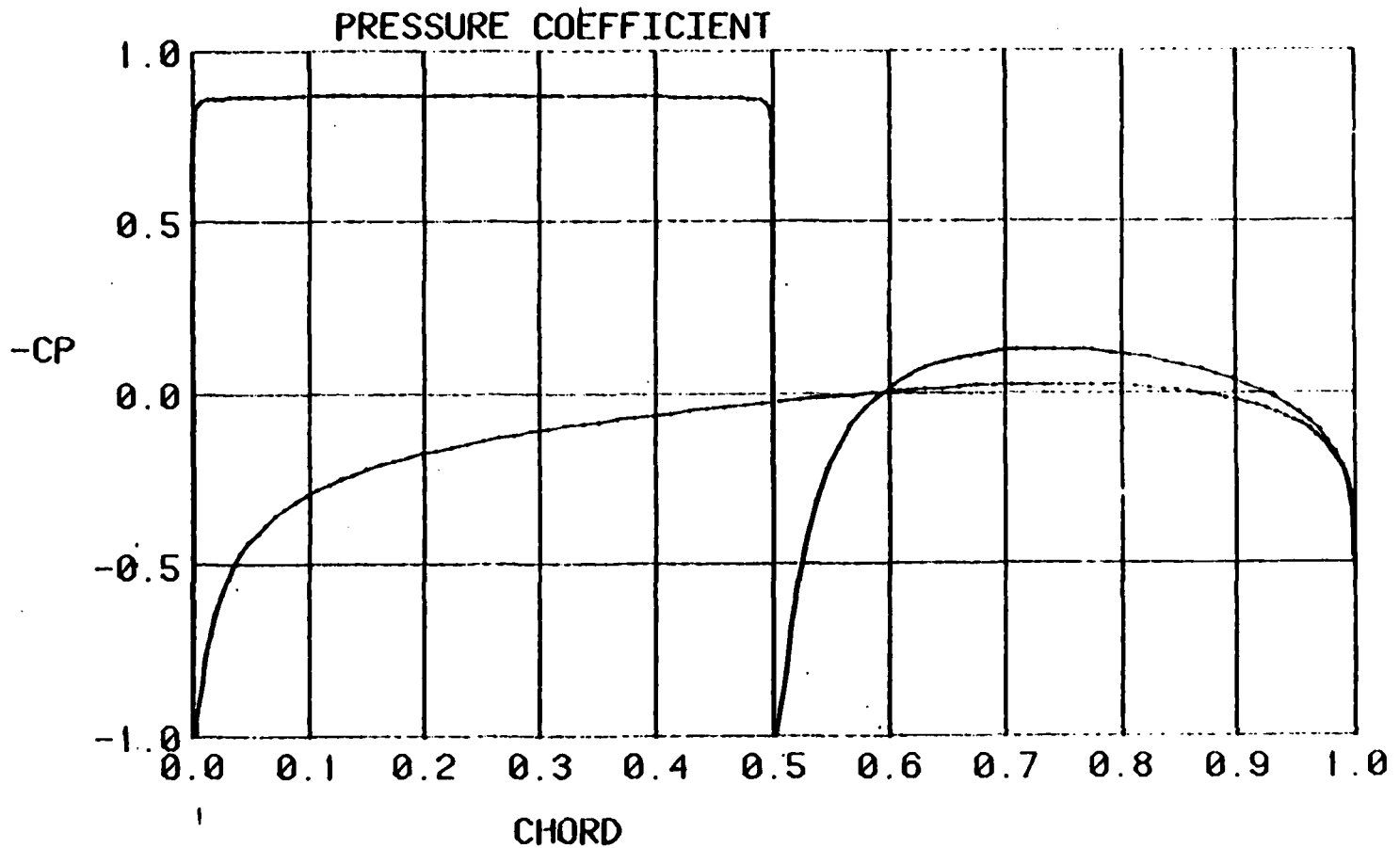


Figure 10

Pressure Distribution
NACA 16-006 Section
$\alpha = 4°$, $\ell/c = 0.50$

Figure 10 shows the corresponding pressure coefficient distribution. As is to be expected the pressure is constant over the cavity and the modified Riabouchinsky cavity termination model produces the desired stagnation point at the trailing edge.

Figure 11 shows the convergence characteristics of Uhlman's method as applied to this case. About 12 iterations are necessary for convergence. It is important to note that an extremely large number of surface elements are needed for accurate results. This is not surprising since an equally large number of elements are required to capture the minimum pressure coefficient of the fully-wetted flow around such a thin section.

Experimental results for steady partially cavitating round-nosed hydrofoils are not plentiful. However, a few data points may be found in the work of Shen and Peterson [25], who performed experiments on a modified Joukowsky section. Table 1 presents a comparison of their results with those of Uhlman's method and the linear method of Van Houten.

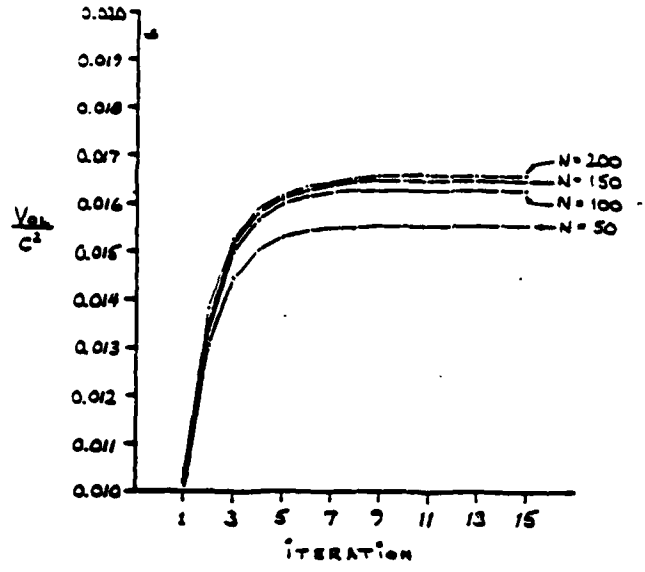


Figure 11

Convergence
Vol/c^2 vs. number of iterations
NACA 16-006 α = 4° t/c = 0.50
for N = 50, 100, 150, 200

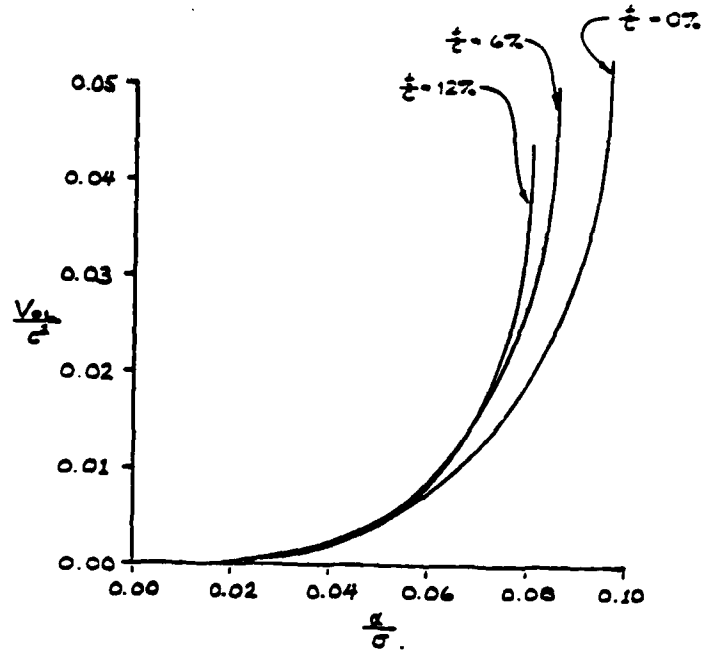


Figure 12

Vol/c^2 vs. α/σ
NACA 16 Series Sections
linear results
w/ thickness
α = 4°

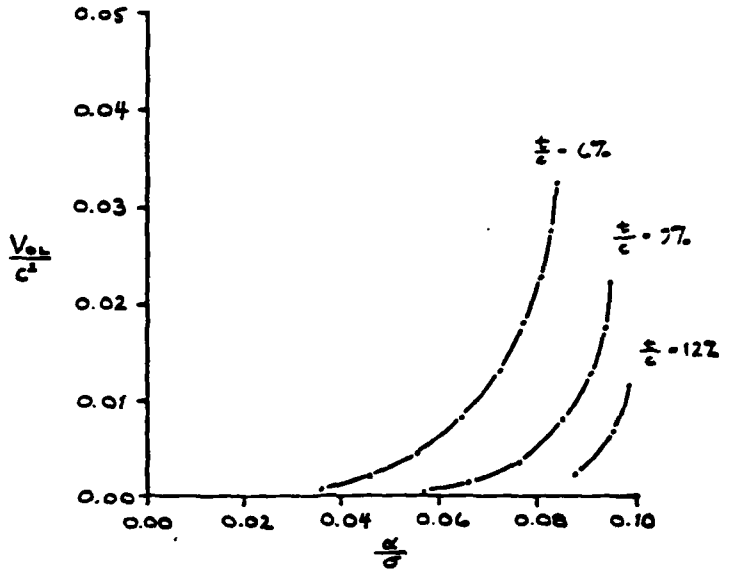


Figure 13

Vol/c^2 vs. a/a
NACA 16 Series Sections
Tulin & Hsu's results
$a = 4°$

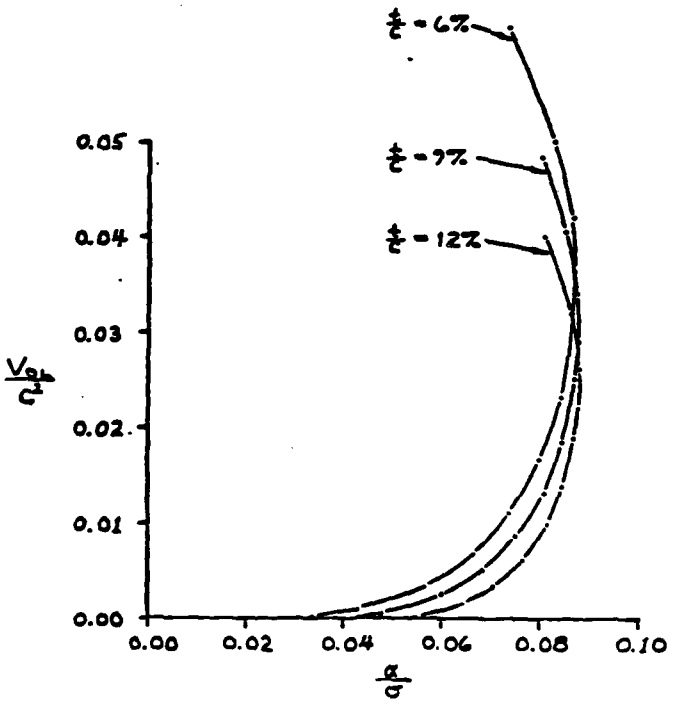


Figure 14

Vol/c^2 vs. a/a
NACA 16 Series Sections
Nonlinear results
$a = 4°$

TABLE 1

	$\ell/c = 0.40$	$\ell/c = 0.30$	$\ell/c = 0.25$
	$\alpha = 4.3^\circ$	$\alpha = 4.2^\circ$	$\alpha = 3.8^\circ$
Experiment	$\sigma = 1.13$	$\sigma = 1.21$	$\sigma = 1.13$
Nonlinear	$\sigma = 1.11$	$\sigma = 1.20$	$\sigma = 1.14$
Linear	$\sigma = 1.37$	$\sigma = 1.53$	$\sigma = 1.51$

The agreement between experimental data and the nonlinear theory is excellent. The linear theory is clearly inferior. Further experimental investigations are presently being pursued at MIT. Figures 12, 13, and 14 show the effect of section thickness on cavity volume as predicted by three different theories. Figure 12 is a linear theory result using the numerical procedure of Van Houten. Figure 13 is from Tulin and Hsu, while figure 14 is from Uhlman's method. These results are all for a cavity length of fifty percent of the chord. In brief, it is apparent that the trend of linear theory is opposite to that of either of the nonlinear theories. The latter both yield the result that increasing section thickness decreases cavity volume. However, this effect is far less pronounced in Uhlman's results than in Tulin's. Even the more moderate influence of thickness predicted by Uhlman, however, is large enough to suggest that significant errors may be incurred in applying linear theory in the propeller problem.

Uhlman's approach has also been applied to the problem of steady

nonlinear super-cavitating flow past two-dimensional hydrofoils. Preliminary results show excellent agreement with analytic theory.

4. FUTURE DIRECTIONS

The use of surface singularity methods to solve the nonlinear problem has been demonstrated by Uhlman for the case of relatively thick sections in steady flow. The analysis of thin foil sections , such as the tip sections of propeller blades, would be improved by incorporating variable element lengths so that the relatively small leading edge region can be adequately modeled. The required number of elements can probably be reduced by the use of curved elements, and by allowing the vorticity to vary over the elements' length. The extension of the nonlinear theory to unsteady flows should also be undertaken.

The development of nonlinear methods to solve cavity flow problems is useful from two points of view. There is obvious value in the ability to calculate the cavitation which develops in any given flow situation. Equally important, however, is the use of these methods to develop insight into the role and importance of the various sources of nonlinearity. These include higher order terms in the foil thickness ratio, similar terms in the thickness ratio of the foil-cavity system, and the nonuniformity of the linear solution at both the foil leading edge and the cavity termination. Were the latter effects to be dominant, one might develop local corrections to the linear solution which would incorporate the bulk of the nonlinear

effects. These corrections could then be added to the propeller analysis program with a minimum of increased cost or complexity. If, on the other hand, this should prove impossible, a surface singularity procedure might be developed for propeller geometries. If this were to be undertaken, it would be imperative to reduce computation costs to a minimum.

Eventually, of course, one must face the limitations implicit in any method which treats solely sheet cavitation originating at the leading edge of the foil. Propeller tip vortex cavities often exceed in volume the sheet cavities on the blades, and must eventually be modeled numerically. In unsteady flow the sheet cavities are often observed to pull back from the leading edge during their collapse phase and may collapse into cloud cavitation. The numerical modeling of these effects, along with the roles of viscosity and nucleation, will have to be addressed in the future.

REFERENCES

1) Tulin, M.P. "Steady Two-Dimensional Cavity Flows About Slender Bodies", DTMB Report 834, Navy Department, Washington, D.C., May 1953.

2) Tulin, M.P. "Supercavitating Flow Past Foils and Struts". Symposium on Cavitation in Hydrodynamics, National Physical Laboratory, Teddington, England, 1955.

3) Acosta, A.J. "A Note on Partial Cavitation of Flat Plate Hydrofoils", California Institute of Technology, Hydrodynamics Laboratory, Report No. E-19.9. October 1955.

4) Geurst, J.A. "Linearized Theory for Partially Cavitated Hydrofoils", Int. Shipbuilding Progress, Vol. 6, No. 60, August 1959.

5) Guerst, J.A. "Linearized Theory for Fully Cavitated Hydrofoils", Int. Shipbuilding Progress, Vol. 7, No. 65 Jan. 1960.

6) Wade, R.B. "Linearized Theory of a Partially Cavitating Plano-Convex Hydrofoil Including the Effects of Camber and Thickness", Journal of Ship Research, Vol. 11, No. 1, March 1967, pp. 20-27.

7) Leehey, P. "Supercavitating Hydrofoil of Finite Span", Proceedings of IUTAM Symmposium on "Non-Steady Flow of Water at High Speeds", Leningrad, June 1971, "NAUKA" Publishing House, Moscow, 1973.

8) Uhlman, J.S. "A Partially Cavitated Hydrofoil of Finite Span", Journal of Fluids Engineering, Vol. 100, No. 3. September 1978, pp. 353-354.

9) Widnall, S.E. "Unsteady Loads on Hydrofoils Including Free Surface Effects and Cavitation". MIT Fluid Dynamics Laboratory Report No. 64-2, June 1964.

10) Golden, D.W. "A Numerical Method for Two-Dimensional, Cavitating, Lifting Flow", MIT, Dept. of Ocean Engineering Report No. 815112-1, May 1975.

11) Jiang, C.W. and P. Leehey "Experimental and Theoretical Investigation of Unsteady Supercavitating Hydrofoils of Finite Span", MIT, Department of Ocean Engineering Report 83481-4, September 1977.

12) James, R.M. "On the Remarkable Accuracy of the Vortex Lattice Method", Computer Methods in Applied Mechanics and Engineering, vol. 1, 1972.

13) Van Houten, R.J. "The Numerical Prediction of Unsteady Sheet Cavitation on High Aspect Ratio Hydrofoils", Fourteenth Symposium on Naval Hydrodynamics, 1982.

14) Tulin, M.P. "An Analysis of Unsteady Sheet Cavitation", Nineteenth American Towing Tank Conference, 1980.

15) Peters, A.S., T.R. Goodman, and J>P> Breslin "A Partially Cavitating Hydrofoil in a Gust", Stevens Institute of Technology, Davidson Laboratory, Report SIT-DL-2118, November 1980.

16) Van Houten, R.J. and H.C. Sayre "Experimental and Theoretical Studies of the Effect of Gas Content on Unsteady Cavity Flows", MIT, Department of Ocean Engineering, Report No. 82-1. January 1982.

17) Lee, C-S. "Prediction of the Transient Cavitation on Marine Propellers by Numerical Lifting Surface Theory", Thirteenth Symposium on Naval Hydrodynamics, Tokyo, October 1980.

18) Kerwin, J.E. and CS. Lee "Prediction of Steady and Unsteady Marine Propeller Performance by Numerical Lifting-Surface Theory, Transactions SNAME, VOL. 86, 1978.

19) Greeley, D.S. and J.E. Kerwin "Numerical Methods for Propeller Design and Analysis in Steady Flow", Transactions SNAME, vol. 90, 1982.

20) Wilson, M.B.,; D.N. McCallum; R.J. Boswell; D.D. Bernhard; A.B. Chase, "Causes and Corrections for Propeller-Excited Airborne Noise and Naval Auxiliary Oiler", Transactions SNAME. vol. 90, 1982.

21) Kerwin, J.E., "Flow Field Computations for Non-Cavitating and Cavitating Propellers", Fourteenth Symposium on Naval Hydrodynamics, Ann Arbor, Michigan, August 1982.

22) Breslin, J.P., R.J. Van Houten, J.E. Kerwin, C-A Johnsson "Theoretical and Experimental Propeller-Induced Hull Pressures Arising from Intermittent Blade Cavitating, Loading, and thickness", Transactions SNAME, vol. 90, 1982.

23) Tulin, M.P., and C.C. Hsu, "The Theory of Leading-Edge Cavitation on Lifting Surfaces with Thickness", Symposium on "Hydrodynamics of Ship and Offshore Propulsion Systems", March 1977.

24) Uhlman, J.S., "The Surface Singularity Method Applied to Partially Cavitating Hydrofoils", Fifth Lips Propeller Symposium, Drunen, The Netherland, May 1983.

25) Shen, Y.T. and F.B. Peterson, "Influence of Hydrofoil Oscillation on Boundary Layer Transition and Cavitation Noise", Thirteenth Symposium on Naval Hydrodynamics, Tokyo, October 1980.

DISCUSSION

Terry Brockett
David W. Taylor Naval Ship Research
and Development Center

First I would like to congratulate the investigators at MIT for the rapid progress they have made in this difficult hydrodynamic area.

The predicted cavitation patterns shown for the A0177 are somewhat different than those observed full scale (presented in author's Reference 20); in particular the predicted cavitation near the hub did not occur full scale and observed full-scale cloud cavitation is not predicted. Will the authors comment on these differences and describe the efforts necessary to improve the prediction



REPORTS OF THE

HIGH SPEED VEHICLE

COMMITTEE

COMMITTEE REPORT
HIGH SPEED VEHICLE COMMITTEE
20th ATTC

The High Speed Vehicle Committee of the 20th American Towing Tank Conference met in session on 1 August 1983 to review technical contributions to the conference and to discuss the current state of technology in high speed vehicles and advanced ships. The committee was composed of the individuals listed in Attachment 1. The committee accepted the ITTC definition of advanced ship for its working basis; namely, that the definition of advanced vehicles was broad enough to cover all marine vehicles moving at or on the water surface but excluding conventional surface ships and submarines.

The goals of the High Speed Vehicle Committee were: (a) to examine recent advances in the state-of-the-art of tow tank testing as related to advanced vehicles, (b) to discuss in committee session recent advances in high speed vehicle design and performance, (c) to examine the current level of research and development specifically for advanced ships and (d) to bring together and correlate the recent experiences of individuals dealing with specific vehicle types with the objective of sharing the common features key to the development of improved tankery for advanced ships.

The first of these goals resulted in a series of discrete and specific project summaries and problem areas. These are enumerated in Attachment 2. The specific items have been designated under one of three categories: (1) Recent Projects (RP), (2) New Tankery Techniques (NT), and (3) Area of Current Important Investigation (AI).

The second objective of presenting recent advances in high speed vehicle design and performance was handled through a balanced presentation program at the High Speed Session of the conference. The program of contributions are listed as Attachment 3 and the specific papers are reprinted in the proceedings.

The third objective was achieved through the timely presentation by Jacques B. Hadler of a conference key note address covering the "State-of-the-Industry." The Committee discussion was well served by Mr. Hadler's presentation.

The Committee received for consideration from K. Yosifov, Deputy Director, Bulgarian Ship Hydrodynamics Center, Varna 9003 (Telephone 7.51.80) the attached description (Attachment 4) of a program for improvement of high speed planing boat performance. Mr. Yosifov has expressed an interest in the exchange of technical information covering planing boat testing of the type noted in the program. He is specifically interested in comparing the performance of the parent model from the MBK series with similar results from Series 62.

The Committee also received for consideration a recent report of a "Survey of High Speed Waterborne Transport World-Wide," as summarized in an article in "High Speed Surface Craft" presented as Attachment 5.

The Urban Mass Transportation Administration has sponsored a specific study of the RHS-200 Hydrofoil. This study resulted in a full-scale trials evaluation of the hydrofoil which is briefly summarized in Attachment 6.

Finally, the Committee presents for consideration and continued compilation a bibliography of selected technical papers published outside of the United States or translated since the last ATTC. The bibliography included as Attachment 7 is not exhaustive nor even representative of the volume of foreign technical publications but does reflect a portion of the technical advances presented abroad for high speed vehicles.

Attachment 1

20th ATTC
HIGH SPEED VEHICLE COMMITTEE
MEMBERSHIP

David D. Moran, Chairman
Head, Special Ship & Ocean Systems Dynamics Branch
Code 1562
David Taylor Naval Ship R&D Center
Bethesda, MD 20084
(301) 227-1228

Timothy Bertch, Ens. USN
Nuclear Power School
7508 F. Serano Circle
Orlando, FL 32807
(305) 646-5366

Donald Blount
Naval Sea Systems Command
Code 6660
Naval Station
Norfolk, VA 23511
(804) 444-9164

Jacques B. Hadler
Director, Center for Maritime Studies
Webb Institute of Naval Architecture
Glen Cove, NY 11542
(516) 671-2356

Robert Latorre
Department of Naval Architecture and Marine
Engineering
The University of Michigan
Ann Arbor, Michigan 48109
(313) 764-6470

John R. Meyer, Jr.
Advanced Hydrofoil Systems Office
Code 1150
David Taylor Naval Ship R&D Center
Bethesda, MD 20084
(301) 227-1796

Eugene Miller
Hydronautics, Inc.
7210 Pindell School Road
Laurel, MD 20810

Daniel Savitsky
Davidson Laboratory
Stevens Institute of Technology
Hoboken, NJ 07030

Michael B. Wilson
Powering Systems Evaluation Branch
Code 152
David Taylor Naval Ship R&D Center
Bethesda, MD 20084

Fred W. Wilson
Program Development Office
Code 1604
David Taylor Naval Ship R&D Center
Bethesda, MD 20084
(301) 227-1476

Attachment 2

HIGH SPEED VEHICLE PROJECT SUMMARIES

The following project summaries and areas of interest to high speed vehicle developments were presented at the High Speed Vehicle Committee meeting of 1 August 1983. The specific items have been designated under one of three categories: (1) Recent Projects (RP), (2) New Tankery Techniques (NT) and (3) Areas of Current Important Investigation (AI)

1. (AI) There exists at all R&D establishments a well identified requirement to taylor tankery to the needs and funds of the sponsor. Extensive tank testing is an historical luxury which in most cases can no longer be tolerated.

2. (AI) The tow point position for narrow and specifically narrow twin hull ships, e.g. SWP7H, SES(Hi L/B), on twin cushion vehicles must be well established experimentally. The traditional method of moment compensation for incorrect tow point is not appropriate for motion evaluations, especially in oblique headings. LCG variations are being attempted in lieu of self-propulsion whenever self-propulsion is either impractical due to model scale or other limiting considerations.

3. (AI) SES cushion densities and cross-structure heights are increasing and this is forcing the tank tester into new areas of concern in cushion air supply and compressibility scaling.

4. (NT) A new technique has been developed to measure the unsteady loads or hydrofoils operating in a wave field. Application to SWATH control foils is presently under consideration.

5. (NT) A new water tunnel technique has been developed to simulate the unsteady pressure excitation on a hull due to propeller unsteady loading in a partial wake or boundary layer. The goal is to examine the effects of propeller clearance to avoid vibration similar to those encountered on high speed ships such as CPIC which were designed with low propeller tip clearance.

6. (RP) The recent ITTC questionnaire on model test techniques is being reviewed at all tank laboratories with respect to high speed vehicle applications.

7. (NT) A wake survey has been performed recently by DTNSRDC on a high speed hull in which the wake was generated with screens following a boundary layer calculation. The method is ideal when there is a requirement to generate on the model a realistic wave field for propulsion or waterjet inlet studies. An assumption of inlet momentum equal to the free stream velocity has been found to be inappropriate in high speed applications.

8. (NT) There is promise showing in a recent Japanese application of liquid crystal thermal transfers for the study of wetted surface area determination. If the hull interior is coated and photographed the wetted surface and spray areas are displayed as color pattern. It is expected that boundary layer transition points will be observable through this technique with no disturbance to the flow field by the instrumentation. There is promise that the technique will work under unsteady conditions and in seakeeping examinations.

The technique uses a temperature sensitive sheet attached to a body at a slightly higher temperature. The liquid crystal sheet will rapidly change its color to the local temperature. In studies of gas turbine blades the color pattern is used to define the temperature distribution using a color key. Recording the color pattern by movies or video allow the dynamics of the temperature change to be studied.

The application of this technique to high speed marine vehicle model testing will require additional test development. With wood or wax models the crystal sheets would be mounted on the hull in the region of interest and underwater photographs/movies/video can be used to record the flow conditions.

An alternative is to form the model surface out of metal and mount the liquid crystal sheets inside the hull. Then the change in the sheet will define the wetted surface, spray region, and boundary layer transition. Movies may define the instantaneous conditions in seakeeping tests.

9. (RP) Recent Full Scale Trials noted included:

1. Suave Lino SWATH Rough Water Trials - SIT
2. Racing Seaknife Trials - NSEA Norfolk
3. RHS-200 Rodriquez Hydrofoil - DTNSRDC

Full scale testing remains a major objection of the naval architect in the assessment of and certification of ship performance and may in many cases be unduplicatable through model testing. Full scale evaluation remains economically viable if the ship already exists.

10. (NT) In a recent waterjet propulsion and high speed hull/propulsion interaction study, the thrust was successfully evaluated through measurements of nozzle discharge pressure and discharge rather than through conventional thrust measurements.

11. (RP) An impulse reaction thruster has been recently investigated. The thruster consists of a rotating chambered cylinder in which chambers are alternatively filled and fired by jet impulse. The thrust was here measured through the reaction on an impulse bucket.

12. (RP) The U.S. Marine Corps is presently attempting to increase the speed of an LVT to 20 mph as a planing hull. The DTNSRDC and Hydronautics wave hull is jointly involved in the design process. The Stevens Institute of Technology is presently testing a 0.55 scale model of the vehicle.

13. (RP) The Webb Institute of Naval Architecture has recently completed a major regression analysis on the resistance of a planing boat series.

ATTACHMENT 3

THE FOLLOWING CONTRIBUTIONS WERE PRESENTED TO THE 19th ATTC, STEVENS INSTITUTE OF TECHNOLOGY, AUGUST 1983, BY THE HIGH SPEED VEHICLE COMMITTEE

1. Ens. Bertch
   Planing Patrol Vessel Feasibility Study

2. R. Meyer, Jr.
   Extended Performance Hydrofoil

3. R.T. Waters, D.D. Moran, F. Messale
   High Speed Maneuvering of Amphibious Hovercraft

4. R. Latorre
   Planing Surface C

5. M.B. Wilson
   Low F Performance of a Hydrofoil in Calm Water and Regular Waves

6. F.W. Wilson
   SES Technology Development

7. E. Miller
   Self-Propelled Waterjet Testing

8. D. Savitsky
   International High Speed Vehicle Tow Tank Testing

9. D.D. Moran
   High Speed Vehicle Committee Summary Report

Attachment 4

Yegorov, I.T., Bun'Kov, M.M., Sandovnikov, Yu.M., Propulsive Performance and Seaworthiness of Planing Vessels,

1. Systematic Series MBK of Small Displacement Planing Vessels

The above-investigated materials on the propulsive performance of large-displacement planing vessels cannot be used to design low-speed vessels as a result of noncorrespondence of their load factors, the principal dimension ratios and also the elements of the propulsion units.

Accordingly, a systematic series of models of planing vessels MBK was developed (42), the basic purpose of the testing of which was to obtain systematic data permitting efficient selection of the lines and principal dimensions and also calculation of the drag of the ships of this class.

The developed systematic series consists of 25 models with hard-chine lines (stepped and stepless) for small planing vessels and also rounded bilge lines characteristic of small launches and pleasure boats designed to operate in the floating mode. The models were developed for four basic groups distinguished from each other both by the ratio of the geometric elements of the hull and the lines (Table 2.18).

Table 2.18. Basic Geometric Elements of the Lines Drawing of Models of the MBK systematic Series

Модель (1)	Длина модели по скуле $L_{ск}$, м (2)	Ширина модели по скуле на миделе $B_{м}$, м (3)	Ширина модели по скуле на транце $B_{т}$, м (4)	Угол внешней килеватости на миделе $\beta_{м}$, ° (5)	Угол внешней килеватости на транце $\beta_{т}$, ° (6)	Относительная длина $L_{ск} : B_{м}$ (7)	Сужение кормовой оконечности $B_{т} : B_{м}$ (8)
			Группа А (9)				
МБК-1	2,05	0,65	0,52	12,5	5,0	3,15	0,80
МБК-2	2,05	0,65	0,52	5,0	5,0	3,15	0,80
МБК-3	2,05	0,65	0,52	12,5	5,0	3,15	0,80
МБК-4	2,05	0,65	0,52	12,5	5,0	3,15	0,80
МБК-5	2,05	0,65	0,52	—10,8	0	3,15	0,80
МБК-6	2,05	0,65	0,52	21,0	21	3,15	0,80
МБК-7	2,52	0,56	0,42	15,5	0	4,5	0,75
МБК-8	2,05	0,65	0,52	12,5	5,0	3,15	0,80
МБК-9	1,90	0,65	0,53	8,5	10	2,92	0,815
			Группа Б (10)				
МБК-10	1,625	0,65	0,52	7,0	5,0	2,50	0,80
МБК-11	2,05	0,65	0,52	7,0	5,0	3,15	0,80
МБК-12	2,44	0,65	0,52	7,0	5,0	3,75	0,80
МБК-13	1,625	0,65	0,52	12,5	5,0	2,50	0,80
МБК-1	2,05	0,65	0,52	12,5	5,0	3,15	0,80
МБК-14	2,44	0,65	0,52	12,5	5,0	3,75	0,80
МБК-15	1,625	0,65	0,52	18,0	5,0	2,50	0,80
МБК-16	2,05	0,65	0,52	18,0	5,0	3,15	0,80
МБК-17	2,44	0,65	0,52	18,0	5,0	3,75	0,80
МБК-18	2,05	0,65	0,52	12,5	8,0	3,15	0,80
МБК-19	2,05	0,65	0,52	12,5	12,5	3,15	0,80
МБК-20	2,05	0,65	0,422 5	12,5	5,0	3,15	0,65
МБК-21	2,05	0,65	0,617 5	12,5	5,0	3,15	0,95
			Группа В(11)				
МБК-22	2,05	0,65	0,52	8,0	5,0	3,15	0,80
МБК-4	2,05	0,65	0,52	12,5	5,0	3,15	0,80
МБК-23	2,05	0,65	0,52	15,0	5,0	3,15	0,80
			Группа Г (12)				
МБК-24	2,05	0,65	0,52	—	—	3,15	0,80
МБК-25	2,05	0,65	0,52	—	—	3,15	0,80

Key:

1. Model
2. Length of model on chine L_{chine}, m
3. Breadth of model on chine midships
4. Breadth of model on chine at the transom
5. Exterior deadrise angle midships
6. Exterior deadrise angle at the transom
7. Relative length L_{chine}:
8. Aft end taper
9. Group A
10. Group B
11. Group C
12. Group D

Group A is made up of models having identical principal dimensions but distinguished by the lines.

Group B consists of models with hard chine stepless lines. The models of Group C have hard-chine stepped hull formations. Group D consists of model with rounded

bilge lines. When constructing the systematic series MBK, the following parameters were varied:

a) The frame lines;

b) Static load factor C_Δ=0.158 to 0.352 (for each model of the series);

c) Relative center of gravity position $\bar{x}_g$=0.35 to 0.45 (for each model of the series);

d) Relative length $L_{chine}: B_x$=2.5 to 3.75 (group B);

e) Exterior deadrise angle midships (on the step):

For group B β_x=7 to 18°;

For group C β_p=8 to 15°.

f) The exterior deadrise angle at the transom β_T=5 to 12.5° (group B);

g) Aft end taper $B_T: B_x$=0.65 to 0.95 (group B).

The lines drawing of the hulls of the models in group A having identical principal dimensions but differing with respect to lines are presented in Figure 2.50.

The model MBK-1 had hard-chine, stepless lines characteristic of small seagoing planing vessels. Model MBK-2 had rounded bilge lines with small exterior deadrise angle in the aft section (from midships to transom); it was equipped with developed gussets which play the role of the chine. The model MBK-3 had mixed lines with hard chine in the stern and molded lines in the bow. For the model MBK-4 stepped formations of the hull were selected with increased exterior deadrise angle on the step β_p=12.5° in contrast to the existing small stepped planing vessels. The model MBK-5 had "sea sled" type lines.

The lines of the model MBK-6 are characterized by the fact that it has increased transverse deadrise in practice with respect to the entire length ($\beta_x = \beta_T = 21°$) and longitudinal steps parallel to the fore-and-aft line.

The model BK-11 (see Table 2.11) which was equipped with hydroskis was used as the model MBK-7.

The lines of model MBK-8 were simplified and were formed by the lines developed on a plane. Model MBK-9 had trimaran lines which were used when developing the plans for a full-scale mass-consumption motorboat.

The geometric elements of the lines drawing, the static load factor and relative center of gravity position of the MBK series models were varied as follows.

On variation of the static load factor $C_\Delta = \frac{\Delta}{\gamma B_x^3}$ the midships beam of the model was kept constant (B_x = 0,65 м) , and the load (displacement) varied: it was 434, 690 and 970 N.

When testing each model of the series the values of relative center of gravity position $\bar{x}_g = x_g/L_{chine} = 0.35,\ 0.40.\ 045.$

Models MBK-1, MBK-13 and MBK-14 were tested for three values of the static load factors and three values of the relative center of gravity position.

On variation of the parameter L_{chine}: B_x the length of the model varied (transverse cross sections remained constant in this case). For variation of the exterior deadrise angle midships the shape of the chine in plan, the relative length, the exterior deadrise angle at the transom and the aft end taper of the model remained constant.

On varying the exterior deadrise angle at the transom the shape of the chine in plan, the relative length, the exterior deadrise angle midships and aft end tap of the model remained unchanged.

The aft end taper was realized as a result of variation of the transom beam on chine with constant midships beam on chine of the model.

During the process of towrope testing of the series MBK models, the drag of the water on the model r(v), the running trim angle of the model $\phi(v)$, expouse of the center of gravity of the model h(v), and wetted length on chine $l_{chine}(v)$ were measured as a function of speed.

All the series models were tested for relative speeds, $Fr_\Delta = 0.5$ to 6.0. In this case the following relations were constructed in dimensionless form for each model:

$$\varepsilon = \frac{r}{\Delta} = f(Fr_\Delta);\ \varphi = f(Fr_\Delta);\ \frac{l_{см}}{L_{см}} = f(Fr_\Delta). \quad (1)$$

Key: 1. chine

The relations obtained for individual models were compared with each other with respect to the most characteristic geometric hull parameters of the series MBK models. During this comparison, unavoidable experimental errors were diminish and reliable hydrodynamic characteristics were established for these models.

An analysis of the results of testing the series MBK models demonstrated that following basic parameters have the most significant influence on the drag for $Fr_\Delta = const$:

a) The frame lines;

b) The static load factor C_Δ;

c) The relative center of gravity position $\bar{x}_g$;

d) Relative length $\bar{L} = L_{chine}$; B_x;

e) The exterior deadrise angle midships β_x.

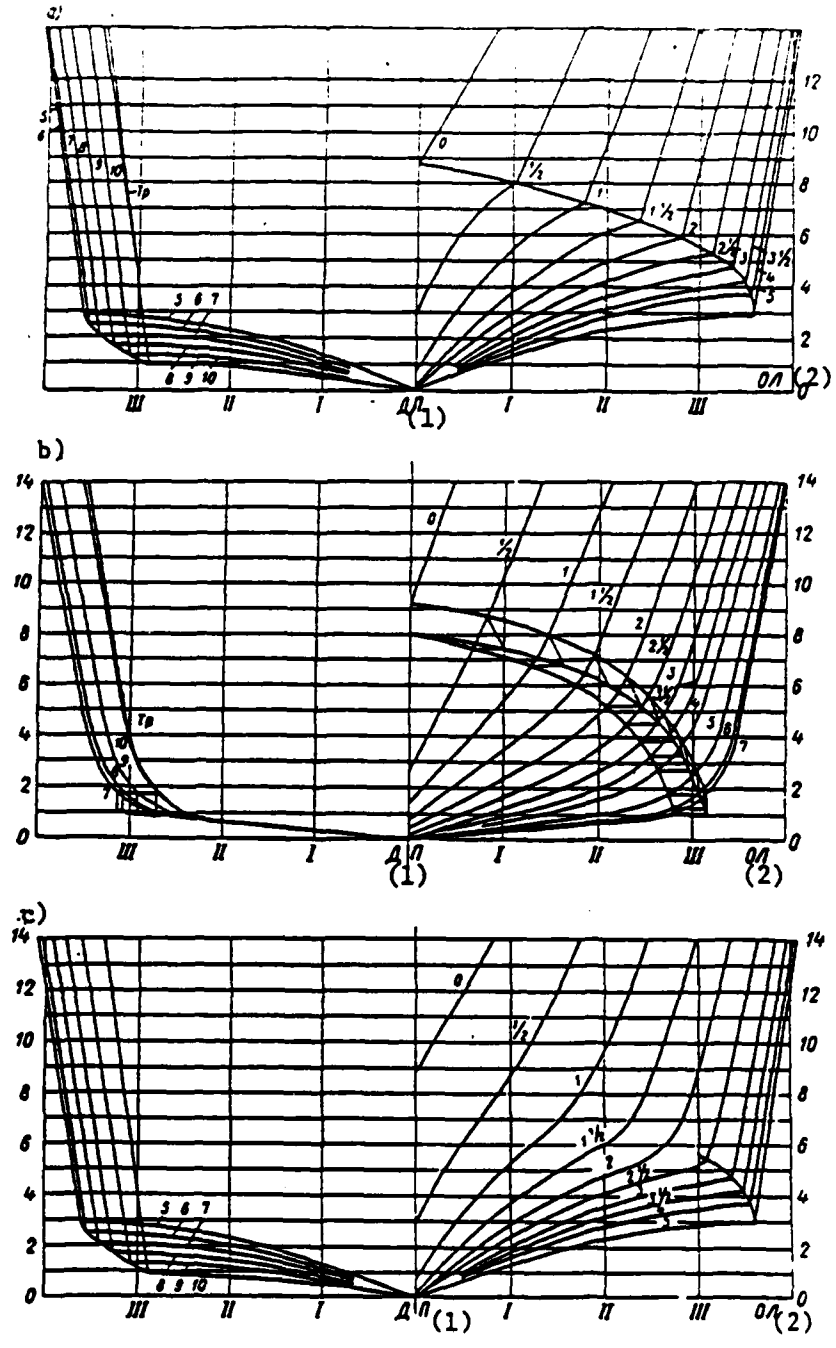
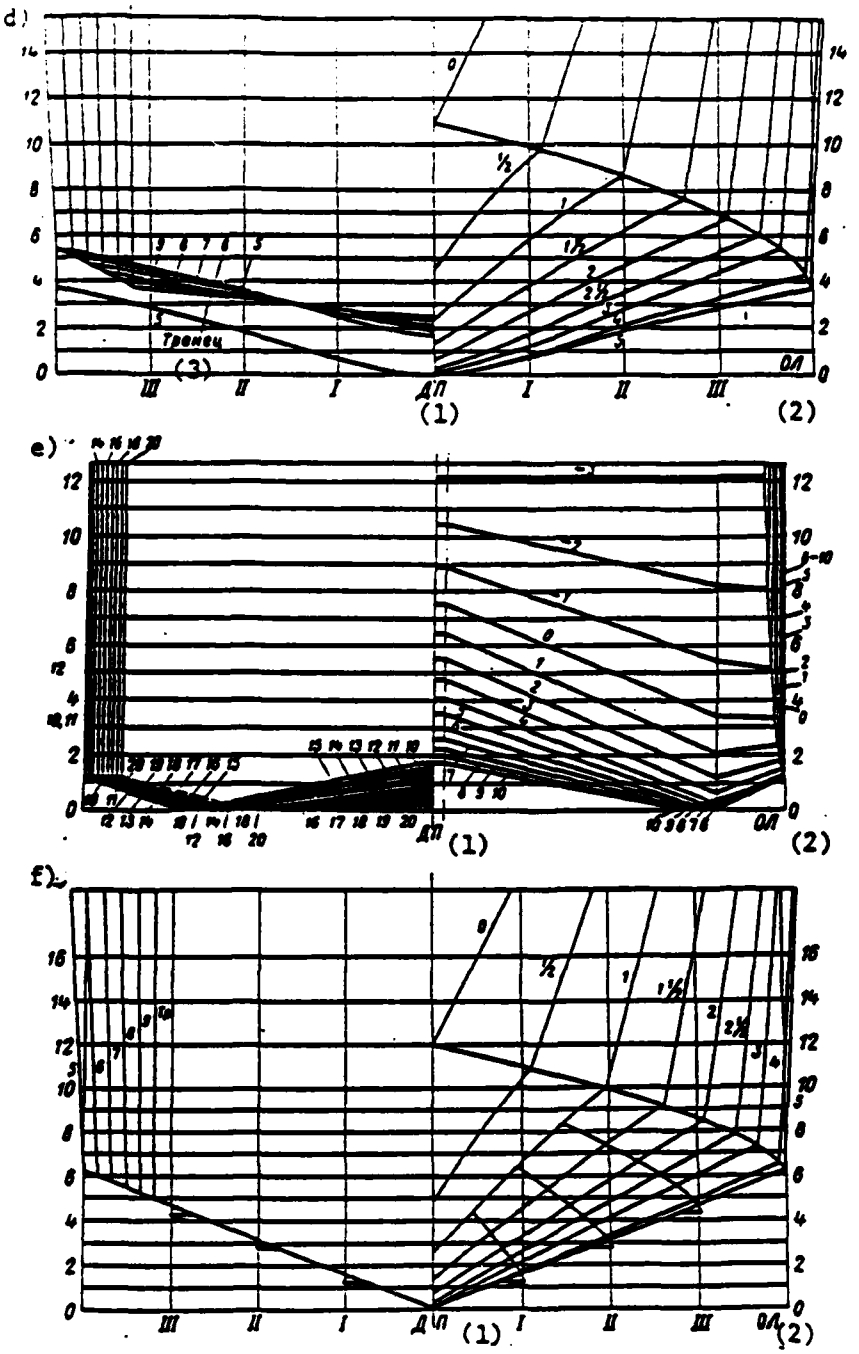


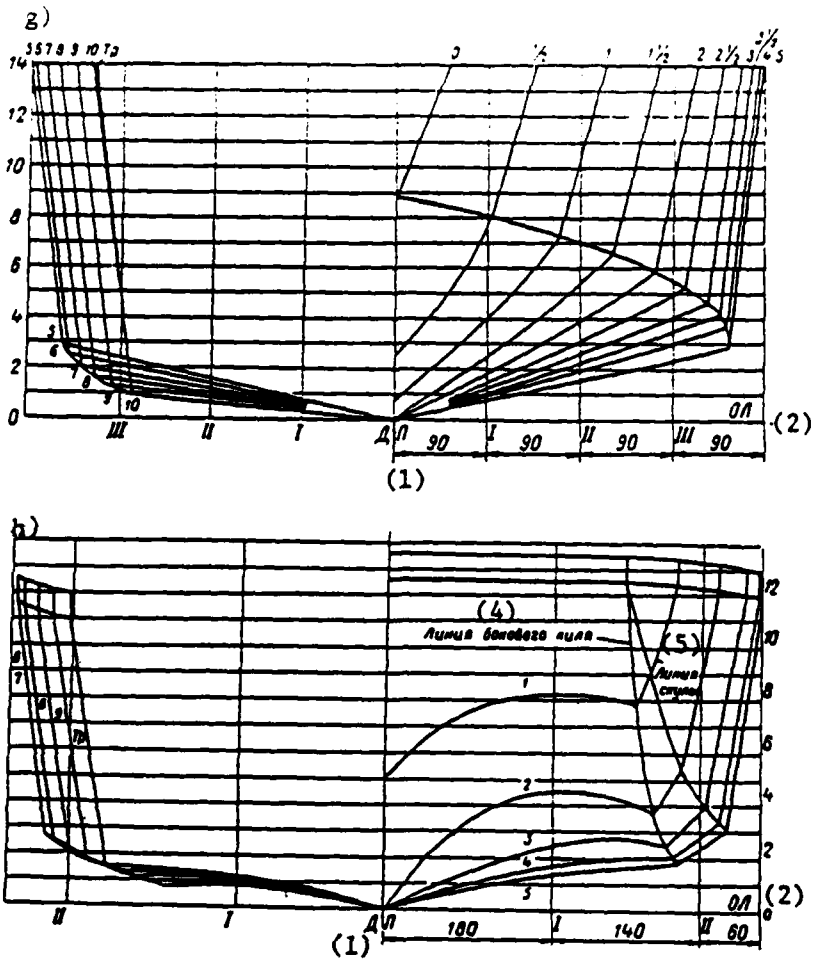
Figure 2.50. Hulls of the group A models of the MBK systematic series: a — MBK-1; b -- MBK-2; c — MBK-3; d -- MBK-4; e — MBK-5; f — MBK-6; g — MBK-8; h -- MBK-9

Key:

1. center plane
2. base line



[Figure 2.50, continued]
Key:
3. transom



[Figure 2.50, continued]
Key:

4. Bilge keel line
5. Chine line

Thus, the inverse lift-drag ratio of a small planing vessel with given frame lines for Fr_Δ=const can be represented as a function of the following parameters:

$$\varepsilon = \varepsilon(\bar{x}_g, C_\Delta, \bar{L}, \beta_x).$$

An anlysis of the experimental relations for the inverse lift-drag ratio of models of the systematic series MBK as a function of the basic parameters indicates that these functions are smooth, differentiable and bounded in the investigated range of basic parameters, including the limits of their variation. The latter permits representation of the inverse lift-drag ratio with constant Froude number analytically in the form of a Taylor series for a function of several variables by a formula analogous to formula (2.34). In the given case in the expansion by the formula $\varepsilon_0(x_{g0}, C_{\Delta 0}, \bar{L}_0, \beta_{x0})$ is the inverse.

Survey of high-speed waterborne transport world-wide

From HIGH SPEED SURFACE CRAFT
Vol. 21, No. 3, 1982

THE CONGRESS OF THE UNITED STATES has appropriated funds for a comprehensive survey and analysis of high-speed waterborne public passenger transportation in the United States and throughout the world. A report is to be submitted to Congress on this survey and analysis no later than 26 January 1983.

While the transportation systems to be examined are of a very specialised type, and are not as prevalent as bus transportation systems, the study is none the less varied and quite large. The study will provide important insights and answers to the heretofore unanswered question as to why a transportation system which seems to thrive in other countries is virtually nonexistent in the United States. The study will also provide insight into the integration of high-speed transportation services with existing transportation modes.

The project

UMTA (Urban Mass Transportation Administration) plans the study and analysis to be a joint effort between the US Department of Transportation (DOT) and an outside contractor. The project team within DOT will consist of an UMTA project manager, financial analyst, an engineer, and a planner,with support from sister agencies within the Department.

It is believed that the inhouse team will complement an outside consultant in the area of governmental financial support (Federal, State, and local) for the establishment of high speed ferry services, and in the analysis of a selected area's ability to economically and environmentally support such services.

Work to be performed

The contractor shall perform the following tasks:

(1) Describe, in detail, the approach to be followed in performing the survey and analysis required by the United States Congress. This description should include, to the best of the contractor's ability, anticipated travel (international and national) necessary to complete the scope of work.

(2) A literature search shall be conducted of those reports which are relevant in the field of high-speed waterborne transportation vessels and operations, world-wide.

(3) Investigate high-speed waterborne passenger transportation operations world-wide. Such investigation shall include patronage, capacity, routes, trip times, trip lengths, operating revenues (by source), operating cost (by function), subsidies (by source), competition, general weather and water conditions, and type of service (recreational, commutation, business and other). The investigation shall also include the planning undertaken to develop the various high-speed waterborne transportation services worldwide, recreational, business, commutation, and other. Interface with other modes will be described in this report. Marketing activities, both prior to initiation of the service and on a continuing, basis, will also be described. If market surveys were conducted, an analysis of the results based on actual utilisation of the service should be included to the extent feasible.

(4) An investigation shall be made of high-speed waterborne vessels (both domestic and international) including engineering and economic comparison with other modes, energy efficiency, maintainability, reliability, ride quality, safety, comfort accessibility to handicapped persons and operating characteristics.

(5) An investigation shall be made of the feasibility of high-speed waterborne passenger transportation in the United States. This investigation shall include the following:

(a) Existing and former US high-speed waterborne transportation operations and analysis of reasons for the success or lack thereof.

(b) Overall assessment of market potential (including suitable sites) in the US

(c) Determination of 6 to 10 most likely areas where high-speed waterborne transportation could feasibly operate in the US. UMTA will make a final determination on the sites for in-depth analysis as follows:

- Assessment of routes, terminals, cost, ridership, tariffs, and problems of such services in these areas. This assessment should also include which high-speed vessel(s) are most appropriate for each site. This analysis should include market research of potential ridership.
- Interface and possible competition with their modes in the area. This should include an analysis of how the high-speed waterborne transportation service would enhance the total transportation service delivery systems within each area. It should also include an analysis of interface with other modes at the site.
- An investigation shall be made to the extent feasible of the interest on the part of the local public and/or private sector in operating a high-speed waterborne transportation service and the capability of operating such service.

(6) The feasibility of introducing foreign high-speed waterborne technology into the US marketplace shall be investigated. This investigation should take into consideration the Jones Act of 1920 as amended (46 USC Section Cite 8830, first proviso) and any other applicable legislation and regulation. Strategies for introduction of this technology should be developed.

RHS-200 HYDROFOIL EVALUATION

A performance and passenger ferry evaluation of a Rodriquez Cantiere Navale RHS-200 surface piercing hydrofoil ship was conducted for the U.S. Coast Guard and the Urban Mass Transportation Administration of DOT by DTNSRDC in May of 1982. Calm and rough water powering characteristics of the 125 ton, 254 passenger, diesel-powered ship were determined. The tests included investigation of ship takeoff power, time and distance requirements. A wide scope of hullborne and foilborne turning trials were performed. Bollard pull and underway towing capabilities were assessed. Emergency stopping distances were also determined. The bow wake of the ship was measured, interior and exterior sound levels were recorded, the spectural definition of structural vibrations were obtained. The rough water trials primarily considered the effect of the flap-controlled Seakeeping Augmentation System on ship motions and accelerations in State 3 and State 5 seas. The ferry service evaluation included ship compliance with USCG applicable requirements and operational and arrangement information pertinent to ferry utilization. A report is currently in process of finalization and submittal to the USCG for review and approval.

RHS 200 TRIAL SCOPE

PART A: CALM WATER SPEED-POWER

- Speed Log Calibration
- Hullborne Speed-Power
- Calm Water Takeoff Trials
- Foilborne Speed-Power & Trim

PART B: CALM WATER TURNING

- Spiral Turning
- Debris Avoidance Maneuvers
- Low Speed Maneuverability
- Tactical Diameter

PART C: RESPONSE CHARACTERISTICS

- Stopping Characteristics
- Tactical Response Time
- Wake Evaluation

PART D: TOWING CHARACTERISTICS

- Bollard Pull Tests
- Towing Capability
- RHS 200 Characteristics Under Tow

PART E: ROUGH WATER TRIALS

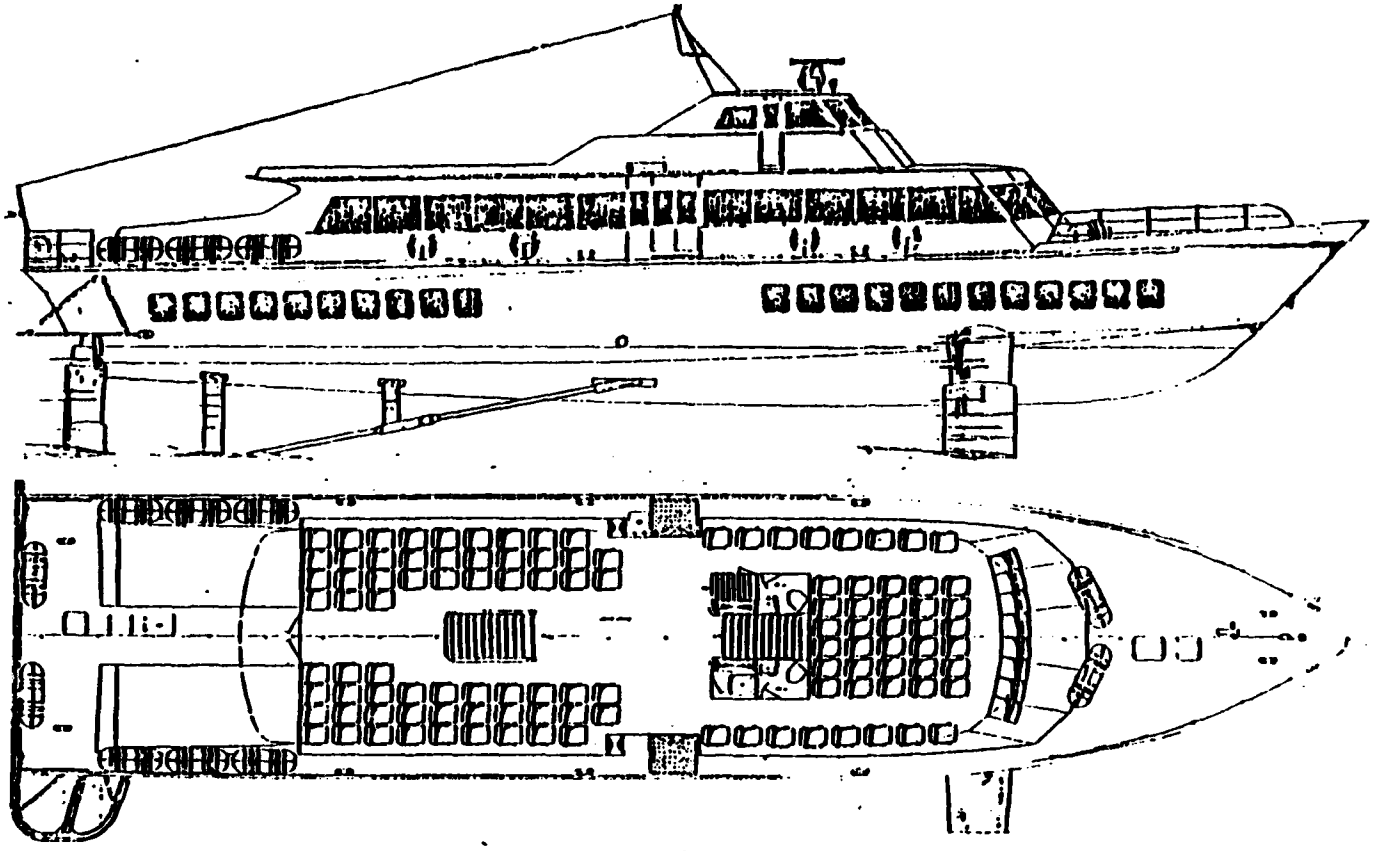
- Hullborne Matrix Trials
- R/W Takeoffs and Landings
- Foilborne Matrix Trials
- R/W Spiral Turning
- R/W Debris Avoidance
- Slamming
- Seakindliness
- Anchoring

PHOTOGRAPHIC COVERAGE

ACOUSTIC & VIBRATION SURVEYS

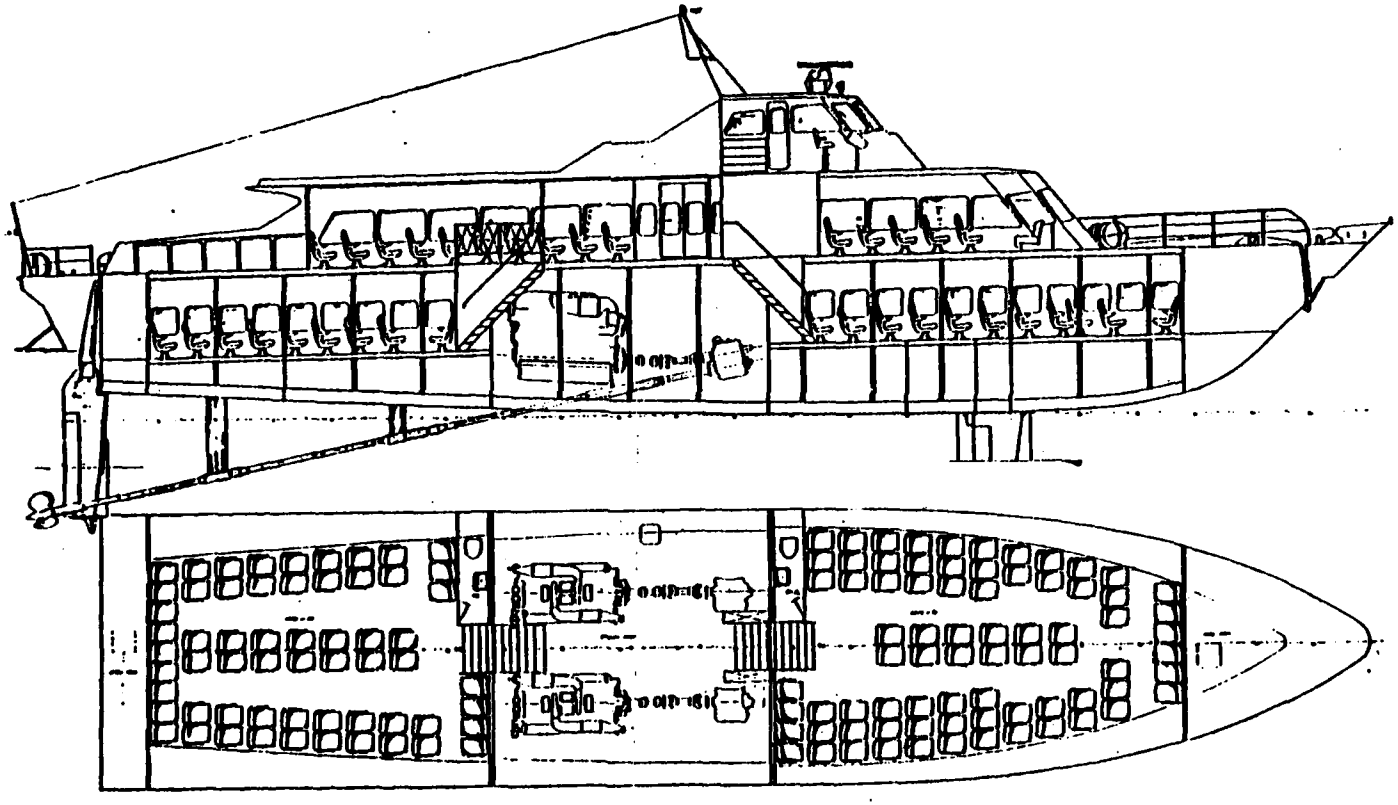
HYDROFOIL BOAT RHS 200 TYPE - 254 PASSENGERS

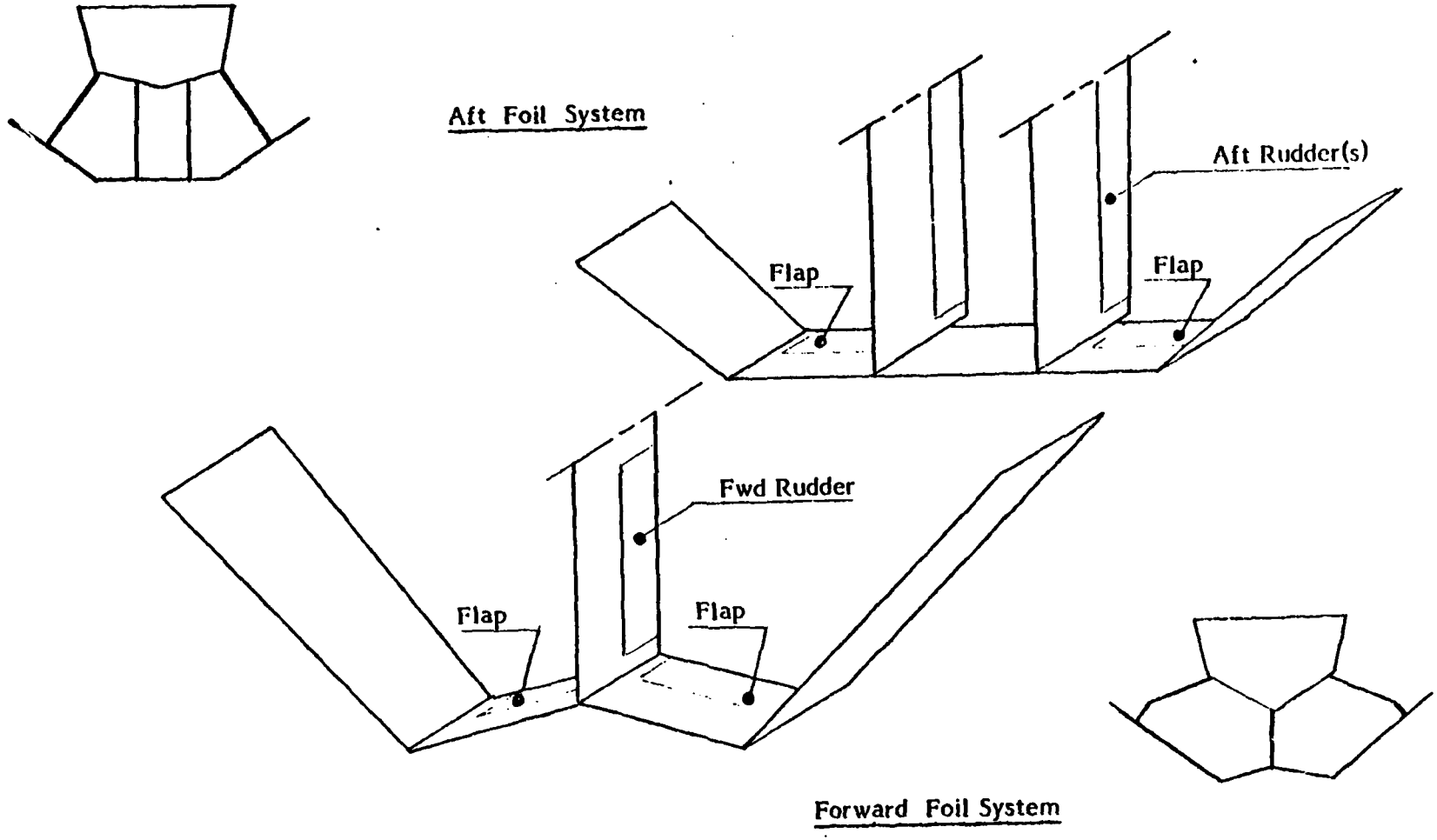
ALISCAFO RHS 200 - 254 PASSEGGERI



Length overall	35.80 m.	Lunghezza f.t.	35.80 m.
Molded breadth	7.00 »	Larghezza f.t.	7.00 »
Width across foils	14.40 »	Larghezza s.a.	14.40 »
Draught, waterborne	4.55 »	Pescaggio da fermo	4.55 »
Draugth, foilborne	2.05 »	Pescaggio in nav.	2.05 »
Displacement	120 tons.	Dislocamento	120 tonn.
Power plant	2x2600 HP	Propulsione	2x2600 HP
Cruising speed	36 knots	Velocità cr.	36 nodi
Cruising range	200 miles	Autonomia	200 mig.
Passengers	254	Passeggeri	254

RHS 200





RHS 200 FOIL SYSTEM SCHEMATIC

Attachment 7

BIBLIOGRAPHY

1. Keuning, J.A., Gerritsma, J., "Resistance Tests of a Series of Planing Hull Forms with 25 Degrees Deadrise Angle," International Shipbuilding Progress, Vol. 29, No. 337, September, 1982

2. Sedov, L.I., Similarity and Dimensional Analysis in Mechanics, MIR Publishers, Moscow, 1982, pp 79-86

3. Shao, S., Wang, Y., "The Influence of Chine Strips on Resistance and Motions of High Speed Hull Forms," High Speed Surface Craft, Vol. 20, No. 1, Jan-Feb., 1981, pp 46-51

4. Takekuma, K., Baba, E., "Hydrodynamic Design and Development of High Speed Craft in MHI," Mitsubishi Technical Bulletin No. 154, Dec. 1982 or High Speed Surface Craft, Feb. 1982

5. Yegorov, I.T., Bun'Kov, M.M., Sandovnikov, Yu. M., Propulsive Performance and Seaworthiness of Planing Vessels, Sudostroeniye, Leningrad, 1978 (In Russian),NAVSEA Translation No. 1965, 1982, available in SNAME Library

6. Fuwa, T., Yoshino, T., Yamamoto, T., Sugai, K., "An Experimental Study on Broaching-to of a Small High Speed Boat," Journal of the Society of Naval Architects of Japan, Vol. 150, Dec., 1981, pp 223-231, in Jap.

7. Shao, S., Wang, Y., "The Influence of Chine Strips on Resistance and Motions of High-Speed Displacement Hull Forms," High Speed Surface Craft, Vol. 20, No. 1, Jan-Feb., 1981, pp 46-51

8. Jin, P., Su, B., Tan, Z., "A Parametric Study on High-Speed Round Bilge Displacement Hulls," High-Speed Surface Craft, Vol. 19, No. 12, pp. 6-13.

9. Yegorov, I.T., Bun'Kov, M.M., Sandovnikov, Yu.M., Propulsive Performance and Seaworthiness of Planing Vessels, Sudostroyeniye, Leningrad 1978 (In Russian) NAVSEA Translation No. 1965, 1982 (Available in SNAME Library)

10. Bailey, D., "The Effect of Shallow Water on the Performance of a High Speed Ship," National Maritime Institute, Report No NMI R 154, February, 1983.

11. Millward, A., "The Effect of Shallow Water on the Resistance of a Ship at High Sub Critical and Super Critical Speeds." Trans RINA Paper W4, 1981

12. Millward, A., "Shallow Water and Channel Effects on Wave Resisatance at High Sub Critical and Super Critical Speeds," Trans RINA Paper W2, 1982

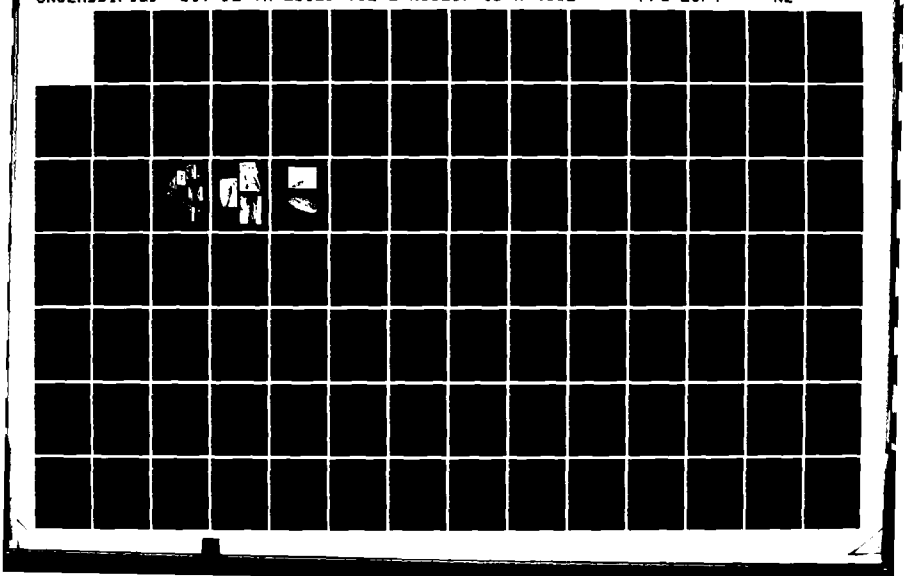
13. Maruo, H., Tachibana, T., "An Investigation into the Sinkage of a Ship at the Transcritical Speed in Shallow Water," Journal of the Society of Naval Architects of Japan, Vol. 150, Dec. 1981, pp. 56-62 (In English)

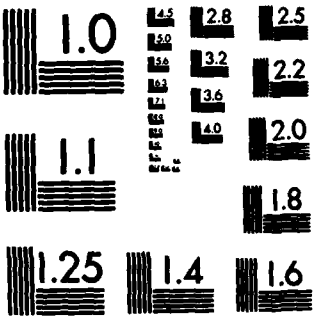
14. Basin, A.M., Velednitsky, I.O., Lyakhovitsky, A.G., Ship Hydrodynamics in Shallow Water, Sudostroeniye, Leningrad, 1976, (In Russian)

15. Kolbizaev, B.A., et. al., Handbook for Design of Ship with Dynamic Lift Support, Sudostroeniye, Leningrad, 1980 (In Russian)

16. Sakic, V., "Approximate Determination of the Propulsive Power of Small Hydrofoil Craft," High Speed Surface Craft, Vol. 21, No. 3, March, 1982, pp. 11-18

AD-A144 226 PROCEEDINGS OF THE GENERAL MEETING OF THE AMERICAN 6/7
TOWING TANK CONFERENCE..(U) STEVENS INST OF TECH
HOBOKEN NJ DAVIDSON LAB D SAVITSKY ET AL. AUG 83
UNCLASSIFIED SIT-DL-TR-13029-VOL-1 N00167-83-M-4062 F/G 20/4 NL





MICROCOPY RESOLUTION TEST CHART
NATIONAL BUREAU OF STANDARDS-1963-A

AD-P003 813

HIGH SPEED MANEUVERING OF AMPHIBIOUS HOVERCRAFT

By

R.T WATERS *

D.D. MORAN **

and

R.F. MESSALLE ***

* Naval Architect, David Taylor Naval Ship R&D Center
** Head, Special Ship and Ocean Systems Dynamics Branch, David Taylor Naval Ship R&D Center
*** Mathematician, David Taylor Naval Ship R&D Center

ABSTRACT

The high speed maneuvering control of amphibious hovercraft involves a careful balance of aerodynamic and hydrodynamic forces and control effectors. Hovercraft maneuvering control can be either extremely precise or practically non-existent according to the selection and placement of control devices. A wide variety of options are avaiable to the hovercraft designer who must match mission requirements against design complexity, reliability and cost considerations. These tradeoffs must be accomplished through reliable methods for maneuvering prediction and analysis including direct and supporting experimental methods. The development of hovercraft simulations is discussed with an emphasis on the practical experience gained in recent years by the U.S. Navy in amphibious hovercraft operations at all speeds over water and solid terrain. A specific data based simulation which requires extensive tow tank testing is presented and the tankery requirements are defined.

INTRODUCTION

Hovercraft are the most maneuverable of marine vehicles. Their air cushion contact to the free surface provides a flexibility for overwater maneuvering which is unmatched at low speed. This low speed advantage becomes a high speed control challenge when the lack of significant yaw and sway resistive forces places the entire maneuvering control burden upon the propulsion forces and the flexibility of the control system. The U.S. Navy Amphibious Assault Landing Craft (AALC) and the subsequent Landing Craft Air Cushion (LCAC) Vehicles have been designed to provide substantial maneuvering ability over both land and water. This maneuvering flexibility has been demonstrated repeatedly throughout the full scale trials phase of the JEFF (A) and JEFF (B) programs. It has been further demonstrated through the companion analytic simulation methods. These studies have been verified through the application of fullscale trials data and control records as inputs to the simulation analyses. The simulated and measured hovercraft trajectories have shown a remarkable degree of equivalency considering the difficulty of mathematical modeling of hovercraft. The analytic simulation developed is based upon fundamental Newtonian mechanics as outlined in the following sections. Implementation of the simulation is dependent upon the use of a large hydrodynamic data base developed through an extensive program of model scale tow tank experiments. These studies include stability towing, model oscillation and rotating arm testing. This simulation method thereby commands a greater commitment of model scale testing than most ship design and performance evaluation procedures.

ACV MANEUVERING EQUATIONS OF MOTION

The horizontal plane motion of an air cushion vehicle can be mathematically described by a series of six linearized Eulerian equations of motion based upon Newton's law of motion, F=ma. These equations, when based upon a coordinate system fixed in the principle axis of the vehicle at the center of gravity, can be represented as follows:

$$X - \text{Force} = m\left[\Delta\,\dot{u} + \bar{z}_c\,\dot{q}\right] \tag{1}$$

$$Y - \text{Force} = m\left[\dot{v} + u_o r + \bar{x}_c\dot{r} - \bar{z}_c\,\dot{p}\right] \tag{2}$$

$$Z - \text{Force} = m\left[\dot{w} - u_o\,q - \bar{x}_c\,\dot{q}\right] \tag{3}$$

$$K - \text{Moment} = I_{44}\,\dot{p} - I_{64}\,\dot{r} - m\,\bar{z}_c\left[\dot{v} + u_o\,r\right] \tag{4}$$

$$M - \text{Moment} = I_{55}\,\dot{q} + m\left[\bar{z}_c\,\Delta\dot{u} - \bar{x}_c\,(\dot{w} - qu_o)\right] \tag{5}$$

$$N - \text{Moment} = I_{66}\,\dot{r} - I_{64}\,\dot{p} + m\,\bar{x}_c\left[\dot{v} + ru_o\right] \tag{6}$$

The six forces and moments are the sums of all the external forces acting on the vehicle. These forces include the aerodynamic forces, hydrodynamic forces and propulsion forces. The aerodynamic forces are those forces which act upon the vehicle due to it's relative movement though the air. This relative motion includes both the vehicle velocity vector and the relative wind velocity vector. The hydrodynamic forces arise because the vehicle's pressure field imparts energy to the free surface when the vehicle moves along the air-water interface and because the seal system used to contain the air cushion can drag along the water surface under certain conditions. The propulsion forces include all of those forces imparted to the vehicle by the propulsion and control systems.

The aerodynamic and hydrodynamic forces can be represented mathematically as functions of the vehicle acceleration, velocity, and displacement vector or state vector. In general however, not all the components of this state vector effect any one of the forces and moments acting on the ship. As an example:

$$X - \text{hydrodynamic} = f(\phi,\Theta,u,v,w,p,q,r,\dot{u},\dot{v},\dot{w},\dot{p},\dot{q},\dot{r}) \tag{7}$$

$$X - \text{aerodynamic} = f(\phi,\Theta,u,w,r,p,q,r,\dot{u},\dot{v},\dot{w},\dot{p},\dot{q},\dot{r})$$

$$K - \text{hydrodynamic} = f(\phi,u,v,p,r,\dot{v},\dot{p},\dot{r})$$

In order to examine these forces and to compare them for different designs, the total force can be represented by a Taylor series expansion. This expansion would take the following form for the hydrodynamic yaw moment.

$$N - \text{hydrodynamic} = N_v\,v + N_r\,r + N_{\dot{v}}\,\dot{v} + N_{\dot{r}}\,\dot{r} + N_p p + \tag{8}$$

$$N_{\dot{p}}\,\dot{p} + N_{vr}\,v\,r + N_{\dot{v}\dot{r}}\,v\,\dot{r} + N_{vu}\,vu + N_{ru}\,ru + \ldots$$

$$+ N_{rr}\,|r|\,r + \ldots\ldots$$

This Taylor expansion can be taken out to an infinite number of terms. For practical purposes, some of these terms can be ignored as they are quite small and representing them in a mathematical model would be very cumbersome.

Hydrodynamic/Aerodynamic forces

The forces acting on the vehicle do to its movement thru the air and water can be obtained by performing model scale experiments in the wind tunnel and the towing tank. Figure 1 presents the results of tow tank experiments on a 1/12th scale model of the LC JEFF (B). In that figure, the nondimensional yaw moment coefficient is presented as a function of drift angle. The Taylor coefficient obtained from this data would be N'_v, N_{vvv}', and N_{vvvv}. The first order term, N_v, would be the slope, $\partial N'/\partial v'$, at zero drift angle. The other two coefficients, N_{vv} and N_{vvv} would be used to account for the curvature of the data results. This figure is typical of the type of results that are obtained from model scale experiments for all fully skirted rectangular planform presents and two problems which occur when studying ACV maneuvering.

First, mathematically representing the model scale data with Taylor series expansions is quite difficult when the results exhibit compound curvature. In order to accurately model these data, one must develop a large number of terms in the Taylor expansion. The problem of mathematically modelling these forces for use in dynamic computer models can be overcome by using a different represention for the data. This representation requires a data base of the forces and moment used to generate the Taylor coefficients instead of the coefficients. A detailed description of this process and its limitations will be discussed later. The second problem occurs on the actual vehicle during a maneuver. As shown in figure 1, the yaw moment which resists the drift angle or sway velocity increases until a drift angle, β, of -15.0 degrees is reached and then drops off rapidly with increasing drift angle. If one looks at a maneuver where the control system is applying a yaw moment to vehicle to overcome the hydrodynamic yaw resisting moment, when the drift angle at which maximum hydrodynamic yaw moment is exceeded, the hydrodynamic force decreases but the control force does not. The excess yaw moment due to the control forces causes the drift angle to increase further and the craft pirouettes. Because the vehcile is cushion borne and the drag increase due to high drift angles is small, it is possible for the vehicle to end up going backwards or sideways at a relatively high speed. This pirouette or spin-out phenomena can occur on most fully-skirted ACVs.

The variation of the nondimensional hydrodynamic yaw moment, N', with nondimensional yaw rate r', is presented in Figure 2. Here, the hydrodynamic yaw restoring moment does not reach a maximum and then drop off. Figures 1 and 2 are typical of all the results for rectangular fully skirted planforms at speeds above hump. For speeds below hump, ACV's do not exhibit the instability in the hydrodynamic yaw restoring moment.

The Taylor series representation of these forces and moments is useful when examining the overall performance of the vehicle over a range of speeds. In Figure 3, the nondimensional hydrodynamic coefficient, N_v, is presented as a function of Froude number, where:

$$N'_v = \left.\frac{\delta N'}{\delta v'}\right|_{v=0} = \left.\frac{\delta N'}{\delta(-\sin\beta)}\right|_{\beta=0}$$

In Figure 3, it is seen that at speeds below hump (Froude number < 0.5), N_v' is a large positive number. As speed is increased to hump, N_v' become negative and then becomes positive again at speeds above hump (Froude number > 0.75). The vehicle maneuvering characteristics can be related to this nondimensional coefficients and the other basic coefficients be using a reduced form of the equations of motion for two degrees of freedom for sway and yaw. Equations 2 and 6 can be reduced to provide a hydrodynamic stability criterion G, which is:

$$G = 1 - \frac{N_v' (Y_r' - m')}{Y_v' \quad N_r'} \tag{11}$$

where $G > 0$ means a stable vehicle

$G = -4.43$ for Froude number = .535

$G = 4.23$ for Froude number = 1.17

$G = 20.67$ for Froude number = 1.66

The negative value of G at a Froude number of 0.535 is due entirely to the fact that N_v' is negative at that speed. For the vehicle, a negative value of G means that if the craft is perturbed in some manner, it will go into a undamped oscillation or divergence in the vehicle path. This representation of the vehicles course keeping stability also can be used to explain the pirouette problem described previously. If the variation of nondimensional yaw moment with sway velocity changes slope at some drift angle, then the local nondimensional hydrodynamic coefficient, N_v', will change sign. By substituting the local N_v' into equation 11 for a Froude number of 1.17 and a drift angle of -17 degrees.

$$G = 4.23\Big|_{\beta=0} \quad \text{for} \quad N_v'\Big|_{\beta=0} = .0011 \quad \text{or} \quad G = -2.23\Big|_{\beta=17} \quad \text{for} \quad N_v'\Big|_{\beta=17} = -0.0012$$

At that drift angle, the vehicle is hydrodynamically unstable so the fixed control forces cause a divergent track i.e. pirouette.

The aerodynamic forces are somewhat more dependant vehicle configuration than the hydrodynamic forces because the superstructure configurations of different vehicles vary more. The results of wind tunnel model experiments on a 1/12 scale model are presented in Figure 4. In this Figure, the nondimensional side force, Y' and nondimensional yaw moment, N', are presented as a function of drift angle. These results are quite undramatic and are as expected, Y_v' (aerodynamic) is negative while N_v' (aerodynamic) is positive. LC JEFF^v(B) has large superstructure forward and the aerodynamic yaw moment presented does not include the effect of propulsors and rudders. For a vehicle with large aerdynamic rudders aft, N_v' (aerodynamic) would be negative.

HYDRODYNAMIC/AERODYNAMIC FORCES - MODEL EXPERIMENTS

The maneuvering data presented previously were obtained from experiments on a LC JEFF (B) model. There are three experiments which must be performed to quantify the aerodynamic and hydrodynamic forces acting on an air cushion vehicle during a maneuver. First, a rotating arm test is performed to obtain the hydrodynamic velocity depentant (damping) forces and the forces dependant upon the roll angle. This procedure requires that a captive model is run in circles at various speeds, drift angles, roll angles and turn radius. The forces acting on the model are recorded, the inertial tares are remove, and the results analized to obtain the velocity dependant hydrodynamic coefficients such as N_v', N_r', $N_{r\phi}'$, Y_v', etc. The acceleration dependant (added mass) hydrodynamic forces are obtained from a Horizontal Planar Motions (HPM) experiment. The procedure involves sinusoudally oscillation of a model in sway and yaw while the model is moving down the tow tank. The hydrodynamic forces and moments acting on the model and the motion of the model are recorded. The equation of motion, the measured forces and the measured motions are analyzed to relate the measured forces to the acceleration of the model. This experiment will provide the acceleration dependant hydrodynamic coefficients such as $Y_v^{\bullet}'$, $N_r^{\bullet}'$ and $Y_{vr}^{\bullet\bullet}'$. Wind tunnel experiments are used to obtain the aerodynamic forces acting on the vehicle. For this procedure, a model is placed in the wind tunnel at various drift angles and the resultant aerodynamic forces are measured.

Typically, for these experiments, the model will consist of a scaled flexible skirt system and a scaled lift system are installed on a platform of the same shape as the full scale vehicle. For hydrodynamic experiments, it is not necessary to model either the superstructure or the propulsion and control systems of the full scale vehicle. For Froude scaled hydrodynamic experiments, it is not possible to model the structrual characteristics of the skirt system. This does not appear to lead to any great errors in the results.

It is very important, however, to model the lift system performance, as differences in lift system air flow rate effect the hydrodynamics forces and moments. Wind tunnel models do not have to model the flexible skirt and lift system, but the superstructure must be accurately modeled.

CONTROL DEVICES

The third type of forces acting on an aircushion vehicle are the propulsion and control forces. These are the forces due to the air propellers, the aerodynamic rudders and the other control devices.

There are several types of control devices normally used on amphibious air cushion vehicles. Due to the amphibious operation requirement these devices are all usually some type of aerodynamic force producer. The simplest device is an aerodynamic rudder mounted at the rear of the vehicle which generates force due to lift when there is air blowing across it. To make these rudders effective at low speed, they are often placed behind and in the outflow of either the main propulsors or some auxillary flow device such as a duct from the cushion. The amount of control authority (force produced) is dependant upon the size of the rudder and the velocity of air flow over it. Therefore, the side force per unit of rudder deflection Y_{δ_r}, is:

$$Y_{\delta_r} = 1/2\ \rho\ s\ v^2\ \frac{\delta\ C_L}{\delta\ \alpha} \tag{12}$$

$$\frac{\delta\ C_L}{\delta\ \alpha} = \frac{0.9\ (2\ \pi)\ a}{\cos\ \Lambda\ ((a^2/\cos^4 \Lambda)+4)^{1/2}+\ 1.8} \tag{13}$$

Note: For fully movable rudders with moderate aspectratios from reference 2.

Λ - Sweep angle at 1/4 - chord
a - Geometric aspect ratio
v - Inflow velocity
ρ - Air density
s - Rudder area

Yaw moment generated by placing the rudder either forward of or aft of the vehicle center of gravity.

$$N_{\delta_r} = Y_{\delta_r} \cdot \text{x distance between rudder stock and vehicle CG}$$

This type of control device has been installed on several air cushion vehicles including the LC JEFF (B), and the SRN-4. An additional benefit of this device is the added directional stability which is obtained when moving at high speeds.

Another method of control can be used if the vehicle has more than one propulsor unit. Typically, an ACV with two or more air propellers can be controlled by developing differential thrust between propellers mounted on opposite sides of the vehicle centerline. This installation will not generate much side force, but differential propulsion can generate considerable yaw moment at low speeds. The disadvantage of this method of control as that at high speeds the amount of control authority is limited by the requirement to provide straight ahead thrust. At the maximum vehicle speed, there is insufficient control authority available to turn the craft without slowing down. Another method of controlling the craft with a air propeller involves rotating the entire propeller to generate vectored thrust. This system is used on the LC JEFF (A) with four shrouded propellers and on the BH-7 with an open propeller. This approach can provide both side force and yaw moment and at low speed is capable of providing a great deal of control authority.

A third technique for providing control authority requires use of air from the lift system. The control force is generated by directing a stream of this pressurized air through some opening in the lift or cushion system. The simplest method is to install a "puff port" in a plenum above the cushion. When the plenum is opened to the atmosphere, the pressure in the cushion force air out into the atmosphere. Control force is generated by conservation of momentum.

$$F = m\ V = \rho\ V^2\ A \tag{14}$$

where m = Mass of air
v = Velocity of air exiting puff port
A = Area of puff-port
ρ = Density of air

$$V = 0.6 \left(\frac{2\Delta\rho}{\rho}\right)^{1/2} \quad (15)$$

where $\Delta\rho$ - Pressure drop from plenum to atmosphere
0.6- Approximate discharge coefficient for square edged port.

Equation 15 is approximate as the discharge coefficient varies with port size, shape, air flow Reynold's number and what type of puff-port cover is used. Puff ports provide control at low speed, however as speed increases the effectiveness is reduced due to free stream air flowing across the port and deflecting the out flow jet. An improvement on the puff-port is the bow thruster. Bow thrusters generate force in the same way as a puff-port, by throwing weight (air) away. Bow thrusters however, can rotate to direct the force in any direction. At speed, the bow thruster can also be directed aft to provide propulsion forces. The amount of bow thruster thrust for the LC JEFF (B) is:

$$T_{\text{Bow Thruster}} = mv = \rho \, Q_{\text{Bow Thruster}} \, V \quad (16)$$

$$\text{Y-Force}_{\text{Bow Thruster}} = F_{\text{Bow Thruster}} \sin \delta_{\text{Bow Thruster}} \quad (17)$$

$$Q = 5.20 \, (2 \rho_{BT}/\rho)^{1/2} \quad (18)$$

$$V = .33 \cdot A \, (2 P_{BT}/\rho)^{1/2} \quad (19)$$

where: A = Bowthruster Duct Area

The total force generated by the bowthruster does drop with increasing speed. This is due to the fact that a speed increases the change in momentum decreases due to the forward velocity.

$$F = m \cdot (V_{\text{thruster}} - V_{\text{vehicle}}) \quad (20)$$

A comparison of the performance of the various control methods is shown in Table 1.

	Zero Speed	Low Speed	High Speed	Side Force	Yaw Moment
Aerodynamic Rudder	Poor	Poor	Good	✓	✓
Aerodynamic Rudder Behind Prop.	Poor	Good	Good	✓	✓
Differential/Prop.	Good	Good	Poor		✓
Rotating Prop	Good	Fair	Poor	✓	
Puff Port	Good	Good	Fair	✓	✓

PREDICTION TECHNIQUES

Coefficient Based Method

To study the maneuvering performance of an air cushion vehicles without use of radio control models or full scale craft, it is necessary to use the Eulerian equations of motion stated previously. Since the calculations involved are very complex and time consuming, this analysis is best performed using a time domair computer simulation which will mathematically model the forces involved. Typically, this computer program would contain the equations of motion, some representation of the forces and moments acting upon the vehicle, a method of providing control input to the model and an integration technique. The program basically works as follows:

1) Some initial set of vehicle displacements, velocities and accelerations are chosen along with a set of control inputs.

2) The computer program then calculates the hydrodynamic, aerodynamic and control forces based upon the initial input.

3) These forms are then used long with the Eulerian equations of motion to calculate new vehicle accelerations.

4) These accelerations are integrated over some small time step (usually less than 0.5 seconds). to obtain new vehicle velocities and the velocities integrated to obtain new displacements.

5) The new set of vehicle displacements, velocities and accelerations replace those used previously in step 2 and the process repeats itself.

This is the basic outline of most mathematical models of a vehicle in maneuvering motion. The differences in programs are found largely in the forces acting on the vehicle represented. As stated previously, a typical approach used for surface ships involves developing a series of maneuvering coefficients and representing the total force as a summation of these coefficients multiplied by the various accelerations, velocities and displacements. An example of this approach for surface ships is presented in Reference 3. This is the "classical" approach to the marine vehicle maneuvering problem. It can be reduced to a simple description of the vehicle by the six coefficients

Y_v', N_v', Y_{δ_r}', N_{δ_r}', Y_r' and N_r'

and the vessel mass. Unfortunately, this approach is not easily adaped to modelling highly nonlinear systems such as ACV's for the reasons stated earlier.

Table Method

A second approach to representing the aerodynamic and hydrodynamic forces in the mathematical model is to construct a table of the force data and apply interpolation between specific points in the table. This "table look-up" tech-

nique presents several advantages over the Taylor series representation. First, the tables of data can be constructed to cover any number or range of variables wished. The amount of nonlinearity in the data base is longer a problem, the interpolation routine can handle any number of variables at the same time. As an example, the table constructed to model the LC JEFF (B) is a four dimensional matrix with speed, sway velocity, roll angle and yaw rate as the axes. Each "point" in the matrix contains the six hydrodynamic forces and moments associated with a specific speed, sway velocity, roll angle and yaw rate. To obtain the hydrodynamic forces and moments at any time step, the computer program performs a four way interpolation between available data points. For the LC JEFF (B), the model data used in the simulation were taken at the design displacement and the pitch angles associated with the different speeds. Other hydrodynamic forces such as those associated with the vehicle accelerations are calculated using the standard Taylor series coefficients.

If a force or moment is a function, F (x,y) of two independent variables x and y, then a polynomial fit to the function may be presented as:

$$F(x,y) = a_0(y) + a_1(y)x + a_2(y)\,x^2 + \ldots.$$

where each coefficient of x is also a polynomial in y. The number of terms to be used then depends on the desired accuracy of the fit. As additional independent variables are introduced the amount of polynomial curve fitting explodes if the function is nonlinear and a close fit is required. For an air cushion vehicle it is not unreasonable to assume that the forces and moments are functions of speed, drift angle, yaw rate, roll angle and even additional variables such as pitch angle and center of gravity location. The central difficulty with a Taylor series expansion or ploynomal fit is the requirement that a small set of coefficients explain a large data set. It is this global requirement that is difficult to satisfy.

Rather than perform a curve fit it is often easier to store the entire table of data values as input to the computer program. When a value of the function is required for a set of independent variables the data table is searched. Further when it is required to estimate the values at points between known data points an interpolation is applied based upon on the local values of the function. The interpolation process is independent of the global values and variations of the function. This requires an interpolation scheme or curve fit that uses all the known data around the unknown point. The most important requirement is that the interpolation method must be continuous. That is, as a known data point is approached the interploated valve must approach the known value. This requirement rules out low order least square fits to the surrounding data points. The simplest ploynomial which has this property in N independent variables has two coefficients and consists of the sum of all possible combinations of products of the independent variables, or

$$F(x,y,z) = \sum_{i=u}^{l} \sum_{j=u}^{l} \sum_{k=u}^{l} a_{ijk}\, x^i\, y^j\, z^k$$

During a computer simulation, the coefficients must be evaluated, but they can be saved and reused as long as the surrounding points are the same. The coefficients are the corresponding partial derivations:

$$a_{ijk} = \frac{\partial^{i+j+k} F}{(\partial_x)^i (\partial_y)^j (\partial_z)^k}$$

which are computed by finite difference of the table of values. In essence then the table look-up method is really a local Taylor series expansion about a given point and required to be exact at the nearest data points. This is easier to achieve than a Taylor series expansion which must be accurate for the global data base. The determination of all points in the data table requires, of course, a very extensive and expensive model testing process.

FULL SCALE RESULTS

The results from the full scale trials of the JEFF craft can be summarized as follows:

(1) The craft are easily able to meet their maneuvering requirement of 4000 feet advance and 6500 feet transfers.
(2) The craft exceed the turning predictions of the DTNSRDC simulation.
(3) The plots appear to use too much control action.
(4) Low speed well deck entry was easily accomplished.

Of particular concern is the fact that the DTNSRDC simulation agreement with full scale data was fair to poor. Figures 5 and 6 show two typical maneuvers and the comparisons were made by using the actual pilot control actions as input to the simulations. The main difficulty appears to be in getting the simulation yaw rate to correspond to full scale experiment. Figure 7 shows that the simulation is producing the proper general behavior but the magnitude is not correct. Additional problems also occur in matching the speed and drift angle.

Several possible difficulties have been identified as the source of the discrepencies. One problem is the lack of accurate information on the initial condition of craft and the wind speed and direction. Further, during the maneuver there is no updated wind information is available. Further, the data base is valid only for speed, drift angle yaw rate and role in calm water and steady motion conditions. Additional rate terms may be important during the turn and are not included in the data base. Another potential defect is the presumed fact that the high speed data base is developed for three speeds (hump speed, 35 knots and 50 knots). Because of these large speed increments, the interpolation scheme is not totally accurate.

The general deficiency is that the data base was necessarily constructed without model test data at all values of the four independent variables. Essentially the test program consisted of varying 3 of the independent variables

while holding the fourth at zero. Typically, a force or moments would be measured for a fixed speed for several roll angles and drift angles at zero yaw rate. The data base was then constructed by assuming that effects at other yaw rates add linearly.

It is recommended that when a table look-up approach is used that proper care be given to the test matrix and all possible combinations be measured. Ideally the table look-up scheme should be on-line during the test to guide the experimenters in where the next test condition should be run. By exercising the table look-up during the test at intermediate conditions the size of interpolation errors can be determined. The high pilot work load is currently under study. Figure (8) shows a typical rudder time history. One assumption presently under consideration is that the operators are not at ease with a central system in which they must wait as the side forces produce yaw rates and heading changes. As time progresses the changes and associated rates grow larger leading to a natural tendency toward overcontrol.

By treating the rudder displacement, thruster displacement and yaw rate values as a time series, it is possible to determine the correlation between them. There appears to be a opne second lag between operator action and yaw response. For short time intervals of 20-30 seconds, 90% yaw rate variation can be explained by a linear model, ie yaw rate = A x thruster angle + B x rudder angle with a one second lag. For larger time intervals the residual error grows and the coefficients A and B change. Current investigations now are examining higher order time series methods.

SUMMARY

Simulation of hovercraft maneuvering is much more difficult than other marine vehicles due to the lack of significant hydrodynamic yaw and sway resistive forces and the potential for horizontal plane instability. These difficulties have necessitated the determination of the hydrodynamic characteristics of hovercraft through extensive tow tank testing, oscillation and rotating arm tests. The dependence upon aerodynamic control forces complicates the simulation accuracy through a need to predict thrust and drag forces and moments in all quadrants without the existence of satisfactory analytic methods. These deficiencies have forced the development of a data based simulation methodology in which the hydrodynamic and aerodynamic coefficients must be obtained through a comprehensive series of model scale towing tank experiments which include (1) stability, (2) oscillation and (3) rotating arm studies. This method has further promoted the use of data tables, extensive interpolation, and computer table searches to provide satisfactory coefficients for the equations of motion. The success of the data table interpolations is dependent upon the quantity and quality of the model test data which are developed in the tow tank. The experimental procedures and programs must be well correlated to insure that the data base is smooth and continuous. The results of the endeavor are presently mixed. There have been difficulties in achieving a good match between predictions and full scale data; however, several deficiencies may be attributed to the nonuniformity of full scale operation falling outside of the present capability of the simulation. The simulation program has been extremely valuable in examining the control options and hovercraft responses in parametric analyses.

REFERENCES

1. Wachnik, Z.G., R.F. Messalle, J.A. Fein, "Control Simulation of Air Cushion Vehicles", Proceedings Forth Ship Control Symposium, October 1975.

2. Larsen, K., "Review of Previously Published Rudder Studies", ETT TM 79, 1946.

3. Strom-Tejsen, J., "A Digital Computer Technique for Prediction of Standard Maneuvers of Surface Ships", Taylor Model Basin Report 2130, December 1965.

4. Fein, J.A., Magnuson, A.H., Moran, D.D., "Dynamic Performance of an Air Cushion Vehicle in a Marine Environment", Jol. Hydronautics, 1974.

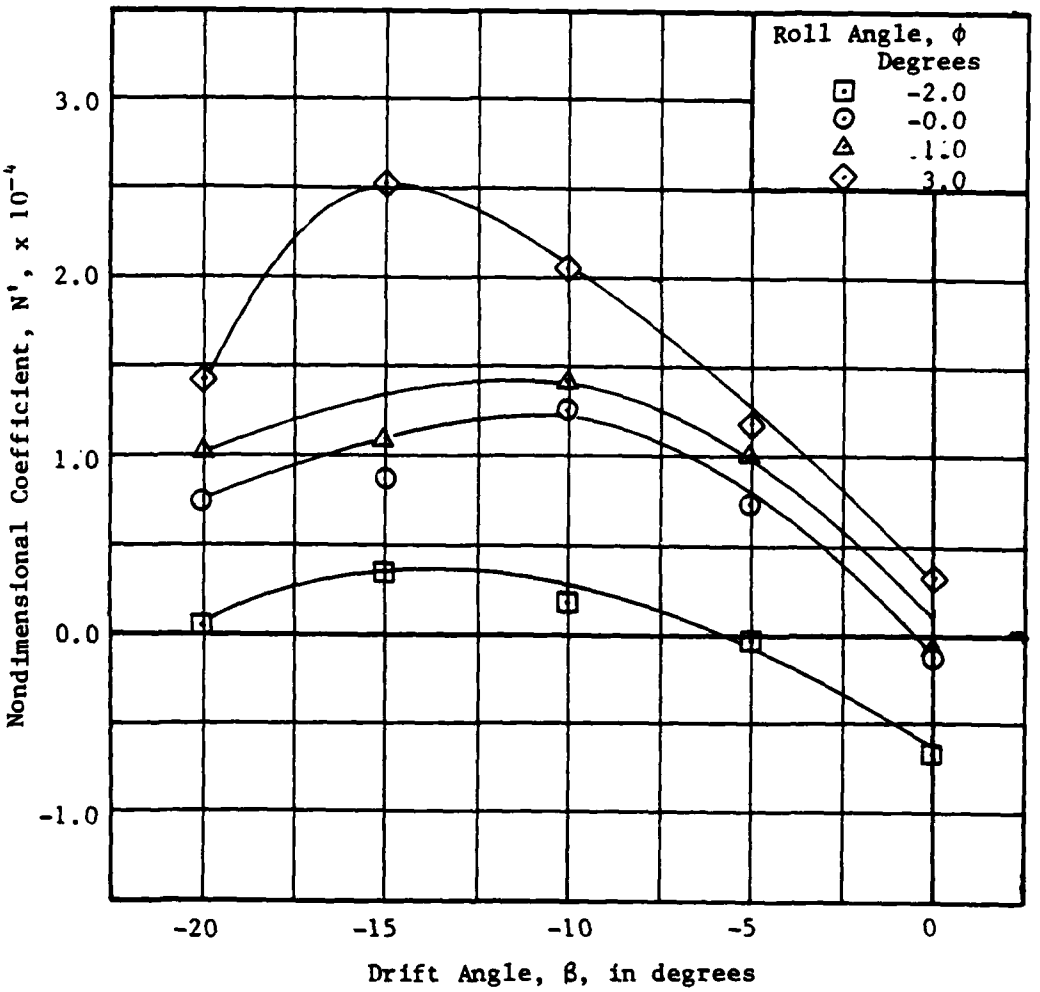


Figure 1 - Variation of Nondimensional Yaw Moment Coefficient with Drift Angle for a Series of Roll Angles, On-Cushion for a 1/12th Scale Model of the LC JEFF(B) at a Froude Number of 0.535

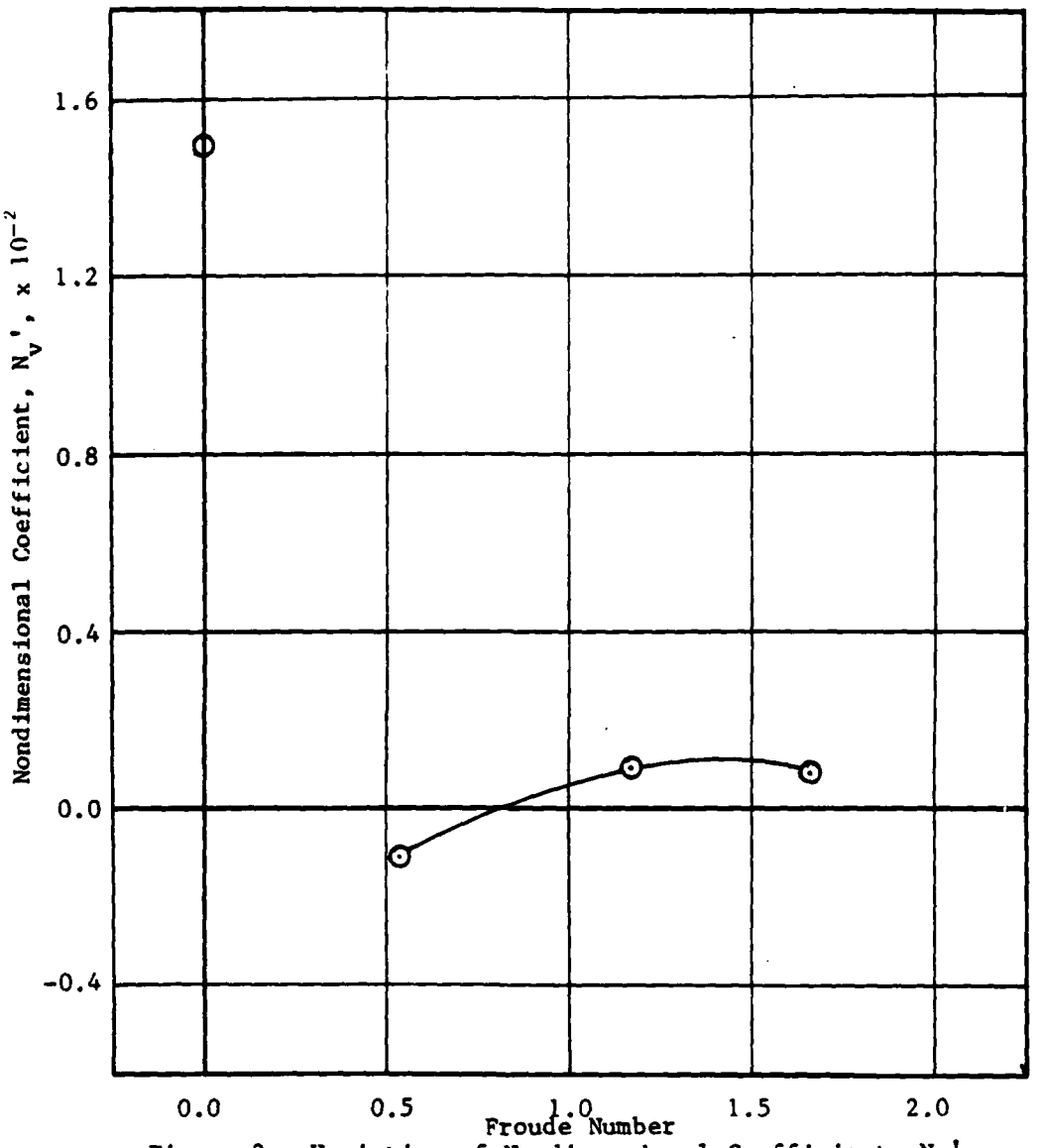


Figure 3 - Variation of Nondimensional Coefficient, N_v', with Froude Number for the LC JEFF(B)

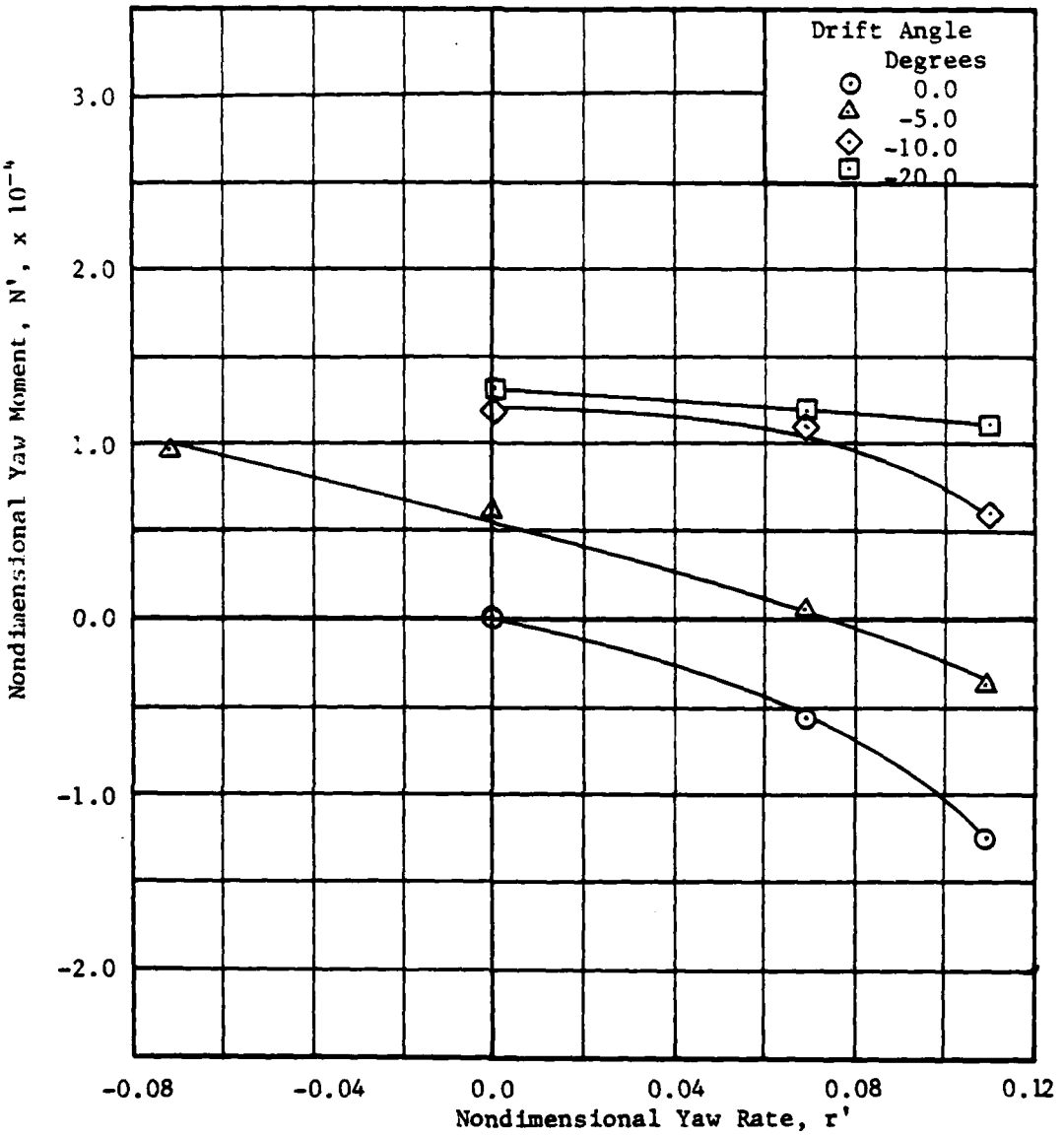
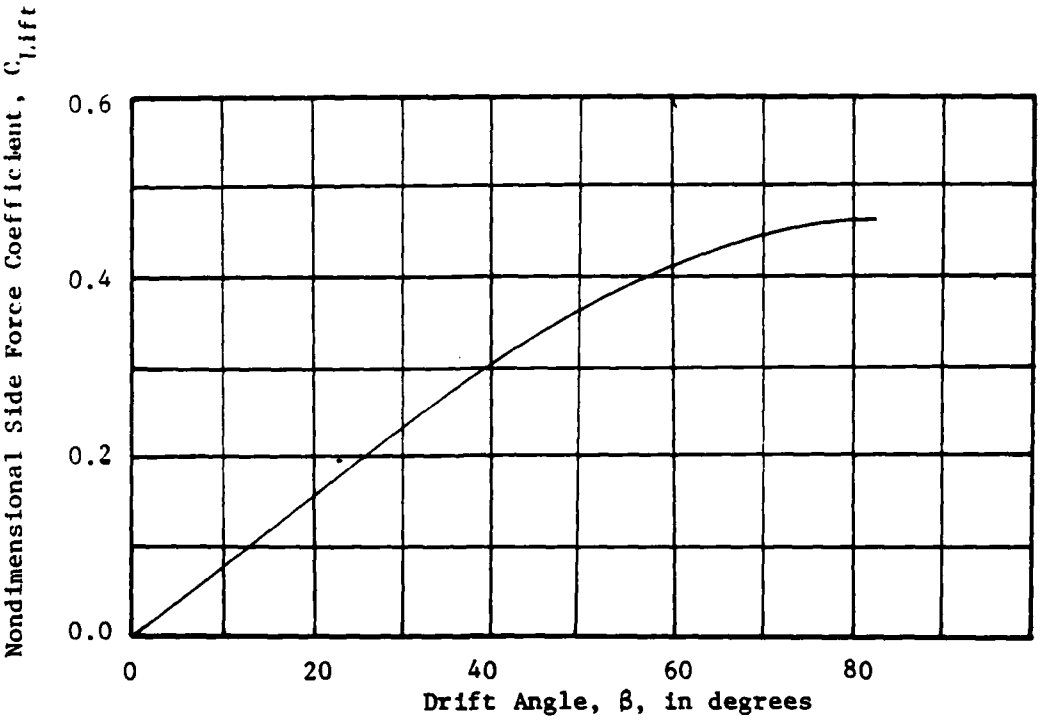
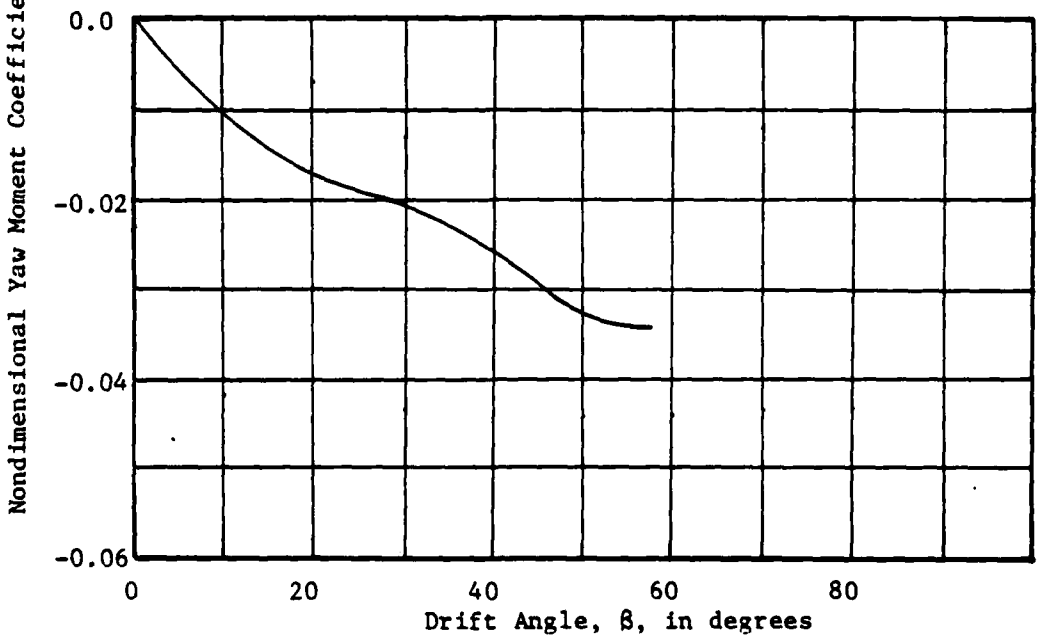


Figure 3 - Variation of Nondimensional Yaw Moment Coefficient with Nondimensional Yaw Rate for the LC JEFF(B) On-Cushion at a Froude Number of 0.535



Variation of Nondimensional Aerodynamic Side Force Coefficient with Drift Angle for a 1/12th Scale Model of the LC JEFF(B)

Figure 4 - Results of Wind Tunnel Experiments on a Model of the LC JEFF(B)



Variation of Nondimensional Aerodynamic Yaw Moment Coefficient with Drift Angle for a 1/12th Scale Model of the LC JEFF(B)

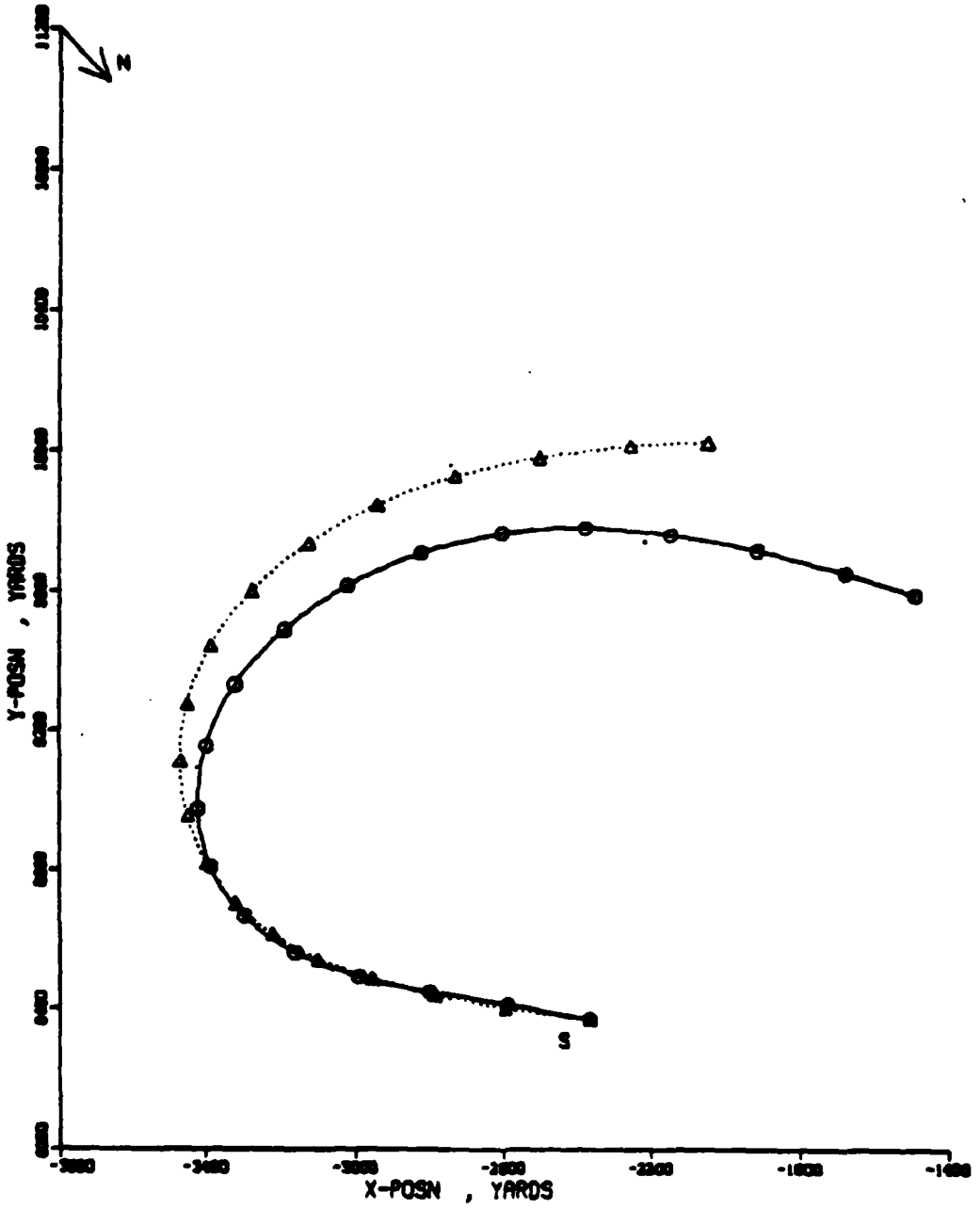


Figure 5 - Comparison of Full Scale Maneuvering Trajectory (O) and Simulated Trajectory (Δ) in a 180° Turn

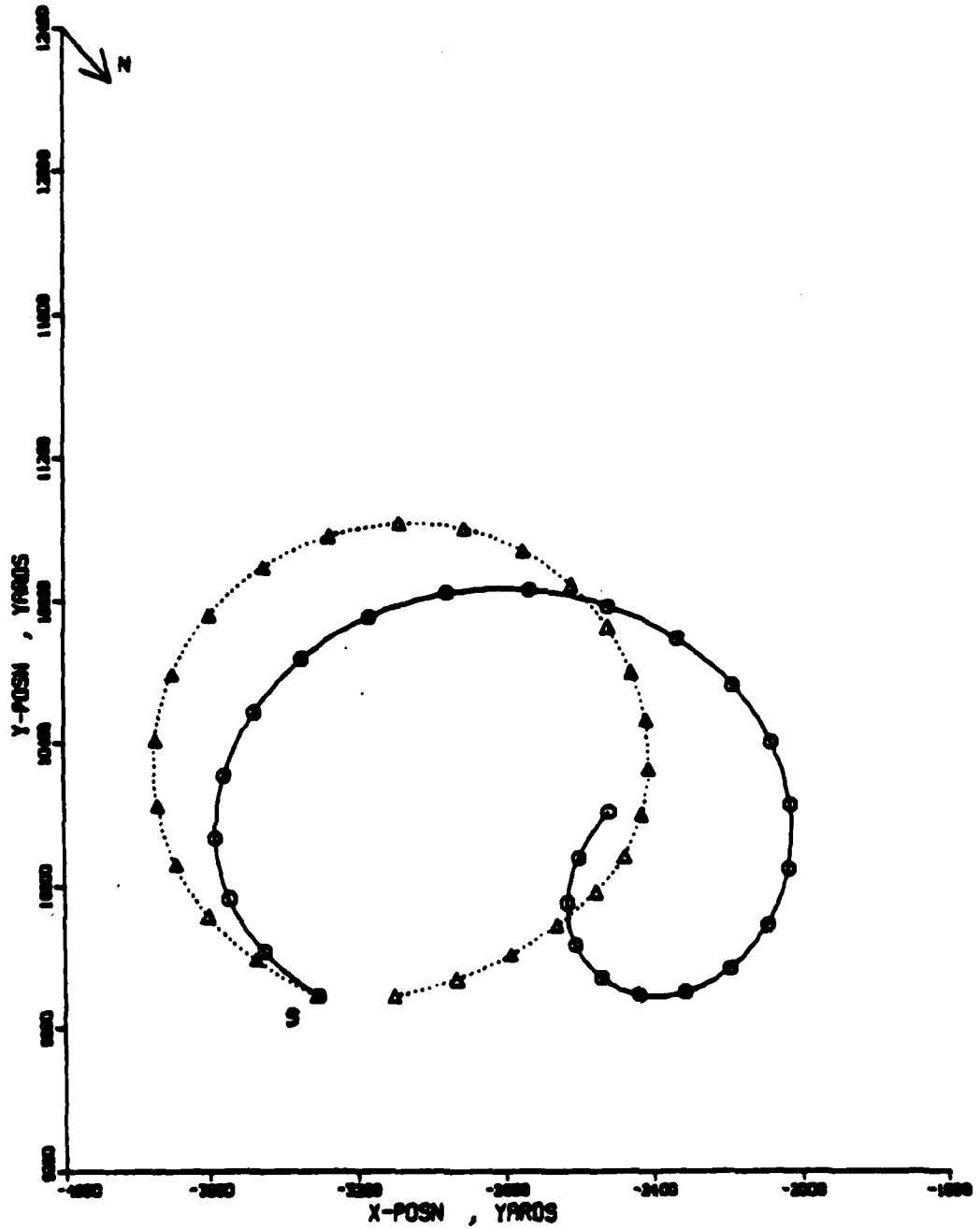


Figure 6 - Comparison of Full Scale Maneuvering Trajectory (O) and Simulated Trajectory (Δ) in a 360° Turn

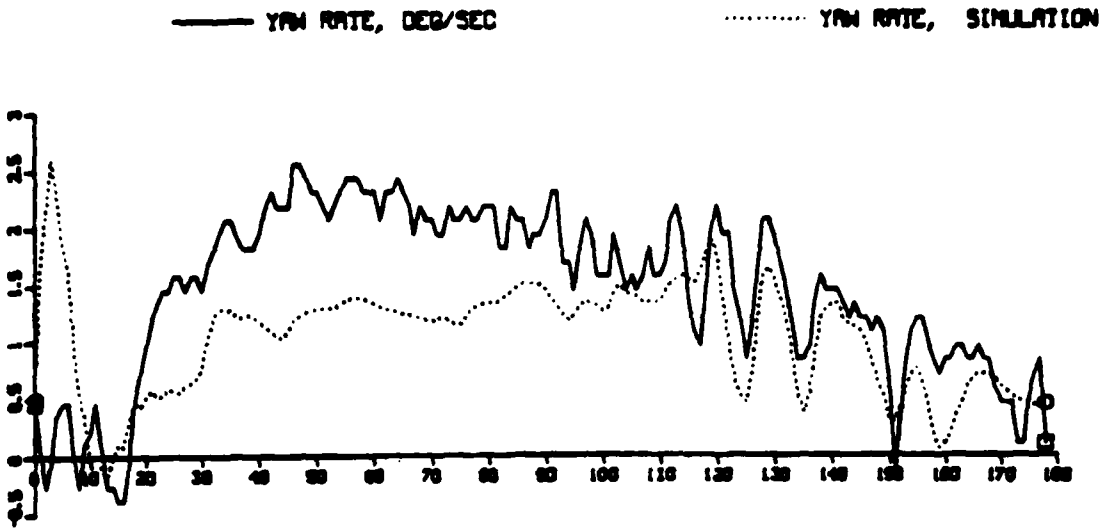


Figure 7 - Comparison of Full Scale Yaw Rate and Simulated Yaw Rate.

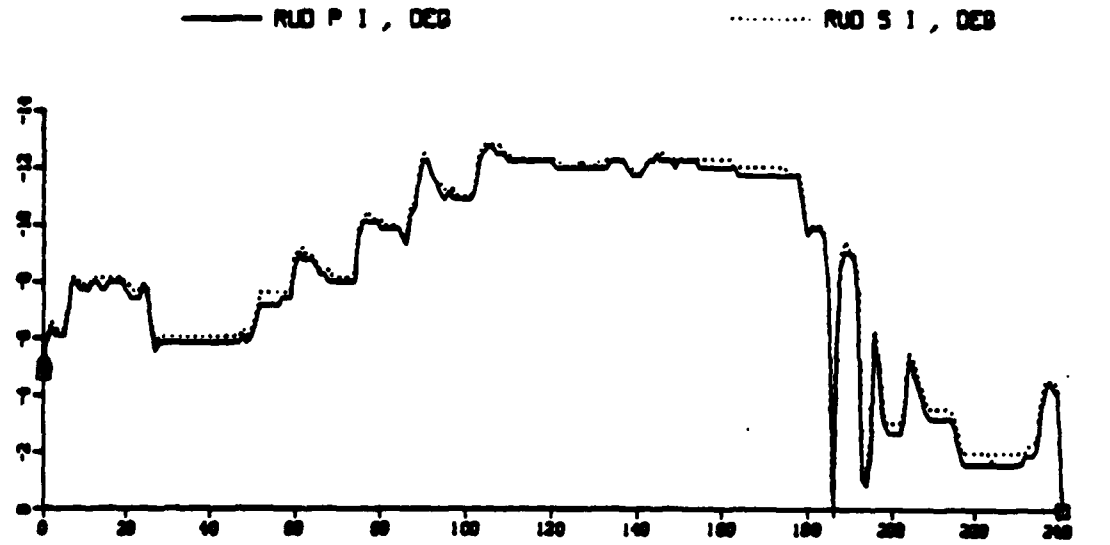


Figure 8 - Full Scale Rudder Control Time Histories for Port and Starboard Rudders Indicating Pilot Work Load.

AD-P003 814

EXTENDED PERFORMANCE HYDROFOIL PROGRAM

by

John R. Meyer

ABSTRACT

This paper traces the origin of the Extended Performance Hydrofoil (EPH) concept from the Hybrid Vehicle Investigations at the ~~David Taylor Naval Ship R&D Center~~ DTNSRDC starting in 1973. The potential mission applications of the EPH are discussed along with extensive model tests, computer simulation, and cavitation analyses. The work completed, design status, and future plans are also described for a demonstration vehicle based on the HIGH POINT (PCH-1) R&D hydrofoil.

AUGUST 2, 1983

20TH AMERICAN TOWING TANK CONFERENCE
HIGH SPEED VEHICLE COMMITTEE

EXTENDED PERFORMANCE HYDROFOIL PROGRAM

by
John R. Meyer

BACKGROUND

The study of hybrid marine vehicles, which eventually led to the concept of the Extended Performance Hydrofoil (EPH), began in 1973 with the inception of a Hybrid Marine Interface Vehicle Program at the David Taylor Naval Ship Research and Development Center. One objective of this program was to explore the advantages to be realized through conceptual hybrid surface ship platforms.

A "hybrid" marine interface vehicle is defined as one having more than one source of sustention over a major portion of its operational speed regime. In this hybrid vehicle program the three types of lift available for surface ships, Buoyancy (often denoted as the X vertex of the "Sustention Triangle" shown in Figure 1), Dynamic Lift (the Y vertex), and Powered Static Lift (the Z vertex), were combined in various proportions using at least two forms of lift. The reason that the Navy began researching and continues to explore hybrid surface ships is the flexibility offered to the ship designer when given a set of mission requirements. Each of the three sources of lift has its advantages and disadvantages with respect to a particular mission's requirement. Combinations of these means of sustention can sometimes capitalize on the advantages of, or alleviate the problems of the different types of lift that are used. Thus, hybrid vehicles can fill in the gaps in performance between different methods of sustention, giving the designer a greater choice of options.

Some early hybrid configurations were: Small Waterplane Area Air Cushion Ship (SWAACS), on the X-Z segment of the Sustention Triangle (see Figure 1); the Hydrofoil Air Cushion Ship (HYACS), on the Y-Z segment; and Small Waterplane Area Single Hull (SWASH) ship, Hydrofoil Small Waterplane Area Ship (HYSWAS), and Large Hydrofoil Hybrid Ship (LAHHS) all on the X-Y segment. It is no accident that the X-Y segment of the Sustention Triangle, combinations of buoyancy and dynamic lift, have drawn more attention than other combinations. Early studies indicated that the combination of buoyancy and dynamic lift provided the potential for relatively high hydrodynamic efficiency, particularly in rough water [Ref 1]. The EPH utilizes these two means of lift with a fully submerged hydrofoil system for dynamic lift and a long, slender buoyancy/fuel tank attached longitudinally to the underside of the foils. Approximately fifty percent of lift is supplied by its foils and fifty percent by the buoyancy/fuel (B/F) tank. This design retains qualities of the hydrofoil such as high speed and excellent sea-keeping characteristics while alleviating its limitations in range, weight sensitivity, and high drag characteristics in the twenty to thirty knot speed regime. The design of the EPH is advantageous between twenty and thirty knots because it tends to have higher lift-to-drag ratios (L/D) than hydrofoils at the lower end of their foilborne speed range and higher L/D than displacement ships in the high end of their speed range.

Because of its advantages, the Extended Performance Hydrofoil has undergone considerable investigation, and is the only hybrid surface vehicle program for which funding is being considered by the U.S. Navy.

EARLY DESIGNS AND MISSION ANALYSES

Some early design work that contributed to development of the EPH includes the Hydrofoil Small Waterplane Area Ship (HYSWAS) shown in Figure 2. This form has a single long strut that connects the submerged buoyancy/fuel tank to the main hull, unlike the EPH which had several struts (as a conventional fully-submerged hydrofoil) to support the ship's weight. This HYSWAS research is documented in Reference 2. The ship functions in nearly the same way as the EPH, i.e., small waterplane area when foilborne, with a submerged tank for buoyancy and fuel storage. The differences are that the EPH has the possibility of wet retraction of its foils, there is the potential for B/F tank removal, and it has little added buoyancy from its struts, while the HYSWAS tank and foil system are fully integrated, and considerable buoyancy is provided by the strut.

The investigations of HYSWAS were, to a large degree, aimed at designing a two thousand ton ship with seventy percent of the weight supported by buoyancy and thirty percent by the foils. Since the HYSWAS was a cross between a fully-submerged hydrofoil and a demi-SWATH (Small Waterplane Area Twin Hull) ship, analytical investigations were largely a product of the technologies of the two parent designs. Results showed the potential for maximum speeds greater than 40 knots, a 4000 mile range at 20 knots, and its efficiency at low, as well as high, speeds. Other important results of this research showed that the ship would be hydrostatically stable when hullborne, and that there was adequate control available to operate in a seaway [Ref 3 and 4]. HYSWAS model tests were run on an 18.25 scale model of the 2000 ton scale ship at Tank #1 of the DTNSRDC Langley Field Towing Basin to predict resistance [Ref 5]. The results verified the significant reduction in hump drag normally associated with hydrofoil take-off conditions.

Various design options for buoyant/dynamic lift hybrids and their effects on vehicle configuration and performance were investigated [Ref 6]. From this study emerged a configuration, shown in Figure 3, which later became known as the EPH. Some of the design parameters examined were ship size, B/F tank size, foil/strut configuration, and foil loading. The effects of changes in these parameters were measured in terms of design speed, range, payload, powering, intact stability, etc. In addition, general conclusions were reached about the differences between the conventional hydrofoil and the hydrofoil with a B/F tank. Some of the more interesting results are as follows. The speed for maximum foilborne range is reduced for the hydrofoil with a B/F tank, and its range is increased. Maximum range improvement potential increases with ship size from about 20% in small sizes (light-ship weight about 205 L. tons) to about 90% for large sizes (light-ship weight about 1860 L. tons). The hullborne range was improved considerably in the ten to twenty knot speed regime for the B/F tank version of the hydrofoil. Minimum foilborne speed of the hydrofoils with tanks can be reduced by five to ten knots, but the design speed would be limited to forty and forty-five knots. This work was later expanded upon by including an additional ship size category and a discussion of progress on other phases of the EPH program [Ref 7].

With the extended range, reduced minimum foilborne speed, and other attributes associated with the Extended Performance Hydrofoil, it was of interest to explore a variety of mission applications. Several such missions have been considered for the EPH as an advanced guided missile frigate (FFHGX). The FFHGX has an advanced weapon system consisting of surface-to-air missiles, HARPOON missiles, over-the-side torpedoes, a close-in weapon system, and sophisticated navigation, surveillance, and terminal engagement radar. The missions suggested for the FFHGX are escort missions for various convoys, from 16-knot

merchant vessel convoys to 32 knot SL-7 fast containership convoys. It was felt that the FFHGX would be well suited because of its AAW and ASW capabilities and, more importantly, because of the high sustained speed of advance as well as high sprint speed while retaining good range characteristics. The conclusion of the investigation was that the FFHGX would be better for several missions than the current FFG-7 class of frigates.

The EPH has also been considered for a role in a Patrol Hydrofoil Missileship (PHM) consort. It was suggested that the EPH could serve as a support ship, supplying fuel to the limited range PHMs so that they could traverse long distances at relatively high speeds to provide strategic mobility. There would be three or four PHMs teamed with one medium to large (900-1900 ton) EPH which could supply ammunition, provisions, and limited repair, as well as fuel to the PHMs.

The application of EPH and conventional hydrofoil designs to specific scenarios associated with battle group escort has also been investigated. Here, EPH was shown to have certain advantages, particularly in the larger size category.

It was anticipated that the B/F tank of the EPH configuration had some potential for sonar installations. An investigation was made, and a report was prepared which presented the approach used for predicting basic sonar performance for various arrays that can be installed on the buoyancy/fuel (B/F) tank of an EPH. Also the concepts for EPH sonars developed during the study and the results and tactical/operational implications of a performance analysis of those sonars were reported. Existing and planned surface ship and submarine sonar systems were reviewed and the array characteristics applicable to the EPH concept were briefly summarized. Operational and geometrical constraints as well as a number of array configurations were investigated. A parametric approach was employed to examine the impact of B/F tank length, EPH speed, and sonar frequency on detection ranges, using three generic sound speed profiles: surface duct, bottom bounce, and convergence zone.

Because the EPH is uniquely suited to certain applications, as indicated by these studies, exploratory development should continue.

EPH RESEARCH

Between 1978 and 1979 EPH feasibility design had come to the point where it was necessary to obtain data that would lead to a full-scale demonstration vehicle. The projected test vehicle was to be the HIGH POINT, PCH-1 R&D hydrofoil. In 1979 a series of experiments were conducted on a 1/20 scale model (79 inches long) of a small hydrofoil with buoyancy/fuel tank. The basic hydrofoil was a model of the PHM that had been built for the Advanced Hydrofoil Office at DTNSRDC in 1974. A B/F tank was designed and built for this model at Stevens Institute of Technology (S.I.T.) as was the original hydrofoil model. Captured model tests were performed using the B/F tank, supported by a sting-support strut, and different combinations of strut and foil elements (upper hull was not included); see Figure 4. The captured model tests were performed at S.I.T. with Davidson Laboratory's Rotating Arm Facility [Ref 8]. In an effort to determine the effects of the B/F tank on stability, control, and maneuvering performance, the six components of force and moment were measured as functions of variables including pitch, drift, and roll angle, turning radius, heave, tangential velocity, submergence, and strut and foil flap deflections. From the measurements taken from several hundred runs, hydrodynamic coefficients were tabulated to be used to assist in the formulation and verification of an ideal motion hybrid ship simulator with the versatility to

evaluate maneuvering, motion, and loads for many buoyant/dynamic lift ships in varying sea conditions.

After the captured model tests, the buoyancy/fuel tank was rebuilt to include a 1-1/2 horsepower electric motor and a balance system for measuring each of the six hydrodynamic forces and moments. With this, a complete 1/20 scale model of an EPH was built from the original PHM model with an automatic control system and force measuring devices, as well as self-propulsion. The struts, foils, and most of the B/F tank of the model were made of aluminum while the hull was made of balsa wood covered with plastic. An umbilical cable of 105 power and signal wires ran between the master control on the carriage and the model. Figure 5 shows the model during a typical run in the Maneuvering and Seakeeping Facility at DTNSRDC. Over three hundred runs were performed in calm water, regular and random waves of heights up to simulated Sea-State 6, at different angles with respect to the wave propagation. Simulated full-scale speeds from 16 to 45 knots were tested. This series of tests supplied data on the hydrodynamic forces and moments induced by the B/F tank, motions, accelerations, and foil flap angles.

The 1/20 scale model of EPH was further tested in an unpowered mode at DTNSRDC for the purpose of measuring bottom pressures produced by the model with and without a B/F tank. A series of runs were made at depth Froude Numbers in the region of 1.0.

After these model tests there were several additional steps taken towards obtaining a working design for an EPH full-scale demonstrator vehicle, namely the PCH-1 fitted with a B/F tank.

A computer simulation of the PCH-1 EPH feasibility demonstration craft was developed at DTNSRDC. The purpose was to determine the craft's motions and the loads developed by the tank under a variety of conditions within the anticipated operating envelope using the present PCH-1 autopilot. The dynamic, digital simulation was constructed by merging an existing six-degree-of-freedom simulation of PCH-1 (having no autopilot changes) with a simulation of the tank assembly. Results of the simulation showed that the vertical member of the cruciform stern, being an active control surface for EPH, must be commanded to move in a way ensuring overall stability, and overcoming part or all of the adverse effects of the tank's presence, especially in turns.

It was found that the craft was stable foilborne in the vertical plane in response to a number of height and pitch step inputs made in calm water. For the horizontal plane, simulation runs were made at speeds from 25 to 40 knots, Sea States 5 and 6, straight line and turns from helm commands of 90 and 135 degrees--with and without the tank in some cases for comparison purposes. Although the tank degrades PCH-1 turn performance, the simulation showed that turn radius increases by only about 15%, and increases somewhat the average control surface angles. Even with this turn rate reduction, maneuverability is considered excellent and consistent with that of fully submerged hydrofoils.

Boeing Marine Systems was contracted to extend the computer simulation for the PCH-1 with B/F tank, as well as do a cavitation analysis in the region of the forward foil/strut and B/F tank. The cavitation analysis, using an advanced three dimensional potential flow panel method program, had an impact on the design of the demonstrator. A preliminary analysis showed that the nose shape of the B/F tank was a potential source of cavitation problems. Sensitivity to configuration and operating conditions was further explored [Ref 9], and the shape of the nose was altered. With the final nose shape established, it was observed that the body would not significantly degrade the forward foil cavitation performance; the flap efficiency increases in the presence of the body while the sensitivity to angle of attack decreases; and the onset of foil cavitation is displaced outwards from the plane of symmetry due to the body.

Therefore it was concluded that no degradation of PCH-1 sea state performance is expected with the B/F tank attached. If the ship trim can be reduced by about 0.5° the analysis indicates that larger leading edge and flap hinge line incipient cavitation margins will be present for the EPH configuration and improved sea state operation can be expected.

EPH DEMONSTRATOR DESIGN

From the model tests and simulation data available at the time, Grumman Aerospace Corporation, under contract with DTNSRDC, performed a feasibility investigation followed by a baseline design of a PCH-1 EPH demonstrator. The purpose of the feasibility investigation was to better define the technical validity of using a buoyancy/fuel tank to improve hydrofoil performance and enhance mission capabilities. This was completed in January 1980. The conclusions dealt mainly with limitations on tank net buoyancy to maintain intact stability up to an 80 knot wind condition, problems with coordinated turns due to aft foil hinge line cavitation, and installation design problems associated with a removable B/F tank. However, it also concluded that the concept of installing a buoyancy/fuel tank on the PCH-1 is practical. The baseline design report of December 1980 (revised in November 1981) followed up on previous recommendations and detail design. This report clearly defines limitations of the demonstrator vehicle that were speculated on in the previous report such as turning degradation, intact stability, and attachment of the B/F tank; and defines other sources of possible improvement such as a more powerful engine and an additional rudder.

CURRENT STATUS AND PLANS

Funding for the EPH program has been curtailed. There are tentative plans to restart the HIGH POINT, PCH-1 EPH demonstration program. Subsequent to design completion and fabrication of the B/F tank and PCH-1 ship alteration, the program would include an extensive trials period during which the speed-sea state envelope would be explored to its limits. These data would confirm structural loads data from model tests described above and computer simulations of motions and maneuvering. This data base will be essential for future EPHs, or similar hybrid ship designs.

REFERENCES

1. Meyer, J.R., "A Comparison of Several Hybrid Surface Ship Concepts," Naval Engineers Journal, pp. 183-190 (April 1977).

2. Meyer, Jr., J.R. and J.H. King, "The Hydrofoil Small Waterplane Area Ship (HYSWAS)," AIAA/SNAME Third Advanced Marine Vehicles Conference, Paper No. 76-875, Arlington, Virginia (September 1976).

3. Lee, C.M., "Determination of Size and Location of Foils for 2000 Ton Hydrofoil Small Waterplane Area Ship (HYSWAS) for Vertical-Plane Stability," David W. Taylor Naval Ship R&D Center, Report No. SPD-648-01 (November 1975).

4. Lee, C.M., R.T. Waters, and K.K. McCreight, "Preliminary Investigation of Roll Controllability of a Hydrofoil Small Waterplane Area Ship (HYSWAS)," David W. Taylor Naval Ship R&D Center, Report No. SPD-808-01 (December 1977).

5. Karafiath, G., "Resistance Prediction for a 2000 Ton HYSWAS (Hydrofoil Small Waterplane Area Ship) Represented by DTNSRDC Model #5355." David W. Taylor Naval Ship R&D Center, Report SPD-675-02 (November 1979).

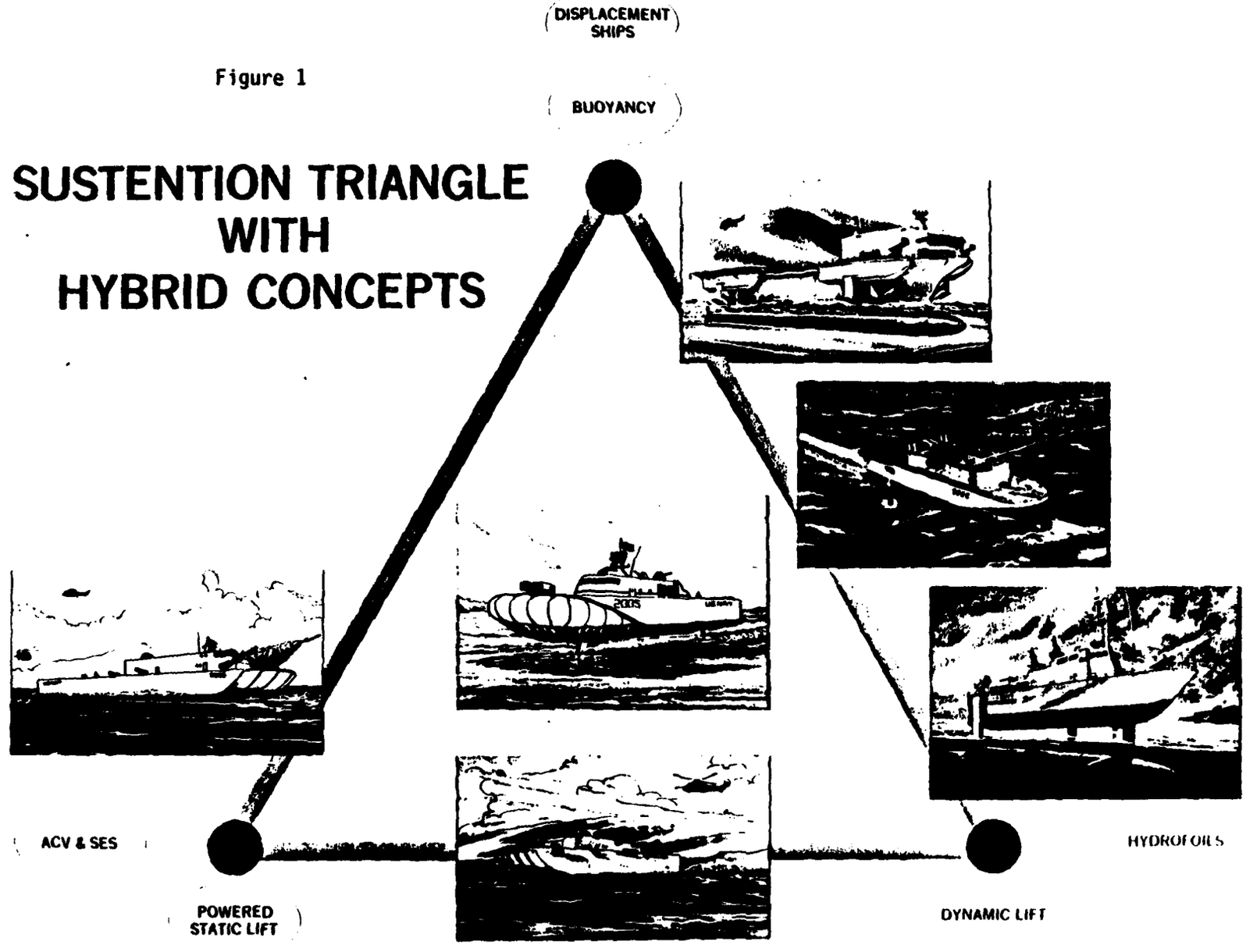
6. Hawkins, S., J. King, and J. Meyer, "Hydrofoil Operational Performance Enhancement Using Hybrid Design Options" AIAA/SNAME Advanced Marine Vehicles Conference, Paper No. 78-750, San Diego, California, (April 1978).

7. Meyer, Jr., J.R., "Extended Performance Hydrofoils," AIAA Sixth Marine Systems Conference, Paper No. 81-2067, Seattle, Washington (September 1981).

8. Suarez, A. and J. Breslin, "The Davidson Laboratory Rotating Arm Facility" DL Technical Note 597 (September 1960).

9. "HIGH POINT Extended Performance Hydrofoil Configuration Forward Foil Cavitation Analysis," The Boeing Co, Document No D321-51327-1 (September 1981).

Figure 1


DISPLACEMENT SHIPS
BUOYANCY
SUSTENTION TRIANGLE WITH HYBRID CONCEPTS
ACV & SES
POWERED STATIC LIFT
DYNAMIC LIFT
HYDROFOILS

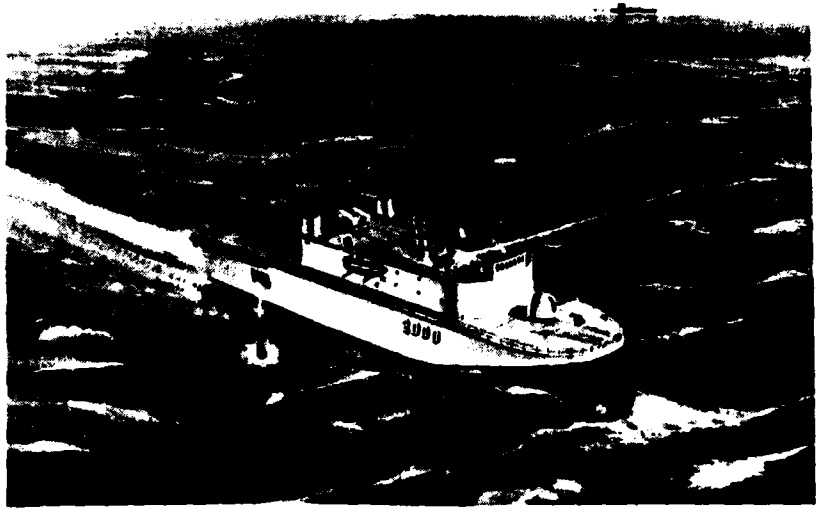


Figure 2 - Hydrofoil Small Waterplane Area Ship (HYSWAS)

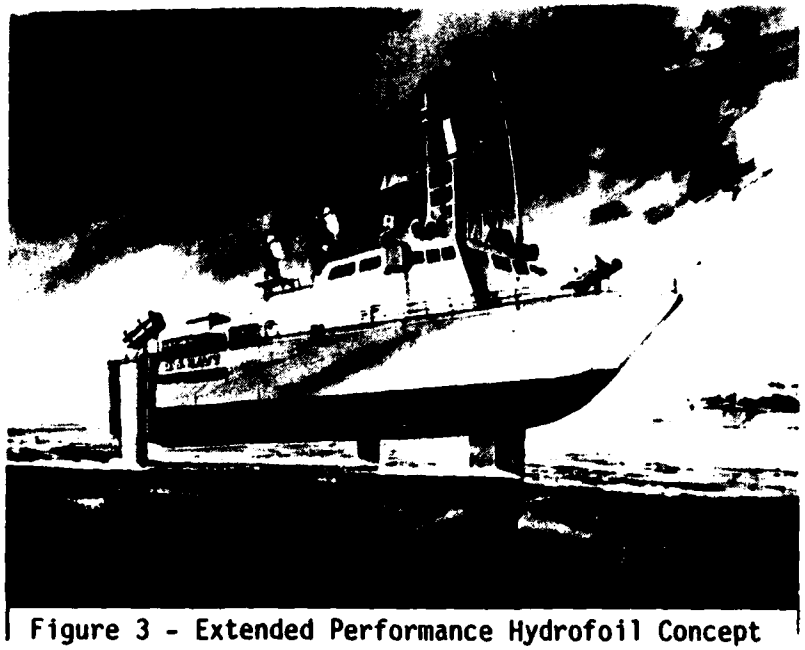


Figure 3 - Extended Performance Hydrofoil Concept



Figure 4 - Captured Model of EPH Lift System

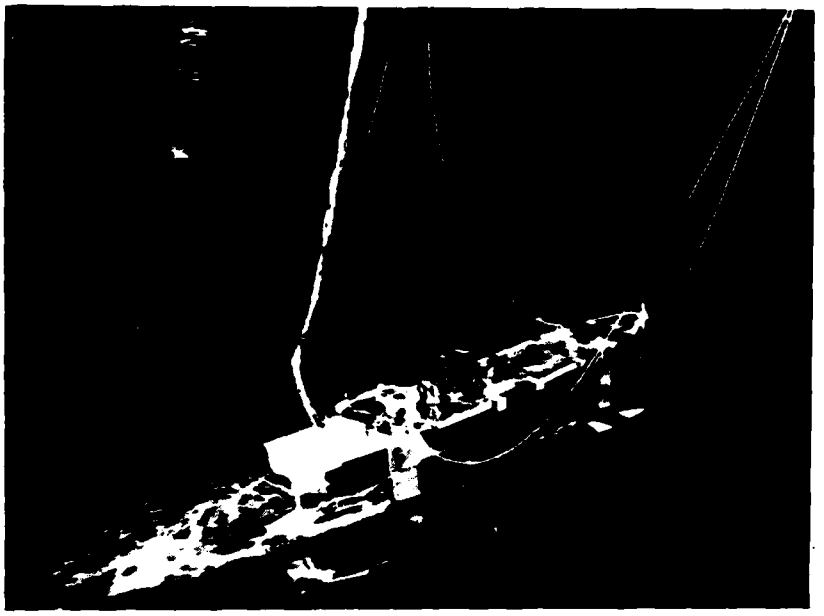


Figure 5 - Self-Propelled EPH Model Under Test at DTNSRDC

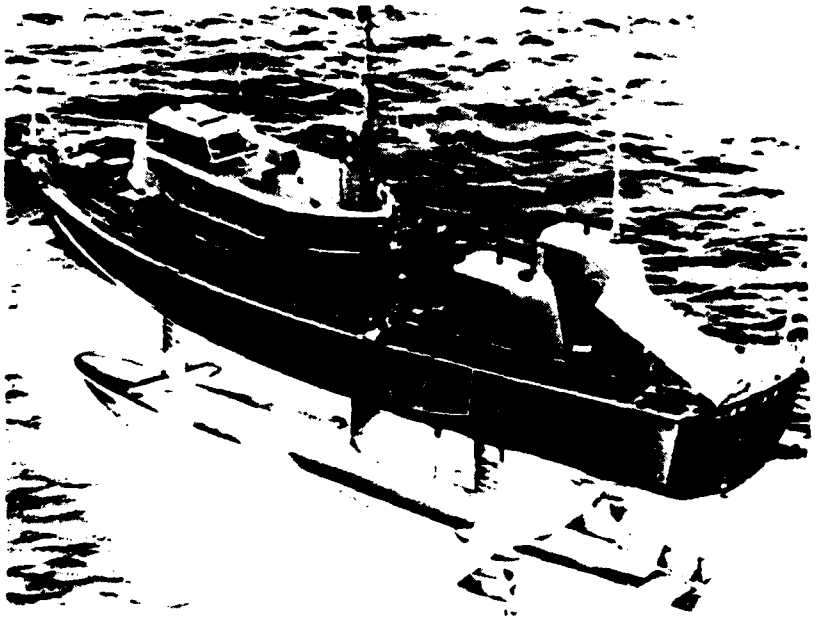


Figure 6 - PCH-1 HIGHPOINT EPH Feasibility Demonstrator

AD-P003 815

PLANING SURFACE C_F [1]

By

R. Latorre[2]

ABSTRACT

For model-full scale resistance estimates the C_f value from the ATTC/ITTC line (1) is used to scale the frictional resistance in calm water resistance tests of planing hulls. Assuming the planing surface is supported by dynamic lift, the force vector analysis gives an expression for C_{f_1}:

$$C_{f_1} = \frac{(R_t - W\tan\tau)}{1/2\ \rho V_1^2\ S}$$

In this contribution C_f values from published data on planing plates, prismatic hulls, and Series 62 models [2]-[8] are compared to the corresponding ATTC C_f values. Here $3\times10^{-3} < C_{f_1} < 4\times10^{-3}$ which is below the ATTC line $Rn < 2\times10^6$ and above the ATTC line for higher Rn.

While the differences are within engineering accuracy ± 10% of the ATTC line, the force vector analysis of the planing test data is appropriate to verify the extent of turbulent flow on the planing surface.

1. INTRODUCTION

This paper is an outgrowth of a study on the effect of shallow water on the viscous resistance of planing vessels in shallow water. The force vector analysis was used to establish the deep water value of C_{f_1} shown in Fig. 5 for the resistance tests of series 62 models.

The results seemed interesting and with the other data collected appeared to be useful for those involved in high speed vechile testing.

With high speed vechiles, the test results should qualify the lift coefficient of the wetted surface as well as the resistance. In the scaling procedure developed for displacement vessels [1]:

$$R_T = R_R + R_F + R_a + \sum_i R_i \qquad 1.1$$

so

$$R_R = R_T - R_F - \sum_i R_i - R_a$$

where R_R : Residuary Resistance

R_F : Frictional Component based on ATTC line Cf

R_a : Correlation = 0

R_i : Additional resistance typically air resistance

The results from series 62 models tested at DWTNSRDC [7] and U of M [8] are compared using the residuary resistance coefficient C_R in Fig. 1.

$$C_R = \frac{R_R}{1/2\rho V^2 S} \qquad 1.2$$

where ρ : Density

V : Velocity

S : Wetted Surface

The particulars of the planing models are summarized in Table 1. The scale factor between these models is $\lambda = 1.71$. The results in Fig. 1 show good agreement. This good agreement is clear in Fig 2a-2c. Figs 1 and 2 are representative of the satisfactory results from present tank practice. Here the value of C_f was obtained from [1] at the Reynolds number Rn determined using the avg. wetted length recorded in the test data.

2. C_f of Planing Surfaces

A comprehensive outline of the many studies of the planing surface C_f is beyond the scope of this paper. Since

TABLE 1 Planing Model Particulars

Item	units	NSRDC 4666[7]	U of M 1174[8]
A_p	ft^2	9.715	3.322
L_p	ft	5.987	3.50
B_{pA}	ft	1.623	0.949
B_{pX}	ft	1.956	1.144
B_{pT}	ft	1.386	0.810
∇	ft^3	1.63	0.326

[1] Contribution to 20th ATTC High Speed Vehicle Committee, 8/2-4/83 Meeting

[2] Associate Professor, Dept. of Naval Arch & Mar. Eng., University of New Orleans, New Orleans, La., (Formerly with Univ. of Michigan)

the investigation of D. Savitsky and E. Ross on the turbulence simulation of planing surfaces [2], there have been several studies of the extent of the laminar flow on the planing surface[3], [4]. A. Cole and A. Millward used miniature Preston tubes to estimate the skin friction and the corresponding C_f value. These results were for Rn < $2x10^6$ and typically were under the ATTC C_f values. [2],[3],[4],[5],[6].

In Yegorov's book, Riman's flat plate C_f experiments are summarized. The details of the tests and the C_f analysis were not described in detail. It was noted that C_f was found to be a strong function of the trim angle τ and to a lesser degree the Reynolds number. The results are shown in Fig. 3.

DuCane describes a practice for checking the test results using the "apparent C_{fa}" given by:

$$C_{fa} = \frac{R_T - W\tan\tau - R_{air}}{1/2\rho V^2 S} \qquad 2.1$$

where W: Weight of planing model

τ: Trim angle

R_{air}: Air resistance

This is illustrated in Fig. 4 [9] where the Model 1 C_{fa} values indicate adequate turbulent flow on the planing surface. On the otherhand, the C_{fa} values of 2 is below the ATTC line indicating the presence of laminar flow. The hook form of the curves are characteristic for planing models as the Series 62 C_f values in Fig. 5 indicate.

It is evident in Fig. 5 that for Rn < $2x10^6$ the C_f values fall below the ATTC line. For tanks with moderate speed this is an area of concern. It is also useful to make another observation of the apparent lack of theoretical work on extending the numerical codes of J. Wellicome and J. Jahangeer [10] and L. Doctors [11] to calculate the boundary layer transistion and C_f.

3. Force Vector Analysis

In the previous section the series 62 test data was introduced. The series 62 C_f values plotted in Fig. 5 were obtained from the results of the following analysis.

Consider the planing surface at an angle τ as shown in Fig. 6. Using a transform matrix it is possible to write:

$$\begin{bmatrix} -X \\ Y \end{bmatrix} = \begin{bmatrix} \cos\tau & -\sin\tau \\ \sin\tau & \cos\tau \end{bmatrix} \begin{bmatrix} -D_f \\ N \end{bmatrix} \qquad 3.1$$

This represents the transform from the body axis (x',y') to the moving axis (x,y). Here the rise in the C.G is neglected. In Fig. 6 the following notation is adopted:

X : Resistance in the horizontal
Y : Lift Force in the vertical
Y = W
D_f: Viscous force acting tangential to the planing suface
N : Lift force normal to the p planing surface
W : Vessel weight assumed to be supported by the planing surface.

From (3.1):

$$-X = -D_f\cos\tau - N\sin\tau \qquad (3.2)$$

$$W = Y = -D_f\sin\tau + N\cos\tau \qquad (3.3)$$

This gives the classical results:

$$X = W\tan\tau + D_f/\cos\tau = (W\sin\tau + D_f)\sec\tau \qquad (3.4)$$

$$X = N/\sin\tau - W\cot\tau \quad \tau \neq 0 = (N - W\cos\tau)\csc\tau \qquad (3.5)$$

In writing the expressions for the frictional drag and dynamic lift, the velocity along the plate surface is defined by V_1.

$$D_f = 1/2\rho V_1^2 S\, C_f \qquad (3.6)$$

$$N = 1/2\rho V_1^2 S\, C_l \qquad (3.7)$$

This leds to writing C_f as:

$$C_f = \frac{(X - W\tan\tau)\cos\tau}{1/2\rho V_1^2 S} \qquad (3.8)$$

$$C_l = \frac{(X + W\cot\tau)\sin\tau}{1/2\rho V_1^2 S} \qquad (3.9)$$

These expressions have appeared in the literature [2],[5],[6]. In [12] V_1 is given by :

$$V_1 = V\sqrt{\frac{1 - 0.0120\tau^{1.1}}{\lambda^{1/2}\cos\tau}\, f(\beta)}$$

where λ = S/b with the deadrise angle denoted by β. In the analysis the following simplification is introduced:

$$V_1 = V\cos\tau$$

giving:

$$C_{f_1} = \frac{(X - W\tan\tau)}{1/2\rho V^2 S\cos\tau} \qquad (3.10)$$

$$C_{l_1} = \frac{(X + W\cot\tau)\sin\tau}{1/2\rho V^2 S\cos^2\tau} \qquad (3.11)$$

The series 62 model tests in Fig. 1 and Fig. 2 were reanalysized using equation (3.11) and the value of C_{f_1} plotted in Fig. 5. The characteristic hooked curves appear for both data sets. It is difficult to explain the higher C_{f_1} values since the wind resistance corrections were not applied to the data.

For a better grasp of the difference the value of C_{f1}/C_{fATTC} is plotted in Fig. 7 for the two tests. For $2 < F_\nabla < 3$ the values of C_{f1}/C_{fATTC} fall between 1.05 - 1.15. In both cases it is clear the flow is turbulent which is expected.

4. Discussion

This paper has reviewed a number of published results from planing plates, prismatic hulls, and tests with the series 62 hull. The U of M tests were shown to be in good agreement with the DWTNSRDC tests of the series 62 planing hull.

The results from an analysis of the force vectors gave C_{f_1} values in the range of $3 \times 10^{-3} < C_{f_1} < 4 \times 10^{-3}$. This is in agreement with Cole and Millward's C_f values estimated from tests with a planing surface fitted with minature Preston tubes. While the differences of the C_{f_1} value from the ATTC C_f values have been presented, it is difficult to make a conclusion since the air resistance was not taken into account. Additional experimental and theoretical work should help clarify this point. From the standpoint of model testing using C_{f_1} is useful to check the extent of turbulent flow on the planing surface.

1. Todd, F.H., "Tables of Coefficients for ATTC and ITTC Model Ship Correlation and Kinematic Viscosity and Density of Fresh and Salt Water," SNAME T&R Bulletin 1-25, 1976.

2. Savitsky, D., and Ross, E.W., "Turbulence Simulation in the Boundary Layer of Planing Surfaces, Part II Preliminary Experimental Investigation," Stevens Institute of Technology, Experimental Towing Tank Report, No. 444, Aug. 1952, 43 pp.

3. Cole, A.J., Millward, A., "The Measurement of Skin Friction on a Planing Hull using a Minature Preston Tube," TRANS. RINA, Vol. 120, 1978, pp.179-185.

4. Latorre, R., "Study of Prismatic Planing Model Spray and Resistance Components," To appear in The Journal of Ship Research, Fall, 1983.

5. Yegorov, I.T., Bun'Kov, M.M., Sandovnikov, Yu.M., PROPULSIVE PERFORMANCE AND SEAWORTHINESS OF PLANING VESSELS, Sudostroeniye, Leningrad, 1978 (In Russian) NAVSEA Translation No. 1965, 1982 available in SNAME Library.

6. Bannikov, Yu.M., Lukashevskiy, V.A., "Experimental Investigation of the Lift and Drag of Hydroplaning Plates," Fluid Mechanics Soviet Research Vol. 6, No.2, March-April, 1977 pp. 78-86.

7. Clement, E.P., Blount, D.L., "Resistance Tests of a Systematic Series of Planing Forms," TRANS. SNAME, Vol. 71, 1963, p. 541 & p. 543.

8. Toro, A.I., "Shallow Water Performance of a Planing Boat," Univ. of Michigan, Department of Naval Architecture and Marine Engineering Report No. 019, April, 1969, p. 22.

9. DuCane, P., HIGH SPEED SMALL CRAFT, John DeGraff, Inc. Tuckahoe, N.Y. 1973, p. 367.

10. Wellicome, J.F., Jahangeer, J.M., "The Prediction of Pressure Loads on Planing Hulls in Calm Water," TRANS. RINA, 1978, pp. 53-70.

11. Doctors, L.J., "Representation of Three-Dimensional Planing Surfaces by Finite Elements," Proceedings, First Conference on Numerical Ship Hydrodynamics,"DWTNSRDC, Washington, D.C., 1975 pp 517-537.

12. Savitsky, D., "Hydrodynamic Design of Planing Hulls," Marine Technology, Vol. 1, No. 1, 1964, pp. 71-95.

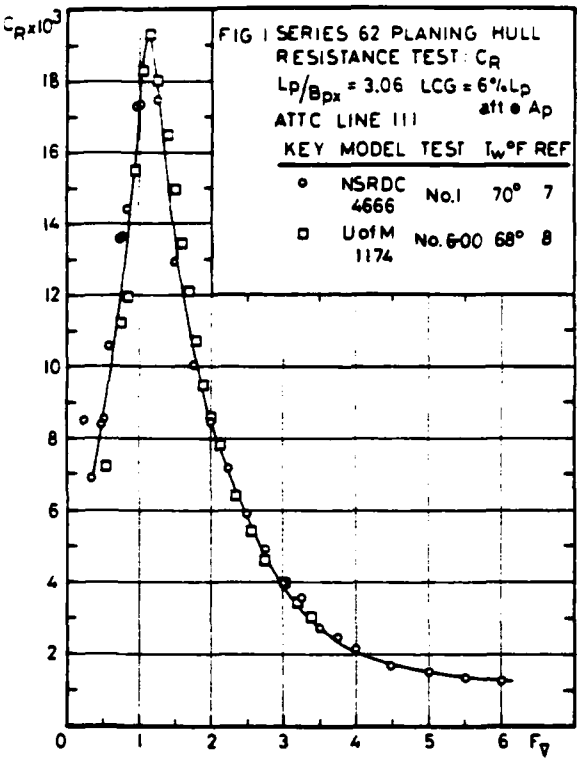
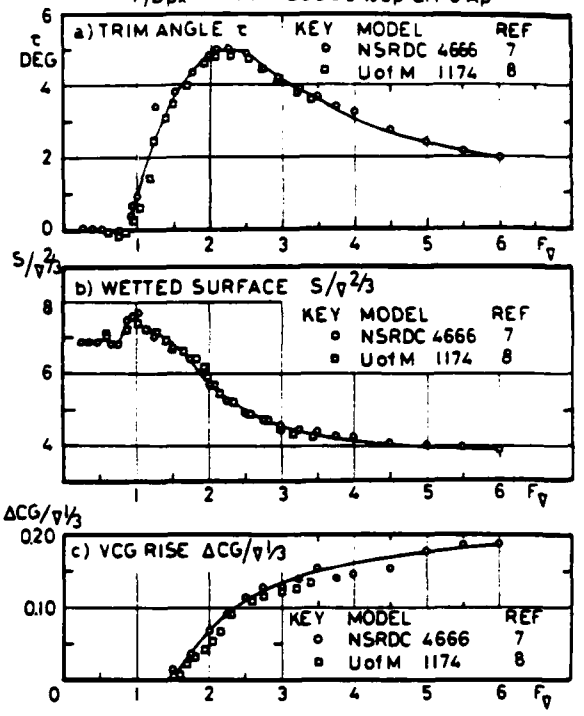


FIG 2 SERIES 62 PLANING HULL TESTS
L_P/B_{px} = 3.06 LCG = 6% L_P aft ● Ap



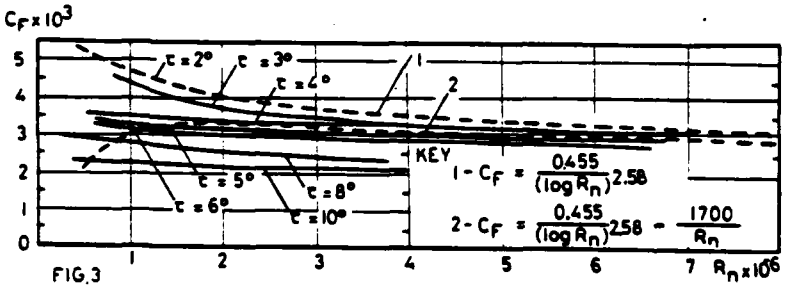


FIG.3
MEASURED C_F FOR FLAT PLANING PLATES [5]
RIMAN EXPERIMENTS L/B = 1.0, 2.5, 5.0 $2° < \tau < 12°$

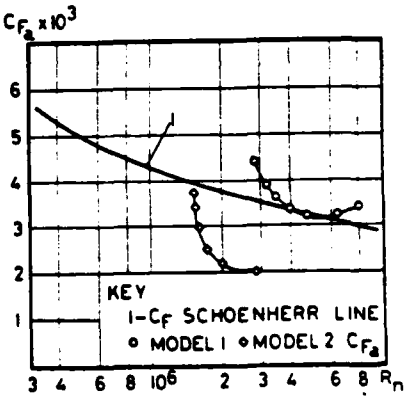


FIG 4 [9]

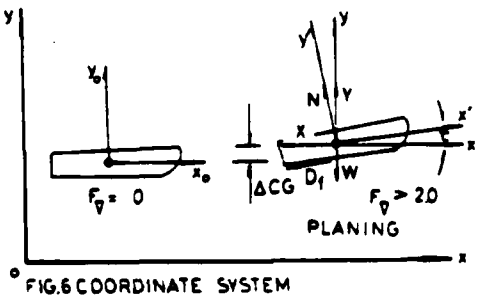


FIG.6 COORDINATE SYSTEM

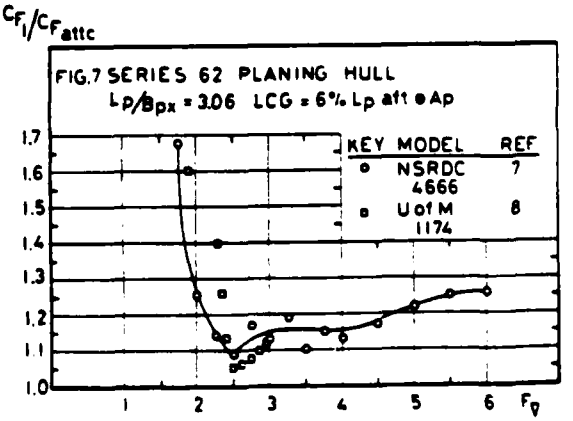
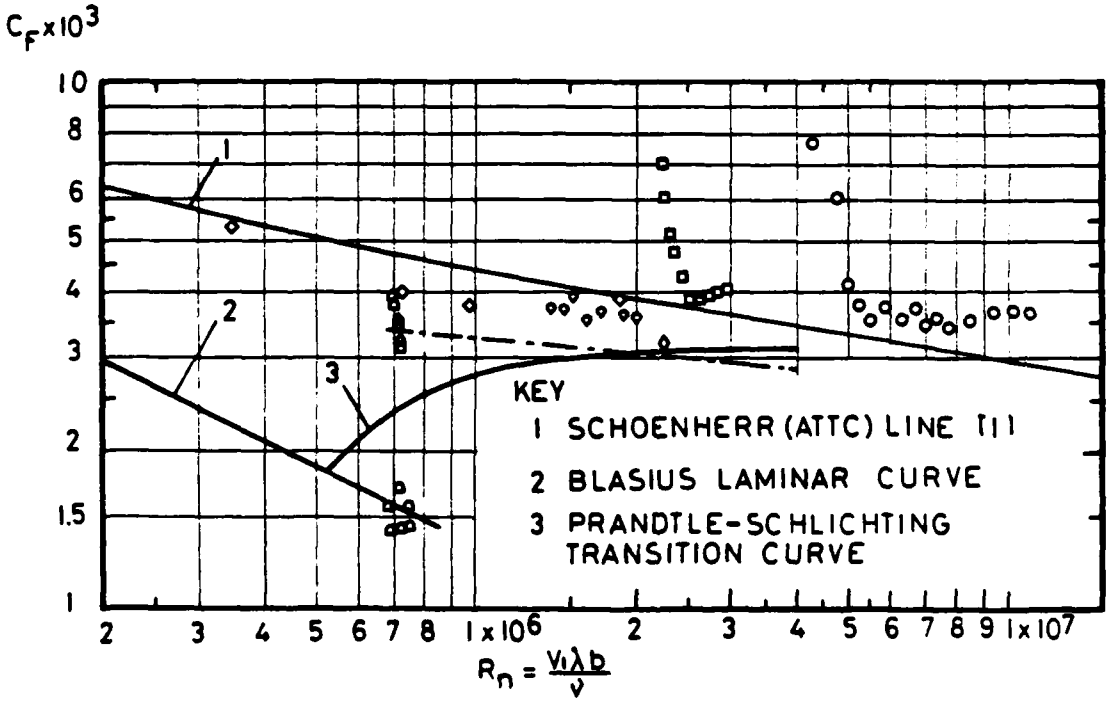


FIG.5 MEASURED PLANING C_F

MODEL	SYMBOL	τ	β	REF	NOTES
FLAT PLATE	○	4-6.5°	0°	3	PRESTON TUBE
	—·—	6°	0°	5	TOWING TEST
PRISMATIC	◇	6°	20°	2	TOWING TEST
	▫	6°	15°	4	TOWING TEST A
	△	6°	15°	4	TOWING TEST B
	◇	1-12°	15°,30°	6	TOWING TEST MEAN C_F
SERIES 62	○	2-5°	12.5°	7	TOWING TEST 1 MODEL 4666
	□	3-5°	12.5°	8	TOWING TEST 6-00 MODEL 1174



AD-P003 816

PLANING PATROL VESSEL FEASIBILITY STUDY

TIMOTHY C. BERTCH
ENSIGN, U.S. NAVY

ABSTRACT

Naval architecture is a field that began as an art using only a few scientific principles, but through research and development has evolved into a science. As ship design has become more complex, naval architects in R&D have become more specialized, a process which necessitates a special effort from the naval architect to keep the "big picture", the Navy's operational requirements. To satisfy these requirements and to allow the best choice of platforms, the U.S. Navy must be given craft information in operational format. The purpose of this paper is to provide some of that information for planing craft.

INTRODUCTION

In the first third of this century naval strength was measured primarily by the number of battleships in a country's navy. As emphasis and funding was concentrated on these vessels, fledgling concepts (such as naval air power) struggled to survive. During peacetime the acceptance and/or reevaluation of a concept requires extensive examination. This process may reduce introduction of marginally valuable concepts but can also delay introduction of badly needed systems. For example, aviation's naval potential was shown by the sinking of the German battleship Ostfriesland in 1921 and the fleet 'attack' exercise on the Panama Canal in 1929. However, acceptance of naval aviation's potential met with resistance which possibly contributed to catastrophes such as Pearl Harbor and the sinking of the ships Repulse and Prince of Wales.

Today, two realities are facing naval planners: the technological advances in guided weapons such as missiles and torpedoes and the rapidly increasing cost of naval platforms. These guided weapons with designs emphasizing compactness, low maintenance requirements and self contained homing capabilities are allowing smaller craft to be as effective as the larger craft that the older systems required. The high cost of naval platforms is (or should be) bringing naval planners to consider smaller craft.

In the naval communities of today when one speaks of modern small craft a discussion of advanced marine vehicles may result. Under this category fall air cushion vehicles, hydrofoils and planing craft. The focus of this paper will be limited to planing craft.

There are two basic types of planing craft, those with a hard chine

hull shape and those with a round bilge hull shape. The former provides more lift and therefore has a greater maximum speed. This type is presently favored by the British, Americans, Soviets and the Scandinavian countries. The latter, while requiring more propulsive power for the same speed than the hard chine, has much better seakeeping characteristics. The Germans, French and Israelis appear to favor this type (Figure 1). As it is beyond the scope of this paper to advocate either type, the term 'planing craft' here will encompass both types.

One of the confusing aspects of naval small patrol vessels is the craft designation. This paper is concerned with patrol craft that are naval vessels whose maximum speed is above 25 knots, displace less than 500 tons, are at least partially dynamically supported at full speed (planing), and are armed with either missiles, guns, torpedoes or any combination of these.

HISTORY

The value of the high speed small craft began to be realized in the early twentieth century when the development of the torpedo made the small craft a potential threat. The first use of the torpedo was in 1891 when a Chilean gunboat sank the insurgent held 3500 ton battleship "Blanco Encalada". The defeat of the Russians at Port Arthur (1904) and Tsurshima (1905) by Japanese torpedo craft alerted the naval world to the value of the high speed small craft and its torpedo. The Turbinia with her steam turbine engine had proved the feasibility of high speed small craft, but the development of the internal combustion engine with its higher power to weight ratio for marine use was a needed breakthrough. This led to the development of the Coastal Motor Boat (CMB) which displaced only 14 tons, was capable of operations in the North Sea and had a speed of 46 knots. Although the First World War was generally uneventful for the CMB, these vessels did succeed in a raid on Kronstadt after the Russian Revolution where they sank one cruiser and damaged two capital ships and two destroyers while only losing one CMB.

These vessels were not mentioned in any of the post-war treaties (Versailles or London Naval Conference of 1930) even though at this time these underrated craft possessed a very effective means of naval torpedo delivery. The high speed small craft were faster and more maneuverable than the larger destroyers but disadvantages which included limited seakeeping ability, vulnerability to being hit and a short range (which increased dependence on a supporting base) prevented extensive use. Other problems were high building costs for the displacement and maintenance required for the high performance engines.

Although the U.S. Navy possessed only 33 patrol vessels on 1 July 1940, the development of this type of vessel had been sufficiently accomplished to allow construction of 1700 of these vessels in the next five years, including over 700 PT boats. While the total tonnage destroyed by these vessels is not impressive (of major vessels only two destroyers and two submarines were sunk) they provided an essential deterrent factor in forward areas where more valuable craft were not risked. In these forward areas, such as the Philippines at the beginning of the war and later at Guadalcanal, these vessels did challenge control of the seas where larger vessels could not be supplied or hidden from enemy air superiority. And although these craft were left to their own devices (and own defense) they suffered fewer percentile losses than aircraft carriers, cruisers or destroyers (Table I).

After World War II the use of the patrol craft waned as military expenditures were reduced. After the construction in 1951 of PT 809-812 (for research in aluminum hulls, hard and soft chine, welding vs. riveting and gas turbine) the small craft program in the Navy halted. When the need for these vessels was realized in the 1960's the Navy purchased the Norwegian 'Nasty' class for service in the VietNam War. Interest in the high speed small craft concept did return in the 1970's with the establishment of the Naval Inshore Warfare Craft Program. The Coastal Patrol Interdiction Craft (CPIC), the technological result of this program, was developed for the Republic of Korea. This vessel may already be obsolete as it was not constructed with missile capability, thought by some to be essential in today's patrol craft. This program was cancelled in 1976 and despite PHM development the Navy is left without a small, inexpensive capable patrol craft.

EFFICIENCY

The value or efficiency of a vessel is determined by how effectively the vessel completes its mission compared with the costs involved in completing its mission. The missions of the Navy vary from holding sea lines of communication to power projection. In any case the heart of the mission of a naval vessel is the ability to fight.

The first measure of the ability to fight is the effectiveness of the weapons systems, but other factors are equally as important. The vessel's fighting ability is not only a factor of the quality and reliability of the vessel's weapons systems but also a function of speed, endurance and seakeeping performance required to reach the area of conflict. Also, the vessel must exhibit adequate habitability standards to allow the crew to perform without degrading its function in the system. The effectiveness is a function of:

- Weapon Systems
- Speed
- Endurance
- Seakeeping
- Habitability

While other factors may or may not exist this effort will be concerned with these five factors only.

The counterbalance to effectiveness is cost. A vessel that can perform every task perfectly is of no value if it can not be afforded. Also a vessel is of limited value if two ships with one half the capability have a lesser combined cost; and finally, an inexpensive vessel is of no value if it has no effectiveness. Therefore, when considering efficiency, the cost of the vessel is as important as all the other factors combined.

Many areas are covered by the term 'cost'. Costs include capital expenditures such as design costs, building costs, and life cycle costs. Other costs include opportunity costs (the loss of the ability to spend the allocation elsewhere) and moral costs (experienced by those who send men out to sea in ships that might enter combat). These noncapital costs and other costs that may exist shall not be discussed in this effort. The mission of the naval architect is to design the vessel with the most effectiveness for the least cost possible, thereby maximizing efficiency.

To simply provide information on the efficiency of the planing patrol vessel would not be adequate without some comparison with another type of vessel. Destroyers and frigates are proven craft and as the definition of each varies between countries which causes overlap of certain characteristics (ie: length and speed in Figure 2) the term "Destroyer/Frigate" shall be used in the comparison for that 'type' of craft.

WEAPONS SYSTEMS

Technological advances in weapon systems indicate that the patrol vessel can carry weapons of nearly equal capability as those of destroyers/frigates. The development of light weight guided missiles has made the smaller patrol craft a potential, if not potent, offensive weapon. Table II shows the characteristics of the most widely used surface to surface missiles. The capabilities of these missiles (size, accuracy, range and lethality) have improved the effectiveness of the patrol vessel. The ability of the patrol craft to carry the same missiles (albeit fewer) and the characteristics of the missile (cannister/box storage for low maintenance and 'fire and forget' self-homing capabilities) gives the patrol craft a first round 'punch' as strong as any destroyer. Surveillance and detection is one area where the patrol craft is less capable than the destroyer/

frigate but tactical information support from support vessels, coastal systems, reconnaissance aircraft and even satellites can equalize this situation. Further comparison of electronic equipment is beyond the scope of this effort. The patrol vessel which might have been considered a minor nuisance to major combatants in the past may be considered a potent threat in the near future.

To compare the effectiveness of the destroyer/frigate and patrol vessel's gun systems the 5in 54cal Mk45 and the 76mm 62cal Mk75 gun mounts are presented. Both are proven systems and are used in several foreign navies as well as the U.S. Navy. The gun characteristics are shown in Table III and for the purposes of this paper the effectiveness of the fire control systems are assumed to be equal. By assuming that the relative effectiveness is equal to the product of the ratio of the ammunition weights, the ratio of the maximum ranges, the ratio of rate of fire and the ratio of maneuverability, and assuming that the patrol vessel is one sixth more maneuverable than the destroyer/frigate, the relative effectiveness of the 5in 54cal is between 1 and 1.4 time(s) as effective as the 76mm 62cal. Ship motion and other effects on gun effectiveness are difficult to quantify and are assumed to be zero. The advantage of the larger gun might be considered marginal and in light of the relative mount weight ratio of 3.5, some of the newer frigate designs include the 76mm instead of the 5in.

The majority of patrol vessels, however, do not carry gun systems as large as 76mm. Due to size constraints smaller patrol vessels and vessels with other main armament (missiles, torpedoes) have lighter gun systems that are used for anti-aircraft defense and combat against surface vessels deemed too small to justify using the main armament. The breakdown is given below:

Gun Barrel Size	Percentage of Patrol Vessels	
larger than 40mm	22	(some vessels
between 30 and 40mm (inclusive)	52	carry multiple
between 20 and 30mm (exclusive)	26	gun mounts of
20mm and less and Machine Gun	34	various sizes)

The use of torpedoes in patrol craft is waning as they are being replaced by smaller, more versatile missile systems but there is one advantage that makes the value of the torpedo too great to have it be completely phased out of patrol craft. A hit below the waterline can cause more damage which is difficult to repair at sea and therefore more likely to sink the vessel. A realistic tactical situation exists where vessels which have been disabled by missiles would be attacked by the shorter range but more damaging torpedoes to prevent salvage/repair. Therefore in a squadron of patrol craft a missile/torpedo mix is desireable.

SPEED

Figure 2 is a plot of vessel length versus the acknowledged maximum speed. This figure illustrates the fact that for approximately the same speed the patrol vessel operates at a higher speed-length ratio, which puts it closer to or in the area called the 'planing regime' where planing vessels have a higher speed for installed horsepower than displacement vessels. This figure also shows that the patrol craft have higher maximum speeds on the average (8%), and along with the better turning characteristics of the smaller patrol vessel (assuming another 8%), the maneuverability of the patrol vessel (found from combining these advantages) may be considered to be one sixth higher than the destroyer/ frigate.

HABITABILITY

Technical advances have allowed the naval architect to provide a suitable level of habitability in all areas except ship motions. Naval systems have advanced so that crew comfort, fatigue, and working efficiency are becoming the primary liabilities in the determination of the need to adjust operations due to sea conditions. While severe motions can be accepted for a period of time due to operational necessity, the vessels motions should not adversely affect the crew's ability to perform its duties under normal patrol conditions. Experimental data have been added to the ISO ship motion standard as per reference (1). The ISO 'Guide for the Evaluation to Whole-Body Vibration' concerns the effect of vehicle (ship) vibrations transmitted to human operators. From this standard as shown in Figure 3 one finds that a planing vessel with a length of 216' can maintain 29.4 kts in Sea State 6 for twenty hours (encounter angle = 180 degrees), before "a significant risk of impaired working efficiency" (9) occurs. With an assumed twelve hour warning (weather information/storm buildup) the patrol vessel has a 940 mile range to find shelter before efficiency begins to be lost. However at a encounter angle of 0 degrees the encounter frequency drops below the range covered by the ISO. In this region the Motion Sickness Incidence (MSI) dominates. The vessel mentioned above has a one hour MSI of 15% under these conditions.

Another method of determining the crew's tolerance to ship motion for planing craft is to evaluate impact limits as proposed by Payne (10). The previous method, ISO-2631, uses RMS acceleration values. Payne's premise is that sharp peak accelerations, which would hardly affect an RMS value, are serious factors in the crew's ability to perform its duty. A Dynamic Response Index (DRI) is defined by the compressions on the spinal column due to peak accelerations. From a time history of accelerations of a vessel in a particular sea state and velocity, the number of times specified

DRIs are exceeded can be found. Plotting on Payne's Impact Ride Quality Index Chart (Figure 4) one can find toleration limits, the percentage of the maximum DRI the crew can withstand.

In summary, Figure 3 shows that a patrol vessel has habitability capabilities that qualify it as an oceangoing vessel. Payne's work provides an alternate standard which has yet to be applied to planing craft. While the patrol vessel's ability to withstand ship motions is obviously less than the destroyer/frigate's, the destroyer/frigate is expected to remain at sea for a much longer period of time which requires the increased habitability. Therefore, for the amount of time deployed the superiority of the higher habitability of the destroyer/frigate may be minimal.

RANGE and ENDURANCE

Endurance is another area where comparison between types of craft requires mission analysis. While the mission of a destroyer/frigate calls for an extended level of endurance to travel to a distant location and be able to remain on station indefinitely, the patrol vessel's mission is more limited.

The patrol craft has a higher range per ton of displacement for the corresponding speed as shown in Figure 5, and as the patrol craft may have a higher payload/displacement ratio, the patrol vessel has a higher range/ton of payload for the corresponding speed. Figure 6 shows the actual range for the corresponding Froude Number. By using the established values for 19 warships curves of mean values for destroyers/frigates and patrol vessels were fitted (curves 1 & 2). These curves intersect at an endurance of 2000 nautical miles, indicating that patrol vessels can operate at a higher Froude Number for the same range under that value. However, for design purposes these curves do not adequately describe the present day situation. To best describe the relationship if vessels were to be built today, these curves are paralleled so that they lie just higher than the highest vessel's value and become curves 3 & 4. These curves describe an apparent "state of technology" which indicates the patrol vessel can operate at a higher Froude Number up to an endurance of 2750 miles. As the Froude Number varies as a function of velocity and the inverse square root of length, knowing the average lengths of destroyers/frigates and patrol vessels shows that the patrol vessel is capable of achieving a higher speed up to an endurance of 1500 miles.

Therefore even before considering the fact that the patrol vessel's mission requires less endurance, it can be shown that the patrol vessel is the faster vessel for missions requiring less than the 1500 mile range.

This includes all but mid-ocean and extended time deployments. In terms of endurance, the patrol vessel is an oceangoing vessel.

SPEED LOSS IN SEAWAY

Although the vessel's seakeeping limits due to ship motions have been already noted, meeting those limits would require a voluntary correction (speed or course change) to improve ride quality. Another aspect of seakeeping is involuntary speed loss due to wave action. Figure 7, a prediction for involuntary speed loss is taken from reference (1). Assuming a linear change of speed loss between the curves in the figure, Figure 8 can be derived. When the curves are extrapolated slightly, despite the fact that the limits of Froude Number and wave height/displacement ratio restrain prediction to only high speeds and for a small number of displacements, Figure 8 shows the effect of vessel displacement, speed and sea state on percent involuntary speed loss.

A standard assumed for seakeeping ability of patrol craft is to be able to maneuver and fight without loss of effectiveness in Sea State 3 and survive in Sea State 6. Figure 9 shows the percentage of time that these sea conditions occur for the world's oceans as found by historical measurements. For a great majority of the time a patrol vessel can be used in almost any location on the globe.

COSTS

One of the early problems with the adoption of patrol craft was the high building cost per unit displacement. This and the craft's limited military capabilities did not allow for extensive construction of patrol vessels. During World War II the average U.S. cruiser/destroyer craft cost 6.7 million dollars while the average patrol vessel cost .58 million dollars (3). Therefore the Navy could purchase just over 11 patrol vessels for one cruiser/destroyer with the patrol vessel having vastly inferior seakeeping and weapons systems. A more favorable cost effectiveness relationship (50:1) exists today with the cost of a destroyer as high as a half billion dollars and a capable patrol vessel costing less than 10 million. However, a more adequate comparison of these types is required to provide a basis for cost appraisal.

Two cost functions have been defined to clarify the nature of ship costs. In the first shown in Figure 10, comparing the destroyer/frigate with the patrol vessel shows that patrol vessels tend to have a lower cost per unit displacement and unit speed. This plot, derived from the characteristics of fourteen warships, can be roughly approximated by a curve, which relates Cost/(Displacement times Maximum Velocity) and Froude Number. By manipulation of the variables the cost may be represented as a function

of velocity (maximum), length and the non-dimensional (L/B), (B/T) and block coefficient. Accordingly, for the same hull form the cost is a function of length and maximum velocity (Figure 11). The relationship implied by Figure 11 (as much as twenty five percent inaccurate due to scatter around the faired curve in Figure 10, inflation and age anomalies) provides an indication of the factors of cost and their relationship. As length increases, cost increases at a rate which, not unexpectedly, is a cubic function (Figure 12). Figure 11 also shows that the additional cost to provide a higher maximum speed also increases as length increases. In summary, the cost of a warship may be represented as a function of its dimensions, block coefficient and maximum velocity. Other factors that may influence costs are not considered in this presentation.

The size of the crew directly affects the size of the warship and therefore its cost. Figure 13 shows that crew size follows a relatively narrow band in functional relationship to ship length. Figure 14 shows that crew size is not a direct function of displacement. An increase in complement does affect vessel design as the addition of "One man to the complement, allowing for an increase of ship size will cost 50,000 pounds ($100,000) in 1980" (8). From the same paper's Table 10 the NATO average volume of living space per man is shown to be 150 cubic feet, a further constraint on crew size.

The greatest impact of crew size on cost is not on construction cost but rather on annual costs. From the annual cost per paygrade (Composite Standard Rates) found in the Navy Comptroller Note 7041 FY 82 and the approximate rank breakdown on a warship, the annual crew cost is shown as a function of length in Figure 15. These costs account for pay and allowances (including moves) only, and do not include other costs such as training. If it is assumed that these are the total personnel costs, then annual operating costs can be found. Figure 4 of reference (8) shows that personnel costs are 14 percent of the annual costs, which makes determination of annual operating costs possible (Figure 16). This conservative estimate for annual costs still shows that in the life of a vessel (20 years) the sum of the annual costs will exceed the construction costs. Therefore increasing the size of a vessel will not only increase its construction cost but also to the same degree, its life cycle cost.

A true cost comparison of a destroyer/frigate and a patrol vessel is now possible. Using the average lengths and operating speeds of the destroyer/frigate and patrol vessel (402 ft/21.7kts and 116ft/23.5kts, respectively) the construction cost function of the destroyer/frigate is greater than the patrol vessel by a factor of 75. For the same average values the annual costs of the destroyer/frigate are 7.5 times as large as the patrol vessel's. Therefore with the construction cost distributed over the twenty year life of a warship the destroyer/frigate annual costs are 11.75 times that of the patrol craft.

SUMMARY

To summarize, it is not possible to compare total military effectiveness of a destroyer/frigate and a patrol vessel without a complete mission analysis. However, the patrol vessel is becoming as effective as a destroyer/frigate in some of what used to be exclusive destroyer/frigate missions. For certain surface combat missions the patrol vessel may be capable of complimenting or even taking the place of the destroyer/frigate. While a patrol vessel usually has only guns and missiles, most destroyer/frigate's torpedoes are intended for use against submarines and are of limited effectiveness in surface combat. Although for most missions the number of missiles carried by a patrol vessel should be adequate, the destroyer/frigate has an advantage with its larger number of missiles. The destroyer/frigate gun system is usually more capable, as well. Overall, in weapons systems the destroyer/frigate is assumed to be approximately twice as capable as the patrol vessel.

The habitability of the destroyer/frigate is superior to the patrol vessel in conditions greater than Sea State 3, but in conditions greater than Sea State 6 the habitability of both types is severly reduced. Assuming the destroyer/frigate is twice as capable by the middle range and knowing that these conditions exist worldwide approximately one-half of the time (Figure 9), the habitability effectiveness of the destroyer/frigate is 1.5 times higher than the patrol vessel. The average endurance of a destroyer/frigate is 3.25 times that of a patrol vessel but the patrol vessel's speed at this endurance is eight percent higher than the destroyer/frigate. Assuming that the patrol vessel has an involuntary speed loss equal to this extra speed, the destroyer/frigate's superior effectiveness is a function of three of the five discussed parameters; weapons systems, habitability and endurance. Combining these factors the destroyer/frigate is approximately ten times as capable (2 x 1.5 x 3.25). Compared with the life cycle cost ratio of 11.75 patrol vessels to one destroyer/frigate, it is concluded that the patrol vessel is approximately 20 percent more efficient than the destroyer/frigate in its mission.

This life cycle value should not be dismissed as overly optimistic. Maintenance and stores are a function of at least the deck area (proportional to the length squared) if not the displacement (proportional to the length cubed). Comparing Figures 13 and 14 will show that crew size is at least a function of length squared. Fuel costs are a function of resistance which also varies as a function of at least length squared. Therefore operating costs vary as at least the square of the length. With the 'destroyer/frigate'/patrol vessel average length ratio of almost 3.5, the operating costs ratio is a factor of twelve, not the factor of 7.5 the author proposed. Therefore the operating cost ratio, the controlling

factor of the life cycle costs, may be considered conservative.

CONCLUSION

The patrol vessel is becoming an increasingly capable platform as the technology of naval platforms and weapons increases. The higher Froude Numbers caused by shorter length and higher maximum speed favor the planing hull shape. The advances in weapons systems technology is giving the patrol craft a combat effectiveness of the same order of magnitude as a destroyer. While the combat effectiveness of a destroyer has also grown this does not necessarily mean the destroyer is the most efficient platform for all of what have been 'destroyer missions'. The much reduced building and life cycle costs as well as improved endurance, habitability and seakeeping ability make the patrol craft an attractive oceangoing naval platform. While the patrol craft can not replace the destroyer, its effectiveness has improved considerably. There is a need for a reevaluation to determine the most effective patrol craft/destroyer combination for a strong Navy.

REFERENCES

1. Savitsky, D. and Gore, J.L., "A Re-evaluation of the Planing Hull Form," American Institute of Aeronautics and Astronautics, Inc., 1979.

2. "Japanese Naval Losses from Pearl Harbor to October 1, 1944," Statistical Section, Division of Naval Intelligence, December 4, 1944.

3. Annual Report from the Secretary of the Navy to the President: Fiscal Year 1945.

4. Bulkley, Robert J., Jr., At Close Quarters. (Washington: Government Printing Office), 1962.

5. McLeavy, Roy. Naval Fast Strike Craft and Patrol Boats. (Poole: Blandford Press), 1978.

6. Polmar, Norman. The Ships and Aircraft of the U.S. Fleet. (Annapolis: Naval Institute Press), 1978.

7. Marriot, John. Fast Attack Craft. (New York: Crane, Russak & Co., Inc.), 1978.

8. Andrews, D. and Brown, D., "Cheap Warships Are Not Simple," SNAME Ship Costs and Energy Symposium, New York, September, 1982.

9. "Guide for the Evaluation of Human Exposure to Whole-Body Vibration," ISO 2631-1974(E), International Organization for Standardization, Switzerland, 1974.

10. Payne, P.R., "On Quantizing Ride Comfort and Allowable Accelerations," AIAA/SNAME Advanced Marine Vehicles Conference, Arlington, Virginia, September, 1976.

11. Von Gierke, H.E., "The ISO Standard 'Guide for the Evaluation of Human Exposure to Whole-Body Vibration'," DOT-TSC-OST-75-40, National Aeronautics and Space Administration, Washington, D.C., November, 1975.

12. Bhattacharyya, Rameswar. Dynamics of Marine Vehicles. (New York: John Wiley & Sons), 1978.

13. Principles of Naval Architecture. Ed. John P. Comstock. (New York: SNAME), 1967.

14. Jane's Fighting Ships, 1981-1982. (New York: McGraw-Hill Book Co.), 1982.

15. Jane's Fighting Ships, 1944-1945. (New York: The McMillan Co.), 1944.

16. Combat Fleets of the World 1982/1983. Ed. Jean Labayle Couhat. (Annapolis, Md: Naval Institute Press), 1982.

FIGURE 1: SMALL COMBATANT FAMILY TREE

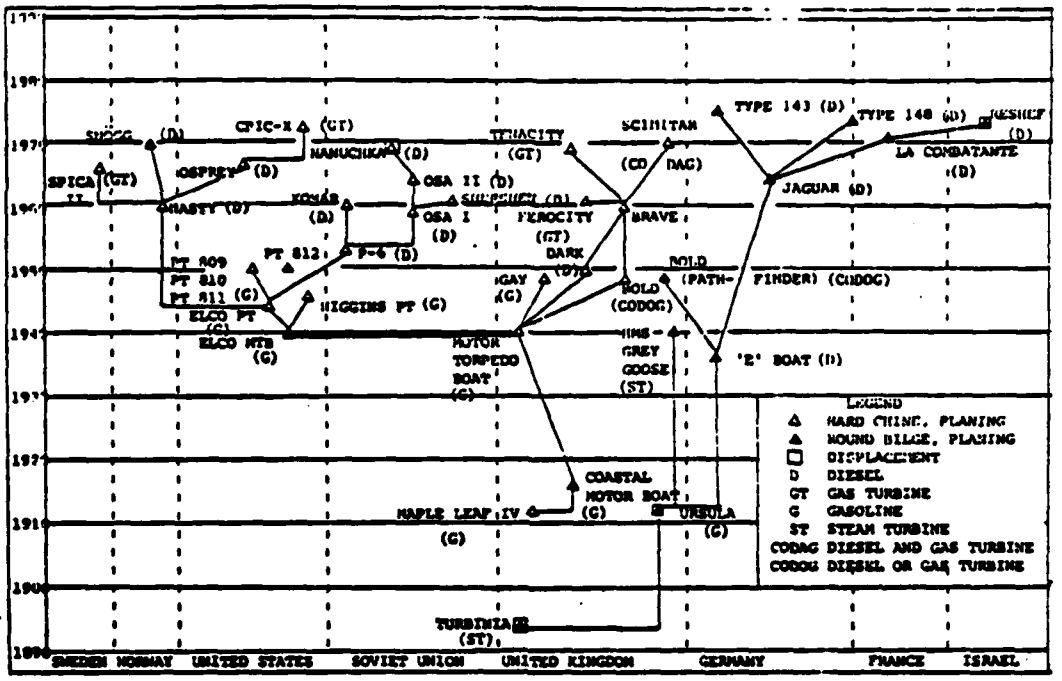


FIGURE 2: PLOT OF VESSEL LENGTH VS MAXIMUM SPEED

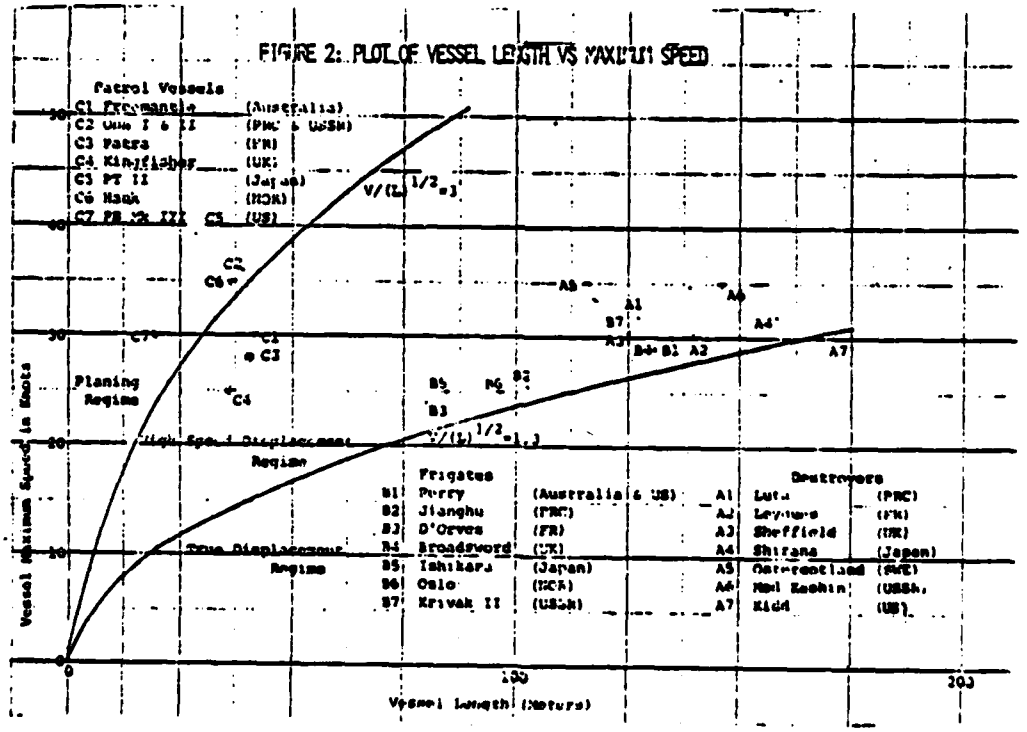


TABLE I: WORLD WAR II SHIP STATISTICS

SHIP TYPE	ON HAND 1 JUL 41	NUMBER BUILT	TOTAL	NUMBER LOST	PERCENT LOST
Aircraft Carrier (CV, CVL)	6	27	33	5	15.2
Cruiser (CA, CL)	37	40	77	10	13.0
Destroyer (DD, DE)	168	862	1030	221	21.5
Torpedo Boats (PT)	29	687	716	69	9.6

TABLE II: MISSILE CHARACTERISTICS

MISSILE (Country Made)	Speed (Mach)	Range (N.M.)	Warhead Wt. (lb)	Vessel Name	Vessel Length (ft)	Number Carried
Exocet (France)	0.9	20.5	330-440	Combattante II	154	4
SS12 (France)	0.75	3.2	62.6	Trident	133.5	6
Otomat (France/Italy)	0.8	32-43	463	Constitucion	121	3
Gabriel (Israel)	0.58	22	397	Reshef	191	7
Penguin (Norway)	0.7	15	264	Jagaren	120	4
Styx (Soviet Union)	0.7	23	---	Osa II	128	4
Harpoon (United States)	0.86	60	510	Jaguar III	191	8

TABLE III: GUN CHARACTERISTICS

Gun	Mount Weight (lb)	Rate of Fire (rounds/min)	Range (yds)	Ammunition Weight (lb)
5in/54cal Mk 45	47,820	16-20	25,909	70
76mm/62cal Mk 75	13,680	75-85	21,000	14
		Rf = .19 to .27	Rr = 1.2	Rw = 5

Relative Effectiveness = Rw * Rr * Rf * Rm
where Rw = ratio of the ammunition weights
Rr = ratio of the maximum ranges
Rf = ratio of the rates of fire
Rm = ratio of maneuverability = .86

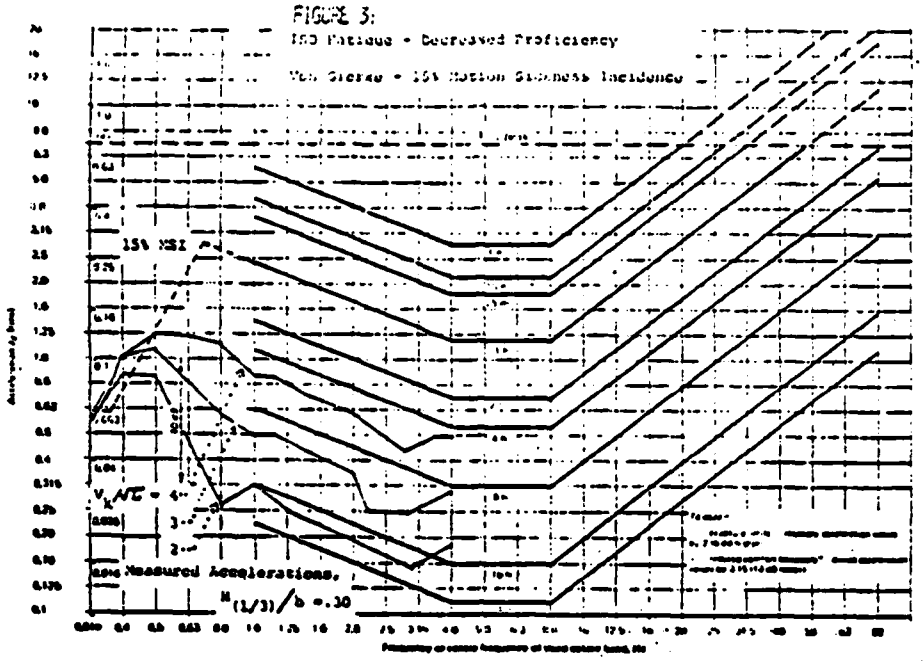
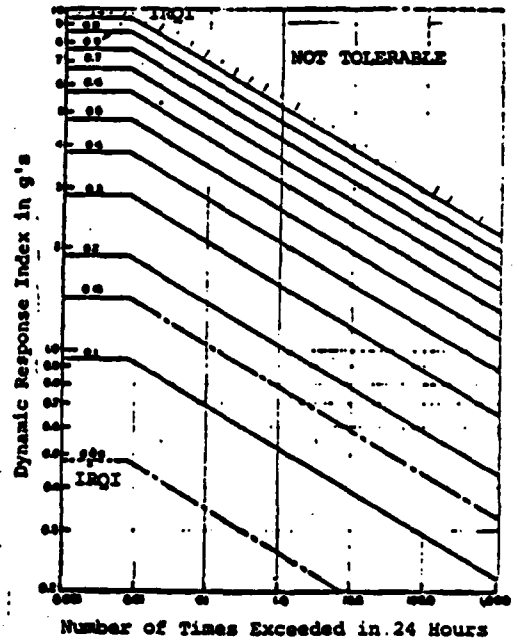
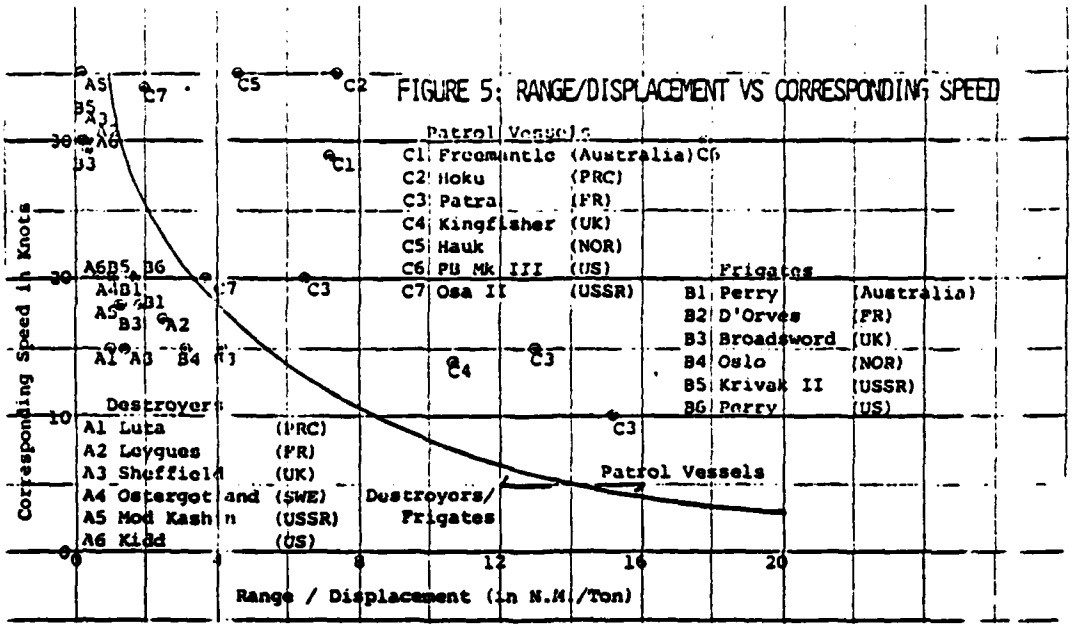


FIGURE 4: IMPACT RIDE QUALITY INDEX CHART




FIGURE 5: RANGE/DISPLACEMENT VS CORRESPONDING SPEED
Patrol Vessels
C1 Freemantle (Australia)
C2 Hoku (PRC)
C3 Patra (FR)
C4 Kingfisher (UK)
C5 Hauk (NOR)
C6 PB Mk III (US)
C7 Osa II (USSR)
Frigates
B1 Perry (Australia)
B2 D'Orves (FR)
B3 Broadsword (UK)
B4 Oslo (NOR)
B5 Krivak II (USSR)
B6 Perry (US)
Destroyers
A1 Luta (PRC)
A2 Loygues (FR)
A3 Sheffield (UK)
A4 Ostergot and (SWE)
A5 Mod Kash n (USSR)
A6 Kidd (US)
Destroyers/ Frigates
Patrol Vessels
Corresponding Speed in Knots
Range / Displacement (in N.M./Ton)

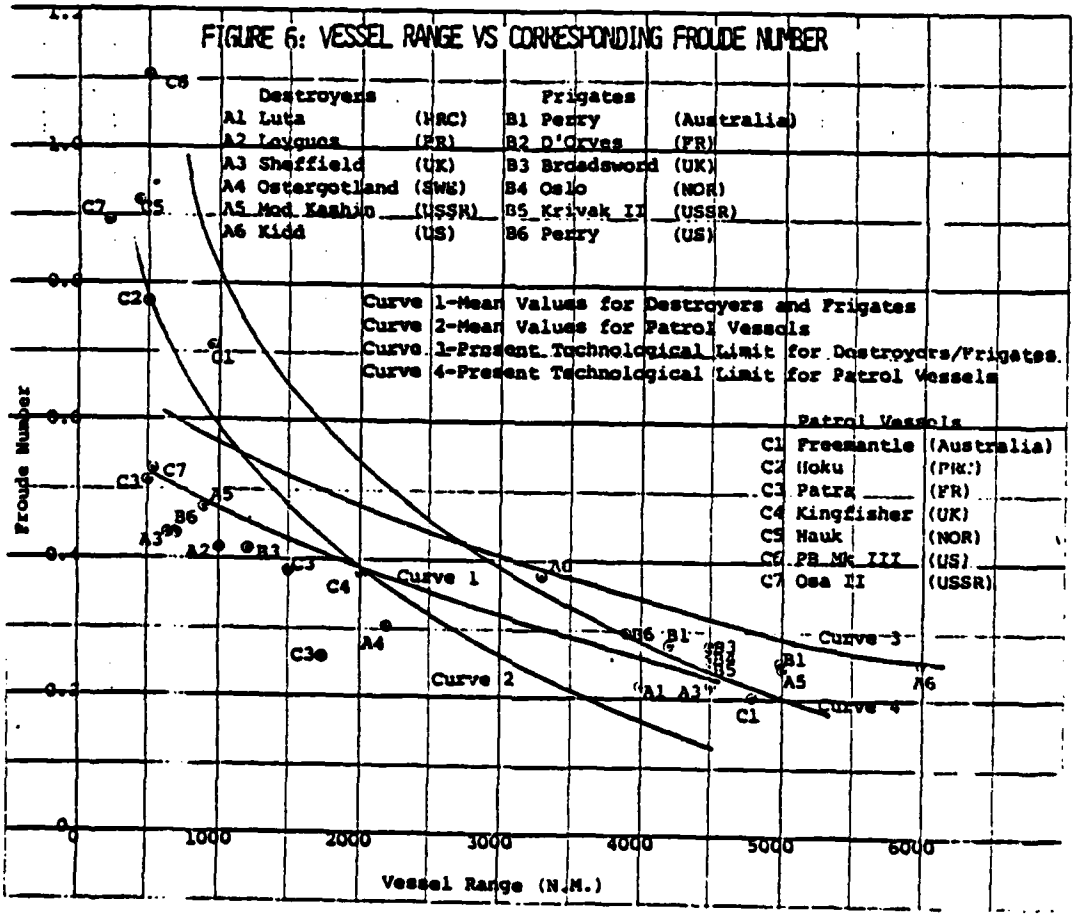

FIGURE 6: VESSEL RANGE VS CORRESPONDING FROUDE NUMBER
Destroyers
A1 Luta (PRC)
A2 Loygues (FR)
A3 Sheffield (UK)
A4 Ostergotland (SWE)
A5 Mod Kashin (USSR)
A6 Kidd (US)
Frigates
B1 Perry (Australia)
B2 D'Orves (FR)
B3 Broadsword (UK)
B4 Oslo (NOR)
B5 Krivak II (USSR)
B6 Perry (US)
Curve 1-Mean Values for Destroyers and Frigates
Curve 2-Mean Values for Patrol Vessels
Curve 3-Present Technological Limit for Destroyers/Frigates.
Curve 4-Present Technological Limit for Patrol Vessels
Patrol Vessels
C1 Freemantle (Australia)
C2 Hoku (PRC)
C3 Patra (FR)
C4 Kingfisher (UK)
C5 Hauk (NOR)
C6 PB Mk III (US)
C7 Osa II (USSR)
Froude Number
Vessel Range (N.M.)

FIGURE 7

VOLUMETRIC FROUDE NUMBER VS PERCENT SPEED LOSS IN HEAD SEAS

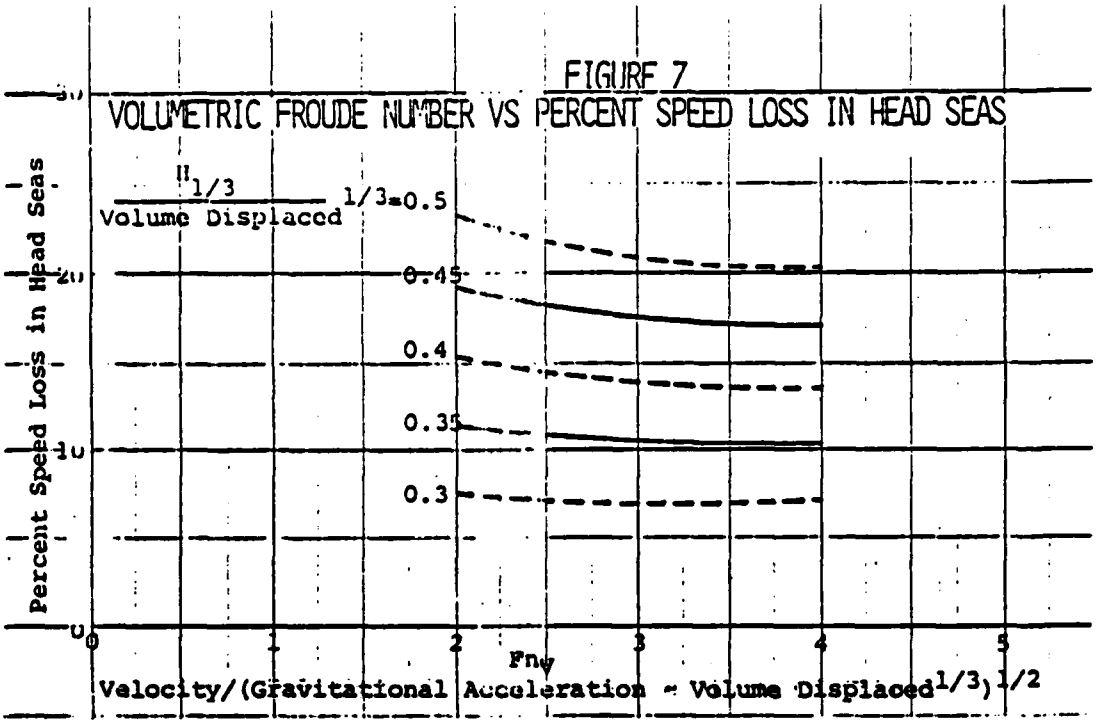


FIGURE 8: VESSEL DISPLACEMENT VS PERCENT INVOLUNTARY SPEED LOSS

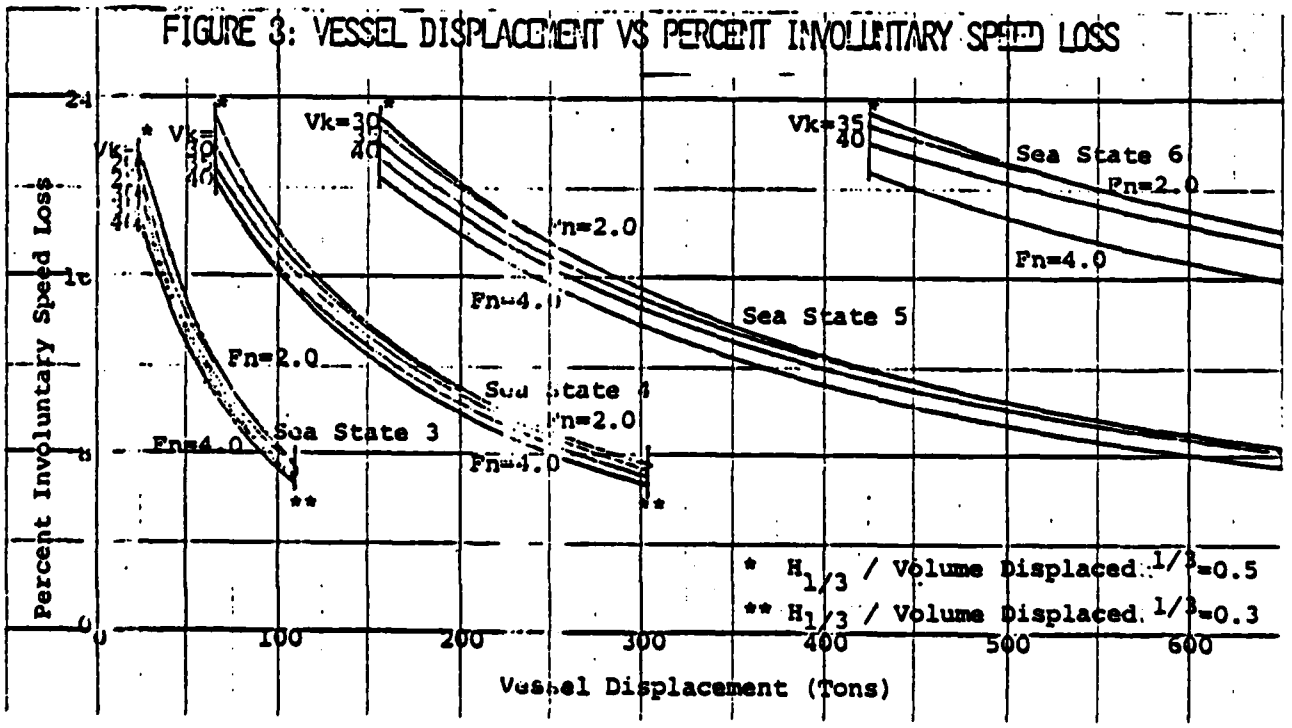
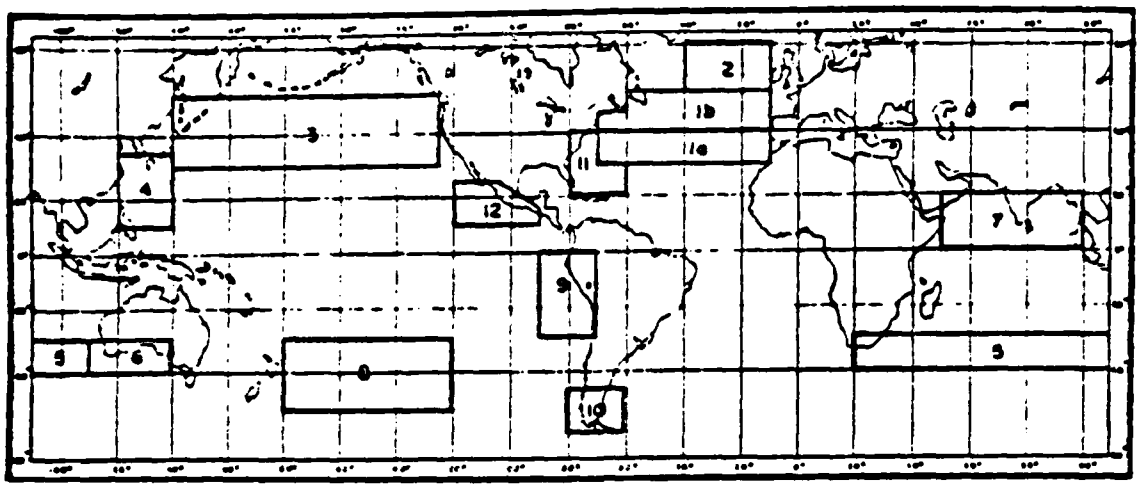
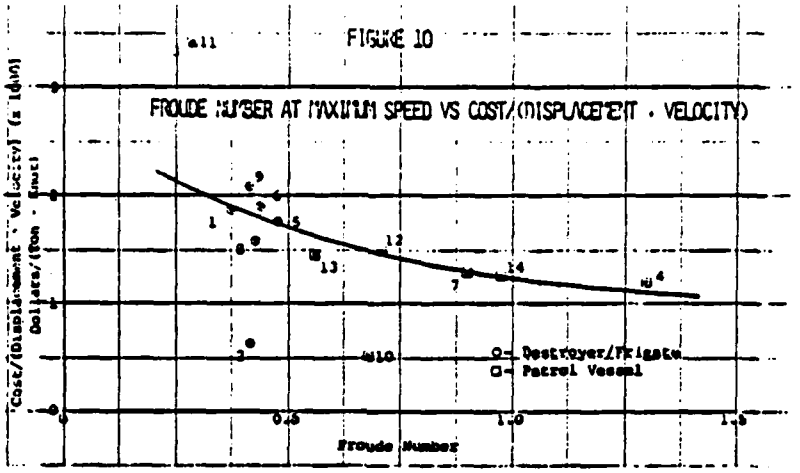
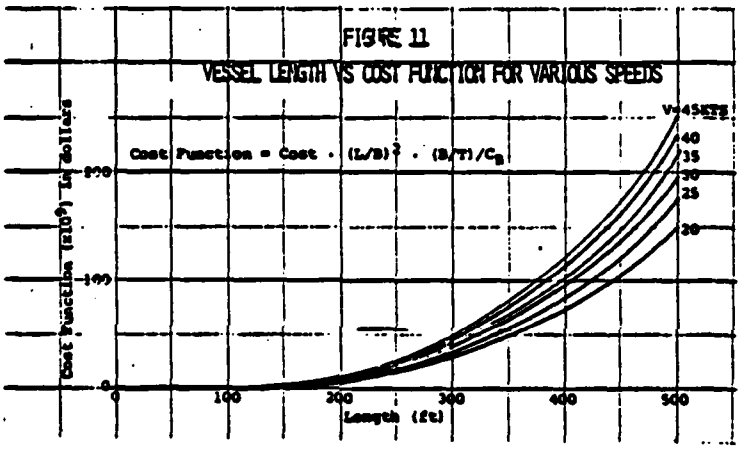


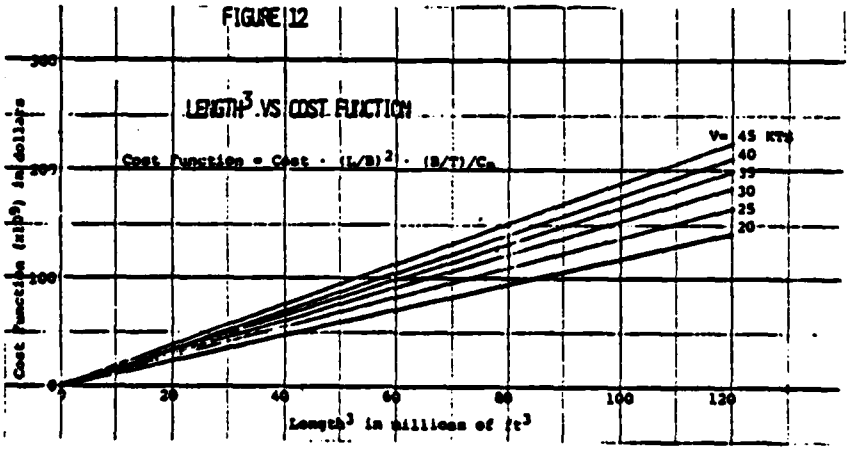
FIGURE 9 - HISTORICAL MEASUREMENTS OF SEA STATE BY REGION

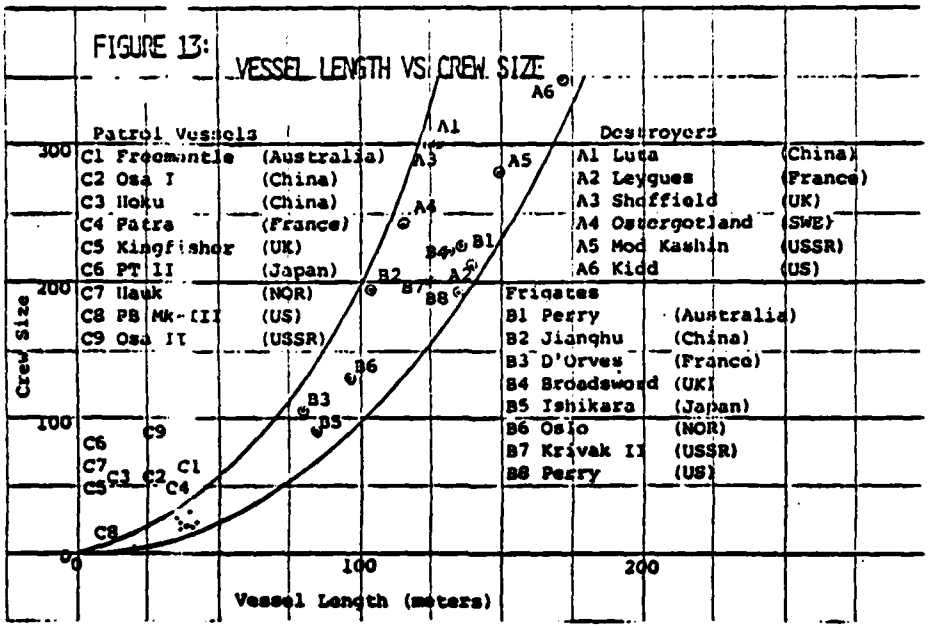


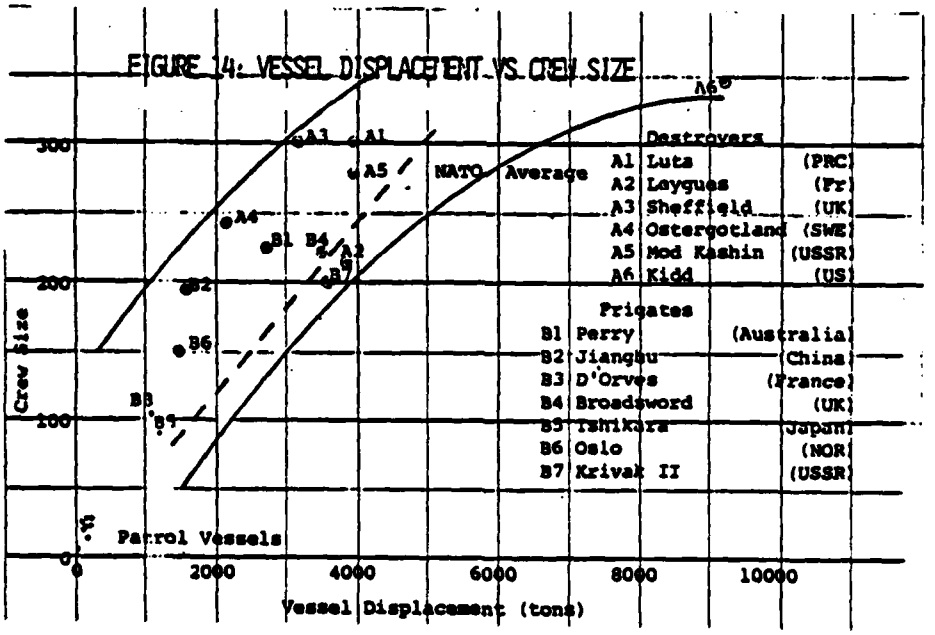
Area	Percent of Observations Sea State 3 and less	Percent of Observations Sea State 6 and less
1a	42.7	98.6
1b	34.0	96.9
2	29.0	95.1
3	37.4	98.0
4	54.9	99.6
5	28.2	98.4
6	26.5	97.4
7	56.2	99.3
8	18.7	97.8
9	61.7	100.0
10	29.8	85.8
11	60.9	99.7
12	76.9	99.9

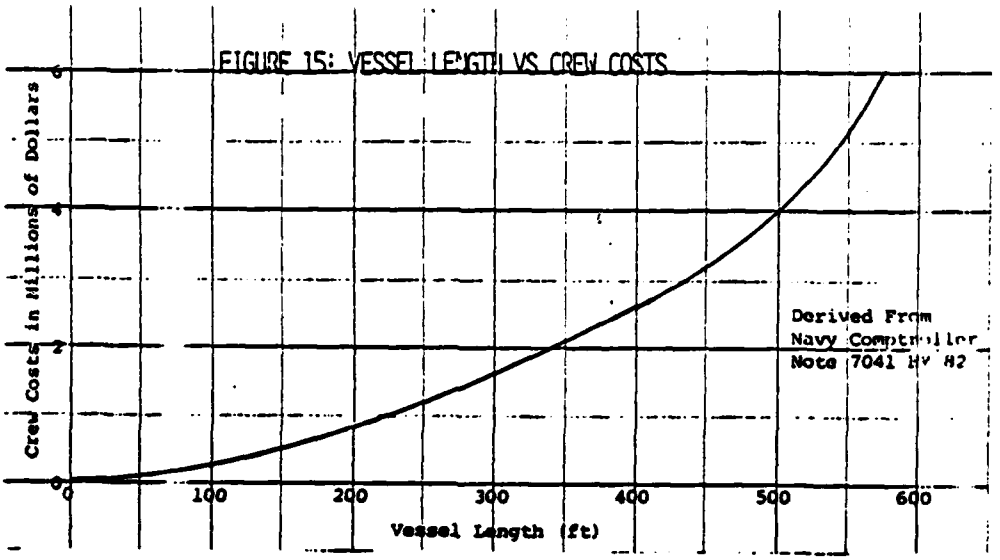

FIGURE 10
FROUDE NUMBER AT MAXIMUM SPEED VS COST/(DISPLACEMENT · VELOCITY)
Froude Number
Destroyer/Frigate
Patrol Vessel

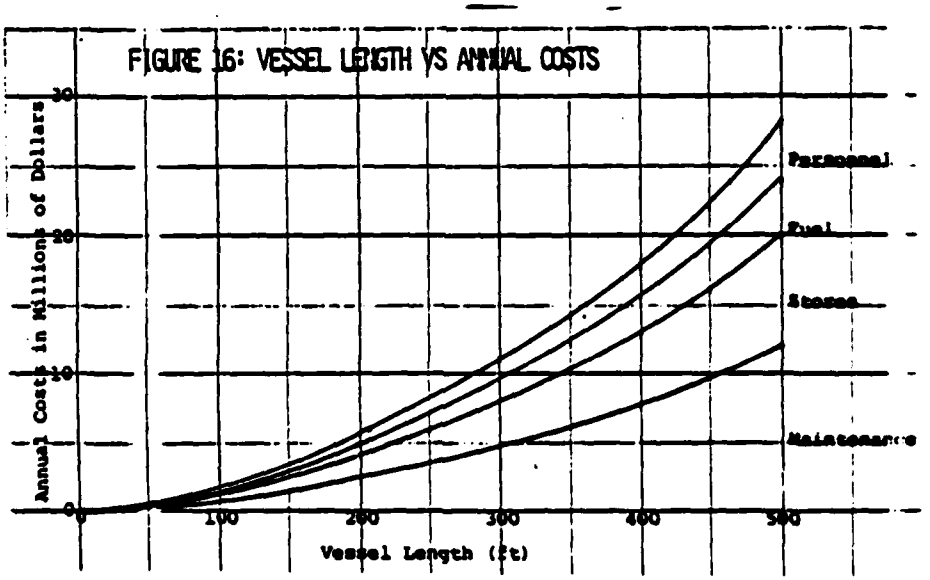

FIGURE 11
VESSEL LENGTH VS COST FUNCTION FOR VARIOUS SPEEDS
Cost Function = Cost · (L/B)² · (B/T)/C_B
Length (ft)


FIGURE 12
LENGTH³ VS COST FUNCTION
Cost Function = Cost · (L/B)² · (B/T)/C_B
Length³ in billions of ft³


FIGURE 13: VESSEL LENGTH VS CREW SIZE
Patrol Vessels
C1 Freemantle (Australia)
C2 Osa I (China)
C3 Hoku (China)
C4 Patra (France)
C5 Kingfisher (UK)
C6 PT II (Japan)
C7 Hauk (NOR)
C8 PB Mk-III (US)
C9 Osa II (USSR)
Destroyers
A1 Luta (China)
A2 Leygues (France)
A3 Sheffield (UK)
A4 Ostergotland (SWE)
A5 Mod Kashin (USSR)
A6 Kidd (US)
Frigates
B1 Perry (Australia)
B2 Jianghu (China)
B3 D'Orves (France)
B4 Broadsword (UK)
B5 Ishikara (Japan)
B6 Oslo (NOR)
B7 Krivak II (USSR)
B8 Perry (US)
Crew Size
300
200
100
0
100
200
Vessel Length (meters)


FIGURE 14: VESSEL DISPLACEMENT VS CREW SIZE
NATO Average
Destroyers
A1 Luta (PRC)
A2 Leygues (Fr)
A3 Sheffield (UK)
A4 Ostergotland (SWE)
A5 Mod Kashin (USSR)
A6 Kidd (US)
Frigates
B1 Perry (Australia)
B2 Jianghu (China)
B3 D'Orves (France)
B4 Broadsword (UK)
B5 Ishikara (Japan)
B6 Oslo (NOR)
B7 Krivak II (USSR)
Patrol Vessels
Crew Size
300
200
100
0
2000
4000
6000
8000
10000
Vessel Displacement (tons)


FIGURE 15: VESSEL LENGTH VS CREW COSTS
Crew Costs in Millions of Dollars
0
2
4
6
0
100
200
300
400
500
600
Vessel Length (ft)
Derived From
Navy Comptroller
Note 7041 BY 82


FIGURE 16: VESSEL LENGTH VS ANNUAL COSTS
Annual Costs in Millions of Dollars
0
10
20
30
0
100
200
300
400
500
Vessel Length (ft)
Personnel
Fuel
Stores
Maintenance

AD-P003 817

EXPERIMENTAL DETERMINATION OF LOW FROUDE NUMBER HYDROFOIL PERFORMANCE IN CALM WATER AND IN REGULAR WAVES

by

Michael B. Wilson
David W. Taylor Naval Ship Research and Development Center

ABSTRACT

Results of experimental investigations are presented for the steady and unsteady hydrodynamic force performance of an aspect ratio 6, NACA 64A010 foil section, plain-flapped, rectangular planform hydrofoil. The forward-leading sting-supported foil model was operated in calm water in the speed range of chord Froude numbers varying from 1.22 to 4.23 at five depth-to-chord ratios. It was run under regular head waves at Froude numbers varying from 1.22 to 3.67 at three depth-to-chord ratios, in a systematic series of wave lengths and amplitudes. These data cover an important low Froude number speed regime. For both the calm water (steady) and the unsteady cases, comparisons are provided between the exeperimental results and analytical predictions. It is shown that at low Froude numbers there is a trend toward exaggerated level of both steady and unsteady hydrodynamic forces on a hydrofoil.

INTRODUCTION

The physical size of certain types of proposed subcavitating hydrofoil systems has grown in recent years in response to design considerations for large hydrofoil ships, for partial hydrofoil supported craft, for applications as antipitch and antiroll fins on surface ships, and for control foils on small waterplane area twin hull (SWATH) ships. This has focused attention on a low Froude number range that has received little attention in most of the

hydrofoil experimental literature that provides basic hyrofoil data, for operation in either calm water or in waves. Chord Froude numbers as small as 1.5 to 2 at submerence ratios of h/c = 0.5 to 2 are conceivable operational values of interest in practical application for large hydrofoil craft at takeoff or for SWATH ships at cruise speed.

For steady operation (in calm water), it is known that a hydrofoil running near the free surface at low Froude numbers at a fixed geometric angle of attack experiences an accentuated drag-due-to-lift (or total induced drag) caused by a hump of the wavemaking drag coefficient centered around a depth Froude number $F_{n_h} = 1.4$. The accompanying lift coefficient shows a local minimum or dip at about the same Froude number. These effects are exaggerated as the submergence ratio decreases. Predictions of general properties of steady hydrofoil force performance using linearized potential theory have been available for a long time. Examples of important fundamental references are the contributions by Nishiyama,[1*], Wu,[2] Breslin,[3] and the numerous works noted in the bibliographies of these papers.

Examples of published presentations of smooth water experimental hydrofoil data include work by: Wadlin, et al,[4], Wilson and Kelley,[5], Jones,[6] Feldman,[7] Dixon, et al[8], and Wilson[9]. The latter experimental project formed part of the basis for the present discussion.

For the case of unsteady force response on a hydrofoil moving under waves, the available results of both theoretical studies and experiments with finite aspect ratio foils have established the expected strong relationship between the characteristics of unsteady force amplitude response and the parameters of reduced frequency of encounter k_e; geometical features such as

---

*A complete listing of references is given starting on page 573.

aspect ratio and depth-to-chord ratio; and have pointed tentatively to an exaggerated unsteady effect for low Froude operation. There is a large body of theoretical work concerned with the prediction of unsteady forces on foil in unbounded flow resulting from either forced pitch and heave motions or from operation in a cross-flow or gust. There are older summaries on unsteady airfoil loads such as Bisplinghoff, et al.[10] and Fung[11] that list much important work that served to inspire later work on the comparable hydrofoil problem. Examples of successful lifting surface work on unsteady subsonic airfoil loads, whose results can be used to assemble approximate predictions for submerged hydrofoils, are Reissner[12], Reissner and Stevens,[13] and Lawrence and Gerber[14].

Some examples of direct contributions to the analysis of finite aspect ratio hydrofoils near a free surface, operating with forced pitch and heave or moving under waves have been reported by Widnall,[15] Widnall and Landahl[16], Widnall,[17] and Tsakonas and Henry[18]. Examples of published experiments conducted on hydrofoils moving under waves include Kaplan,[19] Schuster and Schwanecke,[20] Wetzel and Maxwell,[21] Henry and Ali,[22] Tsakonas and Henry,[18] Steele,[23] Schuster and Schwanecke[24] and Karafiath[25] whose work forms the second major part of this presentation.

The experiments described here were designed to provide steady and unsteady lift and drag force data for foil-alone performance specifically covering a low Froude number range of interest, at sufficiently large Reynolds numbers, with a guarantee of turbulent boundary layer flow, and with minimal hydrodynamic interference from the support system.

As an example application, a recent DTNSRDC concept design of a 11,000 L. Ton SWATH ship calls for chord length 15.5-ft (4.72-m) aft control foils to be operated at nominal depth-to-chord ratio h/c = 1.5 The sustained

speed of 30 knots with cruise speed of 20 knots correspond to control foil chord length Froude numbers of F_{n_c} = 2.27 and 1.5, respectively. The present results could have direct bearing on the design and operation of such a low Froude number hydrofoil system.

DESCRIPTION OF EXPERIMENTS

FACILITY

Both sets of experiments described here were conducted on Carriage 2 in the deep water basin at the David W. Taylor Naval Ship Research and Development Center, Carderock. This towing tank is 1886-ft (574.8-m) long, 51-ft (15.5-m) wide, with a water depth of 22 ft (6.71 m). The pneumatic wavemaker was used to generate regular waves for the unsteady experiments, with the basin water level reduced to 19.5 ft(5.94 m).

MODEL AND MOUNTING SYSTEM

The hydrofoil model manufactured for these experiments is an aspect ratio 6, rectangular planform wing, with a chord lenght of 16 in. (40.64 cm), maximum thickness of 1.6 in (4.064 cm), and squared-off tips. The NACA 64A010 section shape, the offsets of which are given by Loftin,[26] was machined from a solid piece of aluminum, and the final surface finish was produced with emery cloth. Table 1 summarized the important characteristics of the hydrofoil model.

It was important with the calm water experiments to achieve total foil lift coefficients of at least 0.8 to cover conditions expected at low speed takeoff of a lifting hydrofoil system, so a trailing-edge flap was provided with a flap chord ratio of c_f/c = 0.25 and with a generous flap span extending across nearly the full foil span, b_f/b = 0.934. The flap deflection angles were fixed rigidly using a series of 14 angled flap pads. Plastiline putty was

forced into the gaps at the flap knee so the flap system can be described as a "sealed plain flap." Figure 1 is a sketch of the hydrofoil section showing the flap deflection angle δ_f. The flap angle was zero for all the unsteady experiments.

TABLE 1 - HYDROFOIL GEOMETRY AND PARTICULARS

Aspect ratio	A = 6
Foil thickness ratio	t/c = 0.10
Span	b = 8 ft (2.438 m)
Chord length	c = 1.333 ft (0.406 m)
Flap chord ratio	c_f/c = 0.25
Flap span ratio	b_f/b = 0.934
Flap planform area ratios	S_f/S = 0.2357
Planform area; shape	S = 10.67 ft^2 (0.991 m^2); Rectangular, squared-off tips
Foil material	6061-T6 aluminum
Section shape	NACA 64 A010
Turbulence stimulator wire	0.016 in. (0.041 cm)

Turbulence stimulation was provided by 0.016 in. (0.0406 cm) diameter piano wire stretched taut at a distance of 0.02 c or 0.32 in (0.813 cm), back from the leading edge. Each span length of wire was held in place at 1-ft (30.5-cm) intervals, and was thus permitted to strum in the flow over the foil.

The forward-leading sting support for the hydrofoil consists of a long horizontal pipe instrumented for the measurement of lift and drag forces

through two support points. Angle of attack variation for the foil is provided by a series of steel nose pieces, each with an angled slot that accommodates the rear end of the foil. There is a different nose piece for each angle of attack considered, and the slot in each is positioned such that the foil quarter-chord point always lies along the centerline of the sting-nose combination. With this scheme, the sting was always towed submerged in a level orientation, for every angle of attack of the foil.

The dynamometer for this set-up was designed to measure the hydrodynamic forces on the sting-plus-foil and the sting alone. It consists of an assemblage of three standard four-inch DTNSRDC differential reluctance block gauges. Drag force was measured using a single block gauge located in the forward gauge stack. The lift force was determined by the sum of the forward and aft lift gauges, having capacities of 5,000 lb (22.24 KN) and 2,000 lb (8.896 kN), respectively. For positive values of lift, the forward gauge stack was loaded in compression and the aft in tension. A nominal maximum allowable value of total foil lift force of 3,000 lb(13.34 KN) was adhered to during the tests so as not to exceed the rated capacities of any of the force gauges in the system.

Simple streamlined fairings were fitted around the block gauge stacks. These were fastened at the top end only, with gaps at the lower end, so that no forces were transferred through the fairings that would interfere with the force measurements on the sting-plus-hydrofoil combination. Hydrodynamic interferences from the elliptically shaped nose piece and from the sting and fairings are believed to be very small. Figure 2 is a sketch of the sting and dynamometer support system.

CALIBRATIONS

Set up and calibration of this experiment consisted of first calibrating the individual gauges, then recalibrating and adjusting the arrangement of the dynamometer components in the assembled condition on a calibration stand. Without disassembly, the dymamometer was moved to the carriage and the final calibration factors were obtained with the model support system completely assembled.

Owing to the large physical dimensions of this dynamometer, there are small but important elastic deformations of the pipe sting, the struts, and cross support beam that occur under the application of large lift forces typical of this experiment. The resultant force measurment interactions appear predominately as changes in the drag force readings due to various levels of lift force. After extensive calibration, the interaction effect of lift into drag was found to be consistently repeatable, nonlinear, and subject to simple removal from the instrument indicated values. Interaction of drag force into indicated lift was found to be negligibly small, as was the effect of applied moment upon indicated drag. All the final force data presented here have been systematically corrected for dynamometer interaction effects.

Elastic deformation of the sting under load also causes a change in the effective angle of attack, α , measured at the quarter-chord of the hydrofoil. With the assembled dynamometer mounted on the carriage, a deformation calibration was obtained as a factor of angle of attack-change-per-unit lift $\Delta\alpha/L$, which was then used to correct the nose piece angle of attack α_N to account for the amount of measured lift.

In addition to the static calibrations, the dynamic response of the dynamometer (with foil attached) was explored. A small mechanical shaker was

used to produce excitation forces for the response behavior of both the lift and drag gauges. The response for vertically applied exciting force (lift) was obtained with the foil and sting submerged to a depth of a half chord, while the horizontal response was determined with the foil raised out of the water. The latter mode was most convenient, and the added mass associated with horizontal direction was expected to be small. Characteristic resonances were easily identified for both the vertical and horizontal excitations, with flat frequency response regimes determined below 3 Hz for both lift and drag. The maximum value of encounter frequency produced during the experiments in waves was 1.65 Hz, with the majority of the data taken at encounter frequencies between 0.33 and 1.1 Hz. Hence, for the unsteady measurements of both lift and drag, there were assumed to be no dynamic amplification effects.

PROCEDURE

Overall, the experiments were directed at obtaining the hydrodynamic force characteristics on the submerged hyrofoil alone, so that contributions from the supporting sting had to be collected separately, then subtracted away as tares.

Calm Water Experiments

The operating procedure consisted of making runs in the speed range U = 8 to 27.7 ft/sec (2.44 to 8.44 m/s) corresponding to chord length Froude numbers F_{n_c} = 1.22 to 4.23, at each fixed depth of submergence h measured to the hydrofoil quarter-chord (submerged of sting centerline). The first series of tests was run with the sting alone, and fitted with a faired plug having

the same shape as the slotted nose pieces. These tests covered the complete speed range and all the submergences h/c = 0.25, 0.5, 1.0, 2.0, and 4.0. The second series of tests were run with the sting-plus-foil, at the various wing angles of attack provided by the slotted nose pieces α_N = 0, 2, 4, 6, and 8 deg, and with zero flap deflection. The third series of tests were aimed at high lift performance and were run with flap deflection angles δ_f = 7.5 and 15 deg at two different nose piece angles of attack α_N = 4 and 8 deg, at submergence ratios h/c = 0.5, 1.0, 2.0, and 4.0.

Measured water temperature was 68°F (20°C), so the density and kinematic viscosity values used in the data reduction were ρ = 1.9367 slug/ft^3 (998.13 kg/m^3) and ν= 1.0836 x 10^{-5} ft^2/sec (1.0067 x 10^{-6} m^2/s), respectively. The complete range of chord length Reynolds number is R_{n_c} = 0.984 x 10^6 to 3.41 x 10^6. The large size of this hydrofoil model was originally chosen to keep R_{n_c} as large as possible, generally above one million.

Unsteady Experiments in Regular Waves

For the unsteady experiments, the same basic procedure outlined above applied. The nominal (nose piece) angle of attack was constant at α_N = 4 deg. with flap angle δ_f = 0 deg.

These head wave experiments involved variations in foil submergence depth h, forward speed U, wave period T_o, and wave amplitude ζ_a. The foil submergence ratio was held fixed at h/c = 0.5, 1.0, and 2.0 for each series of runs varying speed and the exciting wave parameters. The forward speed range was U = 8 to 24 ft/sec (2.44 to 7.32 m/s) corresponding to chord length Froude numbers of 1.22 to 3.67. Wave period was varied from T_o = 1.75 to 4.25 sec, corresponding to wave lengths of 15.7 to 92.4 ft(4.78 to 28.2 m). The

nominal wave amplitude for the basic regular wave tests was ζ_a = 3.5 in (8.89 cm) and tests for linearity were made at wave amplitudes of 2.0 in (5.08 cm) and 5.0 in (12.7 cm). The corresponding values of wave amplitude-to-semi chord ratios were r = 0.44, 0.5 and 0.625, respectively.

The four primary tests speeds spanned the complete speed range and corresponded to chord length Froude numbers of F_{n_c} = 1.22, 1.83, 2.6, and 3.67. More intermediate speeds were added in order to obtain data for certain constant values of the reduced frequency of encounter

$$k_e = \frac{\omega_e c}{2U} = \frac{\omega c}{2U}(1 + U\omega/g) \qquad (1)$$

where $\omega = (2\pi g/\lambda)^{1/2}$ is the circular frequency of the wave form of wave length λ. Thus the unsteady force response ratios were also determined for nominal values of k_e = 0.183, 0.25, and 0.315 in the range of constant selected chord length Froude numbers.

EXPERIMENTAL RESULTS

CALM WATER LIFT AND DRAG PERFORMANCE

Basic Performance Curves

The basic calm water (steady) hydrofoil lift and drag characteristics with zero flap deflection are presented in Figures 3 through 7 in groups of two graphs for each submergence ratio, for h/c = 4.0, 2.0, 1.0, 0.5, and 0.25, respectively. Displayed are the coefficient C_L versus angle of attack and the drag coefficient C_D versus C_L, plotted with contours of constant speed.

These performance diagrams are classical presentations of the lift and drag for airfoils. For unbounded flows, the results for a range of speeds

typically collapse onto single curves in these types of plots. Of course, for a near free surface hydrofoil this is not the case. the effects of speed (Froude number) tend to become more pronounced as the submergence ratio is decreased, especially for the range of low Froude numbers of these experiments.

For the deepest submergence case of h/c = 4, the lift curves of C_L versus α in Figure 3 follows a single straight line, indicating essentially no influence of free surface waves. Close scrutiny of the drag coefficients for h/c = 4 taken at zero lift shows a speed variation that runs parallel to a flat plate skin friction line, but offset by a constant value due mainly to the turbulence stimulator wire drag.

Lift

The linear relationship between C_L and α for each speed is clearly evident in Figures 3a, 4a, 5a, 6a, and 7a and justifies the usual definition for a zero flap lift-curve slope C_{L_α}. Variations of the inferred values of lift-curve slope with speed and submergence ratio are shown in Figure 8. This plot shows the characteristic reduction of lift with decreasing submergence (at constant α) and the tendency toward a local dip or minimum of lift slope at depth Froude number $F_{n_h} = 1.4$. From the data for the deepest submergence case h/c = 4 the reference lift-curve slope is determined to be

$$(C_{L_\alpha})_\infty = 0.06905 \text{ deg}^{-1}$$

The hydrofoil lift performance with flap deflection has been studied in detail in Reference 9. High values of C_L, in some cases exceeding 1.0, were achieved at the largest flap deflection angle $\delta_f = 15$ deg and the deeper submergence cases. Although there is nearly a linear increase of flap lift

increment ΔC_L due to deflection δ_f at any one speed and submergence, the curve of actual values of ΔC_L that may be attained with a given δ_f shows a distinctive fall-off with decreasing submergence ratio.

Drag Analysis

The hydrofoil drag performance with flap deflection has been studied in detail Reference 9. An example polar plot of C_D vs C_L is shown here in Figure 9 for the foil submergence case h/c = 0.5 to illustrate the unified trend of drag data for the range of unflapped and flapped configurations for this uncambered foil.

The net total drag of the fully submerged, subcavitating hydrofoil with flaps may be divided into components interpreted as the sum of total parasitic drag (or profile drag) plus the drag-due-to-lift and wavemaking (sum of induced and wavemaking drag). Symbolically, then, in coefficient form

$$C_D = C_{D_{parasitic}} + C_r \tag{2}$$

or

$$C_D = \left(C_{D_{p,min}} + \Delta C_{D_{tips}} + \Delta C_{D_p} + \Delta C_{D_{p,flap}} \right) + \left(C_{D,L_{TOT}} + C_{W_t} \right) \tag{3}$$

where $C_{D_{p,min}}$ = minimum wing profile drag, sum of friction drag plus the form drag that includes effects of foil thickness and stimulator wire drag

$\Delta C_{D_{tips}}$ = parasitic drag component due to squared-off tips

ΔC_{D_p} = incremental profile drag, without flap

$\Delta C_{D_{p,flap}}$ = incremental profile drag due to flap deflection

$C_{D,L_{TOT}}$ = $C_{D,L} + K_f(\Delta C_L)^2/\pi A$ = total of induced drag plus wavemaking drag-due-to-lift, plus additional induced drag due to partial span flap arrangement

K_f = induced drag factor for partial span flaps

ΔC_L = incremental lift coefficient due to flap deflection

C_{W_t} = wavemaking drag due to displacement effect of finite thickness foil

The calm water experiment described here was designed with the idea of using the results of the deepest submergence case in order to deduce those parasitic components that are independent of free surface effects.

Certain of the parasitic drag components can be fitted from the trends of the present data or estimated from other sources. For instance, the hydrofoil minimum profile drag is adequately fitted by

$$C_{D_{p,min}} = 2\, C_f(ITTC) + 0.0025$$

where C_f (ITTC) denotes the flat plate turbulent skin friction coefficient approximated by the 1975 ITTC correlation curve, evaluated at the chord length Reynolds number R_{n_c}. Extensive details on all the remaining terms may be found in Reference 9.

For the analysis of components of the measured drag data, the predicted drag-due-to-lift coefficient for the rectangular planform hydrofoil has been estimated here using theoretical results for submerged hydrofoil drag with an elliptic circulation distribution.

$$C_{D,L} = \left(\frac{C_{D,L}}{C_{L_o}^2}\right)_{RECT} C_L^2 \qquad (4)$$

where
$$\left(C_{D,L}/C_{L_o}^2\right)_{RECT} = (1 + \delta_p)\left(C_{D,L}/C_{L_o}^2\right)_{ELLIP} \qquad (5)$$

δ_p = Glauert correction factor for induced drag ($\delta_p = 0.05$ for the A=6 wing).

C_L = hydrofoi lift coefficient

C_{L_o} is a wing reference lift coefficient for elliptic circulation distribution

$(C_{D,L}/C_{L_o}^2)_{ELLIP}$ is the lifting line theory drag-due-to-lift coefficient ratio for elliptic circulation distribution obtained from the results of Wu[2] and evaluated extensively by Wilson[27]

Inferred Hydrofoil Drag-due-to-Lift: Residual Drag

The hydrofoil residual drag coefficient is obtained from the measured total drag

$$C_r = C_{D_{measured}} - C_{D_{parasitic}} \quad (6)$$

where $C_{D_{parasitic}}$ contains all the applicable parasitic drag components (see Equations (2) and (3)). This residual drag is supposed to be dominated by the drag-due-to-lift, but must include a small wavemaking drag due to displacement effect (foil thickness).

Plots of the residual drag ratio C_r/C_L^2 versus Froude number are given in Figures 10 through 12 for the submergence ratios h/c = 2 and 1, 0.5, and 0.25, respectively. These graphs summarize the results for both zero flap and the flapped configurations (high lift). Plotted for comparison are two prediction curves for the drag-due-to-lift ratio $(C_{D,L}/C_L^2)$: (1) the hydrofoil lifting line theory for elliptic distribution distribution $(C_{D,L}/C_L^2)_{o\ ELLIP}$ and (2) the estimate derived from the HANDE analysis by the Boeing Company.[28] The presentation of the residual drag in this manner puts a severe test on the cases of very low levels of lift, because even small errors or the presence of wavemaking drag due to nonlifting origin are amplified by the factor $1/C_L^2$ as $C_L \to \pm 0$. Data from the small nose angle of attack, α_N = 2 deg, seem to suffer

from this problem, as they do not fall into the trends established by the results for the angles of attack α_N = 4, 6, and 8 deg. For the data with moderate to high levels of lift coefficient, the results at a given submergence coalesce toward a single curve, and are bounded below by the lifting line prediction, $(C_{D,L}/C_L^2)_{o\ ELLIP}$, and seem to be bounded above by the HANDE[28] prediction curve.

Another method of data presentation for the residual drag coefficient is a plot of C_r versus C_L^2 illustrated for example in Figure 13 for the case of submergence ratio h/c = 0.5 at three different Froude numbers. The measured data include both unflapped and flapped hyrofoil results. It appears that although the lifting line theory result is generally too low at the smaller Froude numbers shown, the HANDE[28] predictions based on

$$C_{D,L} = C_{DRAG_{IND}} + C_{\Delta DRAG_{WAVE}} \qquad (7)$$

are too high, as shown earlier in Figures 10 through 12. This plot also shows that the values of C_r near zero lift coefficient follow a trend that suggests a small offset at zero lift. The magnitude of the offsets of the C_r curve are larger at the low Froude numbers, and at the shallower submergences. It is plausible that these represent contributions to the hydrofoil residual drag that are attributable to wavemaking resistance due to foil thickness, rather than strictly drag due-to-lift.

UNSTEADY LIFT AND DRAG IN HEAD WAVES

A definition sketch for the hydrofoil operating in regular head waves is given in Figure 14a. The measured time varying force responses in waves were Fourier analysed to determine the amplitude and phase at the first and second harmonic of the fundamental frequency of encounter for head waves

$$\omega_e = \frac{2\pi}{\lambda}(c_w + U) = \omega(1 + U\omega/g) \qquad (8)$$

Thus, lift and drag responses were determined in terms of the following force coefficient decompositions

$$C_L = \bar{C}_L + C_{L1} \cos(\omega_e t + \Phi_{L1}) \qquad (9)$$

$$C_D = \bar{C}_D + C_{D1} \cos(\omega_e t + \Phi_{D1}) + C_{D2} \cos(2\omega_e + \Phi_{D2}) \qquad (10)$$

where C_L = total measured lift coefficient

$\bar{C}_L$ = time average (mean) value of the lift coefficient response

C_{L1} = amplitude of the oscillating part of the lift coefficient response at the fundamental frequency

Φ_{L1} = phase angle of the oscillatory part of the lift response at the fundamental frequency

C_D = total measured drag coefficient

$\bar{C}_D$ = time average (mean) value of the drag coefficient response

C_{D1}, C_{D2} = amplitudes of the oscillatory part of the drag coefficient response at the first and second harmonic of encounter frequency, respectively

Φ_{D1}, Φ_{D2} = phase angles of the oscillatory part of the drag response at the first and second harmonic of encounter frequency, respectively

The definitions of the unsteady amplitude force coefficients are given in the list of notation. Figure 14b illustrates the time varying lift response with respect to the incoming wave. Actually, analysis of the unsteady lift response also included a term at twice the fundamental frequency, with amplitude C_{L2}. This contribution was found to be very small, on the order of 0.01 to 0.02 times the first harmonic response, and was therefore judged to be zero within the accuracy of the experiment.

Foil-alone responses were obtained by removing the sting tare responses from the foil-plus-sting values, accounting for both the magnitude and phase, at both the first and second harmonic of the encounter frequency. All the response data presented here has been reduced to foil-alone values.

Basic Unsteady Lift and Drag Response

Data for the amplitude and phase of the first harmonic lift coefficient respose ratio C_{L1}/r are given in Figures 15, 16, and 17 for the depth-to-chord ratios h/c = 2, 1, and 0.5, respectively. The contours are for constant chord length Froude number. The response ratio C_{L1}/r represents the lift coefficient amplitude per unit wave amplitude, made dimensionless by the semi chord. Nearly all these data were collected at a nominal wave amplitude ratio r_{NOM} = 0.44. The magnitudes of the response are clearly exaggerated at lower Froude numbers and at the shallower depths of submergence.

Measured results for the amplitude of the first harmonic drag coefficient response ratio C_{D1}/r are given in Figures 18, 19, and 20 for the three submergence depths; followed by the results for the second harmonic drag coefficient response ratio C_{D2}/r presented in Figures 21, 22, and 23 for the depth-to-chord ratios h/c = 2, 1, and 0.5, respectively. The second harmonic drag response often shows up as a rather significant fraction of the first harmonic, with some C_{D2} values as large as 70 percent of the corresponding C_{D1} value. Magnitudes of both harmonic components of the unsteady drag response are noticeably exaggerated for the cases of low Froude number and shallow submergence.

Linearity of Unsteady Response

While most of the data were taken at a nominal wave amplitude ratio r_{NOM} = 0.44, checks on the linearity of the unsteady response process were carried

out by runs in regular waves having smaller and larger amplitudes (r_{NOM} = 0.22 and r_{NOM} = 0.6), at three reference Froude numbers, F_n = 1.22, 1.83, and 3.66. To assess the quality of linearity, examples of the cross plots of amplitude and phase of the unsteady force response versus the dimensionless wave amplitude ratio r are given here in Figures 24 and 25 for h/c = 1. Results at the other submergences are very similar in trend. The linearity of the first harmonic lift response is very good, as indicated by the horizontal lines representing contours of constant Froude number. The linearity of the amplitude seems somewhat better than that of the phase angle.

The quality of linearity of both harmonics of the drag response is not nearly as good as that for the lift response. Especially the phase angles seem to show considerable variation with the wave amplitude. It should be noted that the drag response measurement is much less accurate than the lift response measurement, and this is particularly true of the phase angle. This may be attributed to the fact that the magnitudes of the drag response are much smaller than for the lift, and thus considerably more sensitive to the effects of inevitable scatter.

Unsteady Amplitudes and Mean Response

One way to view the relative magnitude of the unsteady lift and drag responses is to compare their values to the time average or mean values of force response. The two ratios $C_{L1}/\overline{C}_L$ and $C_{D1}/\overline{C}_D$ are plotted versus reduced frequency of encounter k_e in Figures 26, 27, and 28 for the depth-to-chord ratios h/c = 2, 1, and 0.5, respectively. These graphs indicate that the amplitude of the first harmonic lift response can reach rather large values with respect to the mean lift level, and that the magnification of the unsteady response

is exaggerated by shallow submergence and very distinctly by low Froude number. The largest observed value of the ratio $C_{L1}/\bar{C}_L = 2.2$ occurs at the lowest chord Froude number $F_{n_c} = 1.22$, at $h/c = 0.5$, $k_e = 0.43$. The corresponding ratio for the first harmonic drag response is $C_{D1}/\bar{C}_D = 1.1$.

Even at the depth-to-chord ratios $h/c = 1$ or 2, the unsteady lift response amplitude will reach significant levels, about comparable with the mean lift, in the low Froude number range around $F_{n_c} = 1.22$.

Comparison with Gust-Response Approximation

It is helpful to have some prediction scheme to compare with the experimentally determined force response. Ideally, comparisons should be carried out using the results of a comprehensive lifting surface theory specifically designed to handle free surface problems such as the Widnall wing analysis computer program developed at M.I.T by Ashley, et al[29] and Widnall[17] and carried out in detail by Widnall. The convergence and accuracy characteristics of this work were explored by Besch and Rood[30]. However, a simpler approach was adopted here, and comparisons have been made using a non-free surface "gust-response approximation." Following the development by Henry and Ali[22], Karafiath[25] worked out several cases of predictions that made use of existing lifting surface results for finite aspect ratio wings in unbounded flow.

For the flow and axis definitions of Figure 14a, a passing wave of infinitesimal amplitude $\zeta_a = r(c/2)$ in deep water has wave elevation (in x-coordinate fixed on the foil) given by

$$\zeta(x,z,t) = r(c/2)\cos\kappa[x - (U+c_w)t] \tag{11}$$

where κ = wave member = $2\pi/\lambda$

C_w = wave celerity = $g/\omega = (g\lambda/2\pi)^{1/2}$

λ = wave length

ω = circular frequency = $(2\pi g/\lambda)^{1/2}$

The induced vertical velocity component down in the fluid is

$$w(x,z,t) = r(c/2)\,\omega e^{\kappa z}\sin\kappa[x-(U+C_w)t] \tag{12}$$

Along $-c/2 < x < c/2$, at $z = -h$, and for $\lambda/(c/2) >> 1$, the vertical cross flow velocity can be approximated by

$$w(x,-h,t) = r(c/2)\,\omega e^{-\kappa h}\,[\kappa x\cos\omega_e t - \sin\omega_e t] \tag{13}$$

where ω_e = encounter frequency = $\kappa(U + c_w)$

In the Henry and Ali[22] work the gust response operator is represented as

$$(\frac{C_{L1}}{r})\cos(\omega_e t + \Phi_{L1}) \tag{14}$$

so that the response to the sinusoidal gust is sinusoidal with a phase shift Φ_{L1}. Henry and Ali[22] gave an equivalent combination of heave and pitch that gave the same velocity distribution as Equation (13), and then suggested using existing published results for the unsteady lift loadings of finite aspect

ratio wings that occur in response to the equivalent sinusoidal heave and pitch. In making this adaptation, it is important to use the reduced frequency of encounter k_e to account for the effect of wave celerity. Only results for the lift response C_{L1}/r, were obtained in this manner,[22,25] and of course the hydrodynamic effect of the free surface is not accounted for in this approximation.

Examples of comparisons between the present measurements and the approximated gust-response predictions are given in Figures 29 and 30. In Figure 29, the results for C_{L1}/r and Φ_{L1} are shown plotted versus reduced frequency of encounter k_e for submergence ratio h/c = 2, nominal wave amplitude ratio r_{nom} = 0.44, with contours of speed (Froude number), and where use has been made of the lift response predictions from Reissner[12,13]. In Figure 30, the results for C_{L1}/r and Φ_{L1} are plotted versus submergence ratio h/c for the constant value of k_e = 0.185 and r_{nom} = 0.44, with contours of speed, and where the results of Lawrence and Gerber[14] have been extrapolated to cover the case of aspect ratio A = 6. In general, the gust response approximations overestimate the lift response ratio and the phase angle, with progressively worse predictions at shallower submergences and at higher frequencies (larger k_e). This is the expected trend because the approximate theory uses spanwise distributions of lift loading applicable to unbounded flow over a wing rather than the actual distributions for a lifting foil near the free surface. It is known, for example from these experiments at low Froude numbers, that the steady lift capability of the hydrofoil is decreased as the foil nears the surface (lift curve slope falls off). The effect is anticipated to influence unsteady lift performance as well.

SUMMARY AND DISCUSSION

Extensive experimental data are presented for the foil-alone lift and drag forces experienced by an aspect ratio 6 hydrofoil operated at several

submergences in a range of low Froude numbes in both calm water and in regular head waves. The following conclusions and observations can be made:

- For calm water operation, the experimental results given here for the inferred drag-due-to-lift with flap deflection provide useful hydrofoil data including cases at relatively high lift coefficients up to about 1.0.
- From calm water results, measured (inferred) values of residual drag coefficients C_r for the entire range of lift coefficient, appear likely to contain wavemaking resistances contributions due to foil thickness that are noticeable only at the lowest Froude numbrs $F_{n_c} < 2$, and for the shallow submergences. For the higher Froude numbers and deeper submergences, the C_r values appear to be predominantly drag-due-to-lift.
- The two prediction schemes for calm water drag-due-to-lift considered here give results that coalesce and are both relatively accurate for Froude numbers higher than around $F_{n_c} = 3$. For lower Froude numbers, the lifting line estimate for elliptic circulation distributions gives $C_{D,L}$ values too low, while the HANDE predition formula gives values that are a little high.
- For wave-induced unsteady loading, it was found that speed (Froude number) has a strong influence on the amplitude and phase angle of the first harmonic lift response and the first and second harmonics of drag response, where the fundamental frequency is the encounter frequency ω_e. Froude number effects are more important as the foil submergence decreases.
- The second harmonic of lift response was found to be very small, essentially zero.
- The first harmonic lift response amplitude and phase angle are linear with wave amplitude.

- The drag response amplitudes and phase angles (both first and second harmonics) do not appear to be linear with wave amplitude. However the magnitude of the measured oscillating drag was small, creating difficulties in data resolution, especially with phase angle.
- Prediction of the first harmonic lift response amplitude at submergence h/c = 2 is overpredicted by about 11 to 16 percent by the gust-response approximation using the Reissner theory results, and by about 6 to 10 percent using the extrapolated Lawrence and Gerber results. For shallower submergences, the predictions by the gust-response approximation become much much poorer.
- The amplitude of the first harmonic unsteady response can reach values over twice as high as the mean hydrofoil lift force for the case of Froude number F_{n_c} = 1.22, at h/c = 0.5, and for reduced frequency of encounter k_e = 0.315. At deeper submergences of h/c = 1 or 2, operation at such low Froude number in waves will produce oscillating lift response about the same magnitude as the mean lift. These ratios apply to the operation of the hydrofoil with nominal angle of attack α_N = 4 deg, so that the mean lift coefficient for F_{n_c} = 1.22 runs around $C_L \approx 0.12$ and 0.2 at h/c = 0.5 and 1.0, respectively. It should be noted that the magnitude of oscillating lift response does not depend on the mean lift.

ACKNOWLEDGMENTS

The work described here was authorized by the Naval Material Command funded under NAVSEA's Ships, Subs and Boats Exploratory Development Program, and administered by the Ship Performance Department of DTNSRDC.

For the calm water experiments the author gratefully acknowledges the work of D. Mullinix, A. Feller, D. Gregory, G. Karafiath, P. Lafrance, J. Peck, A. Sobolewski, and B. Young. The unsteady experiments were carried out and reported on by G. Karafiath with the help of B. Peters, M. Davis, D. Moir, and W. Mitchell.

NOTATION

		Units*
A	Hydrofoil planform aspect ratio; $A = b^2/S$	-
b	Hydrofoil span	ℓ
b_f	Hyrofoil flap span	ℓ
C_D	Drag coefficient; $C_D = D/\frac{1}{2}\rho U^2 S$	-
$\overline{C_D}$	Mean (time average) drag coefficient in waves	-
C_{D1}	First harmonic oscillatory drag amplitude coefficient; $C_{D1} = D_1/\frac{1}{2}\rho U^2 S$	-
C_{D2}	Second harmonic oscillatory drag amplitude coefficient, $C_{D2} = D_2/\frac{1}{2}\rho U^2 S$	-
$C_{D,L}$	Drag-due-to-lift coefficient, sum of induced drag plus wavemaking drag-due-to-lift	-
$C_{D,L_{TOT}}$	Total hydrofoil drag due-to-lift, sum of induced drag plus wavemaking drag due-to-lift plus additional drag-due-to partial span flap arrangements; $C_{D,L} + K_f(\Delta C_L/\pi A)$	-
$C_{Dp,min}$	Minimum wing profile drag coefficient	-
$C_{Dparasitic}$	Sum of all parasitic drag coefficient components	-
$C_{DRAG_{IND}}$	Hydrofoil induced drag coefficient, including biplane effect for large Froude number; estimated using HANDE[28] formula	-
C_f	Skin friction drag coefficient	-
$C_{\Delta DRAG_{WAVE}}$	Hydrofoil wave resistance coefficient; estimated using HANDE[28] formula	-
C_L	Lift coefficient; $C_L = L/\frac{1}{2}\rho U^2 S$	-
$\overline{C_L}$	Mean (time average) lift coefficient in waves	-
C_{L_α}	Hydrofoil wing lift-curve slope	-
$(C_{L_\alpha})_\infty$	Wing lift-curve slope in unbounded flow	-
C_{L_o}	Wing reference lift coefficient for elliptic circulation distribution at infinite depth	-

* ℓ = length, M = mass, T = time, F = force = $M\ell/T^2$

C_{L1}	First harmonic oscillatory lift amplitude coefficient; $C_{L1} = L_1 / \frac{1}{2}\rho U^2 S$	-
C_r	Hydrofoil residual drag coefficient; measured drag less all estimated parasitic drag components	-
C_{W_t}	Hydrofoil wavemaking drag coefficient due to thickness	-
c	Hydrofoil chord length	ℓ
c_f	Flap chord length	ℓ
c_w	Wave celerity	ℓT^{-1}
D	Hydrofoil drag force, drag component	F
D_1	Amplitude of first harmonic oscillatory drag response	F
D_2	Amplitude of second harmonic oscillatory drag response	F
F_{n_c}	Froude number based on chord length; $F_{n_c} = U/(gc)^{1/2}$	-
F_{n_h}	Froude number based on depth of submergence of quarter chord	-
g	Acceleration due to gravity	ℓT^{-2}
h	Depth of submergence to hydrofoil quarter chord	ℓ
K_f	Induced drag factor for partial span flap	-
k	Reduced frequency; $k = \omega c/2U$	-
k_e	Reduced frequency of encounter; $k_e = \omega_e c/2U = k(1 + U\omega/g)$	-
L	Hydrofoil lift force	F
L_1	Amplitude of first harmonic oscillatory lift response	F
R_{n_c}	Reynolds number based on chord length; $R_{n_c} = Uc/\nu$	-
r	Wave amplitude-to-semi chord ratio; $r=\zeta_a/(c/2)$	-
r_{NOM}	Nominal test value of r	-
S	Hydrofoil planform area; $S = bc$	ℓ^2
S_f	Planform area of flaps; $S_f = b_f c_f$	ℓ^2
T_o	Wave period; $T_o = (2\pi\lambda/g)^{1/2}$	T
t	Hydrofoil section maximum thickness, also time	ℓ

U	Freestream velocity, speed of hydrofoil	ℓT^{-1}
$w(x,z,t)$	Vertical component of fluid velocity	ℓT^{-1}
x	Coordinate horizontal axis	ℓ
z	Coordinate vertical axis	ℓ
α	Hydrofoil resultant angle of attack of chord line with respect to freestream direction; $\alpha = \alpha_N + (\Delta\alpha/L)L$	deg
α_N	Nose piece angle of attack	deg
δ_f	Flap deflection angle	deg
δ_P	Glauert planform shape correction factor for induced drag coefficient	-
$\Delta\alpha/L$	Change of angle of attack-per-lift due to sting deformation under lift load	deg/F
ΔC_{D_p}	Incremental profile drag coefficient (due to angle of attack), without flap	-
$\Delta C_{D_{p,flap}}$	Incremental profile drag coefficient due to flap deflection	-
ΔC_L	Incremental lift coefficient due to flap deflection	-
ζ	Wave elevation	ℓ
ζ_a	Wave amplitude	ℓ
κ	Wave number; $\kappa = 2\pi/\lambda$	ℓ^{-1}
λ	Wave length; $\lambda = 2\pi g/\omega^2$	ℓ
ν	Kinematic viscosity	$\ell^2 T^{-1}$
ρ	Mass density of water	$M\ell^{-3}$
Φ_{D1}	Phase angle of first harmonic of oscillatory drag response	deg
Φ_{D2}	Phase angle of second harmonic of oscillatory drag response	deg
Φ_{L1}	Phase angle of first harmonic of oscillatory lift response	deg
ω	Circular frequency; $\omega = (g\kappa)^{1/2}$	rad T^{-1}
ω_e	Circular frequency of encounter; $\omega_e = \omega(1 + U\omega/g) = \kappa(c_w + U)$	rad T^{-1}

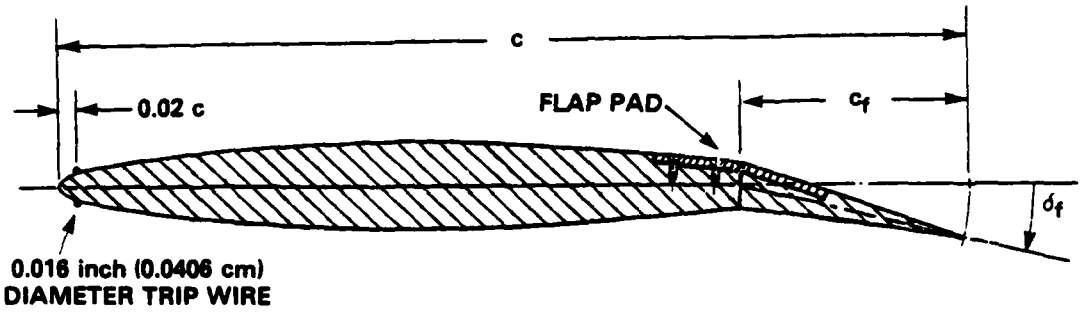


Figure 1 - Hydrofoil NACA 64 A010 Section With 0.25c Plain Flap

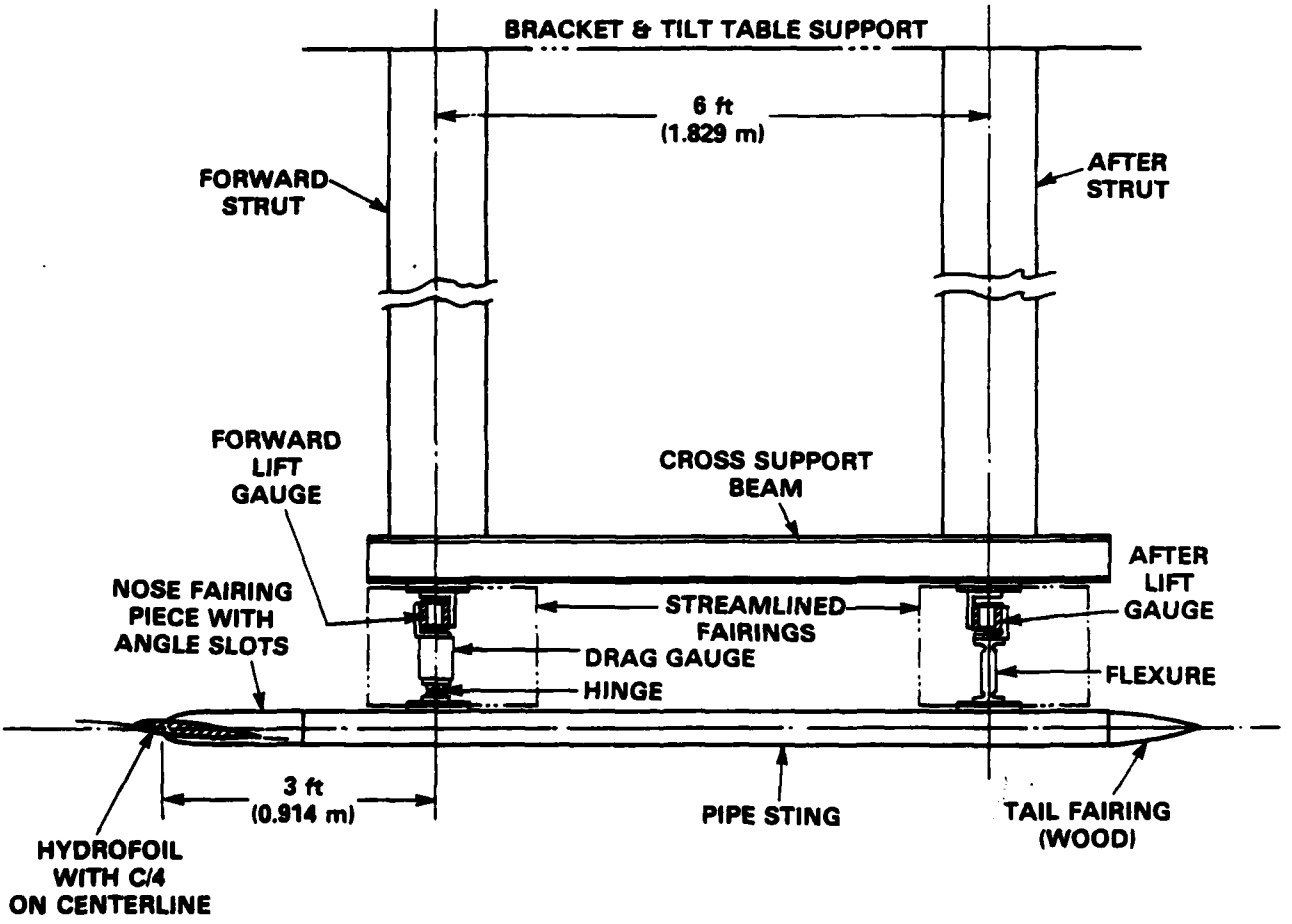


Figure 2 - Sketch of Hydrofoil Forward-Leading Sting and Dynamometer Support System

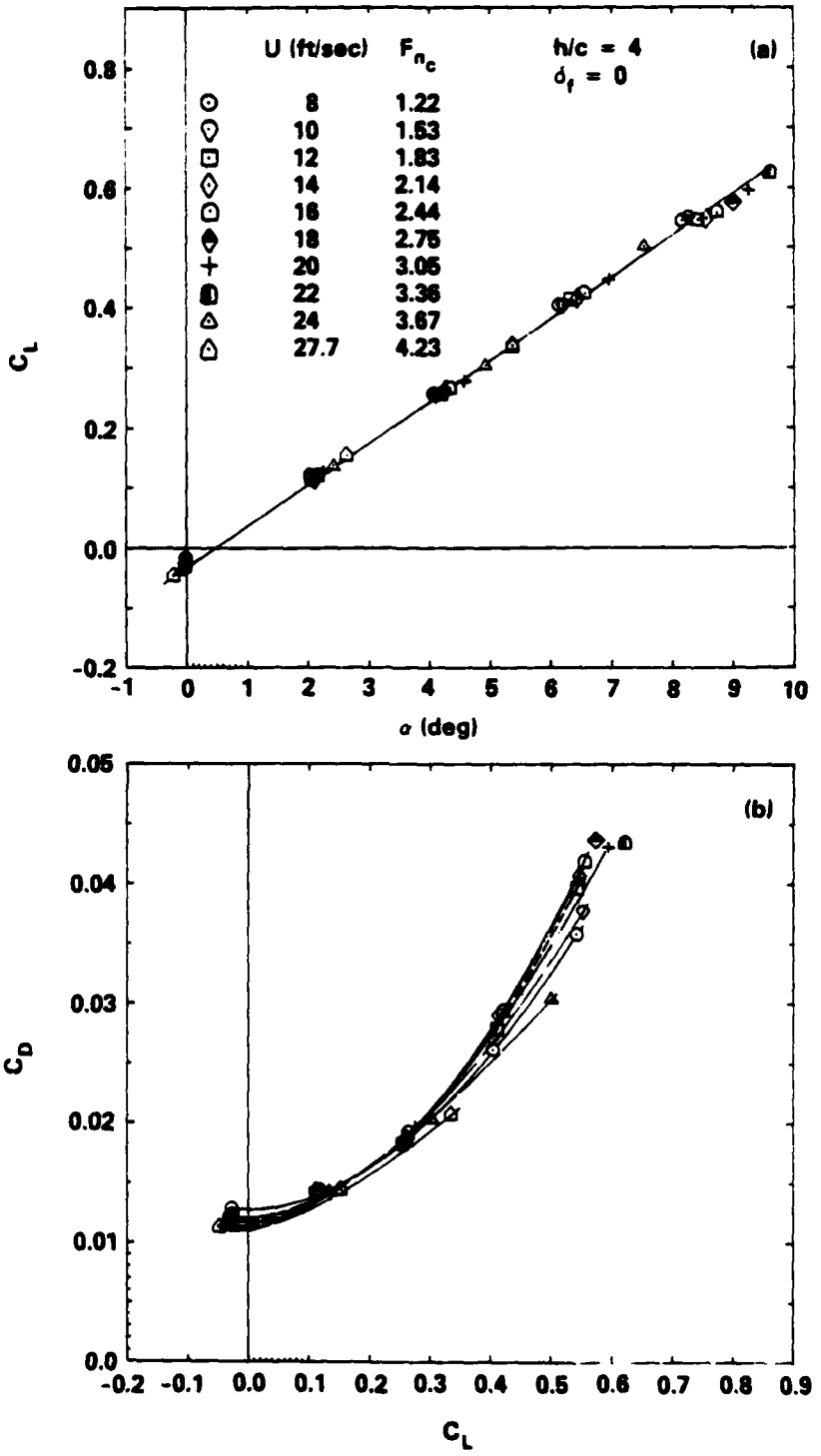


Figure 3 - Measured Hydrofoil Lift and Drag Coefficients for Submergence Ratio h/c = 4, Zero Flap, Contours of Speed

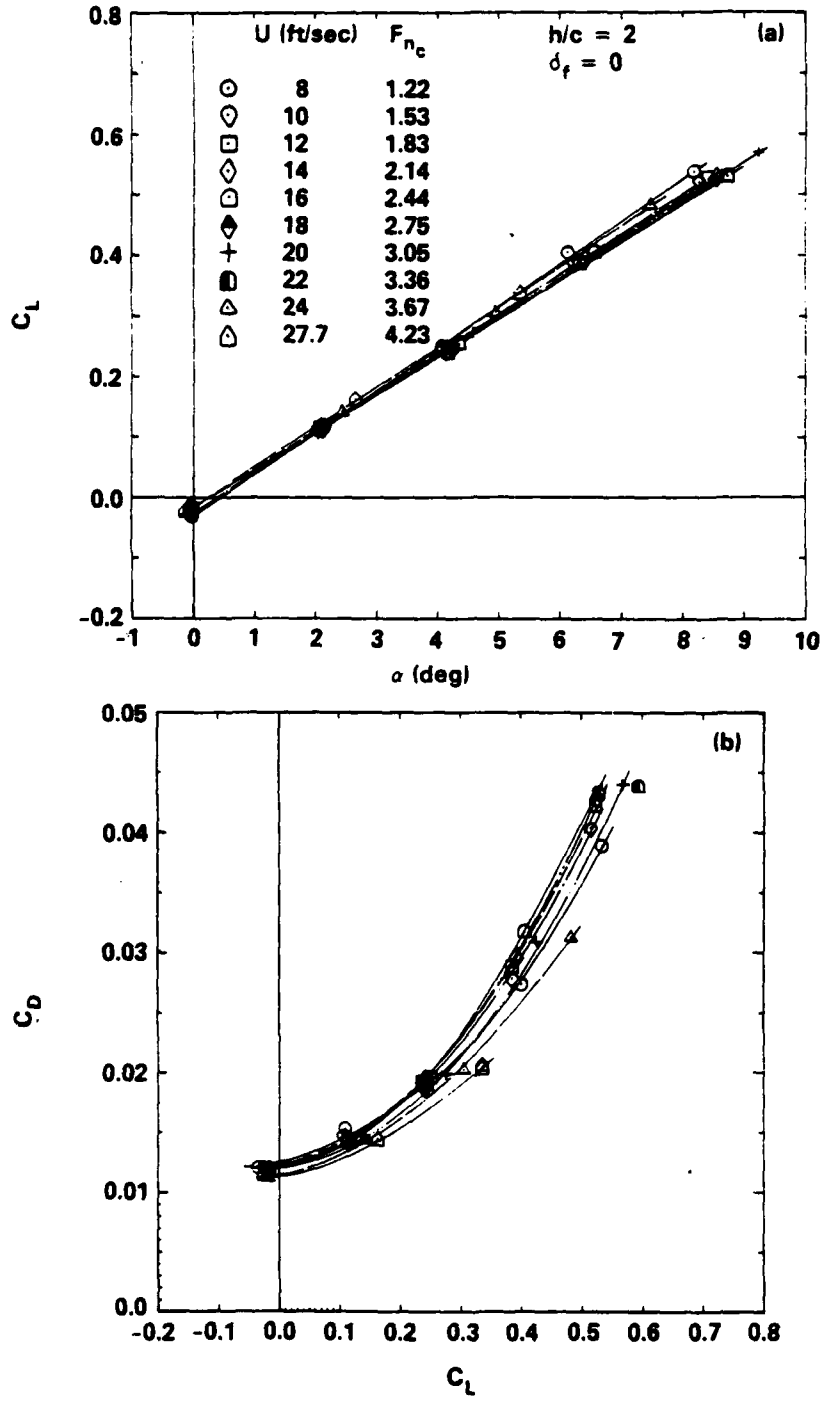


Figure 4 - Measured Hydrofoil Lift and Drag Coefficients for Submergence Ratio h/c = 2, Zero Flap, Contours of Speed

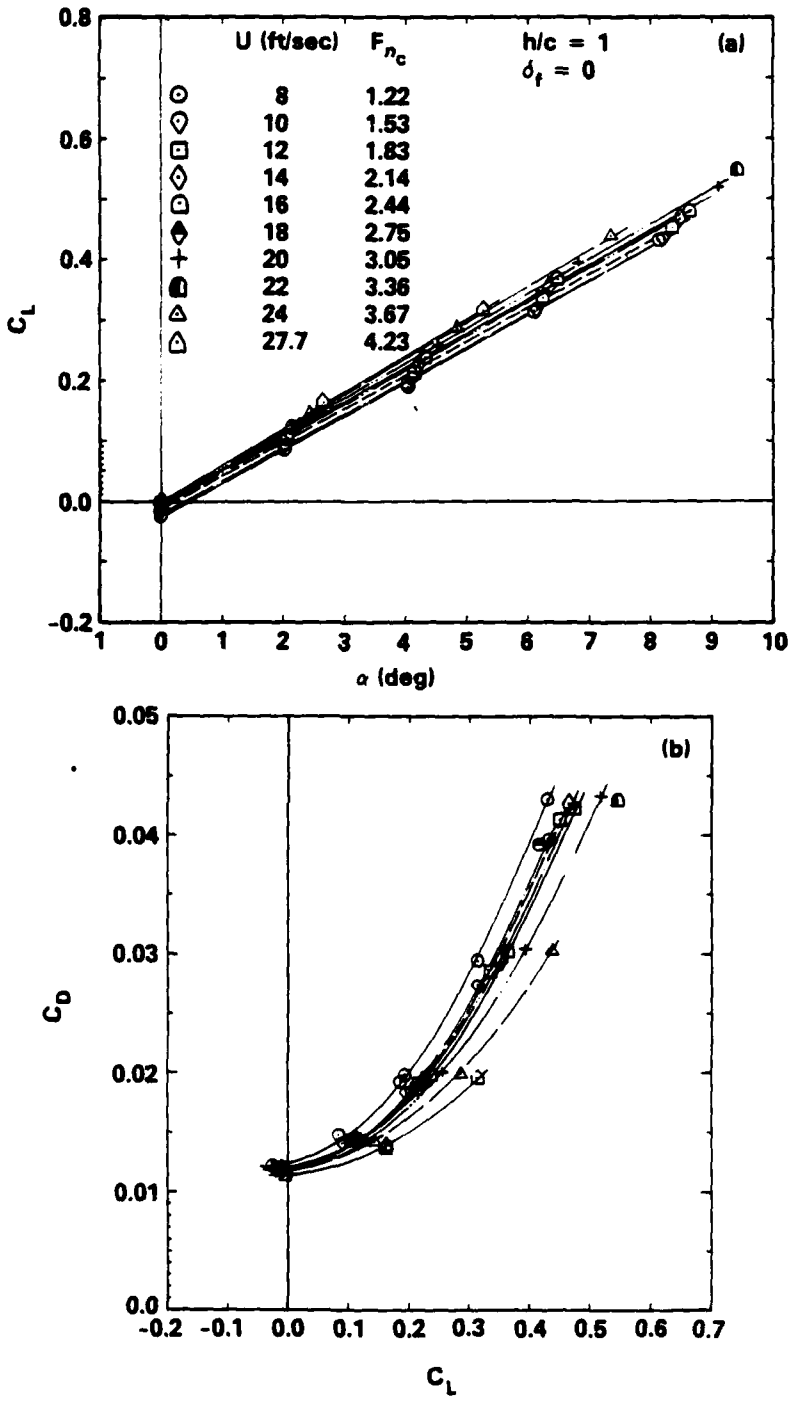


Figure 5 - Measured Hydrofoil Lift and Drag Coefficients for Submergence Ratio h/c = 1, Zero Flap, Contours of Speed

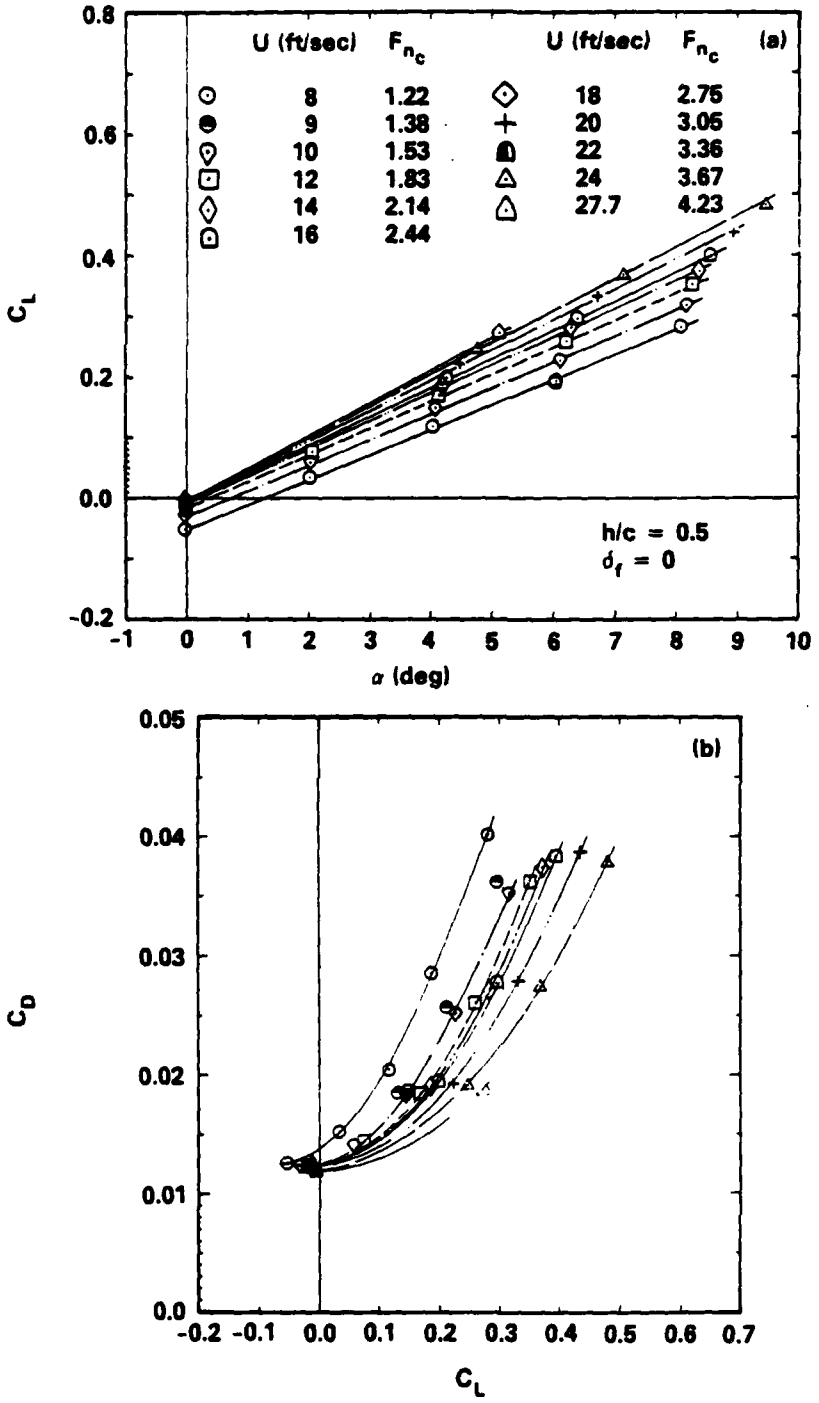


Figure 6 - Measured Hydrofoil Lift and Drag Coefficients for Submergence Ratio h/c = 0.5, Zero Flap, Contours of Speed

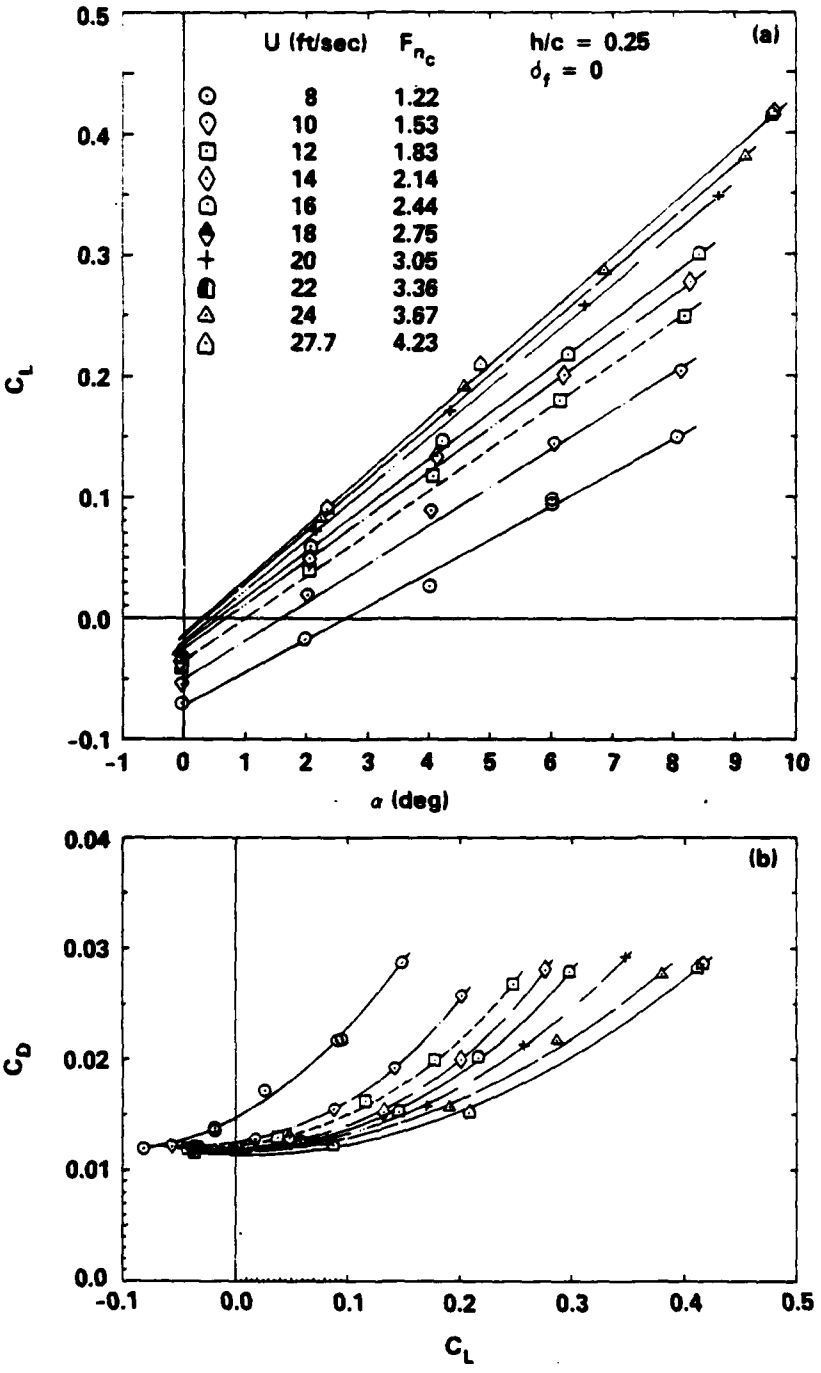


Figure 7 - Measured Hydrofoil Lift and Drag Coefficients for Submergence Ratio h/c = 0.25, Zero Flap, Contours of Speed

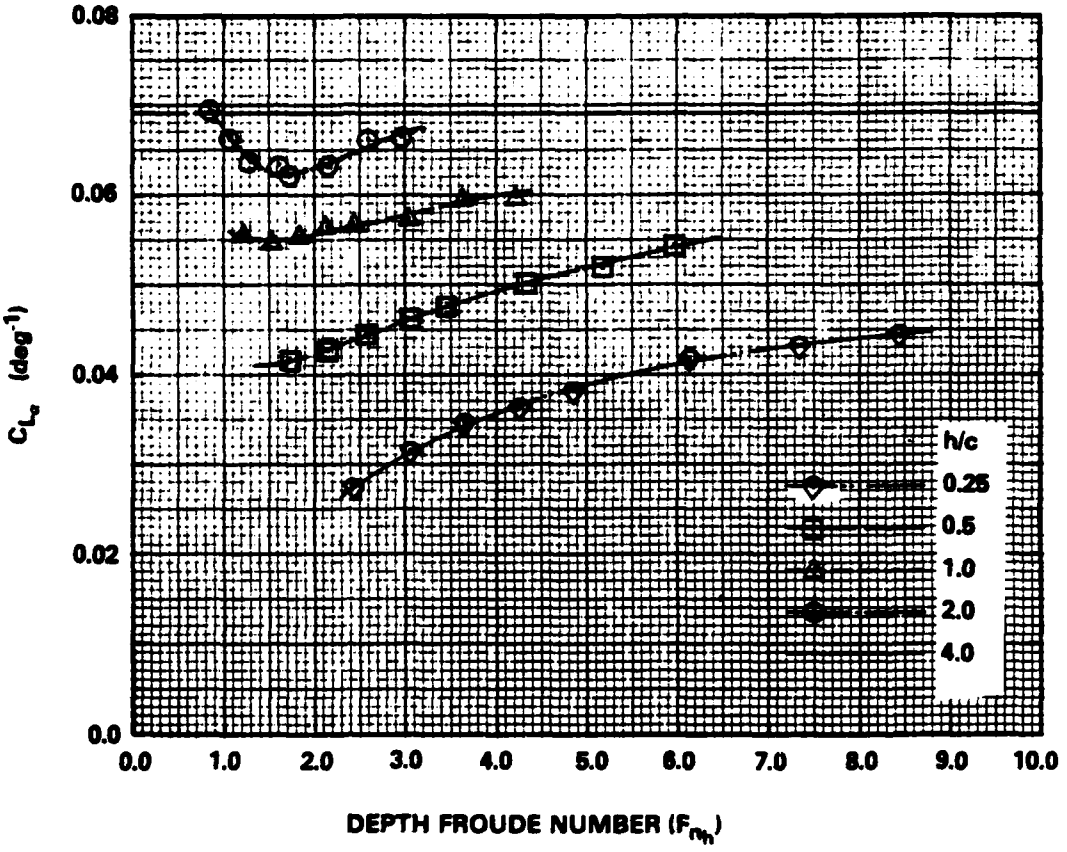


Figure 8 - Variation of Hydrofoil Lift-Curve Slope versus Depth Froude Number, Contours of Submergence

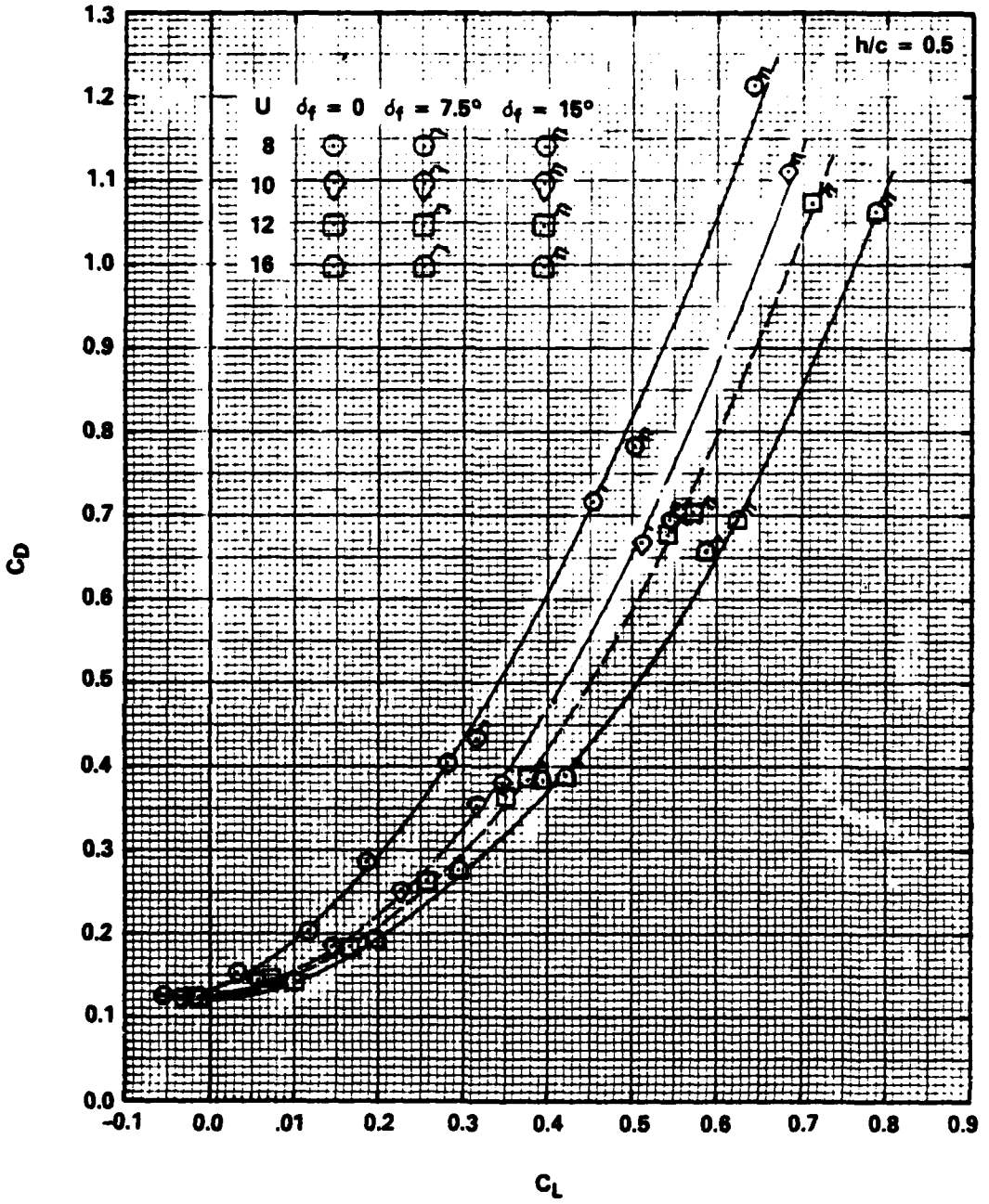


Figure 9 - Drag Polar of Measured C_D versus C_L for Flapped and Zero Flapped Hydrofoil at Submergence Ratio h/c = 0.5

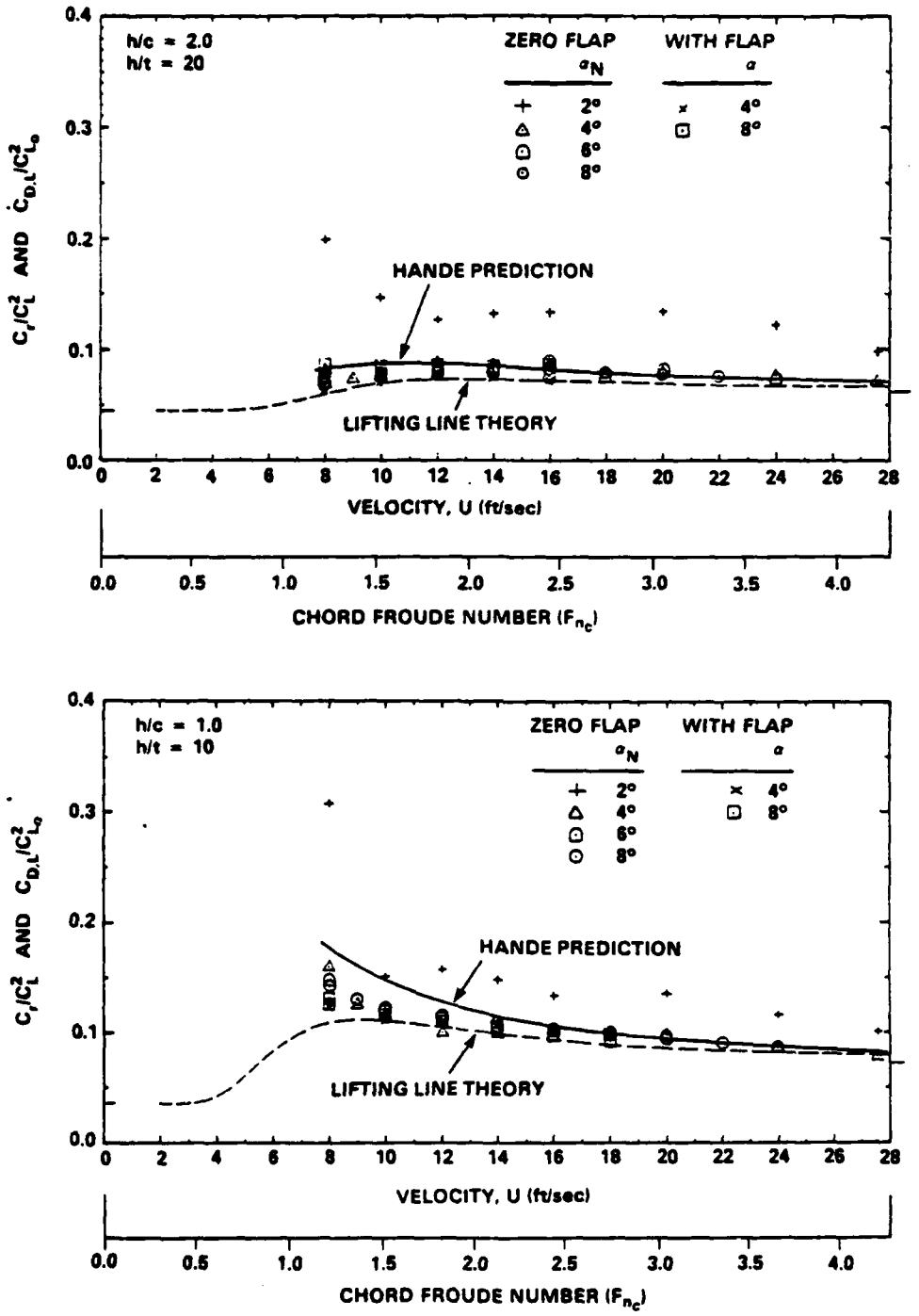


Figure 10 - Summary Plot of Total Drag-due-to-Lift Ratio versus Speed; Experiment and Predictions, at Submergence Ratio h/c = 2.0 and 1.0

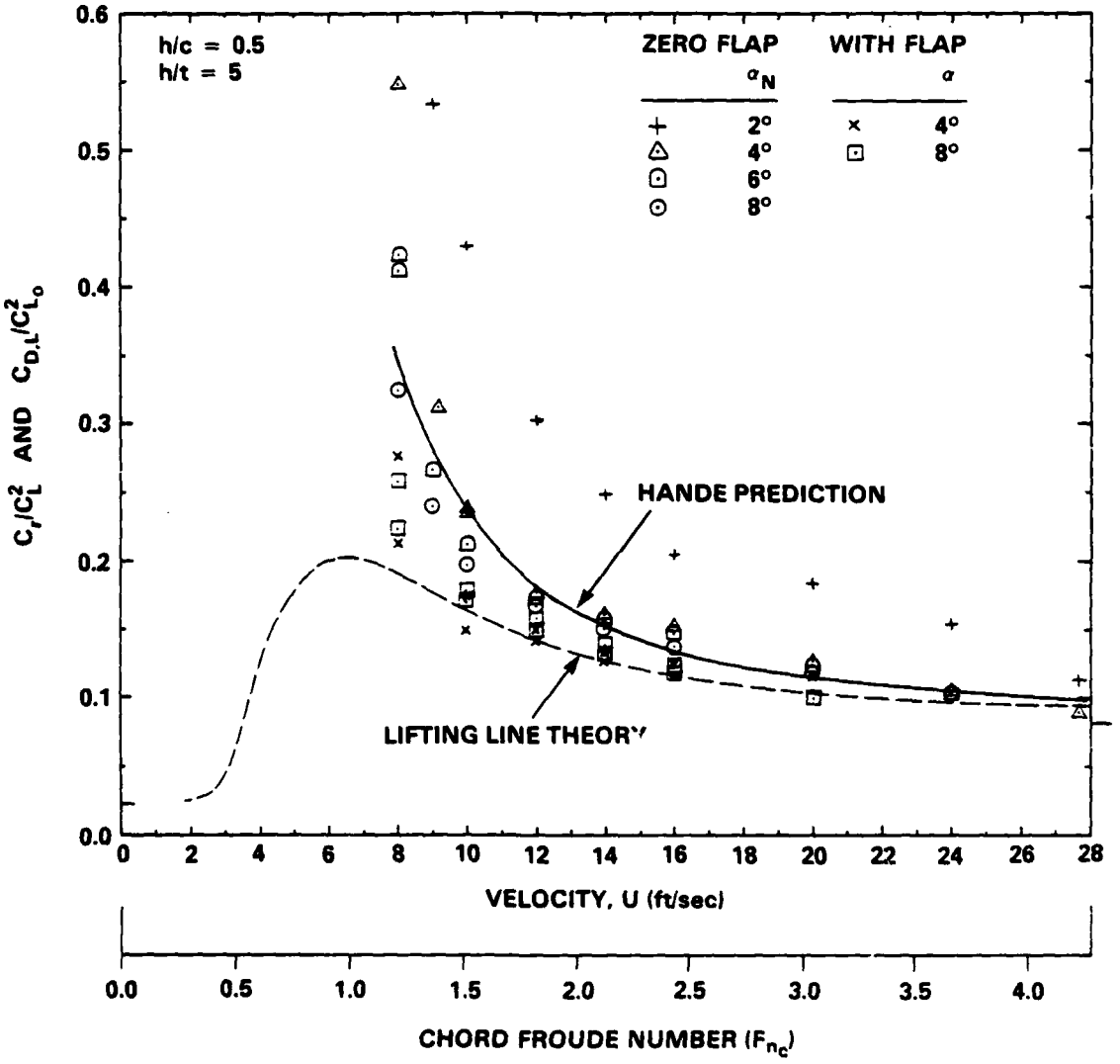
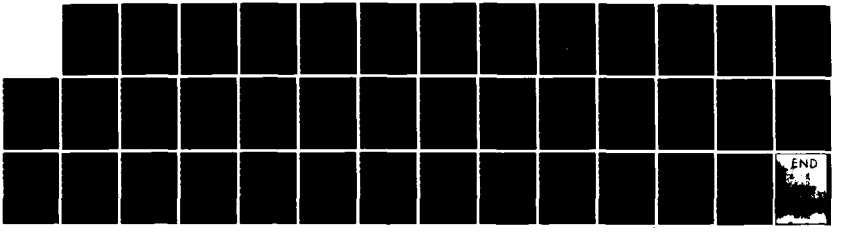
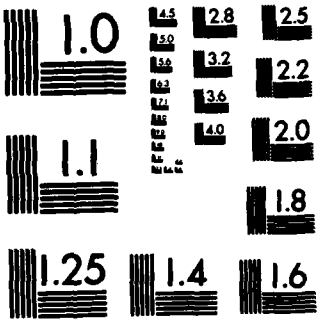


Figure 11 - Summary Plot of Total Drag-due-to-Lift Ratio versus Speed; Experiment and Predictions, at Submergence Ratio h/c = 0.5

AD-A144 226 PROCEEDINGS OF THE GENERAL MEETING OF THE AMERICAN TOWING TANK CONFERENCE. (U) STEVENS INST OF TECH HOBOKEN NJ DAVIDSON LAB D SAVITSKY ET AL. AUG 83 7/7

UNCLASSIFIED SIT-DL-TR-13029-VOL-1 N00167-83-M-4062 F/G 20/4 NL





MICROCOPY RESOLUTION TEST CHART
NATIONAL BUREAU OF STANDARDS-1963-A

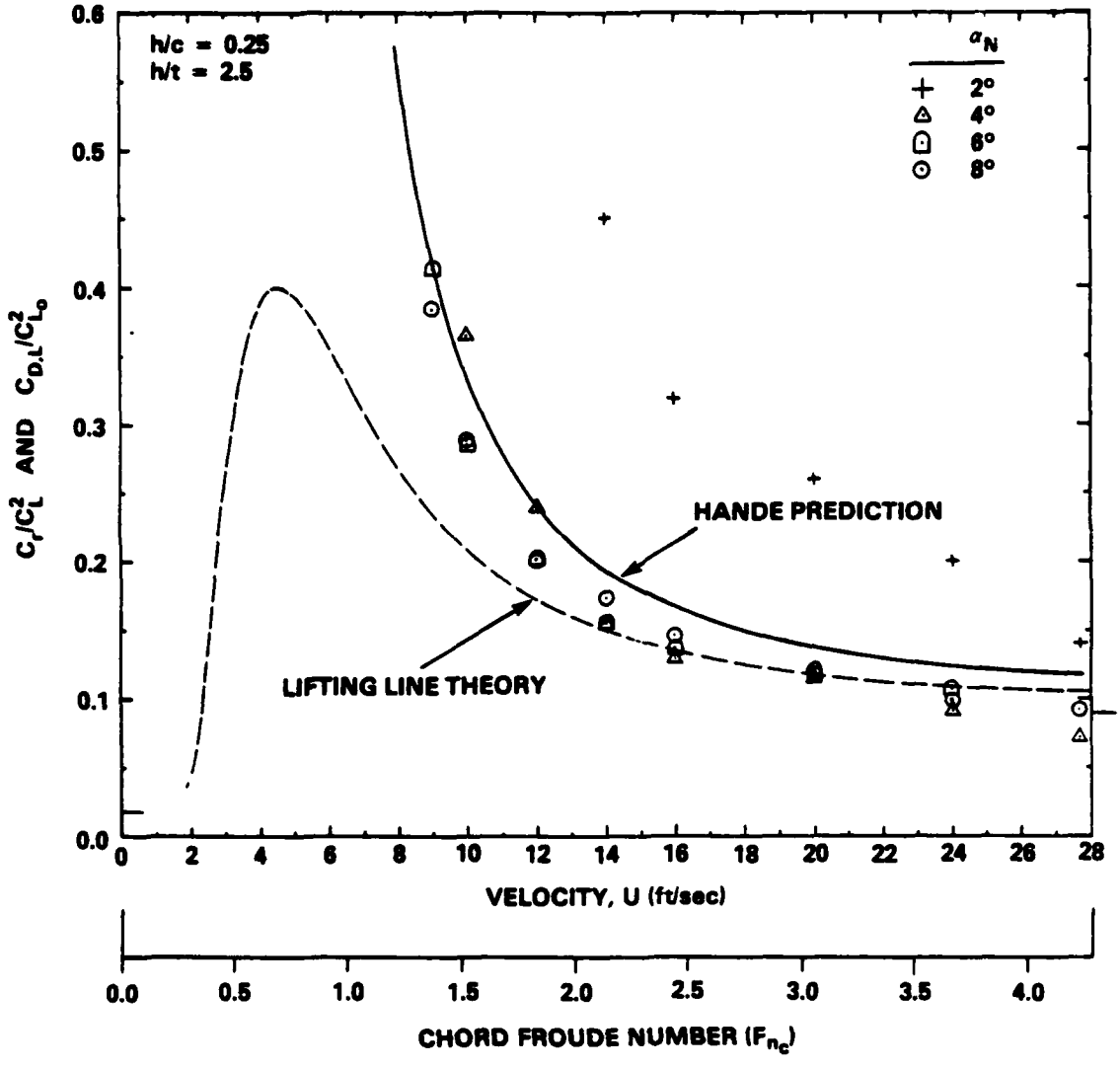


Figure 12 - Summary Plot of Total Drag-due-to-Lift Ratio versus Speed; Experiment and Predictions, at Submergence Ratio h/c = 0.25

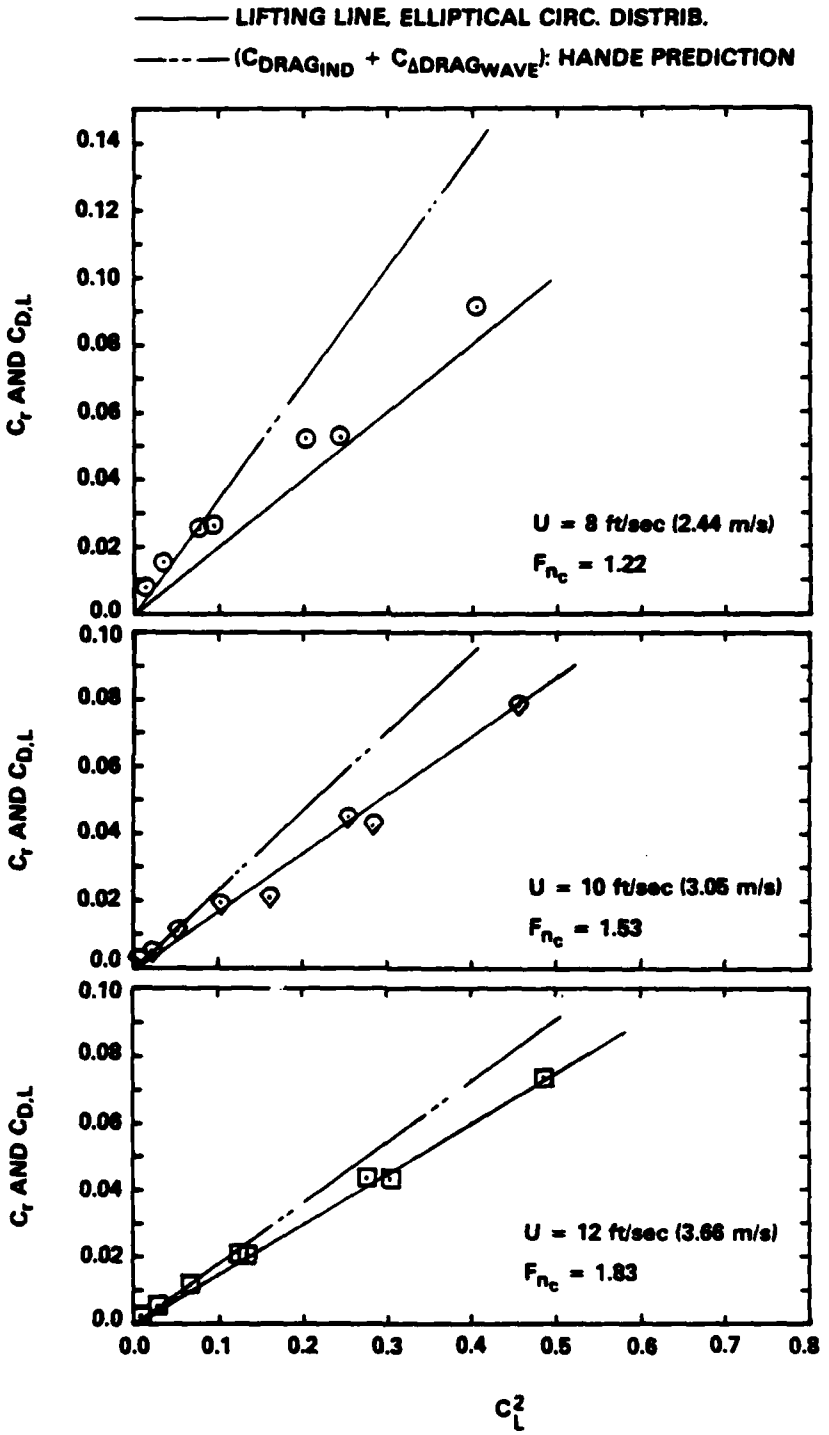


Figure 13 - Comparison of Measured C_r with Predictions of $C_{D,L}$ versus C_L^2, for Submergence Ratio h/c = 0.5

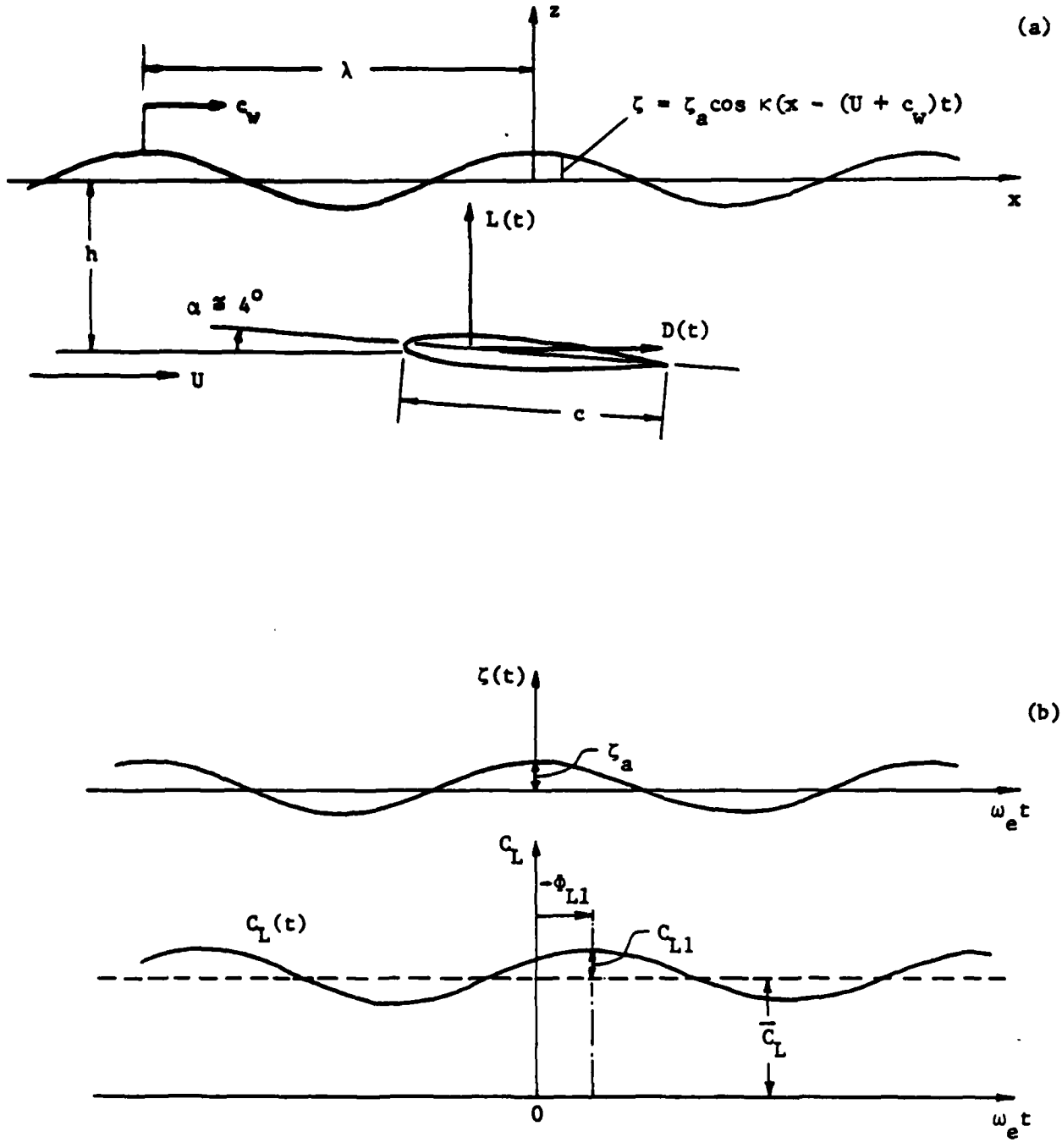


Figure 14 - Definition Sketch for Wave Geometry and Unsteady Lift Response Amplitude and Phase Angle

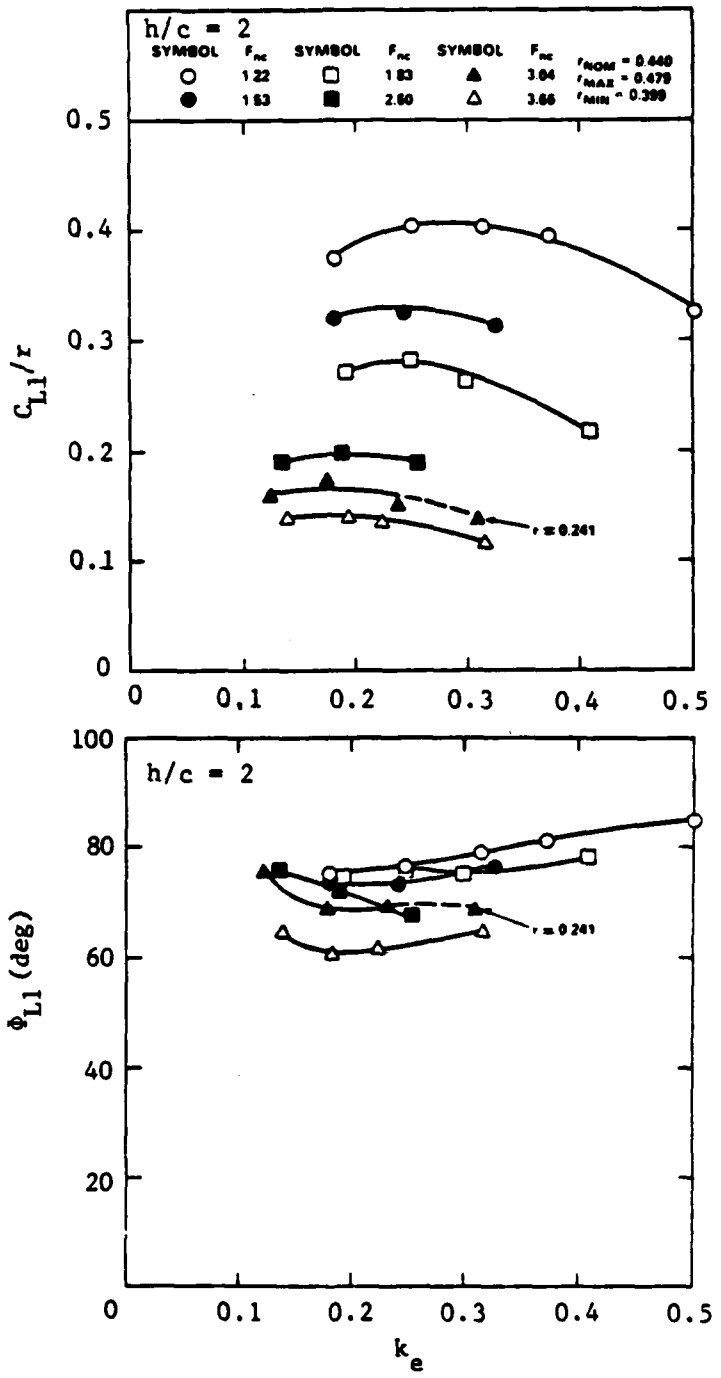


Figure 15 - Oscillatory Lift Response Amplitude Ratio and Phase Angle at the Fundamental Frequency; for h/c = 2.0

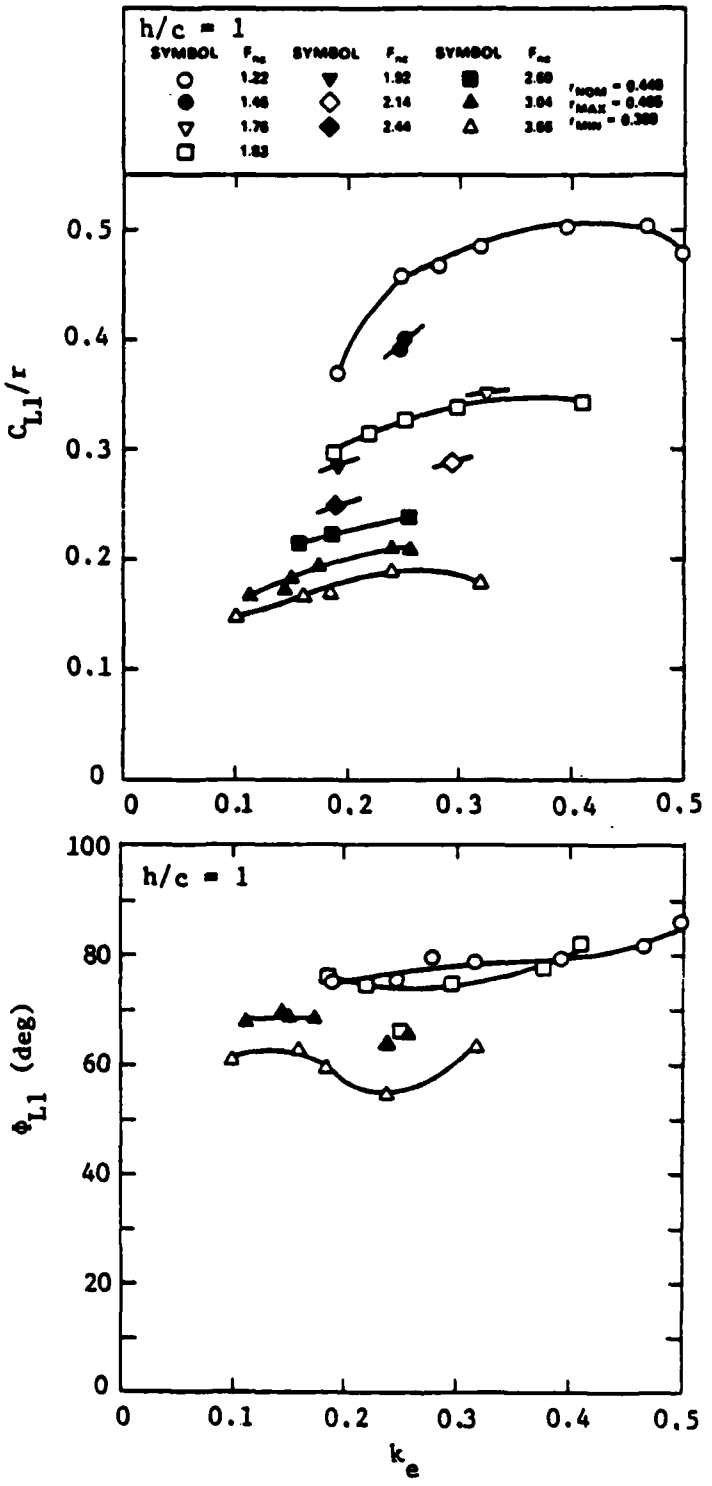


Figure 16 - Oscillatory Lift Response Amplitude Ratio and Phase Angle at the Fundamental Frequency; for h/c = 1.0

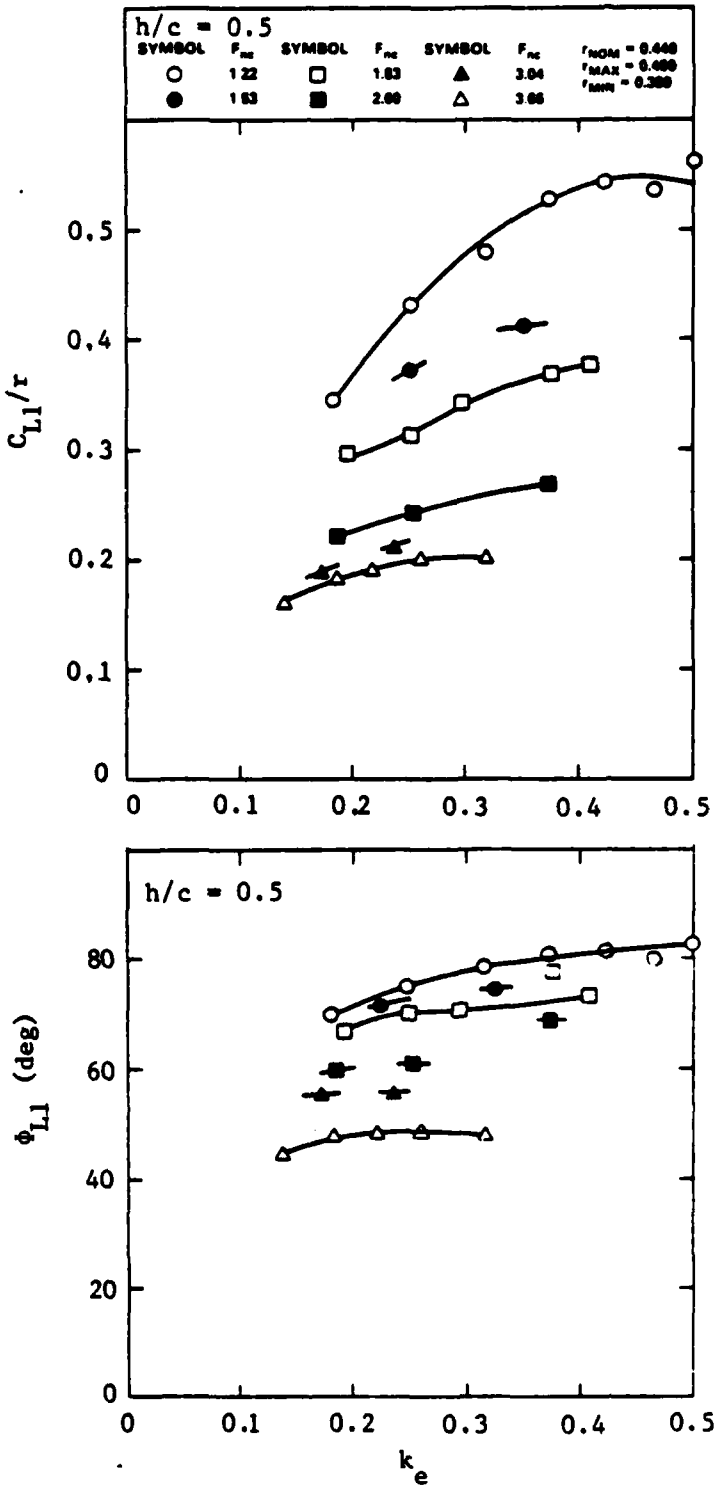


Figure 17 - Oscillatory Lift Response Amplitude Ratio and Phase Angle at the Fundamental Frequency; for h/c = 0.5

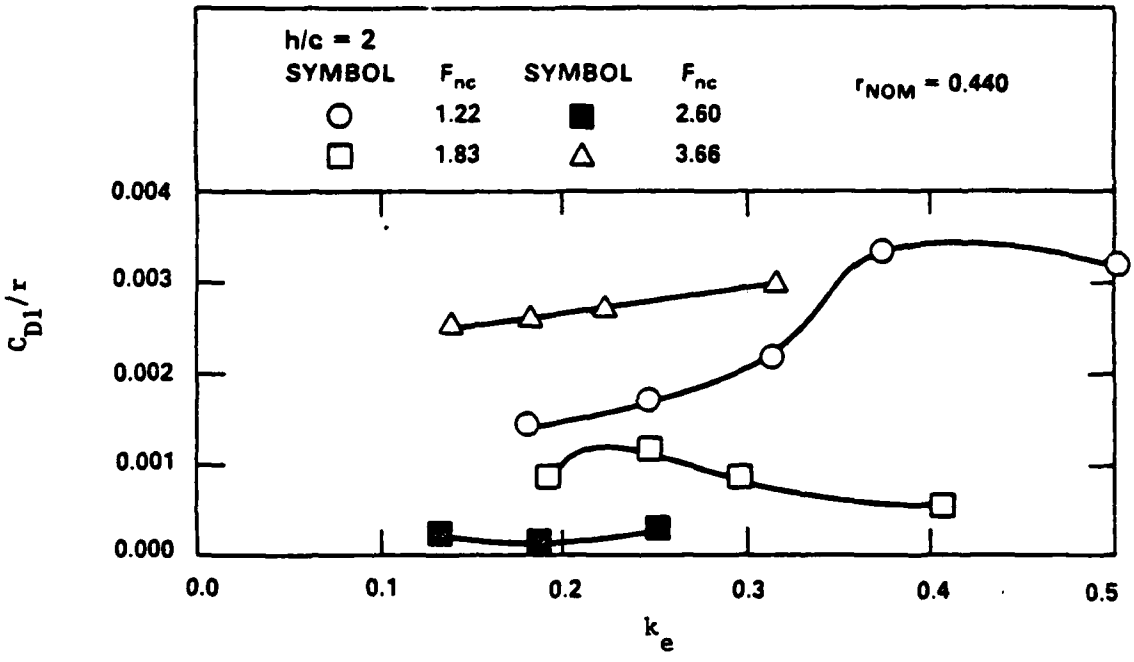


Figure 18 - Oscillatory Drag Response Amplitude Ratio at the Fundamental Frequency; for h/c = 2.0

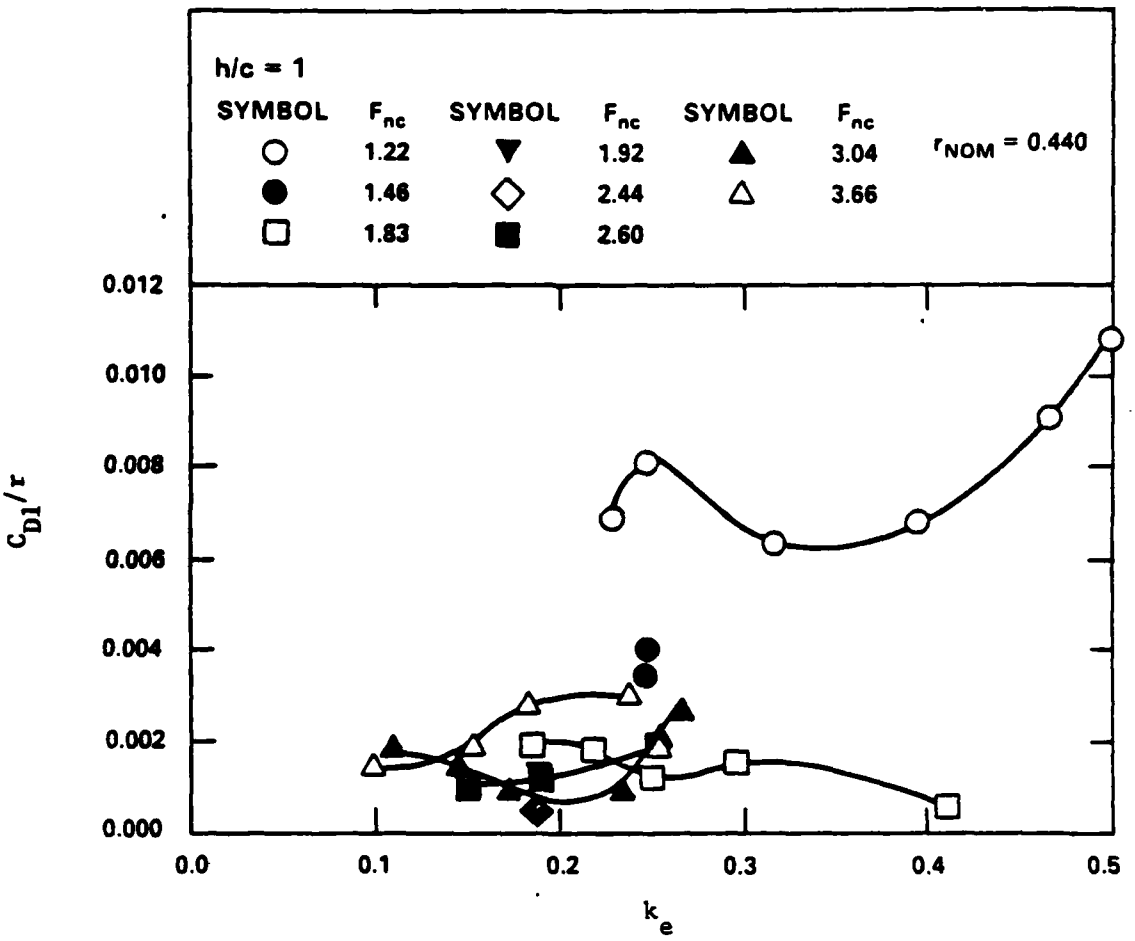


Figure 19 - Oscillatory Drag Response Amplitude Ratio at the Fundamental Frequency; for h/c = 1.0

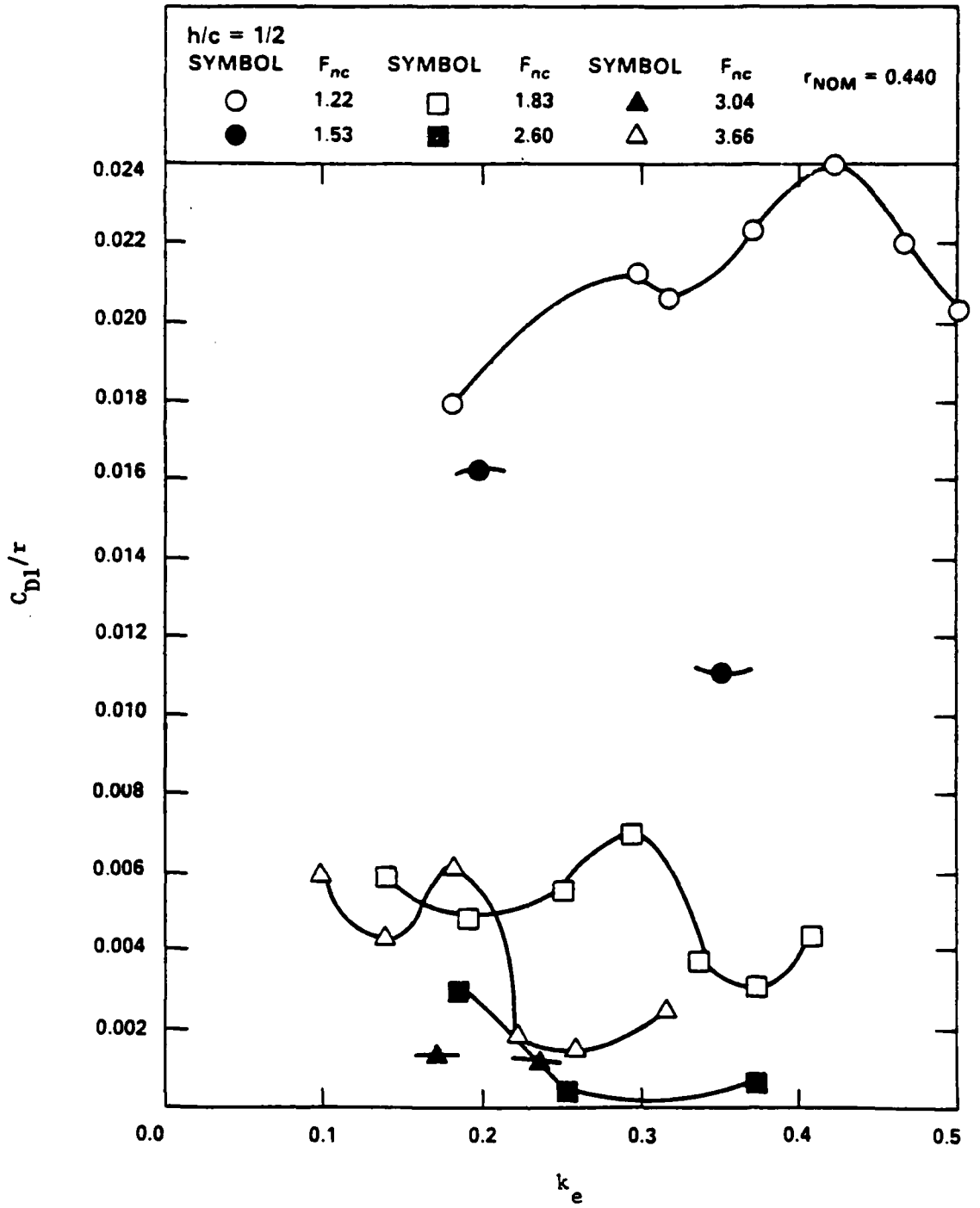


Figure 20 - Oscillatory Drag Response Amplitude Ratio at the Fundamental Frequency; for h/c = 0.5

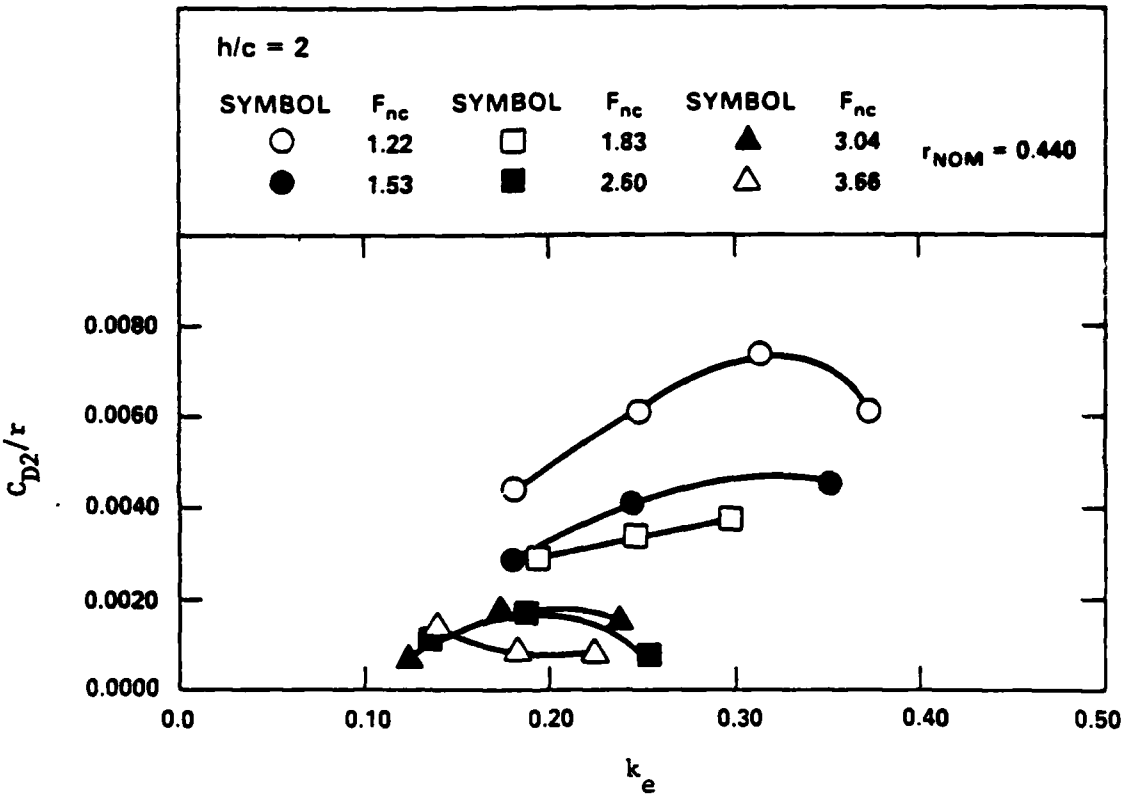


Figure 21 - Oscillatory Drag Response Amplitude Ratio at Twice the Fundamental Frequency; for h/c = 2.0

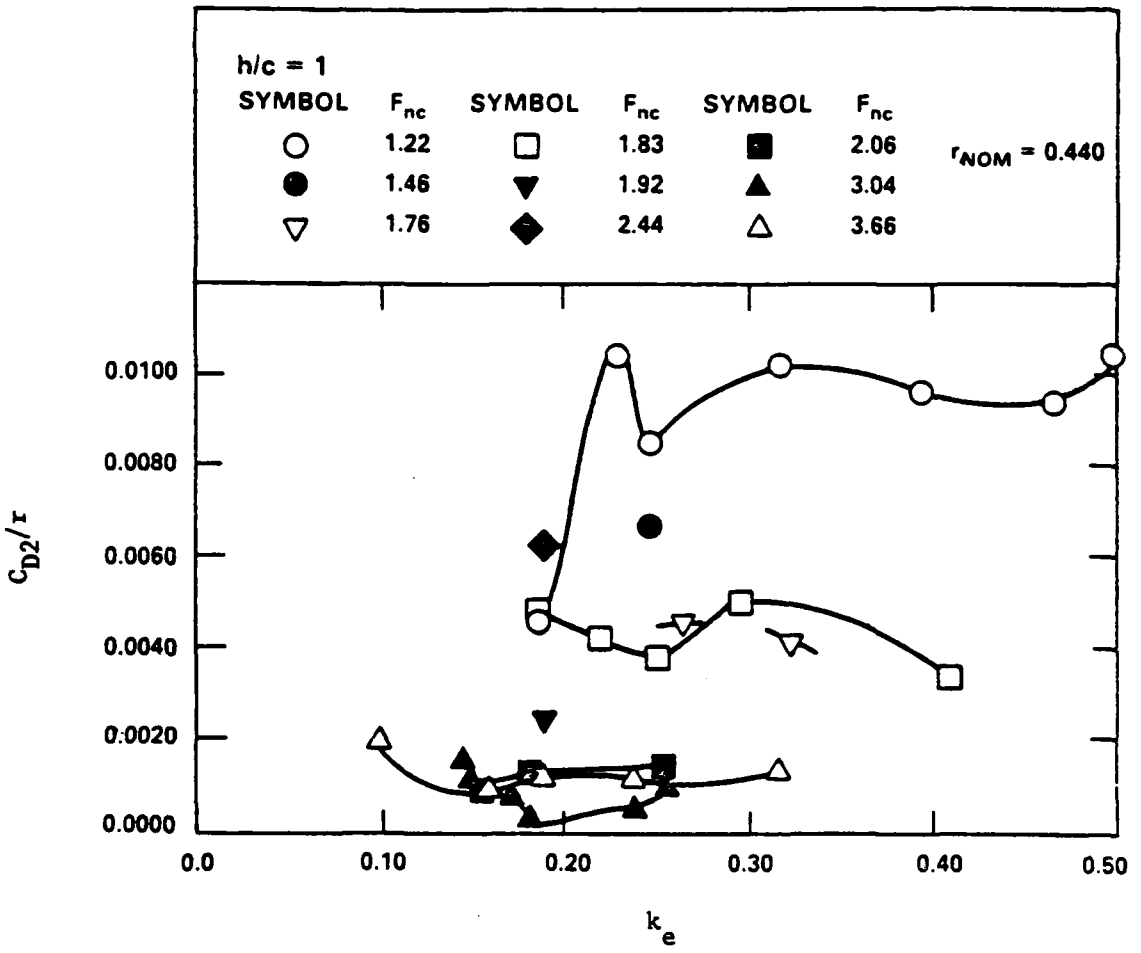


Figure 22 - Oscillatory Drag Response Amplitude Ratio at Twice the Fundamental Frequency; for h/c = 1.0

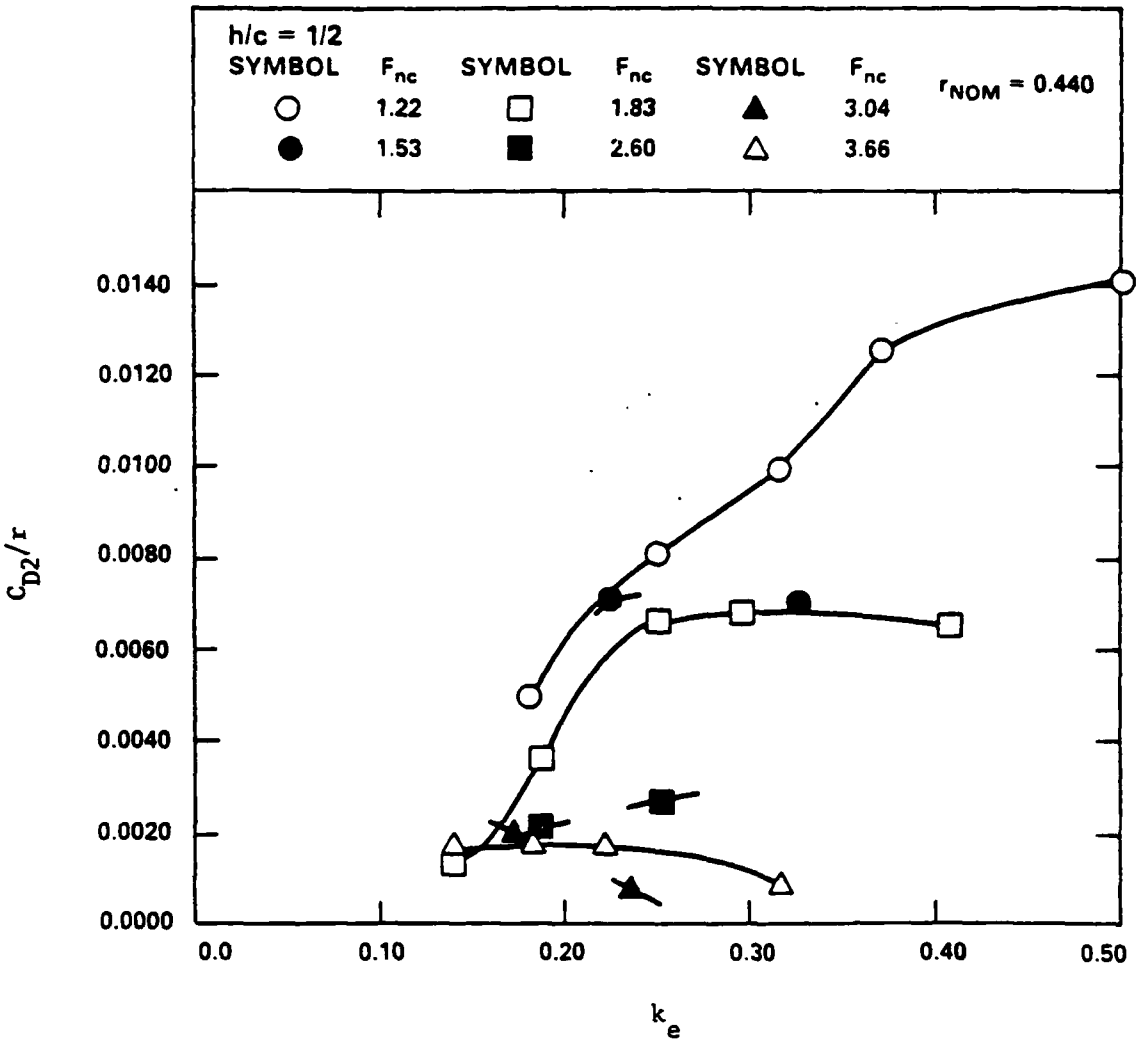


Figure 23 - Oscillatory Drag Response Amplitude Ratio at Twice the Fundamental Frequency; for h/c = 0.5

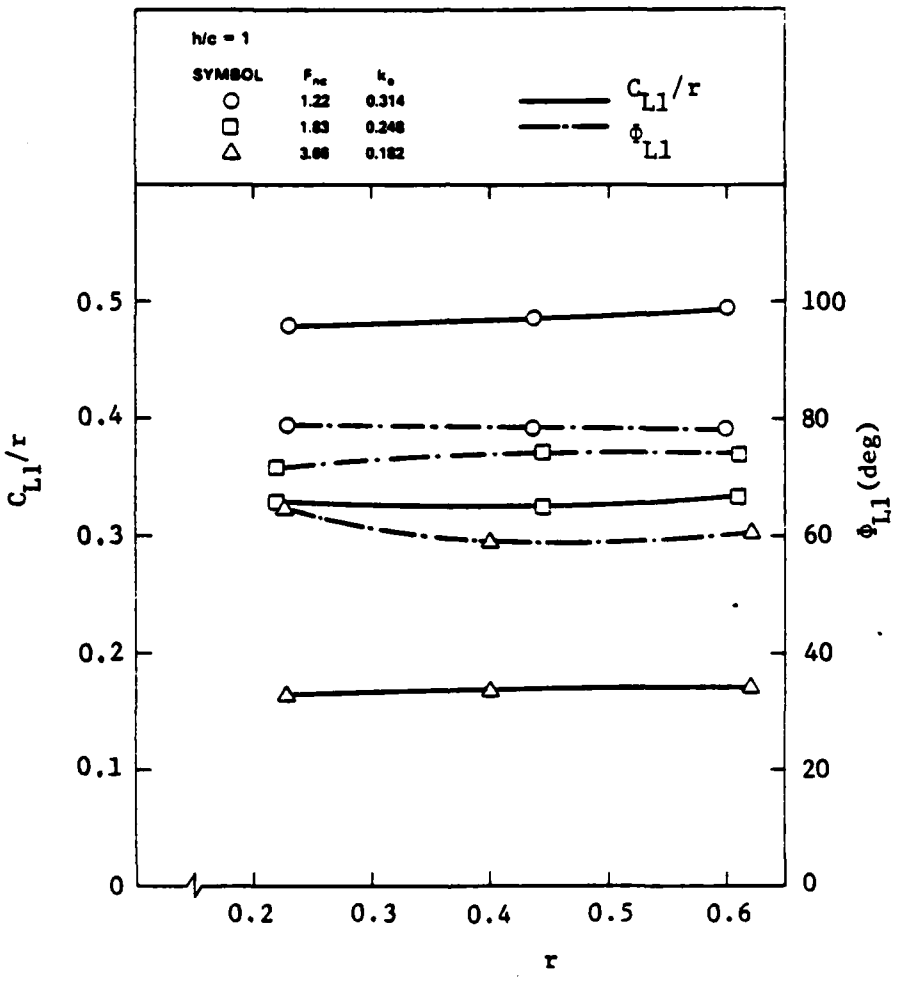


Figure 24 - Linearity Check on First Harmonic Oscillatory Lift Response Ratio; for h/c = 1.0

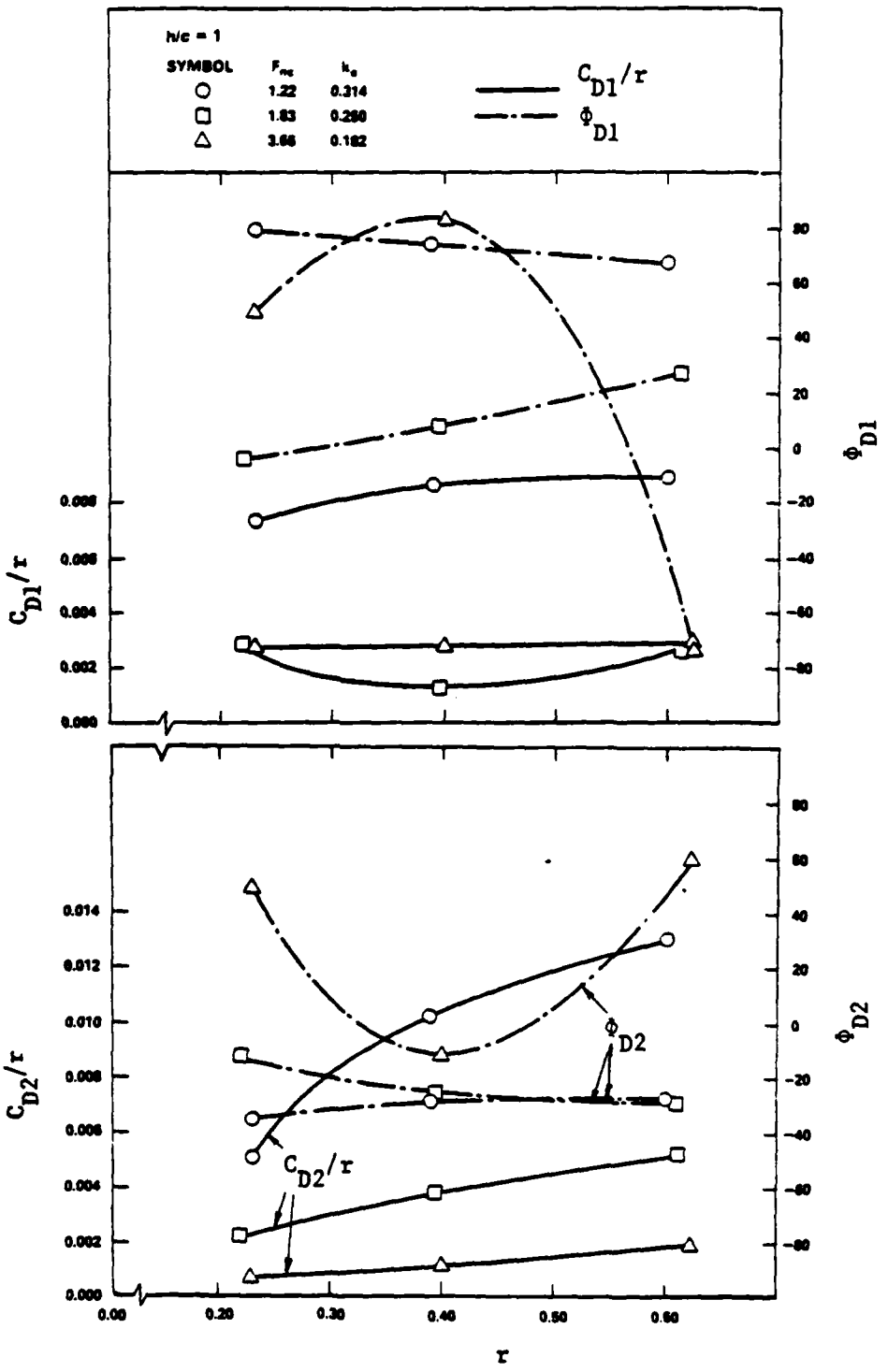


Figure 25 - Linearity Check on First and Second Harmonic Oscillatory Drag Response Ratio; for h/c = 1.0

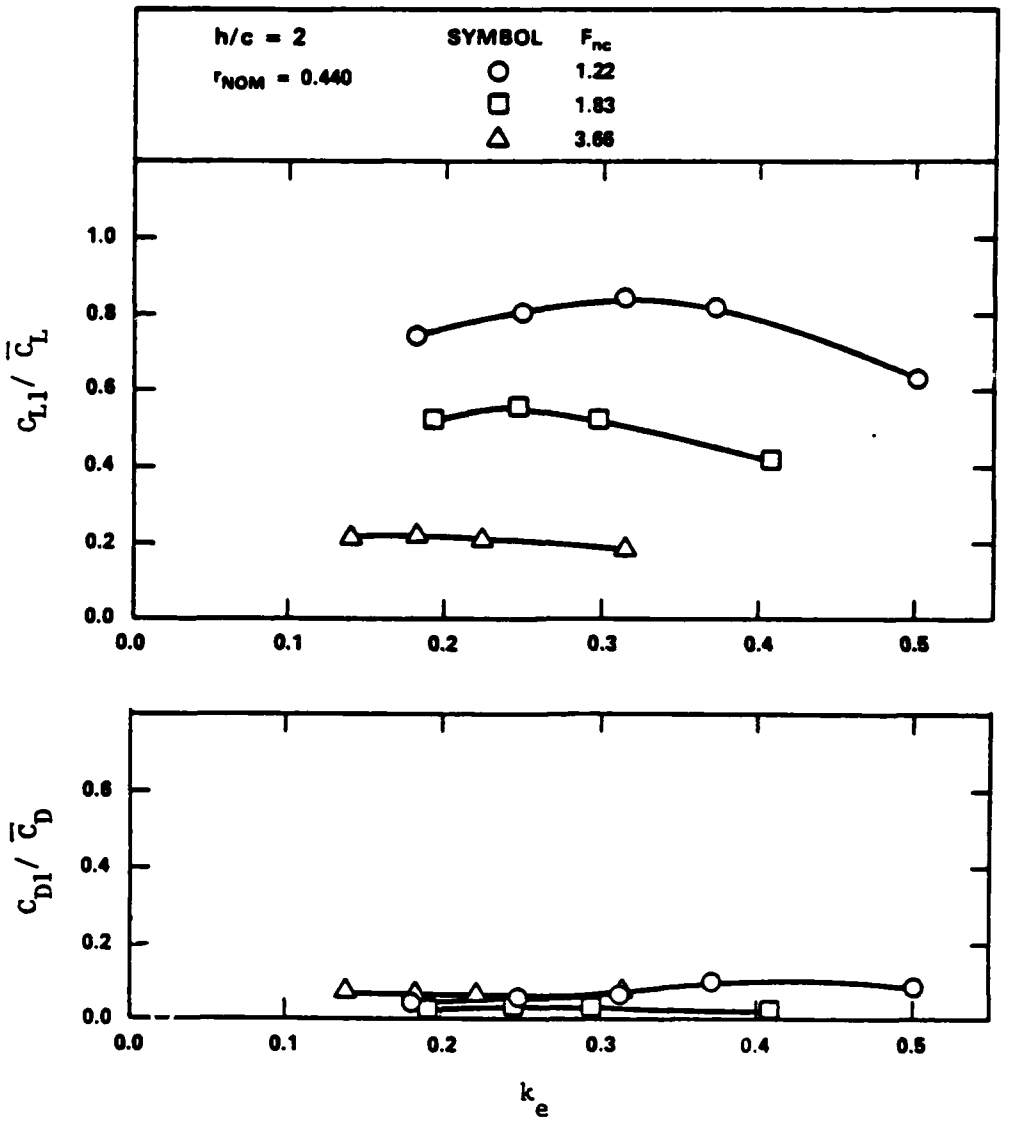


Figure 26 - Ratio of First Harmonic Response Amplitude-to-Mean Value, for Lift and Drag; at h/c = 2.0

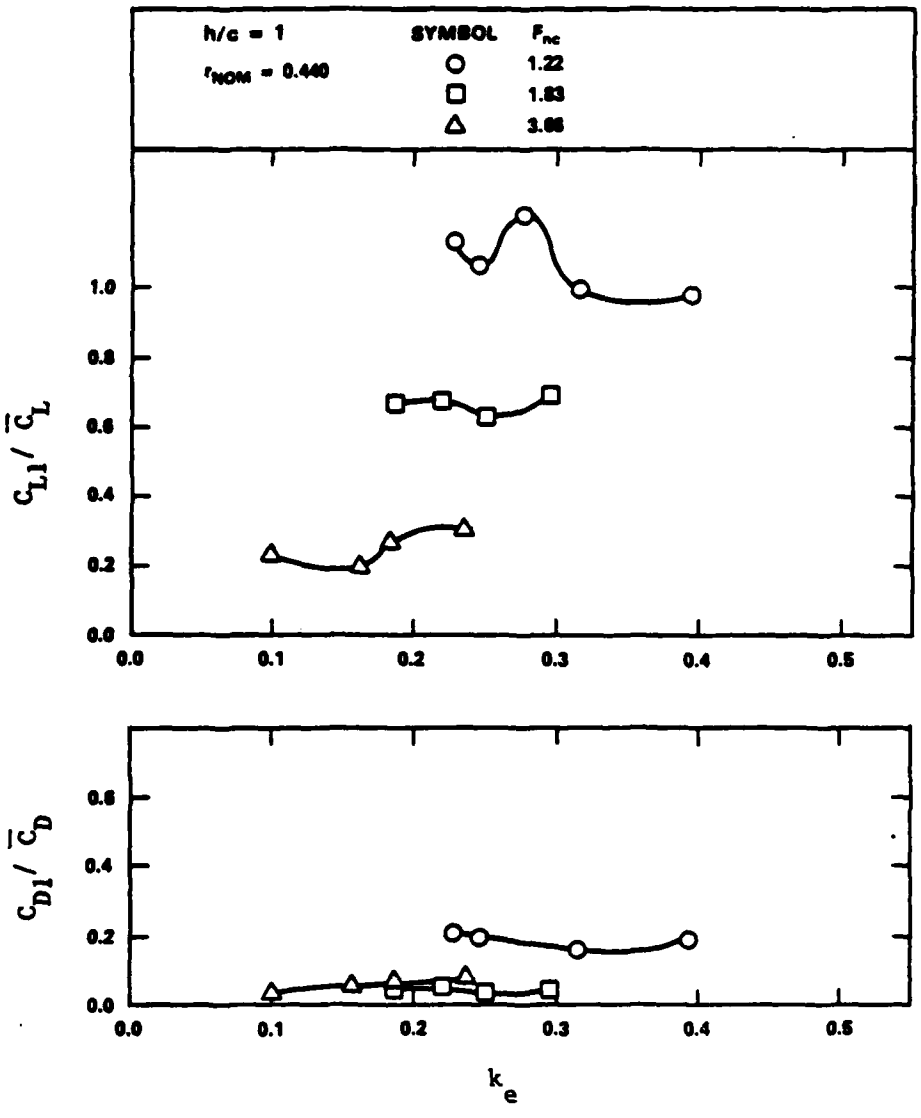


Figure 27 - Ratio of First Harmonic Response Amplitude-to-Mean Value, for Lift and Drag; at h/c = 1.0

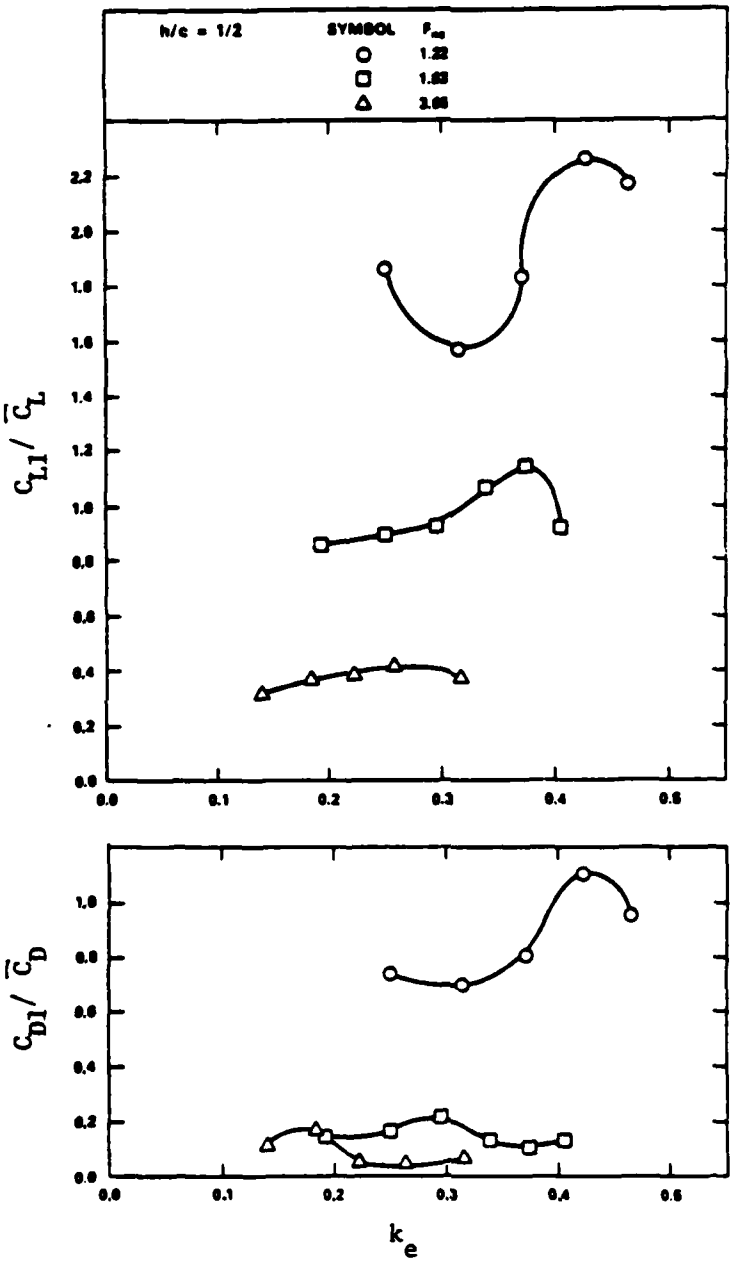


Figure 28 - Ratio of First Harmonic Response Amplitude-to-Mean Value, for Lift and Drag; at h/c = 0.5

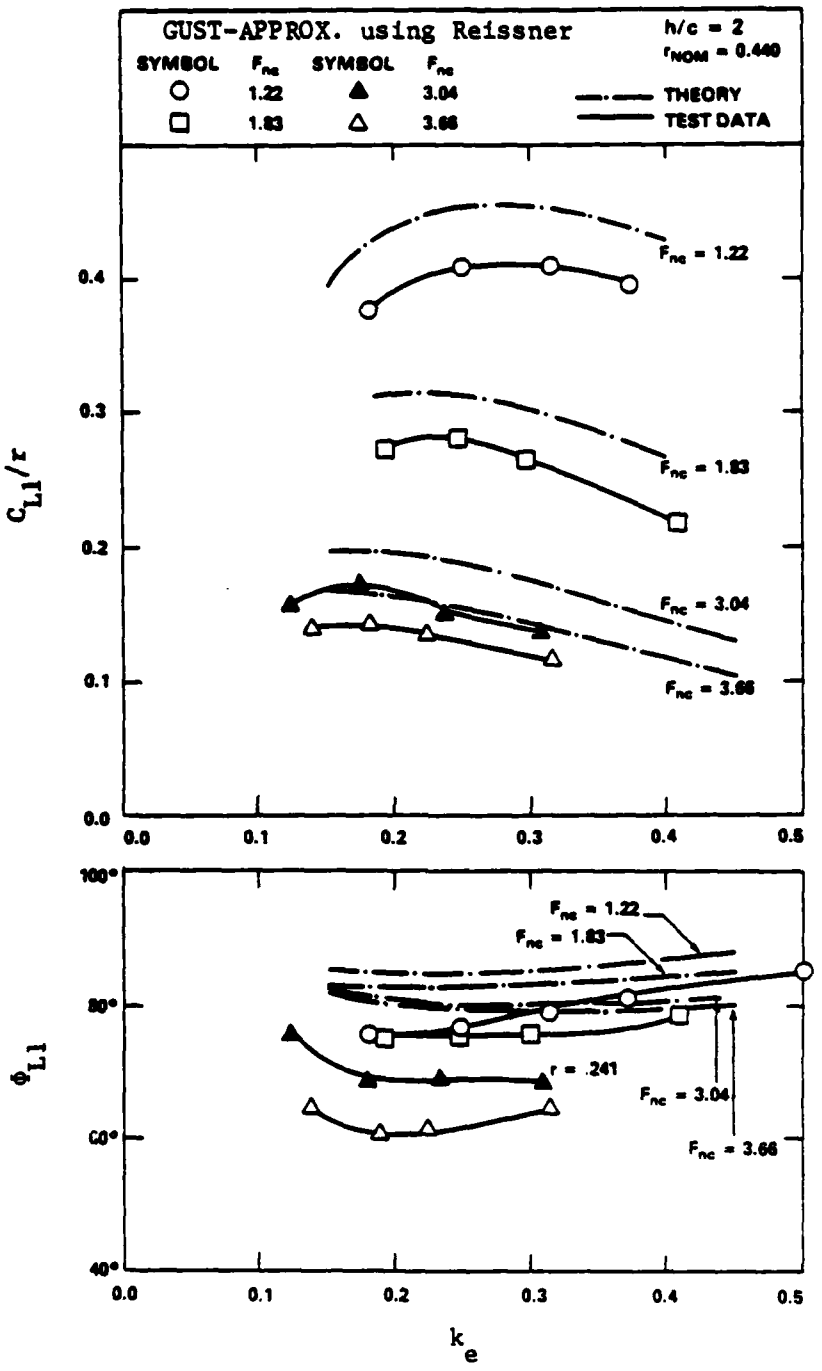


Figure 29 - Comparison of Measured First Harmonic Lift Response Amplitude Ratio and Phase Angle with Approximate Gust-Response Prediction using Reissner Results; for h/c 2.0

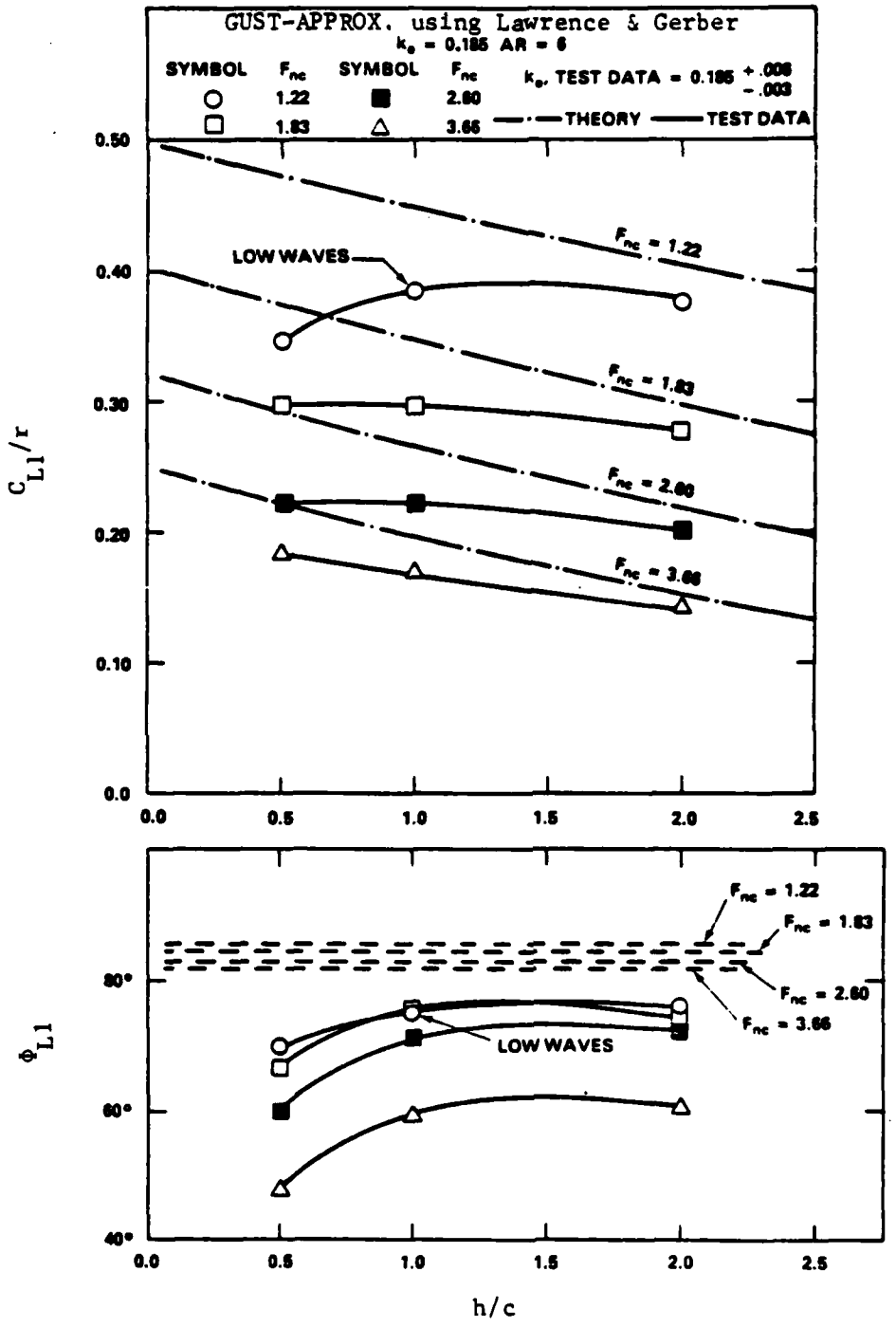


Figure 30 - Comparison of Measured First Harmonic Lift Response Amplitude Ratio and Phase Angle with Approximate Gust-Response Prediction using Lawrence and Gerber Results; for k_e = 0.185

REFERENCES

1. Nishiyama, T., "Linearized Steady Theory of Fully Wetted Hydrofoils," Advances in Hydroscience, Vol. 3, Edited by Ve Te Chow, Academic Press, pp. 237-342 (1966).

2. Wu, T.Y., "A Theory for Hydrofoils of Finite Span," Journal of Mathematics and Physics, Vol. 33, pp. 207-248 (1954/1955); also California Institute of Technology Hydrodynamics Laboratory Report 26-8 (May 1953).

3. Breslin, J.P., "Application of Ship-Wave Theory to the Hydrofoil of Finite Span," Journal of Ship Research Vol. 1, No. 1, pp. 27-35 (1957).

4. Wadlin, K.L., C.L. Shuford and J.R. McGehee, "A Theoretical and Experimental Investigation of Hydrofoils at Subcritical and Supercritical Speeds," NACA Report 1232 (1955).

5. Wilson, M.B. and J.R. Kelley, "Low Froude Number Performance of a Flat Plate Hydrofoil," DTNSRDC Ship Performance Department Report SPD-743-01 (Dec 1976).

6. Jones, C.E., "Flapped Hydrofoils in Smooth Water Subcavitating Flow," General Dynamics/Convair Report ZH-153 (Nov 1961).

7. Feldman, J., "Experimental Investigation of Near-Surface Hydrodynamics Force Coefficients for a Systematic Series of Tee Hydrofoils DTMB Series HF-1," David Taylor Model Basin Report 1801 (Dec 1963).

8. Dixon, R. J., M. Schmiechen, L.C. Shrout, and R.K. Watanabe, "An Experimental Investigation of the Hydrodynamic Characteristics of a Partially Cavitating Hydrofoil," Proc. 19th ATTC, University of Michigan, Ann Arbr, Michigan (Jul 1980).

9. Wilson, M.B., "Experimental Performance of a Flappd Hydrofoil in Calm Water at Low Froude Numbers," DTNSRDC Report 82/002 (Jun 1982).

10. Bisplinghoff, R.L., Ashley, H., and Halfman, R.L., Aeroelasticity, Addison-Wesley Publishing Co., Inc., Reading, Massachusetts, 1957.

11. Fung, Y.C., The Theory of Aeroelasticity, John Wiley & Sons Inc. New York, 1955.

12. Reissner, E. "Effect of Finite Span on the Airload Distribution for Oscillating Wings Part I - Aerodynamic Theory of Oscillating Wings of Finite Span", NACA Tn 1194, 1947.

13. Reissner, E., and Stevens J.E., "Effect of Finite Span on the Airload Distributions for Oscillating Wings Part II - Methods of Calculation and Examples of Application", NACA TN 1195, 1947.

14. Lawrence, H.R., and Gerber, E.H., "Aerodynamic Forces on Low Aspect Ratio Wings Oscillating in an Incompressible Flow", Journal of the Aeronautical Sciences, Vol. 19, No. 11 (Nov 1952).

15. Widnall, S.E., "Unsteady Loads on Hydrofoils Including Free Surface Effects and Cavitation," M.I.T. Fluid Dynamics Laboratory Report 64-2 (Jun 1964).

16. Widnall, S. and Landahl, M., "Digital Calculation of Steady and Oscillatory Hydofoil Loads Including Free Surface Effects," Mass. Inst. Technol. Tech. Note, Navy Contract Nonr 1841(81) (Jul 1965).

17. Widnall S.E., "Unsteady Loads on Supercavitating Hydrofoils of Finite Span", Journal of Ship Research, Vol. 10, No. 2, June 1966.

18. Tsakonas, S. and C.J. Henry," Finite Aspect Ratio Hydrofoil Configurations in a Free Surface Wave System," Stevens Institute of Technology Davidson Lab Report R-1118 (Jun 1966).

19. Kaplan, P., "The Forces and Moments Acting on a Tandem Hydrofoil System in Waves," Stevens Institute of Technology, Experimental Towing Tank Report No. 506 (Dec 1955).

20. Schuster, S. and H. Schwanecke, "On Oscillating Hydrofoils, Part 1," Berlin Towing Tank, ONR Contract No. N62 558-2236 (Dec 1960).

21. Wetzel, J.M. and W.H.C. Maxwell, "Tandem Interference Effects of Flat Noncavitating Hydrofoils," St. Anthony Falls Hydraulic Laboratory Project Report 61 (May 1962).

22. Henry, C.J. and M.R. Ali, "Hydrofol Lift in Head Seas," Stevens Institute of Technology, Davidson Laboratory Report R-982 (Oct 1963).

23. Steele,J.M., "The Unsteady Lift Force on a Restrained Hydrofoil in Regular Waves," NSRDC Report 3386 (Nov 1970).

24. Schuster, S. and H. Schwanecke, "On Oscillating Hydrofoils, Part II," Berln Towing Tank, ONR Contract No. N62 558-2236 (Jun 1962).

25. Karafiath, G., "Experimental Investigation of Hydrofoil Force Response in Regular Seas at Low Chord Froude Numbers," DTNSRDC Ship Performance Dept. Report SPD-0956-01 (Feb 1981).

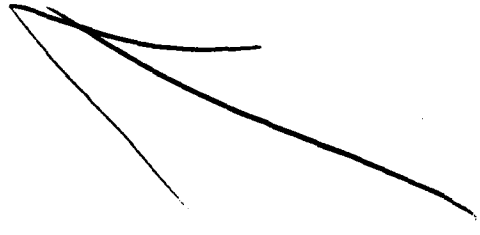
26. Loftin, L.K., "Theoretical and Experimental Data for a Number of NACA 6A-Series Airfoil Sections," NACA Report 903 (1948).

27. Wilson, M.B., "Lifting Line Calculations for Hydrofoil Performance at Arbitrary Froude Number and Submergence. Part I Fixed Shape Elliptical Circulation Distribution," DTNSRDC Ship Performance Department Report DTNSRDC/SPD-0839-01 (Jun 1978).

28. Boeing Company, "Hydrofoil Analysis and Design Program (HANDE). Theory Manual Vol. 2," Boeing Document D321-51312-2 (Jul 1976).

29. Ashley, et al, "New Directions in Lifting Surface Theory", Journal of the American Institute of Aeronautics and Astronautics, Vol. 3, No. 1 pp. 3-16

30. Besch, P.K. and Rood, E.P., "Accuracy of Hydrofoil Loading Predictions Obtained form a Lifting Surface Computer Program,", DTNSRC Report 79/039 (Sep 1979).



REVIEW OF ACTIVITIES OF HIGH SPEED MARINE VEHICLE COMMITTEE OF INTERNATIONAL TOWING TANK CONFERENCE

BY

DANIEL SAVITSKY*

In 1978 the 15th ITTC recognized the increasing utilization of towing tanks in the development of high-speed marine vehicles and created a High Speed Marine Vehicle Panel. Their charge was to identify the status of model test procedures unique to high speed marine craft and to identify the hydrodynamic problems related to high speed vessel model tests and their full scale extrapolation procedures.

The panel was composed of eight members representing seven countries: United States, England, France, West Germany, Japan, The Netherlands and the USSR. A series of rather extensive reports were prepared whose total volume exceeded the publication limit set by the 16th ITTC. This problem was solved when the David W. Taylor Naval Ship Research and Development Center agreed to publish all the material as one of their reports and an extensive summary of that work was published in the official 16th ITTC Proceedings (August 1981).

The title of the DWTNSRDC report is: "Status of Hydrodynamic Technology as Related to Model Tests of High Speed Marine Vehicles", DTNSRDC-81/026, July 1981. It contains separate status reports related to model test procedures for SWATH, semidisplacement round bilge hulls, planing hulls, semisubmerged hydrofoils, surface effects ships and air cushion vehicles. In addition the report presents a listing of some 35 recommendations of technology studies for the 6 high speed vehicle types. It is recommended that members of the ATTC obtain copies of this report for their libraries.

The 16th ITTC, during its meeting in Leningrad in 1981, recommended that the High Speed Panel become a full committee of the ITTC. This new High Speed Marine Vehicle Committee is currently preparing a report dealing with the following recommendations approved by the Executive Committee of the 16th ITTC. This report will be presented at the 17th ITTC to be held in Sweden in September 1984.

1. Prepare and circulate a questionnaire to the ITTC membership to solicit their opinions on the various aspects of testing high speed marine vehicles.

2. Prepare a state of the art report on the testing of submerged hydrofoils.

---

*Acting Director, Davidson Laboratory, Stevens Institute of Technology

3. Prepare a bibliography on all high speed marine vehicles.

4. Undertake a review of symbols, definitions, etc. for inclusion in the ITTC Dictionary of Ship Hydrodynamics and List of Standard Symbols.

5. Encourage existing ITTC technical committees to undertake some of the 35 technical recommendations presented in their report.

In addition, the following technology items are being considered:

1. Appendage scaling.

2. Free-to-surge and fixed-surge model test techniques.

3. Skin friction coefficients.

4. Cavitation influence on test procedures.

5. Aerodynamic interference effects on towing tank carriages.

Some of the general results of the replies to the questionnaire may be of interest to the ATTC membership:

1. The greatest activity in high speed vehicle model testing is with round bilge semi-displacement hulls and planing craft.

2. There are three times as many test establishments conducting model tests on semidisplacement craft and planing hulls than with any other vehicle type.

3. There has been a significant increase in the number of establishments that have tested SWATH vessels for the first time in the past three years.

4. The most common type of testing on high speed vehicles is resistance, followed by powering and to a lesser extent seakeeping.

5. For the vast majority of member establishments, high speed craft testing represents less than 20 percent of their total model test activities and 80 percent of this work is developmental.

It is timely that the 20th ATTC has just incorporated a High Speed Vehicle Committee into its organization. The list of technology studies recommended by the ITTC High Speed Marine Vehicle Committee is long and complex indicating the large number and variety of unresolved problems in this area of tankery. The ITTC invites the newly formed ATTC committee on High Speed Vehicles to join with them in providing solutions to our problems.

BANQUET

ADDRESS

THE UNCERTAIN 80'S

By: Dean J. B. Hadler
Webb Institute of Naval Architecture

Mr. Chairman, Members and Guests of the 20th American Towing Tank Conference:

My talk today is entitled "The Uncertain 80's". Any industry, just like life, is fraught with uncertainties. We are now experiencing more uncertainties than at any time I can recall. I suspect we are at a turning point in which our industry will encounter many changes throughout the next few years - hence, the title.

Tonight, as Dan Savitsky asked, I would like to make a few projections on possible trends in towing tank work. This is a new role for me - projecting into the future - rather then reporting on research accomplished or design problems solved.

In undertaking this task, I bring a number of different perspectives which I would like to identify so you know the biases which I bring to my observations. My first perspective is that of an academician who has the task of reviewing and helping to reshape a naval architecture educational program for the future. My second is as Director of a college research center which is primarily concerned with commercial shipping and my last is as a consultant to a wide variety of shipbuilding and ship design organizations in the United States.

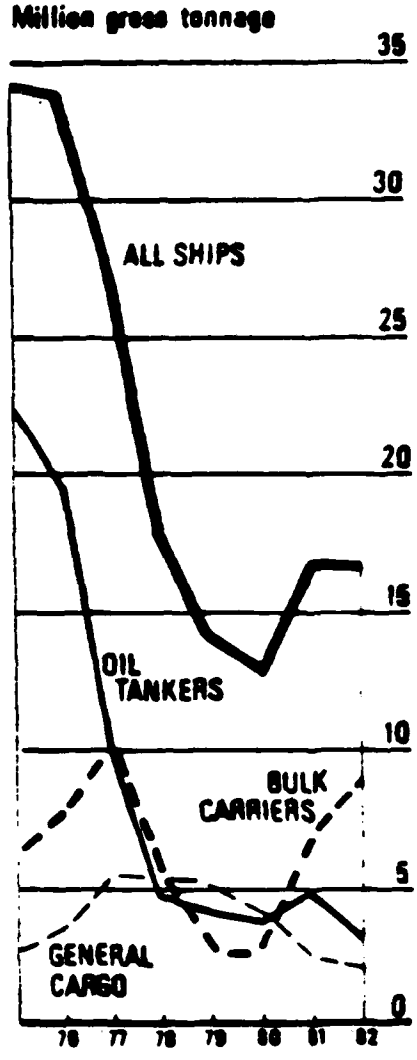
Since towing tanks act as a business in support of the shipbuilding and ocean exploitation industry, I think it wise to look at the projections for these industries before looking into those for towing tanks. My observations are limited to the commerical sector.

I would now like to highlight a few of the statistical observations from the shipbuilding and ship operating portions of the industry. I will first examine the shipping and shipbuilding situation from the world perspective.

Figure 1 shows the annual tonnage of ships constructed by type over the last seven years. From this figure, we can see the decline in the number of ships constructed - particularly of tankers. Although there has been a temporary increase in bulk carriers, recent reports show that they too are decreasing. Of the ships under construction, about 50 percent are being built in Japan and 10 percent in South Korea. Korea's market share is rising a couple of percentage points per year at the expense of other countries. Korea's price is about 10 percent less than Japan's; thus, it can be expected that their growth trend will continue. China, as well as other developing countries, is trying to break into the world market. Only Finland, of the developing countries, is booming. They are building ice breakers, cruise liners and special vessels for Russia and western clients. Analysis of the world stock pile of ships shows an excess of about 15 percent, much of which is in laid-up tankers. This results in low freight rates and low profitability. All of this leads to the conclusion that there is too much shipbuilding capacity in the world and it is shifting from the developed to the developing countries.

The shipping industry is now waiting to see when the largest shipping companies in Hong Kong - Sir Pao and C. Y. Tung - start buying surplus ships. This would be a sign that an upsurge in shipping is expected. However, the industry does not expect this to happen for another year or two.

Let us now examine the shipping and shipbuilding industries from the United States perspective. The United States flag fleet has gone from 1,100 ships in 1950 to less than 500 today. Our foreign trade has dropped from 42 percent to less than 5 percent in the same time.



Annual Completions By Ship Types

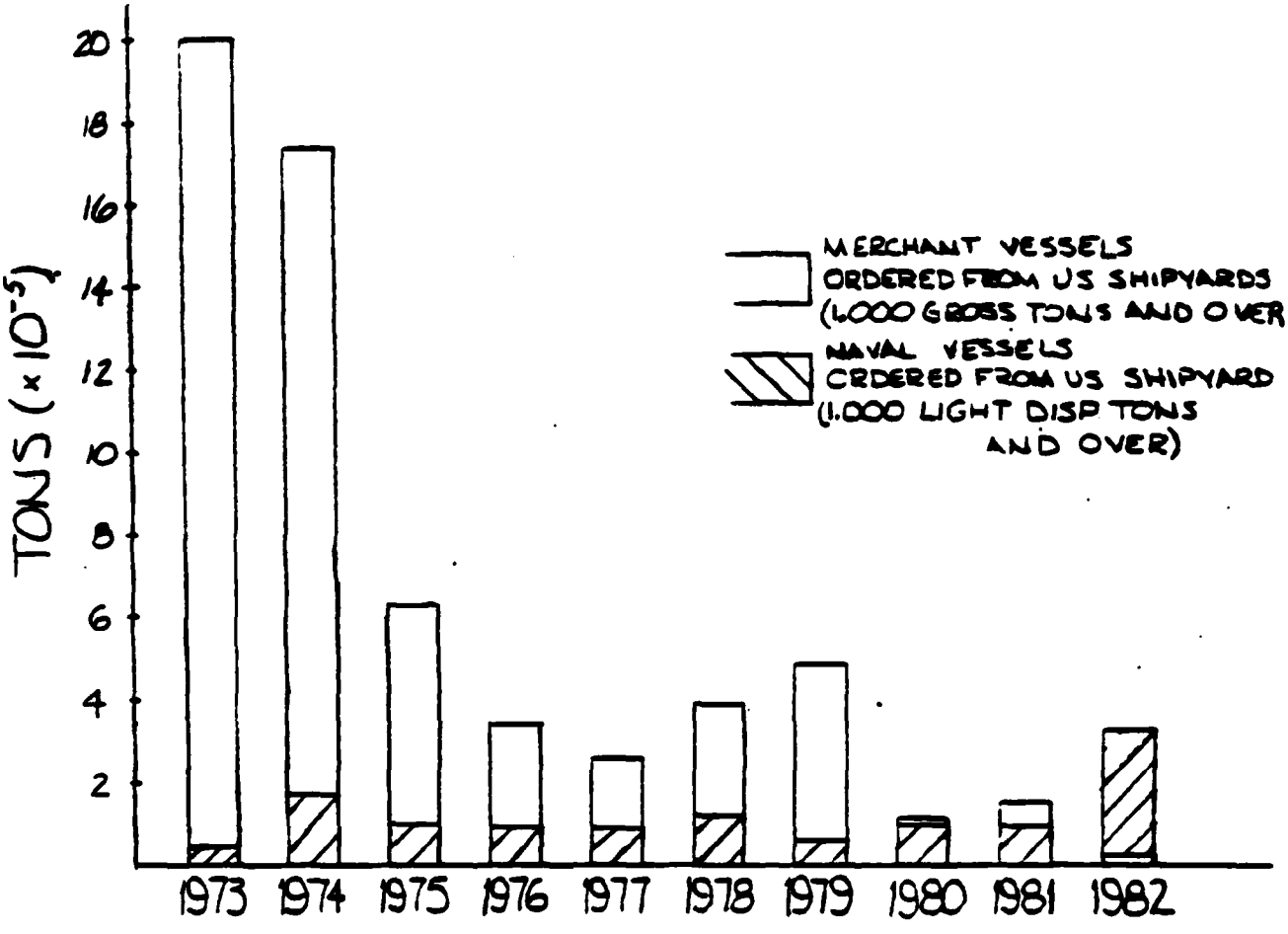
Figure 1

Figure 2 shows the tonnage of merchant or merchant-like ships ordered from the United States yards over the past nine years. The graph shows the rather rapid decline in United States shipbuilding. The recession and the actions of the Reagan administration have accelerated this decline. This decline has been partially mitigated by the rise in commercial ship construction for military use, particularly the "T" class or prepositioning ships for MSTS, which should hold the nucleus of the commercial yards together for a couple of years. After that, the future is very uncertain.

Let us examine the offshore oil exploration industry. It has gone down the same pike as shipbuilding. Today, only two new rigs are under construction in the United States. The oil glut and recession have depressed the market for oil; hence, the limited need for rigs, but the overall picture is brighter than for shipbuilding because oil shortages are likely to occur in the future. Also, American companies are shifting more of their exploration to American shores. The expected opening of new leases (twice as many as over the last 19 years) in the Gulf of Mexico will create a demand for more rigs, particularly for those which can operate at depths greater than 700 feet.

Turning to the inland waterways, the river tug-barge shipping industry also tends to rise and fall with the economic health of the nation. Cost of inland water transportation is about half that of rail. However, new federal laws could change that if river tolls are increased substantially. The demand for coal, one of the major commodities carried, can go up or down with world energy demands.

A newer industrial frontier is Arctic exploration for oil, gas and minerals. As these items become more scarce, the Arctic becomes more attractive. Much research and development will be necessary in order to economically extract resources from this environment. Some estimates indicate that in the next ten years, 20 billion dollars will be required for developing the Arctic area north of Canada alone.


TONS (x 10⁻⁵)
20
18
16
14
12
10
8
6
4
2
1973
1974
1975
1976
1977
1978
1979
1980
1981
1982
MERCHANT VESSELS ORDERED FROM US SHIPYARDS (1,000 GROSS TONS AND OVER
NAVAL VESSELS ORDERED FROM US SHIPYARD (1,000 LIGHT DISP TONS AND OVER)

Deep ocean mining, which will also require extensive research and development, is being greatly delayed pending achievement of an international agreement on the "law of the sea".

With all of the uncertainty about the future of the shipbuilding industry, where do model basins stand? This uncertainty is reflected upon us. To analyze it further, we need to identify our numerous roles.

A) Help ship designers develop and predict the performance of their designs.

B) Solve special ship operation or design problems.

C) Applied research either at the behest of sponsors or on the initiative of the model basin.

The first two roles are heavily dependent upon the state of the shipping and shipbuilding industries, whereas the latter will be concerned with the evolving industries such as Arctic exploration.

In spite of the limitations on shipbuilding, I have noted a number of trends which augment the work of the model basin:

1) The high cost of ships, together with competition between builders, has resulted in much more comprehensive model test programs, i.e., some ship hull designs have gone through a development program involving 8 to 10 model configurations. All of these were tested for their resistance characteristics and at least half were tested self-propelled with stock propellers and with wake surveys at two displacements.

2) The specialized nature of each design frequently creates specialized hydrodynamic or structural problems which require comprehensive effort on the part of model basins to solve; i.e., severe propeller-induced vibration and noise problems on container-type ships.

3) The growing concern with production is now requiring special effort on the part of model basins to develop hulls that are hydrodynamically efficient and less costly to build; i.e., how can the hull be reproportioned so that it can be built faster and cheaper without loosing any of its hydrodynamic efficiency? Closer ties between the designer, the basin and shipbuilder are required to achieve this goal.

4) An area that I suspect will become more important in the future is the smaller vessels such as ocean fishing vessels. They are facing some of the same economic pressures as the larger vessels and will need more efficient and more sophisticated designs in order to compete.

5) The biggest problem for the United States model basins is to be both cost and time competitive with foreign model basins in all aspects of the ship design and test role. This is the same problem the United States shipyards face.

Let us now look at the last role of model basins, that of applied research in both sponsored and self-generated areas. In the United States, most basins, except DTNSRDC, are dependent upon sponsored research. Let us take a look at the trends:

1) Government-sponsored research is level-funded or decreasing. With inflation, the net effect is a decrease in funding.

2) The recession has also resulted in a decline in corporate research.

3) The research which is going on appears to be of two types:

   A) Trying to improve the propulsive efficiency of current ships and of possible new construction. Only a few years ago, fuel was about 7 percent of the operating cost. Today, it is as high as 40 to 50 percent of total operating costs.

   B) Looking ahead to future operations such as Arctic exploration.

Although I cannot foresee who will sponsor it, I believe that the following work must be done by model basins.

1) Where analytical means are not available, build experimental data basis for future design work. I find much of the past experimental work has been put into forms that are easily used in design synthesis models. There are many gaps, however, which need to be filled.

2) Basic research to build up our banks of knowledge - both analytical and experimental.

I must also note that politicians and many businessmen are short sighted. They tend to take the short-term approach and do not build for the future. We need to turn this around by more aggressive action in political and business circles.

In summary, I reach the following conclusions:

1) There will be some contraction in model basin work in parallel with the shipbuilding industry.

2) The model basins, particularly those in the United States, have to improve their efficiency and effectiveness just as does the shipbuilding industry if they are to be competitive.

3) The vigor of the shipping industry and the model basins will also be heavily dependent upon the action of governments, particularly the United States.

4) Privately sponsored research may start to increase as the recession subsides, but it probably will tend to go in the direction of new opportunities or into improving the productivity of the shipping industry.

5) Model basins need to work more closely with our industry to improve the effectiveness of both.

6) These are changing and challenging times. They require imagination, flexibility and perseverance to develop and exploit the opportunities that are before us.

Thank you for letting me share these thoughts with you.

END

FILMED

9-83

DTIC